

In the format provided by the authors and unedited.

The highly surprising behaviour of diphosphine ligands in iron-catalysed Negishi cross-coupling

Antonis M. Messinis^{ID}¹, Stephen L. J. Luckham^{ID}¹, Peter P. Wells^{2,3,4}, Diego Gianolio³, Emma K. Gibson^{ID}^{4,5}, Harry M. O'Brien^{ID}¹, Hazel A. Sparkes¹, Sean A. Davis¹, June Callison^{4,6}, David Elorriaga^{ID}¹, Oscar Hernandez-Fajardo¹ and Robin B. Bedford^{ID}^{1*}

¹School of Chemistry, University of Bristol, Bristol, UK. ²School of Chemistry, University of Southampton, Southampton, UK. ³Diamond Light Source, Harwell Science and Innovation Campus, Didcot, UK. ⁴UK Catalysis Hub, Research Complex at Harwell, Rutherford Appleton Laboratory, Didcot, UK. ⁵School of Chemistry, University of Glasgow, Glasgow, UK. ⁶Department of Chemistry, University College London, London, UK.
*e-mail: r.bedford@bristol.ac.uk

Supplementary Information

The Highly Surprising Behaviour of Diphosphine Ligands in Iron-Catalysed Negishi Cross-Coupling

Antonis M. Messinis,¹ Stephen L. J. Luckham,¹ Peter P. Wells,^{2,3,4} Diego Gianolio,³ Emma K. Gibson,^{4,5} Harry M. O'Brien,¹ Hazel A. Sparkes,¹ Sean A. Davis,¹ June Callison,^{4,6} David Elorriaga,¹ Oscar Hernandez Fajardo,¹ Robin B. Bedford,^{1}*

1. School of Chemistry, University of Bristol, Cantock's Close, Bristol, BS8 1TS, U.K.

2. School of Chemistry, University of Southampton, Highfield, Southampton SO17 1BJ, U.K.

3. Diamond Light Source, Harwell Science and Innovation Campus, Chilton, Didcot OX11 0DE, U.K.

4. UK Catalysis Hub, Research Complex at Harwell, Rutherford Appleton Laboratory, Harwell, Oxon, Didcot OX11 0FA, U.K.

5. School of Chemistry, Joseph Black Building, University Avenue, University of Glasgow, Glasgow, G12 8QQ, U.K.

6. Department of Chemistry, University College London, 20 Gordon Street, London WC1H 0AJ, U.K.

Contents

1 General Considerations	3
2 Negishi cross-coupling with various diphosphines.....	7
3 An examination of the variation of phosphine properties on catalyst performance 21	
4 Synthesis of diphosphine complexes of FeBr₂.....	60
5 Comparison of the catalytic performances of iron(I) vs. iron(II).	80
6 X-ray Absorption Fine Structure (XAFS) spectroscopic studies.....	85
7 Synthesis of ZnBr₂ diphosphine complexes.....	102
8 Competition for diphosphine coordination between FeBr₂ and excess ZnBr₂. 138	
9 DFT calculations on equilibration of dpbz between Fe(II) and Zn(II).....	153
10 Operando NMR spectroscopic investigation of the dpbz-complex speciation in the Negishi cross-coupling.....	165
11 Examining Aryl-Zn/Fe transmetallation	171
12 Kinetic investigations on the Negishi coupling of 1 with 2a using <i>in situ</i> FT-IR spectroscopy	200
13 Crystallographic data.....	219
Supplementary References.....	230

Supplementary methods

1 General Considerations

1.1 Experimental techniques

Unless otherwise stated, all manipulations were carried out under an atmosphere of dry nitrogen using standard Schlenk line techniques or in an argon-filled MBraun glovebox. All glassware was dried at 180 °C, evacuated and back filled with nitrogen gas prior to use. All Schlenk vessels used were equipped with threaded Rodaviss joints and J. Youngs taps, eliminating the need for high vacuum grease. In a few instances, Glindemann PTFE sealing rings were used. Schlenk line air-sensitive filtrations were performed using stainless steel cannula filters fitted with a layer of glass micro-fiber filter paper and a second layer of filter paper mounted with PTFE tape. Filtrations in the glove box were performed by syringing the mixture through a Millipore milex PVDF 0.45 µm filter. NMR spectra of air-sensitive samples were acquired in J. Youngs NMR tubes or in airtight screw top NMR tubes. In order to avoid contamination with other transition metals (especially palladium), all reactions and experiments were performed with new glassware which were used exclusively with iron and thoroughly cleaned in “iron-only” base and acid baths. All catalytic reactions were performed in the specially designed Schlenk shown in Supplementary Figure 1.

Accurate measurement of the volume of solvents, reagents and stock solutions was achieved using newly bought gas tight Hamilton micro syringes, volumetric flasks and recently calibrated Gilson pipettes. In all the kinetic experiments, each reagent addition was performed with a designated syringe and stainless-steel needle ensuring reproducibility and minimising the chances of contamination.

Dry CH₂Cl₂, acetonitrile, toluene, diethyl ether, THF and hexane were obtained from a solvent purification system (passed over alumina). All other solvents were dried over molecular sieves (3 Å) apart from acetone which was distilled from boric anhydride. All solvents were deoxygenated prior to use.

GC-FID analyses were performed using, internal standard, by collecting 0.1 – 0.2 mL aliquots from the reaction mixture followed by: quenching with 0.7 mL of 0.5 M HCl solution, dilution with 1.5 mL of distilled water and extraction with 1 mL of CH₂Cl₂. Prior to GC-FID analysis and quantitation of unknown samples, seven-point calibration of the GC-FID instrument for BnBr (**1**), Bn(4-tolyl) (**3**), Bn₂ (**11**) and (4-tolyl)₂ (**10**) using *n*-dodecane as the internal standard was performed with a coefficient of determination (*r*²) of over 0.9999 for each analyte.

1.2 Materials

Anhydrous NMR spectroscopic solvents were purchased from Sigma-Aldrich or Apollo Scientific, stored over molecular sieves (3 Å) and deoxygenated prior to use. FeBr₂ (99.9995%), ZnBr₂ (99.9995%), potassium metal, graphite, 4,4'-dimethylbiphenyl (**10**), 1,2-diphenylethane (**11**), 1,2-bis(diphenylphosphino)ethane (dppe), 1,2-bis(diethylphosphino)ethane (depe), 1-bromo-3,5-di-*tert*-butylbenzene and 4-iodotoluene were purchased from Sigma-Aldrich and used as received. Cyclooctadiene and *n*-dodecane were purchased from Sigma-Aldrich, stored over molecular sieves (3 Å) and deoxygenated prior to use. Benzyl bromide (BnBr) was purchased from Sigma-Aldrich, distilled under vacuum, stored over molecular sieves (3 Å), filtered, deoxygenated and kept in the freezer of an Ar-filled glove box. 4-Tolylmagnesium bromide solution 1.0 M in THF and methylmagnesium bromide solution 3.0 M in diethyl ether were purchased from Sigma-Aldrich and titrated prior to use with the method reported by Hoye *et. al.*¹ 1,3-Bis(diphenylphosphino)propane (dppp), *cis*-1,2-bis(diphenylphosphino)ethylene (*cis*-dppen), 1,2-Bis[(2*R*,5*R*)-2,5-dimethyl-1-phospholanyl]benzene (MeDuphos), 1,2-Bis[(2*R*,5*R*)-2,5-diisopropyl-1-phospholanyl]benzene (iPrDuphos), diphenylchlorophosphine, *n*-butyllithium and *trans*-1,2-bis(diphenylphosphino)ethylene (*trans*-dppen) were purchased from Alfa-Aesar and used as received. 1,2-Bis(diphenylphosphino)benzene (dpbz) and (2*R*,3*R*)-(−)-2,3-bis(diphenylphosphino)bicyclo[2.2.1]hept-5-ene (norphos) were purchased from TCI and used as received. 4-Methyldiphenylmethane was purchased from Santa Cruz Biotechnology Inc. and used as received. 1,2-Bis(dichlorophosphino)benzene was purchased from Apollo scientific and used as received. 3,4-Dibromothiophene was purchased from Strem and used as received. Potassium graphite,² 3,4-bis(diphenylphosphino)thiophene (dpth),³ Li(4-tolyl),⁴ and 1,2-bis(bis(3,5-di-*tert*-butylphenyl)phosphino)benzene (sciopp)⁵ were synthesised according to literature procedures.

1.3 General instrumentation

Elemental analysis (CHN) was performed on a Euro Vector EA3000 elemental analyzer at the University of Bristol or were obtained by Elemental Microanalysis Ltd, UK.

Mass spectra were recorded on a MicrOTOF II instrument as a solution in toluene:THF (1:4) using HR-ESI as the ionisation mode.

Gas chromatographic analyses were performed with an Agilent Technologies 7820A GC-FID equipped with an Agilent 19091J-413, 325 °C, 30 m x 320 µm x 0.25 µm HP-5 column

using the oven programme: 90 °C hold for 0.5 min; 50 °C/min to 150 °C and hold for 0.5 min; 40 °C/min to 210 °C and hold for 0.5 min; 40 °C/min to 250 °C and hold for 2 min.

Solution phase NMR spectra were collected on a Jeol ECS 300, Jeol ECS 400, Varian 400-MR or a Varian VNMR S500 spectrometer at ambient probe temperatures (25°C). Chemical shifts (δ) are reported in ppm and were referenced to residual proton impurities in the deuterated solvent as reported by Fulmer *et al.*,⁶ in ppm, while multiplicities are indicated as: s (singlet), d (doublet), dd (doublet of doublet), t (triplet), dt (doublet of triplet), td (triplet of doublet), q (quartet), quint (quintet), h (heptet), m (multiplet), br s (broad singlet); coupling constants (J) are in Hertz (Hz). Half-height peak widths for broad peaks are reported in Hz in parentheses after the broad singlet (br s) annotation. Virtual multiplets are reported as simple multiplets as they appear on the spectrum.

In situ FT-IR measurements were performed using a Mettler Toledo ReactIR 15 equipped with an AgX 6 mm x 1.5 m (Silver halide) fiber and DiComp (Diamond) tip probe or with an AgX 9.5 mm x 1.5 m (Silver halide) fiber and SiComp (Silicon) tip probe. Spectra processing was performed using the iC IR software.

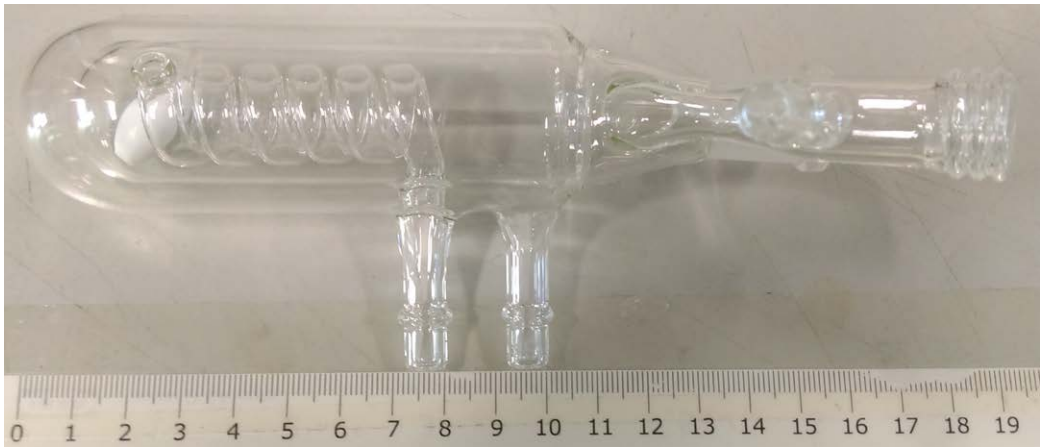
UV-Vis spectra were acquired with an Ocean Optics TP300-series transmission probe or with a 1 cm quartz glass cuvette fitted with a J. Youngs tap coupled to a USB2000+UV-Vis spectrometer with a DT-MINI-2-GS light source. Spectra were collected using Ocean View software and processed using SpectraGryph 1.1.

Samples for electron microscopy analysis were imaged using a JEOL 2100 TEM operating at 200 kV. TEM images were acquired using a Gatan Orius SC1000 digital camera. Energy dispersive X-ray (EDX) analyses and elemental mapping were performed in HAADF-STEM mode with a spot size of 1.5 nm using an Oxford Instruments Aztec X-ray system.

Accurate temperature control of reactions (± 0.05 °C) was achieved with a Julabo F81-ME cryostat.

1.4 Custom-made equipment and experimental setup

Kinetic experiments and reaction monitoring was performed at constant temperature using custom made jacketed Schlecks fitted with an internal cooling coil made by Mr Duncan Tarling in the University of Bristol (Supplementary Figure 1). The complete experimental setup for reaction monitoring using FT-IR spectroscopy is presented in Supplementary Figure 2. Reactions were monitored using UV-vis spectroscopy in a similar fashion.



Supplementary Figure 1. Jacketed Schlenk used to perform kinetic experiments and reaction profiling at constant temperature.



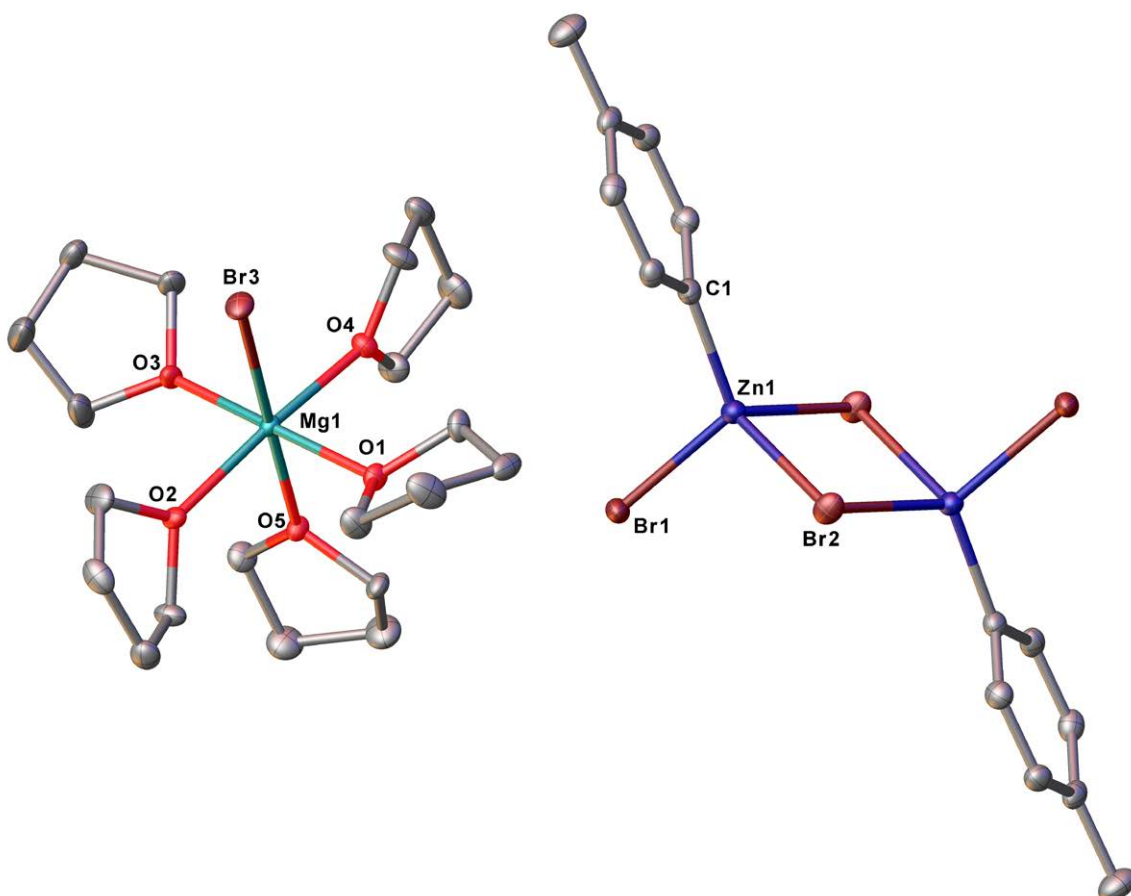
Supplementary Figure 2. Experimental setup for reaction monitoring using *in situ* FT-IR or UV-Vis spectroscopy.

2 Negishi cross-coupling with various diphosphines

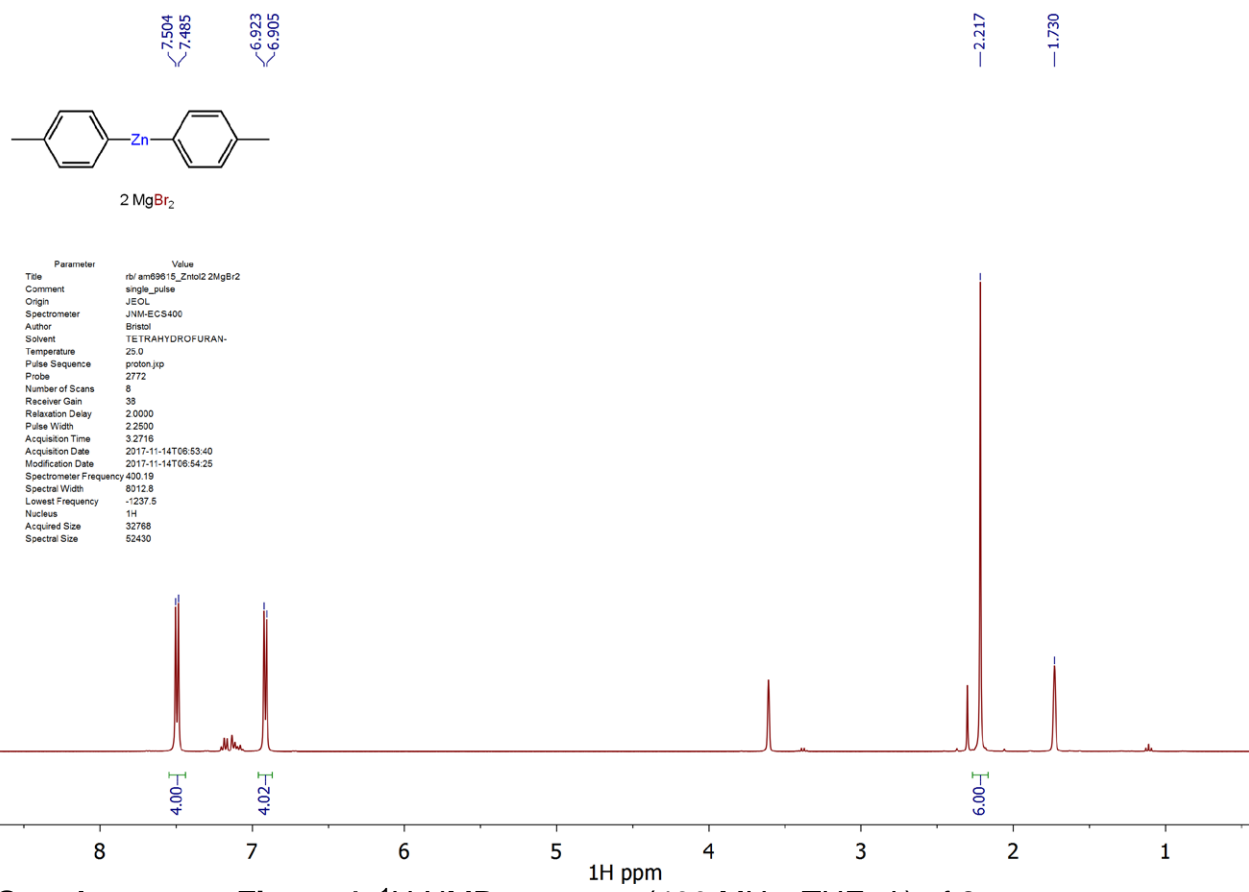
2.1 Synthesis of ZnAr₂/2 MgBr₂ reagents (2a, Ar = 4-tolyl; 2b, Ar = mes)

2.1.1 Zn(4-tolyl)₂/2 MgBr₂ (2a)

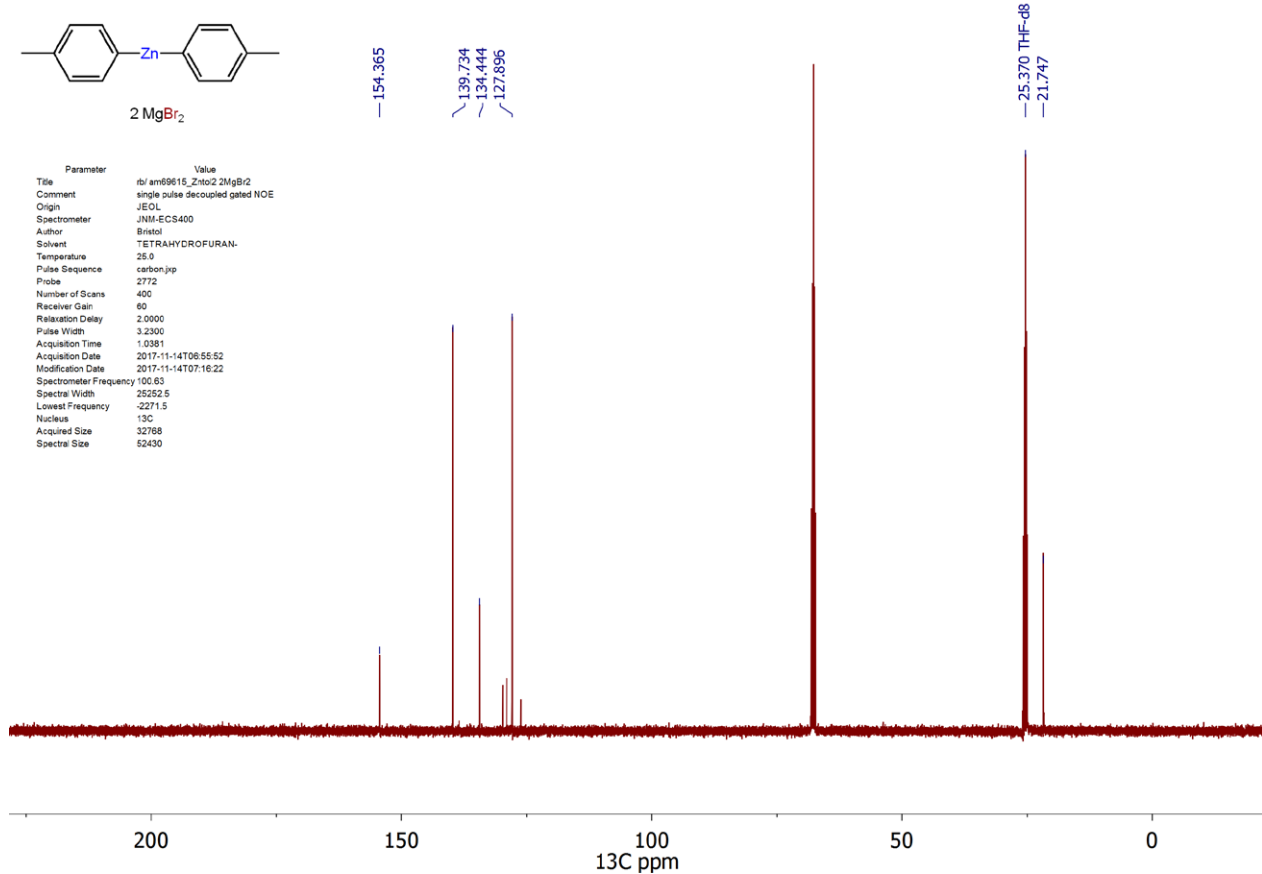
An ampoule was loaded with ZnBr₂ (5.6185 g, 24.95 mmol), THF (76.8 mL) and (4-tolyl)MgBr (1.04 M, 48 mL, 49.9 mmol) to give a 200 mM solution of **2a** which was used without further purification. Trace amounts of (4-tolyl)₂, **10**, present in the solutions of **2a** were determined by quantitative GC-FID analysis. ¹H NMR (400 MHz, THF-d₈) δ = 7.49 (d, J=7.5, 4H), 6.91 (d, J=7.3, 4H), 2.22 (s, 6H). ¹³C NMR (101 MHz, THF-d₈) δ = 154.4, 139.7, 134.4, 127.9, 21.8. Note: during storage of solutions of **2a**, formation of a white precipitate can occur, which can be easily re-dissolved by warming the mixture at 35 °C. On one occasion, colourless crystals suitable for an X-ray crystallographic analysis formed in one of the solutions after prolonged storing (5 months) which were found to be [MgBr(THF)₅]₂[{ZnBr(4-tolyl)(μ-Br)}₂] (**29**) (Supplementary Figure 3).



Supplementary Figure 3. Single-crystal X-ray structure of [MgBr(THF)₅]₂[{ZnBr(4-tolyl)(μ-Br)}₂] (**29**). Hydrogen atoms are omitted for clarity and thermal ellipsoids are set at the 50% probability level.



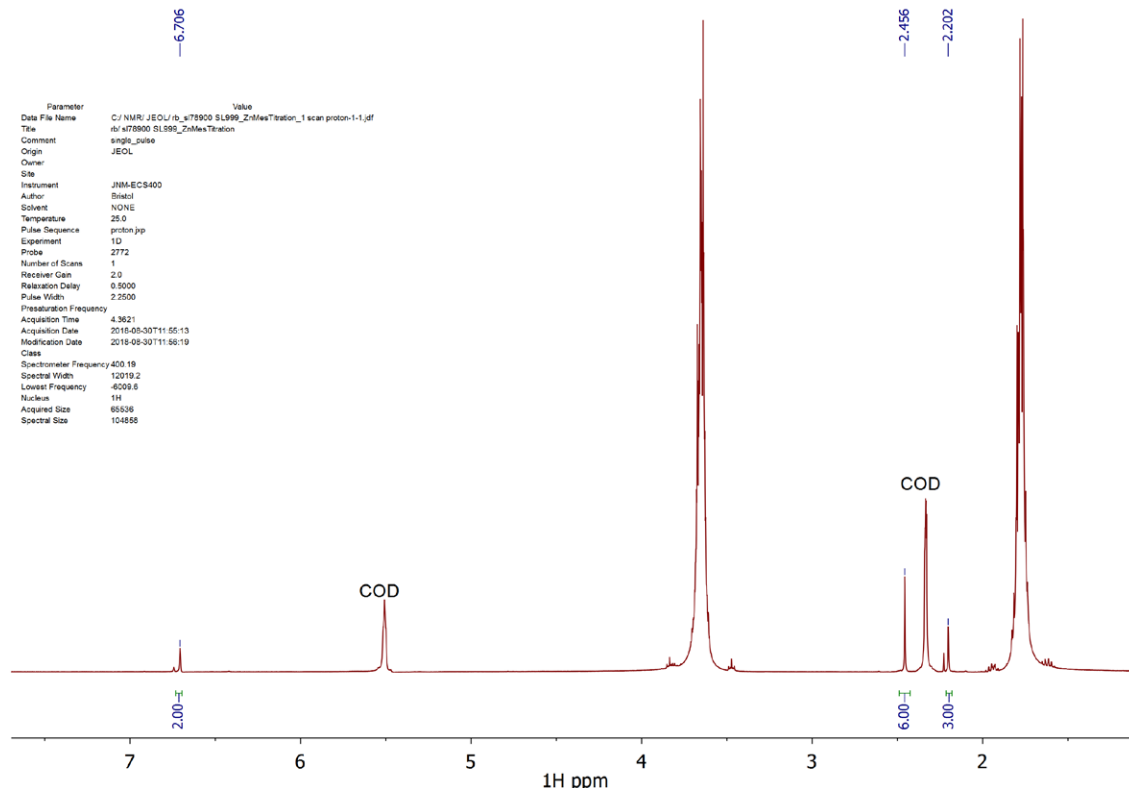
Supplementary Figure 4. ^1H NMR spectrum (400 MHz, THF- d_8) of **2a**.



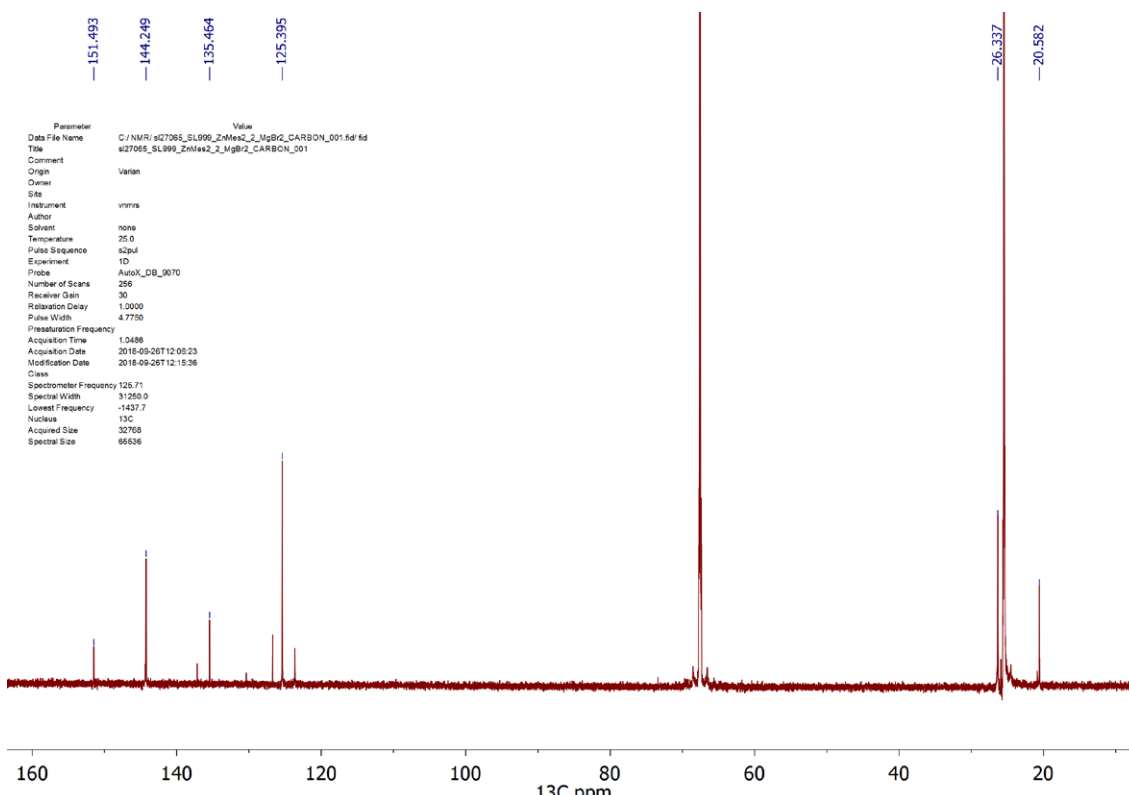
Supplementary Figure 5. ^{13}C NMR spectrum (100 MHz, THF- d_8) of **2a**.

2.1.2 Zn(4-tolyl)₂/2 MgBr₂ (2b)

An ampoule was loaded with ZnBr₂ (2.809 g, 12.48 mmol), THF (76.8 mL) and MesMgBr (0.97 M, 25.7 mL, 24.95 mmol) to give a 100 mM solution of **2b** which was used without further purification. ¹H NMR (400 MHz, THF-*d*₈) δ = 6.71 (s, 2H), 2.46 (s, 6H), 2.20 (s, 3H). ¹³C NMR (126 MHz, THF-*d*₈) δ = 151.49, 144.25, 135.46, 125.39, 26.34, 20.58.



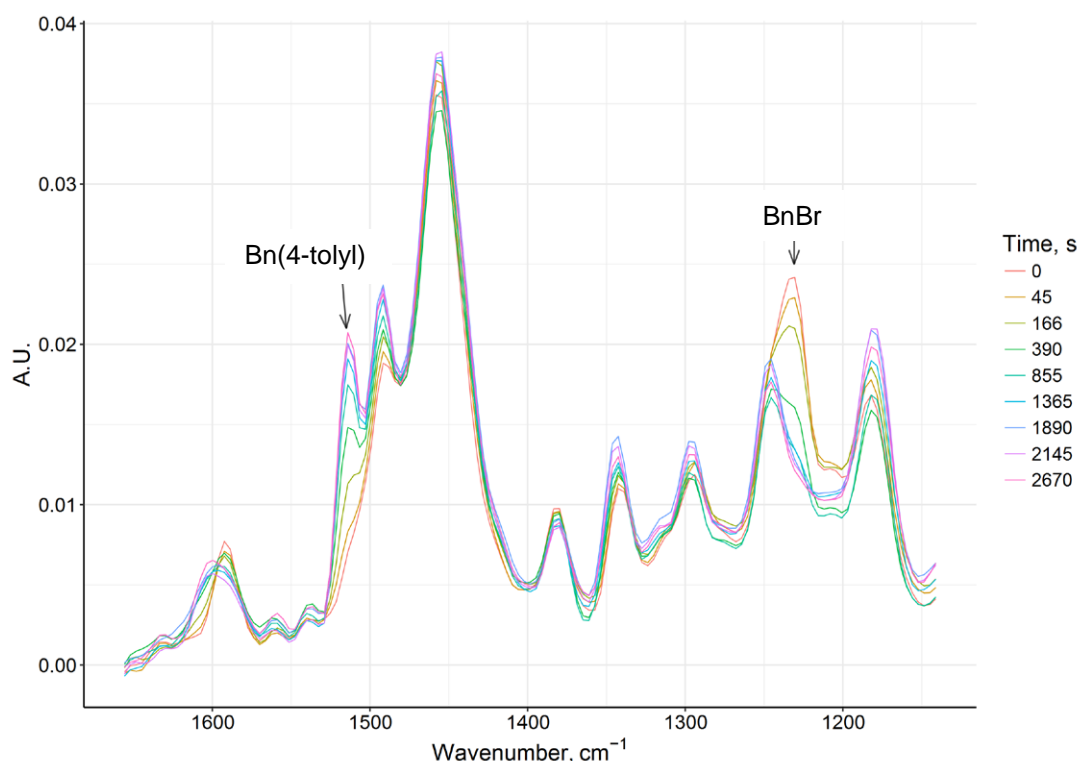
Supplementary Figure 6. ¹H NMR spectrum (400 MHz, THF-*d*₈) of **2b** with 1,5-cyclooctadiene (COD) added as a titration standard.



Supplementary Figure 7. ¹³C NMR spectrum (100 MHz, THF-*d*₈) of **2b**.

2.2 General procedure for following the Negishi reaction using *in situ* FT-IR spectroscopy

A jacketed Schlenk (Supplementary Figure 1) equipped with an internal cooling coil was stored at 180 °C for 10 minutes and then evacuated while still hot. Once cool, it was back-filled with dry nitrogen followed by insertion of the ReactIR 15 probe equipped with a rubber stopper to form an air-tight seal (Supplementary Figure 2). The Schlenk was evacuated and back-filled with dry nitrogen for a second time and the cryostat connected and set at 7.00 °C. The appropriate amount of THF was added and a background IR spectrum collected. Subsequently, *n*-dodecane (1.00 mL, 500 mM stock solution, 0.50 mmol) was added followed by a THF solution of **2a** or Mg-free **2a** (200 mM stock solution in Zn) and the mixture was stirred using a PTFE coated stir-bar at 500 rpm. IR spectra were collected at a rate of one spectrum every 15 seconds (50 scans per spectrum) and BnBr (2500 mM THF stock solution) was subsequently added followed by addition of phosphine (80.0 mM THF stock solution). The reaction was initiated by addition of the Fe-containing compound (20 mM THF stock solution) with the time of addition accurately recorded. The reaction profiles for BnBr (**1**) consumption and Bn(4-tolyl) (**3**) formation were obtained by monitoring the peak area between 1241 cm⁻¹ and 1223 cm⁻¹ and 1529 cm⁻¹ and 1503 cm⁻¹ respectively over time with a two-point baseline correction applied at the edges of each integration region. Example of the IR spectra collected over time are presented in Supplementary Figure 8.



Supplementary Figure 8. IR spectra collected at various times in the reaction of **1** and **2a** catalysed by [FeBr₂(dpbz)₂] (**7a**) in THF.

The amounts of **1** and **3** present in each reaction mixture over time were determined by quantifying the corresponding peak areas to mM. This was achieved by collecting 5 – 9

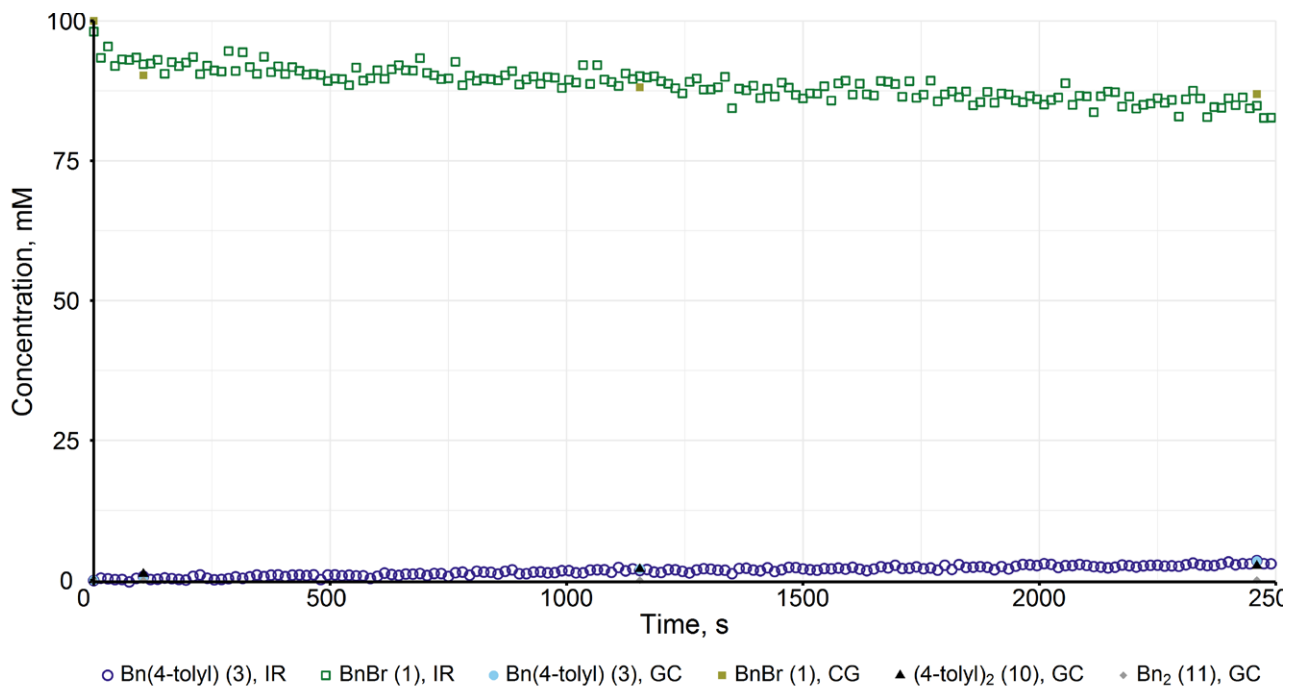
aliquots from each run and analysing them by GC-FID analysis. The concentration values obtained were input into the iC IR software and used to calibrate the response of the React IR instrument for each experiment in mM, with a coefficient of determination (r^2) of 0.950-0.999 for **1** and 0.995-1.000 for **3**. Note: towards the end of most catalysis experiments (at approximately 75% conversion to product) a white precipitate formed resulting in solvent peaks shifting within the measured regions preventing further quantitation by FT-IR spectroscopy. The amounts of Bn_2 (**11**) and $(4\text{-tolyl})_2$ (**10**) were determined by GC-FID only, with $(4\text{-tolyl})_2$ (**10**) corrected for any amount already present in the stock solution of **2a**.

Supplementary Table 1 summarises the reagent quantities and reaction conditions used for each catalytic reaction monitored by *in situ* FT-IR spectroscopy. The individual reaction profiles are shown in Supplementary Figure 9 to Supplementary Figure 25.

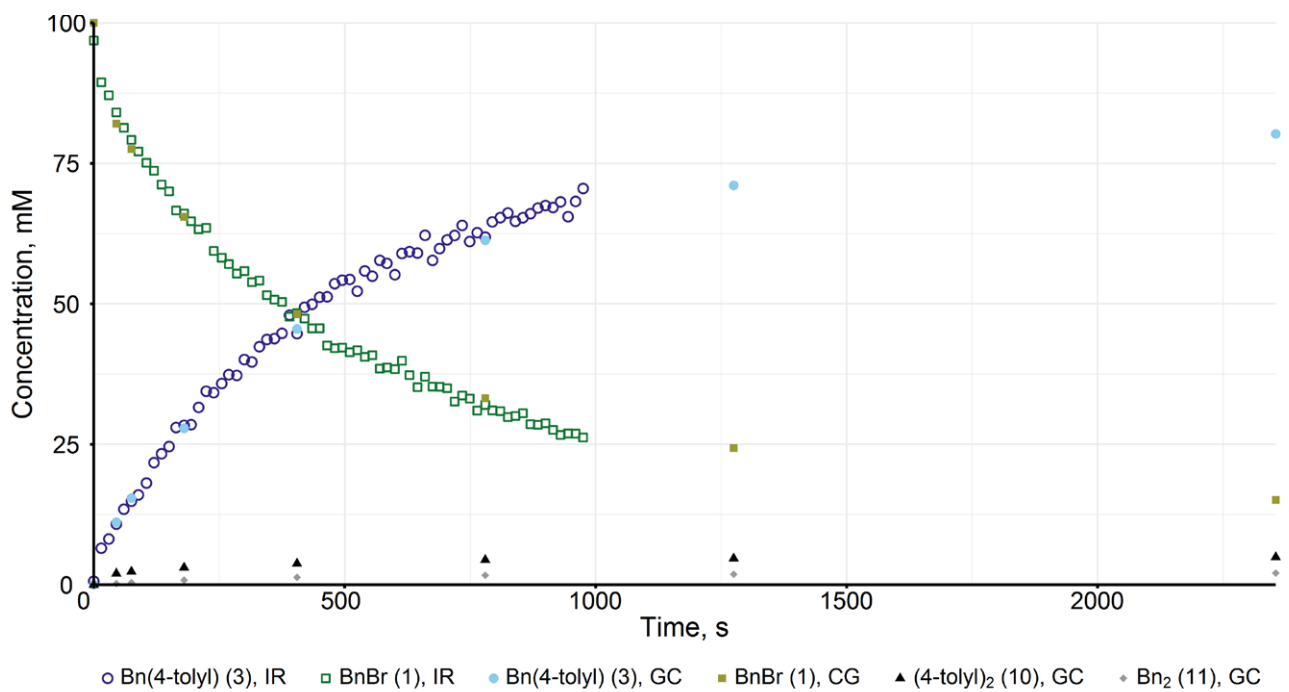
Supplementary Table 1. Summary of catalytic reactions monitored with *in situ* FT-IR spectroscopy.^a

Entry #	Pro-initiator (mM)	Nucleophile (mM)	BnBr (mM)	Phosphine (mM)
S1	FeBr ₂ (1.00)	2a (100)	100	–
S2	FeBr ₂ (1.00)	2a (100)	100	dpbz (2.00)
S3	FeBr ₂ (1.00)	2a (100)	100	dpth (2.00)
S4	FeBr ₂ (1.00)	2a (100)	100	MeDuphos (2.00)
S5	FeBr ₂ (1.00)	2a (100)	100	dppp (2.00)
S6	FeBr ₂ (1.00)	2a (100)	100	norphos (2.00)
S7	FeBr ₂ (1.00)	2a (100)	100	cis-dppen (2.00)
S8	FeBr ₂ (1.00)	2a (100)	100	iPrDuphos (2.00)
S9	FeBr ₂ (1.00)	2a (100)	100	sciopp (2.00)
S10	FeBr ₂ (1.00)	2a (100)	100	dppe (2.00)
S11	FeBr ₂ (1.00)	2a (100)	100	trans-dppen (2.00)
S12	FeBr ₂ (1.00)	2a (100)	100	depe (2.00)
S13	FeBr ₂ (1.00)	2a (100)	100	dmbz (2.00)
S14	FeBr ₂ (1.00)	2a (100)	100	dpbz (2.00) then dmbz (2.00)
S15 ^b	FeBr ₂ (1.00)	2a (100)	100	No ligand then dpbz (2.00)
S16	FeBr ₂ (1.00)	2a (100)	100	trans-dppen (2.00) then dpbz (2.00)
S17	[FeBr ₂ (dpbz)] (1.00)	2a (100)	100	–

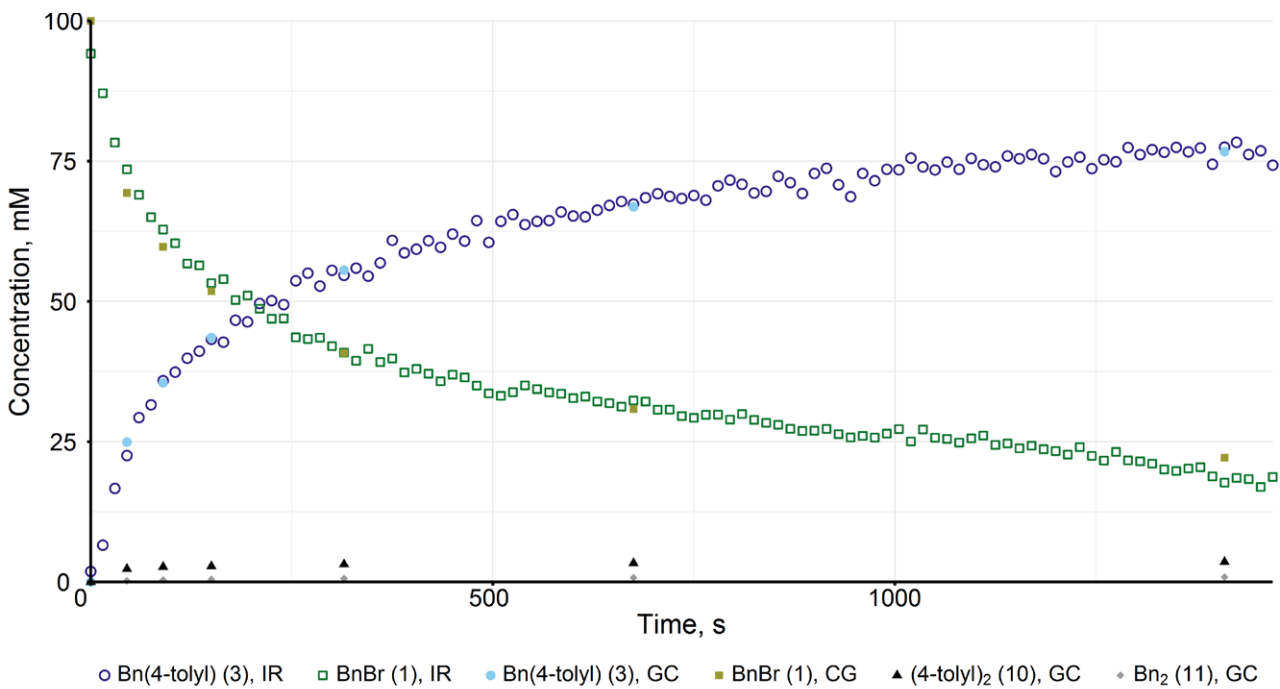
^a General conditions: Reactions were performed in THF at a total volume of 10 mL and monitored with FT-IR spectroscopy at 7.00 °C. **1** stock solution = 2500 mM, **2a** stock solution = 200 mM, 0.5 mmol of *n*-dodecane added as a 500 mM stock solution, Fe stock solution = 20 mM. All reactions were activated by addition of the Fe stock solution. ^bDpbz was added 20 minutes after addition of the rest of the reagents and FeBr₂.



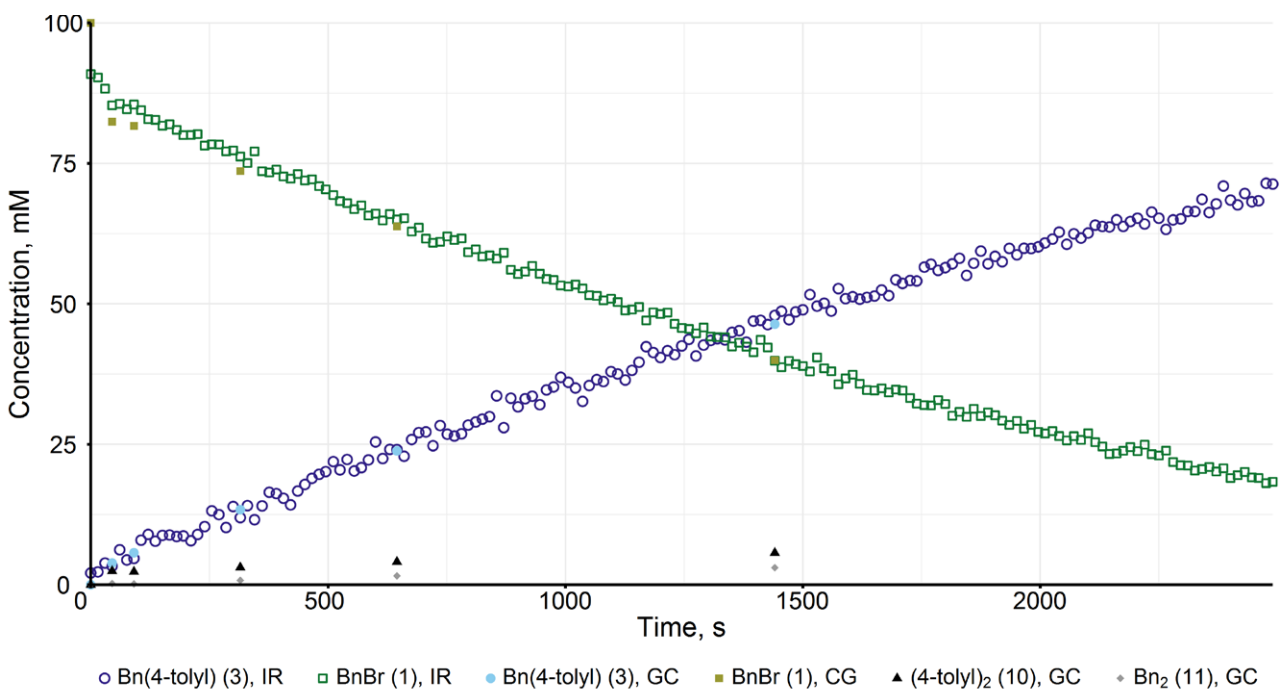
Supplementary Figure 9. Negishi coupling between **1** (100 mM) and **2a** (100 mM) catalysed by FeBr_2 (1.00 mM) at 7.00 °C and a total volume of 10.0 mL (entry S1, Supplementary Table 1).



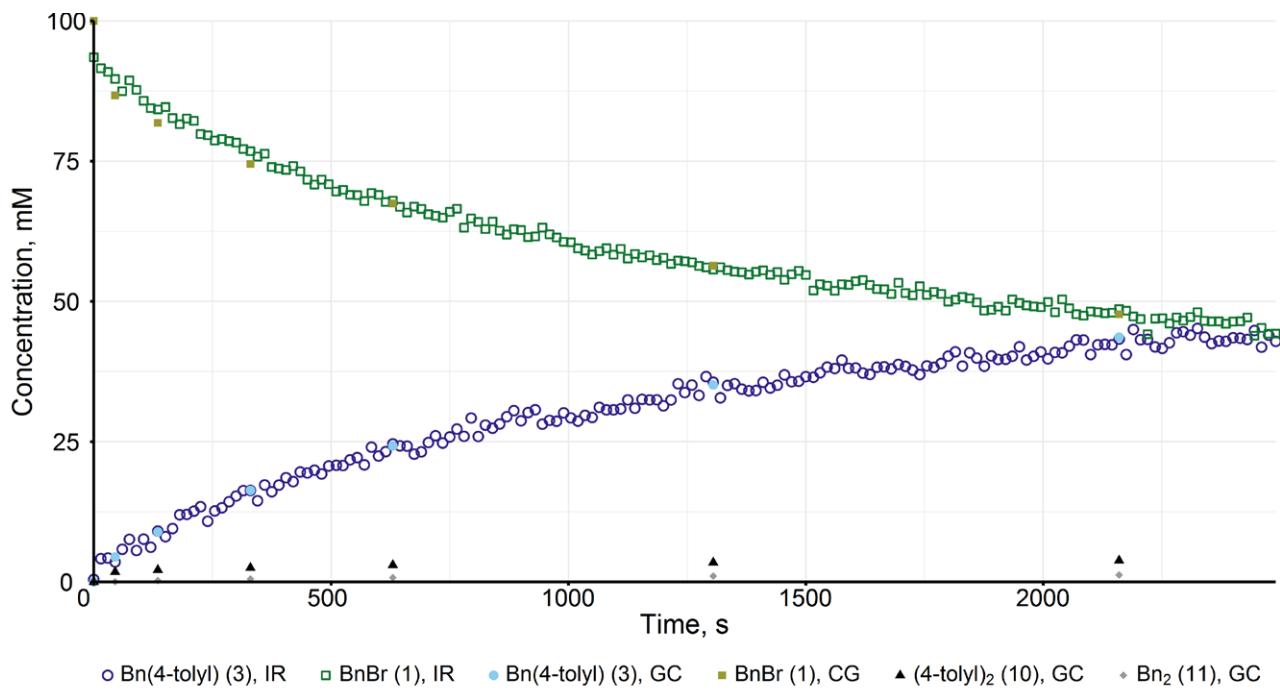
Supplementary Figure 10. Negishi coupling between **1** (100 mM) and **2a** (100 mM) catalysed by FeBr_2 (1.00 mM) + dpbz (2.00 mM) at 7.00 °C and a total volume of 10.0 mL (entry S2, Supplementary Table 1).



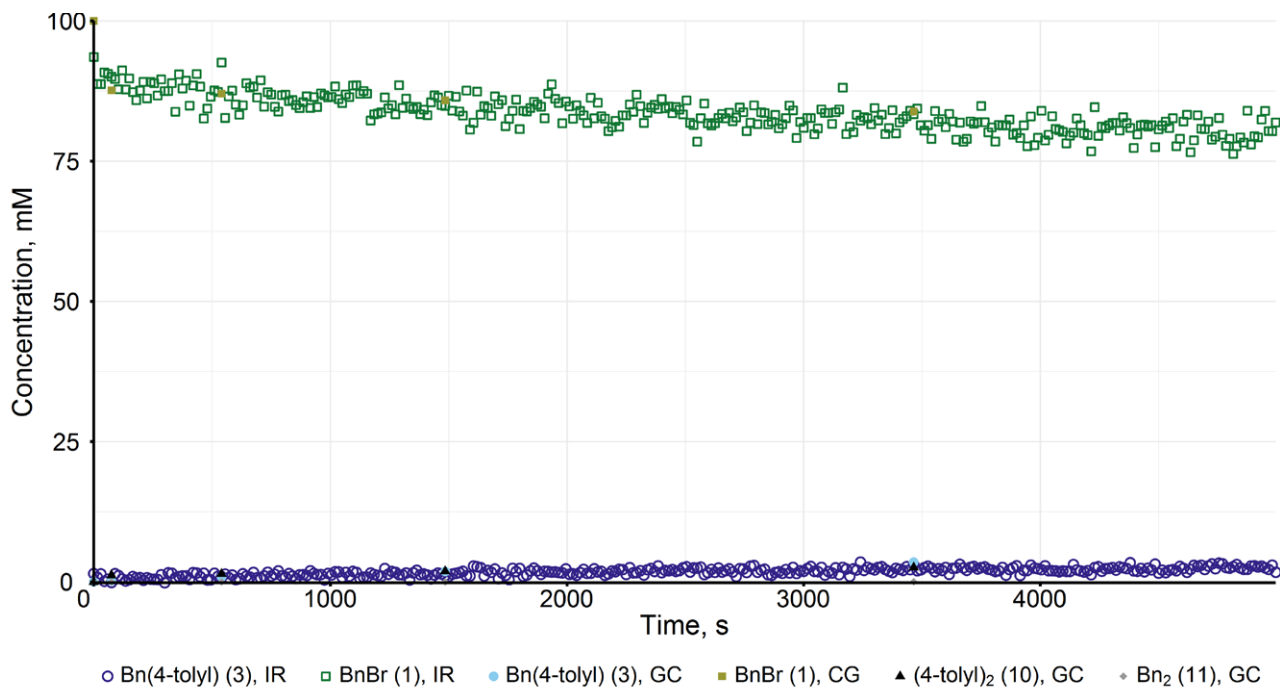
Supplementary Figure 11. Negishi coupling between **1** (100 mM) and **2a** (100 mM) catalysed by FeBr_2 (1.00 mM) + dpth (2.00 mM) at 7.00 °C and a total volume of 10.0 mL (entry S3, Supplementary Table 1).



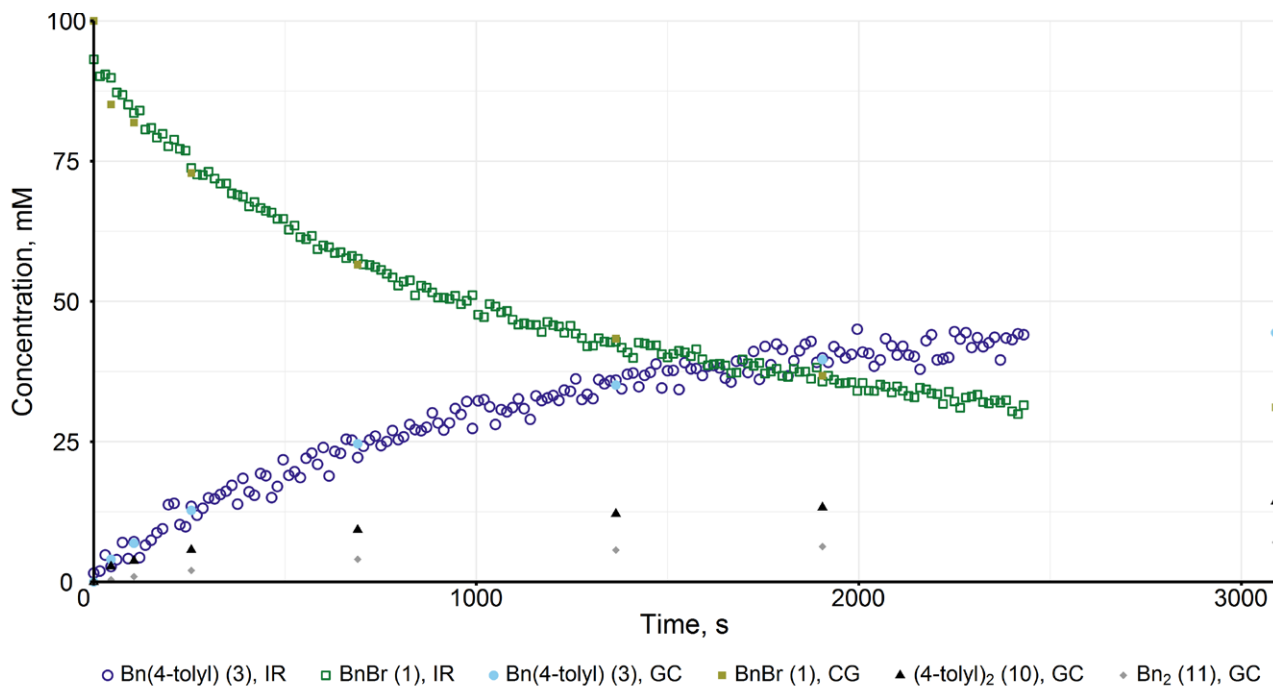
Supplementary Figure 12. Negishi coupling between **1** (100 mM) and **2a** (100 mM) catalysed by FeBr_2 (1.00 mM) + MeDuphos (2.00 mM) at 7.00 °C and a total volume of 10.0 mL (entry S4, Supplementary Table 1).



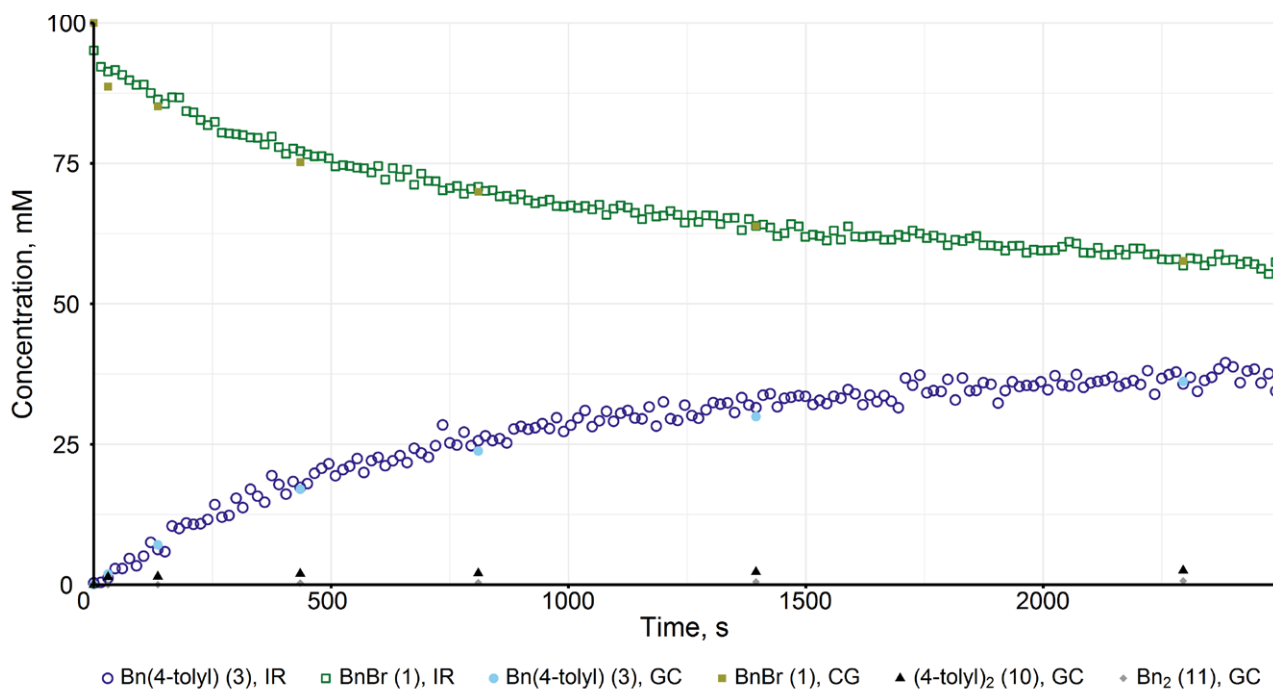
Supplementary Figure 13. Negishi coupling between **1** (100 mM) and **2a** (100 mM) catalysed by FeBr_2 (1.00 mM) + dppp (2.00 mM) at 7.00 °C and a total volume of 10.0 mL (entry S5, Supplementary Table 1).



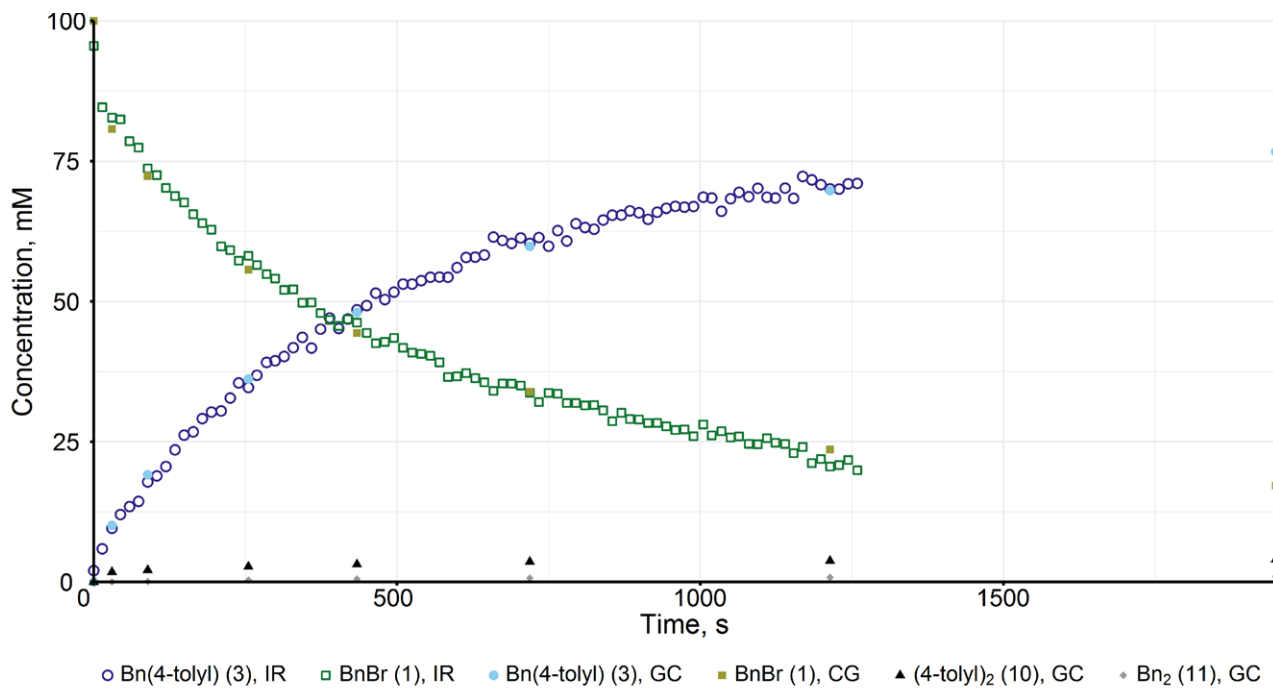
Supplementary Figure 14. Negishi coupling between **1** (100 mM) and **2a** (100 mM) catalyzed by FeBr_2 (1.00 mM) + norphos (2.00 mM) at 7.00 °C and a total volume of 10.0 mL (entry S6, Supplementary Table 1).



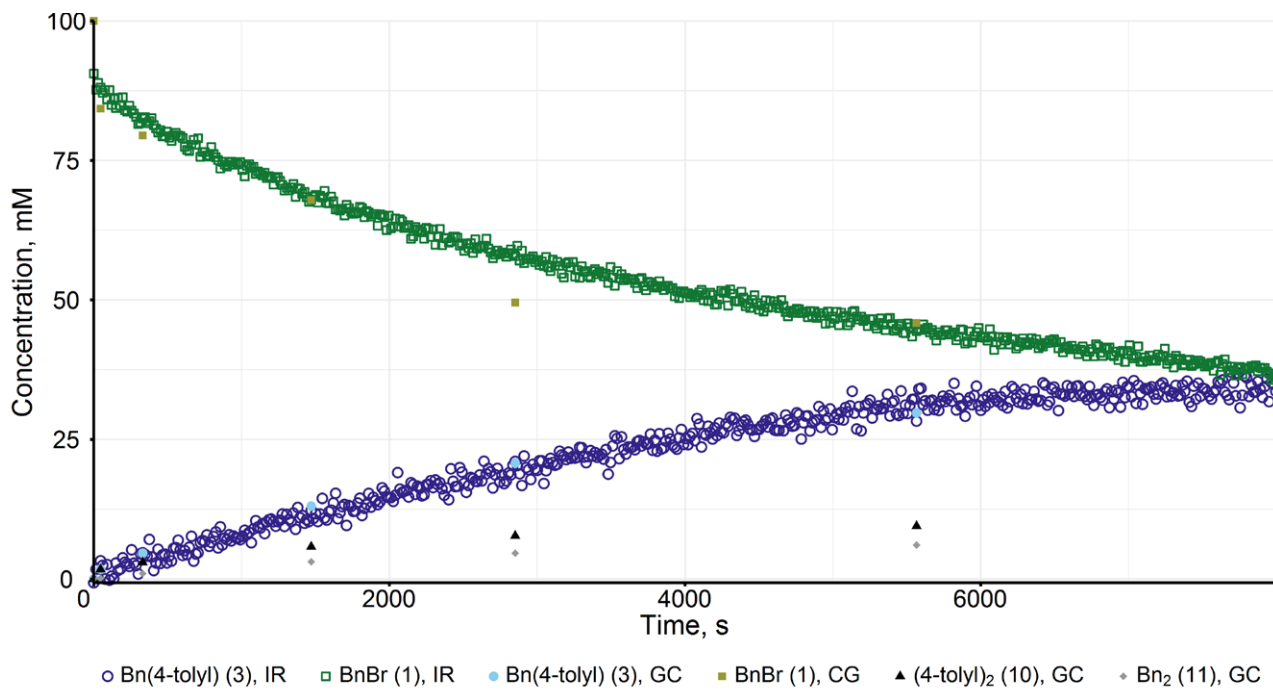
Supplementary Figure 15. Negishi coupling between **1** (100 mM) and **2a** (100 mM) catalysed by FeBr_2 (1.00 mM) in presence of *cis*-dppen (2.00 mM) at 7.00 °C and a total volume of 10.0 mL (entry S7, Supplementary Table 1).



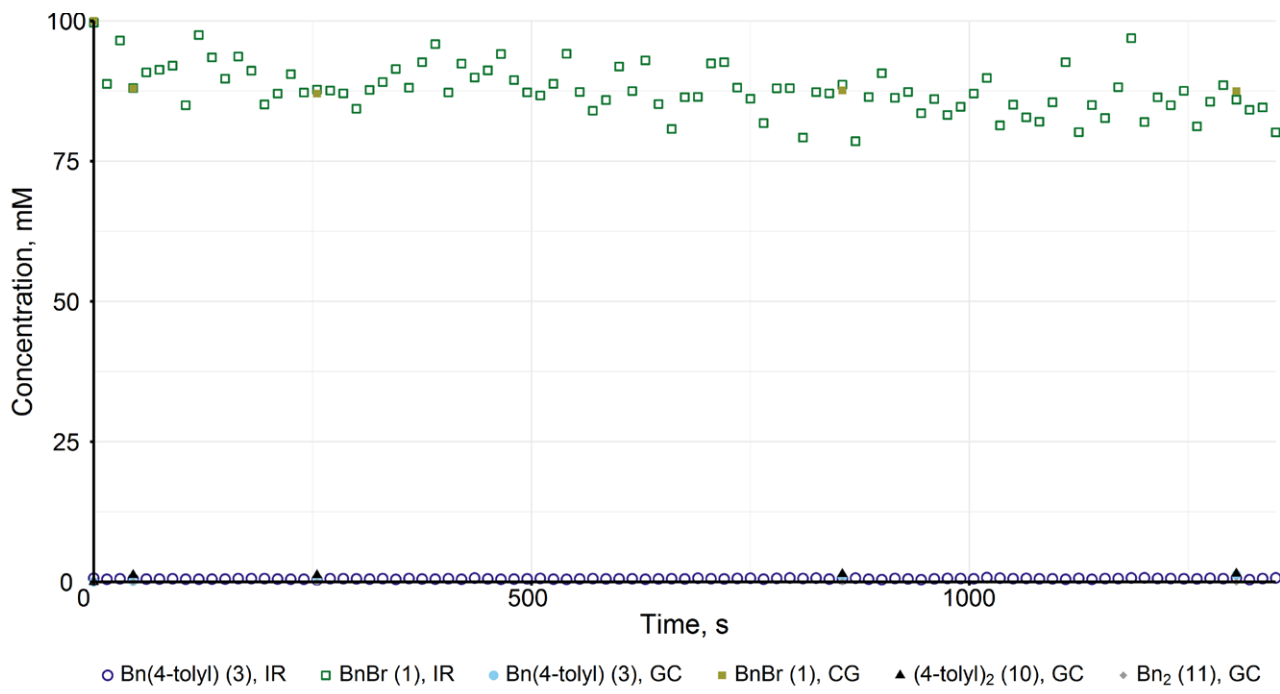
Supplementary Figure 16. Negishi coupling between **1** (100 mM) and **2a** (100 mM) catalysed by FeBr_2 (1.00 mM) + iPrDuphos (2.00 mM) at 7.00 °C and a total volume of 10.0 mL (entry S8, Supplementary Table 1).



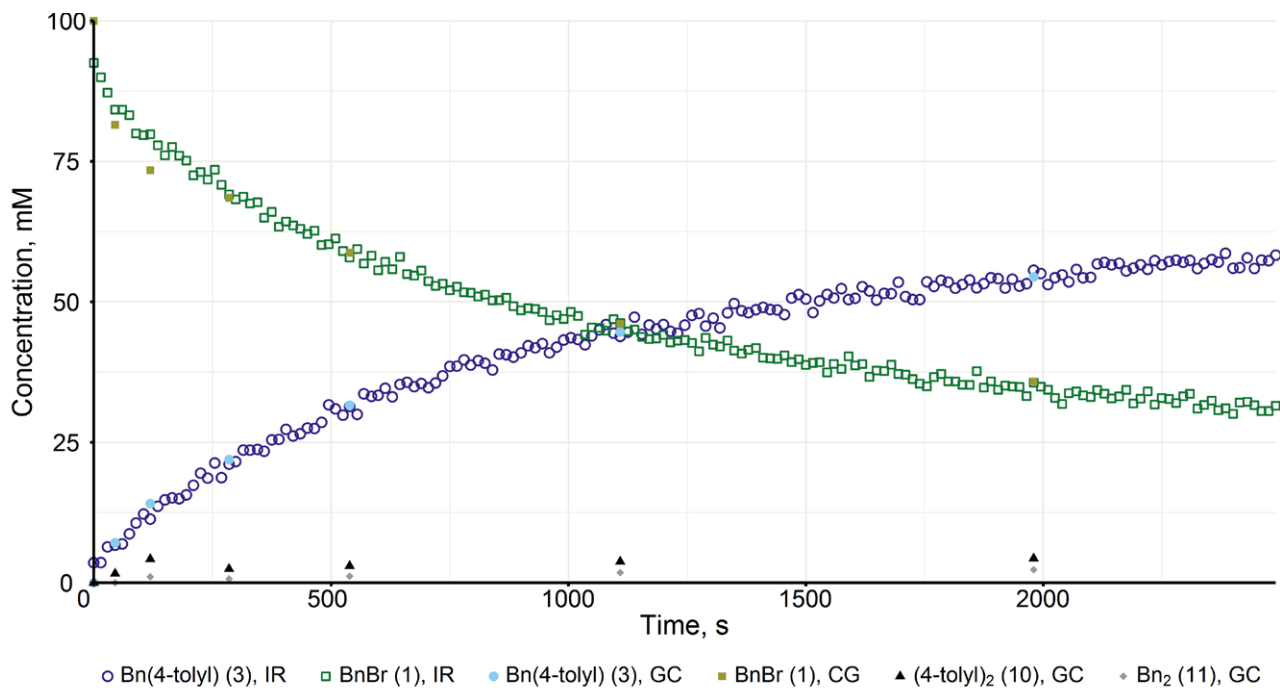
Supplementary Figure 17. Negishi coupling between **1** (100 mM) and **2a** (100 mM) catalysed by $[\text{FeBr}_2(\text{sciopp})]$, **4h**, (1.00 mM) + sciopp (1.00 mM) at 7.00 °C and a total volume of 10.0 mL (entry S9, Supplementary Table 1).



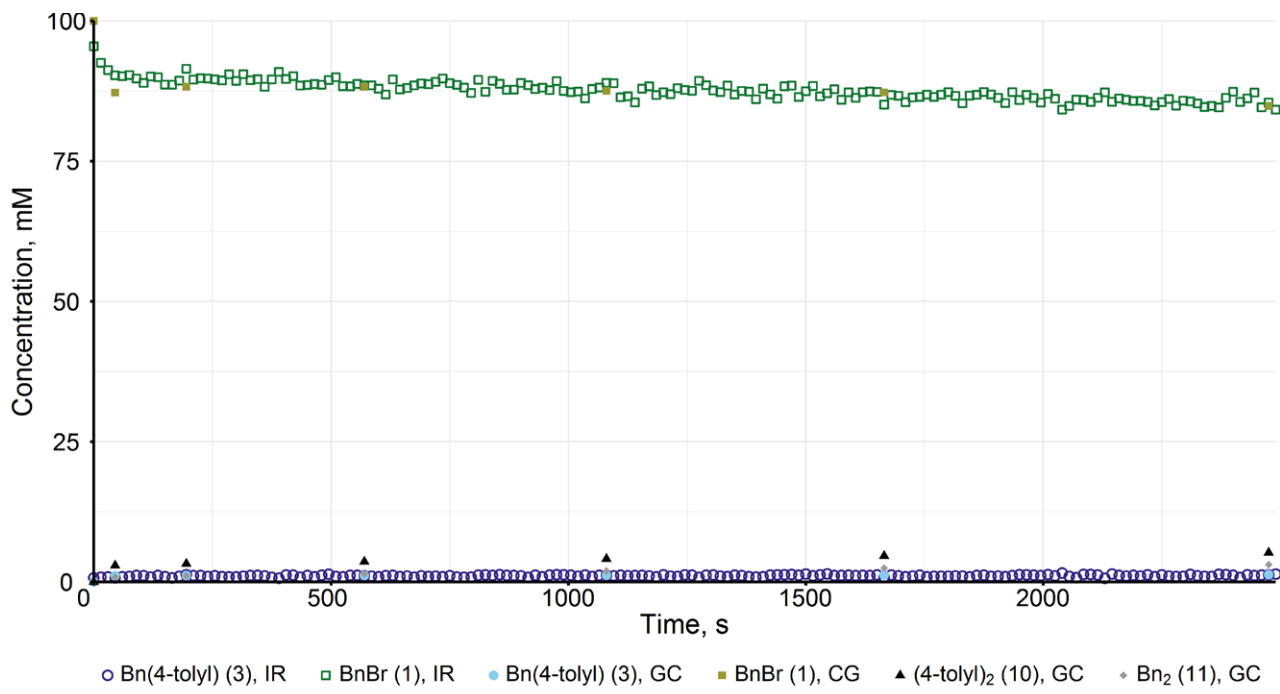
Supplementary Figure 18. Negishi coupling between **1** (100 mM) and **2a** (100 mM) catalysed by FeBr_2 (1.00 mM) + dppe (2.00 mM) at 7.00 °C and a total volume of 10.0 mL (entry S10, Supplementary Table 1).



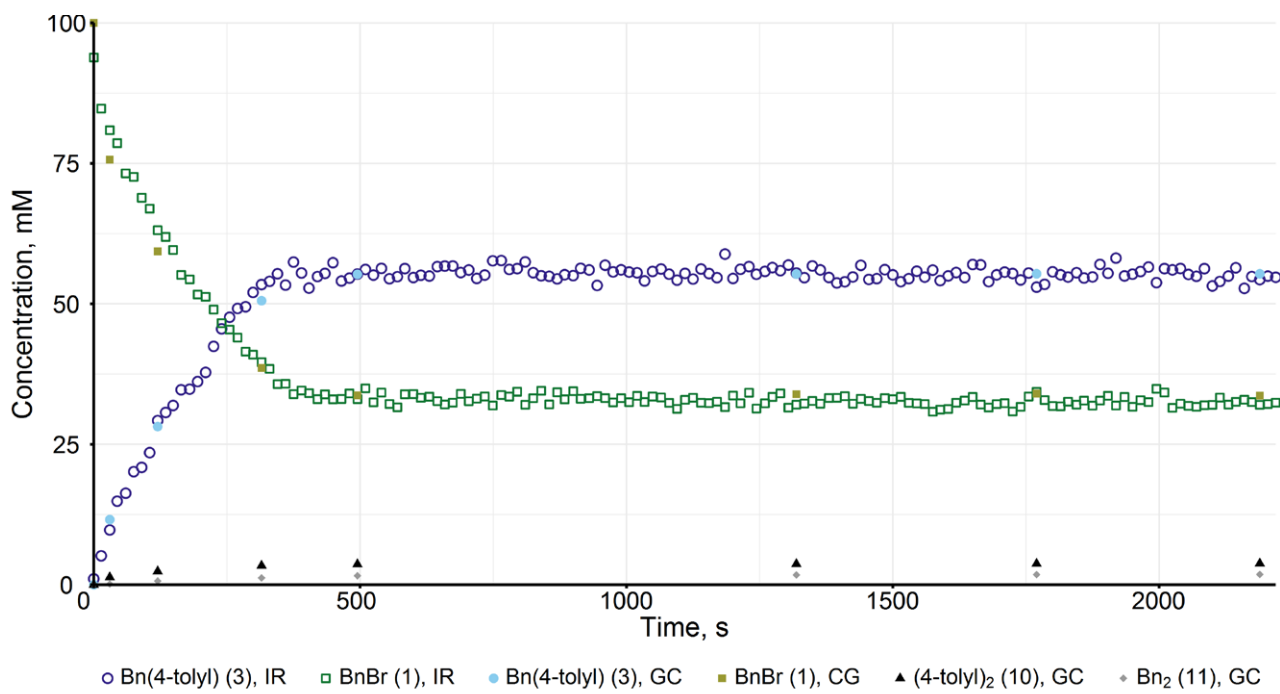
Supplementary Figure 19. Negishi coupling between **1** (100 mM) and **2a** (100 mM) catalysed by FeBr_2 (1.00 mM) + *trans*-dppen (2.00 mM) at 7.00 °C and a total volume of 10.0 mL (entry S11, Supplementary Table 1).



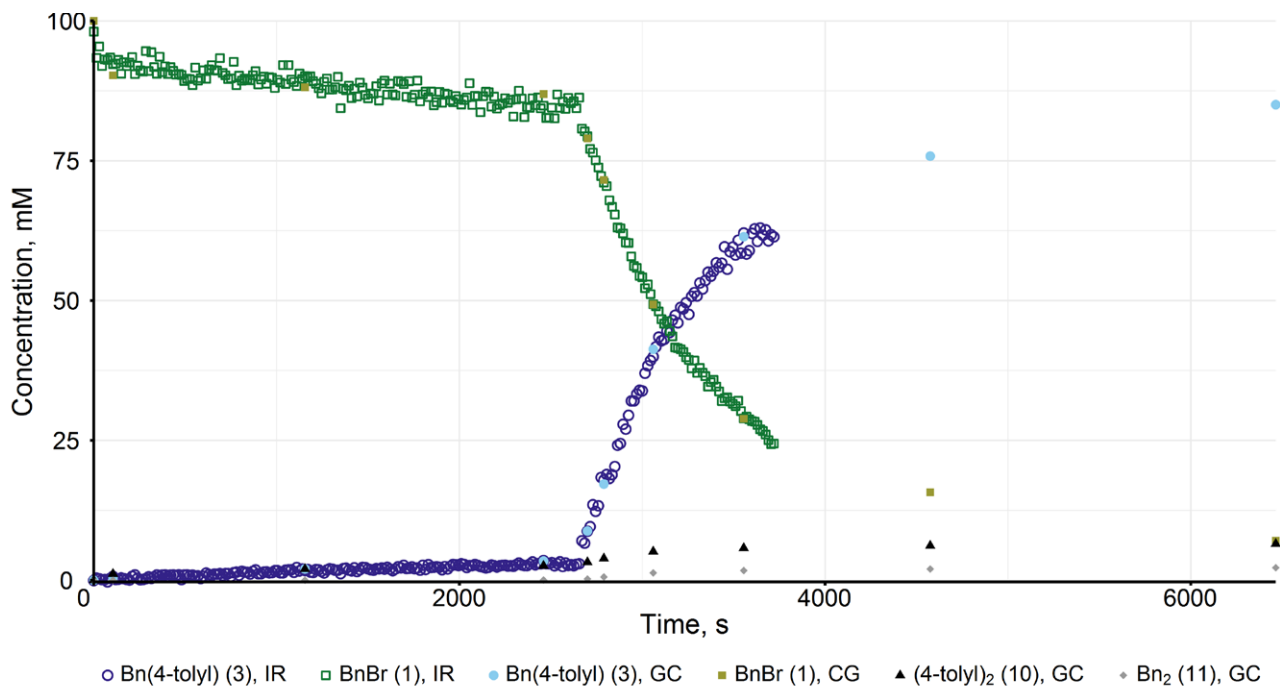
Supplementary Figure 20. Negishi coupling between **1** (100 mM) and **2a** (100 mM) catalysed by FeBr_2 (1.00 mM) + depe (2.00 mM) at 7.00 °C and a total volume of 10.0 mL (entry S12, Supplementary Table 1).



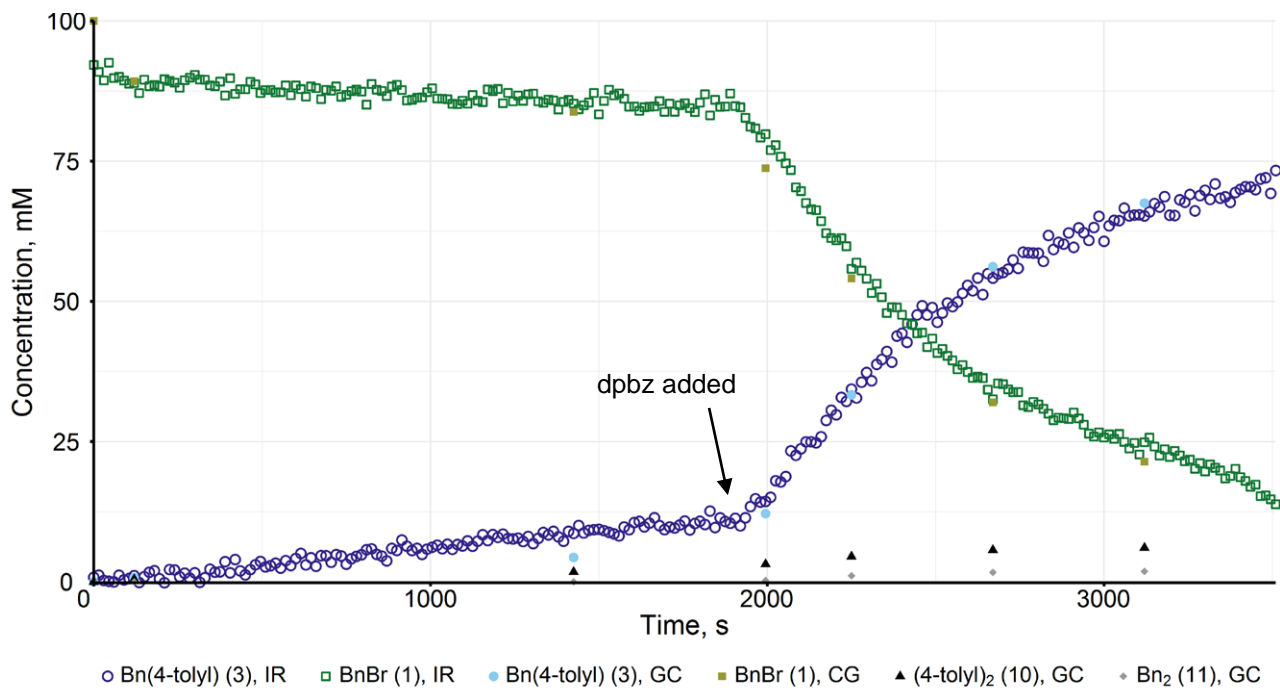
Supplementary Figure 21. Negishi coupling between **1** (100 mM) and **2a** (100 mM) catalysed by FeBr_2 (1.00 mM) + dmbz (2.00 mM) at 7.00 °C and a total volume of 10.0 mL (entry S13, Supplementary Table 1).



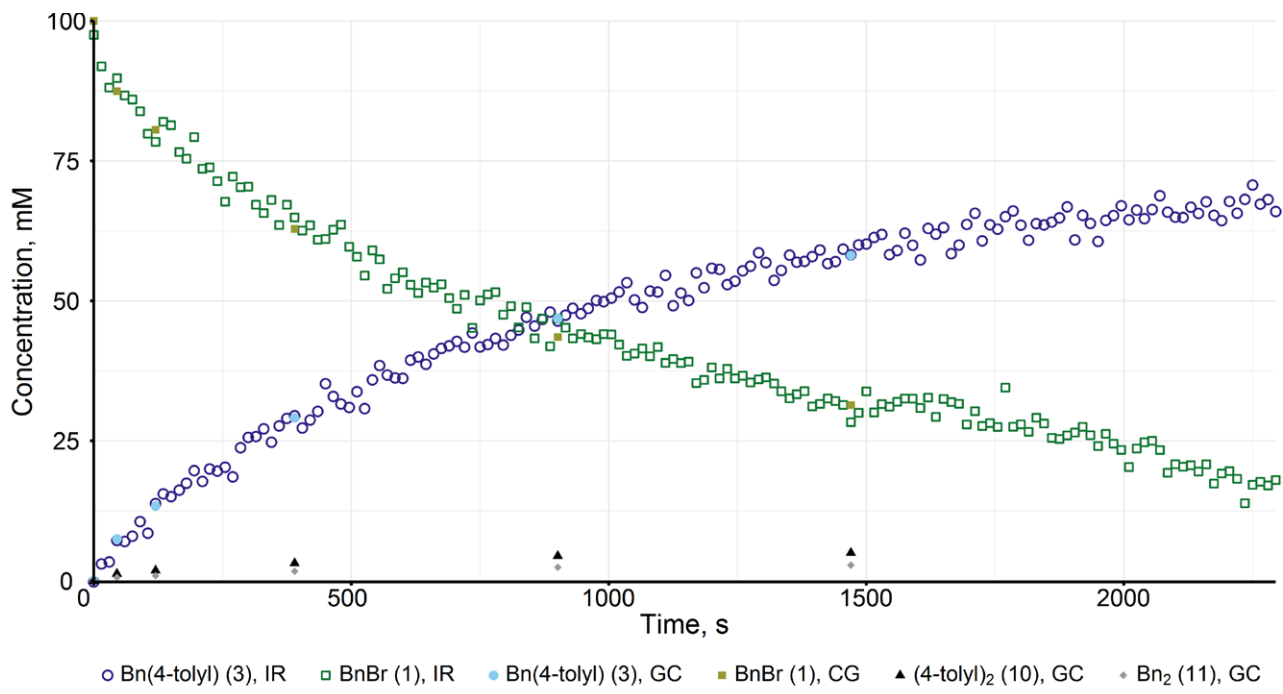
Supplementary Figure 22. Negishi coupling between **1** (100 mM) and **2a** (100 mM) catalysed by FeBr_2 (1.00 mM) + dpbz (2.00 mM) followed by addition of dmbz (2.00 mM) after 360 s at 7.00 °C and a total volume of 10.0 mL (entry S14, Supplementary Table 1).



Supplementary Figure 23. Negishi coupling between **1** (100 mM) and **2a** (100 mM) catalysed by FeBr₂ (1.00 mM) at 7.00 °C, followed by the addition of dpbz (1.00 mM) at 2400 s to give a total volume of 10.0 mL (entry S15, Supplementary Table 1).



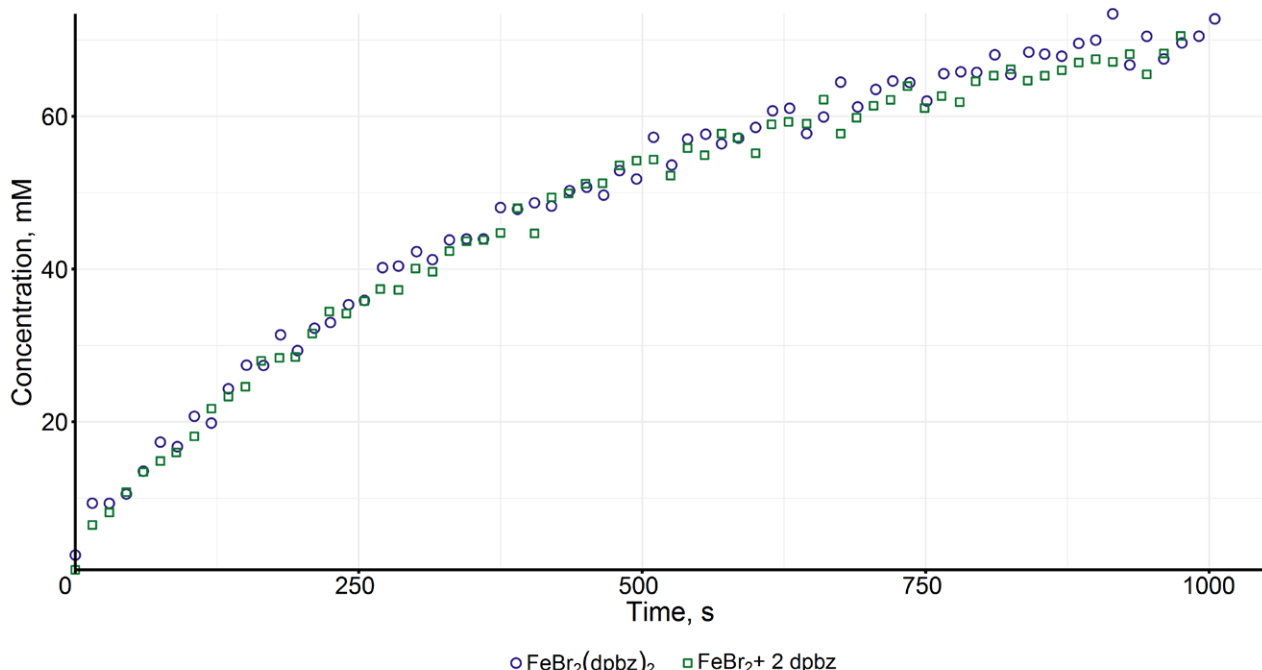
Supplementary Figure 24. Negishi coupling between **1** (100 mM) and **2a** (100 mM) catalysed by FeBr₂ (1.00 mM) + *trans*-dppen (2.00 mM) followed by addition of dpbz (2.00 mM) after 1910 s at 7.00 °C and a total volume of 10.0 mL (entry S16, Supplementary Table 1).



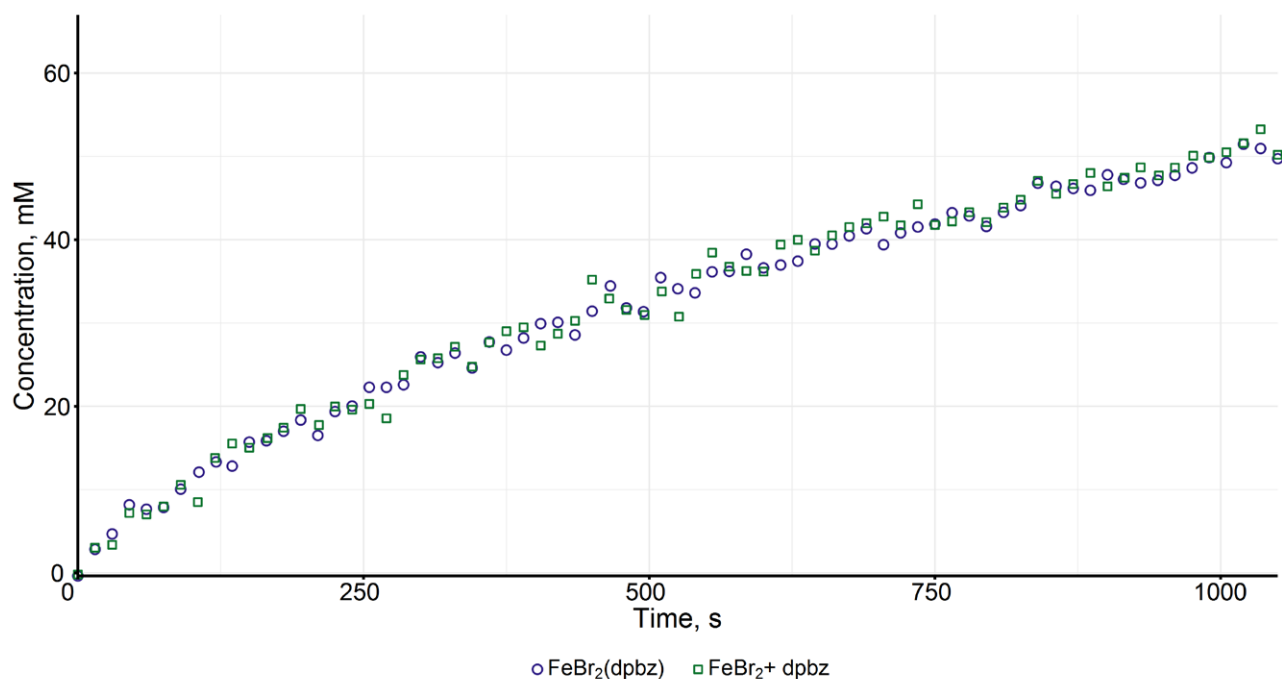
Supplementary Figure 25. Negishi coupling between **1** (100 mM) and **2a** (100 mM) catalysed by $[\text{FeBr}_2(\text{dpbz})]$, **4a**, (1.00 mM) at 7.00 °C and a total volume of 10.0 mL (entry S17, Supplementary Table 1).

2.3 Comparison of the use of $[\text{FeBr}_2(\text{dpbz})_n]$ or $\text{FeBr}_2 + n \text{ dpbz}$ ($n = 1$ or 2) in the Negishi reaction

Supplementary Figure 26 and Supplementary Figure 27 compare the reaction profiles for the coupling of **1** with **2a** using either $[\text{FeBr}_2(\text{dpbz})_n]$ or $\text{FeBr}_2 + n \text{ dpbz}$ ($n = 1$ or 2) as the pre-catalysts (conditions as per sections 2 and 12). As can been seen, it makes no difference whether or not the dpbz is coordinated to the Fe at the beginning of the reaction.



Supplementary Figure 26. Comparison of the Negishi coupling between **1** (100 mM) and **2a** (100 mM) catalysed by either $[\text{FeBr}_2(\text{dpbz})_2]$, **7a**, (1.00 mM) or $\text{FeBr}_2 + 2$ eq. dpbz at 7.00 °C (Supplementary Figure 10 and Supplementary Figure 60).



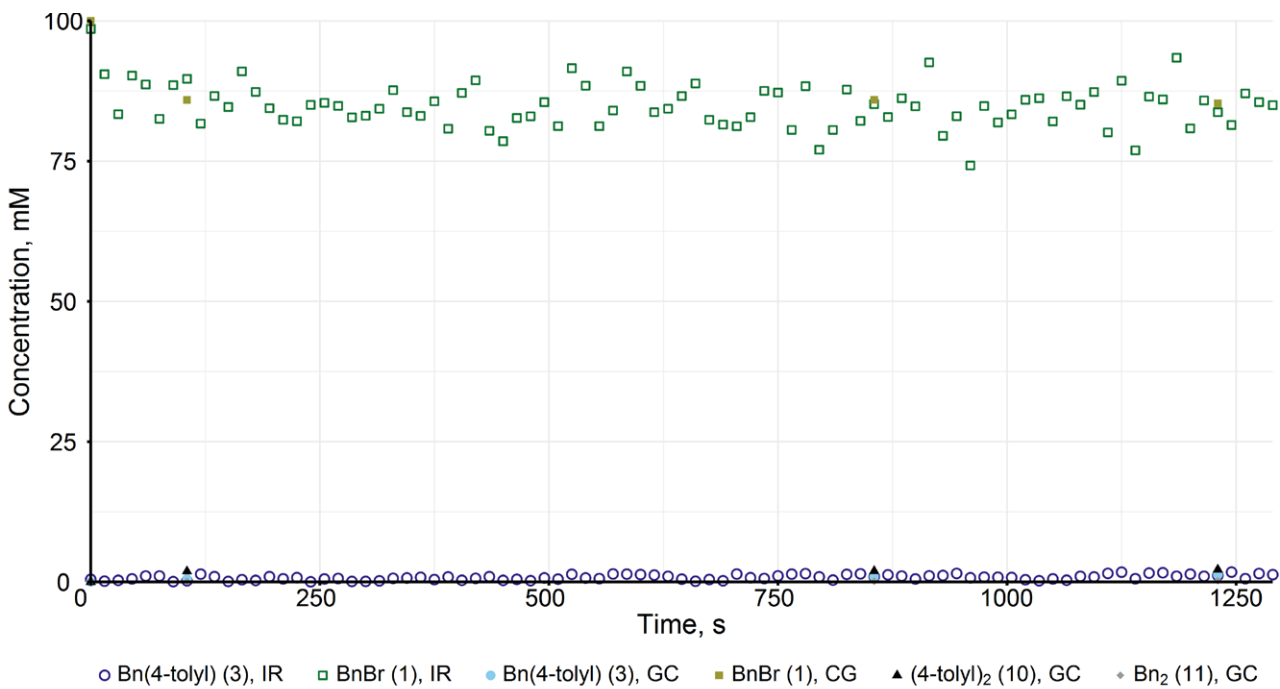
Supplementary Figure 27. Comparison of the Negishi coupling between **1** (100 mM) and **2a** (100 mM) catalysed by either [FeBr₂(dpbz)], **4a**, (1.00 mM) or FeBr₂ + 1 eq. dpbz at 7.00 °C. (Supplementary Figure 25 and Supplementary Figure 214).

3 An examination of the variation of phosphine properties on catalyst performance

In order to examine whether or not any trends could be drawn from the variation of phosphine ligands on catalyst performance, we investigated: (a) the importance of chelation; (b) the effect of variation in bite angle; (c) steric effects, using a percentage buried volume approach; (d) electronic influence, determined by DFT-calculated [(PP)Ni(CO)₂] $\nu(\text{CO})_{\text{symm}}$ values and (e) a Ligand Knowledge Base analysis and these approaches are outlined below. Summarising, beyond noting that chelating diphosphines are essential for activity, no clear trends could be established.

3.1 Importance of chelation

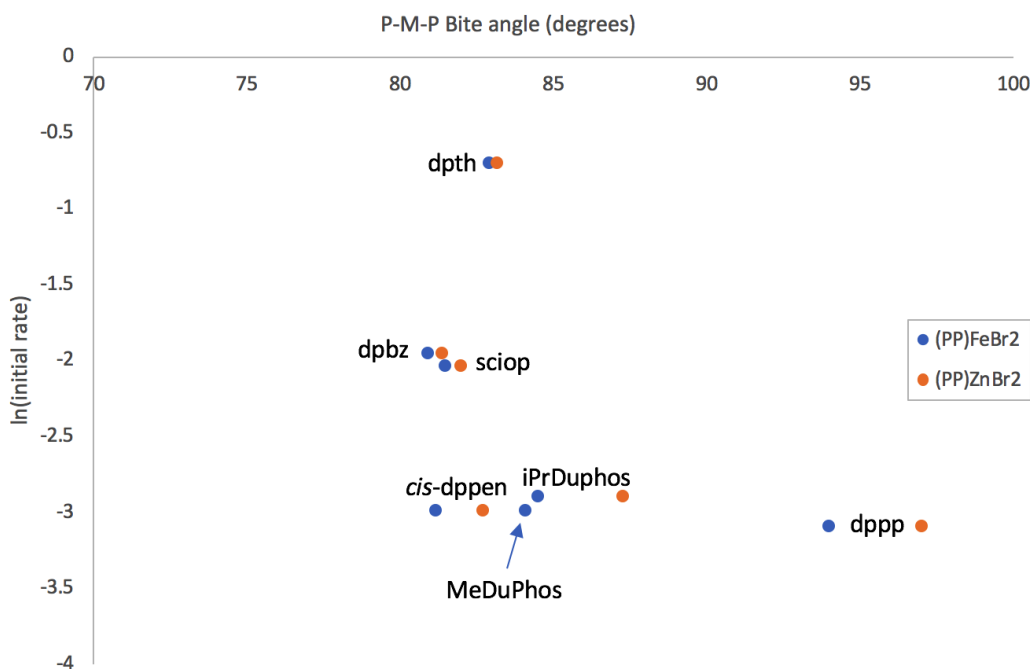
Firstly, we have established that a chelate ring is necessary – the use of PPh₃ in place of dpbz led to no activity (conditions as per section 2.2), as indicated in Supplementary Figure 28, despite the fact that PPh₃ may be considered as the monodentate equivalent of dpbz, one of the best performing ligands.



Supplementary Figure 28. Negishi coupling between **1** (100 mM) and **2a** (100 mM) catalysed by FeBr_2 (1.00 mM) + PPh_3 (2.00 mM) at 7.00 °C and a total volume of 10.0 mL (entry S18, Supplementary Table 1).

3.2 Variation in bite angle.

The data summarised in Supplementary Figure 29, show the variation in (non-zero) catalyst performance against the bite angle of the P-M-P for $\text{MBr}_2(\text{PP})$ ($\text{M} = \text{Fe}, \text{Zn}$) complexes, as determined by crystallography, for the diphosphines that form simple chelates. It is clear from these plots that there is no specific correlation between activity and bite angle, with a slight decrease in bite angle between dpbz/sciop giving reduced activity, but a similar bite angle between dpbz/sciop and *cis*-dppen giving a significantly reduced activity in the latter case. Meanwhile increasing the bite angle in the series *cis*-dppen, MeDuPhos, iPrDuPhos and dppp has only a marginal impact on the initial rate. The P-Fe-P bite angle in $\text{FeBr}_2(\text{norphos})$ is 86.85(6)°, while that of $\text{ZnBr}_2(\text{norphos})$ is 90.41(3)°, placing the ligand firmly in the middle of the scattered data, and yet no activity is observed when this ligand is employed.

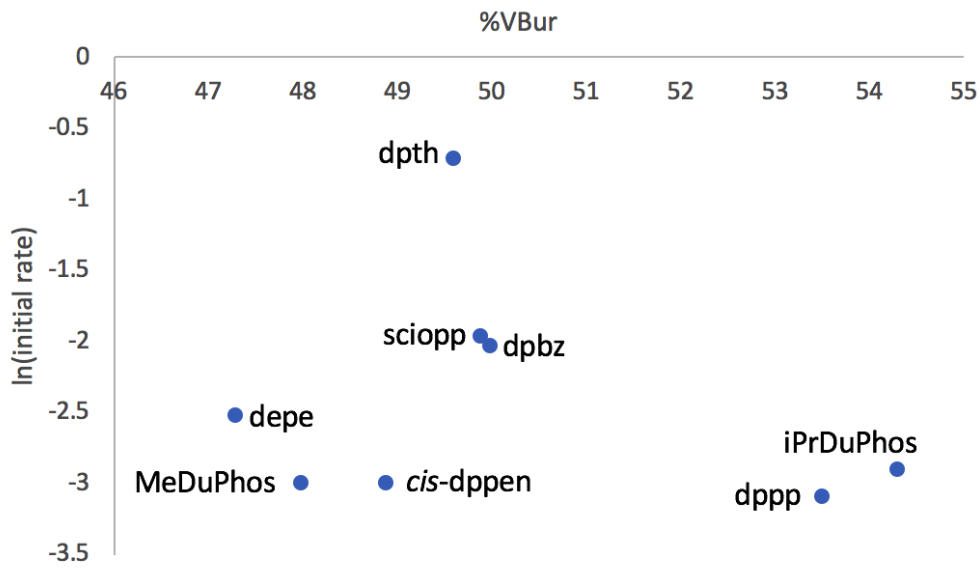


Supplementary Figure 29. Variation in catalyst performance versus chelating diphosphine bite angle in $\text{MBr}_2(\text{PP})$ ($\text{M} = \text{Fe}, \text{Zn}$) as determined crystallographically.

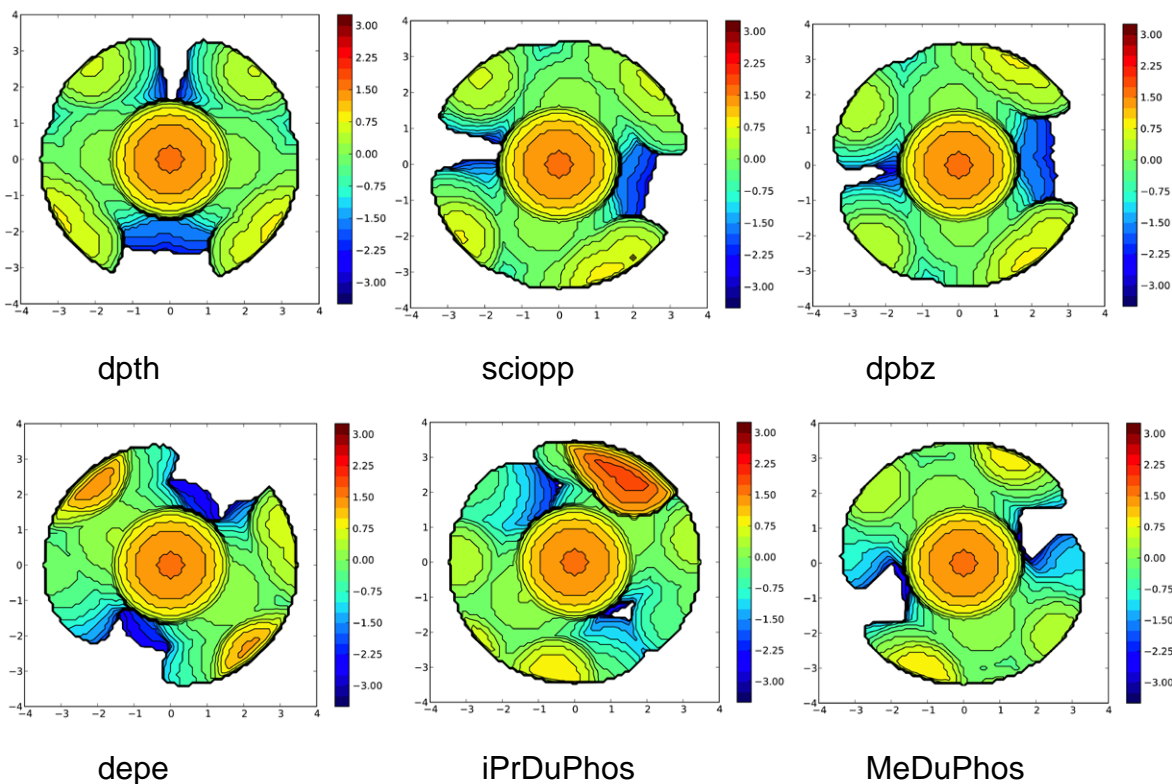
3.3 Steric effect – the percentage buried volume approach.

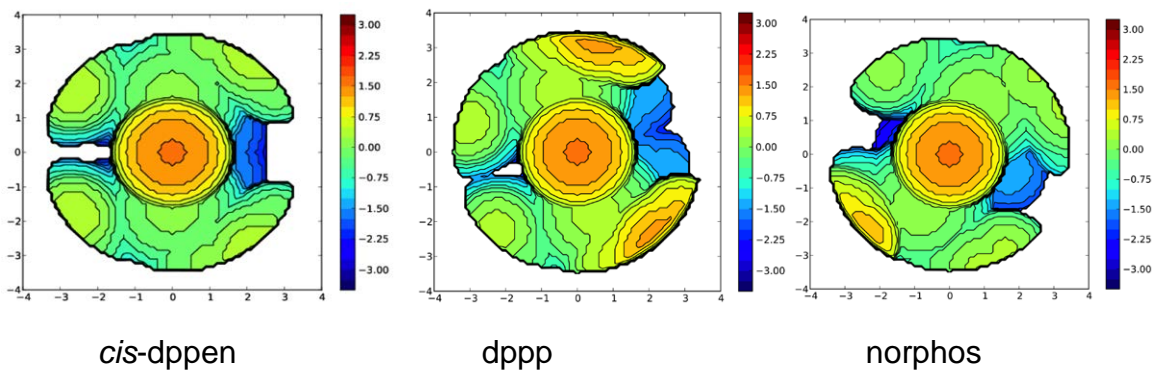
Clearly, the bite angle of a chelating diphosphine is by no means the only metric that is likely to impact on performance, with the steric effects at the metal centre being potentially extremely important and informed by the size and arrangement of the substituents on the phosphorus donors as well as the bite angle of the ligand. In order to quantify a steric metric, we employed SambVca 2, a tool developed by Cavallo and co-workers⁷ to determine both the percent buried volume ($\% V_{\text{Bur}}$) and to produce topographic maps of the ligands' steric profile at the metal centre in selected $\text{ZnBr}_2(\text{PP})$ complexes. Note that while the models employed are based on the zinc complexes, the order, if not the absolute values, would be expected to be the same for $\text{FeBr}_2(\text{PP})$ adducts. The geometries of the selected $\text{ZnBr}_2(\text{PP})$, were first optimised using DFT on Gaussian 09 Rev. D⁸ using the BP86 functional,^{9,10} with the TZVP basis set¹¹ on all atoms except zinc, for which the Stuttgart–Dresden effective core potential and associated basis set were used.¹² Where available, the crystal structure geometry was used as the starting point for geometry optimisation. A frequency calculation was performed on each optimised structure, which confirmed it was a minimum with no imaginary stretching frequencies obtained. Optimised cartesian coordinates are given below (section 3.6). The DFT-optimised geometries were then submitted as .xyz files for SambVca 2 analysis at <https://www.molnac.unisa.it/OMtools/sambvca2.0/index.html>, with the following settings: zinc atom chosen as the atom “coordinated to the center of the sphere”; Zn and the two P atoms selected for “z axis definition” and “z-negative” selected; Zn and the two P atoms selected for “xz-plane definition”; the two Br atoms selected for deletion;

all other settings left as default values, except “include H atoms in the calculations” which was selected. Supplementary Figure 30 summarises the effect of changing %V_{Bur} on the initial rate of catalysis for selected ligands which show activity. From this data it is clear that there is no apparent trend, rather a scatter is obtained. Norphos, which shows no activity, has an almost identical steric profile to dpth, the most active ligand, with a %V_{Bur} = 49.4. Supplementary Figure 31 shows the steric maps calculated for the nine ligands investigated, from this it is clear that the profiles of the ligands from the metal’s perspective is broadly similar.



Supplementary Figure 30. Variation in catalyst performance versus %V_{bur} values for selected DFT-optimised complexes (PP)FeBr₂.

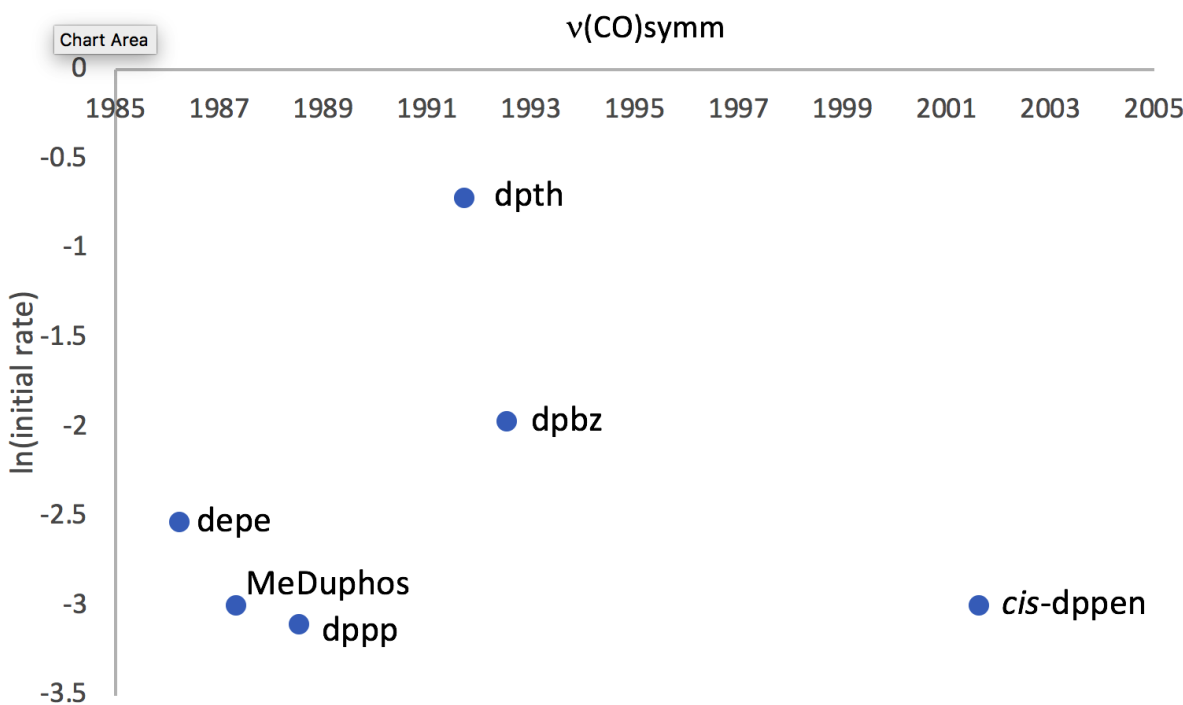




Supplementary Figure 31. Steric maps for selected complexes $\text{ZnBr}_2(\text{PP})$, Br ligands removed, centre = Zn. For details of the meaning of these maps see Cavallo and co-workers.⁷

3.4 Electronic influence.

We next explored the impact of the variation of electronic properties of the diphosphine ligands on the observed catalytic performance. This was undertaken by determining the DFT-calculated $\nu(\text{CO})_{\text{symm}}$ for selected $\text{Ni}(\text{CO})_2(\text{PP})$ complexes, a method previously found to give good results for predicting the net donor properties of chelating diphosphines.¹³ The selected $(\text{PP})\text{Ni}(\text{CO})_2$ structures were optimised using DFT as implemented on Gaussian 09 Rev. D⁸ using the BP86 functional,^{9,10} with the def2-TZVP basis set on all atoms.¹¹ A frequency calculation was performed on each optimised structure, which confirmed it was a minimum with no imaginary stretching frequencies obtained. Optimised cartesian coordinates are given below (section 3.6). This calculation also yielded the calculated value of $\nu(\text{CO})_{\text{symm}}$. Supplementary Figure 32 summarises the calculated $\nu(\text{CO})_{\text{symm}}$ versus initial rate of catalysis. Once again, no clear trend is apparent, with the net electron-donor properties of the more active ligands investigated, dpbz and dpth, lying at the heart of a scatter. Norphos (not shown) has a calculated $\nu(\text{CO})$ of 1990.5, close to the two most active ligands, yet shows no performance in catalysis.

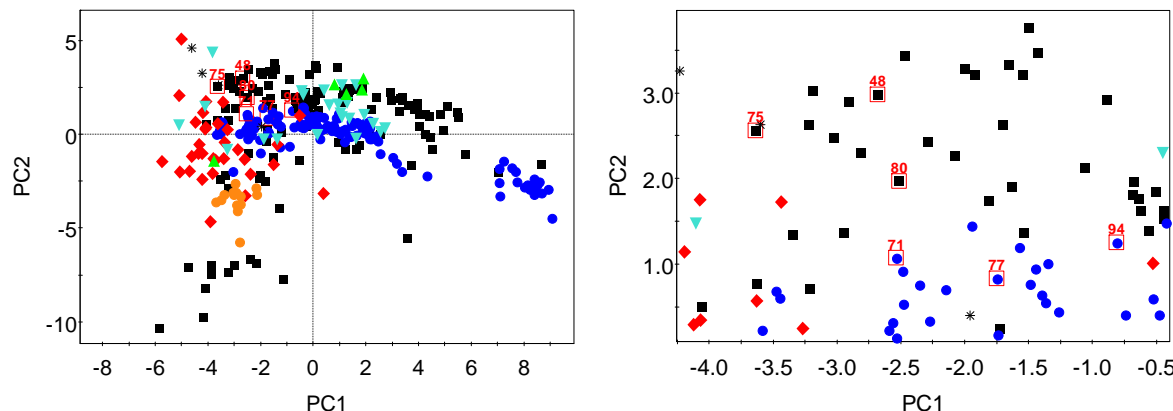


Supplementary Figure 32. Variation in catalyst performance versus DFT-calculated values of $\nu(\text{CO})_{\text{symm}}$ for selected $\text{Ni}(\text{CO})_2(\text{PP})$ complexes, a measure of net electron-donor properties of the PP ligands.

3.5 Ligand Knowledge Base analysis

It is clear from the studies outlined above that no single metric for the diphosphine ligands yields a meaningful correlation with catalyst performance. Accordingly, we finally examined where selected ligands lie in the Ligand Knowledge Base (LKB) for bidentate P,P-donor ligands.^{14,15} The LKB is a collection of 28 ligand descriptors extracted from DFT-calculations for each ligand and a number of representative complexes, which are then computed by principal component analysis into fewer variables (PCs), which optimally capture key contributions. This allows simpler, two- or three-dimensional maps to be produced that chart what one might term ligand chemical space, capturing ligand similarity by their proximity on principal component plots. Supplementary Figure 33 (left) shows the relative positions of six of the ligands used in the iron-catalysed Negishi reaction in Figure 2 on the relevant LKB map of bidentate ligand space, and an expansion of the north-west quadrant, in which the ligands lie (right), while Supplementary Table 2 shows the ligands examined, their LKB identifiers¹⁵ and initial rate data from the Negishi cross-coupling reaction. In this map, Principal Component 1 (PC1) includes descriptors capturing sterics ($\text{He}_8\text{-wedge}$, $n\text{He}_8$, see relevant references for details), ligand bite angles (in $[\text{ZnCl}_2(\text{PP})]$ and $[\text{PdCl}_2(\text{PP})]$ complexes) and terms broadly associated with σ -bonding effects (for instance M-P distances) and the responsiveness of the ligand to coordination (P-R distances and R-P-R angles in different complexes). PC2 loads highly for partial NBO charges and LUMO energies for the P-donors, as well as the change in Zn-P distance compared to a reference compound. Most other descriptors load relatively highly on both PCs, suggesting that they

measure a combination of these effects. For full details of the 28 ligand descriptors and their relative contributions to PC1 and PC2 see the work by Newland and co-workers.¹⁴ Beyond noting that all of the ligands examined lie in the NW quadrant, no clear trends can be identified, with, for instance, the second most active ligand (depe, **48**) lying removed from the most active (dpbz, **77**) and adjacent to dmbz (**75**) which poisons the catalyst.



Supplementary Figure 33. Relative positions of six of the diphosphine ligands used in the catalysis on the Ligand Knowledge Base map for diphosphine ligands (left) and an expansion of the north-west quadrant (right) where all six lie. The LKB identifiers are summarised in Supplementary Table 2, which also summarises the rates of catalysis obtained with these ligands.

Supplementary Table 2. Ligand Knowledge Base identifiers for the six ligands investigated, along with the initial rates of catalysis.

Ligand	LKB Identifier	Ln(initial rate)
dpbz	77	-1.97
depe	48	-2.53
cis-dppen	71	-3.00
MeDuPhos	80	-3.00
dppp	94	-3.10
dmbz	75	No reaction

3.6 Optimised Cartesian Coordinates

3.6.1 %V_{Bur} studies (BP86/TZVP/SDD)

(a) (dpth)ZnBr₂

SCF Energy: -4730041.4431862 a.u.

C	-2.12675	-2.15821	0.50895
C	-0.76221	-2.13038	0.33307
C	-0.24116	-0.78234	0.27603
C	-1.22799	0.16742	0.40966
S	-2.79924	-0.55505	0.61315

H	-2.77223	-3.02611	0.62200
H	-1.11929	1.24901	0.44071
P	1.56918	-0.46651	0.16710
P	0.36498	-3.58503	0.28646
Zn	2.47874	-2.57240	1.22365
C	-0.55863	-4.92038	1.17295
C	-1.23403	-5.94512	0.48981
C	-0.54121	-4.90953	2.58002
C	-1.90387	-6.94062	1.21024
H	-1.23108	-5.97220	-0.60148
C	-1.21837	-5.90475	3.28998
H	0.01330	-4.13274	3.11516
C	-1.90002	-6.92043	2.60885
H	-2.42512	-7.73654	0.67356
H	-1.19887	-5.89260	4.38182
H	-2.42010	-7.70108	3.16843
C	0.41374	-4.11402	-1.48331
C	1.54895	-4.82015	-1.91917
C	-0.63326	-3.85170	-2.38278
C	1.61935	-5.27882	-3.23842
H	2.38647	-4.98714	-1.23666
C	-0.55264	-4.30813	-3.70206
H	-1.50772	-3.28682	-2.05258
C	0.57094	-5.02540	-4.12947
H	2.50503	-5.82343	-3.57212
H	-1.36817	-4.09965	-4.39828
H	0.63251	-5.37916	-5.16106
C	1.93070	-0.23450	-1.62957
C	3.24665	-0.48207	-2.05897
C	0.96074	0.18425	-2.55569
C	3.59025	-0.28360	-3.39982
H	3.99268	-0.85486	-1.35209

C	1.31049	0.37323	-3.89661
H	-0.06721	0.35754	-2.22965
C	2.62551	0.14455	-4.31828
H	4.61301	-0.47994	-3.72812
H	0.55267	0.69706	-4.61359
H	2.89596	0.29196	-5.36624
C	1.79676	1.20270	0.93081
C	1.96035	2.36268	0.15585
C	1.83554	1.28644	2.33490
C	2.14136	3.60089	0.78236
H	1.95426	2.29984	-0.93393
C	2.01068	2.52869	2.95089
H	1.74329	0.37983	2.94050
C	2.16336	3.68632	2.17836
H	2.27018	4.49942	0.17473
H	2.04231	2.58743	4.04094
H	2.30864	4.65350	2.66467
Br	2.13494	-2.34040	3.57313
Br	4.45730	-3.38672	0.22437

(b) (sciopp)ZnBr₂

SCF Energy: -5317700.0200575 a.u.

Br	19.59146	10.74088	5.48822
Br	15.76886	9.24626	4.98352
Zn	18.00278	9.00666	5.80802
P	18.82619	6.72096	5.26608
P	17.85663	8.07707	8.11562
C	18.34792	5.87666	3.68871
C	17.08990	6.17701	3.14603
H	16.45571	6.91580	3.64462
C	16.65657	5.55747	1.96249
C	17.52388	4.64053	1.34281

H	17.20118	4.15646	0.42274
C	18.79545	4.33201	1.85631
C	19.19800	4.96707	3.04347
H	20.18298	4.76233	3.46765
C	15.27651	5.92097	1.38031
C	15.26225	7.42771	1.02143
H	15.44962	8.05899	1.90220
H	14.27992	7.70757	0.60790
H	16.02960	7.65935	0.26644
C	14.18168	5.63915	2.43854
H	14.17173	4.57533	2.72349
H	13.19006	5.89434	2.03164
H	14.33212	6.23689	3.34895
C	14.94311	5.11369	0.11113
H	15.66116	5.30803	-0.70071
H	13.94673	5.40460	-0.25502
H	14.92180	4.02956	0.30501
C	19.75008	3.33770	1.16326
C	19.14337	2.73355	-0.11790
H	18.21965	2.17134	0.08955
H	19.86278	2.03338	-0.56967
H	18.91703	3.50554	-0.86945
C	20.07895	2.17708	2.13368
H	20.56144	2.53970	3.05306
H	20.76599	1.46132	1.65422
H	19.16538	1.63373	2.42113
C	21.05896	4.07048	0.77963
H	20.85532	4.90101	0.08661
H	21.75553	3.37394	0.28589
H	21.56682	4.48634	1.66198
C	20.65175	6.46505	5.39015
C	21.45612	7.36603	4.68246

H	20.98971	8.21778	4.18133
C	22.85158	7.19146	4.62242
C	23.40093	6.10964	5.32398
H	24.48103	5.96107	5.29566
C	22.62118	5.20575	6.07385
C	21.23264	5.39430	6.09191
H	20.59146	4.71317	6.65128
C	23.70800	8.17887	3.80575
C	25.20287	7.80520	3.81615
H	25.62449	7.82106	4.83334
H	25.76617	8.53553	3.21550
H	25.38294	6.80941	3.38094
C	23.55336	9.60088	4.39611
H	22.50550	9.93468	4.40201
H	24.13653	10.32162	3.80073
H	23.92086	9.63671	5.43281
C	23.22148	8.18197	2.33543
H	23.31779	7.18267	1.88314
H	23.82449	8.88665	1.74088
H	22.16983	8.49181	2.25318
C	23.31285	4.05535	6.83158
C	24.07905	3.15994	5.82695
H	23.39258	2.71888	5.08801
H	24.58353	2.33705	6.35827
H	24.84722	3.72431	5.27799
C	22.30813	3.16989	7.59372
H	21.74568	3.74225	8.34726
H	22.84785	2.36787	8.12032
H	21.58511	2.69105	6.91538
C	24.31409	4.64499	7.85466
H	25.09221	5.24815	7.36394
H	24.81601	3.83400	8.40633

H	23.79873	5.29044	8.58206
C	18.04380	5.67295	6.59193
C	17.81557	4.30345	6.36981
H	18.12716	3.85607	5.42346
C	17.17039	3.51796	7.32780
H	17.00306	2.45585	7.13566
C	16.72097	4.09985	8.51746
H	16.19811	3.49703	9.26332
C	16.92548	5.46264	8.74523
H	16.53922	5.92457	9.65639
C	17.59534	6.26108	7.80150
C	16.44118	8.55760	9.20668
C	16.64386	9.02914	10.51195
H	17.65671	9.07284	10.91121
C	15.55517	9.44518	11.29645
C	14.27270	9.36397	10.73122
H	13.41756	9.68541	11.33061
C	14.03807	8.90187	9.42405
C	15.14723	8.50929	8.66029
H	15.01643	8.18675	7.62609
C	15.72657	9.98192	12.73167
C	17.20211	10.00458	13.17482
H	17.64853	8.99818	13.16825
H	17.27203	10.39120	14.20314
H	17.81395	10.65592	12.53241
C	14.93916	9.08345	13.71644
H	13.86604	9.05676	13.47668
H	15.04412	9.46280	14.74562
H	15.31555	8.04897	13.69296
C	15.17855	11.42827	12.80730
H	15.71894	12.09053	12.11396
H	15.29750	11.82727	13.82736

H	14.10952	11.47508	12.55209
C	12.60038	8.87383	8.86789
C	12.05656	10.32286	8.80776
H	11.02693	10.32579	8.41547
H	12.04017	10.79292	9.80249
H	12.67739	10.94678	8.14748
C	11.69907	8.02577	9.79805
H	12.06505	6.98933	9.86332
H	10.67007	8.00029	9.40531
H	11.65523	8.43415	10.81873
C	12.53560	8.27109	7.45189
H	13.13385	8.84531	6.72878
H	11.49204	8.27368	7.10072
H	12.88928	7.22833	7.43710
C	19.35582	8.17522	9.19705
C	20.18811	9.28985	9.05439
H	19.98433	10.01040	8.25714
C	21.29117	9.47621	9.91323
C	21.52302	8.50569	10.89511
H	22.37317	8.63249	11.56663
C	20.70758	7.36506	11.05607
C	19.61948	7.21234	10.18970
H	18.96442	6.34596	10.27978
C	22.18509	10.71819	9.73667
C	23.32179	10.77696	10.77525
H	22.93784	10.81951	11.80684
H	23.92024	11.68538	10.60820
H	24.00230	9.91488	10.69270
C	21.32224	11.99515	9.88812
H	20.52597	12.04171	9.13151
H	21.95127	12.89124	9.76534
H	20.85402	12.03970	10.88387

C	22.81285	10.69267	8.32195
H	23.43745	9.79581	8.18789
H	23.44945	11.58013	8.17603
H	22.04570	10.69463	7.53382
C	21.03463	6.35096	12.17106
C	22.44481	5.75936	11.93216
H	22.49119	5.23010	10.96831
H	22.69758	5.04176	12.72921
H	23.21895	6.54060	11.92539
C	20.02476	5.18862	12.22039
H	19.00253	5.54280	12.42477
H	20.30268	4.49442	13.02814
H	20.01030	4.61562	11.28051
C	21.01033	7.06933	13.54269
H	21.75063	7.88109	13.59364
H	21.23980	6.35545	14.34990
H	20.01904	7.50447	13.74190

(c) (dpbz)ZnBr₂

SCF Energy: -4528485.0895198 a.u.

Br	12.96849	3.89871	3.53120
Br	12.35016	0.72763	6.22182
C	9.35033	5.42589	5.60733
C	7.99606	5.79998	5.62767
H	7.24643	5.12512	6.04632
C	7.60425	7.03665	5.10469
H	6.54970	7.32114	5.12078
C	8.55834	7.90446	4.56138
H	8.24941	8.86995	4.15458
C	9.90594	7.52914	4.52910
H	10.65209	8.19507	4.09060
C	10.30436	6.29087	5.04181

H	11.35202	5.98468	4.97987
C	10.32735	4.21105	8.09323
C	11.05419	3.25841	8.83159
H	11.39476	2.33608	8.35138
C	11.35474	3.50239	10.17460
H	11.92079	2.76005	10.74135
C	10.95061	4.69599	10.78434
H	11.19546	4.88567	11.83177
C	10.24317	5.65102	10.04653
H	9.93443	6.58856	10.51437
C	9.93117	5.41314	8.70337
H	9.38597	6.16556	8.13023
C	8.49257	2.70672	6.36048
C	7.63354	2.67565	7.47101
H	7.83084	3.33487	8.31898
C	6.54912	1.79487	7.51131
H	5.89281	1.78208	8.38419
C	6.31891	0.92254	6.44296
H	5.48064	0.22311	6.47371
C	7.17388	0.93302	5.33727
H	7.01214	0.22876	4.51828
C	8.26011	1.82161	5.27762
C	9.27983	0.12060	3.11156
C	9.90156	-0.94386	3.79144
H	10.45367	-0.75456	4.71673
C	9.83127	-2.23791	3.26906
H	10.31803	-3.05846	3.80050
C	9.16035	-2.47877	2.06394
H	9.11559	-3.49056	1.65498
C	8.55733	-1.41903	1.37868
H	8.04063	-1.59919	0.43330
C	8.61534	-0.12055	1.89757

H	8.14850	0.70303	1.35421
C	8.68770	2.95059	2.58772
C	9.56036	3.60006	1.69709
H	10.64173	3.47431	1.80096
C	9.04414	4.43266	0.69856
H	9.72783	4.93664	0.01223
C	7.66380	4.63108	0.59031
H	7.26459	5.28557	-0.18780
C	6.79382	3.99823	1.48625
H	5.71593	4.15856	1.41056
C	7.30161	3.16038	2.48385
H	6.61882	2.67334	3.18338
P	9.96758	3.83624	6.31873
P	9.43550	1.81318	3.83806
Zn	11.58379	2.55731	4.89636

(d) (depe)ZnBr₂

SCF Energy: -4050296.0887307 a.u.

Br	0.50560	7.98901	7.79810
Br	3.21467	5.12627	6.03083
Zn	2.59611	7.23335	6.95734
P	3.43927	9.00914	5.46163
P	4.50315	7.80164	8.45357
C	2.27590	10.37274	4.95249
C	1.15821	9.86768	4.02993
H	1.55173	9.48831	3.07494
C	4.33055	8.46662	3.91381
C	4.99444	9.55137	3.05962
H	4.26458	10.28485	2.68646
C	4.72534	9.88462	6.51251
H	4.16254	10.56531	7.17244
C	5.56286	8.89355	7.34455

H	6.12782	8.21655	6.68385
C	5.70071	6.44160	8.89686
C	5.14205	5.39876	9.87310
H	4.21228	4.95634	9.48728
C	4.30160	8.86313	9.98494
C	3.15438	8.42781	10.90736
H	2.19737	8.41265	10.36567
H	5.37755	10.51690	5.88933
H	6.30280	9.43347	7.95824
H	5.86896	4.58360	10.00711
H	4.94027	5.82587	10.86605
H	5.93729	5.95642	7.93621
H	6.62714	6.89985	9.28256
H	5.26818	8.89061	10.51665
H	4.11166	9.88362	9.61306
H	3.06145	9.12709	11.75242
H	3.31981	7.42432	11.32390
H	2.84386	11.19696	4.49136
H	1.84382	10.74948	5.89326
H	0.45825	10.68416	3.79803
H	0.58664	9.06186	4.51301
H	5.48147	9.09842	2.18223
H	5.77067	10.10111	3.61345
H	3.58056	7.90619	3.33299
H	5.05671	7.70566	4.24206

(e) (iPrDuPhos)ZnBr₂

SCF Energy: -4440637.3775802 a.u.

Br	4.03551	10.90572	13.38359
Br	2.36839	8.49685	10.44893
Zn	4.04945	8.90655	12.08633
P	6.37969	8.58647	11.38019

P	4.34680	6.76186	13.30454
C	4.11549	6.43998	15.17050
H	5.11243	6.13232	15.52598
C	8.39814	9.71830	13.26093
H	9.04417	8.84004	13.07566
C	7.53613	10.08766	9.48245
H	8.13508	10.20983	8.56739
H	6.70519	10.81262	9.42526
C	6.95219	6.96757	12.10273
C	6.63418	5.05142	13.56422
H	6.01461	4.46585	14.24506
C	3.13626	5.38692	12.80697
H	2.19681	5.97085	12.86780
C	5.89195	8.28074	8.53800
H	4.97929	8.85919	8.76843
C	7.55645	9.97218	11.98958
H	6.83925	10.78205	12.21881
C	3.15194	4.40501	13.99051
H	2.28263	3.72812	13.95022
H	4.04742	3.76468	13.94514
C	3.18232	4.80910	11.37189
H	3.35536	5.66486	10.69731
C	8.26120	6.51489	11.85269
H	8.91122	7.08822	11.18791
C	6.10804	6.21093	12.96072
C	7.93778	4.62047	13.31163
H	8.31254	3.71389	13.79169
C	3.71065	7.70893	15.96910
H	4.43179	8.49924	15.69777
C	6.97197	8.65598	9.57586
H	7.81252	7.94205	9.48288
C	6.34285	8.63511	7.10928

H	6.49609	9.71566	6.97525
H	5.57921	8.31777	6.38307
H	7.28413	8.12106	6.84926
C	3.13408	5.23865	15.28242
H	3.37728	4.62344	16.16245
H	2.11321	5.62173	15.43438
C	8.37760	10.34745	10.73635
H	8.70385	11.39749	10.78589
H	9.29252	9.72789	10.69925
C	3.84212	7.45280	17.48152
H	3.12742	6.68685	17.82400
H	3.63373	8.37351	18.04745
H	4.85605	7.11531	17.74980
C	8.75402	5.34988	12.44243
H	9.77406	5.02055	12.23316
C	7.53264	9.43348	14.49684
H	6.82638	10.25724	14.68135
H	8.16587	9.30907	15.38908
H	6.94210	8.51306	14.38143
C	1.80184	4.23511	10.99893
H	1.52611	3.38409	11.64338
H	1.80513	3.87336	9.95922
H	1.01823	5.00300	11.08245
C	2.31229	8.24257	15.62462
H	2.18040	8.38991	14.54184
H	2.15973	9.22543	16.09316
H	1.51382	7.57527	15.98639
C	4.28024	3.76150	11.13531
H	5.28469	4.14576	11.35919
H	4.27323	3.44523	10.08101
H	4.11714	2.85871	11.74616
C	9.31737	10.92452	13.54053

H	10.03081	11.10905	12.72439
H	9.89997	10.75134	14.45838
H	8.72342	11.84088	13.69001
C	5.53729	6.79019	8.62287
H	6.41210	6.16158	8.38381
H	4.73346	6.54115	7.91476
H	5.18222	6.51190	9.62604

(f) (MeDuPhos)ZnBr₂

SCF Energy: -4243237.7311368 a.u.

Br	0.03359	8.04302	5.19600
Br	-1.98646	4.34059	5.55902
P	1.48796	4.71885	7.09054
P	-0.71557	6.63274	8.68521
C	0.73280	5.87443	11.02340
H	0.01724	6.49717	11.56443
C	-2.28376	6.48893	9.74808
H	-1.95577	6.09979	10.72674
C	1.57579	4.93658	8.94115
C	3.27975	4.86095	6.47225
H	3.91592	4.83186	7.37321
C	0.62861	5.74302	9.62501
C	2.57823	4.28483	9.68516
H	3.30756	3.65497	9.17159
C	1.73620	5.22471	11.74399
H	1.79400	5.34546	12.82792
C	1.35735	2.85655	6.73625
H	0.75939	2.85408	5.80720
C	-1.49727	8.83223	10.12127
H	-1.04029	8.62957	11.10656
H	-1.74715	9.90585	10.10399
C	-0.49632	8.49504	8.99886

H	-0.86196	8.92301	8.04830
C	2.66245	4.42173	11.07150
H	3.44863	3.90309	11.62441
C	2.79551	2.40804	6.41007
H	3.33941	2.17156	7.34252
H	2.78287	1.48327	5.80999
C	0.61554	2.01587	7.77392
H	1.11163	2.03769	8.75605
H	0.57501	0.96667	7.43975
H	-0.42072	2.36290	7.89555
C	-2.74011	7.95427	9.92366
H	-3.28243	8.27702	9.01807
H	-3.44635	8.03512	10.76579
C	0.93496	8.98050	9.21892
H	1.39102	8.52763	10.11251
H	0.93927	10.07390	9.35473
H	1.56862	8.75456	8.34917
C	3.56641	6.14306	5.68724
H	2.89765	6.24233	4.81999
H	4.60680	6.13691	5.32321
H	3.43038	7.04235	6.30440
C	3.49199	3.55810	5.66945
H	3.05013	3.67405	4.66460
H	4.56830	3.36978	5.52589
C	-3.34874	5.55863	9.16225
H	-3.65024	5.87674	8.15371
H	-4.24331	5.55861	9.80626
H	-2.99097	4.52266	9.08076
Zn	-0.46522	6.00636	6.31574

(g) (*cis*-dppen)ZnBr₂

SCF Energy: -4432057.1498603 a.u.

Br	3.76761	14.17876	5.38626
Br	-0.35550	14.17876	4.47525
Zn	1.92878	14.17876	3.87477
P	2.56877	12.52612	2.07912
C	1.29055	12.04241	0.83503
C	1.62593	11.69566	-0.48661
H	2.66765	11.71358	-0.81400
C	0.62471	11.32258	-1.38690
H	0.88961	11.05532	-2.41235
C	-0.71387	11.29182	-0.97514
H	-1.49449	10.99970	-1.68112
C	-1.05027	11.63958	0.33652
H	-2.09343	11.62564	0.65912
C	-0.05366	12.01977	1.24317
H	-0.32239	12.31881	2.26064
C	3.48935	10.97721	2.48192
C	3.06743	9.71190	2.04258
H	2.17972	9.61587	1.41490
C	3.78814	8.57021	2.40957
H	3.45525	7.58881	2.06445
C	4.92683	8.68333	3.21420
H	5.48590	7.78949	3.49937
C	5.34083	9.94275	3.66312
H	6.21813	10.03590	4.30672
C	4.62244	11.08818	3.30919
H	4.92150	12.06474	3.69963
C	3.81032	13.50566	1.13112
H	4.59407	12.95580	0.59853
P	2.56877	15.83138	2.07911
C	1.29055	16.31509	0.83503
C	1.62593	16.66185	-0.48661
H	2.66766	16.64392	-0.81400

C	0.62472	17.03493	-1.38691
H	0.88962	17.30219	-2.41235
C	-0.71387	17.06568	-0.97515
H	-1.49448	17.35780	-1.68112
C	-1.05027	16.71792	0.33652
H	-2.09343	16.73187	0.65911
C	-0.05366	16.33774	1.24317
H	-0.32239	16.03869	2.26063
C	3.48935	17.38030	2.48191
C	3.06744	18.64561	2.04257
H	2.17972	18.74164	1.41489
C	3.78814	19.78729	2.40956
H	3.45526	20.76870	2.06444
C	4.92683	19.67417	3.21419
H	5.48591	20.56801	3.49936
C	5.34083	18.41476	3.66312
H	6.21813	18.32161	4.30671
C	4.62244	17.26932	3.30919
H	4.92150	16.29276	3.69963
C	3.81032	14.85184	1.13112
H	4.59407	15.40170	0.59852

(h) (dPPP)ZnBr₂

SCF Energy: -4457497.1931204 a.u.

Br	3.49237	9.00316	5.52344
Br	4.66677	13.03117	4.91160
Zn	4.94664	10.69671	4.60226
P	7.20398	9.85540	5.20608
P	5.15516	9.99020	2.23231
C	7.54882	9.47904	6.98880
C	6.55000	8.83116	7.73930
H	5.58724	8.58998	7.27944

C	6.77895	8.51739	9.08217
H	5.99683	8.01593	9.65633
C	7.99131	8.85888	9.69194
H	8.16294	8.61871	10.74354
C	8.97862	9.51818	8.95268
H	9.92359	9.79729	9.42431
C	8.76167	9.82914	7.60589
H	9.53667	10.35024	7.04098
C	8.65508	10.85261	4.64701
C	9.88116	10.27573	4.26917
H	10.01007	9.19113	4.27641
C	10.95459	11.08718	3.88846
H	11.90190	10.62961	3.59432
C	10.81638	12.48008	3.88963
H	11.65729	13.11236	3.59611
C	9.59998	13.05931	4.26561
H	9.48514	14.14532	4.26509
C	8.51884	12.25245	4.63539
H	7.56277	12.70892	4.91016
C	7.40165	8.17794	4.38981
H	8.35907	7.74834	4.72405
H	6.60558	7.55586	4.82991
C	7.31913	8.15063	2.85008
H	7.99311	8.90794	2.41715
H	7.72360	7.17570	2.52829
C	5.91353	8.27284	2.22905
H	5.19304	7.64328	2.77583
H	5.92683	7.91007	1.18942
C	6.23792	11.00885	1.13459
C	6.94710	10.46899	0.04619
H	6.89160	9.40124	-0.17701
C	7.72206	11.29820	-0.77051

H	8.27084	10.87014	-1.61246
C	7.78971	12.67259	-0.51258
H	8.39250	13.31908	-1.15430
C	7.08558	13.21489	0.56727
H	7.13685	14.28581	0.77473
C	6.31761	12.38855	1.39466
H	5.78088	12.81320	2.24899
C	3.58967	9.75521	1.26698
C	2.51956	9.07989	1.88337
H	2.61326	8.72776	2.91463
C	1.32272	8.88614	1.18785
H	0.49745	8.36342	1.67617
C	1.17449	9.37529	-0.11488
H	0.23448	9.22981	-0.65173
C	2.23030	10.06184	-0.72297
H	2.11821	10.45607	-1.73557
C	3.43482	10.25364	-0.03742
H	4.24977	10.79739	-0.51804

(i) (norphos)ZnBr₂

SCF Energy: -4553875.3614710 a.u.

Br	0.71157	6.97342	7.10475
Br	4.09141	4.92974	5.54186
Zn	3.00039	6.79822	6.54588
P	3.73282	8.93596	5.33454
P	4.61535	7.42468	8.40824
C	2.42095	10.21978	5.14049
C	1.26431	9.84196	4.43337
H	1.17200	8.82666	4.04125
C	0.22273	10.75318	4.24601
H	-0.67044	10.44570	3.69841
C	0.31200	12.04410	4.77971

H	-0.50756	12.75238	4.64061
C	1.44899	12.42067	5.50098
H	1.52195	13.42386	5.92702
C	2.49995	11.51389	5.68146
H	3.37856	11.82672	6.24766
C	4.62685	8.94017	3.71407
C	4.70350	10.09935	2.92091
H	4.20588	11.01687	3.24239
C	5.40386	10.07430	1.71174
H	5.45705	10.97658	1.09806
C	6.02708	8.89496	1.28381
H	6.56976	8.87755	0.33596
C	5.93918	7.73741	2.06359
H	6.40604	6.80989	1.72511
C	5.23604	7.75266	3.27367
H	5.14075	6.83673	3.86510
C	4.91158	9.58584	6.64018
H	4.21263	9.96493	7.40797
C	6.01272	10.69998	6.45430
H	5.61402	11.67910	6.16392
C	7.15183	10.15753	5.60058
H	7.32622	10.41794	4.55761
C	7.80751	9.23576	6.33073
H	8.61154	8.57880	5.99721
C	7.08816	9.11523	7.67253
H	7.63850	8.62479	8.48374
C	5.73403	8.40756	7.26410
H	5.96208	7.65547	6.48844
C	6.65228	10.58833	7.86959
H	5.93385	10.73928	8.68889
H	7.51278	11.26074	7.99345
C	5.68093	6.12997	9.17706

C	6.57948	5.39580	8.38006
H	6.67433	5.60695	7.31384
C	7.33044	4.35863	8.94006
H	8.02303	3.79700	8.30959
C	7.18396	4.02855	10.29167
H	7.76881	3.21408	10.72425
C	6.27364	4.73756	11.08207
H	6.14070	4.47747	12.13453
C	5.52179	5.77926	10.52993
H	4.81036	6.32011	11.15625
C	4.09918	8.54313	9.78560
C	5.00945	9.07305	10.72136
H	6.06681	8.80443	10.67190
C	4.56082	9.93126	11.72846
H	5.27213	10.33732	12.45132
C	3.20276	10.26675	11.81343
H	2.85523	10.93527	12.60434
C	2.29399	9.73829	10.89232
H	1.23318	9.98860	10.95948
C	2.73627	8.87700	9.88030
H	2.01954	8.45322	9.16909

3.6.2 (PP)Ni(CO)₂ complexes for calculated $\nu(\text{CO})_{\text{symm}}$ studies (BP86/def2-TZVP)

(a) (dptb)Ni(CO)₂

SCF Energy: -2445223.9973996 a.u.

P	5.23177	2.04768	3.69799
P	5.71537	4.00620	6.12189
S	2.12560	1.56701	6.75525
C	4.40170	2.92301	2.30368
C	5.20306	0.28747	3.13294
C	4.21340	2.94883	6.15973
C	5.08902	5.70320	5.75957

C	6.02789	6.67047	5.35885
H	7.07948	6.39265	5.25801
C	3.99094	2.05756	5.05156
C	5.15721	3.15496	1.13944
H	6.19376	2.81311	1.08861
C	6.17473	4.11196	7.90894
C	3.27265	2.79118	7.15490
H	3.21341	3.29929	8.11454
C	4.59724	3.82655	0.05205
H	5.19610	3.99607	-0.84510
C	6.76749	2.98410	8.50465
H	6.94463	2.08739	7.90708
C	3.73768	6.06963	5.85753
H	2.99502	5.32895	6.15903
C	2.88798	1.25349	5.24063
H	2.50389	0.47179	4.58957
C	6.11242	-0.61311	3.71102
H	6.83420	-0.24993	4.44531
C	5.62554	7.97790	5.07890
H	6.36725	8.71724	4.77010
C	4.30150	-0.18406	2.16331
H	3.60284	0.50623	1.68648
C	3.08178	3.39597	2.36016
H	2.48334	3.23197	3.25800
C	5.97983	5.26547	8.68532
H	5.52960	6.15374	8.23935
C	6.94032	4.15763	10.61715
H	7.24128	4.17659	11.66654
C	3.27933	4.29415	0.11665
H	2.84519	4.82858	-0.73068
C	6.36441	5.28696	10.03078
H	6.21092	6.19335	10.62047

C	4.27606	8.33361	5.17725
H	3.95948	9.35267	4.94603
C	7.13865	3.00400	9.84962
H	7.59634	2.11926	10.29698
C	4.30319	-1.53213	1.79196
H	3.60051	-1.88457	1.03369
C	3.33400	7.37613	5.56259
H	2.27778	7.64457	5.63462
C	5.20317	-2.42393	2.38306
H	5.20624	-3.47534	2.08845
C	2.52646	4.08113	1.27344
H	1.49952	4.44782	1.33469
C	6.10810	-1.96091	3.34363
H	6.82259	-2.64822	3.80127
Ni	7.02595	3.03580	4.59078
C	7.75959	4.19480	3.44375
C	8.20922	1.92351	5.32760
O	8.26395	4.92468	2.69662
O	9.01360	1.22917	5.79690

(b) (dpbz)Ni(CO)₂

SCF Energy: -2244172.7490717 a.u.

C	9.35279	5.62687	5.80938
C	8.00638	6.01385	5.72137
H	7.22006	5.28317	5.89711
C	7.66611	7.33300	5.40131
H	6.61367	7.61568	5.32849
C	8.66464	8.28344	5.17673
H	8.39764	9.31211	4.92643
C	10.00995	7.90746	5.26360
H	10.79314	8.64076	5.08018
C	10.35112	6.58868	5.56699

H	11.39816	6.29135	5.61237
C	10.34148	3.99708	7.97686
C	10.93880	2.86714	8.56362
H	11.13962	1.98638	7.94667
C	11.28051	2.86546	9.91666
H	11.74270	1.97927	10.35650
C	11.04727	4.00018	10.70204
H	11.32540	4.00290	11.75789
C	10.46603	5.13223	10.12562
H	10.28573	6.02404	10.72982
C	10.11051	5.13141	8.77219
H	9.65661	6.01669	8.33313
C	8.34386	2.91148	6.21199
C	7.41534	2.96879	7.26316
H	7.59224	3.64286	8.10414
C	6.28453	2.14848	7.25603
H	5.57594	2.19195	8.08584
C	6.07355	1.25891	6.19743
H	5.19938	0.60438	6.19659
C	6.99218	1.19305	5.14656
H	6.83650	0.47968	4.33420
C	8.12980	2.01593	5.14177
C	9.41574	0.17345	3.32996
C	10.12970	-0.73458	4.13146
H	10.67862	-0.36283	4.99832
C	10.14786	-2.09546	3.82165
H	10.70737	-2.78682	4.45515
C	9.46603	-2.56860	2.69499
H	9.48970	-3.63134	2.44554
C	8.76347	-1.67264	1.88505
H	8.23400	-2.03267	1.00019
C	8.73401	-0.30991	2.20079

H	8.18342	0.38018	1.56398
C	8.64880	2.78504	2.37487
C	9.45852	3.01184	1.24608
H	10.49892	2.68907	1.26313
C	8.94310	3.64950	0.11689
H	9.58072	3.81547	-0.75029
C	7.61475	4.09016	0.10333
H	7.21482	4.60001	-0.77542
C	6.80720	3.88343	1.22391
H	5.77166	4.23055	1.22490
C	7.31802	3.23087	2.35173
H	6.67923	3.07077	3.21900
P	9.90871	3.90735	6.18193
P	9.43714	1.95460	3.82393
Ni	11.23334	2.93256	4.68583
C	11.83328	3.90033	3.74588
C	12.24702	1.95374	5.31051
O	12.56821	4.97999	2.67999
O	13.32248	0.99576	5.92406

(c) (depe)Ni(CO)₂

SCF Energy: -1765738.7414837 a.u.

P	3.40944	8.56613	5.60635
P	4.57266	7.84034	8.42687
C	2.02779	9.63288	4.96987
C	1.00203	8.85307	4.13951
H	0.61268	7.99330	4.70391
C	4.35352	8.10902	4.06553
C	4.51277	9.82497	6.44653
H	3.83961	10.50112	6.99957
C	5.48034	9.12722	7.41535
H	6.25178	8.57554	6.85273

C	5.97910	6.86283	9.14525
C	3.91224	8.80138	9.88027
Ni	3.05808	6.94247	7.07807
C	1.42754	7.00338	7.79510
C	3.55877	5.35773	6.43523
O	3.88165	4.32326	6.01441
O	0.36486	7.03925	8.26514
H	5.05391	10.44555	5.71436
H	6.00969	9.85585	8.05053
H	3.31619	8.07844	10.46003
H	6.70186	7.54070	9.62985
H	0.15175	9.49558	3.86578
H	1.44016	8.46969	3.20571
H	1.54538	10.05284	5.86745
H	2.43647	10.48257	4.39761
H	3.75355	7.32235	3.58031
C	4.89928	9.54123	10.78773
H	4.36181	10.07461	11.58718
H	5.60550	8.85250	11.27408
H	5.48843	10.29016	10.23755
C	5.51819	5.76645	10.11298
H	4.78377	5.10283	9.63377
H	6.37025	5.15228	10.44086
H	5.04937	6.18869	11.01449
H	3.17444	9.49764	9.44913
H	6.49218	6.41103	8.28076
C	4.70899	9.21387	3.06579
H	5.27883	8.79903	2.21988
H	3.81190	9.69553	2.64968
H	5.32955	10.00097	3.51997
H	5.26011	7.59626	4.42645

(d) (MeDuphos)Ni(CO)₂

SCF Energy: -1958514.3828110 a.u.

P	3.15978	8.63589	8.70886
P	4.97922	6.80737	6.93950
C	1.30577	9.78433	6.77898
H	0.62873	8.91726	6.78145
C	1.96093	9.99196	8.14309
H	2.62832	10.86897	8.07615
C	0.99319	10.22759	9.31639
H	0.52957	11.22604	9.25034
H	0.16815	9.49446	9.27859
C	1.79765	10.05386	10.60999
H	1.15635	10.06388	11.50634
H	2.50880	10.89189	10.71705
C	2.58343	8.72945	10.51476
H	1.87605	7.89391	10.65218
C	3.71033	8.59822	11.53810
H	4.46910	9.38167	11.39462
C	2.43109	7.04059	8.09310
C	1.12150	6.62241	8.38911
H	0.48351	7.23855	9.02594
C	0.61248	5.42753	7.87771
H	-0.40761	5.12110	8.11871
C	1.41177	4.63029	7.05281
H	1.02234	3.69403	6.64741
C	2.71365	5.03337	6.75094
H	3.32546	4.40023	6.10488
C	3.24244	6.23025	7.26660
C	5.66774	4.50235	8.59117
H	5.51593	5.11995	9.48858
C	6.10421	5.35010	7.39720
H	7.03843	5.87086	7.67115

C	6.35798	4.57558	6.09188
H	7.28324	3.97945	6.16106
H	5.53626	3.85988	5.91251
C	6.42019	5.60108	4.95332
H	6.45099	5.12156	3.96134
H	7.34192	6.20226	5.04524
C	5.19316	6.52691	5.07442
H	4.29990	5.96623	4.74985
C	5.29782	7.81198	4.25515
H	4.38919	8.42512	4.33837
H	6.44141	3.75495	8.82941
H	4.73029	3.96341	8.38898
H	6.14430	8.42836	4.59212
H	5.44764	7.57713	3.18863
H	3.31273	8.68997	12.56209
H	4.22010	7.62721	11.46245
H	2.05822	9.62354	5.99282
H	0.71658	10.67210	6.49856
Ni	5.24551	8.72494	8.00056
C	6.50203	8.54098	9.25315
C	5.47248	10.17033	6.98150
O	7.35039	8.42347	10.03820
O	5.62142	11.13835	6.35636

(e) (*cis*-dppen)Ni(CO)₂

SCF Energy: -2147471.0718350 a.u.

P	2.14984	12.61526	1.75750
C	1.15296	11.38754	0.81622
C	0.73058	11.63398	-0.50014
H	1.05633	12.53984	-1.01631
C	-0.11210	10.73129	-1.15680
H	-0.42925	10.93569	-2.18165

C	-0.54780	9.57456	-0.50550
H	-1.20677	8.87106	-1.01798
C	-0.13917	9.32543	0.80972
H	-0.47984	8.42681	1.32828
C	0.70175	10.22482	1.46684
H	1.01172	10.02221	2.49472
C	3.51449	11.56621	2.43798
C	4.11057	10.53782	1.68546
H	3.73453	10.30286	0.68716
C	5.17187	9.79981	2.21343
H	5.62592	9.00320	1.62012
C	5.64955	10.07690	3.49961
H	6.47718	9.49641	3.91236
C	5.05977	11.09332	4.25536
H	5.42177	11.30927	5.26262
C	3.99788	11.83397	3.72650
H	3.52994	12.62466	4.31584
C	3.05986	13.50787	0.42714
H	3.63231	12.93840	-0.31426
P	2.14984	15.74225	1.75751
C	1.15298	16.96997	0.81622
C	0.73052	16.72347	-0.50011
H	1.05621	15.81757	-1.01624
C	-0.11216	17.62617	-1.15678
H	-0.42936	17.42172	-2.18160
C	-0.54778	18.78295	-0.50551
H	-1.20675	19.48644	-1.01800
C	-0.13908	19.03213	0.80967
H	-0.47970	19.93079	1.32820
C	0.70184	18.13275	1.46680
H	1.01186	18.33539	2.49466
C	3.51449	16.79130	2.43800

C	4.11066	17.81960	1.68543
H	3.73471	18.05449	0.68708
C	5.17195	18.55762	2.21341
H	5.62608	19.35416	1.62005
C	5.64953	18.28063	3.49964
H	6.47715	18.86112	3.91240
C	5.05965	17.26431	4.25544
H	5.42157	17.04843	5.26276
C	3.99778	16.52364	3.72658
H	3.52977	15.73302	4.31596
C	3.05987	14.84965	0.42715
H	3.63232	15.41911	-0.31424
Ni	1.11076	14.17875	2.94359
C	-0.62827	14.17875	2.51285
C	1.38435	14.17870	4.70463
O	-1.75630	14.17877	2.25275
O	1.49835	14.17868	5.86107

(f) (dppp)Ni(CO)₂

SCF Energy: -2172906.8716062 a.u.

P	7.16937	9.98196	5.06687
P	5.32261	9.86986	2.23155
C	7.32725	9.62053	6.87880
C	6.21590	9.79435	7.71561
H	5.28070	10.16024	7.28672
C	6.30308	9.51113	9.08309
H	5.42845	9.65215	9.72149
C	7.50455	9.05306	9.62854
H	7.57436	8.83278	10.69581
C	8.62266	8.88443	8.80328
H	9.56762	8.53550	9.22549
C	8.53589	9.16969	7.43934

H	9.42337	9.05410	6.81234
C	8.67295	11.02666	4.79847
C	9.87184	10.56517	4.23063
H	9.96979	9.52813	3.90598
C	10.96457	11.42508	4.06918
H	11.88594	11.04776	3.62006
C	10.87980	12.75620	4.48221
H	11.73348	13.42548	4.35834
C	9.69142	13.22732	5.05221
H	9.61318	14.26668	5.37784
C	8.59762	12.37344	5.19988
H	7.66910	12.75410	5.63164
C	7.63652	8.33120	4.34664
H	8.63272	8.03811	4.71471
H	6.92295	7.61696	4.78943
C	7.58993	8.23841	2.80910
H	8.18277	9.05084	2.35679
H	8.09476	7.30216	2.51678
C	6.18071	8.21958	2.18692
H	5.54000	7.50711	2.73263
H	6.24942	7.87468	1.14251
C	6.23471	10.78637	0.90713
C	6.10223	10.45471	-0.45316
H	5.41262	9.66375	-0.75765
C	6.82788	11.14686	-1.42492
H	6.71021	10.88487	-2.47872
C	7.69703	12.17847	-1.05077
H	8.26042	12.72193	-1.81222
C	7.83261	12.51722	0.29763
H	8.50205	13.32620	0.59668
C	7.10133	11.82765	1.27089
H	7.19243	12.10074	2.32436

C	3.70516	9.53168	1.41449
C	3.32030	8.28020	0.90668
H	3.99856	7.42697	0.95994
C	2.05747	8.10470	0.32798
H	1.77160	7.12261	-0.05500
C	1.16784	9.17715	0.24052
H	0.18304	9.03832	-0.20997
C	1.54247	10.42919	0.74227
H	0.85076	11.27219	0.68510
C	2.79441	10.60133	1.33253
H	3.07060	11.57411	1.74665
Ni	5.21850	10.71816	4.28255
C	5.08657	12.49920	4.30854
C	3.85996	9.85777	5.05754
O	4.96243	13.65381	4.33968
O	2.94894	9.31023	5.52505

(g) (norphos)Ni(CO)₂

SCF Energy: -2269288.3083274 a.u.

P	3.59818	8.93936	5.52006
P	4.57240	7.62384	8.33276
C	2.35445	10.18727	4.99750
C	1.48202	9.84526	3.94633
H	1.60252	8.88869	3.43221
C	0.46130	10.71161	3.55471
H	-0.20325	10.42809	2.73591
C	0.28196	11.93305	4.21420
H	-0.52036	12.60869	3.91162
C	1.13281	12.27839	5.26638
H	1.00002	13.22757	5.79004
C	2.16225	11.41375	5.65519
H	2.81327	11.70549	6.48095

C	4.56579	8.66567	3.97127
C	4.79799	9.69329	3.03838
H	4.36883	10.68396	3.20203
C	5.56155	9.45257	1.89444
H	5.72920	10.25772	1.17561
C	6.10743	8.18381	1.66649
H	6.70152	7.99694	0.76951
C	5.87715	7.15497	2.58303
H	6.28731	6.15868	2.40550
C	5.10503	7.39345	3.72471
H	4.90260	6.58258	4.42756
C	4.75360	9.81601	6.68621
H	4.04462	10.14505	7.46874
C	5.74126	11.02503	6.48471
H	5.25361	11.95422	6.16668
C	6.95324	10.58649	5.67426
H	7.13340	10.84331	4.63166
C	7.67986	9.75280	6.44013
H	8.56001	9.18285	6.14028
C	6.93544	9.57880	7.76315
H	7.50730	9.17343	8.60529
C	5.67544	8.72917	7.31974
H	6.00129	8.03488	6.52500
C	6.35239	11.00415	7.91791
H	5.60318	11.09789	8.71801
H	7.13958	11.75972	8.05193
C	5.63795	6.22716	8.87588
C	6.94608	6.02186	8.40751
H	7.40834	6.74094	7.72983
C	7.67537	4.89366	8.79981
H	8.69061	4.75010	8.42365
C	7.11115	3.95818	9.66957

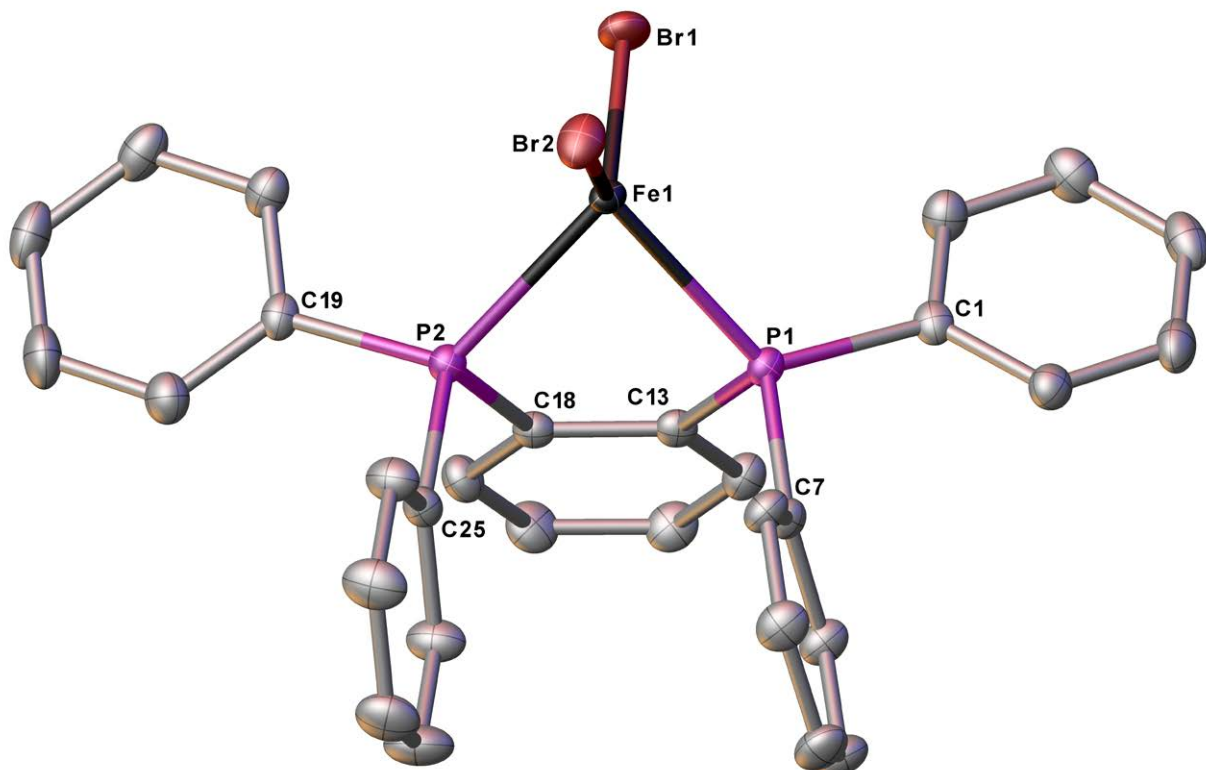
H	7.68081	3.07848	9.97531
C	5.80769	4.15223	10.14177
H	5.35501	3.42240	10.81616
C	5.07586	5.27096	9.74323
H	4.05251	5.40286	10.10310
C	4.29458	8.54788	9.90895
C	5.26748	8.60721	10.92394
H	6.20297	8.05490	10.81307
C	5.03856	9.35188	12.08310
H	5.80090	9.38541	12.86452
C	3.83560	10.04862	12.24624
H	3.65689	10.62678	13.15517
C	2.85963	9.99008	11.24810
H	1.91208	10.51789	11.37457
C	3.08559	9.23921	10.08973
H	2.31200	9.17109	9.32184
Ni	2.91367	7.23455	6.84548
C	1.25647	7.57794	7.41245
C	3.10633	5.58904	6.18143
O	3.19509	4.50483	5.77597
O	0.16385	7.76886	7.75525

4 Synthesis of diphosphine complexes of FeBr₂

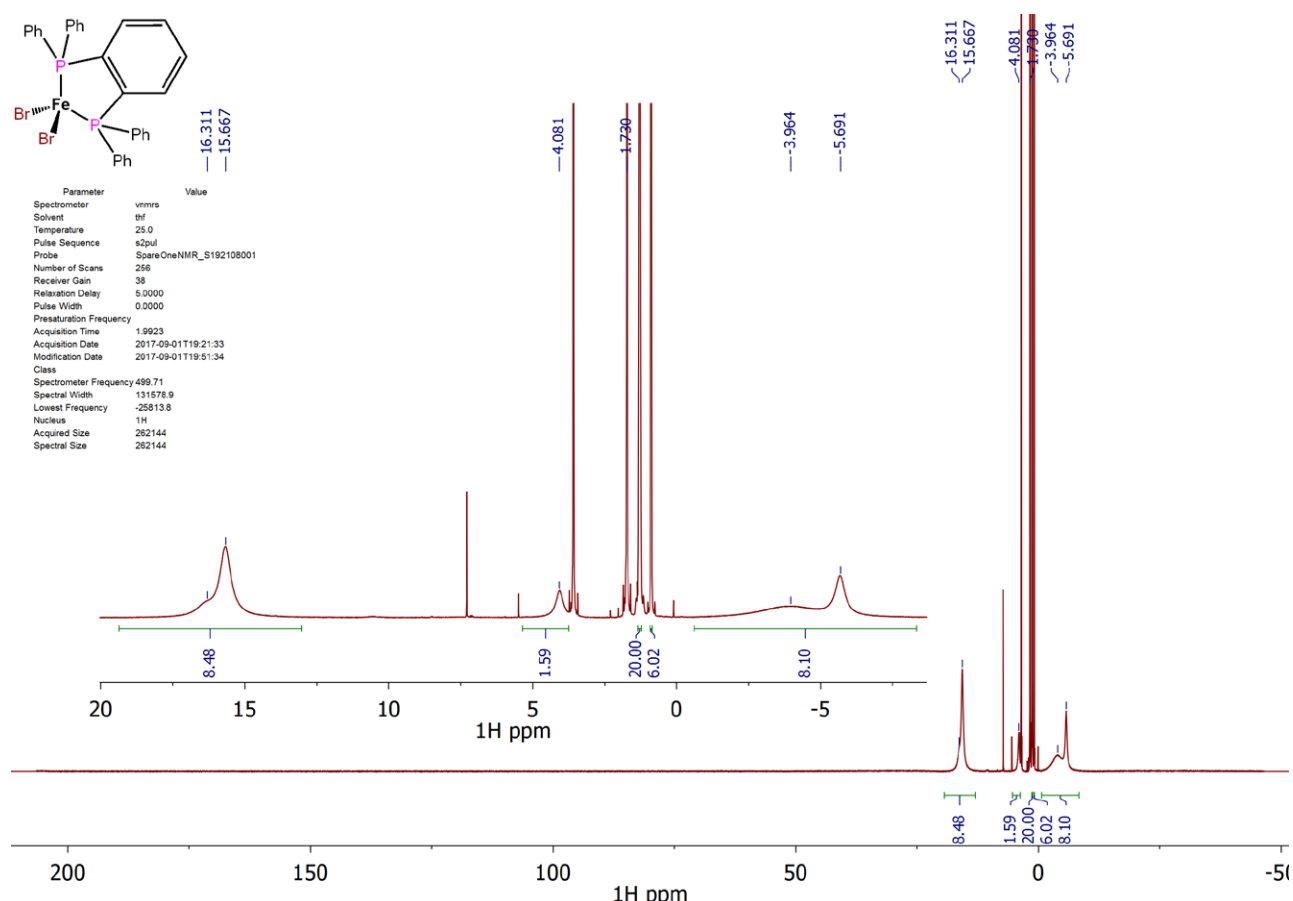
4.1 [FeBr₂(dpbz)] (**4a**)

A Schlenk was loaded with FeBr₂ (465 mg, 2.20 mmol), dpbz (982 mg, 2.20 mmol), CH₂Cl₂ (20 mL) and 10 drops of THF. The mixture was stirred and sonicated until an orange solution was obtained. The solution was then filtered and the filtrate layered with hexane (30 mL) resulting in the formation of grey crystals of [FeBr₂(dpbz)] (**4a**)·CH₂Cl₂ suitable for an X-ray crystallographic study. The crystals were isolated by filtration, ground and dried under reduced pressure for 2 hours to give a light grey powder of [FeBr₂(dpbz)] (**4a**)·CH₂Cl₂ (1.33 g, 81%). The complex can also be crystallised by layering a THF solution with hexane to give [FeBr₂(dpbz)] (**4a**)·THF. ¹H NMR (500 MHz, THF-*d*₈) δ = 16.3 (br s, 340), 15.7 (br s, 235), 4.1 (br s, 146), -4.0 (br s, 1319), -5.7 (br s, 216). Anal. Calcd for C₃₁H₂₆Br₂Cl₂FeP₂: C,

49.84; H, 3.51 Found: C, 50.49; H, 3.53. Anal. Calcd for $C_{34}H_{32}Br_2FeOP_2$: C, 55.62; H, 4.39. Found: C, 56.09; H, 4.37. HRMS (ESI/Q-TOF) m/z: [M+Na]⁺ Calcd for $C_{31}H_{26}Br_2NaP_2Fe$ 682.8967; Found 682.8965.



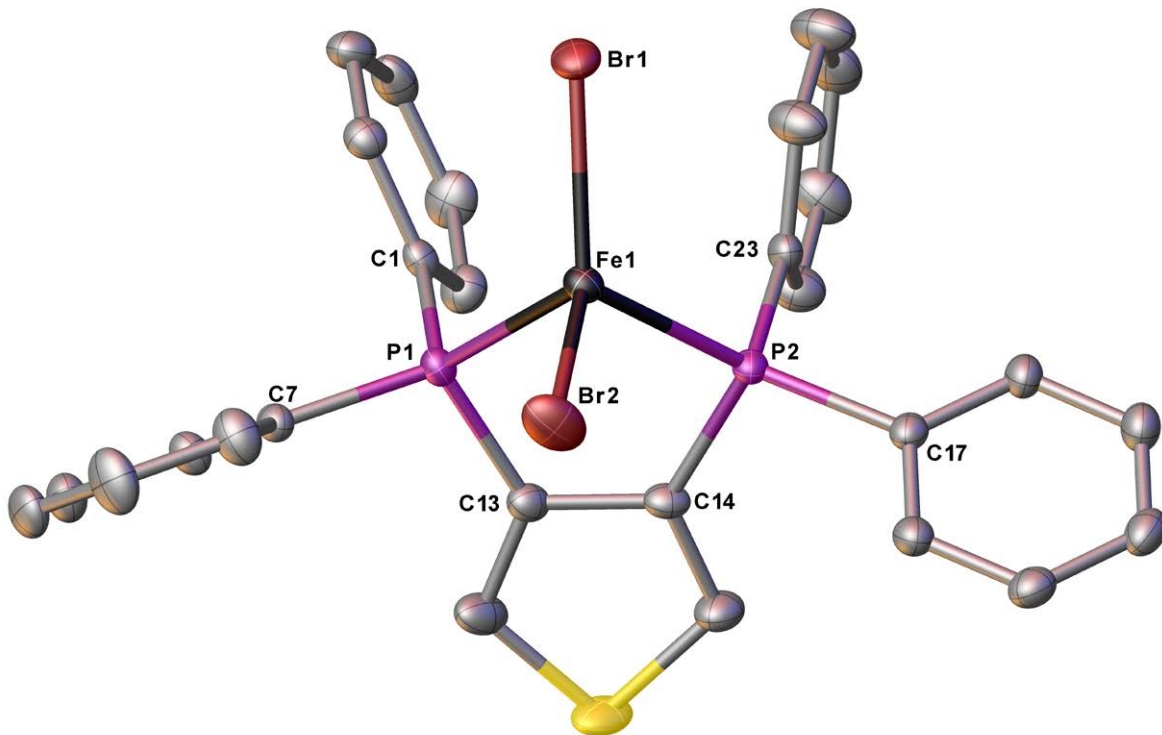
Supplementary Figure 34. Single-crystal X-ray structure of $[FeBr_2(dpbz)]$ (**4a**). Hydrogen atoms and solvent molecules are omitted for clarity. Thermal ellipsoids are set at the 50% probability level.



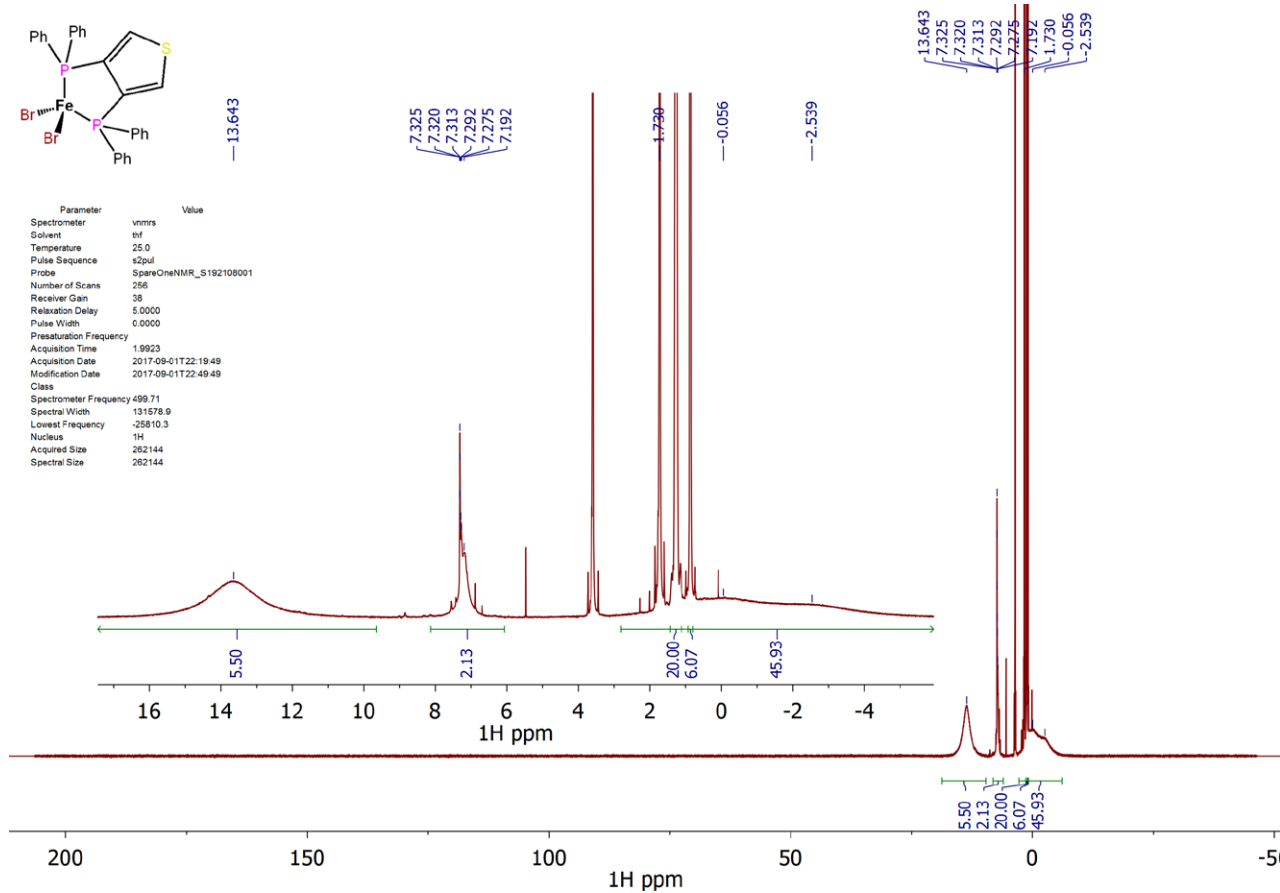
Supplementary Figure 35. 1H NMR spectrum (500 MHz, THF-*d*₆) of $[FeBr_2(dpbz)]$ (**4a**).

4.2 [FeBr₂(dpth)] (4b)

In an argon filled glove box, a vial was loaded with dpth (93.7 mg, 0.207 mmol), FeBr₂ (44.7 mg, 0.207 mmol), CH₂Cl₂ (2 mL) and 7 drops of THF. After standing for 48 hours a yellow-brownish solution formed which was filtered and layered with hexane (4 mL). After 24 hours, yellow-brownish crystals suitable for an X-ray crystallographic analysis formed which were isolated by decanting the supernatant solution, dried under reduced pressure, ground and further dried under reduced pressure for 12 hours to give [FeBr₂(dpth)] (**4b**) (114.2 mg, 83%) as a pale orange-brownish powder. ¹H NMR (500 MHz, THF-*d*₈) δ = 13.6 (br s, 806), 7.32 (br s, 8), 7.29 (s), 7.28 (s), 7.2 (br s, 112), -0.1 (br s, 1640), -2.5 (br s, 1092). Anal. Calcd for C₂₈H₂₂Br₂P₂FeS: C, 50.33; H, 3.32 Found: C, 50.43; H, 3.32. HRMS (ESI/Q-TOF) m/z: [M+Na]⁺ Calcd for C₂₈H₂₂Br₂NaP₂FeS 688.8531; Found 688.8529.



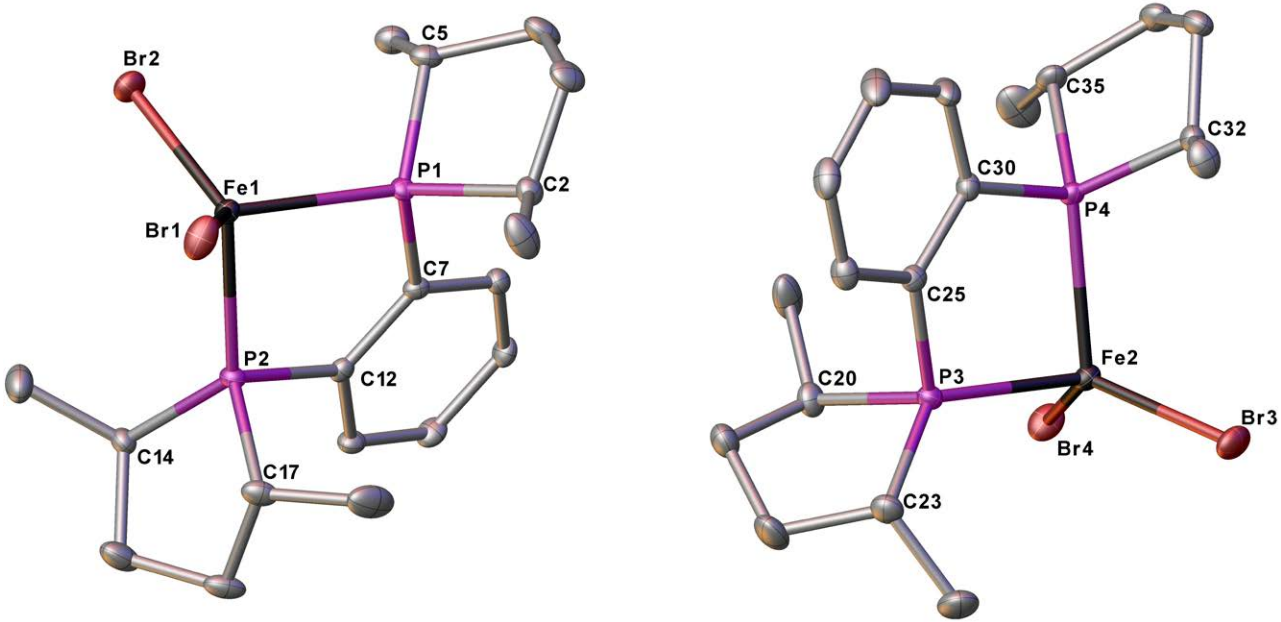
Supplementary Figure 36. Single-crystal X-ray structure of [FeBr₂(dpth)] (**4b**). Hydrogen atoms and solvent molecules are omitted for clarity. Thermal ellipsoids are set at the 50% probability level.



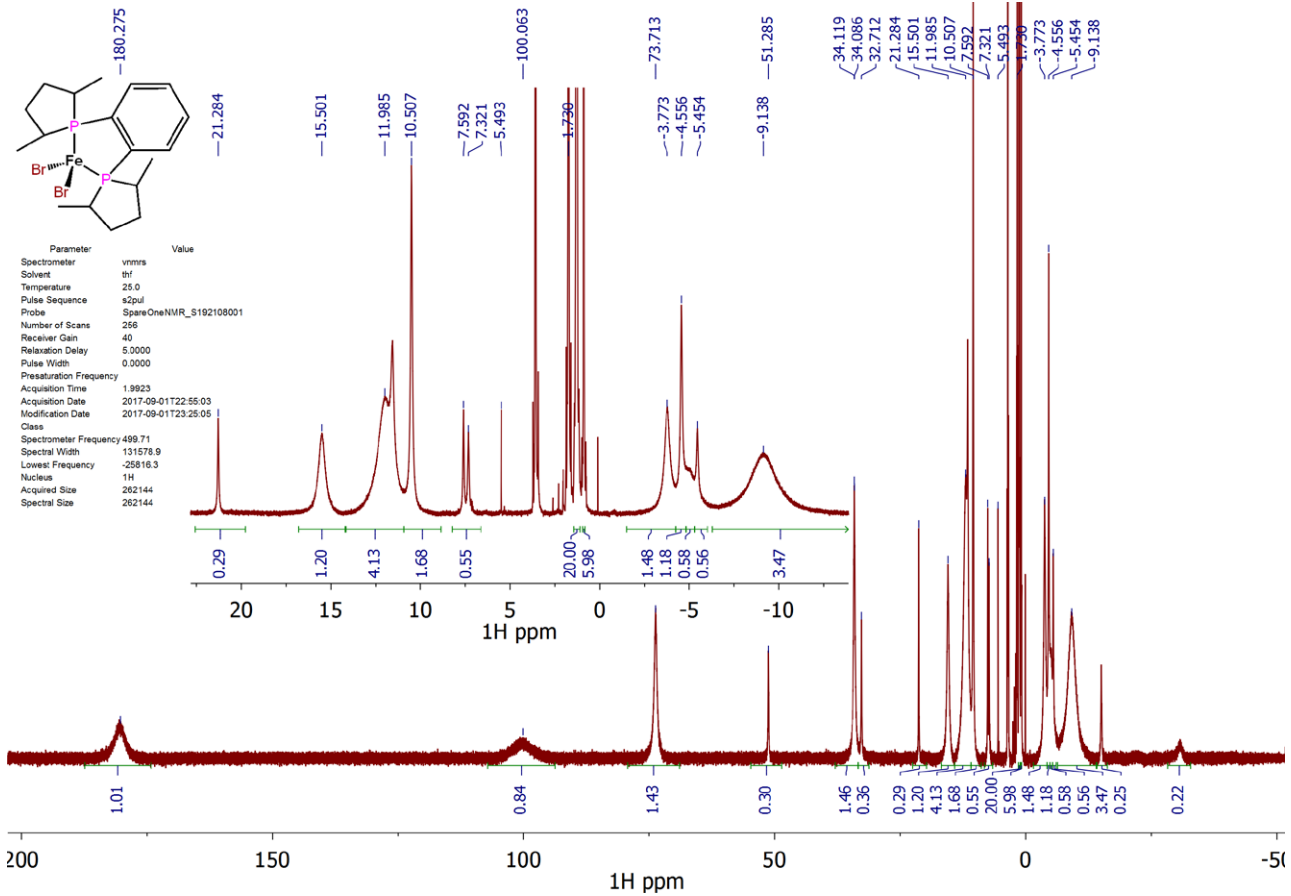
Supplementary Figure 37. ^1H NMR spectrum (500 MHz, THF- d_8) of $[\text{FeBr}_2(\text{dpth})]$ (**4b**).

4.3 $[\text{FeBr}_2(\text{MeDuphos})]$ (**4c**)

In an argon filled glove box, a vial was loaded with MeDuphos (50.2 mg, 0.164 mmol), FeBr_2 (28.9 mg, 0.164 mmol), CH_2Cl_2 (2 mL) and 7 drops of THF. After standing for 48 hours a yellow solution formed which was filtered and layered with hexane (4 mL). After 24 hours, yellow crystals suitable for an X-ray crystallographic analysis formed which were isolated by decanting the supernatant solution, dried under reduced pressure, ground and further dried under reduced pressure for 12 hours to give $[\text{FeBr}_2(\text{MeDuphos})]$ (**4c**)· $\frac{1}{2}\text{CH}_2\text{Cl}_2$ (65.6 mg, 71%) as a yellow powder. ^1H NMR (500 MHz, THF- d_8) δ = 180.3 (br s, 1236), 100.1 (br s, 2265), 73.7 (br s, 291), 51.3 (br s, 81), 34.1 (br s, 166), 32.7 (br s, 68), 21.3 (br s, 37), 15.5 (br s, 218), 12.0 (br s, 464), 11.6 (br s, 122), 10.5 (br s, 108), 7.6 (br s, 35), 7.3 (br s, 45), -3.8 (br s, 192), -4.6 (br s, 62), -5.5 (br s, 82), -9.1 (br s, 831), -15.1 (br s, 91), -30.7 (br s, 536). Anal. Calcd for $\text{C}_{18.5}\text{H}_{29}\text{Br}_2\text{ClP}_2\text{Fe}$: C, 39.36; H, 5.18 Found: C, 40.37; H, 5.27. HRMS (ESI/Q-TOF) m/z: No $[\text{M}]^+$ or $[\text{M}+\text{A}]^+$ peak observed.



Supplementary Figure 38. Single-crystal X-ray structure of the two independent molecules of $[\text{FeBr}_2(\text{MeDuphos})]$ (**4c**). Hydrogen atoms are omitted for clarity and thermal ellipsoids are set at the 50% probability level.

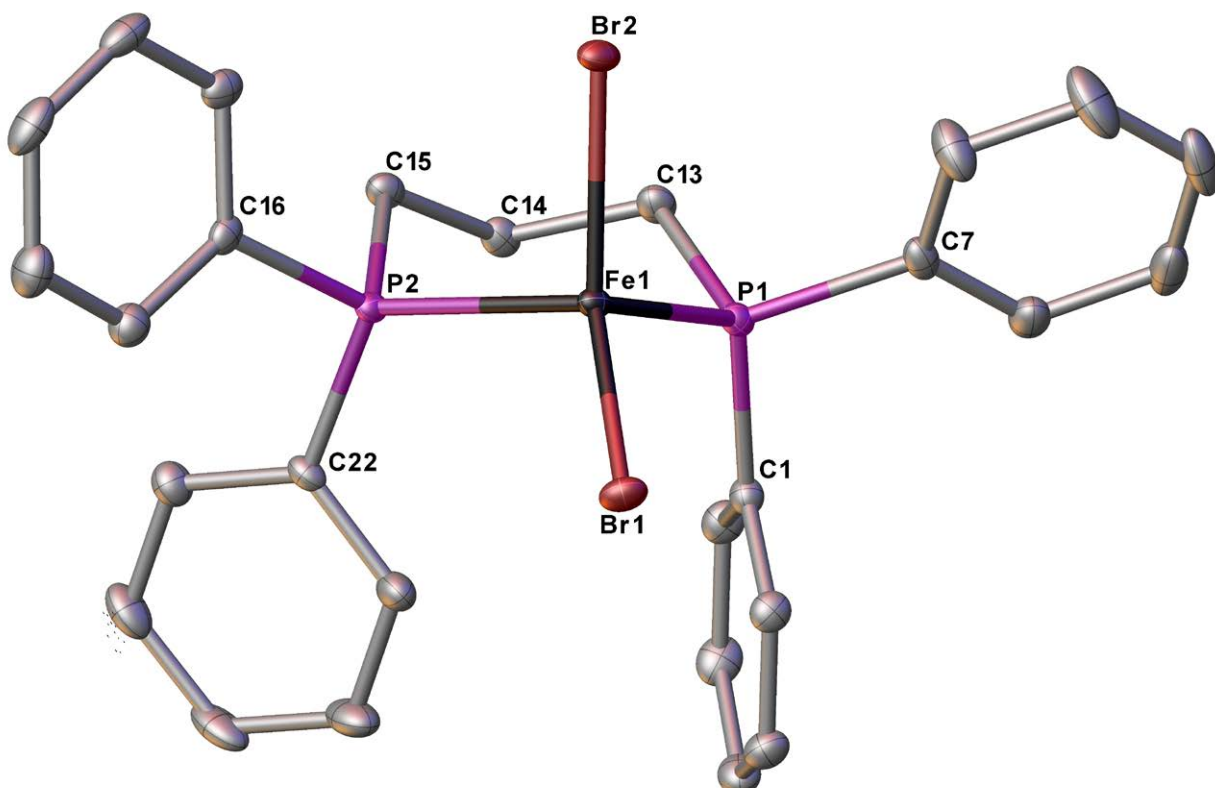


Supplementary Figure 39. ^1H NMR spectrum (500 MHz, THF-*d*₈) of $[\text{FeBr}_2(\text{MeDuphos})]$ (**4c**).

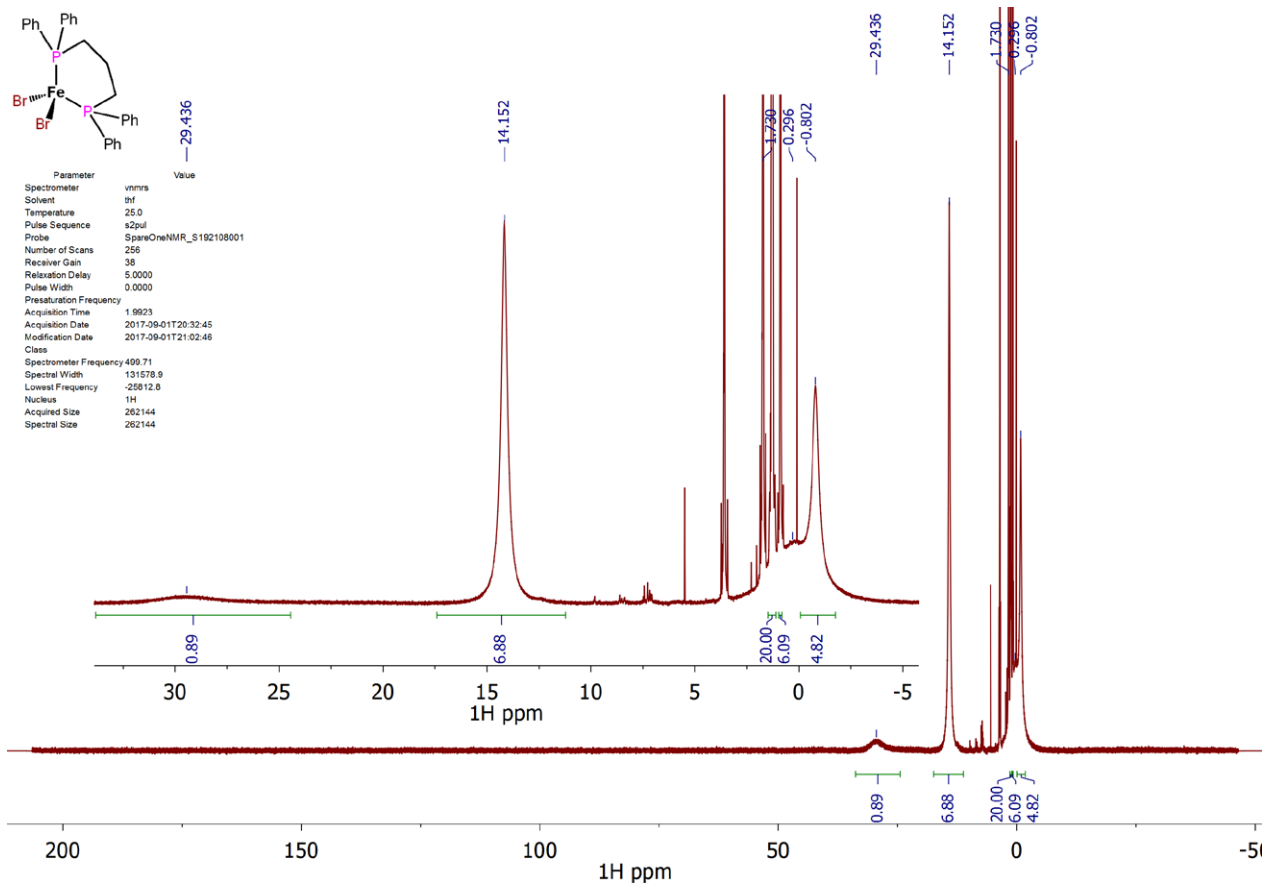
4.4 $[\text{FeBr}_2(\text{dppp})]$ (**4d**)

In an argon filled glove box, a vial was loaded with dppp (97.8 mg, 0.237 mmol), FeBr_2 (51.1 mg, 0.237 mmol), CH_2Cl_2 (4 mL) and 7 drops of THF. After standing for 48 hours a white solid precipitated. The mixture was heated at reflux temperature until the solid fully dissolved to give a brownish-orange solution which was filtered. The filtrate was layered

with hexane (4 mL) and after 24 hours large green-brown dichroic crystals were formed suitable for an X-ray crystallographic analysis. The crystals were isolated by decanting the supernatant solution, dried under reduced pressure, ground and further dried under reduced pressure for 12 hours to give $[\text{FeBr}_2(\text{dppp})]$ (**4d**) (129.4 mg, 87%) as a pale green powder. ^1H NMR (500 MHz, THF- d_8) δ = 29.4 (br s, 1603), 14.2 (br s, 181), 0.30 (br s, 1526), -0.80 (br s, 214). Anal. Calcd for $\text{C}_{27}\text{H}_{26}\text{Br}_2\text{P}_2\text{Fe}$: C, 51.63; H, 4.17 Found: C, 51.55; H, 4.18. HRMS (ESI/Q-TOF) m/z: [M+Na]⁺ Calcd for $\text{C}_{27}\text{H}_{26}\text{Br}_2\text{NaP}_2\text{Fe}$ 648.9124; Found 648.9121.

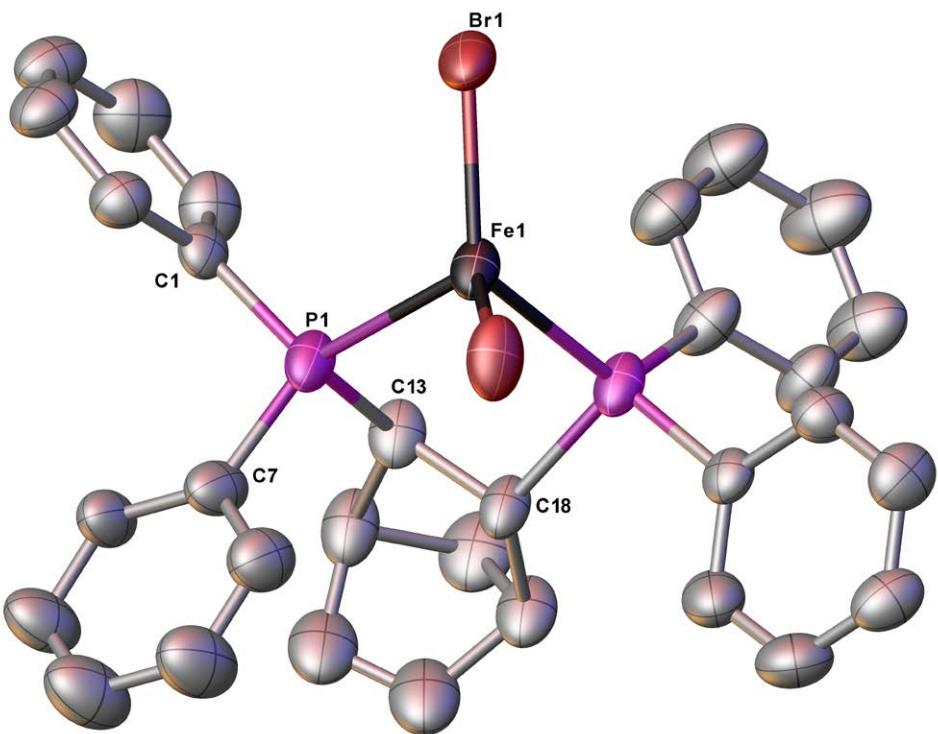


Supplementary Figure 40. Single-crystal X-ray structure of $[\text{FeBr}_2(\text{dppp})]$ (**4d**). Hydrogen atoms are omitted for clarity. Thermal ellipsoids are set at the 50% probability level.

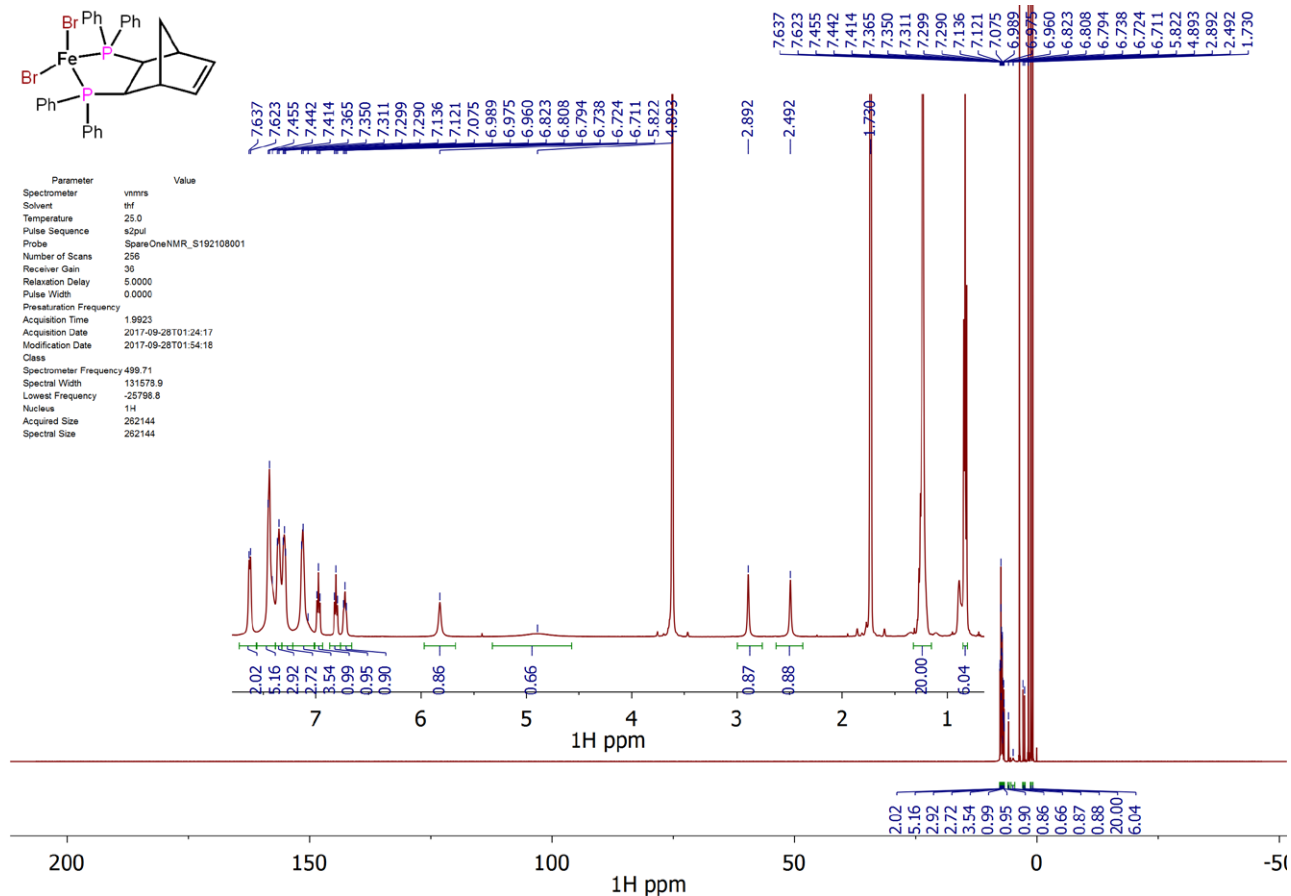


4.5 $[\text{FeBr}_2(\text{norphos})]$ (4e)

In an argon filled glove box, a vial was loaded with norphos (46.5 mg, 0.101 mmol), FeBr_2 (21.7 mg, 0.101 mmol), CH_2Cl_2 (2 mL) and 7 drops of THF. After standing for 48 hours a pale orange solution formed which was filtered and layered with hexane (4 mL). After 24 hours, pale orange crystals suitable for an X-ray crystallographic analysis formed which were isolated by decanting the supernatant solution, dried under reduced pressure, ground and further dried under reduced pressure for 12 hours to give $[\text{FeBr}_2(\text{norphos})]$ (4e) $\cdot\frac{1}{2}\text{C}_6\text{H}_{14}$ (55.6 mg, 78%) as a pale orange powder. ^1H NMR (500 MHz, THF- d_8) δ = 7.63 (br d, $J=7.2$), 7.45 (br d, $J=6.3$), 7.36 (br d, $J=7.5$), 7.31 (br s, 22), 7.13 (br s, 17), 6.97 (t, $J=7.2$), 6.81 (t, $J=7.1$), 6.73 (t, $J=7.7$), 5.82 (br s, 13), 4.89 (br s, 133), 2.89 (br s, 7), 2.49 (br s, 8). Anal. Calcd for $\text{C}_{34}\text{H}_{35}\text{Br}_2\text{P}_2\text{Fe}$: C, 56.62; H, 4.89 Found: C, 56.24; H, 4.92. HRMS (ESI/Q-TOF) m/z: [M+Na]⁺ Calcd for $\text{C}_{31}\text{H}_{28}\text{Br}_2\text{NaP}_2\text{Fe}$ 698.9280; Found 698.9278.



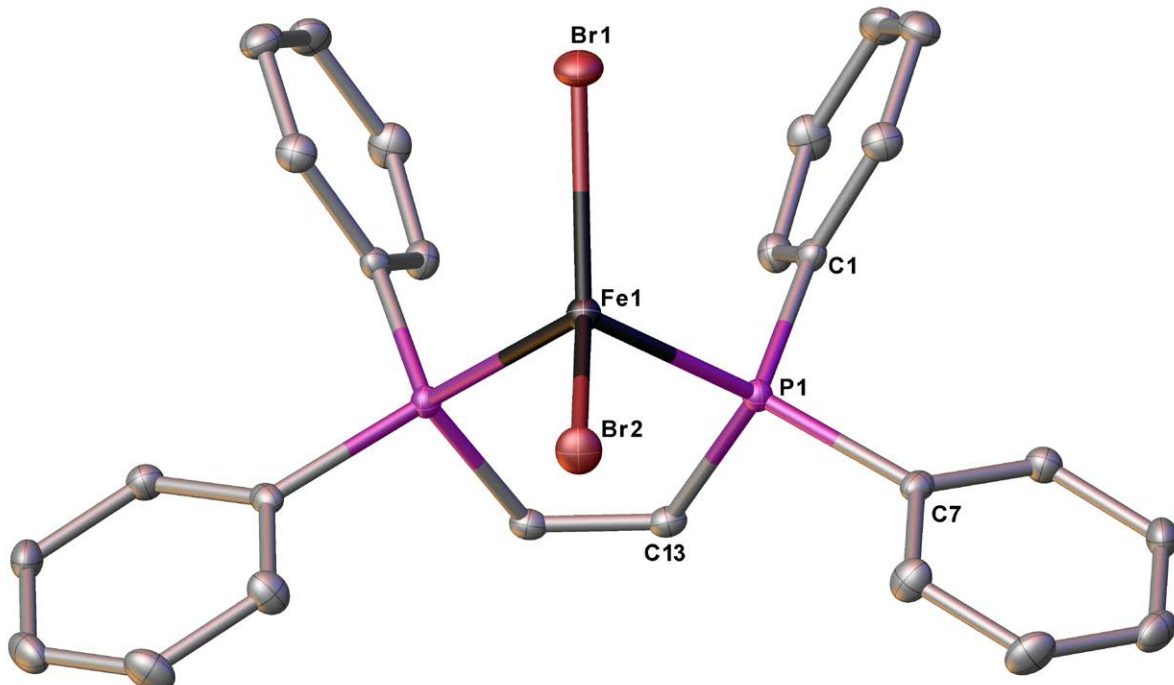
Supplementary Figure 42. Single-crystal X-ray structure of $[\text{FeBr}_2(\text{norphos})]$ (**4e**). Hydrogen atoms, disordered atoms and solvent molecules are omitted for clarity while thermal ellipsoids are set at the 50% probability level.



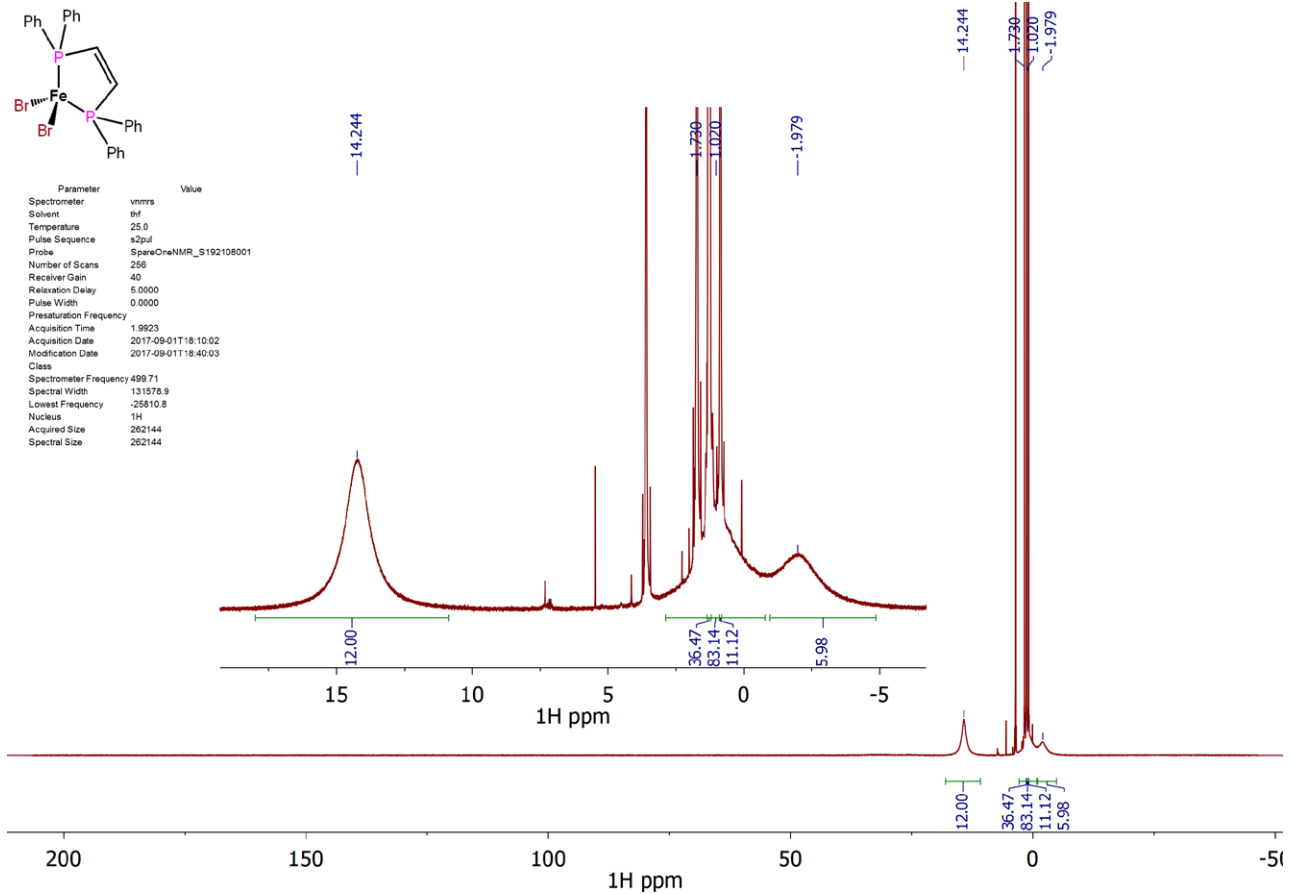
Supplementary Figure 43. ^1H NMR spectrum (500 MHz, $\text{THF}-d_8$) of $[\text{FeBr}_2(\text{norphos})]$ (**4e**).

4.6 [FeBr₂(*cis*-dppen)] (**4f**)

In an argon filled glove box, a vial was loaded with *cis*-dppen (108.6 mg, 0.274 mmol), FeBr₂ (59.1 mg, 0.274 mmol), CH₂Cl₂ (2 mL) and 7 drops of THF. After standing for 48 hours brownish orange crystals of [FeBr₂(*cis*-dppen)] (**4f**) formed which were found to be suitable for an X-ray crystallographic analysis. The crystals were dissolved by heating the mixture to give a clear orange solution which was filtered while still hot. Upon cooling, the filtrate gave crystals of pure [FeBr₂(*cis*-dppen)] (**4f**). In order to improve the yield, the final mixture was layered with hexane (2 mL) and after 24 hours the resultant crystals were isolated by decanting the supernatant solution, dried under reduced pressure, ground and further dried under reduced pressure for 12 hours to give [FeBr₂(*cis*-dppen)] (**4f**) (150.8 mg, 90%) as a pale orange powder. ¹H NMR (500 MHz, THF-*d*₈) δ = 14.2 (br s, 540), 1.1 (br s, 942), -2.0 (br s, 908). Anal. Calcd for C₂₆H₂₂Br₂P₂Fe: C, 51.02; H, 3.62 Found: C, 51.02; H, 3.55. HRMS (ESI/Q-TOF) m/z: [M+Na]⁺ Calcd for C₂₆H₂₂Br₂NaP₂Fe 632.8811; Found 632.8808.



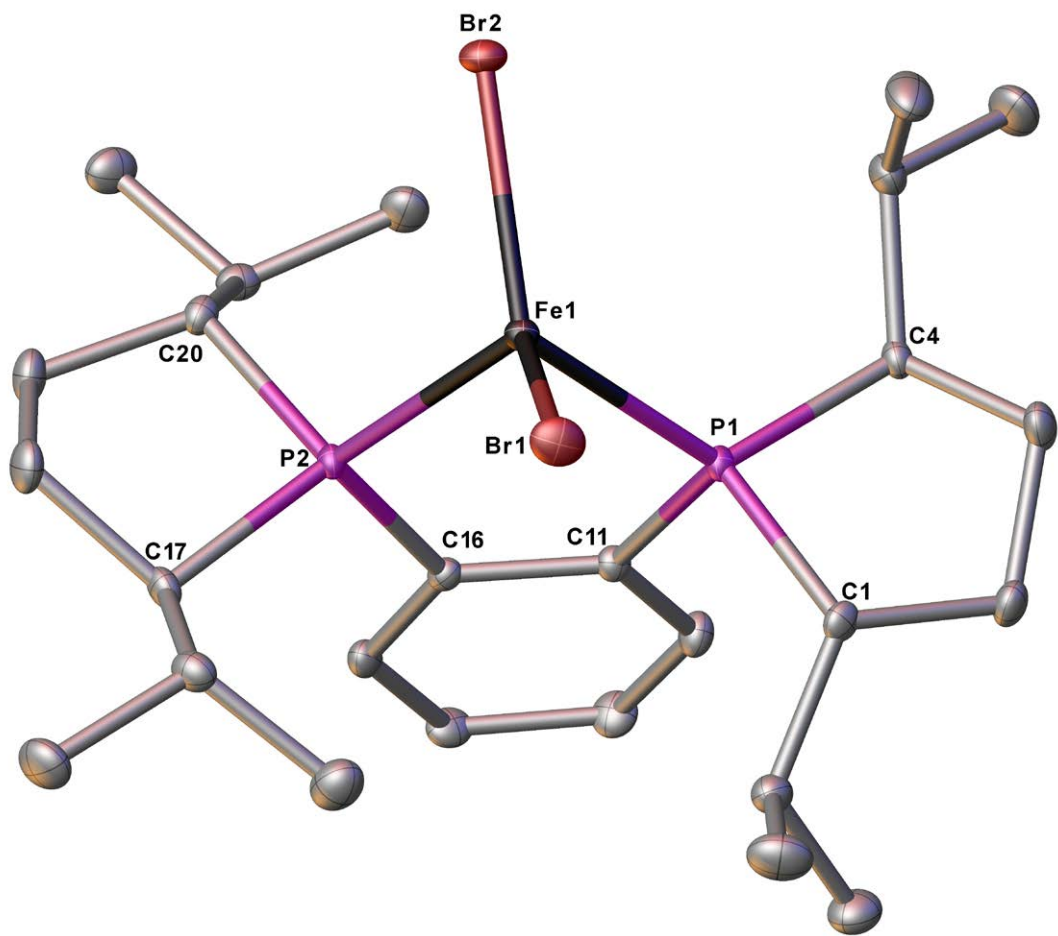
Supplementary Figure 44. Single-crystal X-ray structure of [FeBr₂(*cis*-dppen)] (**4f**). Hydrogen atoms are omitted for clarity while thermal ellipsoids are set at the 50% probability level.



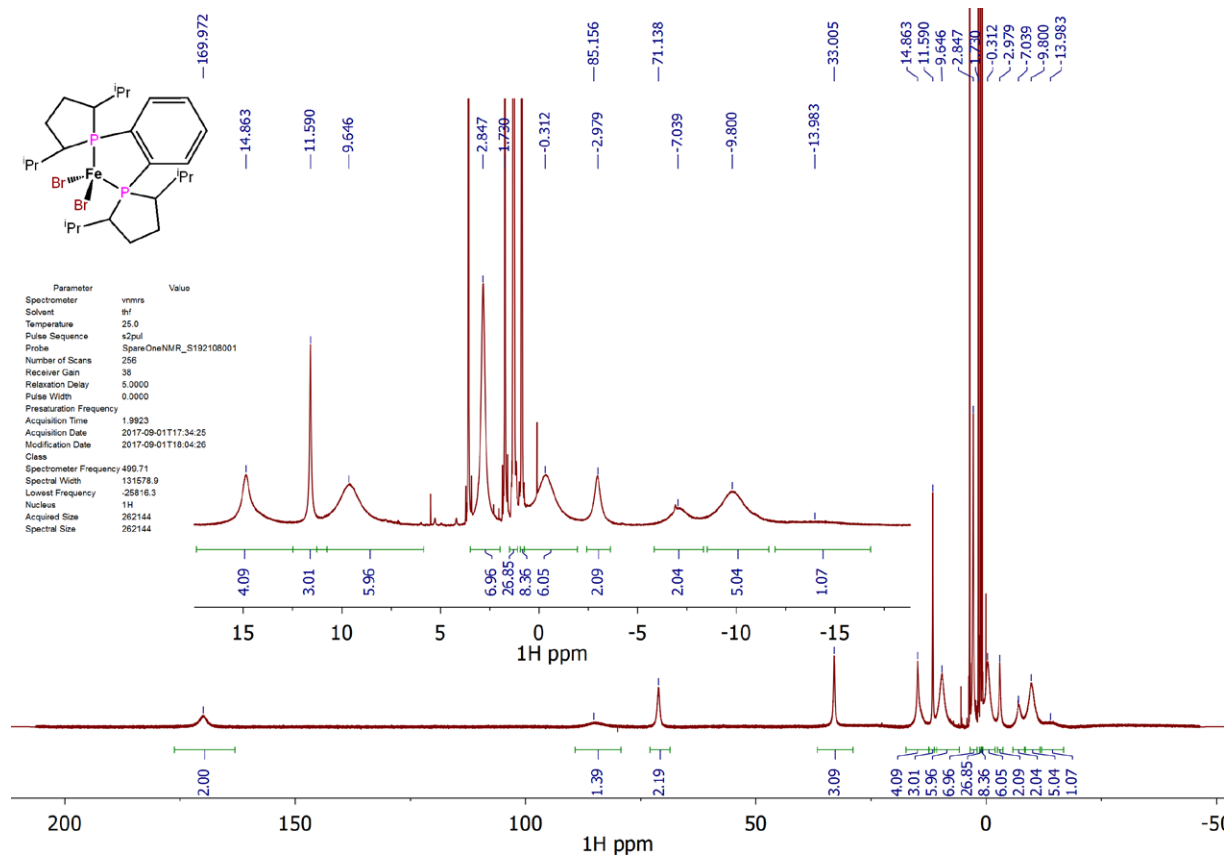
Supplementary Figure 45: ^1H NMR spectrum (500 MHz, $\text{THF}-d_8$) of $[\text{FeBr}_2(\text{cis-dppen})]$ (4f).

4.7 $[\text{FeBr}_2(\text{iPrDuphos})]$ (4g)

In an argon filled glove box, a vial was loaded with iPrDuphos (56.1 mg, 0.134 mmol), FeBr_2 (28.9 mg, 0.134 mmol), toluene (2 mL) and 7 drops of THF. After standing for 48 hours a clear solution formed which was filtered and layered with hexane (4 mL). After 24 hours, pink crystals suitable for an X-ray crystallographic analysis formed which were isolated by decanting the supernatant solution, dried under reduced pressure, ground and further dried under reduced pressure for 12 hours to give $[\text{FeBr}_2(\text{iPrDuphos})]$ (4g) (28.9 mg, 76%) as a pink powder. ^1H NMR (500 MHz, $\text{THF}-d_8$) δ = 170.0 (br s, 998), 85.2 (br s, 2345), 71.1 (br s, 303), 33.1 (br s, 180), 14.9 (br s, 253), 11.6 (br s, 49), 9.7 (br s, 587), 2.9 (br s, 108), -0.3 (br s, 548), -3.0 (br s, 182), -7.0 (br s, 557), -9.8 (br s, 707), -14.0 (br s, 1362). Anal. Calcd for $\text{C}_{26}\text{H}_{44}\text{Br}_2\text{P}_2\text{Fe}$: C, 49.24; H, 6.99 Found: C, 49.37; H, 7.07. HRMS (ESI/Q-TOF) m/z: [M+Na]⁺ Calcd for $\text{C}_{26}\text{H}_{44}\text{Br}_2\text{NaP}_2\text{Fe}$ 655.0532; Found 655.0530.



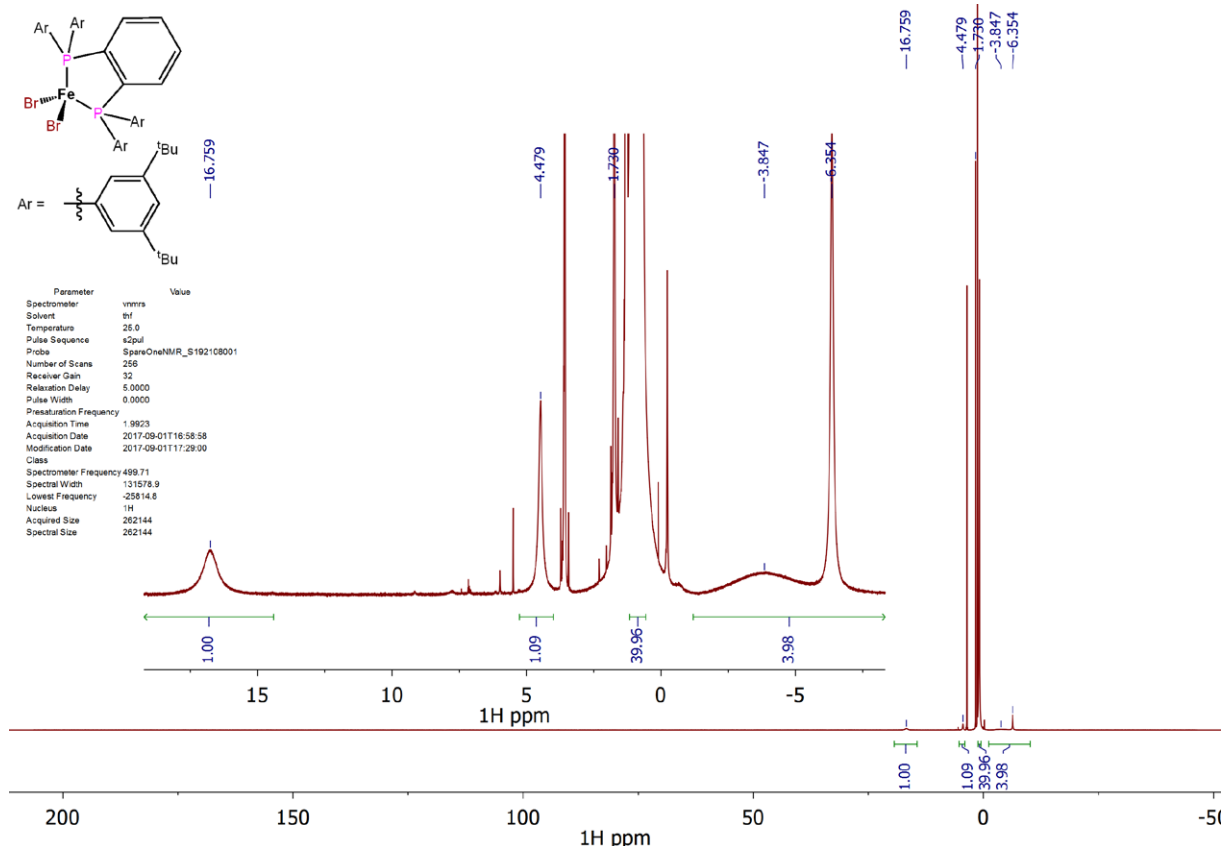
Supplementary Figure 46. Single-crystal X-ray structure of $[\text{FeBr}_2(\text{iPrDuphos})]$ (**4g**). Hydrogen atoms are omitted for clarity. Thermal ellipsoids are set at the 50% probability level.



Supplementary Figure 47. ^1H NMR spectrum (500 MHz, THF-*d*₈) of $[\text{FeBr}_2(\text{iPrDuphos})]$ (**4g**).

4.8 [FeBr₂(sciopp)] (4h)

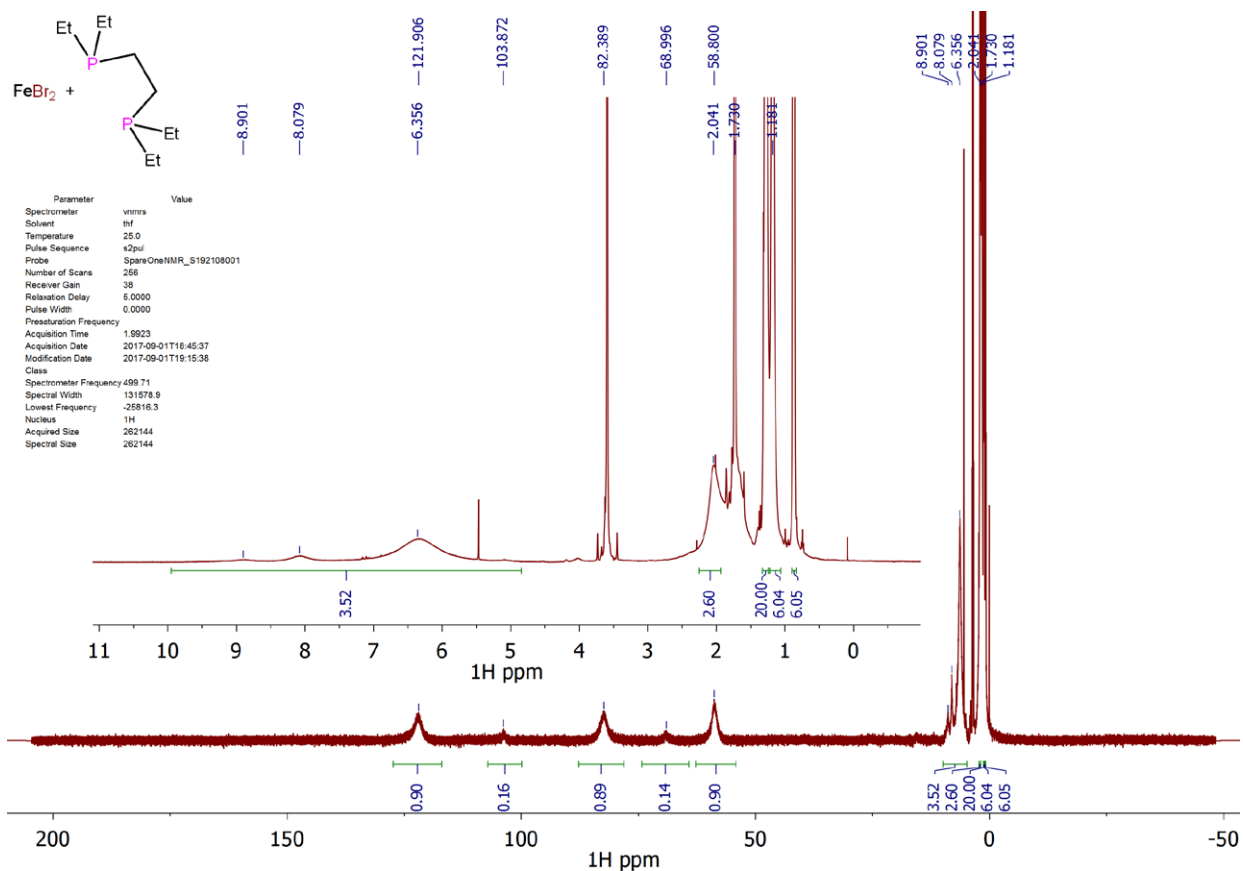
This compound has been reported previously.¹⁶ The spectrum presented in Supplementary Figure 48 is in good agreement with reported ¹H NMR spectroscopic data.



Supplementary Figure 48. ¹H NMR spectrum (500 MHz, THF-*d*₈) of [FeBr₂(sciopp)] (4h).

4.9 Reaction of FeBr₂ with depe

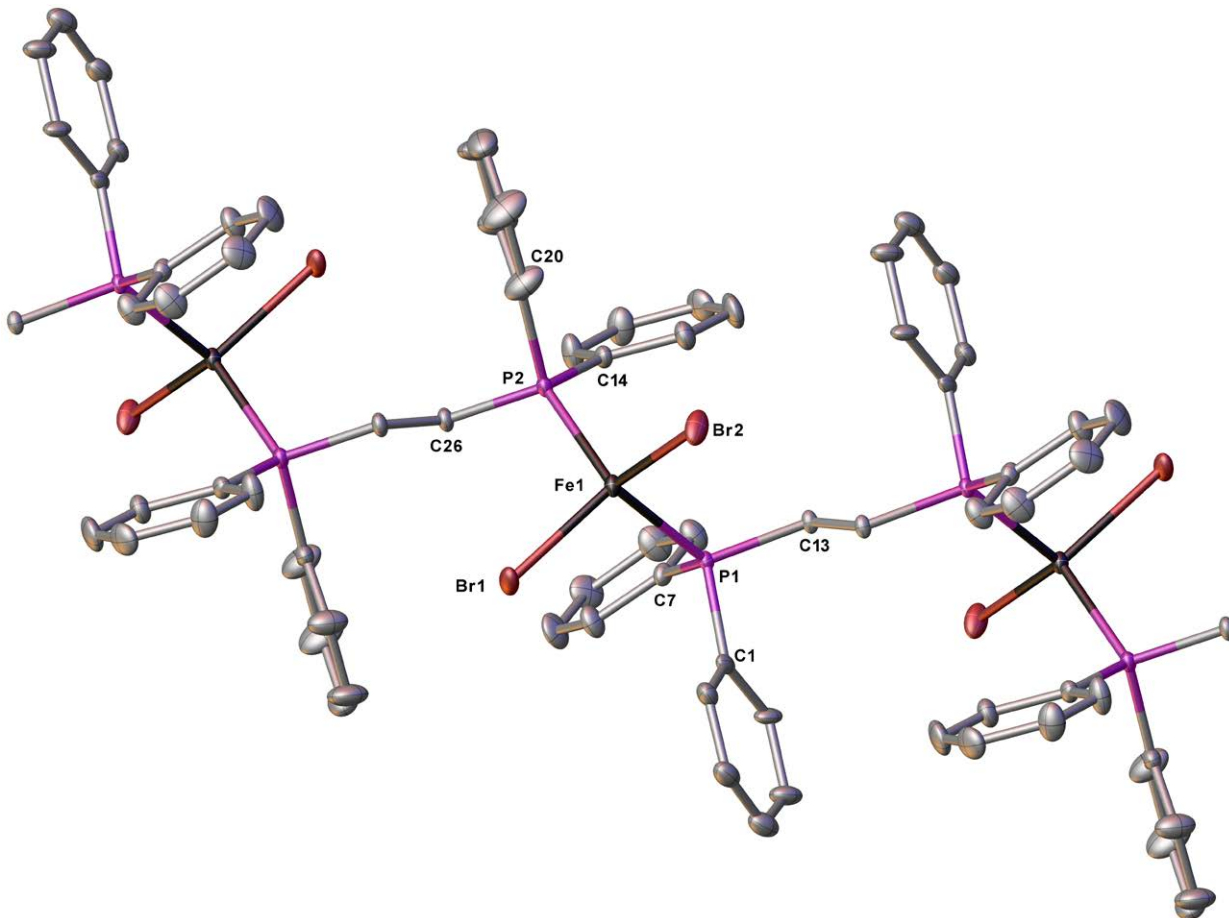
In an argon filled glove box, a vial was loaded with depe (100.0 mg, 0.485 mmol), FeBr₂ (104.6 mg, 0.485 mmol) and CH₂Cl₂ (2 mL) to give a dark green solution which was filtered and layered with hexane (4 mL). After 24 hours, a green oil formed. ¹H NMR data was obtained from a 1:1 mixture of FeBr₂ and depe in THF-*d*₈. ¹H NMR (500 MHz, THF-*d*₈) δ = 122 (br s, 1036), 104 (br s, 576), 82 (br s, 960), 69 (br s, 652), 59 (br s, 704), 8.90 (br s, 259), 8.08 (br s, 184), 6.36 (br s, 333), 2.04 (br s, 118), 1.18 (br s, 23).



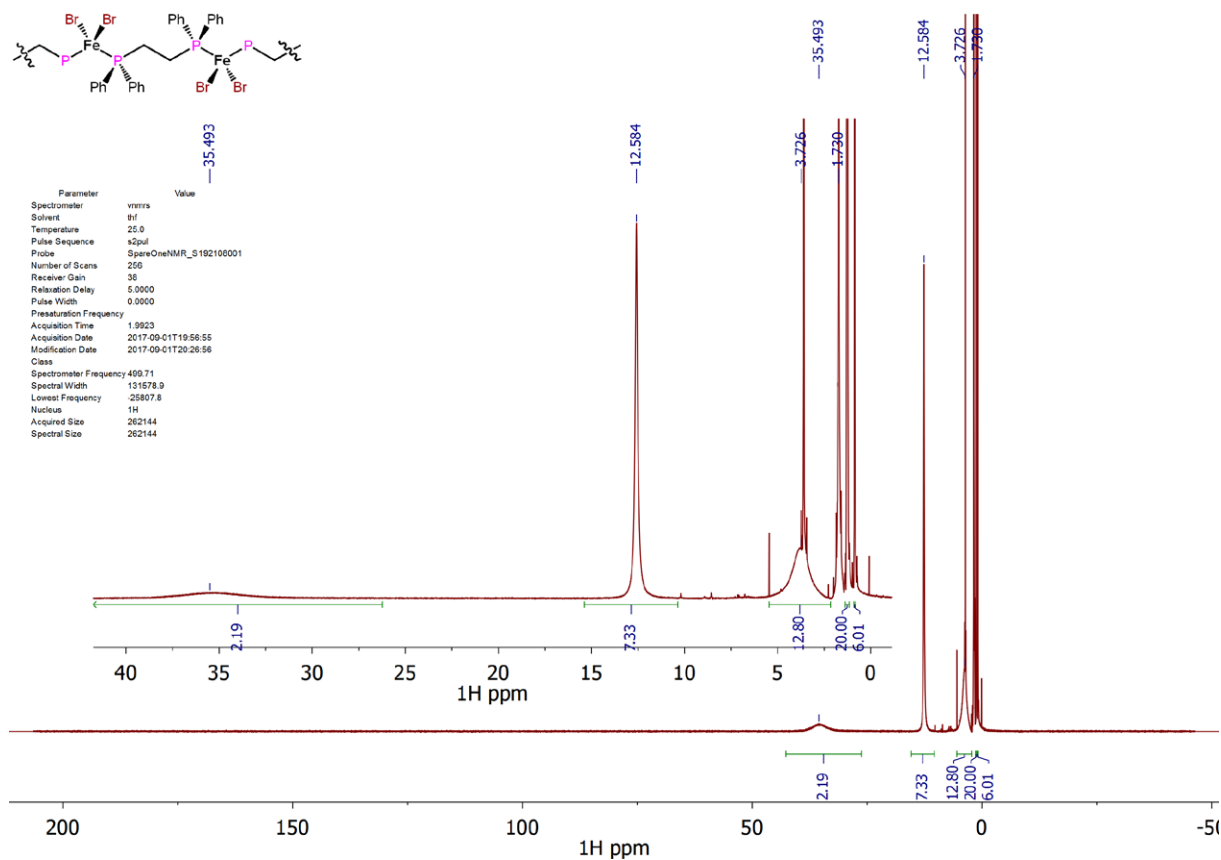
Supplementary Figure 49. ^1H NMR spectrum (500 MHz, $\text{THF}-d_8$) of $\text{FeBr}_2 + \text{one eq. depe.}$

4.10 $[\{\text{FeBr}_2(\mu^2\text{-dppe)}\}_n]$ (5)

In an argon-filled glove box, a vial was loaded with dppe (113.4 mg, 0.285 mmol), FeBr_2 (61.4 mg, 0.285 mmol), CH_2Cl_2 (2 mL) and 7 drops of THF. After standing for 48 hours, long, brown-green dichroic crystals of $[\{\text{FeBr}_2(\mu^2\text{-dppe)}\}_n]$ (5) formed which were found to be suitable for an X-ray crystallographic analysis. The crystals were dissolved by heating the mixture to give a clear orange solution which was filtered while still hot. Upon cooling, the filtrate gave crystals of pure $[\{\text{FeBr}_2(\mu^2\text{-dppe)}\}_n]$ (5). In order to improve the yield, the final mixture was layered with hexane (2 mL) and after 24 hours the crystals formed were isolated by decanting the supernatant solution, dried under reduced pressure, ground and further dried under reduced pressure for 12 hours to give 5 (146.4 mg, 84%) as a pale green powder. ^1H NMR (500 MHz, $\text{THF}-d_8$) δ = 35.49 (br s, 1763), 12.58 (br s, 74), 3.73 (br s, 492). Anal. Calcd for $\text{C}_{26}\text{H}_{24}\text{Br}_2\text{FeP}_2$: C, 50.85; H, 3.94 Found: C, 50.00; H, 3.89.



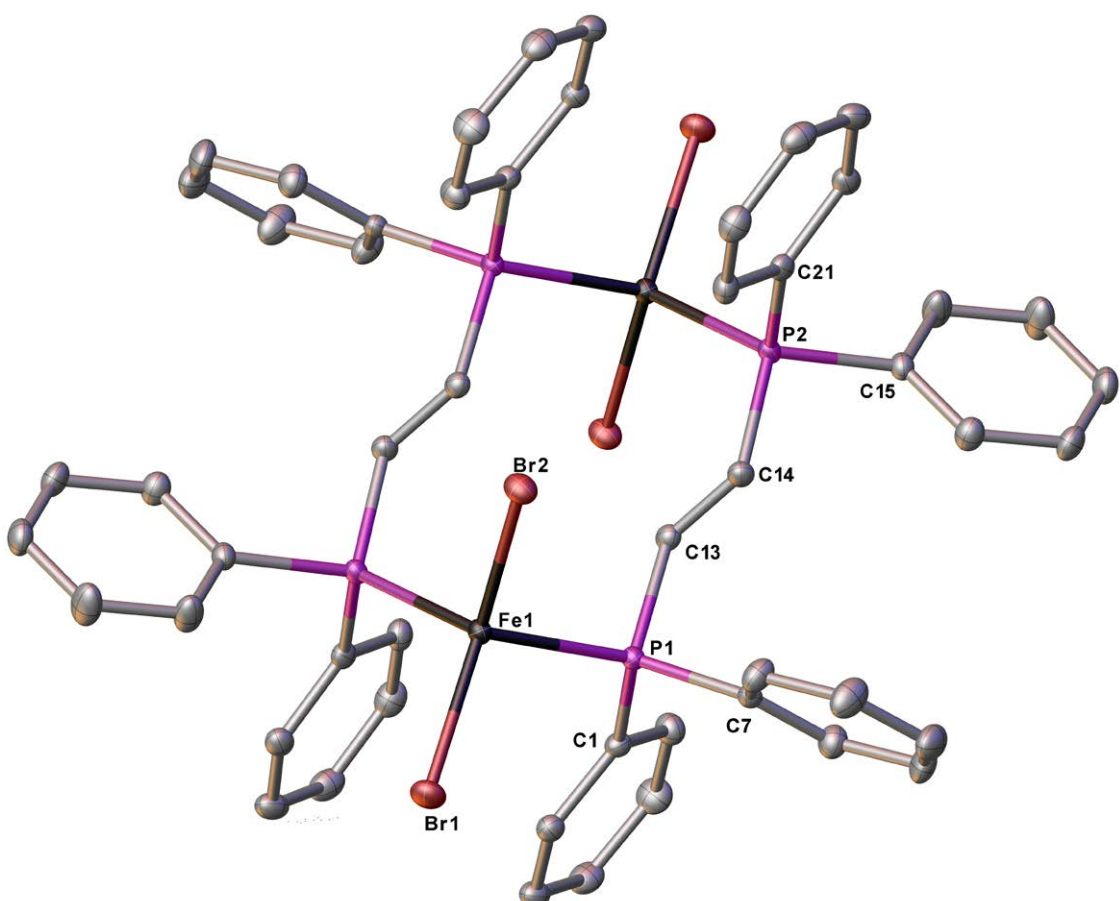
Supplementary Figure 50: Single-crystal X-ray structure of a segment of the coordination polymer of $\left[\{\text{FeBr}_2(\mu^2\text{-dppe})\}_n\right]$ (**5**). Hydrogen atoms and solvent molecules are omitted for clarity. Thermal ellipsoids are set at the 50% probability level.



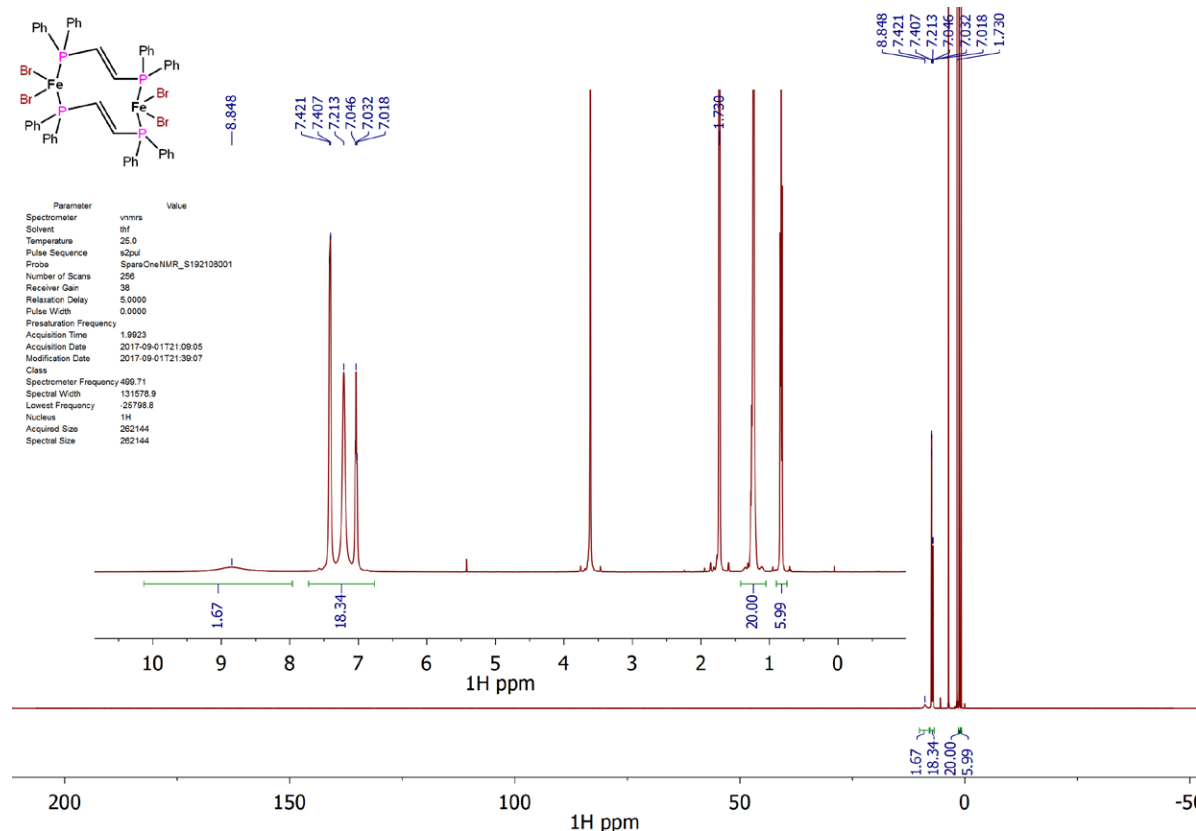
Supplementary Figure 51. ^1H NMR spectrum (500 MHz, $\text{THF}-d_8$) of $\left[\{\text{FeBr}_2(\mu^2\text{-dppe})\}_n\right]$ (**5**).

4.11 $\{(\text{FeBr}_2)(\mu\text{-trans-dppen})\}_2$ (6)

In an argon filled glove box, a vial was loaded with *trans*-dppen (90.5 mg, 0.228 mmol), FeBr_2 (49.2 mg, 0.228 mmol), CH_2Cl_2 (2 mL) and 7 drops of THF. After standing for 48 hours yellow crystals of $\{(\text{FeBr}_2)(\mu\text{-trans-dppen})\}_2$ (6) formed which were found to be suitable for an X-ray crystallographic analysis. The crystals were dissolved by heating the mixture to give a yellow solution which was filtered while still hot. Upon cooling, the filtrate gave crystals of pure 6. In order to improve the yield, the final mixture was layered with hexane (2 mL) and after 24 hours the resultant crystals were isolated by decanting the supernatant solution, dried under reduced pressure, ground and further dried under reduced pressure for 12 hours to give 6 (90.1 mg, 64%) as a yellow powder. ^1H NMR (500 MHz, $\text{THF}-d_8$) δ = 8.9 (br s, 227), 7.4 (br d, $J=3.9$), 7.2 (br s, 23). Anal. Calcd for $\text{C}_{52}\text{H}_{44}\text{Br}_4\text{P}_4\text{Fe}_2$: C, 51.02; H, 3.62 Found: C, 51.11; H, 3.61. HRMS (ESI/Q-TOF) m/z: No $[\text{M}]^+$ or $[\text{M}+\text{A}]^+$ peak observed.



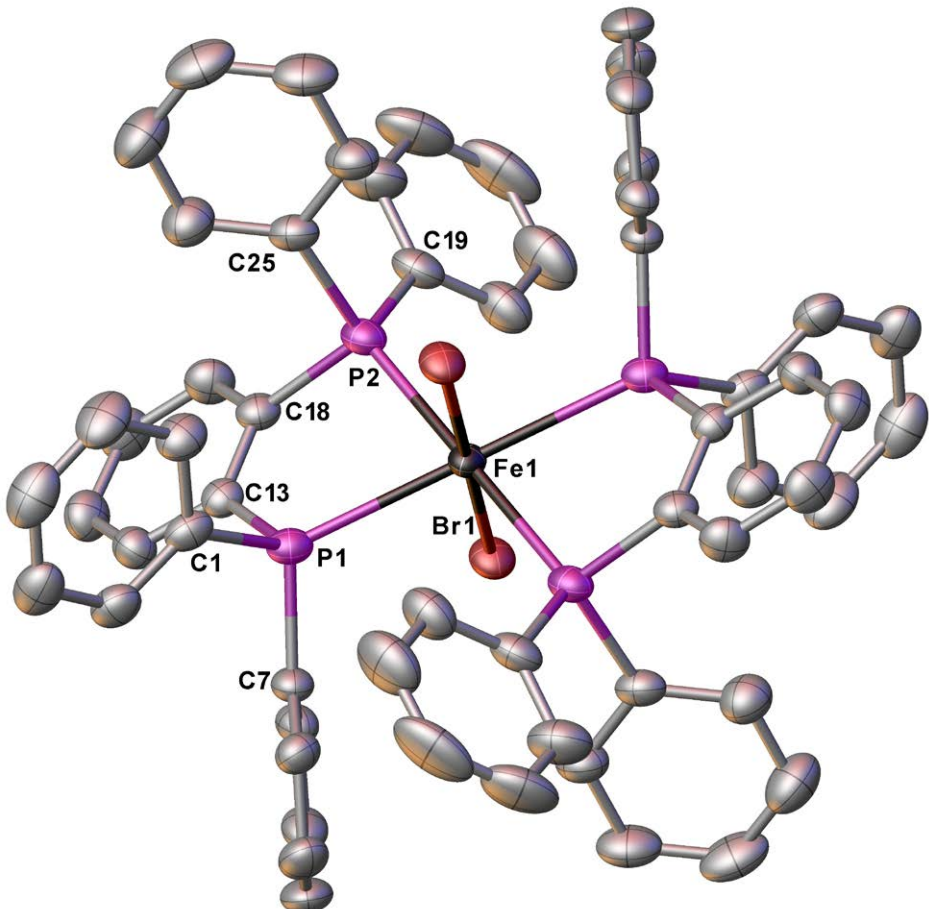
Supplementary Figure 52. Single-crystal X-ray structure of $\{(\text{FeBr}_2)(\mu\text{-trans-dppen})\}_2$ (6). Hydrogen atoms and solvent molecules are omitted for clarity while thermal ellipsoids are set at the 50% probability level.



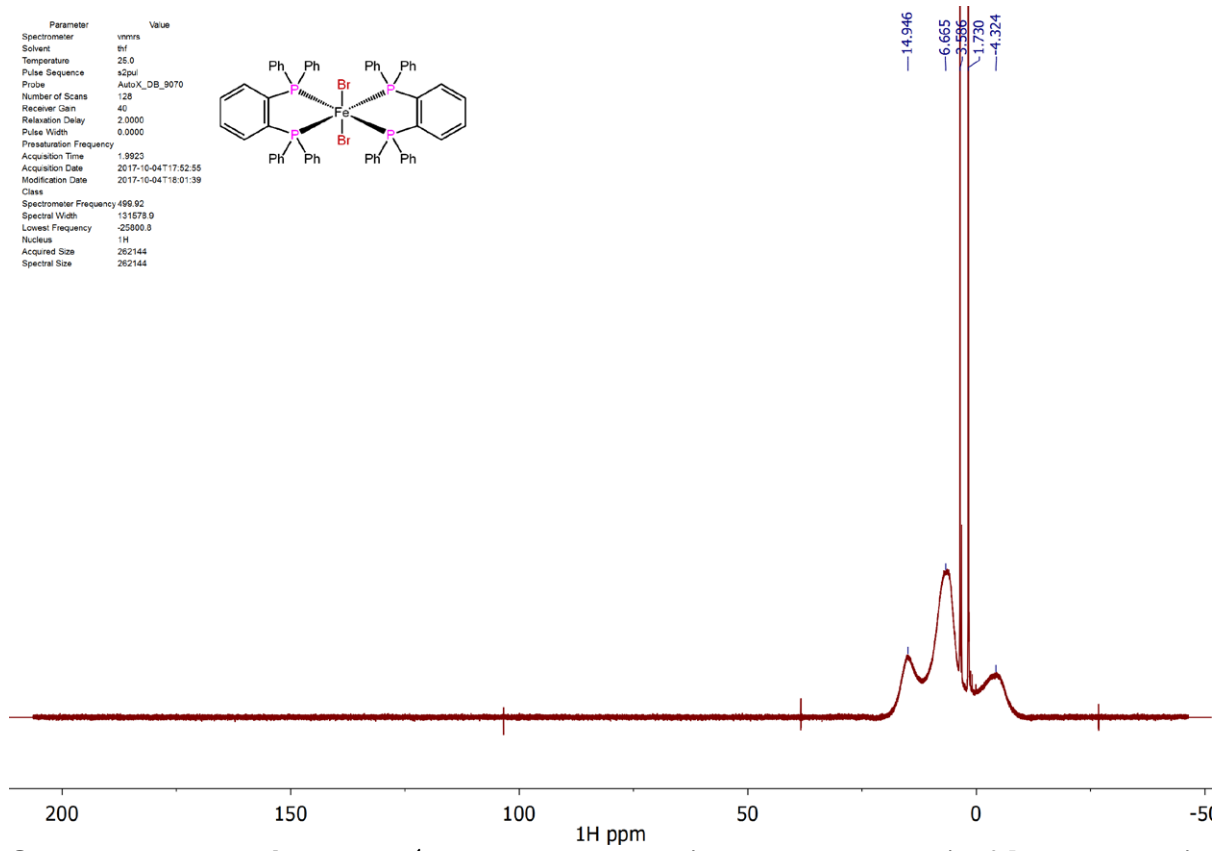
Supplementary Figure 53. ^1H NMR spectrum (500 MHz, THF- d_8) of $[(\text{FeBr}_2)(\mu\text{-trans-dppen})_2]$ (6).

4.12 [trans-FeBr₂(dpbz)₂] (7a)

[trans-FeBr₂(dpbz)₂] (7a) was synthesised using a modification of a previously reported procedure.¹⁷ A Schlenk was loaded with FeBr₂ (465 mg, 2.20mmol) followed by addition of THF (5 mL) and dpbz (1.964 g, 4.40 mmol). The mixture was heated at reflux temperature until FeBr₂ was completely dissolved and then the solvent was removed *in vacuo*. The yellow residue was dissolved in CH₂Cl₂ (20 mL), filtered and the solution layered with hexane (20 mL) to give bright yellow crystals of the 7a suitable for an X-ray crystallographic analysis. The yellow crystals were separated and dried under reduced pressure to form a yellow powder of 7a (1.60 g) while the filtrate was dried, re-dissolved in CH₂Cl₂ (10 mL) and layered with hexane (20 mL) to give a second crop of the material which was combined with the first crop (2.14 g, 88%). Anal. Calcd for C₆₀H₄₈Br₂FeP₄: C, 65.01; H, 4.36. Found: C, 65.52; H, 4.35. ^1H NMR (500 MHz, THF- d_8) δ = 15.0 (br s, 1956), 6.7 (br s, 2287), -4.3 (br s, 3231). ^{31}P NMR (202 MHz, THF- d_8) δ = -13.4. (Note: The observed NMR resonances correspond to 4a in equilibrium with dpbz rather than 7a in solution).

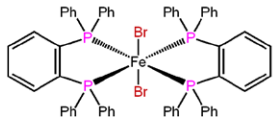


Supplementary Figure 54. Single-crystal X-ray structure of $[trans\text{-}FeBr_2(dpbz)_2]$ (**7a**). Hydrogen atoms and solvent molecules are omitted for clarity. Thermal ellipsoids are set at the 50% probability level.

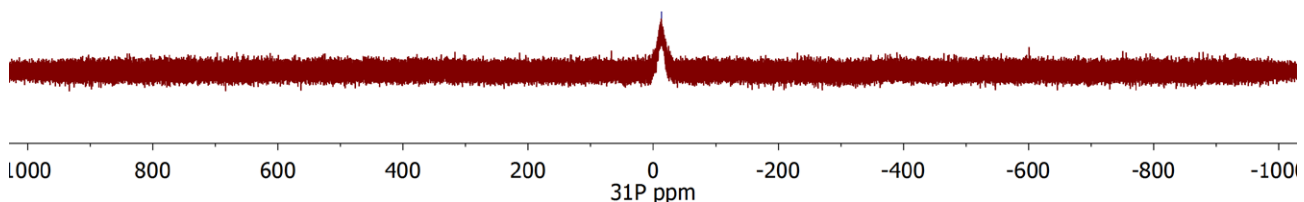


Supplementary Figure 55. ^1H NMR spectrum (500 MHz, THF-*d*₈) of $[trans\text{-}FeBr_2(dpbz)_2]$ (**7a**).

Parameter	Value
Spectrometer	Varian
Solvent	THF
Temperature	25.0
Pulse Sequence	s2pul
Probe	AutoX_DB_9070
Number of Scans	1024
Receiver Gain	50
Relaxation Delay	1.0000
Pulse Width	0.0000
Presaturation Frequency	
Acquisition Time	0.6291
Acquisition Date	2017-10-04T18:04:08
Modification Date	2017-10-04T18:32:05
Class	
Spectrometer Frequency	202.36
Spectral Width	416666.7
Lowest Frequency	-208333.4
Nucleus	³¹ P
Acquired Size	262144
Spectral Size	262144



—13.384



Supplementary Figure 56: ³¹P NMR spectrum (202 MHz, THF-*d*₈) of [trans-FeBr₂(dpbz)₂] (**7a**). Note: the broad signal corresponds to free dpbz in equilibrium with an NMR-silent dpbz-Fe species.

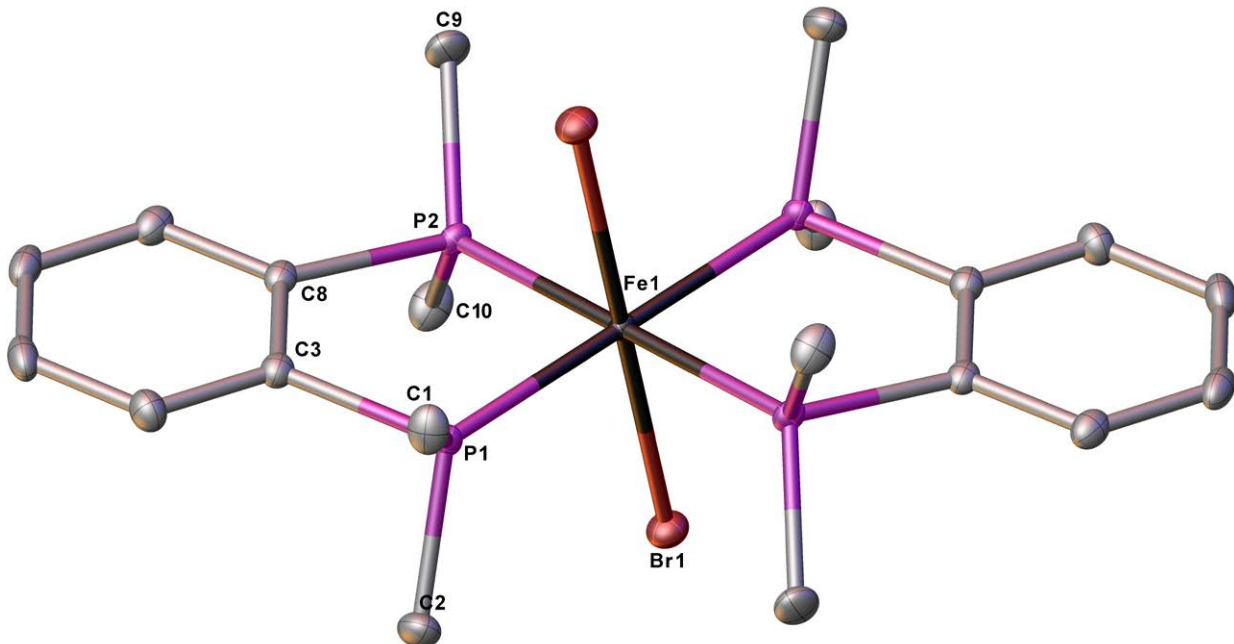
4.13 [trans-FeBr₂(dmbz)₂] (**7b**) and [(dmbz)₂Fe(μ-Br)₂FeBr₂] (**8**)

In an argon filled glove box, a vial was loaded with dmbz (100 mg, 0.504 mmol), FeBr₂ (108.8 mg, 0.504 mmol) and CH₂Cl₂ (4 mL). Instant formation of an insoluble green solid was observed. The reaction was briefly heated to reflux temperature and once cooled it was sonicated for 30 min. The mixture was then left to stand for 12h and the heating/sonication cycle was repeated another two times, during which time no change was apparent. The green solid was isolated by decanting the supernatant solution, washed 3 times with THF (2 mL), dried under reduced pressure, ground and further dried under reduced pressure for 12 hours to give a green powder (79.0 mg, 51%) which was air-stable and insoluble in CH₂Cl₂, THF, hexane, toluene, fluorobenzene, 1,2 difluorobenzene, diethyl ether and acetone. Crystals suitable for an X-ray crystallographic analysis were grown with the use of an H-tube by adding FeBr₂ (27.2 mg, 0.126 mmol) in one arm of the H-tube and dmbz (25.0 mg, 0.126 mmol) in the other. The H-tube was filled slowly with sufficient CH₂Cl₂ to fill the arms and to partially fill the central horizontal tube. After 10 days, green and red crystals were formed (Supplementary Figure 57) which were submitted for X-ray crystallographic analyses. The green crystals corresponded to the [trans-FeBr₂(dmbz)₂] (**7b**) complex (Supplementary Figure 58) while the red crystals to its FeBr₂ adduct: [(dmbz)₂Fe(μ-Br)₂FeBr₂] (**8**) (Supplementary Figure 59). Complexes similar to the [trans-FeBr₂(dmbz)₂]

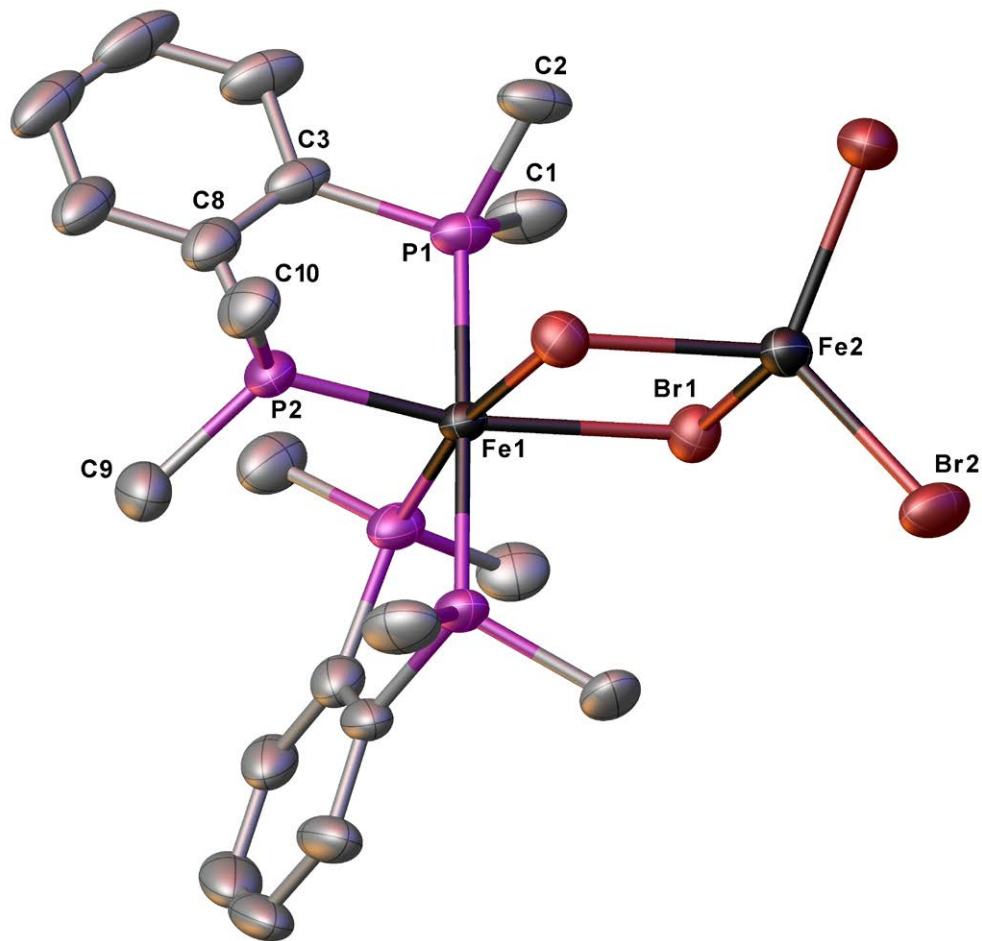
(7b) have been previously reported by Bennett *et al.* such as: [*trans*-FeCl₂(dmbz)₂], which was found to be insoluble in most solvents as well.¹⁸



Supplementary Figure 57. Crystals formed from the reaction of FeBr₂ with dmbz in CH₂Cl₂ in an H tube: green = [*trans*-FeBr₂(dmbz)₂] (7b), red = [(dmbz)₂Fe(μ-Br)₂FeBr₂] (8), yellow = unreacted FeBr₂.



Supplementary Figure 58. Single-crystal X-ray structure of [*trans*-FeBr₂(dmbz)₂] (7b). Hydrogen atoms are omitted for clarity while thermal ellipsoids are set at the 50% probability level.



Supplementary Figure 59. Single-crystal X-ray structure of $[(\text{dmbz})_2\text{Fe}(\mu\text{-Br})_2\text{FeBr}_2]$ (**8**). Hydrogen atoms are omitted for clarity while thermal ellipsoids are set at the 50% probability level.

4.14 $[\text{FeBr}(\text{dpbz})_2]$ (**9a**)

The synthesis of $[\text{FeBr}(\text{dpbz})_2]$ (**9a**) has been previously reported by Bedford *et al.* using BnMgBr as the reducing agent.¹⁹ Here it was synthesised in two separate alternative ways.

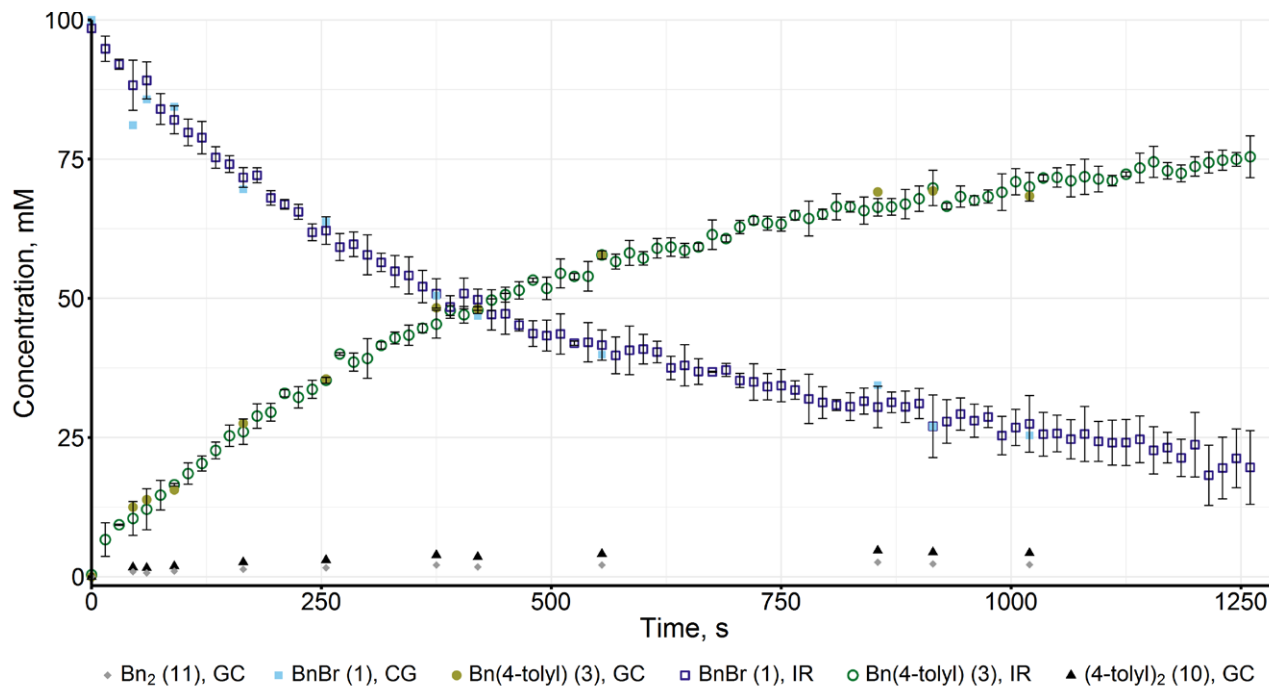
Method A. A Schlenk was loaded with FeBr_2 (483.1 mg, 2.24 mmol) and dpbz (2.00 g, 4.48 mmol) followed by addition of THF (10 mL) and the mixture was heated at reflux temperature until all solids dissolved. Once cooled to room temperature, KC_8 (7.522 mmol/g, 327.6 mg, 2.464 mmol) was added to the solution and the resultant dark red mixture was left stirring at room temperature for 12h. The dark red mixture was then filtered *via* cannula and the filtrate was layered with hexane (10 mL) to give a first crop of the target compound, while the residue was extracted with hot fluorobenzene. The combined extracts were condensed to 25 mL and upon standing for 12h at room temperature produced a second crop of $[\text{FeBr}(\text{dpbz})_2]$ (**9a**) which was isolated *via* filtration while the filtrate was layered with hexane (20 mL) to give a third crop. All three crops were combined and dried under reduced pressure for 2 hours to give $[\text{FeBr}(\text{dpbz})_2]$ (**9a**) as a dark red solid (1.429 g, 62%). Anal. Calcd for $\text{C}_{60}\text{H}_{48}\text{BrFeP}_4$: C, 70.06; H, 4.70 Found: C, 69.79; H, 4.75.

Method B. FeBr_2 (233.4 mg, 1.08 mmol) was dissolved in minimal THF and the solution then dried under reduced pressure. The residue was dissolved in dry acetone (20 mL) followed by addition of dpbz (918 mg, 2.16 mmol) and the mixture was heated to reflux temperature which gave a yellow precipitate. The mixture was dried and the yellow residue dissolved in toluene (20 mL) followed by addition of (4-tolyl) MgBr (2.5 eq, 2.7 mL, 1M, 2.7 mmol) and left stirring for 2h. Dioxane (0.35 mL, 1.5 eq dioxane to MgBr_2) was added and the mixture was stirred for an additional 30 minutes during which time a fine white powder formed which was filtered off. The dark red filtrate was left standing for 48 hours resulting in formation of $[\text{FeBr}(\text{dpbz})_2]$ (**9a**) (750 mg, 68% yield). Anal. Calcd for $\text{C}_{60}\text{H}_{48}\text{BrFeP}_4$: C, 70.06; H, 4.70 Found: C, 70.47; H, 4.75.

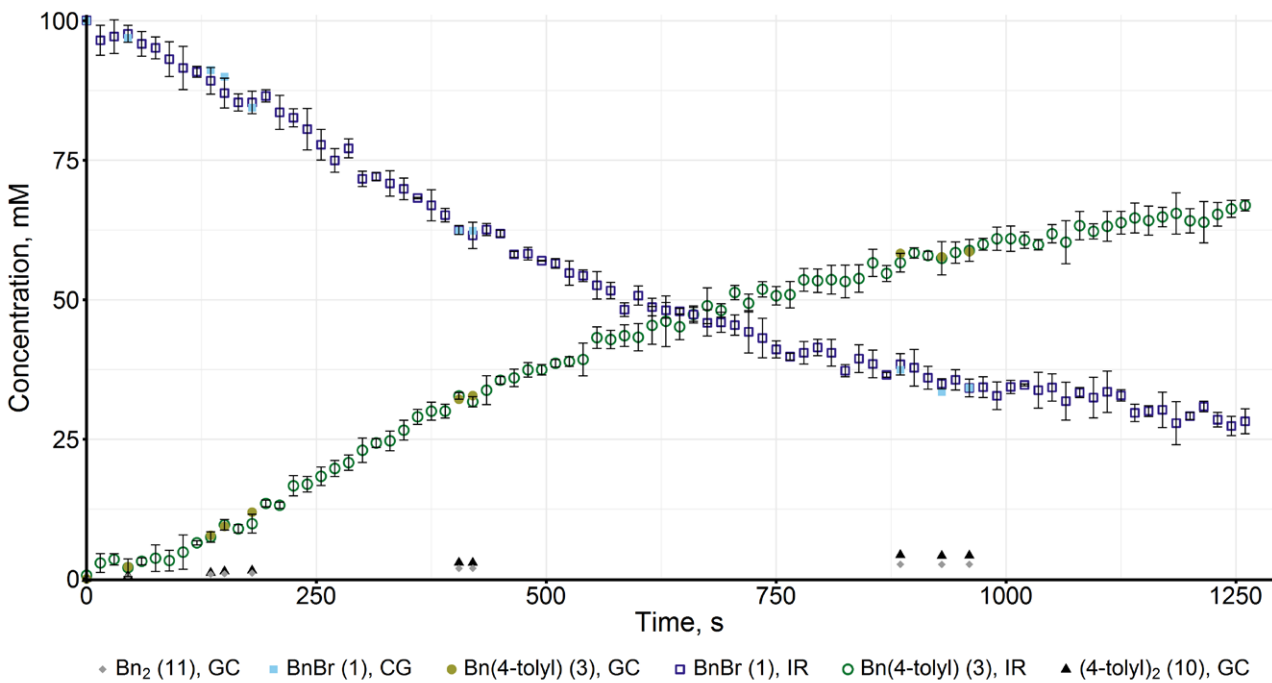
5 Comparison of the catalytic performances of iron(I) vs. iron(II).

5.1 *In situ* FT-IR spectroscopic monitoring of the Negishi coupling of **1** and **2a** catalysed by **7a** or **9a**.

The reaction progress profiles were obtained as described in section 2 using **1** (1.00 mmol) **2a** (1.00 mmol in Zn) and *n*-dodecane (internal standard, 0.5 mmol) catalysed by **7a** (0.0100 mmol) or **9a** (0.0100 mmol). Each experiment was performed three times demonstrating good reproducibility of the results (Supplementary Figure 60 and Supplementary Figure 61).



Supplementary Figure 60. Negishi coupling between **1** (100 mM) and **2a** (100 mM) initiated by **7a** (1.00 mM) at 7.00 °C and a total volume of 10.0 mL. The reaction was performed three times and the results were averaged with the error bars representing standard deviation.

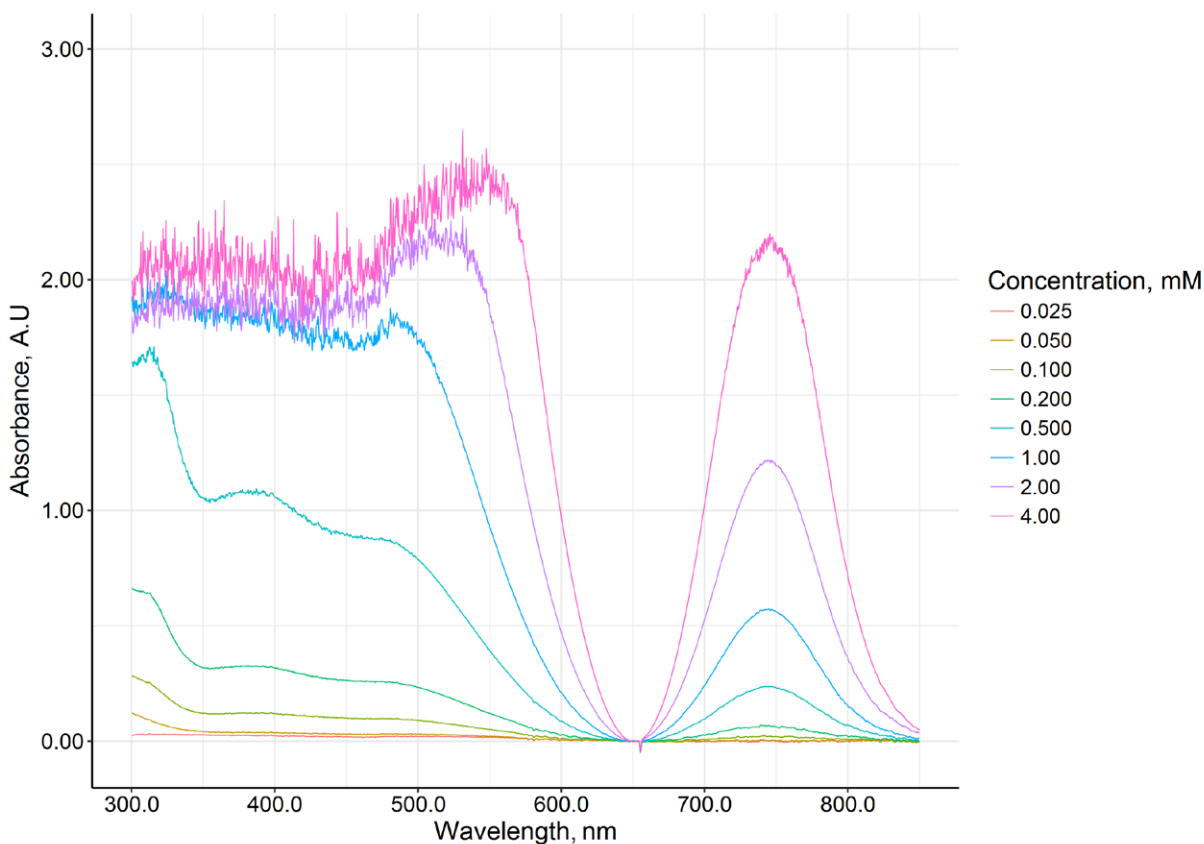


Supplementary Figure 61. Negishi coupling between **1** (100 mM) and **2a** (100 mM) catalysed by **9a** (1.00 mM) at 7.00 °C and a total volume of 10.0 mL. The reaction was performed three times and the results were averaged with the error bars representing standard deviation.

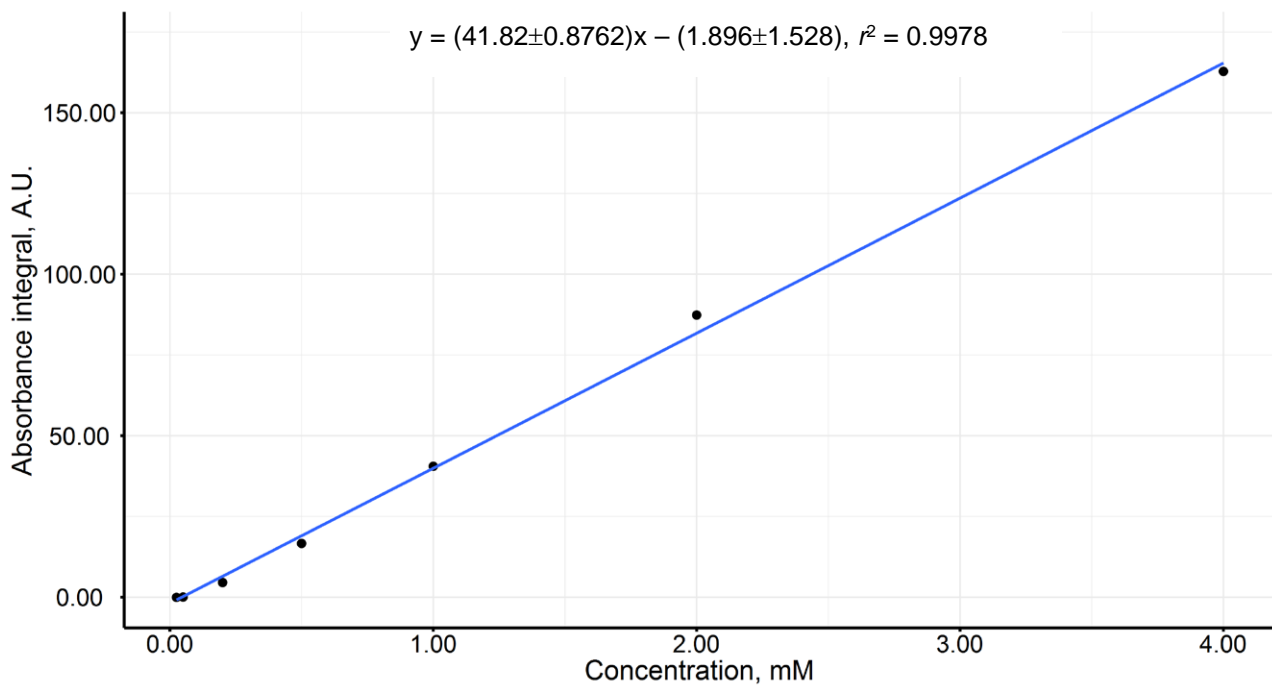
5.2 Calibration of the UV-Vis spectrometer for **9a**.

The UV-Vis spectrometer was first calibrated for **9a** using the PEEK dip probe and the J. Youngs tap fitted cuvette. For the dip probe calibration, a Schlenk was loaded with **9a** (41.1 mg, 0.040 mmol) and THF (10.0 mL) providing a 4.0 mM solution of **9a** whose UV-Vis spectrum was recorded. Subsequently, the solution in the Schlenk was diluted to half its initial concentration (2.00 mM) and the spectrum recorded again. This procedure was repeated until no signal could be detected at 745 nm. The collected spectra were baseline corrected and integrated in the region between 660 nm and 780 nm (Supplementary Figure 62). The data collected were then used to construct the calibration curve presented in Supplementary Figure 63. Similarly, in order to calibrate the cuvette, a 1.00 cm wide quartz glass cuvette fitted with a J. Youngs tap was loaded with **9a** (20.6 mg, 0.020 mmol) and THF (4.00 mL) providing a 5.00 mM solution whose UV-vis spectrum was recorded. Subsequently, the solution in the cuvette was diluted to half its initial concentration (2.5 mM) and the spectrum recorded again. This procedure was repeated until no signal could be detected at 745 nm. The collected spectra were baseline corrected, integrated in the region between 700 nm and 800 nm (Supplementary Figure 64) and the integral values used to construct the calibration curve presented in Supplementary Figure 65.

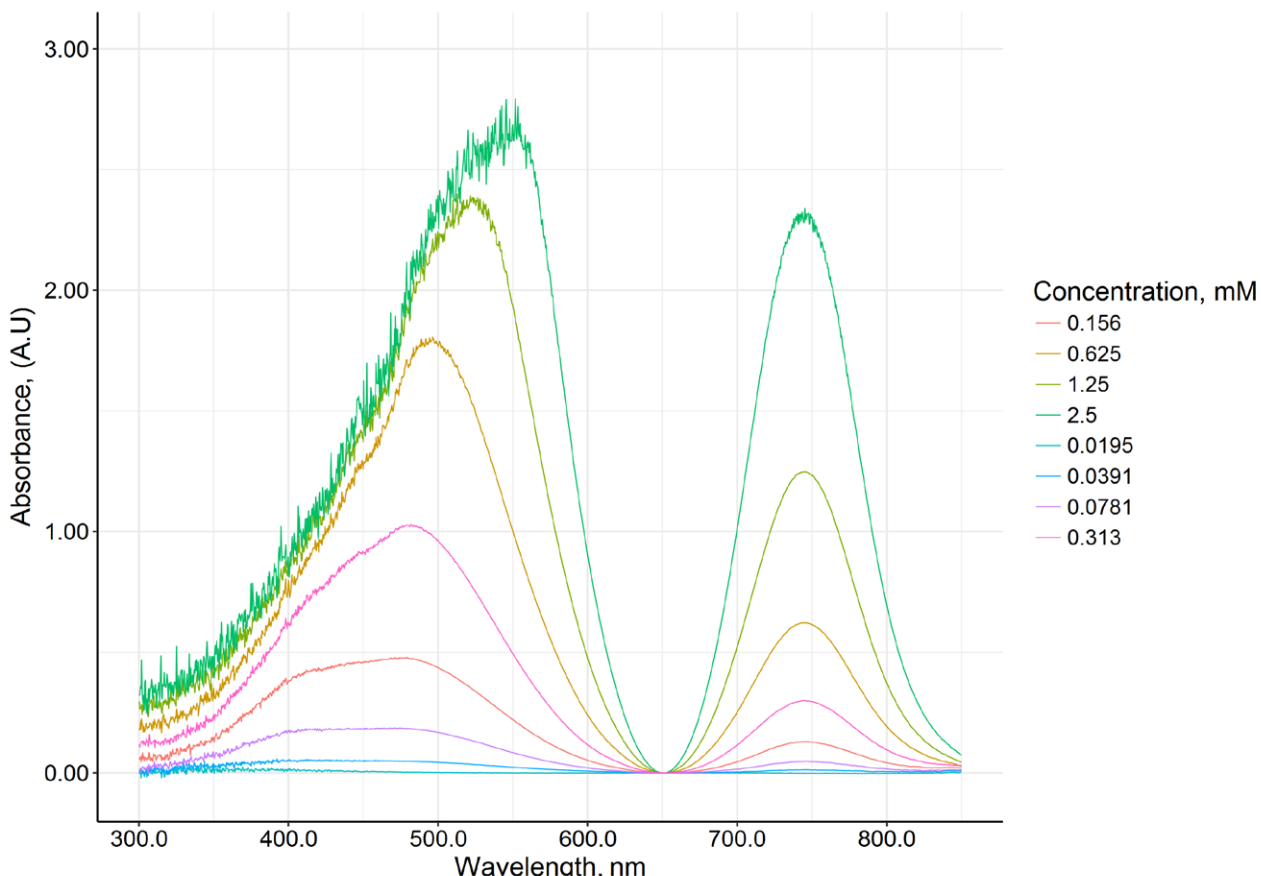
Separately, in order to demonstrate that **9a** can be produced from **7a** and **2a** under catalytically relevant conditions, **7a** was treated with excess (200 equivalents) of **2a** and the UV-Vis spectrum of the mixture was compared with that of **9a** and **7a**. The spectra are shown in Supplementary Figure 66.



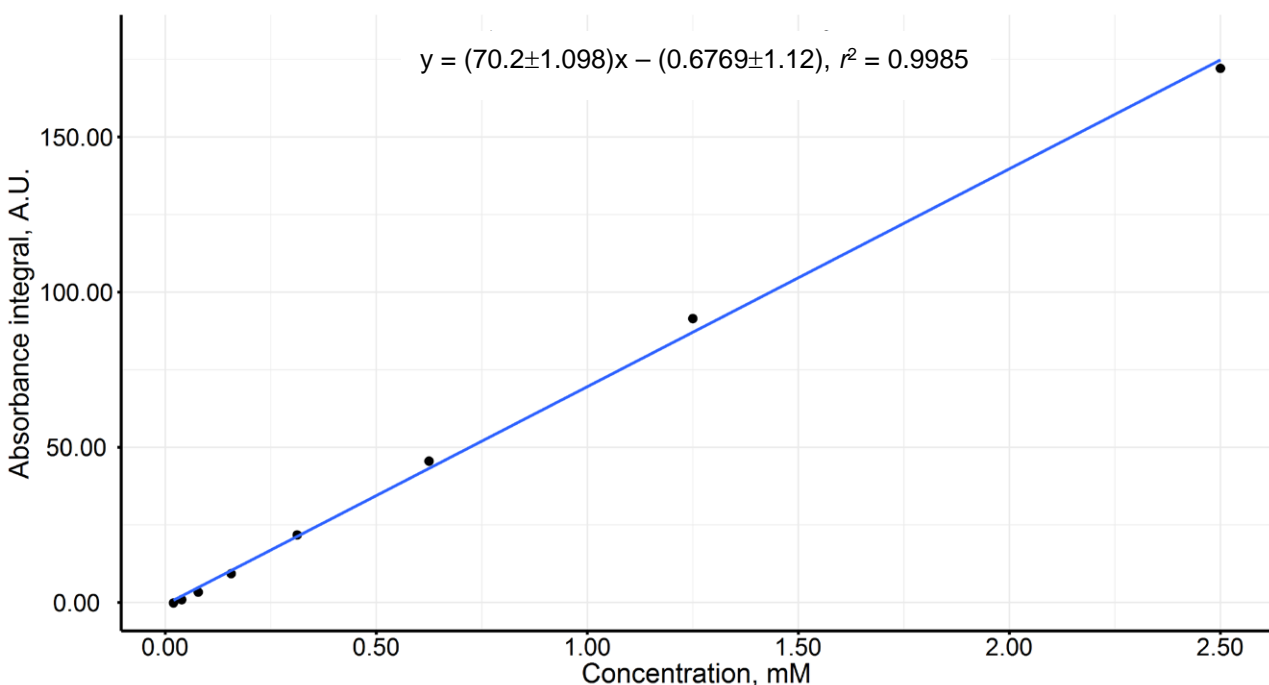
Supplementary Figure 62. Superimposed UV-Vis spectra of a series of THF solutions of **9a** used to calibrate the spectrometer with the dip probe at 6 mm optical pathlength.



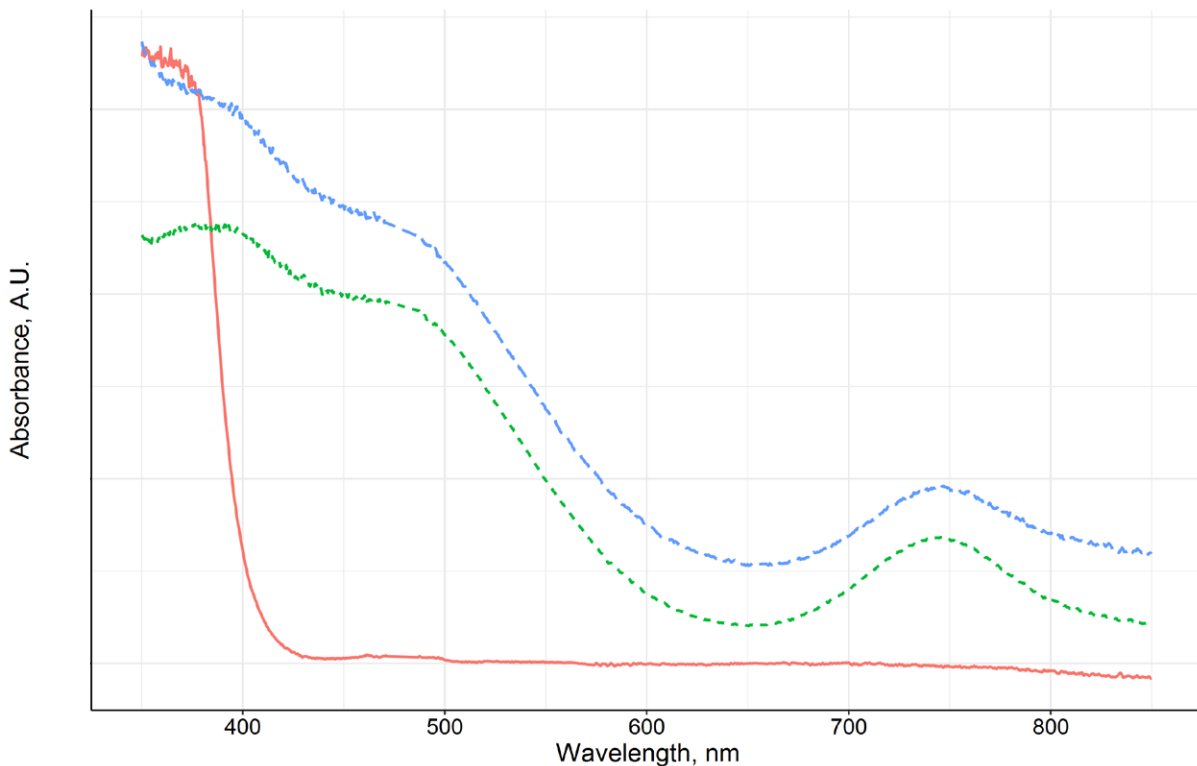
Supplementary Figure 63. UV-Vis calibration curve for a series of THF solutions of **9a** using a dip probe set at a 6 mm optical pathlength. Standard errors are included in the fitted equation.



Supplementary Figure 64. Superimposed visible spectra of a series of THF solutions of **9a** used to calibrate the spectrometer with a 1.00 cm wide quartz glass cuvette.



Supplementary Figure 65. UV-Vis calibration curve for a series of THF solutions of **9a** using a 1.00 cm wide quartz glass cuvette. Standard errors are included in the fitted equation.



Experiment: — $\text{FeBr}_2(\text{Dpbz})_2$ 0.5 mM - - $\text{FeBr}(\text{Dpbz})_2$ 0.5 mM - · $\text{FeBr}_2(\text{Dpbz})_2$ 0.5 mM + $\text{Zn}(p\text{-Tol}_2)/2 \text{ MgBr}_2$

Supplementary Figure 66. UV-Vis spectra of a 0.5 mM solution of $[\text{FeBr}_2(\text{dpbz})_2]$ (**7a**), $[\text{FeBr}(\text{dpbz})_2]$ (**9a**) and the end point of the reaction between 0.5 mM $[\text{FeBr}_2(\text{dpbz})_2]$ (**7a**) and 100 mM **2a** in THF.

5.3 Investigating the amount of **9a** in the Negishi reaction between **1** and **2a**, using **7a** or **9a** as the pe-catalyst (Figure 4b and c).

A jacketed Schlenk was heated in an oven at 180 °C for 20 minutes and then evacuated while still hot. Once cool, it was back filled with dry nitrogen followed by insertion of the UV-Vis dip probe equipped with a rubber stopper to form an air tight seal. The Schlenk was evacuated and back filled with dry nitrogen again and cooled at 7.00 °C using a cryostat. After the UV-Vis instrument was set up (integration time = 40 ms, number of averaged scans = 75), THF (3.10 mL) and n-dodecane (internal standard, 1.00 mL, 500 mM stock solution, 0.5 mmol) and a background spectrum was collected. Subsequently, **2a** (5.00 mL, 200 mM stock solution, 1.00 mmol) was added and stirred using an oval stir-bar at 500 rpm (all additions were performed with gas tight Hamilton syringes). Collection of spectra began and **1** (0.40 mL, 2500 mM stock solution, 1.00 mmol) was added. The reaction was activated by adding **7a** or **9a** (0.50 mL, 20.0 mM stock solution, 0.0100 mmol). The characteristic peak of Fe(I) was monitored at 745 nm by integrating the area between 660 nm and 780 nm.

6 X-ray Absorption Fine Structure (XAFS) spectroscopic studies

6.1 General considerations

X-ray absorption fine structure (XAFS) measurements at the Fe K-edge were carried out on the B18 (core XAFS) beamline at the Diamond Light Source, Didcot, UK. Spectra were recorded using a QEXAFS set-up with a fast-scanning Si (111) double crystal monochromator. All solutions were measured in fluorescence mode using a 36-element solid state germanium detector; transmission data was collected in parallel with ion chamber detectors. Solution XAFS spectra for reference compounds and reaction end points were collected in an air tight sealed (Swagelok fittings were used) polyimide tube (OD = 1.99 mm, ID = 1.93 mm) loaded in an argon filled glove box. For the *operando* flow studies, typically 12 scans were acquired to improve the signal averaging, with a spectral time resolution of 70 s per spectrum ($k_{\max} = 15$, step size 0.3 eV), with a focused beam size of 200 x 200 μm . All measurements were carried out with an Fe foil placed between I_t and I_{ref} for an internal calibration of edge position. XAFS data processing was performed using IFEFFIT²⁰ with the Horae package²¹ (Athena and Artemis). For EXAFS fitting with Artemis, S_0^2 was used as a fixed input parameter ($S_0^2 = 0.8$) derived from fitting the initial reference Fe complex. XANES simulations were performed with FEFF8.4 code starting from data from crystallographic cif files. Simulations were run on the Fe K edge and using self-consistent-field (SCF) molecular electron densities calculated over a cluster (radius 4.2 Å) including 18 atoms. The full multiple scattering contributions have been calculated using a sphere of 5.5 Å including about 40 atoms. Energy resolution was set to 0.2 eV near the edge and 0.05 Å⁻¹ in the near EXAFS region up to 6 Å⁻¹. Projected Density of States were calculated for all the elements present in the structure in an energy range from -20 to +30 eV around the absorption edge. S_0^2 amplitude has been fixed to 1.

6.2 Description of the flow cell used for the *operando* XAFS studies

Time resolved XAFS studies were performed using a custom-made flow cell (Supplementary Figure 67). The body of the cell was constructed from PEEK polymer and was machined in the mechanical workshop of the University of Bristol Physics department by Mr Bartosz Dworzanski. The channel in the cell was grooved with a milling machine and measured 6918 mm long, 1 mm wide and 0.6 mm deep. The long and narrow construction of the cell's channel allowed for high fluid speeds to be achieved with minimal consumption of starting materials, while the zig-zag pattern helped with mixing the reaction mixture throughout the cell by favouring turbulent flow. The top of the cell was sandblasted and sealed with a 75 micron thick polyimide film using Masterbond EP41S-5 two component solvent-proof adhesive which was applied with a small roller constructed from a PEEK rod. The flow cell was connected with the two reagent-containing 50 mL gas-tight syringes using

1/16" OD PEEK tubing and fittings. Reagent addition at a set flow rate was achieved with the use of two syringe pumps. Since efficient initial mixing of the two reaction components in the flow cell is crucial, the cell was designed in such a way that the two solutions collide at high speed upon entering the cell through two narrow (0.2 mm) openings placed opposite each other (see Supplementary Figure 67). Moreover, the first compartment of the cell was loaded with borosilicate glass beads further assisting with initial mixing of the reaction's components. The total volume of the cell was found to be 4.20 mL. The experimental setup for the XAFS studies conducted in the B18 beamline in Diamond, UK is presented in Supplementary Figure 69 while details for the flow experiment are included in Supplementary Table 3.

Supplementary Table 3. Experimental details for the *operando* flow experiment.

Flow cell experimental parameters

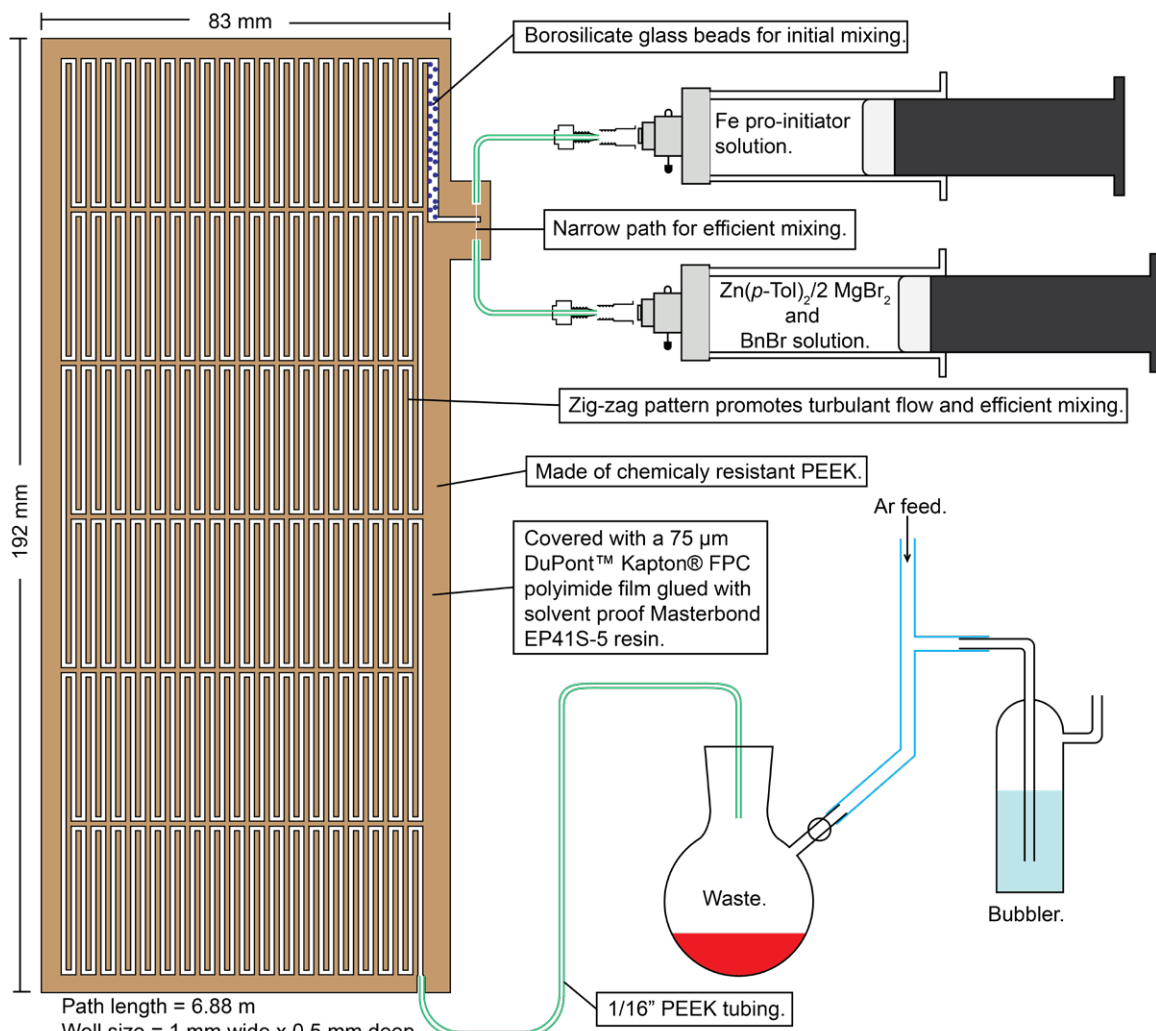
Cell length =	6918 mm	[1] and [2a] in syringe A =	150 mM
Cell width =	1.00 mm	[7a] in syringe B =	3.00 mM
Cell depth =	0.60 mm	[1] and [2a] in cell =	100 mM
Cell volume =	4.20 mL	[7a] in cell =	1.00 mM
Residence time in cell =	1000 s	Flow from syringe A =	0.168 mL/min
Continuous run time =	5 h	Flow from syringe B=	0.084 mL/min
Fluid velocity =	6.918 mm/s	Total flow in cell =	0.252 mL/min

The time necessary for the solvent front to reach each position in the flow cell where the XAFS collection occurred was determined by replicating the experiment using THF, introducing an air bubble in the channel and recording the time required for the air bubble to reach the point of interest.

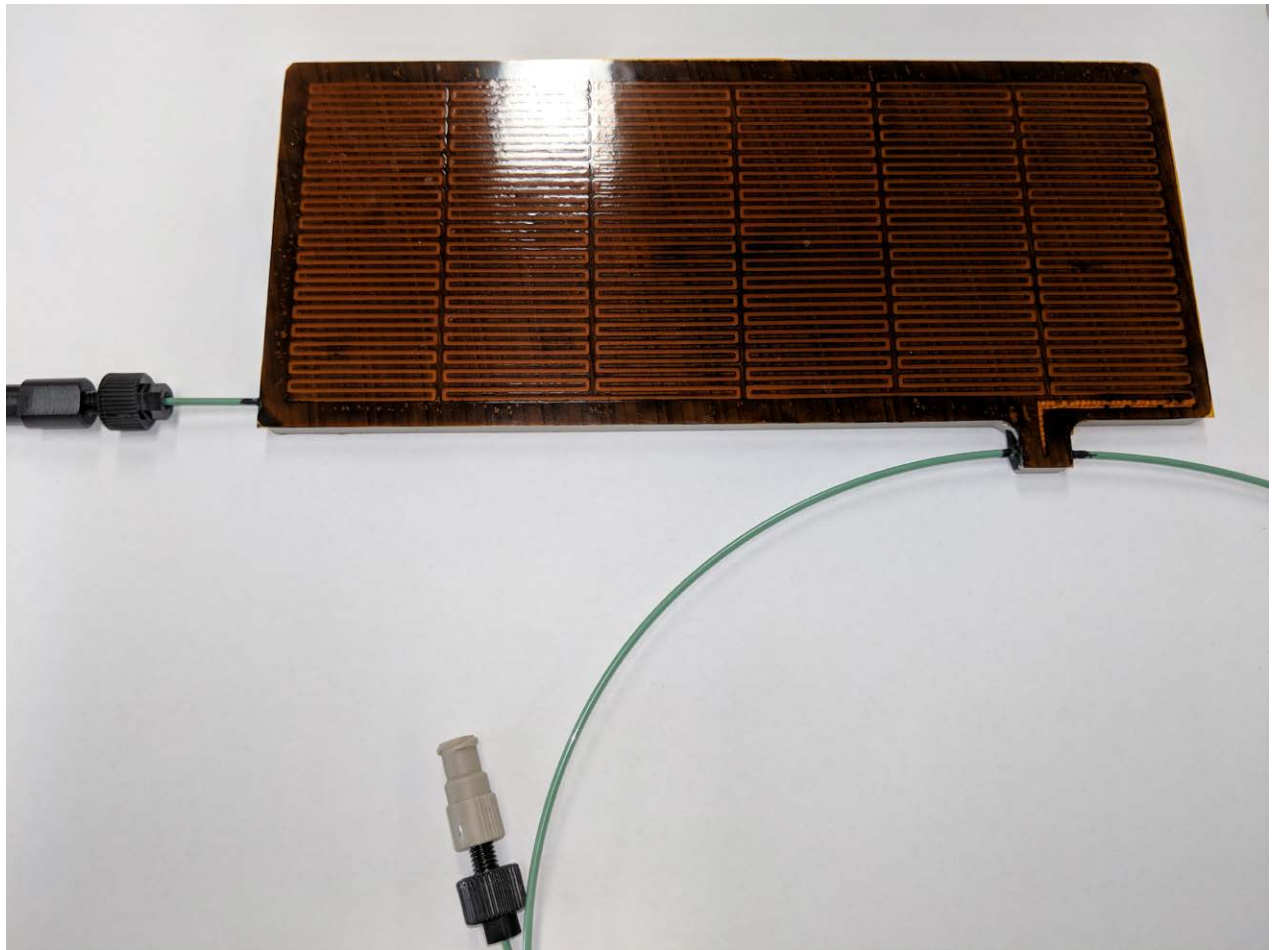
Separately, the profile of the Negishi reaction between BnBr (**1**) and Zn(4-tolyl)₂/2MgBr₂ (**2a**) was obtained under the same temperature and concentrations that the flow cell operated at: a jacketed Schlenk tube equipped with a cooling coil was loaded with THF (3.35 mL), n-dodecane (1.00 mL, 500 mM solution in THF, 0.50 mmol), **2a** (5.00 mL, 200 mM solution in THF, 1.00 mmol) and **1** (0.40 mL, 2500 mM solution in THF, 1.00 mmol). The temperature was set at 22.00 °C and stirring at 500 rpm. Addition of [FeBr₂(dpbz)₂] (**7a**) (0.250 mL, 20.0 mM solution in THF, 0.0100 mmol) followed and the reaction was sampled (0.1 mL - 0.2 mL aliquots) over the course of 40 minutes. Each sample collected was quenched with HCl(aq) (0.5 M) and the time recorded resulting in the profile obtained in Figure 5a and b which was then used to calculate the reaction's composition in each time position where the XAFS were recorded. The results are summarised in Supplementary Table 4.

Supplementary Table 4. Reaction progress for the Negishi coupling of **1** with **2a** under the conditions employed for the XAFS studies.

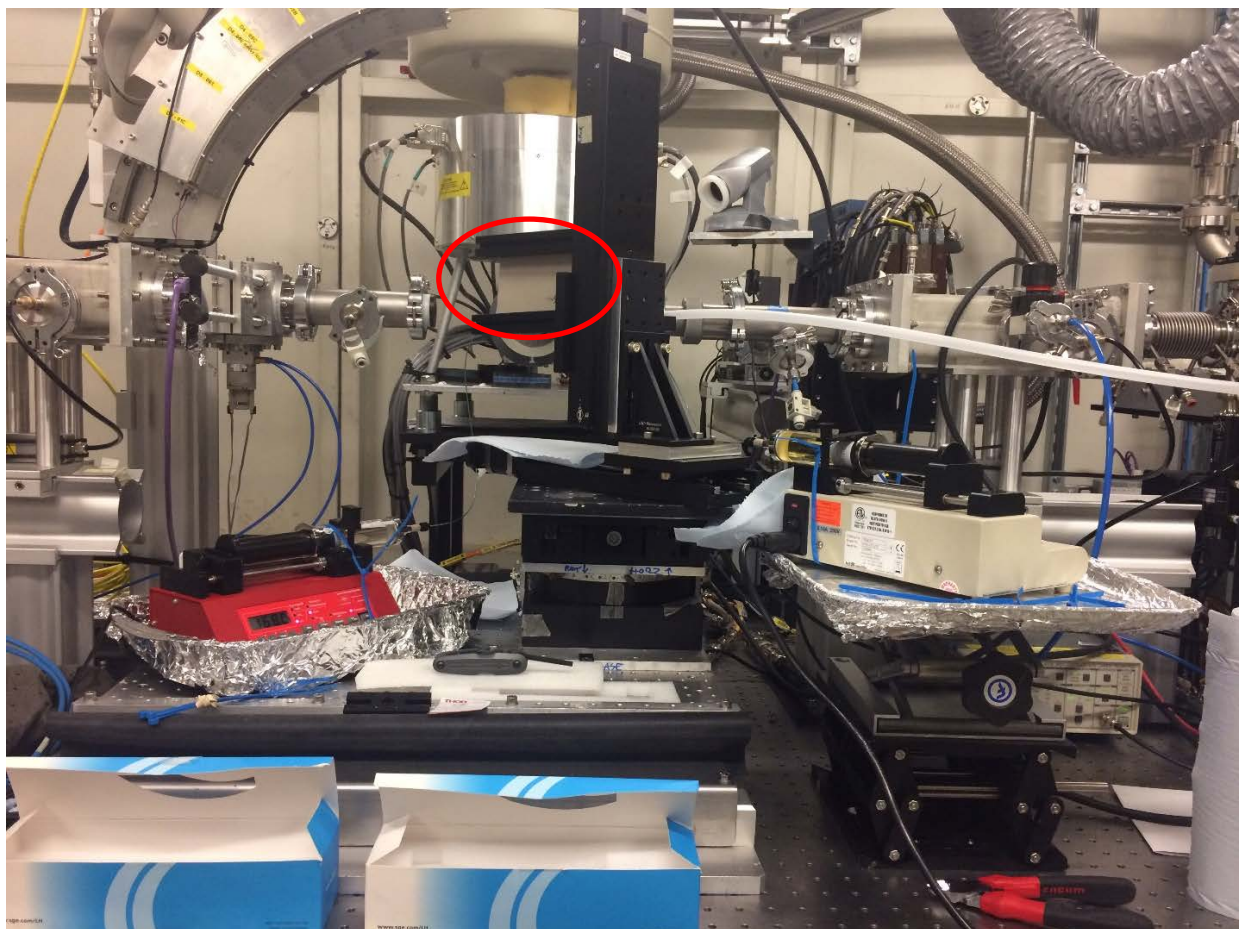
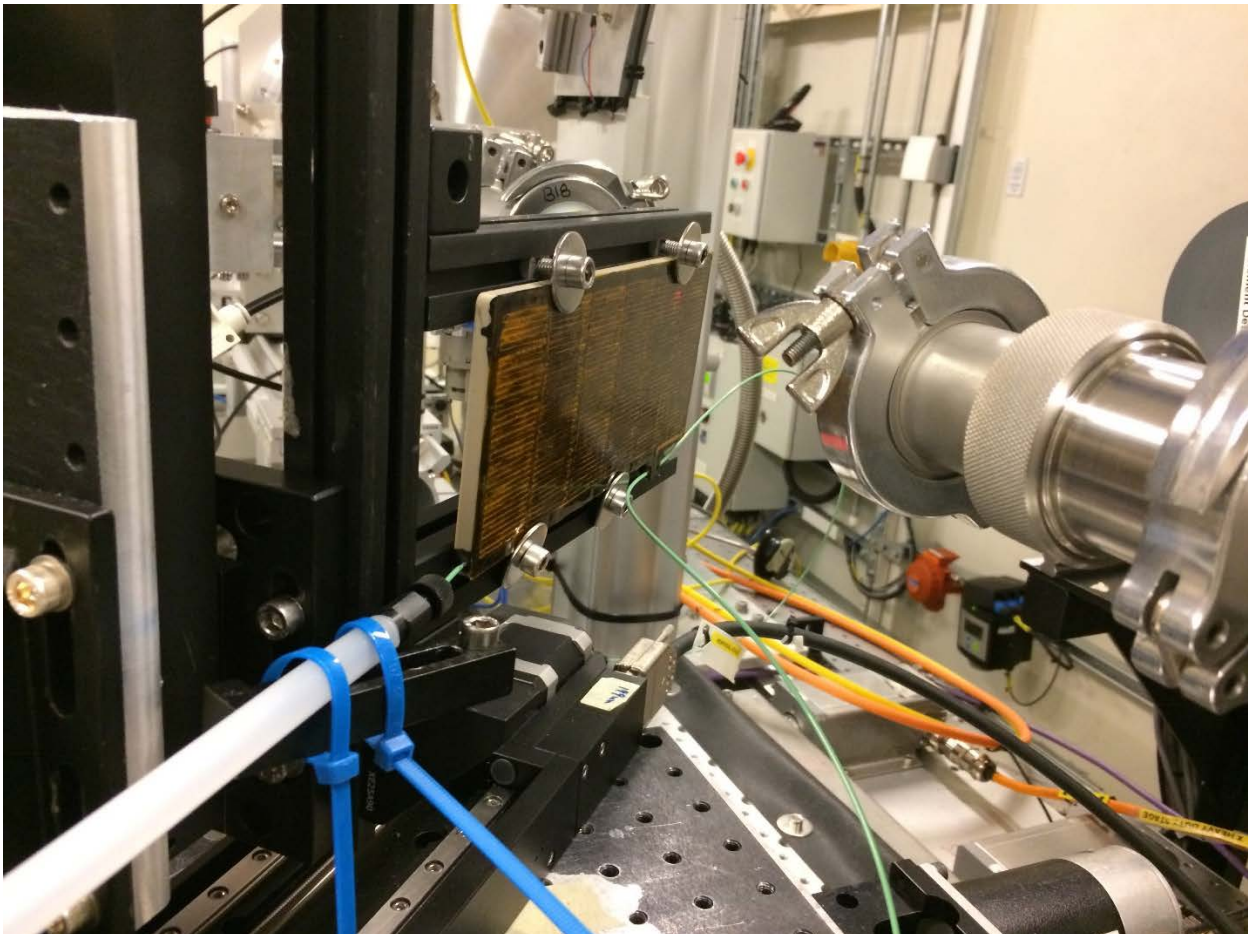
Position on cell	Time (s)	1 (mM)	3 (mM)	10 (mM)	11 (mM)
A	6	85	4.6	0.721	0.00
B	166	48	39	3.49	1.72
C	482	26	65	4.67	2.51
D	817	17	78	5.16	2.81



Supplementary Figure 67. Diagram of the flow cell used for the *operando* XAFS studies.



Supplementary Figure 68. The assembled flow cell used for the *operando* XAFS studies.



Supplementary Figure 69. Setup for time resolved XAFS measurements using a flow cell.

6.3 XAFS spectra and simulations under static solution conditions

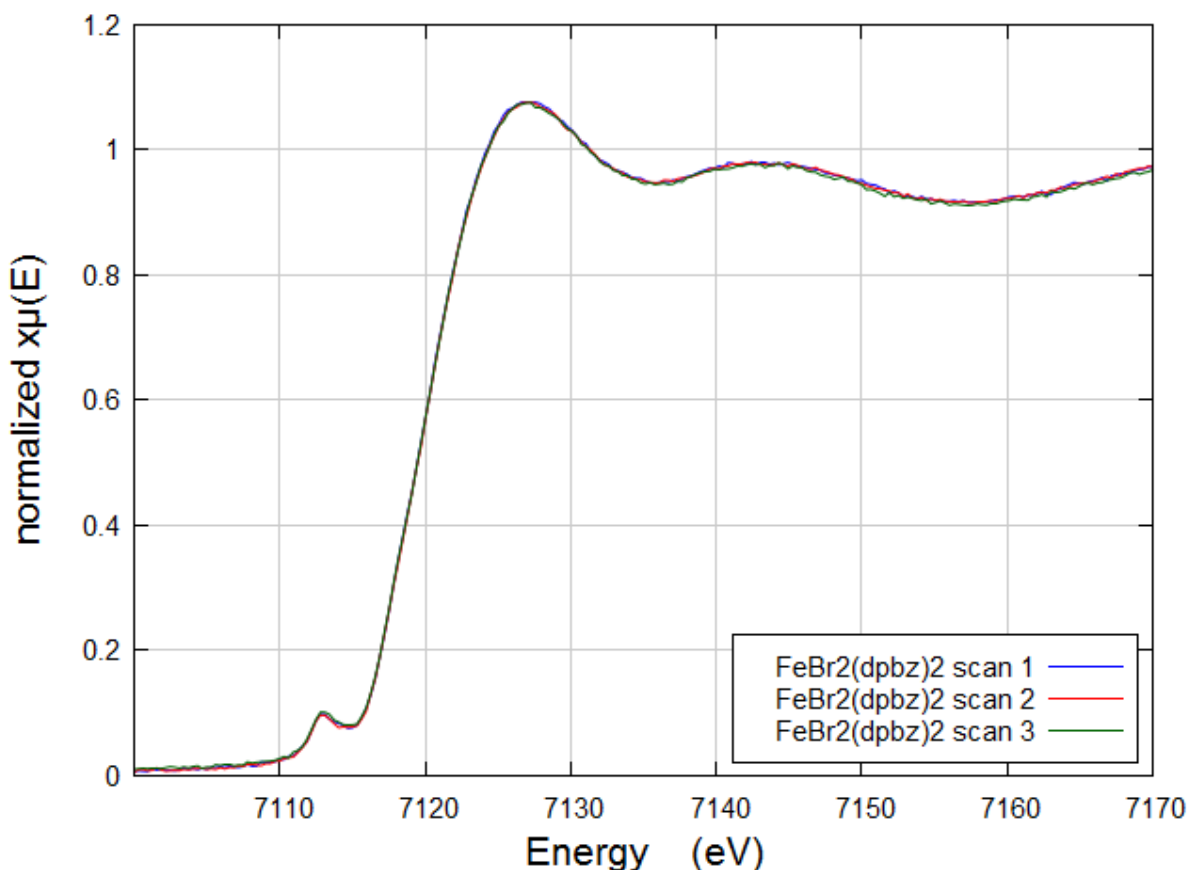
6.3.1 Stability of samples with respect to radiation damage

The XAFS spectra of a wide range of representative species (Supplementary Table 5) in THF stock solutions were each recorded three times for the following durations: 190s per scan for Fe K edge, 121s for Br K edge and 147s per run for Zn K edge. No change was observed between runs in each case, indicating that the samples were stable to radiation damage over the time-frames investigated. By way of example, Supplementary Figure 70 shows the normalized XANES spectra of individual scans for a static solution of the starting complex $[\text{FeBr}_2(\text{dpbz})_2]$, **7a**. The spectra overlay perfectly, which confirms there is no change in speciation during the data acquisition and that the beam has not induced any transformations. Importantly, using the flow rate data coupled with the beam size allows us to determine that the dwell time for the reactions studied in flow (see below) was only 28 ms giving us confidence that no radiation damage was caused in flow.

Supplementary Table 5. Summary of the composition of the solutions used for collecting the XAFS reference spectra of isolated compounds and reaction end points in THF.^a

Entry #	Solution composition (mM)	Edge collected
1	FeBr_2 (40)	Fe, Br
2	FeBr_3 (40)	Fe
3	$[\text{FeBr}_2(\text{dpbz})_2]$ (40)	Fe, Br
4	$[\text{FeBr}_2(\text{dpbz})]$ (40)	Fe, Br
5	$[\text{FeBr}(\text{dpbz})_2]$ (20)	Fe, Br
6	ZnBr_2 (20)	Zn, Br
7	$[\text{ZnBr}_2(\text{dpbz})]$ (20)	Zn, Br
8	ZnPh_2 (50)	Zn
9	$\text{ZnPh}_2/2 \text{MgBr}_2$ (40)	Zn
10	$\text{ZnPh}_2/\text{PhMgBr}$ (40)	Zn
11	BnBr (40)	Br
12	MgBr_2 (40)	Br
13	FeBr_3 (40)/dpbz (40)	Fe
14	FeBr_3 (40)/dpbz (80)	Fe

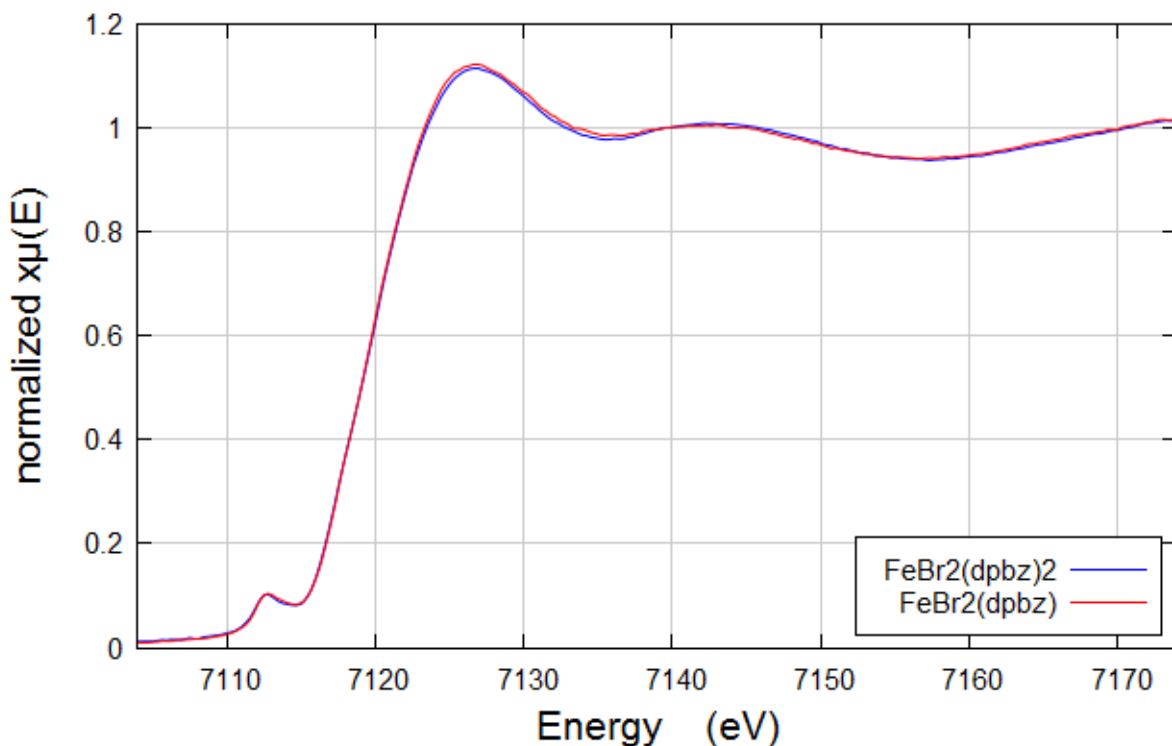
^a All solutions were prepared in an argon sealed glove box and loaded in an air tightly sealed (Swagelok fittings were used) polyimide tube (OD = 1.99 mm, ID = 1.93 mm). $\text{ZnPh}_2/2 \text{MgBr}_2$ solution was prepared *in situ* by reacting ZnBr_2 with PhMgBr .



Supplementary Figure 70. Normalized Fe K edge XANES spectra of $[\text{FeBr}_2(\text{dpbz})_2]$ recorded over 3 x 190 second scans, indicating no apparent radiation damage.

6.3.2 XAFS Spectroscopic investigation of the solution phase structure of FeBr_2 dpbz adducts

Supplementary Figure 71 shows the Fe K edge normalized XANES spectra recorded for THF solutions of mono and bis-chelate complexes $[\text{FeBr}_2(\text{dpbz})]$, **4a**, and $[\text{FeBr}_2(\text{dpbz})_2]$, **7a**. It is clear that the same species is formed in solution, most likely corresponding to the loss of one equivalent of dpbz from **7a** to give **4a**. Supplementary Table 6 and Supplementary Table 7 show the EXAFS fitting parameters with fixed coordination numbers and fixed S_0^2 respectively, meanwhile Supplementary Figure 72 shows the fit of these models. The suggested mono-dissociation of dpbz from **7a** to give **4a** as the main species in solution was confirmed by ^{31}P NMR spectroscopy, as shown in Supplementary Figure 73. The spectrum of **4a** is NMR silent, due to coordination of the dpbz ligand to the paramagnetic the Fe(II) centre. Meanwhile a solution of **7a** showed approximately one equivalent of free dpbz (confirmed by addition of a capillary containing a standardised solution of PPh_3 , not shown), broadened by exchange with the paramagnetic centre. Supplementary Figure 74 shows the simulation of the XANES spectrum performed with FEFF8.4 code, which indicates that features before the main edge can be assigned to a Fe 1s – Br 4p dipolar transition as evident when overlapping the simulated spectra with the projected density of states.



Supplementary Figure 71: Fe K edge normalised XANES spectra of $[\text{FeBr}_2(\text{dpbz})_2]$ (**7a**) and $[\text{FeBr}_2(\text{dpbz})]$ (**4a**) solutions in THF.

Supplementary Table 6. Simulated EXAFS fitting parameters for $[\text{FeBr}_2(\text{dpbz})]$ (**4a**), based on fixed coordination numbers.

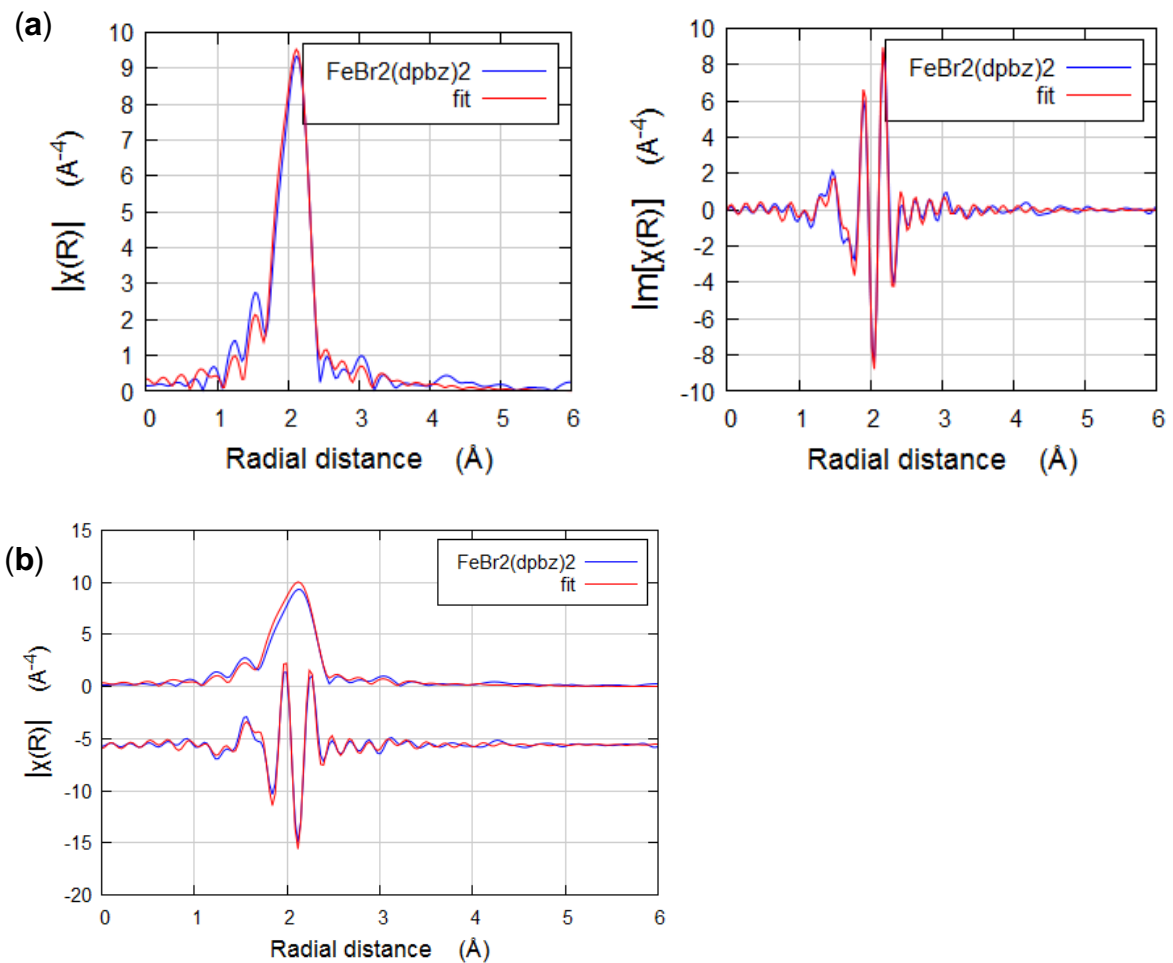
Sample	Abs Sc	N	R / Å	$2\sigma^2 / \text{\AA}^2$	E_f / eV	R _{factor}
$[\text{FeBr}_2(\text{dpbz})_2]$	Fe-Br	2	2.31 (1)	0.003 (1)	0 (1)	0.03
	Fe-P	2	2.46 (1)	0.003 (1)		

Fitting parameters: $S_0^2 = 0.8$; Fit range $3 < k < 15.3$, $1 < R < 2.7$; # of independent points = 13

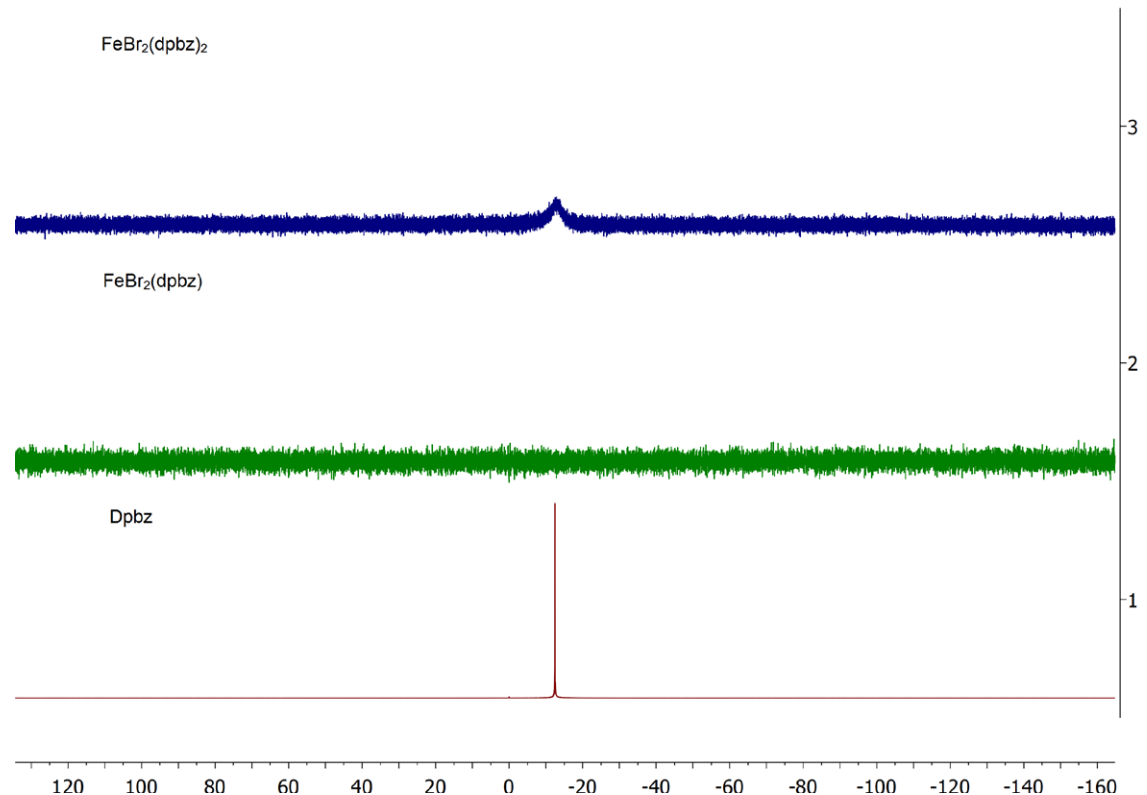
Supplementary Table 7. Simulated EXAFS fitting parameters for **4a**, S_0^2 fixed

Sample	Abs Sc	N	R / Å	$2\sigma^2 / \text{\AA}^2$	E_f / eV	R _{factor}
$[\text{FeBr}_2(\text{dpbz})_2]$	Fe-Br	2.3 (1)	2.31 (1)	0.003 (1)	0 (1)	0.02
	Fe-P	2.2(1)	2.46 (1)	0.003 (1)		

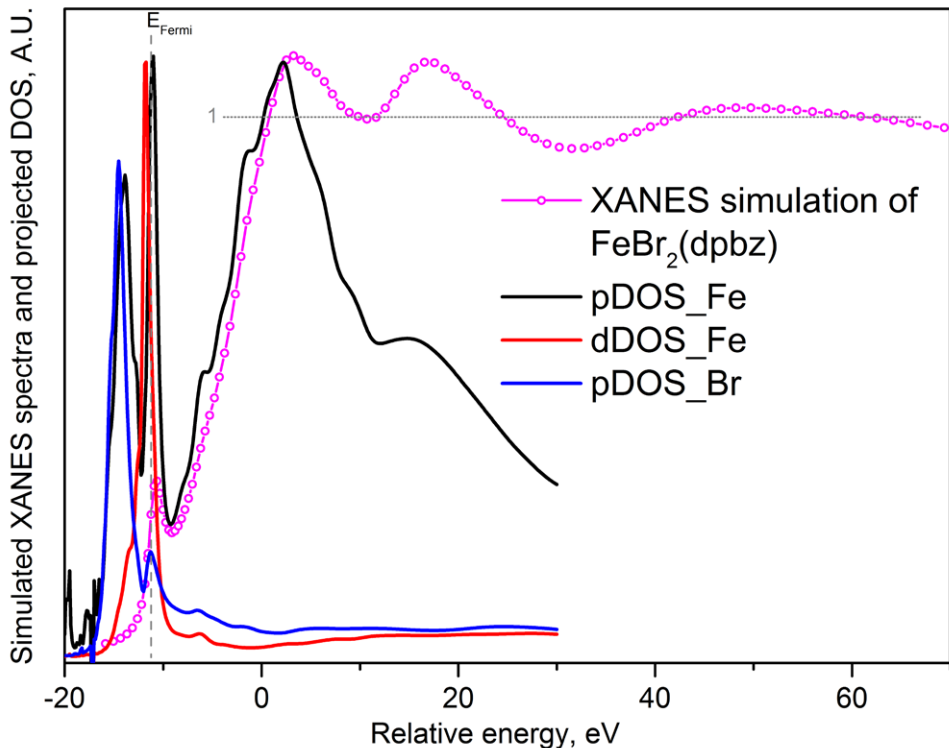
Fitting parameters: $S_0^2 = 0.8$; Fit range $3 < k < 15.3$, $1 < R < 2.7$; # of independent points = 13



Supplementary Figure 72. **(a)** Magnitude and imaginary k^3 Fourier transform data with simulated fit for $[\text{FeBr}_2(\text{dpbz})_2]$ **(7a)** solution in THF, fit consistent with the structure $[\text{FeBr}_2(\text{dpbz})]$ **(4a)** in solution, fixed coordination number **(b)** fixed S_0^2 .



Supplementary Figure 73. ^{31}P NMR spectra (122 MHz, $\text{THF}-d_8$) of dpbz, $[\text{FeBr}_2(\text{dpbz})]$ **(4a)** and $[\text{FeBr}_2(\text{dpbz})_2]$ **(7a)**.



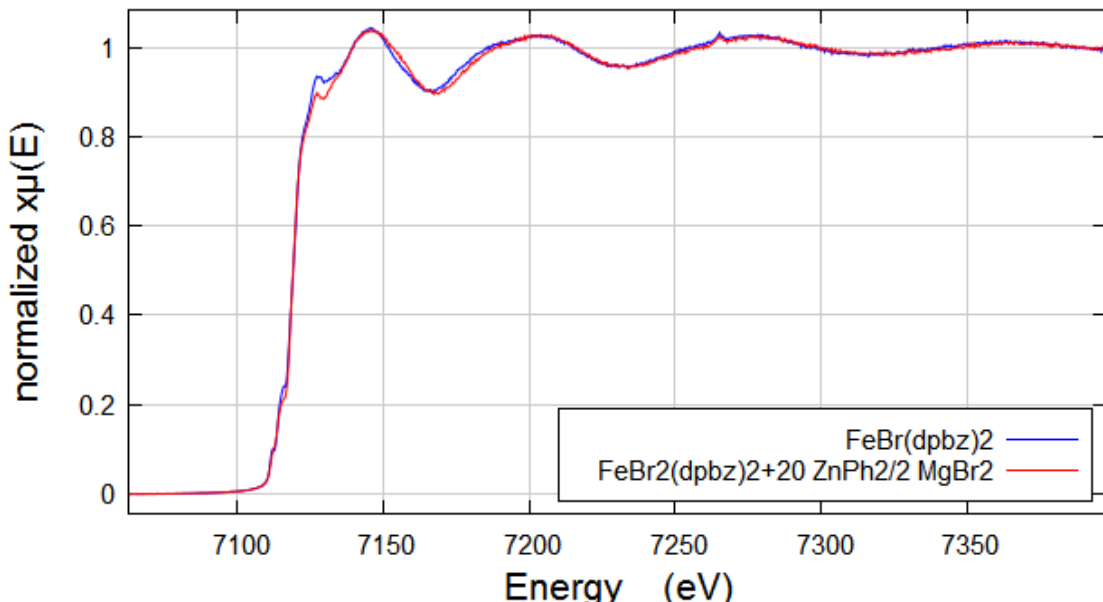
Supplementary Figure 74. XANES simulation of $[\text{FeBr}_2(\text{dpbz})]$ (**4a**) obtained using the FEFF8.4 code.

6.3.3 XAFS Spectroscopy of solutions of iron(I) complex of dpbz and the reduction of Fe(II) to Fe(I)

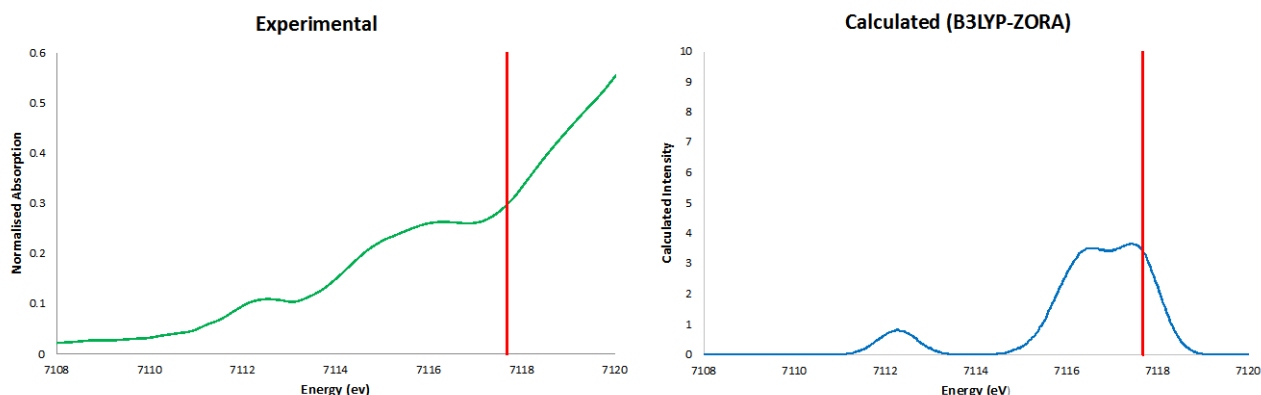
Supplementary Figure 77 shows the Fe K-edge normalized XANES spectra of the pre-formed iron(I) $[\text{FeBr}(\text{dpbz})_2]$ (**9a**) and the reaction mixture obtained on reacting the iron(II) precursor $[\text{FeBr}_2(\text{dpbz})_2]$ (**7a**) with 20 equivalents of $\text{ZnPh}_2/2 \text{MgBr}_2$. It is clear from the very close similarity of the spectra that **7a** is readily reduced to **9a** by the addition of the diarylzinc reagent.

To the best of our knowledge, this is the first example of an XAFS spectrum being recorded for a mononuclear, low spin Fe(I) complex. We therefore explored modelling the spectrum using TD-DFT as implemented in Orca 3.0.0,²² using a previously calculated geometry for $[\text{FeBr}(\text{dpbz})]$, **9a**.¹⁹ The near-edge region of the XAFS spectrum of complex **9a** was modelled using TD-DFT with the B3LYP functional,²³⁻²⁶ in combination with the ZORA-def2-TZVP basis set and def2-TZVP/J auxiliary basis sets and scalar relativistic effects were introduced using the zeroth order regular approximation (ZORA).²⁷⁻²⁹ The calculation was accelerated by using the RIJCOSX approximation.³⁰ A dense integration grid (grid4 nofinalgrid) was used, with a special grid integration accuracy of 7 specified for iron to increase the radial integration accuracy. Only singlet excitations from localised iron 1s orbitals were allowed. The maximum number of expansion vectors allowed in the iterative solution were 500, and 50 roots were used. A constant energy shift of 23.5 eV was applied to the calculated spectrum. Supplementary Figure 76 shows an expansion of the pre-edge/rising edge region (top) and the calculated spectrum is shown beneath. The red line

on both plots represents the position of the ionisation threshold of the 1s orbital. It should be noted that TD-DFT cannot realistically model near or beyond this point, therefore only data to the left of the threshold can be compared. It is clear that the pre-edge features below the ionisation threshold are well modelled by the TD-DFT analysis.



Supplementary Figure 75. Fe K edge normalised XANES spectra of $[\text{FeBr}(\text{dpbz})_2]$ (**9a**) and a mixture of $[\text{FeBr}_2(\text{dpbz})_2]$ (**7a**) with 20 equivalents of $\text{ZnPh}_2/2 \text{MgBr}_2$.



Supplementary Figure 76. The near-edge region of the XAFS spectrum of $[\text{FeBr}(\text{dpbz})_2]$ (**9a**) (left) and TD-DFT calculated spectrum for the near-edge region (right). The red vertical line on both plots indicates the calculated ionisation threshold (7117.7 eV) for the Fe 1s orbital.

6.4 Operando Flow-XAFS investigations of the iron speciation during the $[\text{FeBr}_2(\text{dpbz})_2]$ (**7a**) catalysed Negishi cross-coupling

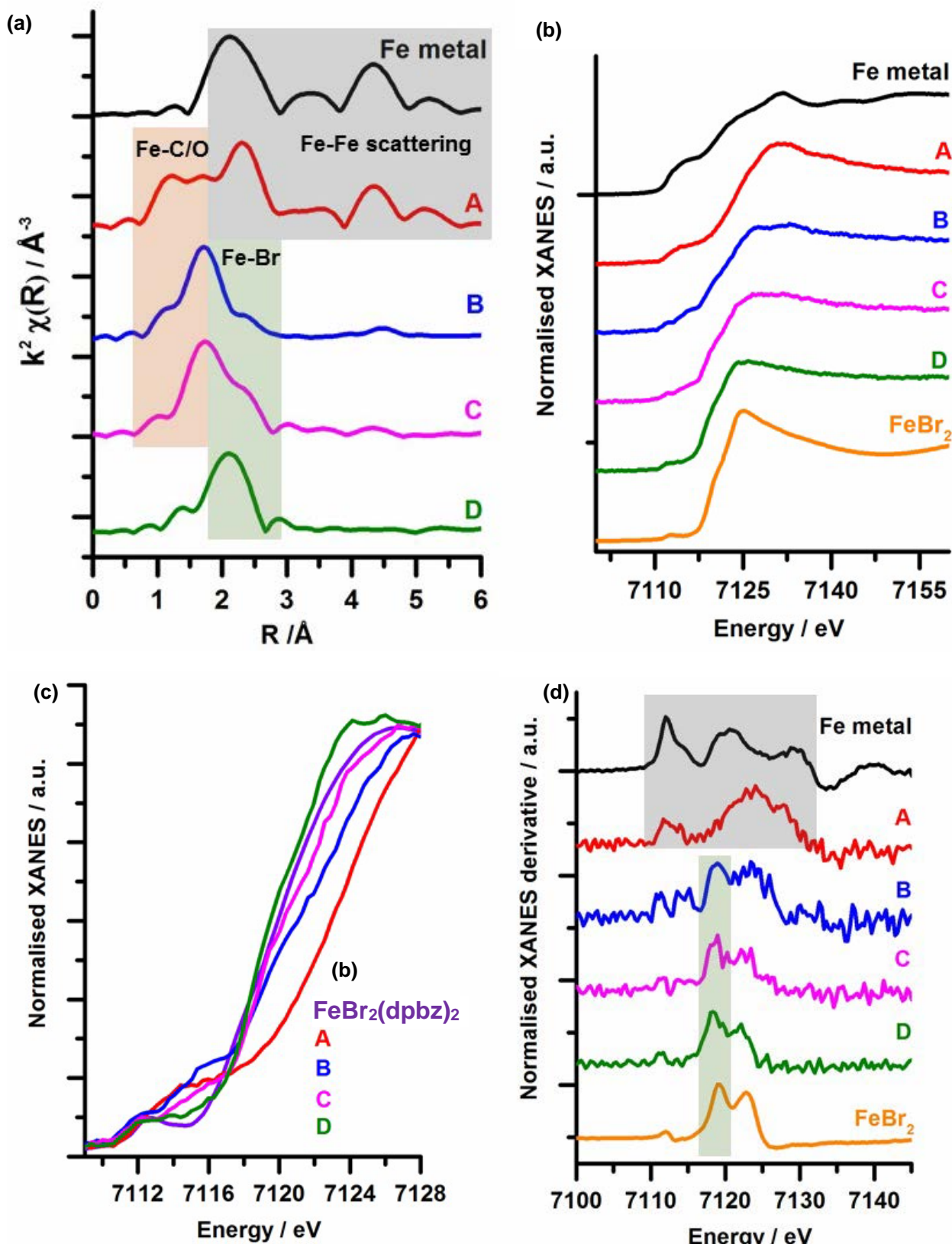
Using the continuous flow reactor described above (section 6.2) and the conditions outlined in Supplementary Table 3 the speciation of the iron was studied in the Negishi coupling of **1** with **2a** using **7a** as a pre-catalyst at four distinct time-points (**A – D**, Supplementary Table 4) using a combination of both the X-ray absorption near edge structure (XANES) and extended X-ray absorption fine structure (EXAFS). This showed significant changes to the catalyst structure during the course of the reaction (Supplementary Figure 77). At time point

A the EXAFS data (Supplementary Figure 77(a)) indicate significant long-range ordering and there are readily identifiable scattering paths consistent with metallic Fe⁰. The EXAFS data are well-modelled (Supplementary Figure 78, Supplementary Table 8) using scattering paths from metallic Fe and additional Fe-C/O scattering paths at 1.85 and 2.05 Å. Inclusion of additional Fe-Br and Fe-P paths was detrimental to the agreement of the experimental and simulated EXAFS data (Supplementary Table 9 and Supplementary Figure 79). A comparison of the XANES spectrum at time-point **A** (Supplementary Figure 77(b)-(d)) with that for Fe metal shows the broad nature of the pre-edge feature observed at 7115 eV is characteristic of Fe metal and supports the observations in the EXAFS data. No build-up of Fe(0) at time point **A**, or the other time points sampled, was observed. Were Fe(0) precipitates to have been deposited on the Kapton window then the fluorescence yield measured from the solid state Ge detector would have increased with increasing time; this was not observed, for example see the overlaid raw K edge data at time point **A** in Supplementary Figure 81.

The XANES spectra at time points **A – D** (Supplementary Figure 77 (b)-(d)) show a shift of the main edge to higher energy as the reaction progresses. The shift to higher energy is most commonly linked to a change in oxidation state, however here it can be correlated to a loss of halide. Previous studies have shown that the 1st row transition metal halides have apparent edge positions much lower than expected as a result of transitions to *p* orbitals arising from the coordinated ligand.³¹ A comparison of the XANES spectra of FeBr₃ and Fe₂O₃ (Supplementary Figure 80) show ~ 5 eV shift in edge position and confirm this is also the case for systems with Br coordinated to Fe.

At time point **B** the EXAFS data (Supplementary Figure 77(a)) show a loss of metallic structure, with the XANES confirming the presence of halide neighbours by a shift of the main edge to lower energy (Supplementary Figure 77(c)). This shift to lower energy is manifested in the derivative of the XANES spectrum (Supplementary Figure 77 (d)) by a peak at 7119 eV, which is readily identifiable in the reference spectrum of FeBr₂. A simulation of the EXAFS data (Supplementary Figure 78, Supplementary Table 8) collected from position **B** is achieved by a fitting model incorporating three scattering paths of Fe-C/O, Fe-C/O and Fe-Br. Assessing further positions along the flow channel (point **C**, t = 482 s, yield = 65% & point **D**, t = 817 s, yield = 78%) further changes to the Fe speciation are observed; at further time points there is a reduction in Fe-C/O scattering interactions, whilst Fe-Br scattering events increase (Supplementary Figure 78, Supplementary Table 8). At point **D** the EXAFS data can be modelled in their entirety with a primary coordination sphere consisting solely of Fe-Br. An alternative fit which includes Fe-P paths is shown in Supplementary Table 10 and Supplementary Figure 82. When the coordination number was

allowed to refine, the CN for Fe-P refines to 0.3 ± 0.2 , good evidence that there are no Fe-P interactions present. On allowing σ^2 to refine, a negative value was achieved, which is not physically possible – further evidence that there are no Fe-P scattering paths present.



Supplementary Figure 77. **(a)** magnitude k^2 Fourier transform data of Fe foil and the $[\text{FeBr}_2(\text{dpbz})_2]$ (**7a**) mediated cross-coupling reaction between **1** and **2a** in THF at different time points along a continuous flow path; position **A**: $t = 6 \text{ s}$, position **B**: $t = 166 \text{ s}$, position **C**: $t = 482 \text{ s}$ and position **D**: $t = 817 \text{ s}$; **(b)** normalised XANES spectra of Fe foil, FeBr_2 and

positions **A** – **D**; (**c**) normalised XANES data showing close up of edge position of $[\text{FeBr}_2(\text{dpbz})_2]$ (**7a**) and positions A-D; and (**d**) normalised XANES derivative spectra of Fe foil, FeBr_2 and positions **A** – **D**.

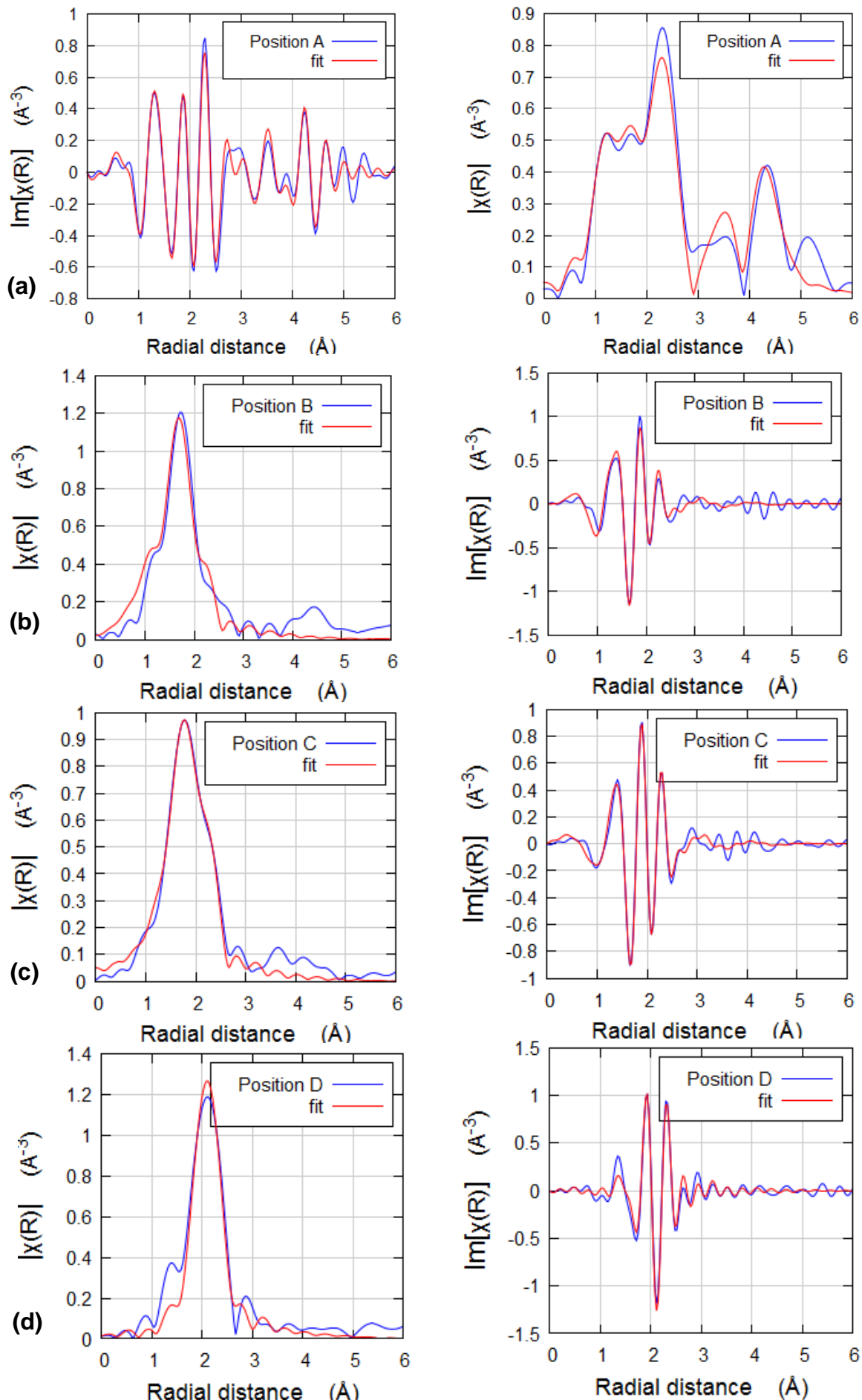
Supplementary Table 8. Simulated EXAFS fitting parameters for the $[\text{FeBr}_2(\text{dpbz})_2]$ (**7a**) mediated cross-coupling reaction between **1** and **2** in THF at different time points along a continuous flow path; position **A**: $t = 6$ s, position **B**: $t = 166$ s, position **C**: $t = 482$ s and position **D**: $t = 817$ s.

Sample	Abs Sc	N	R / Å	$2\sigma^2 / \text{\AA}^2$	E_f / eV	R _{factor}
Position A ^a (Fit 53)	Fe-C/O	2.0	1.85 (2)	0.003 (4)	-4 (2)	0.03
	Fe-C/O	2.0	2.04 (2)	0.003 (4)		
	Fe-Fe	2.4	2.492 (1)	0.008 (1)		
	Fe-Fe	1.8	2.876 (1)	0.008 (1)		
	Fe-Fe-Fe	14.4	3.96 (3)	0.008 (4)		
	Fe-Fe	3.6	4.10 (3)	0.008 (4)		
	Fe-Fe-Fe	14.4	4.556 (2)	0.03 (3)		
	Fe-Fe	7.2	4.762 (2)	0.03 (3)		
Position B ^b	Fe-C/O	1	1.75 (5)	0.002 (2)	-4 (3)	0.03
	Fe-C/O	3	1.98 (2)	0.002 (2)		
	Fe-Br	2	2.36 (3)	0.005 (2)		
Position C ^b	Fe-C/O	1.6 (2)	2.05 (3)	0.003 (2)	6 (3)	0.01
	Fe-Br	4 (1)	2.42 (1)	0.009 (3)		
Position D ^b	Fe-Br	2	2.33 (5)	0.004 (3)	-4 (5)	0.04
	Fe-Br	2	2.45 (3)	0.002 (2)		

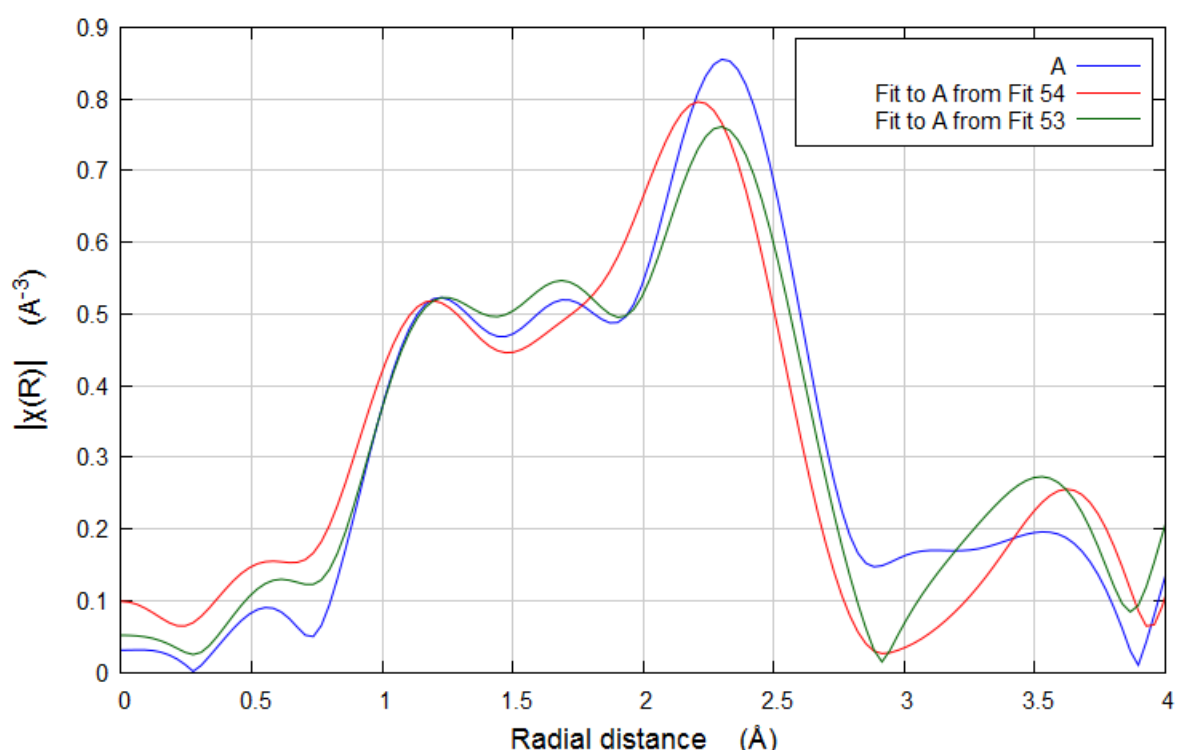
Fitting parameters: $S_0^2 = 0.8$ as deduced by $[\text{FeBr}_2(\text{dpbz})_2]$ standard; ^a Fit range $3 < k < 9.5$, $1 < R < 5$; number of independent points = 16; ^b Fit range $3 < k < 10.8$, $1 < R < 3$; number of independent points = 9;

Supplementary Table 9. Simulated EXAFS fitting parameters for the reaction of $[\text{FeBr}_2(\text{dpbz})_2] + \text{ZnPh}_2 + \text{BnBr} + \text{MgBr}_2$ at time position A, $t = 6$ s, using a fitting model incorporating Fe-Br and Fe-P paths.

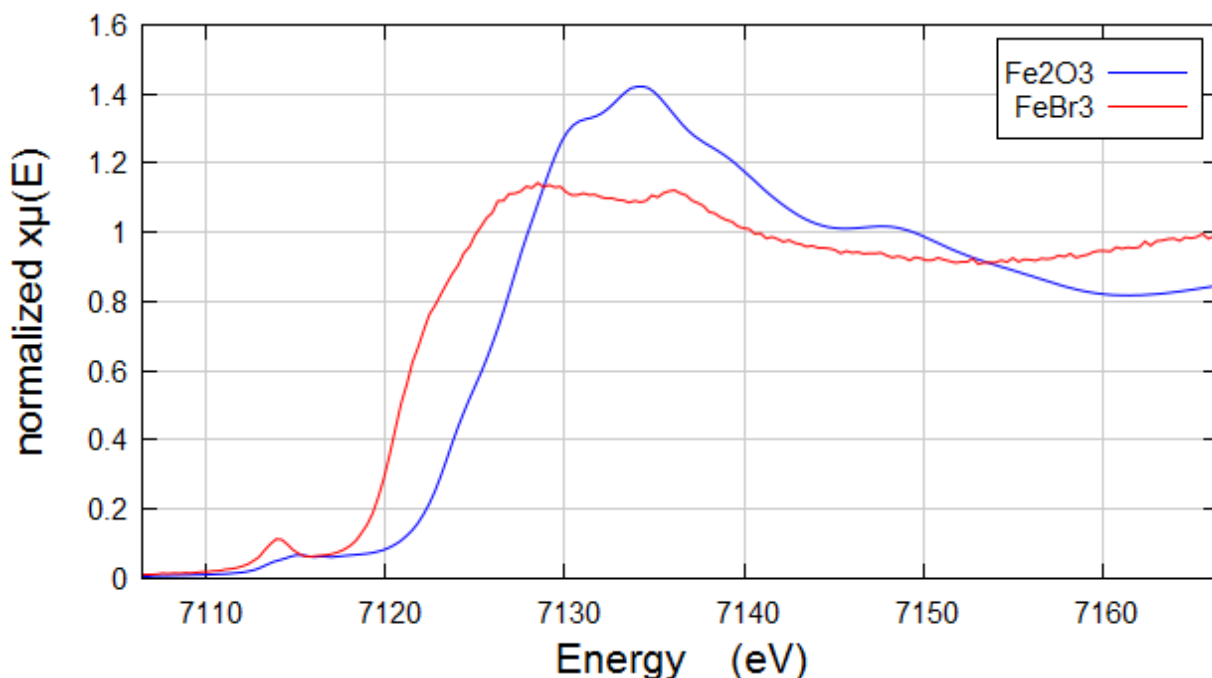
Sample (Fit)	Abs Sc	N	R / Å	$2\sigma^2 / \text{\AA}^2$	E_f / eV	R _{factor}
Position A (Fit 54)	Fe-P	1.6	1.73(3)	0.015 (4)	0 (2)	0.05
	Fe-Br	1.6	2.41 (4)	0.007 (5)		
	Fe-Fe	2.4	2.52 (4)	0.013 (1)		
	Fe-Fe	1.8	2.90 (4)	0.013 (1)		
	Fe-Fe-Fe	14.4	3.99 (7)	0.009 (4)		
	Fe-Fe	3.6	4.13 (7)	0.009 (4)		
	Fe-Fe-Fe	14.4	4.56 (7)	0.006 (3)		
	Fe-Fe	7.2	4.82(1)	0.07(3)		



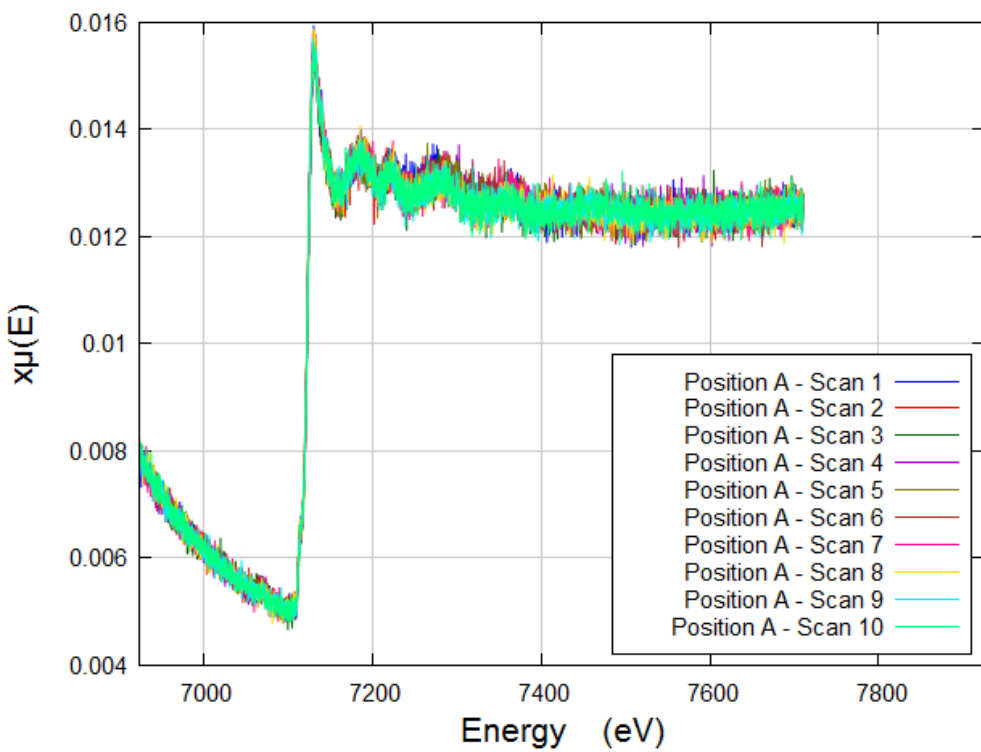
Supplementary Figure 78. Magnitude and imaginary k^2 Fourier transform data with simulated fit for the **7a** mediated cross-coupling reaction between **1** and **2** in THF at different time points along a continuous flow path **(a)** = position **A**, $t = 6$ s, **(b)** = position **B**, $t = 166$ s, **(c)** = position **C**, $t = 482$ s and **(d)** = position **D**, $t = 817$ s.



Supplementary Figure 79. Fourier transform k^2 weight EXAFS data for the reaction of $[\text{FeBr}_2(\text{dpbz})_2] + \text{ZnPh}_2 + \text{BnBr} + \text{MgBr}_2$ at time position **A**, $t = 6$ s, and associated fit: (i) Fit 54 – red line – is the model including Fe-Br and Fe-P scattering paths, (ii) Fit 53 is the model including Fe-C/O scattering paths.



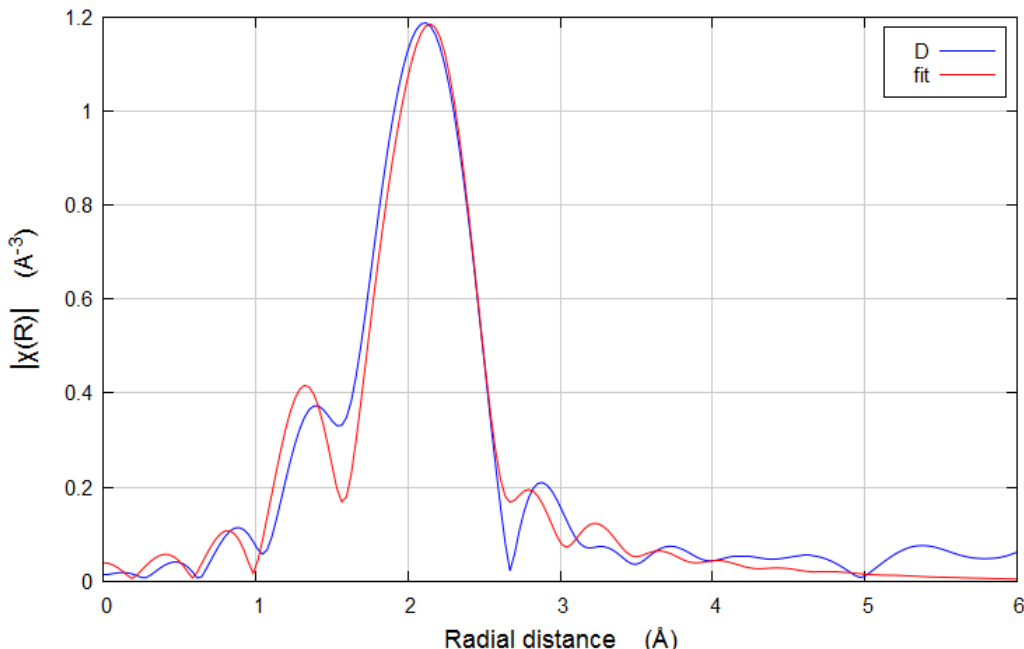
Supplementary Figure 80. Fe K edge normalized XANES spectra of Fe_2O_3 and FeBr_3 .



Supplementary Figure 81. Raw Fe K edge XAS data of position A during sequential measurement of 10 scans, each of 70 s.

Supplementary Table 10. Alternative simulated EXAFS fitting parameters for the reaction of $[\text{FeBr}_2(\text{dpbz})_2] + \text{ZnPh}_2 + \text{BnBr} + \text{MgBr}_2$ at time position **D**, using a fitting model with Fe-P scattering paths

Sample	Abs Sc	N	R / Å	2σ² / Å²	E _f / eV	R _{factor}
Position D#	Fe-P	0.3(2)	1.79 (5)	0.003	0 (6)	0.05
	Fe-Br	2.5 (3)	2.44 (1)	0.003		

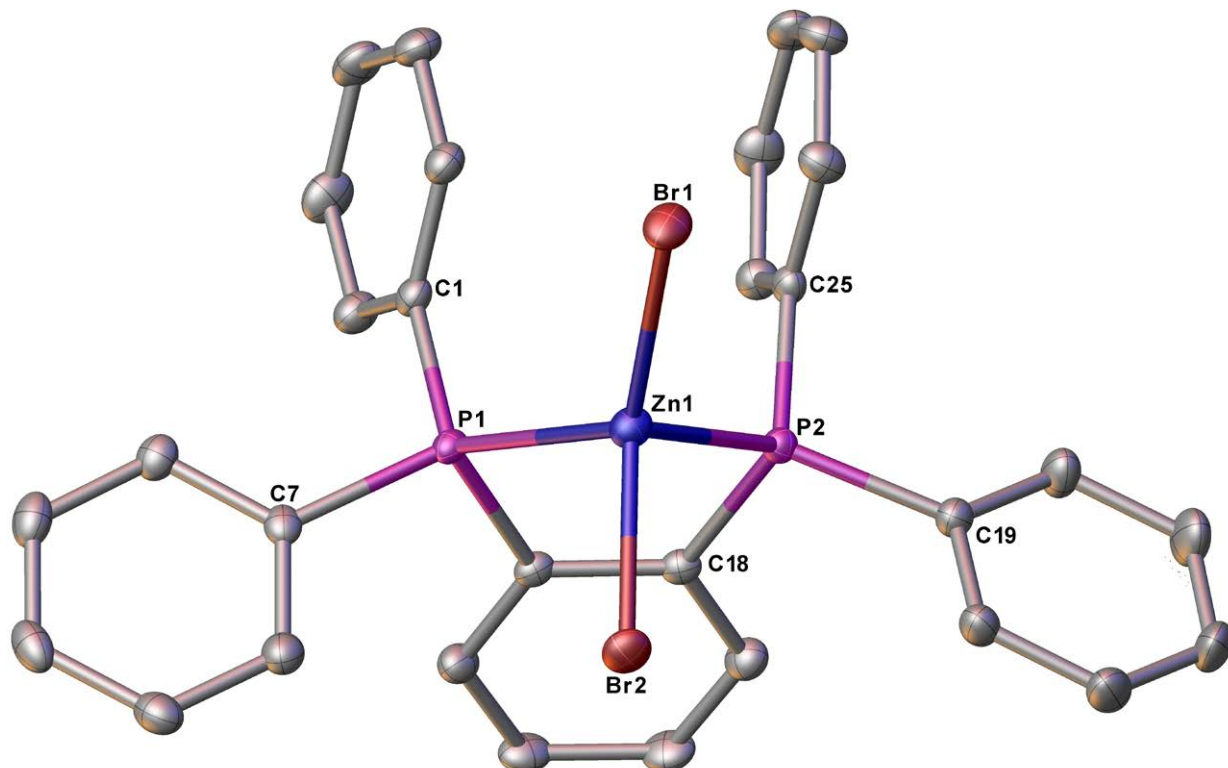


Supplementary Figure 82. Fourier transform k^2 weight EXAFS data for the reaction of $[\text{FeBr}_2(\text{dpbz})_2] + \text{ZnPh}_2 + \text{BnBr} + \text{MgBr}_2$ at time position **D**, and alternative associated fit, achieved with scattering paths of Fe-P and Fe-Br.

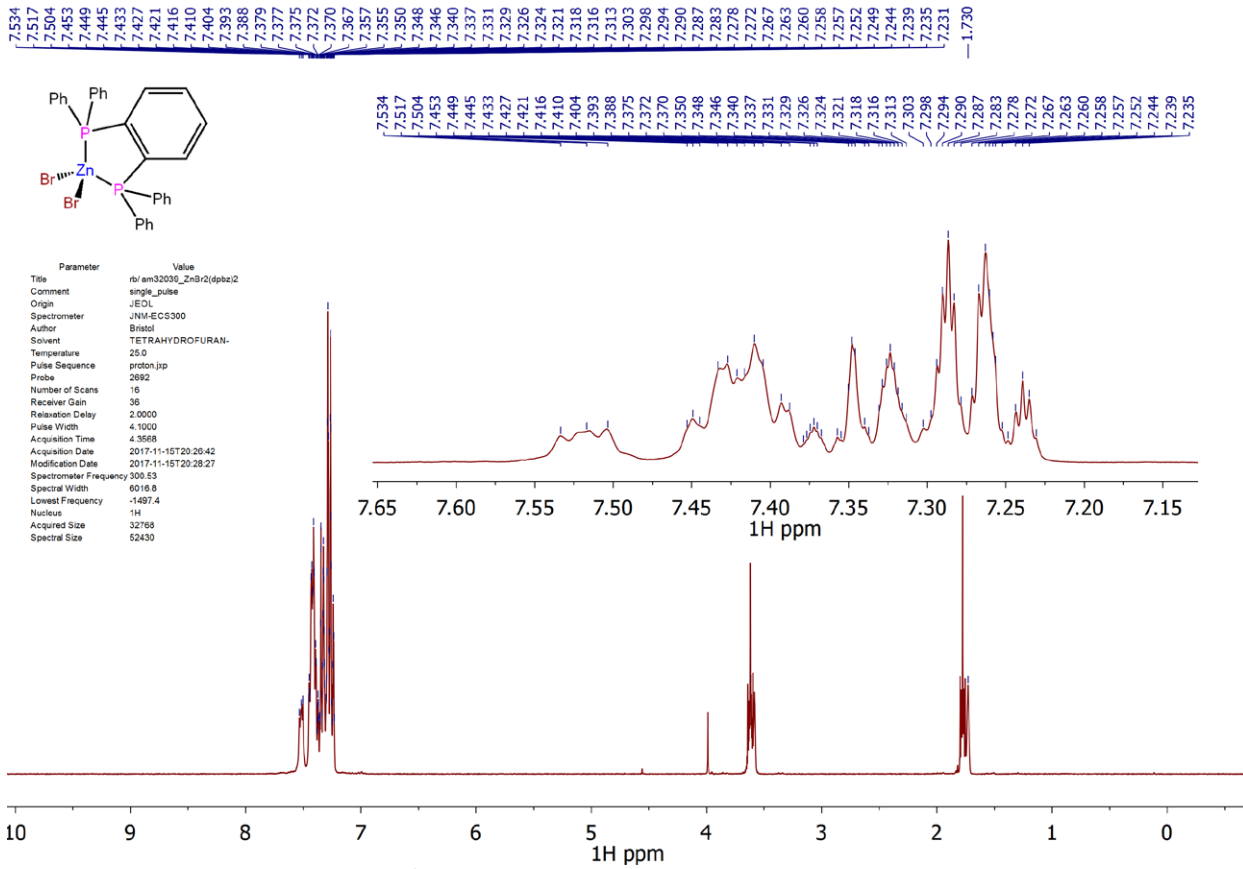
7 Synthesis of ZnBr₂ diphosphine complexes.

7.1 [ZnBr₂(dpbz)] (12a)

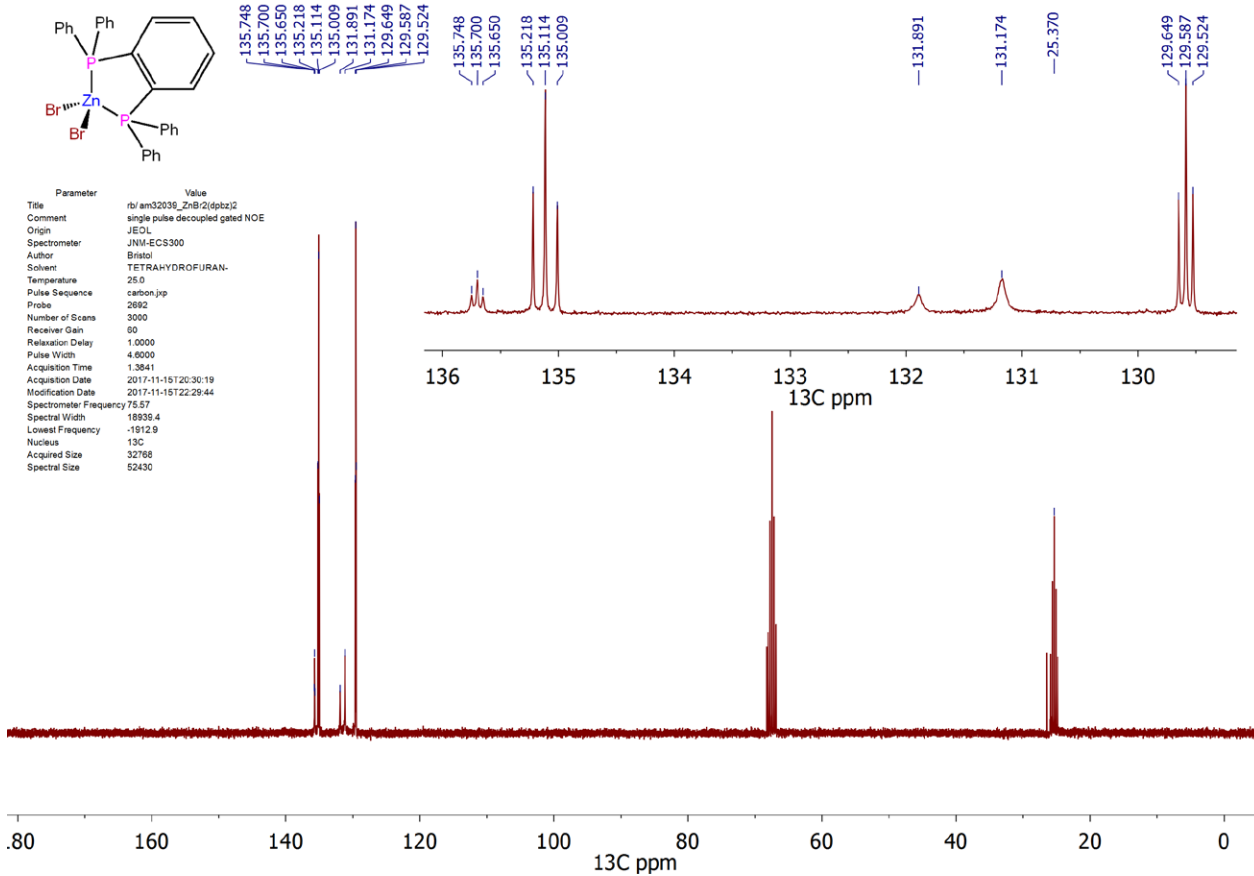
A Schlenk was loaded with ZnBr₂ (250 mg, 1.11 mmol), dpbz (495.6 mg, 1.11 mmol) and THF (16 mL) and the mixture was heated with a heat gun until all components dissolved. Upon cooling, colourless crystals were formed which were isolated by decanting the supernatant and washed with THF (3 mL). The crystals were ground and the resultant powder was left under vacuum for 12h to give **12a** THF (671 mg, 81%) as a white solid. Crystals of **12a** suitable for an X-ray crystallographic analysis were grown by allowing a boiled solution of the compound in THF to slowly cool to room temperature. ¹H NMR (301 MHz, THF-*d*₈) δ = 7.57-7.49 (m, 2H), 7.48-7.16 (m, 22H). ¹³C NMR (76 MHz, THF-*d*₈) δ = 135.7 (t, *J*=3.7), 135.1 (t, *J*=7.9), 131.9 (br s, 5.31), 131.2 (br s, 5.63), 129.6 (t, *J*=4.7). ³¹P NMR (122 MHz, THF-*d*₈) δ = -22.2 (br s, 254.3). Anal. Calcd for C₃₄H₃₂Br₂OP₂Zn: C, 54.91; H, 4.34 Found: C, 54.96; H, 4.32. HRMS (ESI/Q-TOF) m/z: [M+Na]⁺ Calcd for C₃₀H₂₄Br₂NaP₂Zn 690.8909; Found 690.8904.



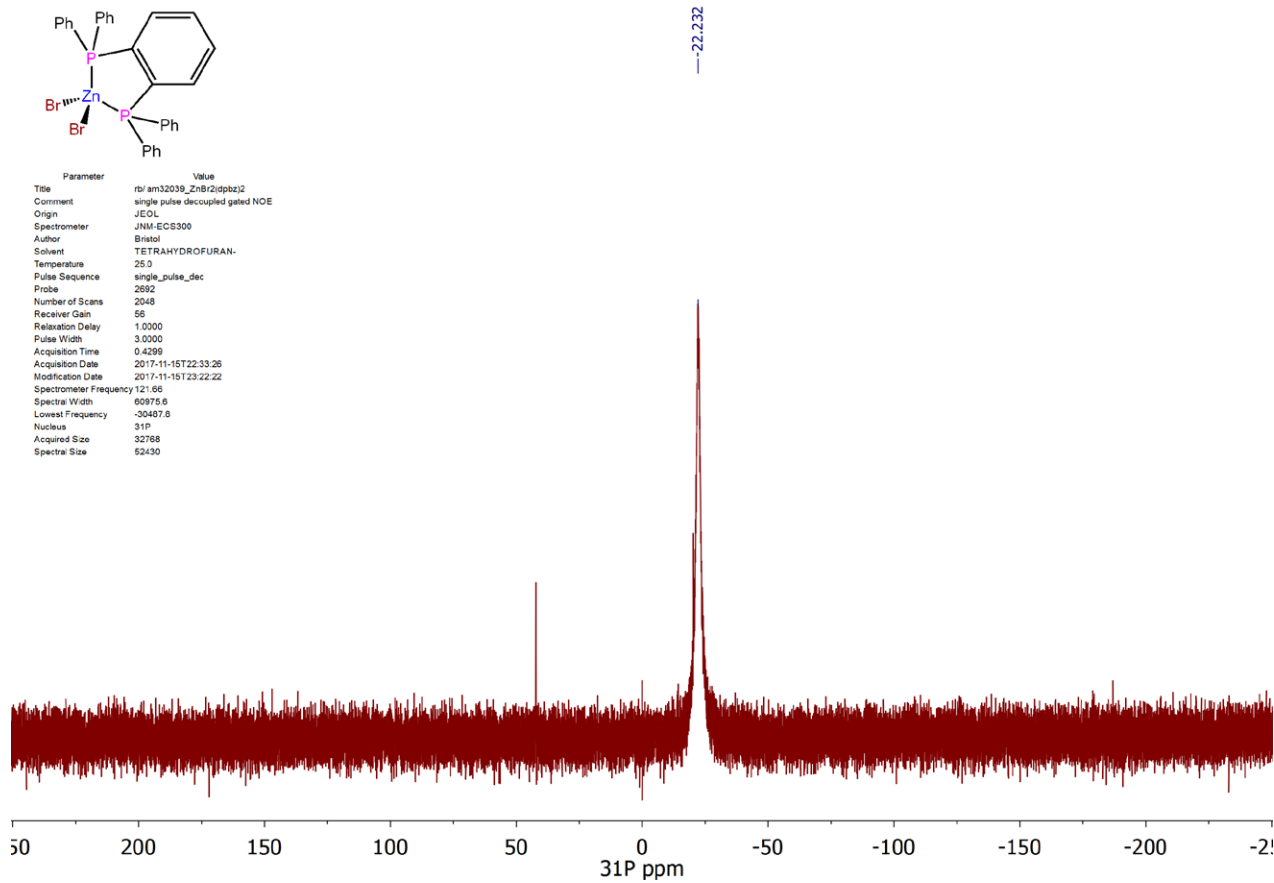
Supplementary Figure 83. Single-crystal X-ray structure of [ZnBr₂(dpbz)] (**12a**). Hydrogen atoms and solvent molecules are omitted for clarity. Thermal ellipsoids are set at the 50% probability level.



Supplementary Figure 84. ^1H NMR spectrum (300 MHz, THF- d_8) of **12a**.



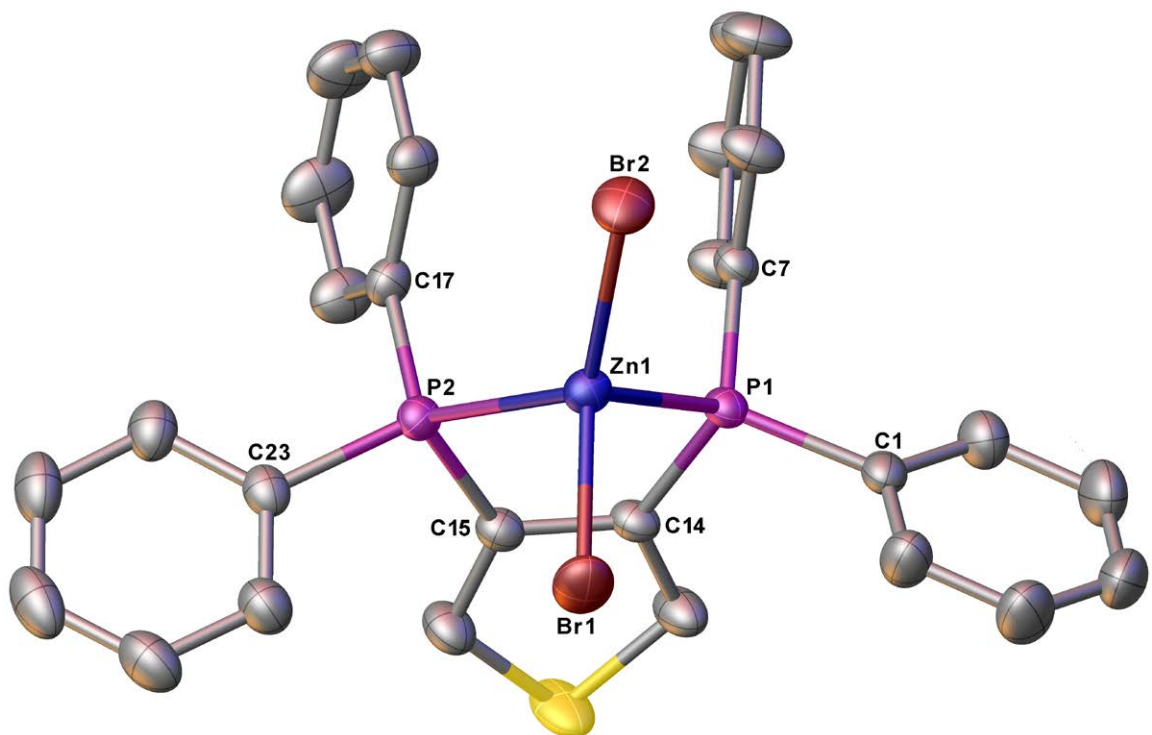
Supplementary Figure 85. ^{13}C NMR spectrum (76 MHz, THF- d_8) of **12a**.



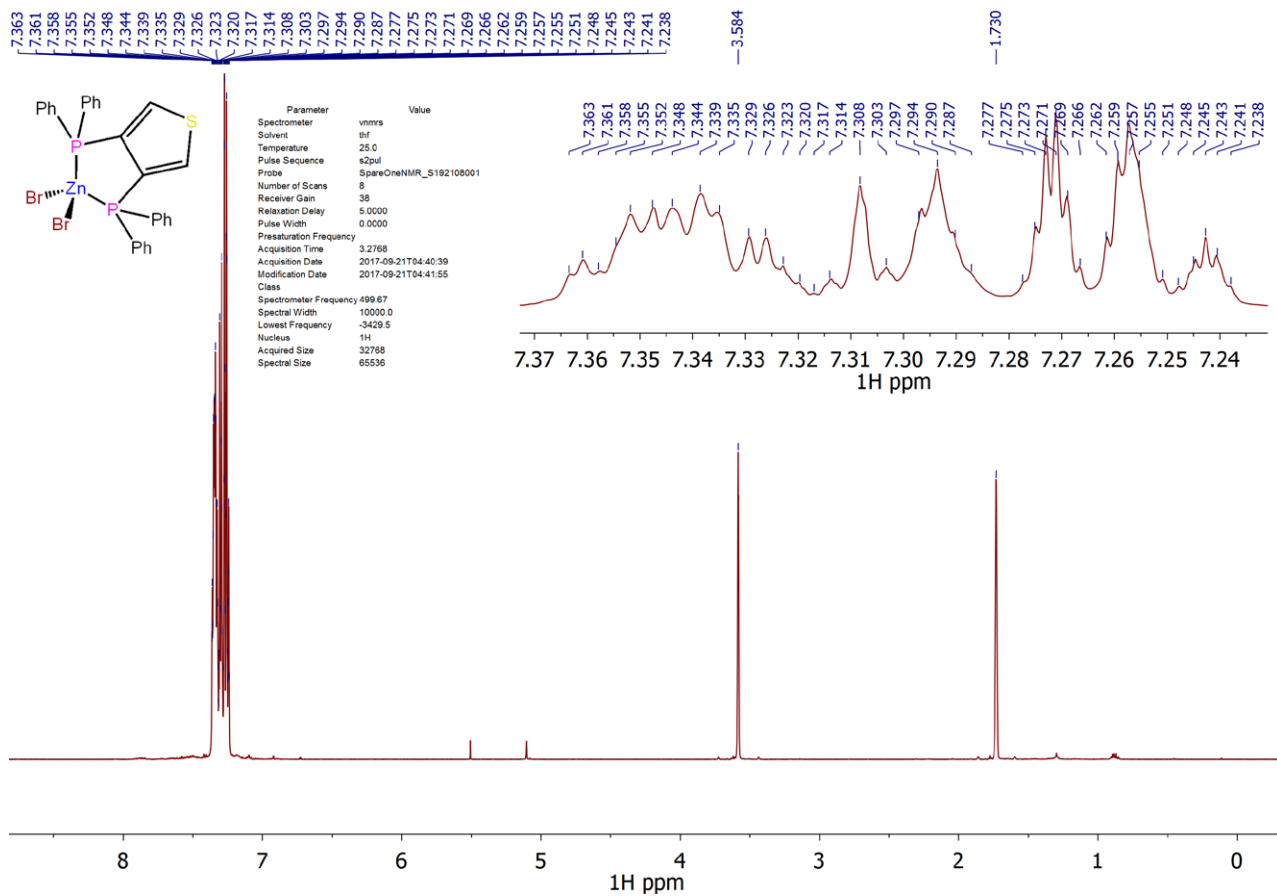
Supplementary Figure 86. ^{31}P NMR spectrum (122 MHz, THF- d_8) of **12a**.

7.2 $[\text{ZnBr}_2(\text{dpht})]$ (12b)

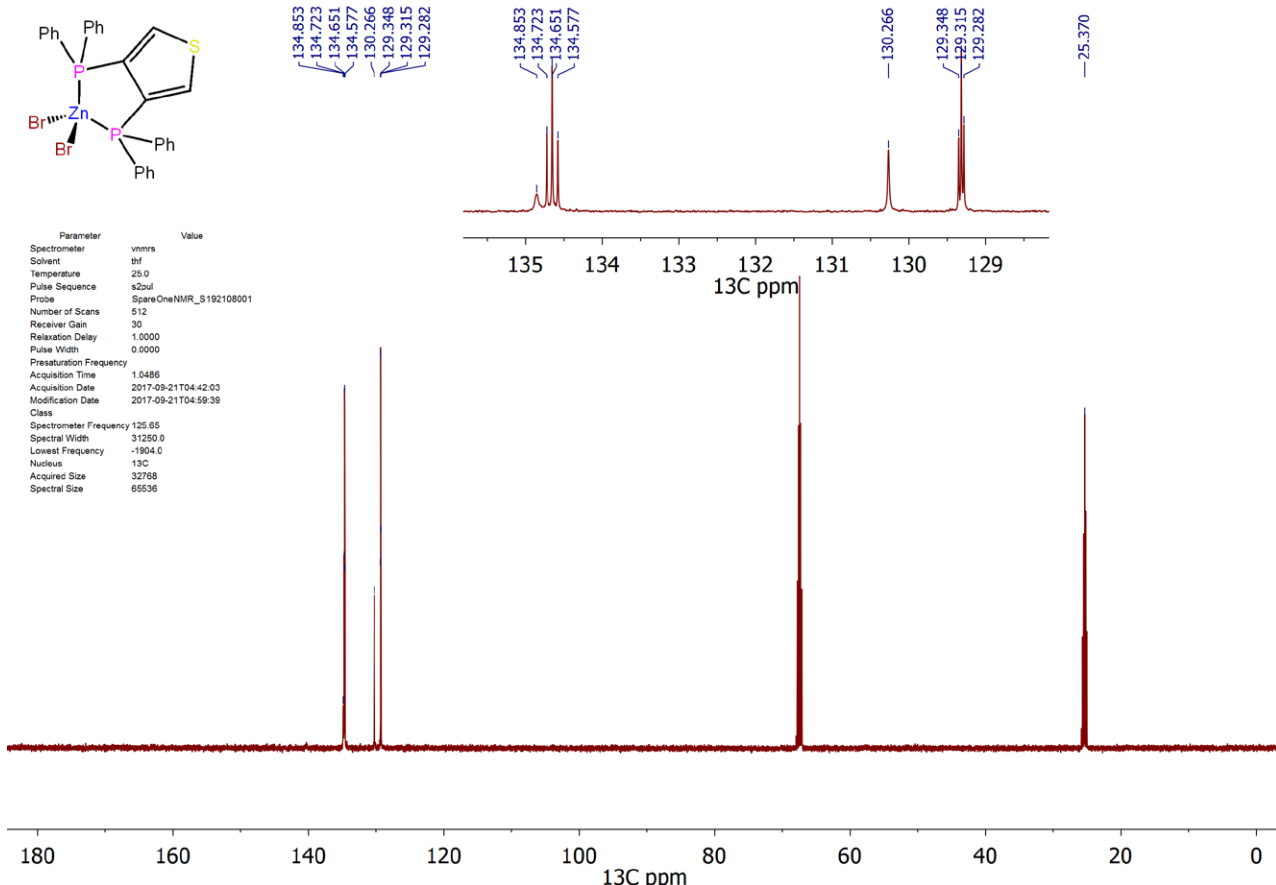
In an argon filled glove box, a vial was loaded with dpht (93.6 mg, 0.207 mmol), ZnBr_2 (46.6 mg, 0.207 mmol), CH_2Cl_2 (2 mL) and 7 drops of THF. After standing for 12 hours a colourless solution formed which was filtered and layered with hexane (4 mL). After 24 hours, colourless crystals suitable for an X-ray crystallographic analysis formed which were isolated by decanting the supernatant solution, dried under reduced pressure, ground and further dried under reduced pressure for 12 hours to give **12b**-1/3 CH_2Cl_2 (129.9 mg, 88%) as a white powder. ^1H NMR (500 MHz, THF- d_8) δ = 7.41-7.19 (m, 22H). ^{13}C NMR (126 MHz, THF- d_8) δ = 134.9, 134.7 (t, $J=9.2$), 130.3, 129.3 (t, $J=4.1$). ^{31}P NMR (202 MHz, THF- d_8) δ = -27.2. Anal. Calcd for $\text{C}_{28.33}\text{H}_{22.67}\text{Br}_2\text{Cl}_{0.67}\text{P}_2\text{S}\text{Zn}$: C, 48.20; H, 3.24 Found: C, 48.62; H, 3.19. HRMS (ESI/Q-TOF) m/z: [M+Na]⁺ Calcd for $\text{C}_{28}\text{H}_{22}\text{Br}_2\text{NaP}_2\text{S}\text{Zn}$ 696.8473; Found 696.8468.



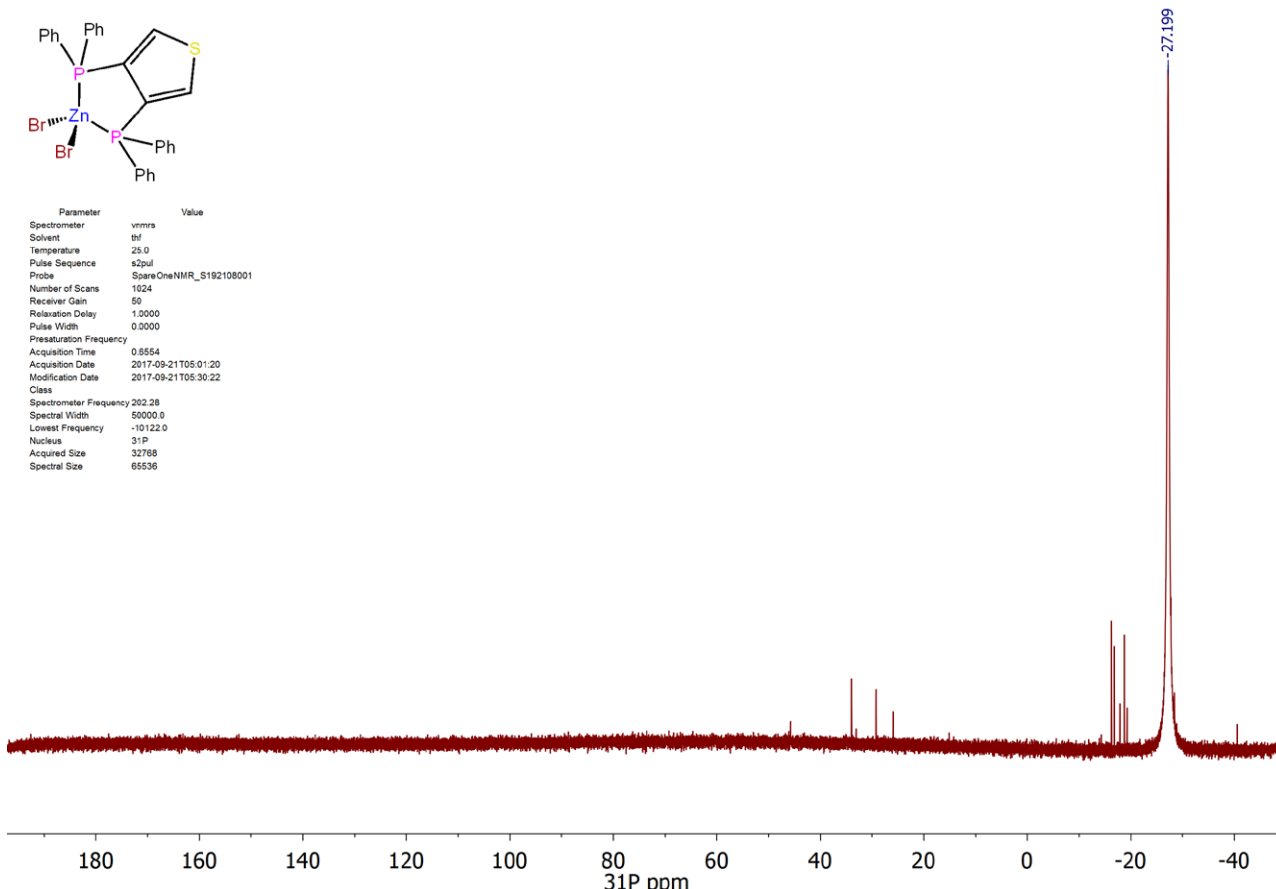
Supplementary Figure 87. Single-crystal X-ray structure of $[\text{ZnBr}_2(\text{dpht})]$ (**12b**). Hydrogen atoms and solvent molecules are omitted for clarity. Thermal ellipsoids are set at the 50% probability level.



Supplementary Figure 88. ^1H NMR spectrum (500 MHz, THF- d_8) of 12b.



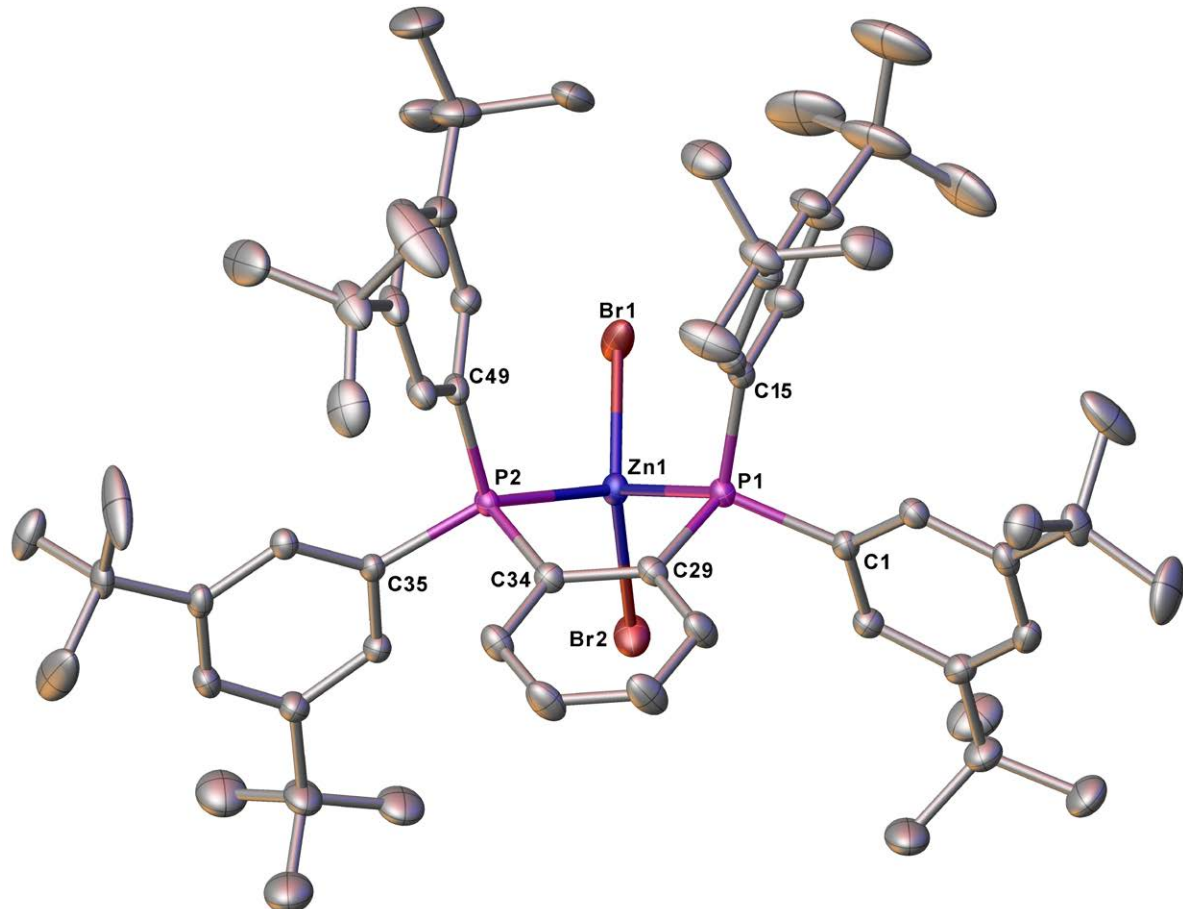
Supplementary Figure 89. ¹³C NMR spectrum (126 MHz, THF-*d*₈) of **12b**.



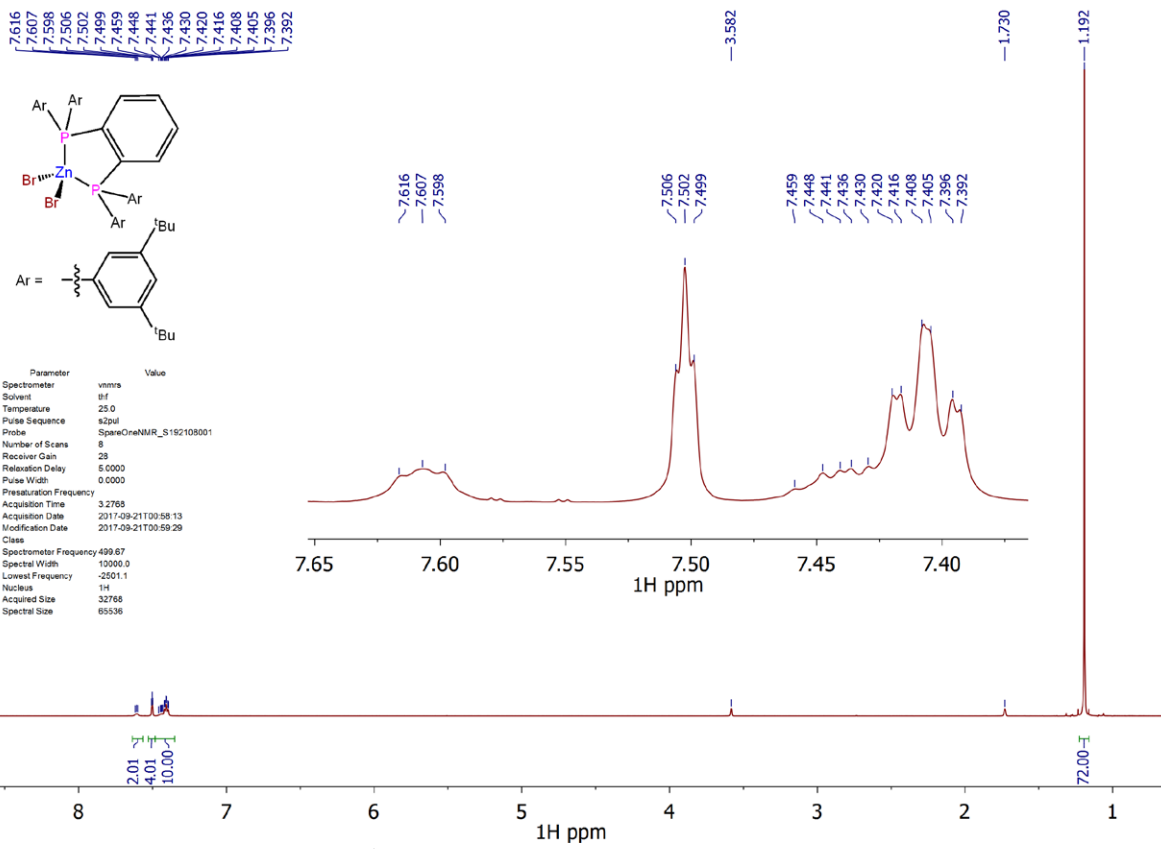
Supplementary Figure 90. ³¹P NMR spectrum (202 MHz, THF-*d*₈) of **12b**.

7.3 [ZnBr₂(sciopp)] (12c)

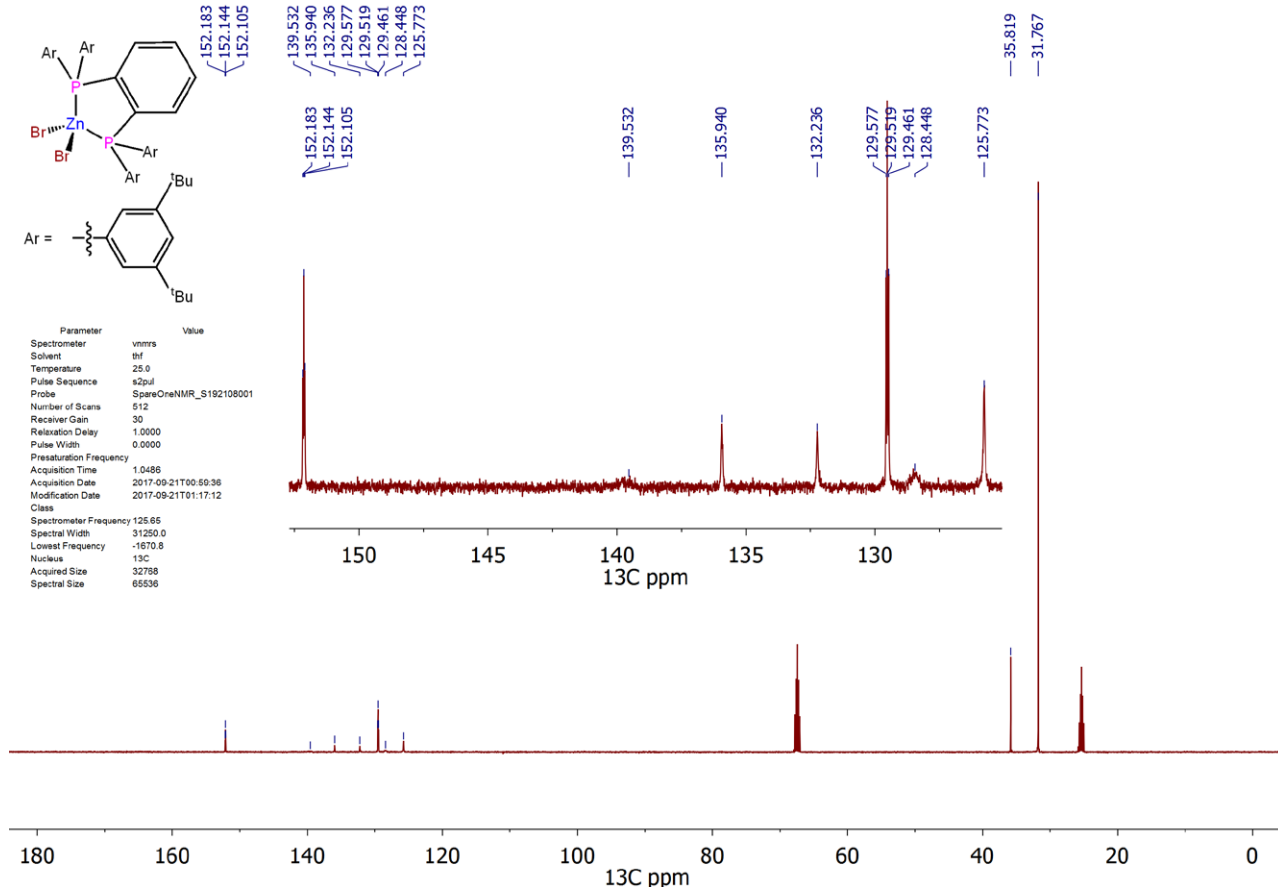
In an argon filled glove box, a vial was loaded with sciopp (87.7 mg, 0.098 mmol), ZnBr₂ (22.1 mg, 0.098 mmol) and toluene (2 mL). After standing for 12 hours a colourless solution formed which was filtered and layered with hexane (4 mL). After 24 hours, colourless crystals suitable for an X-ray crystallographic analysis formed which were isolated by decanting the supernatant solution, dried under reduced pressure, ground and further dried under reduced pressure for 12 hours to give **12c**·0.5 (C₇H₈) (80.4 mg, 70%) as a white powder. ¹H NMR (500 MHz, THF-d₈) δ = 7.61 (t, J=4.6, 2H), 7.50 (t, J=1.8, 4H), 7.47-7.37 (m, 10H), 1.19 (s, 72H). ¹³C NMR (126 MHz, THF-d₈) δ = 152.1 (t, J=4.9), 139.5 (br s, weak), 135.9, 132.2, 129.5 (t, J=7.3), 128.5 (br s. weak), 125.8, 35.9, 31.8. ³¹P NMR (202 MHz, THF-d₈) δ = -23.8. Anal. Calcd for C_{65.5}H₉₂Br₂P₂Zn: C, 67.44; H, 7.95 Found: C, 67.42; H, 8.16. HRMS (ESI/Q-TOF) m/z: [M+Na]⁺ Calcd for C₆₂H₈₈Br₂NaP₂Zn 1139.3917; Found 1139.3912.



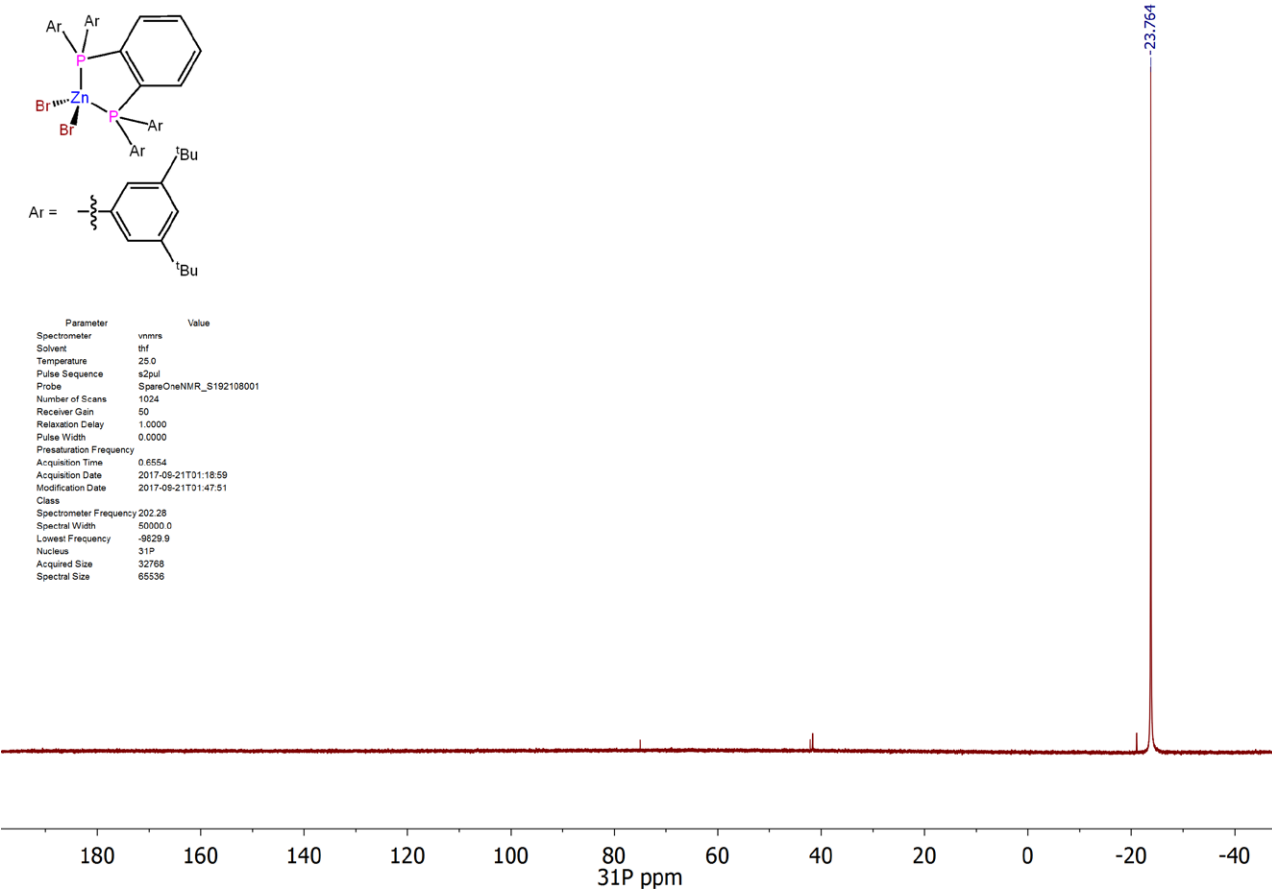
Supplementary Figure 91. Single-crystal X-ray structure of **12c**. Hydrogen atoms and solvent molecules are omitted for clarity while thermal ellipsoids are set at the 50% probability level.



Supplementary Figure 92. ^1H NMR spectrum (500 MHz, $\text{THF}-d_8$) of **12c**.



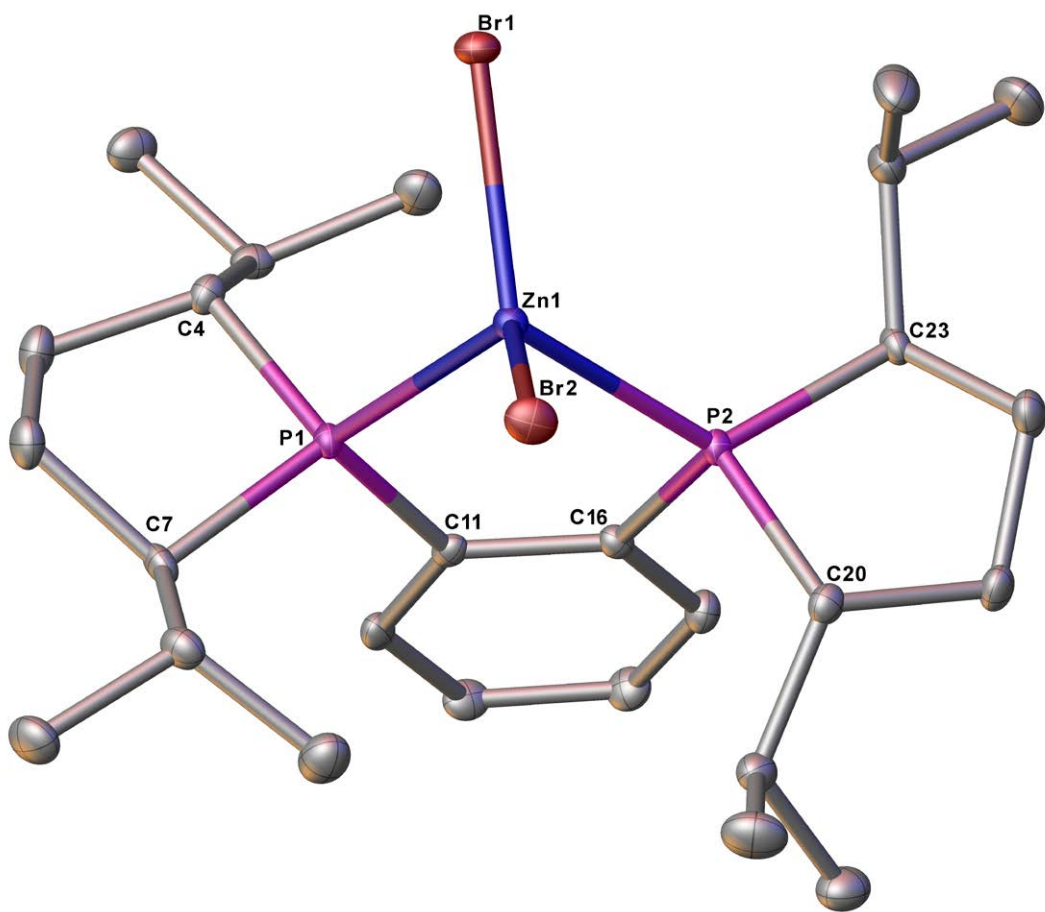
Supplementary Figure 93. ^{13}C NMR spectrum (126 MHz, $\text{THF}-d_8$) of **12c**.



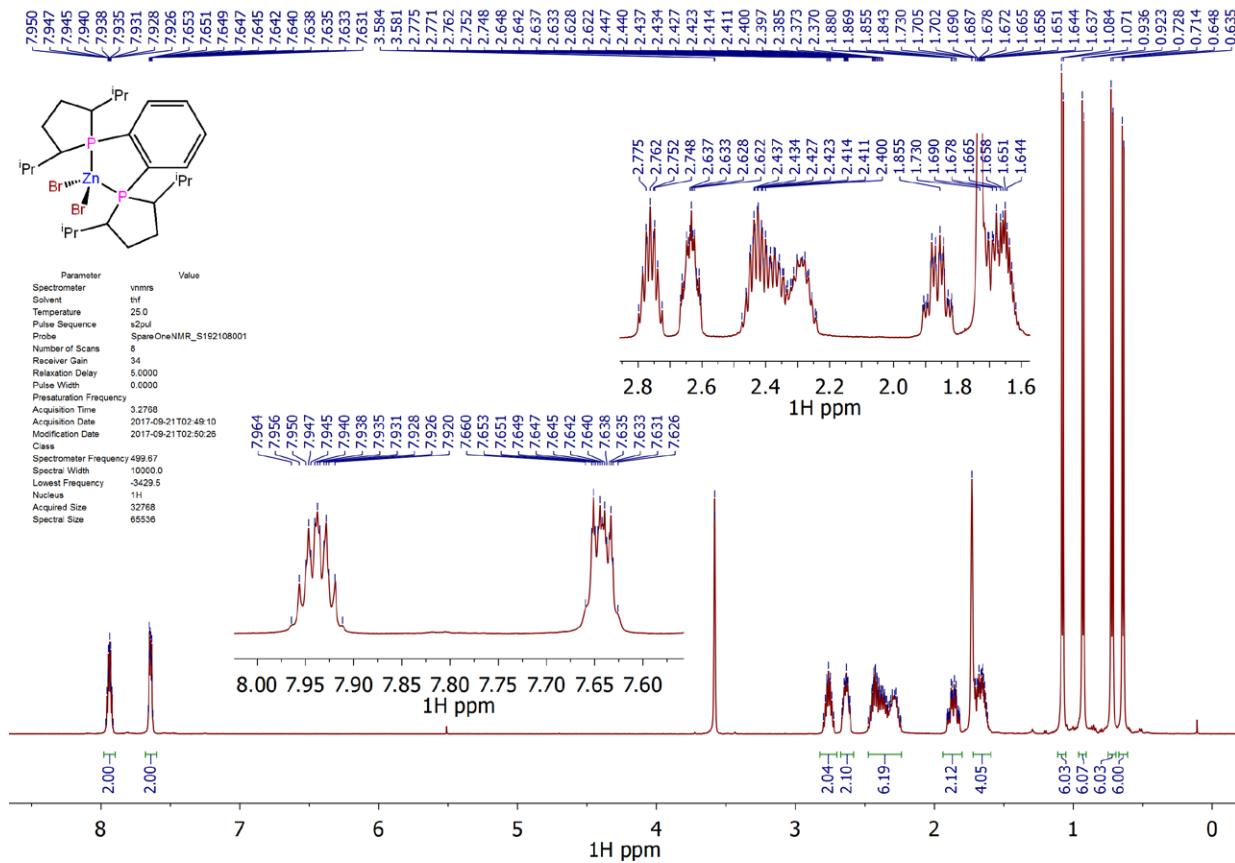
Supplementary Figure 94. ^{31}P NMR spectrum (202 MHz, THF- d_8) of **12c**.

7.4 $\text{ZnBr}_2(\text{iPrDuphos})$ (**12d**)

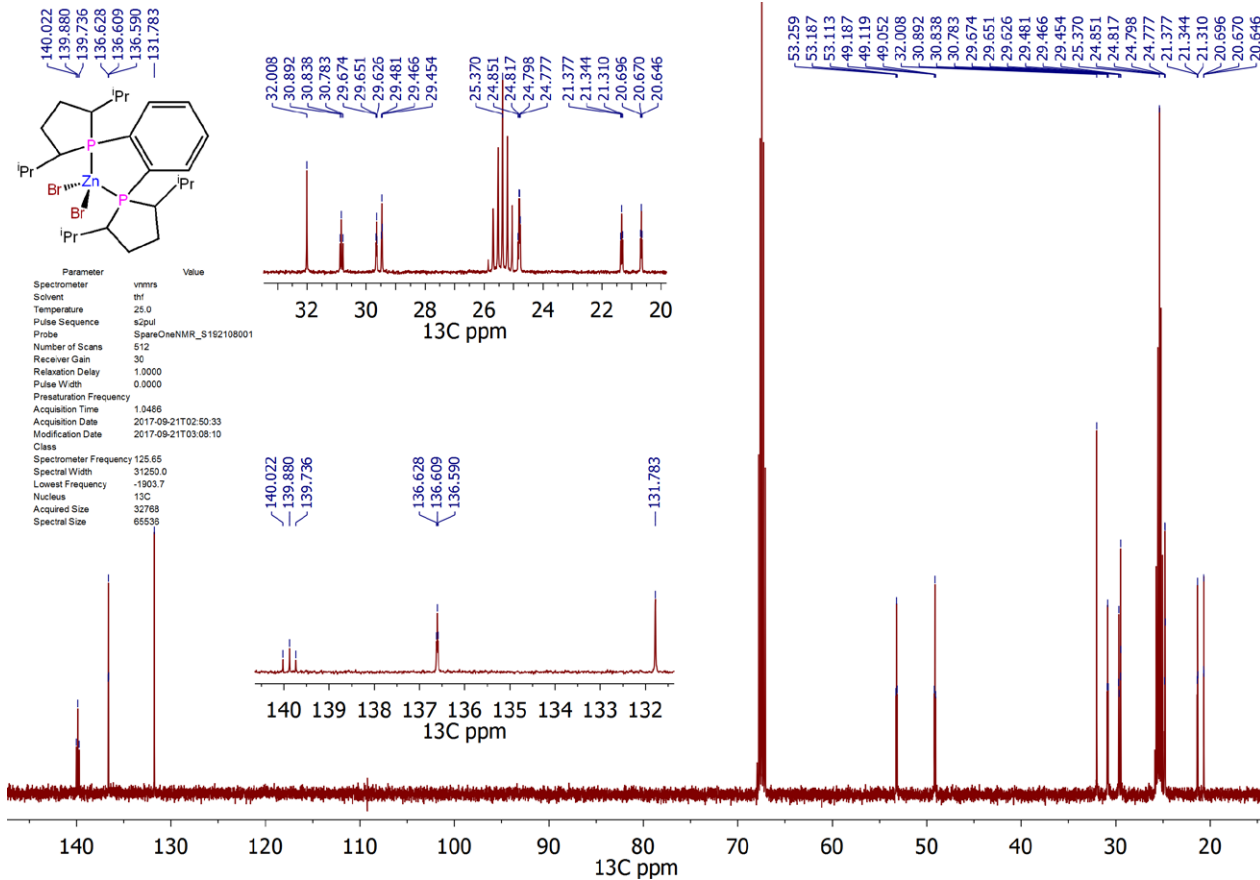
In an argon filled glove box, a vial was loaded with iPrDuphos (55 mg, 0.131 mmol), ZnBr_2 (29.6 mg, 0.131 mmol), toluene (2 mL) and 7 drops of THF. After standing for 12 hours a colourless solution formed which was filtered and layered with hexane (4 mL). After 24 hours of layering, colourless crystals suitable for an X-ray crystallographic analysis formed which were isolated by decanting the supernatant solution, dried under reduced pressure, ground and further dried under reduced pressure for 12 hours to give **12d** (75.9 mg, 90%) as a white powder. ^1H NMR (500 MHz, THF- d_8) δ = 7.97-7.91 (m, 2H), 7.68-7.59 (m, 2H), 2.80-2.72 (m, 2H), 2.67-2.60 (m, 2H), 2.50-2.22 (m, 6H), 1.86 (qdt, J =12.5, 5.6, 1.5, 2H), 1.71-1.57 (m, 4H), 1.08 (d, J =6.6, 6H), 0.93 (d, J =6.6, 6H), 0.72 (d, J =6.7, 6H), 0.64 (d, J =6.6, 6H). ^{13}C NMR (126 MHz, THF- d_8) δ = 139.9 (t, J =18.0), 136.6 (t, J =2.4), 131.8, 53.2 (t, J =9.2), 49.1 (t, J =8.5), 30.8 (t, J =6.9), 29.7 (t, J =3.0), 29.5 (d, J =1.5), 24.8 (d, J =4.2), 24.8 (d, J =2.7), 21.3 (t, J =4.2), 20.7 (t, J =3.1). ^{31}P NMR (202 MHz, THF- d_8) δ = -10.2. Anal. Calcd for $\text{C}_{26}\text{H}_{44}\text{Br}_2\text{P}_2\text{Zn}$: C, 48.51; H, 6.89 Found: C, 48.57; H, 6.87. HRMS (ESI/Q-TOF) m/z: [M+Na]⁺ Calcd for $\text{C}_{26}\text{H}_{44}\text{Br}_2\text{NaP}_2\text{Zn}$ 663.0474; Found 663.0469.



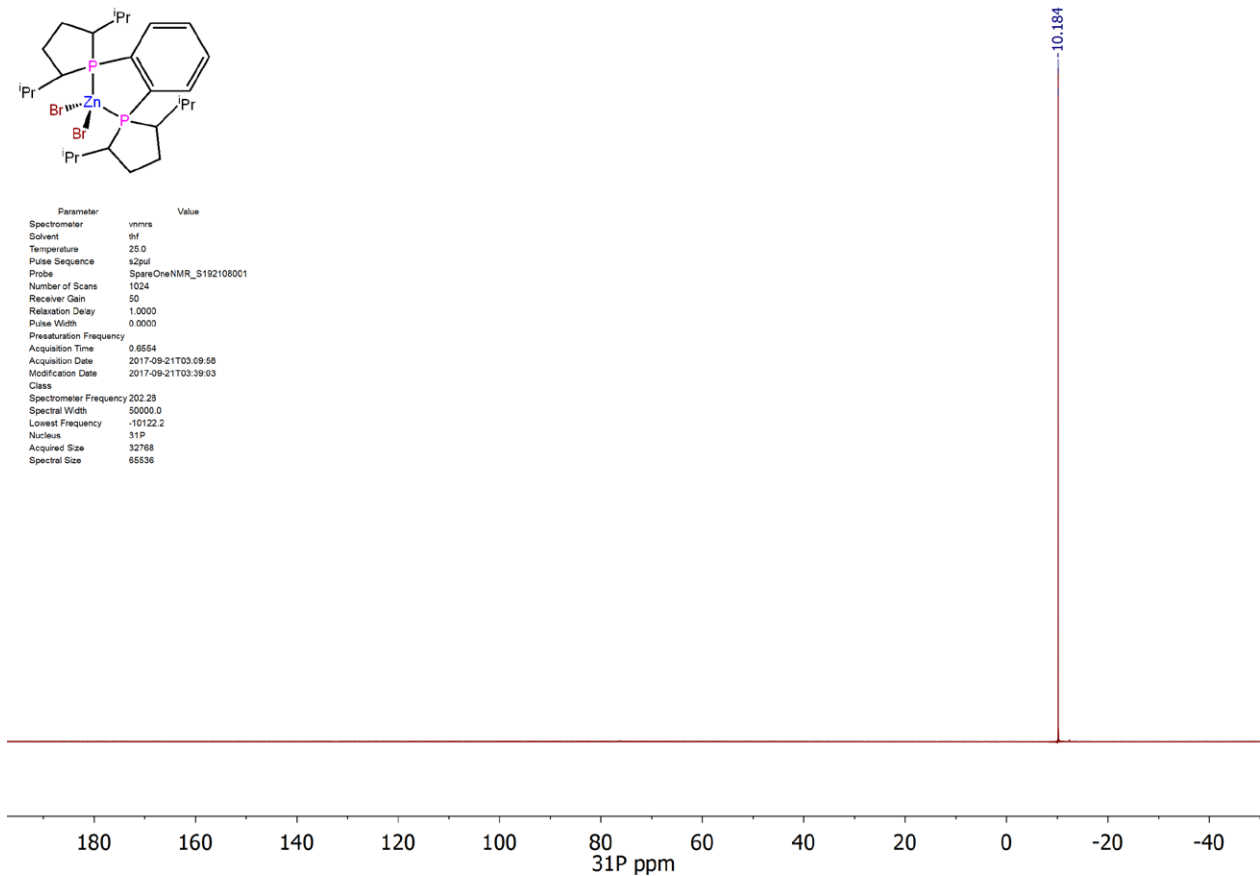
Supplementary Figure 95. Single-crystal X-ray structure of **12d**. Hydrogen atoms are omitted for clarity. Thermal ellipsoids are set at the 50% probability level.



Supplementary Figure 96. ^1H NMR spectrum (500 MHz, THF- d_8) of **12d**.



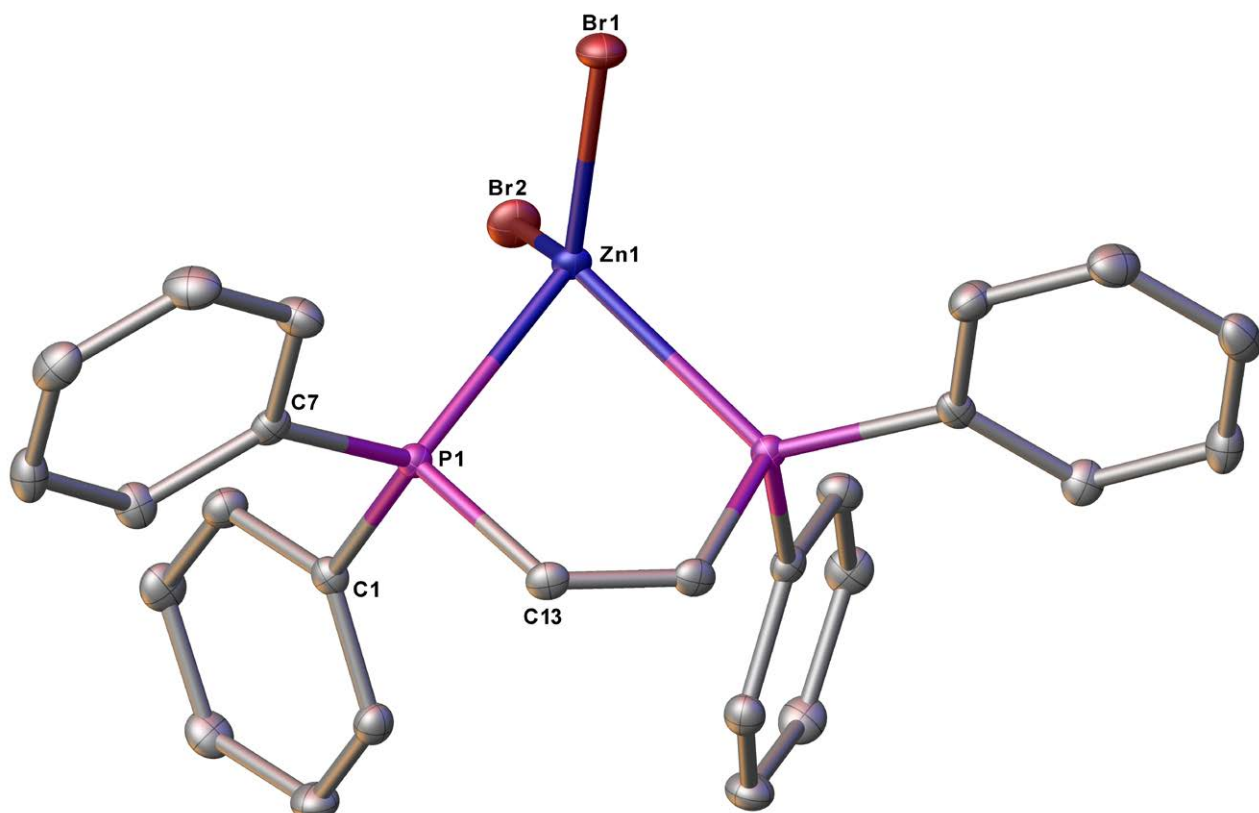
Supplementary Figure 97. ^{13}C NMR spectrum (126 MHz, THF- d_8) of **12d**.



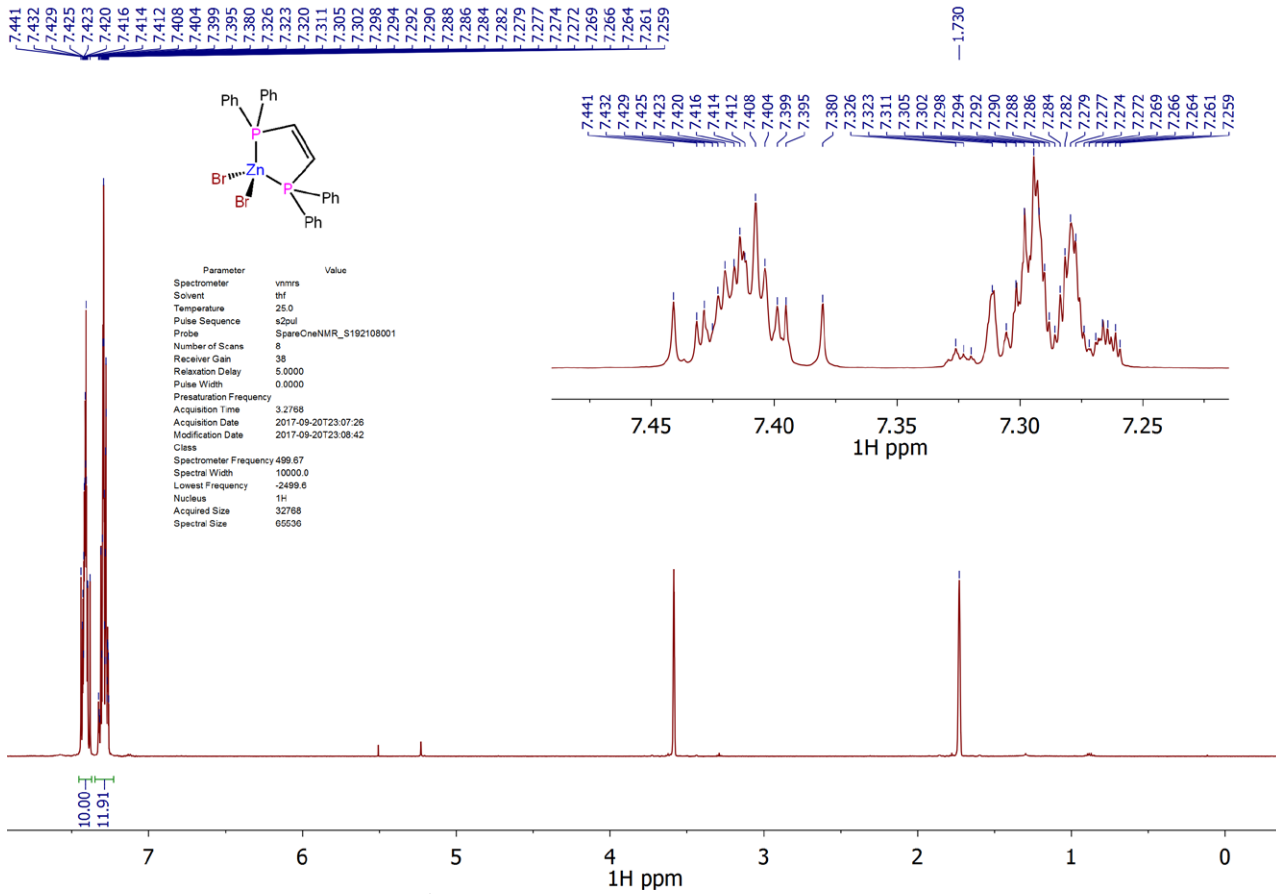
Supplementary Figure 98. ^{31}P NMR spectrum (202 MHz, THF- d_8) of **12d**.

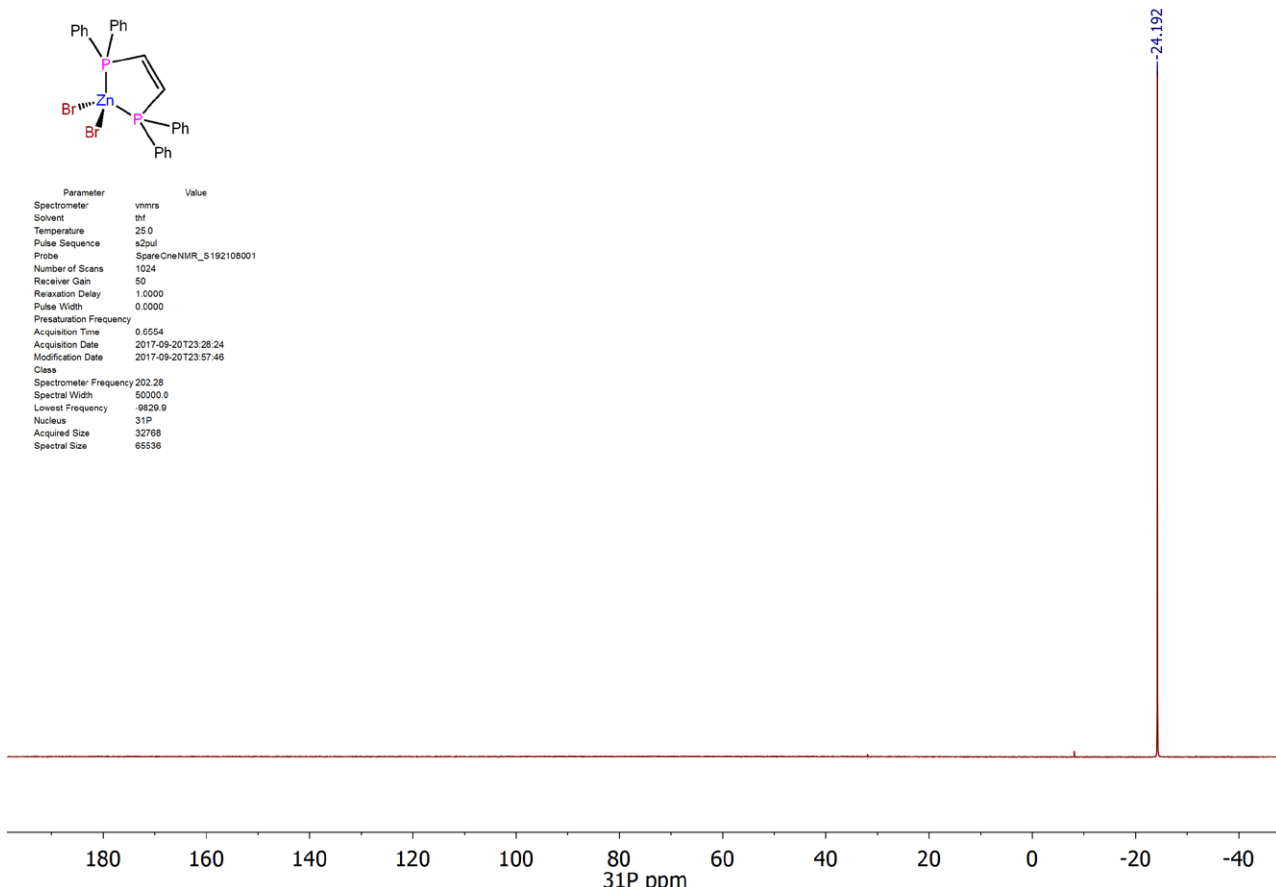
7.5 [ZnBr₂(*cis*-dppen)] (**12e**)

In an argon filled glove box, a vial was loaded with *cis*-dppen (102 mg, 0.257 mmol), ZnBr₂ (57.9 mg, 0.257 mmol), CH₂Cl₂ (2 mL) and 7 drops of THF. After standing for 12 hours colourless crystals suitable for a crystallographic analysis were obtained. The crystals were dissolved by addition of THF and heating, the solution filtered while still hot and layered with hexane (4 mL). After 24 hours of layering, colourless crystals formed which were isolated by decanting the supernatant solution, dried under reduced pressure, ground and further dried under reduced pressure for 12 hours to give **12e** (139.7 mg, 87%) as a white powder.¹H NMR (500 MHz, THF-*d*₈) δ = 7.47-7.37 (m, 10H), 7.34-7.24 (m, 12H).¹³C NMR (126 MHz, THF-*d*₈) δ = 146.9 (t, *J*=11.5), 137.0 (br s, 12.37), 133.9 (t, *J*=9.1), 130.0, 129.4 (t, *J*=3.8).³¹P NMR (202 MHz, THF-*d*₈) δ = -24.2. Anal. Calcd for C₂₆H₂₂Br₂P₂Zn: C, 50.24; H, 3.57 Found: C, 50.21; H, 3.59. HRMS (ESI/Q-TOF) m/z: [M+Na]⁺ Calcd for C₂₆H₂₂Br₂NaP₂Zn 640.8753; Found 640.8747.



Supplementary Figure 99. Single-crystal X-ray structure of **12e**. Hydrogen atoms are omitted for clarity and thermal ellipsoids are set at the 50% probability level.

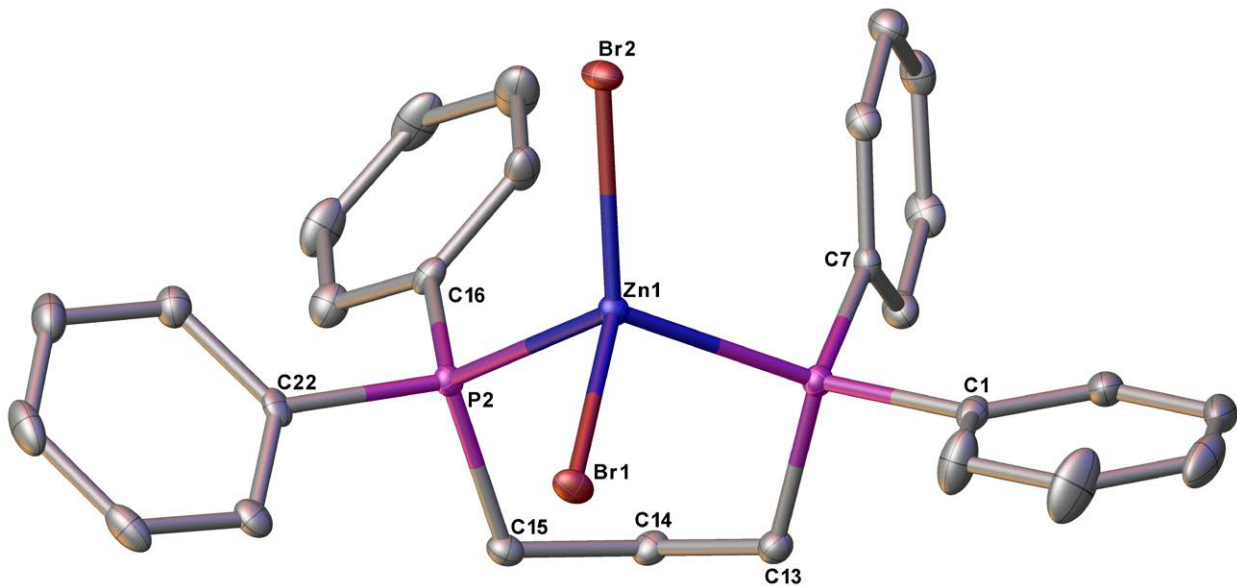




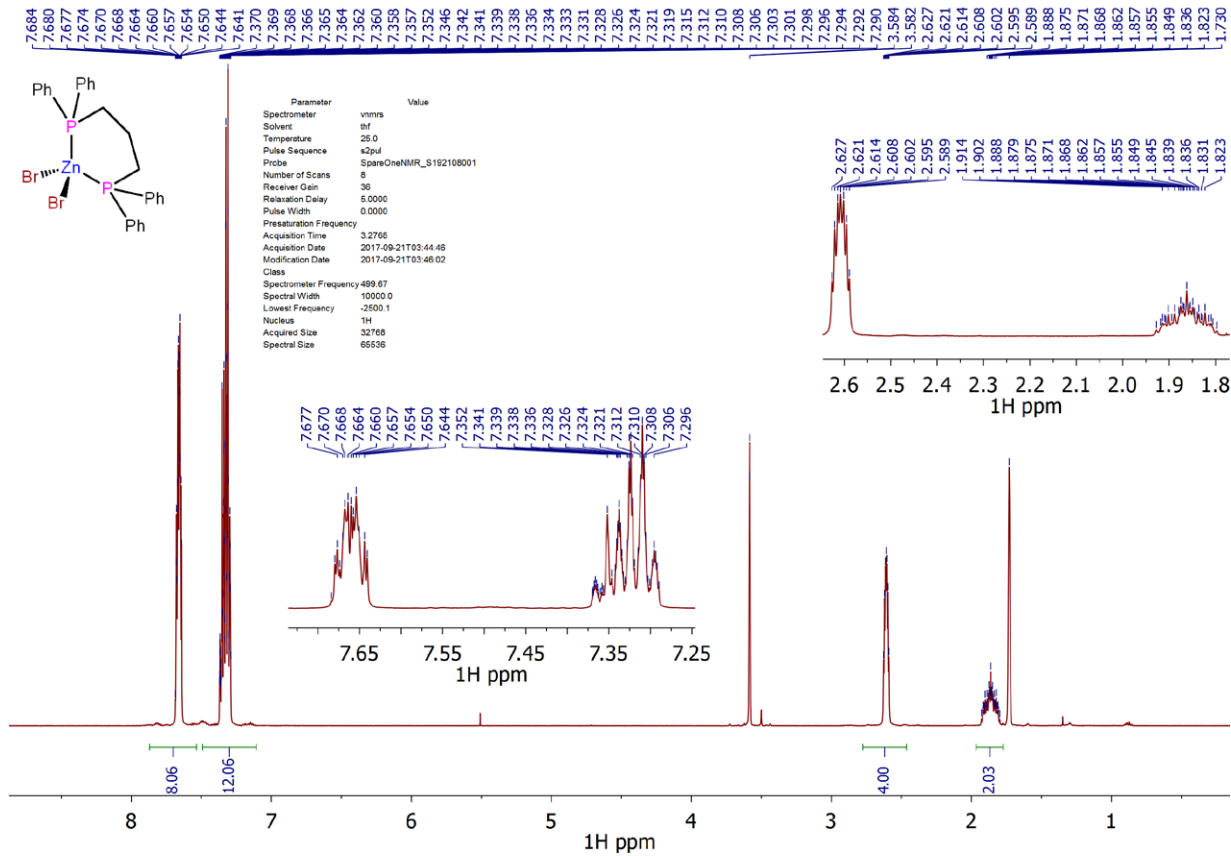
Supplementary Figure 102. ^{31}P NMR spectrum (202 MHz, THF- d_8) of **12e**.

7.6 $[\text{ZnBr}_2(\text{dPPP})]$ (**12f**)

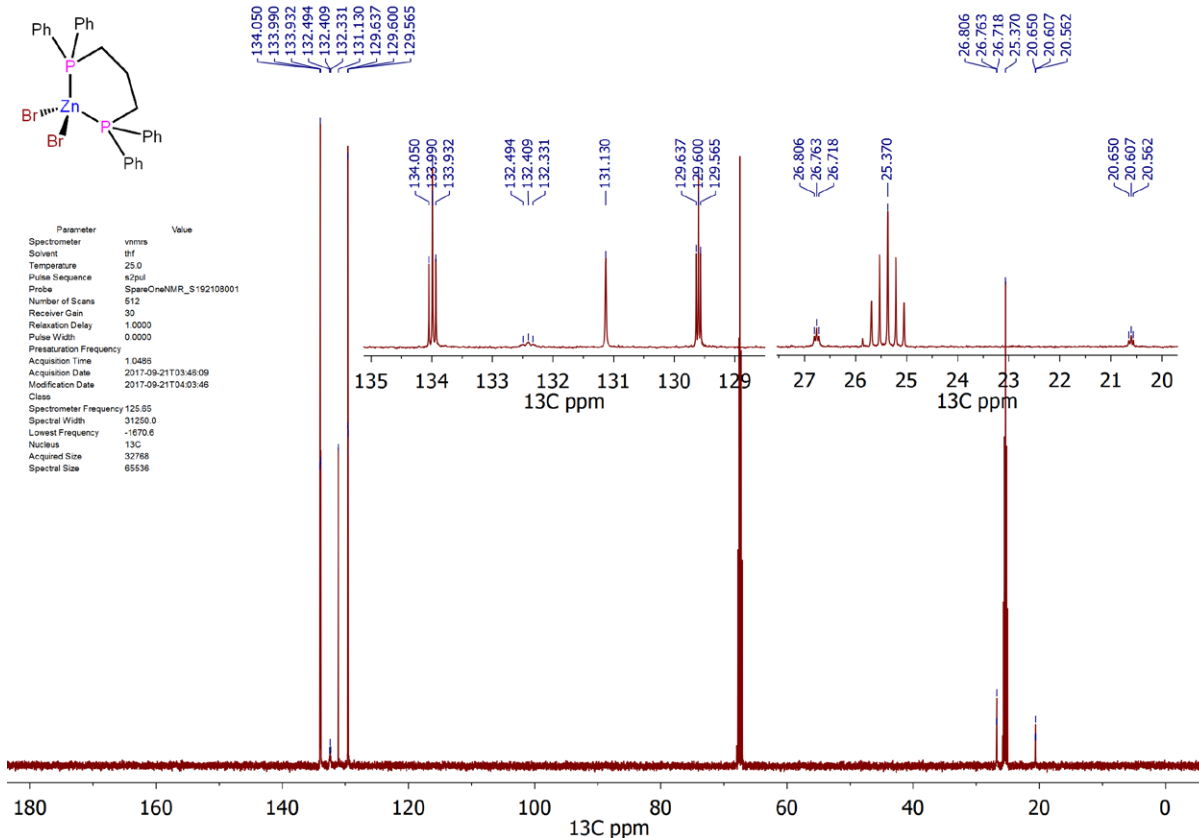
In an argon filled glove box, a vial was loaded with dPPP (96.0 mg, 0.233 mmol), ZnBr_2 (52.4 mg, 0.233 mmol), CH_2Cl_2 (2 mL) and 7 drops of THF. After standing for 12 hours a colourless solution formed which was filtered and layered with hexane (4 mL). After 24 hours of layering, colourless crystals suitable for an X-ray crystallographic analysis formed which were isolated by decanting the supernatant solution, dried under reduced pressure, ground and further dried under reduced pressure for 12 hours to give **12f** (129.2 mg, 87%) as a white powder. ^1H NMR (500 MHz, THF- d_8) δ = 7.70-7.62 (m, 8H), 7.38-7.28 (m, 12H), 2.61 (tt, J =6.2, 3.0, 4H), 1.94-1.79 (m, 2H). ^{13}C NMR (126 MHz, THF- d_8) δ = 134.0(t, J =7.4), 132.41 (t, J =10.2), 131.1, 129.6 (t, J =4.5), 26.8 (t, J =5.5), 20.6 (t, J =5.6). ^{31}P NMR (202 MHz, THF- d_8) δ = -21.5. Anal. Calcd for $\text{C}_{27}\text{H}_{26}\text{Br}_2\text{P}_2\text{Zn}$: C, 50.86; H, 4.11 Found: C, 50.77; H, 4.08. HRMS (ESI/Q-TOF) m/z: [M+Na]⁺ Calcd for $\text{C}_{27}\text{H}_{26}\text{Br}_2\text{NaP}_2\text{Zn}$ 656.9066; Found 656.9060.



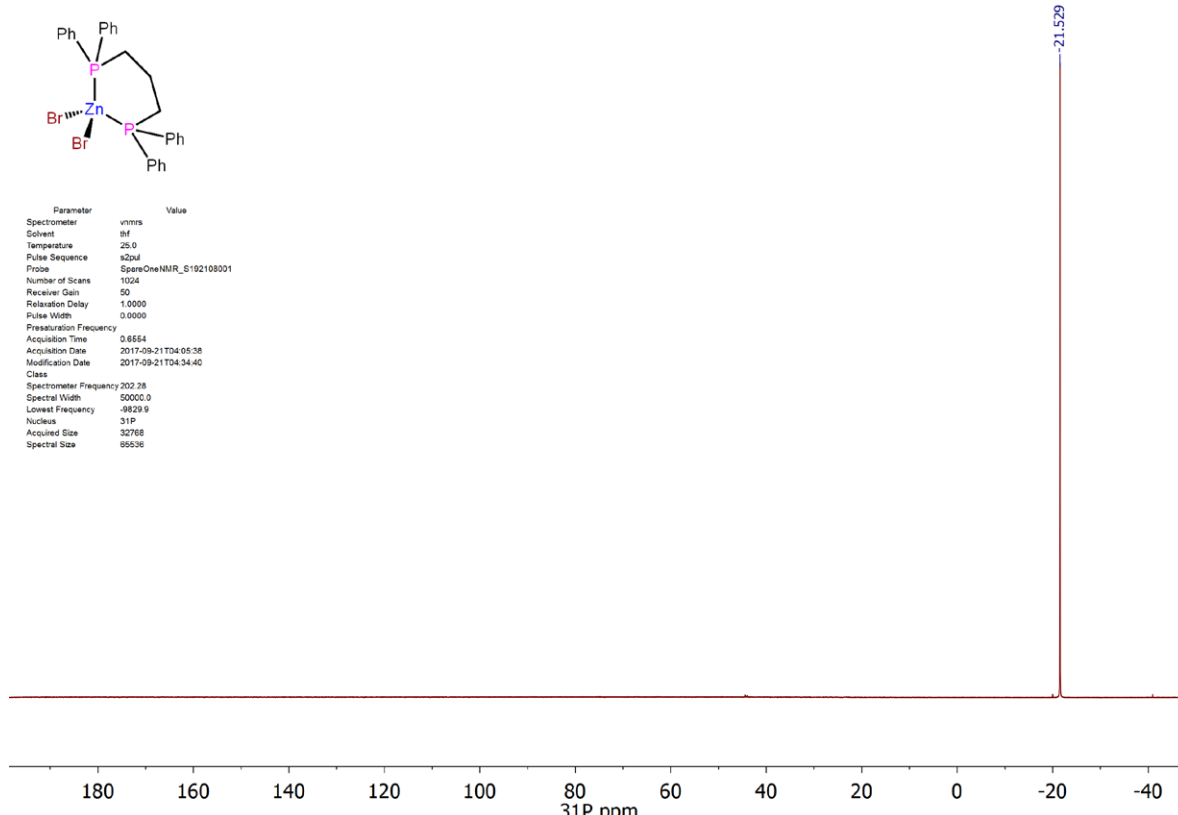
Supplementary Figure 103. Single-crystal X-ray structure of **12f**. Hydrogen atoms are omitted for clarity and thermal ellipsoids are set at the 50% probability level.



Supplementary Figure 104. ¹H NMR spectrum (500 MHz, THF-*d*₈) of **12f**.



Supplementary Figure 105. ^{13}C NMR spectrum (126 MHz, THF- d_8) of **12f**.

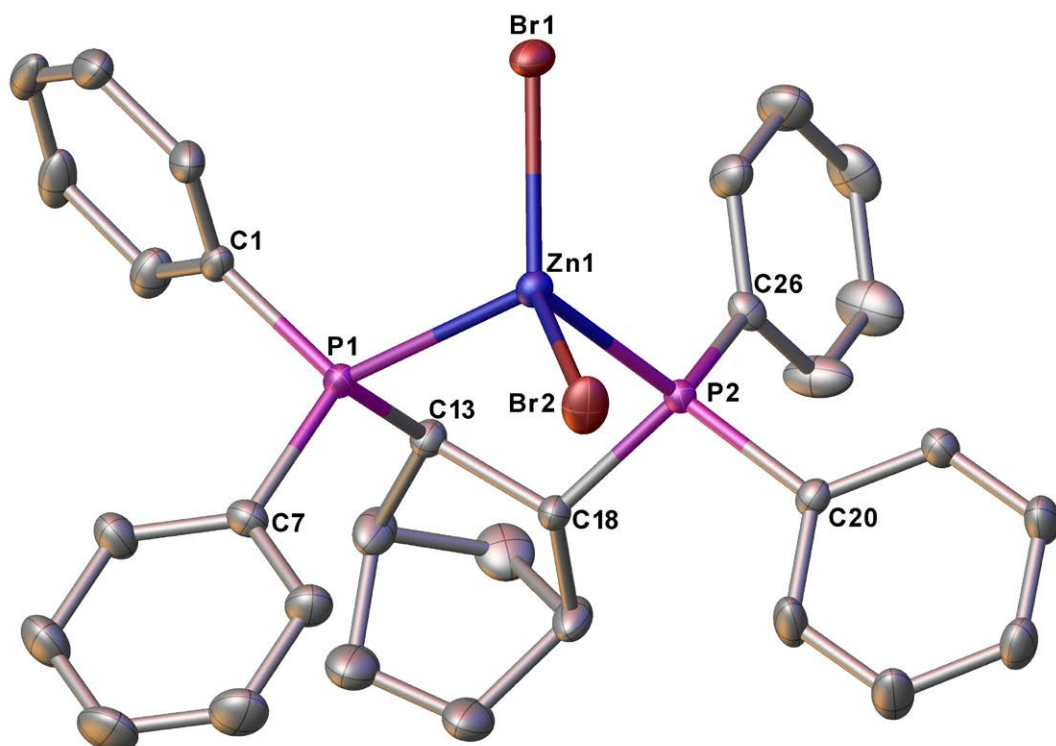


Supplementary Figure 106. ^{31}P NMR spectrum (202 MHz, THF- d_8) of **12f**.

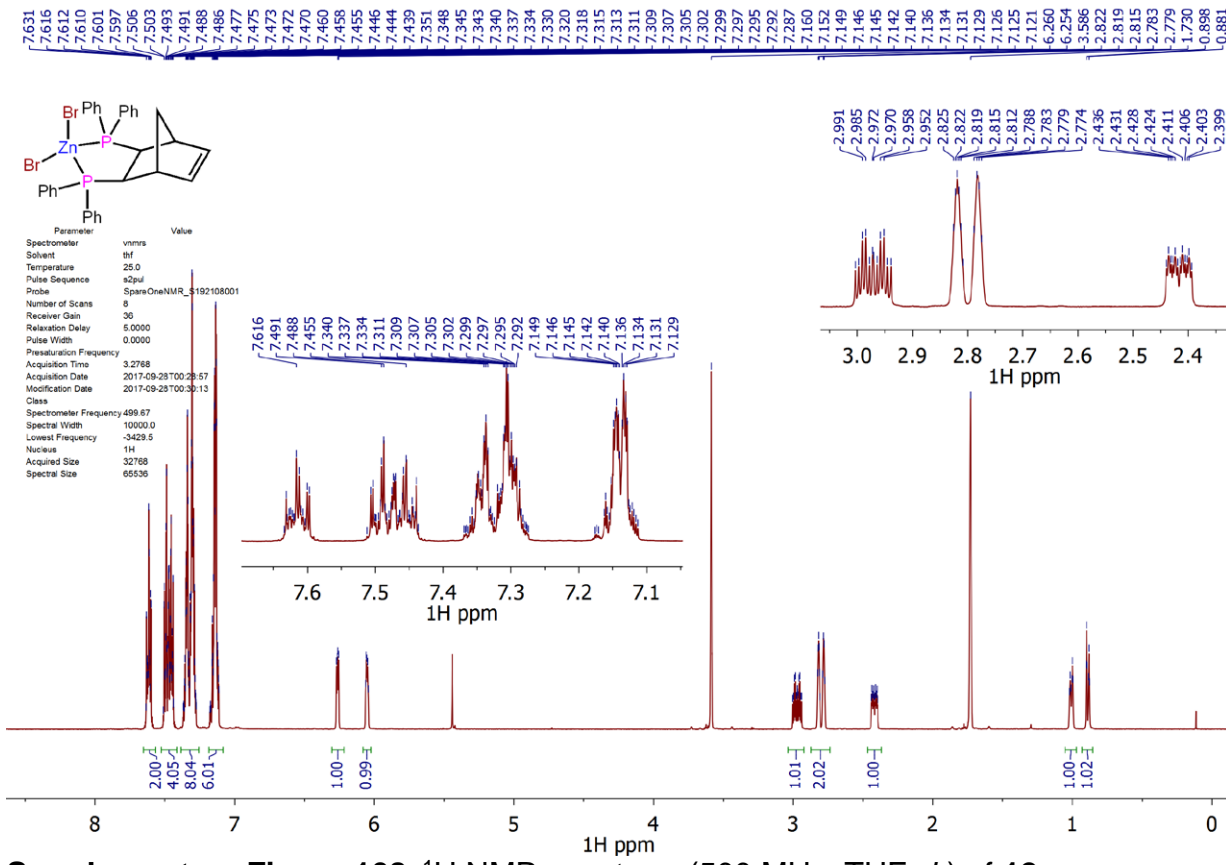
7.7 $[\text{ZnBr}_2(\text{norphos})]$ (12g)

In an argon filled glove box, a vial was loaded with norphos (53.8 mg, 0.116 mmol), ZnBr_2 (26.2 mg, 0.116 mmol), CH_2Cl_2 (2 mL) and 7 drops of THF. After standing for 12 hours a

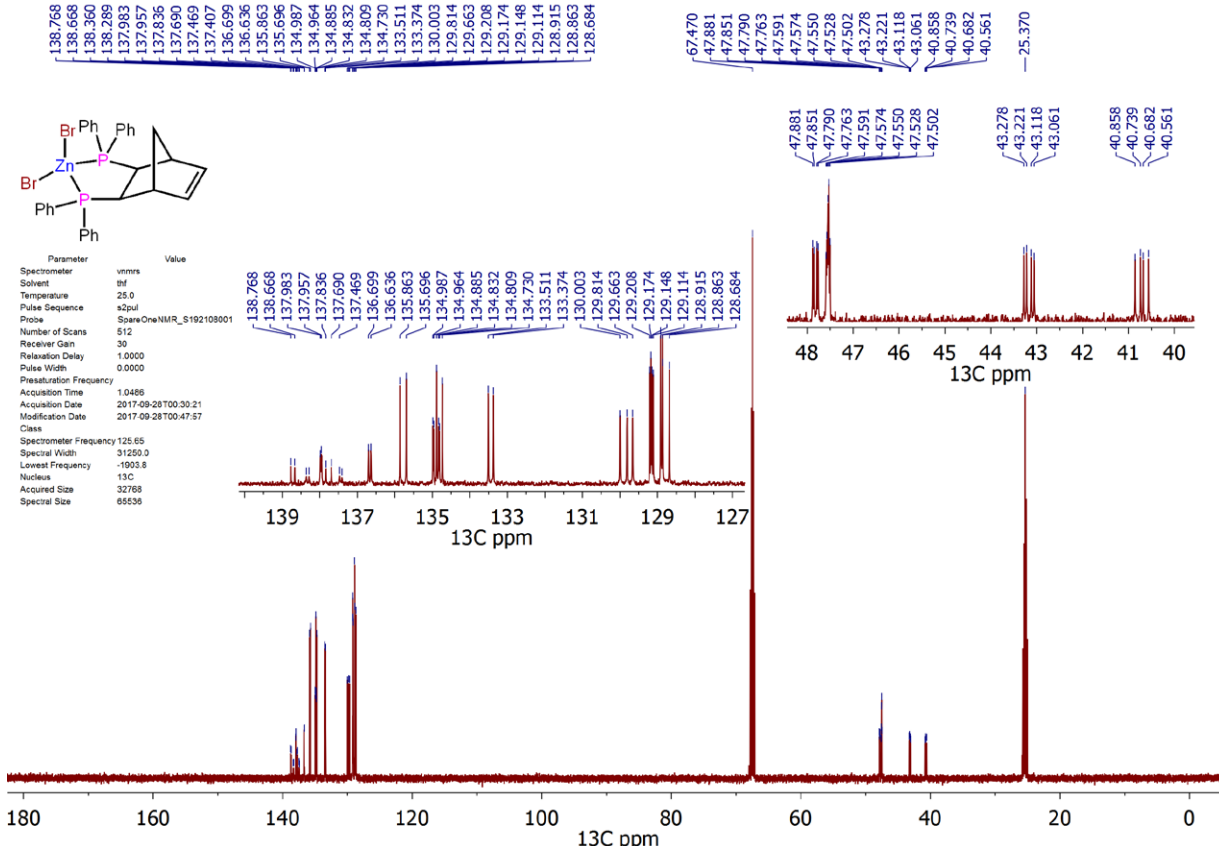
colourless solution formed which was filtered and layered with hexane (4 mL). After 24 hours, colourless crystals suitable for an X-ray crystallographic analysis formed which were isolated by decanting the supernatant solution, dried under reduced pressure, ground and further dried under reduced pressure for 12 hours to give **12g** (54.0 mg, 68%) as a white powder.¹H NMR (500 MHz, THF-*d*₈) δ = 7.69-7.58 (m, 2H), 7.53-7.40 (m, 4H), 7.39-7.27 (m, 8H), 7.18-7.07 (m, 6H), 6.26 (dd, *J*=5.6, 3.1, 1H), 6.07-6.04 (m, 1H), 2.97 (dtd, *J*=16.5, 6.3, 3.1, 1H), 2.84-2.76 (m, 2H), 2.42 (ddt, *J*=12.5, 6.0, 2.1, 1H), 1.01 (dt, *J*=8.5, 2.2, 1H), 0.89 (dt, *J*=1.6, 1H), 0.88 (d, *J*=8.6, 1.6, 1H). ¹³C NMR (126 MHz, THF-*d*₈) δ = 140.0(d, *J*=16.3), 139.3 (d, *J*=15.2), 138.9 (d, *J*=15.6), 138.4 (d, *J*=20.6), 137.5 (dd, *J*=3.4, 1.5), 136.7 (d, *J*=8.4), 135.8 (d, *J*=21.2), 134.9 (dd, *J*=21.0, 2.9), 134.6 (d, *J*=20.5), 133.3 (d, *J*=17.6), 129.8, 129.4, 129.3, 129.1 (dd, *J*=7.2, 2.4), 128.8, 128.8, 128.7, 128.5, 47.8 (dd, *J*=12.6, 3.8), 47.5 (t, *J*=3.0), 43.1 (dd, *J*=20.6, 12.0), 40.9 (dd, *J*=23.6, 16.5). ³¹P NMR (202 MHz, THF-*d*₈) δ = -1.1 (d, *J*=4.4), -3.2 (d, *J*=4.2). Anal. Calcd for C₃₁H₂₈Br₂P₂Zn: C, 54.14; H, 4.10 Found: C, 53.40; H, 3.97. HRMS (ESI/Q-TOF) m/z: [M+Na]⁺ Calcd for C₃₁H₂₈Br₂NaP₂Zn 706.9222; Found 706.9217.



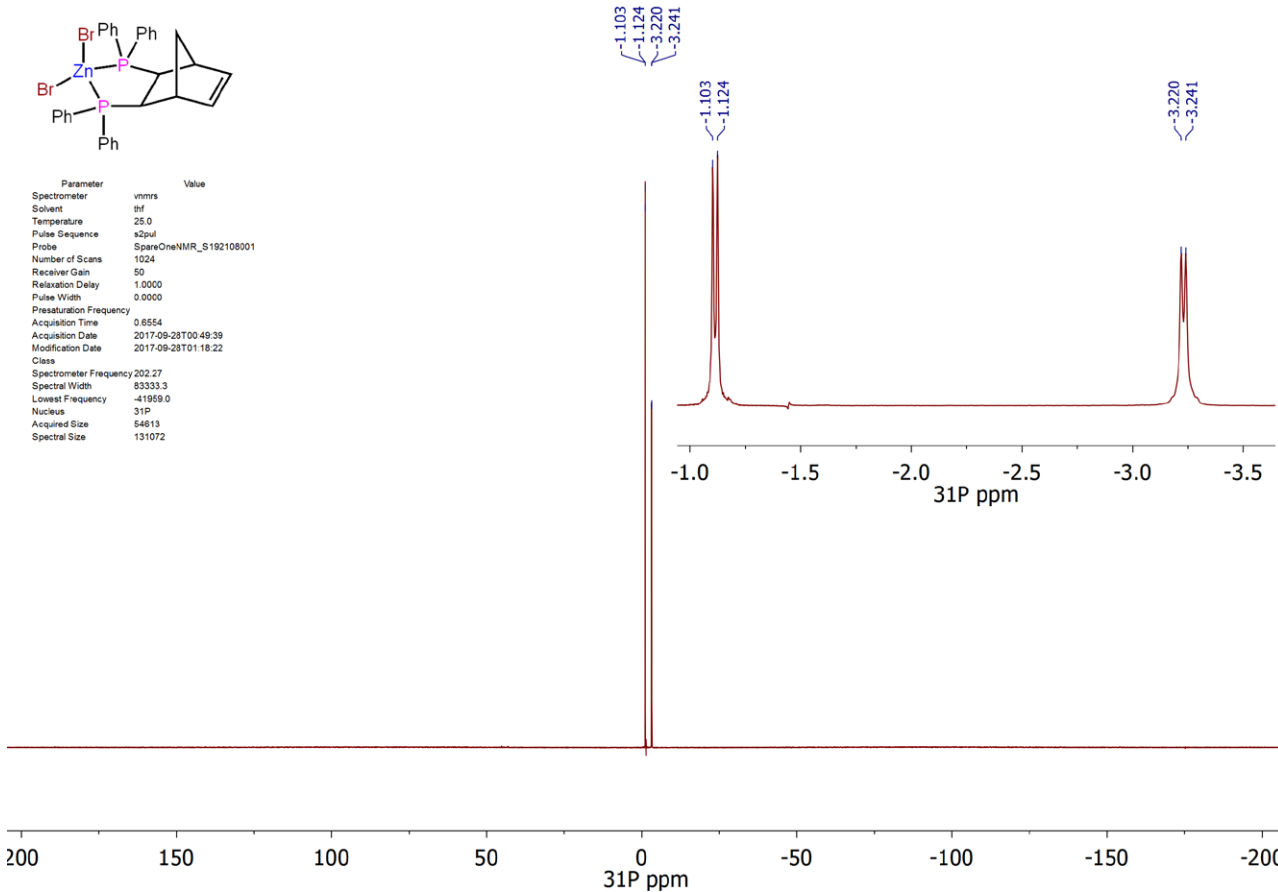
Supplementary Figure 107. Single-crystal X-ray structure of **12g**. Hydrogen atoms and solvent molecules are omitted for clarity. Thermal ellipsoids are set at the 50% probability level.



Supplementary Figure 108. ^1H NMR spectrum (500 MHz, THF- d_8) of **12g**.



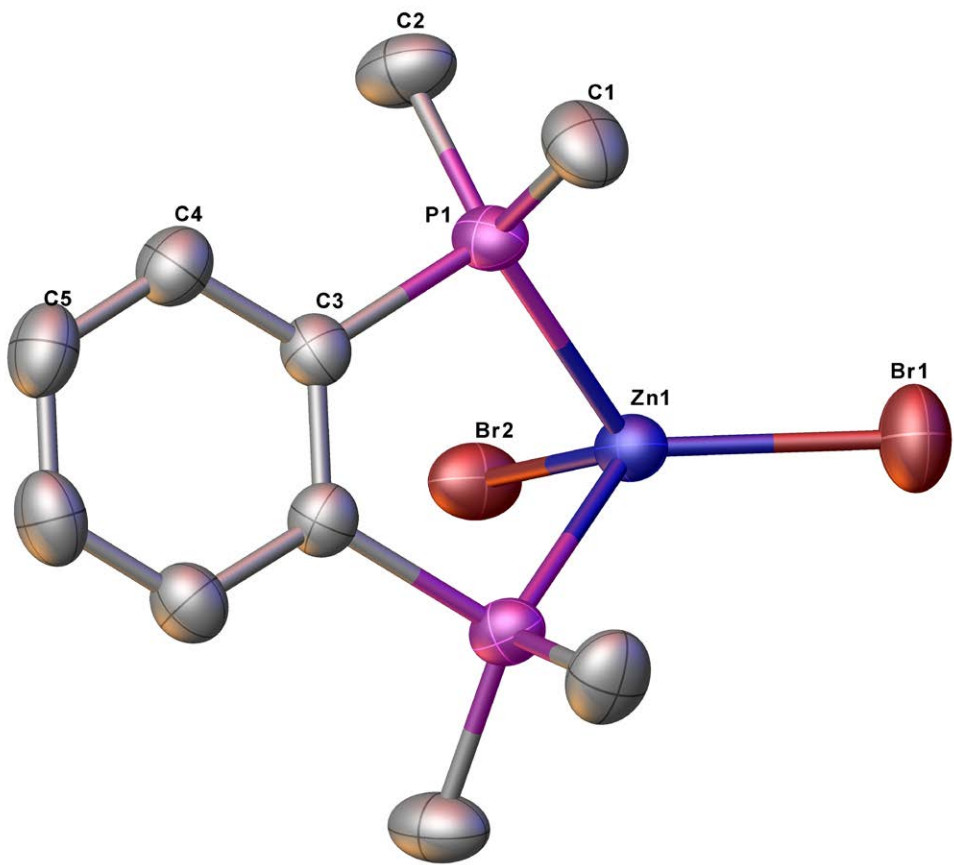
Supplementary Figure 109. ^{13}C NMR spectrum (126 MHz, THF- d_8) of 12g.



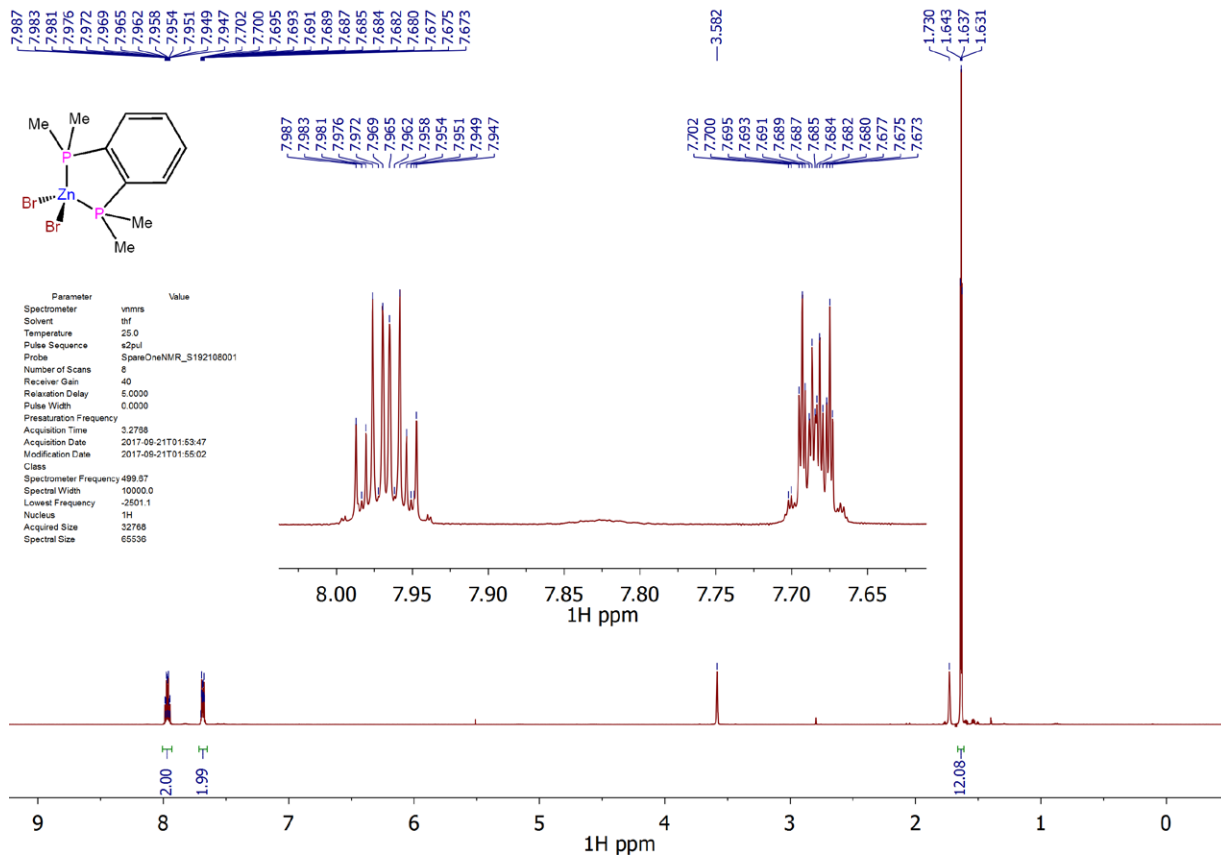
Supplementary Figure 110. ^{31}P NMR spectrum (202 MHz, THF- d_8) of **12g**.

7.8 [ZnBr₂(dmbz)] (12h)

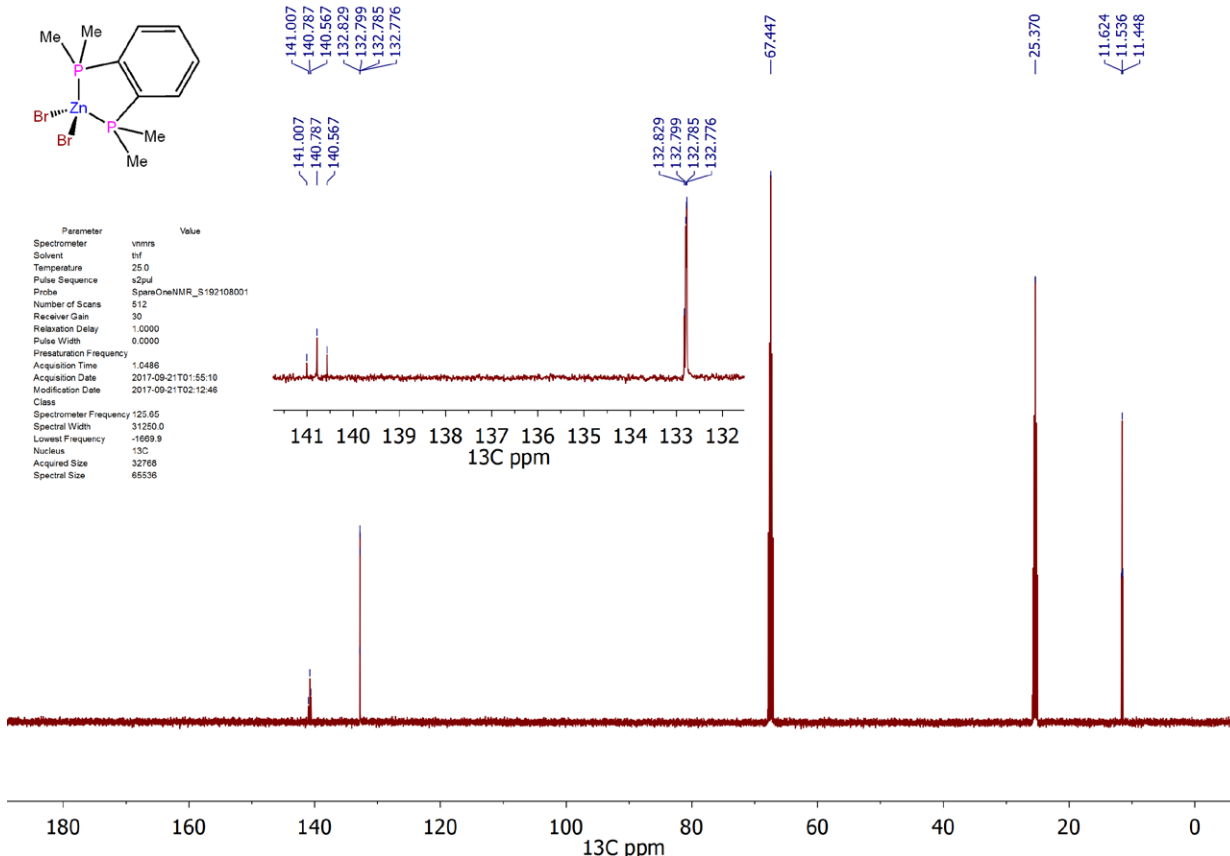
In an argon filled glove box, a vial was loaded with dmbz (33.4 mg, 0.169 mmol), ZnBr₂ (38.0 mg, 0.169 mmol), CH₂Cl₂ (2 mL) and 7 drops of THF. After standing for 12 hours a colourless solution formed which was filtered and layered with hexane (4 mL). After 24 hours, colourless crystals suitable for an X-ray crystallographic analysis formed which were isolated by decanting the supernatant solution, dried under reduced pressure, ground and further dried under reduced pressure for 12 hours to give **12h** (67.3 mg, 94%) as a white powder. ^1H NMR (500 MHz, THF- d_8) δ = 7.97 (ddd, J =11.1, 5.5, 3.4, 2H), 7.68 (ddt, J =5.8, 3.2, 1.0, 2H), 1.64 (t, J =3.0, 12H). ^{13}C NMR (126 MHz, THF- d_8) δ = 140.8 (t, J =27.7), 132.9-132.8 (m), 11.5 (t, J =11.0). ^{31}P NMR (202 MHz, THF- d_8) δ = -44.0. Anal. Calcd for C₁₀H₁₆Br₂P₂Zn: C, 28.37; H, 3.81 Found: C, 28.43; H, 3.81. HRMS (ESI/Q-TOF) m/z: [M+Na]⁺ Calcd for C₁₀H₁₆Br₂NaP₂Zn 442.8283; Found 442.8278.



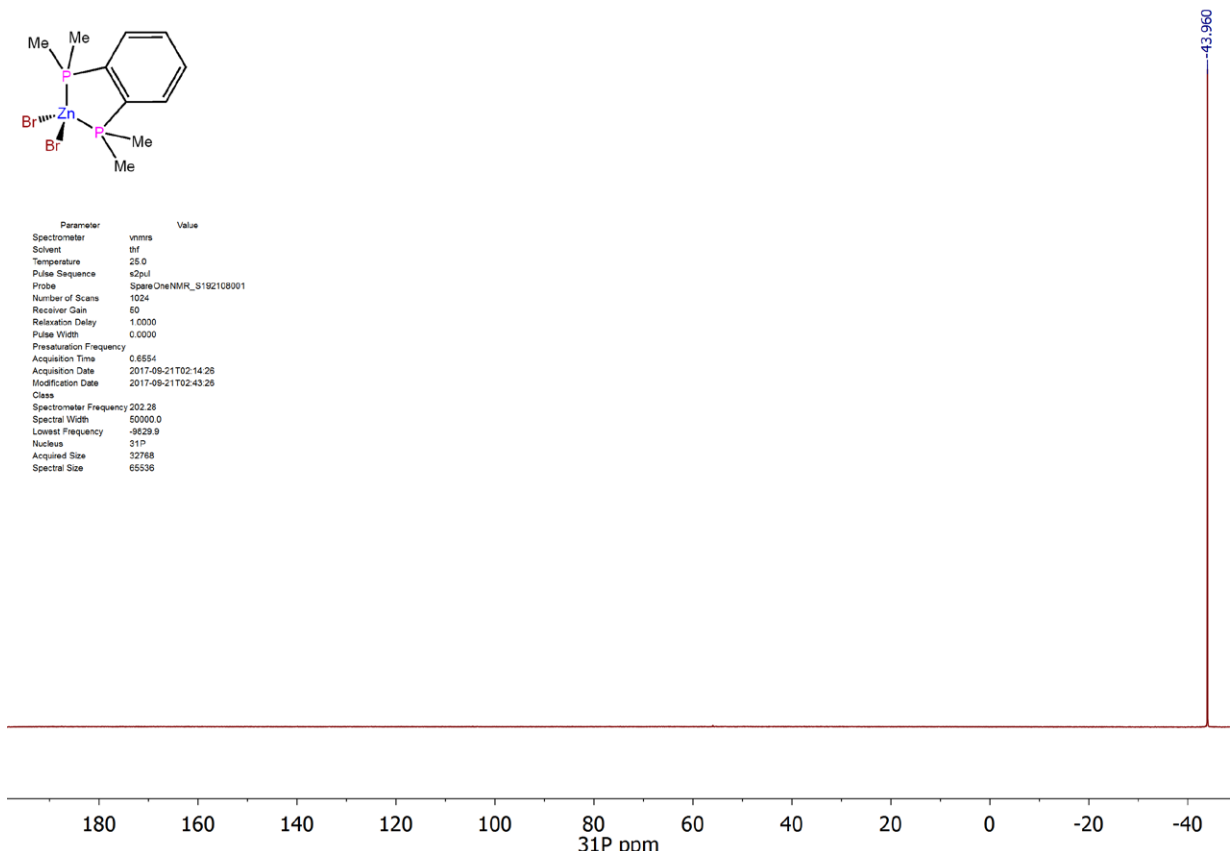
Supplementary Figure 111. Single-crystal X-ray structure of **12h**. Hydrogen atoms and solvent molecules are omitted for clarity while thermal ellipsoids are set at the 50% probability level.



Supplementary Figure 112. ^1H NMR spectrum (500 MHz, $\text{THF}-d_8$) of **12h**.



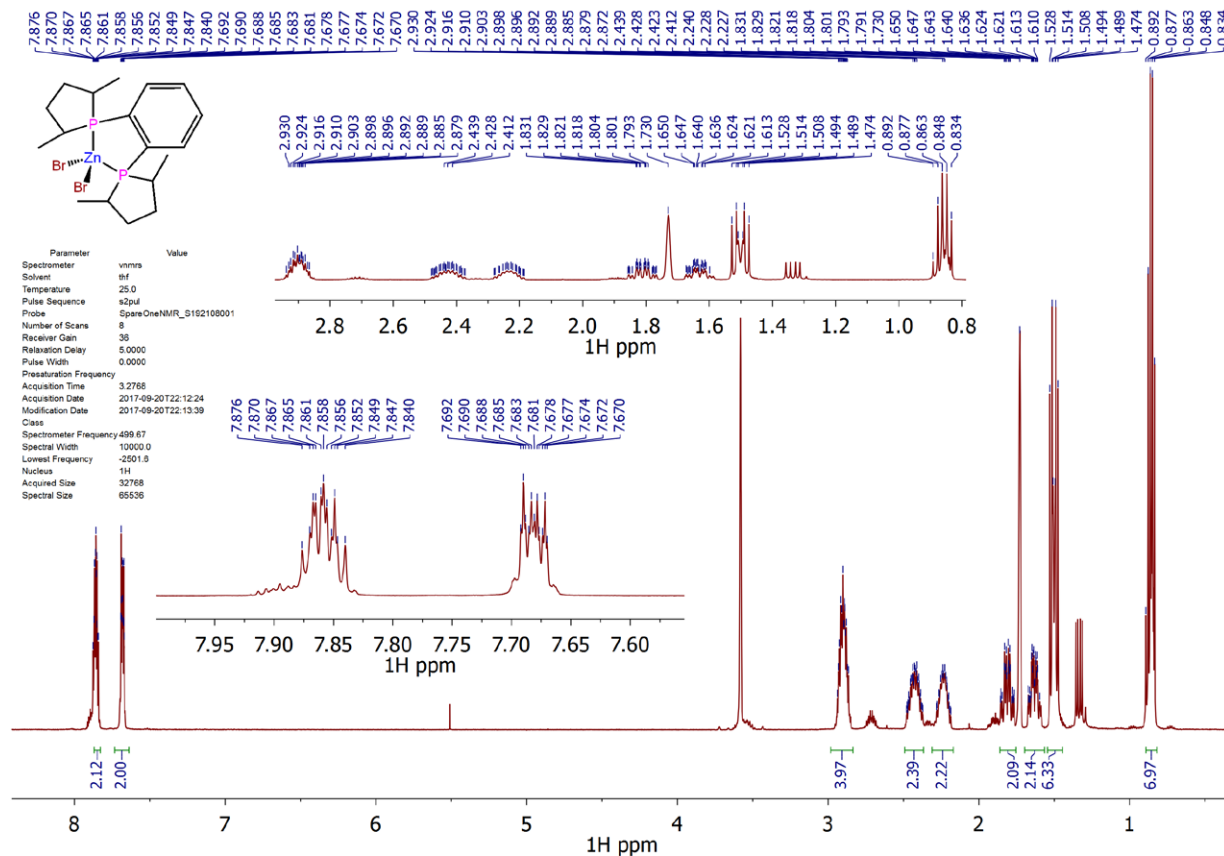
Supplementary Figure 113. ^{13}C NMR spectrum (126 MHz, THF- d_8) of **12h**.



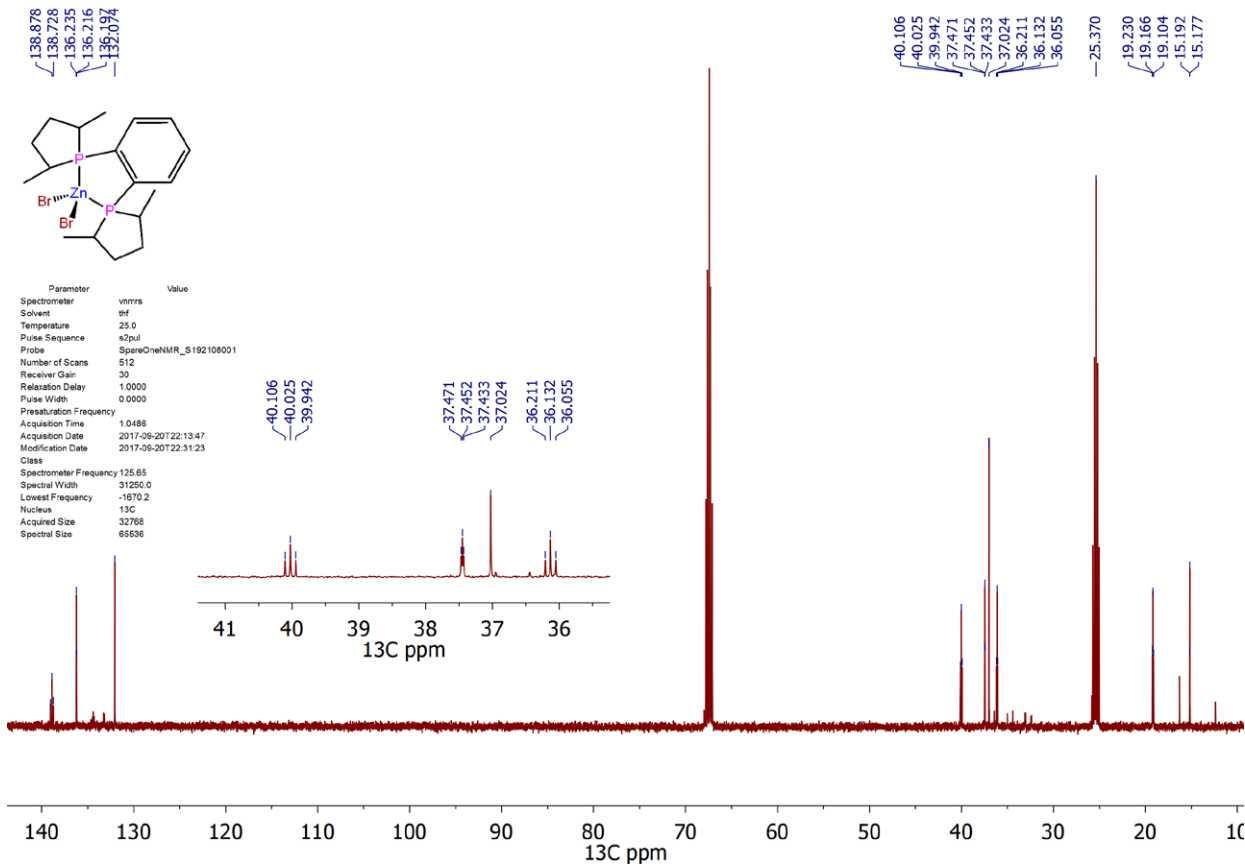
Supplementary Figure 114. ^{31}P NMR spectrum (202 MHz, THF- d_8) of **12h**.

7.9 [ZnBr₂(MeDuphos)] (12i)

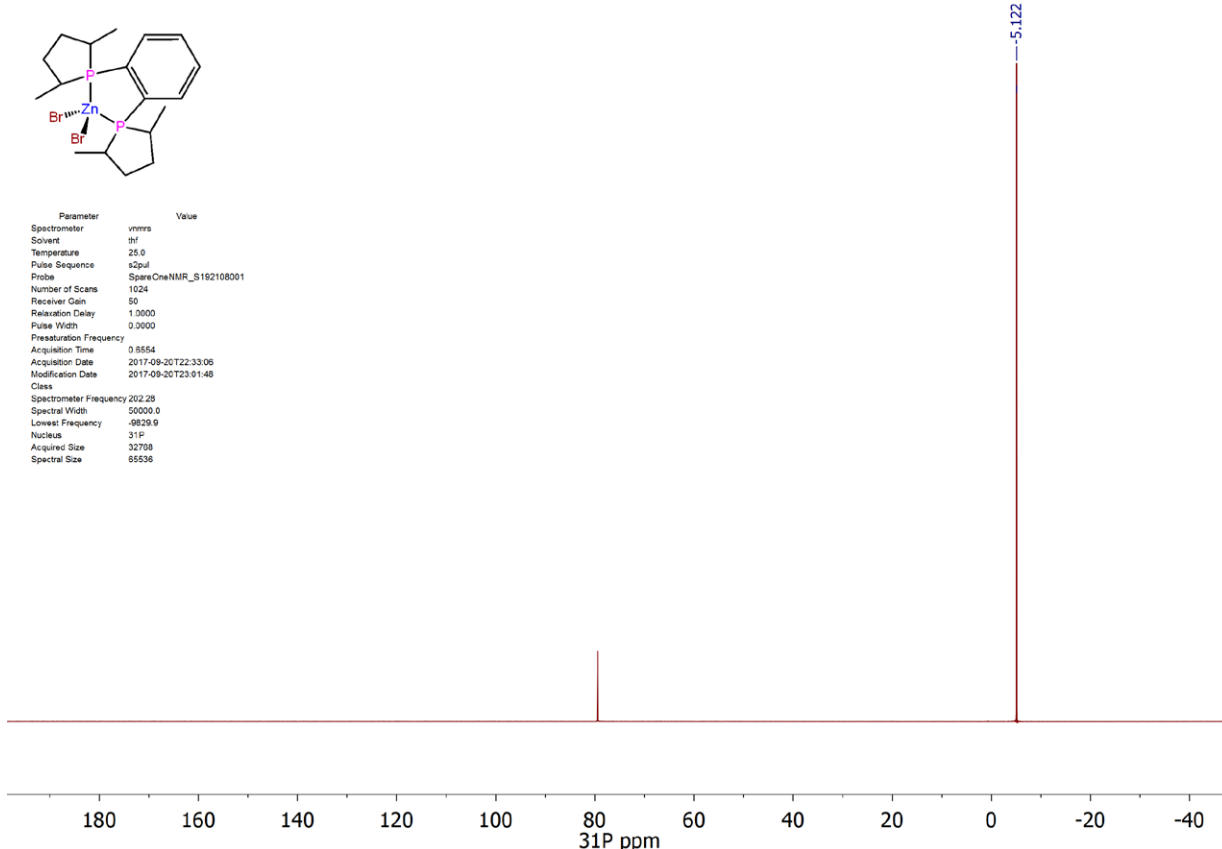
In an argon filled glove box, a vial was loaded with MeDuphos (50.2 mg, 0.164 mmol), ZnBr₂ (45.8 mg, 0.164 mmol), CH₂Cl₂ (2 mL) and 7 drops of THF. After standing for 12 hours a colourless solution formed which was filtered and layered with hexane (4 mL). After 24 hours, colourless microcrystals formed which were isolated by decanting the supernatant solution, dried under reduced pressure, ground and further dried under reduced pressure for 12 hours to give **12i·½CH₂Cl₂** (27.8 mg, 24%) as a white powder. ¹H NMR (500 MHz, THF-*d*₈) δ = 7.86 (dtd, *J*=5.8, 4.5, 3.2, 2H), 7.71-7.65 (m, 2H), 2.95-2.85 (m, 4H), 2.50-2.36 (m, 2H), 2.32-2.14 (m, 2H), 1.90-1.76 (m, 2H), 1.69-1.57 (m, 2H), 1.56-1.45 (m, 6H), 0.86 (dt, *J*=14.3, 7.3, 6H). ¹³C NMR (126 MHz, THF-*d*₈) δ = 139.8-138.3 (m), 136.2 (t, *J*=2.4), 132.1, 40.0 (t, *J*=10.3), 37.5 (t, *J*=2.4), 37.0, 36.1 (t, *J*=9.8), 19.2 (t, *J*=7.9), 15.2 (d, *J*=1.9). ³¹P NMR (202 MHz, THF-*d*₈) δ = -5.1. Anal. Calcd for C_{18.5}H₂₉Br₂CIP₂Zn: C, 38.71; H, 5.09 Found: C, 39.33; H, 5.07. HRMS (ESI/Q-TOF) m/z: No [M]⁺ or [M+A]⁺ peak observed.



Supplementary Figure 115. ¹H NMR spectrum (500 MHz, THF-*d*₈) of **12i**.



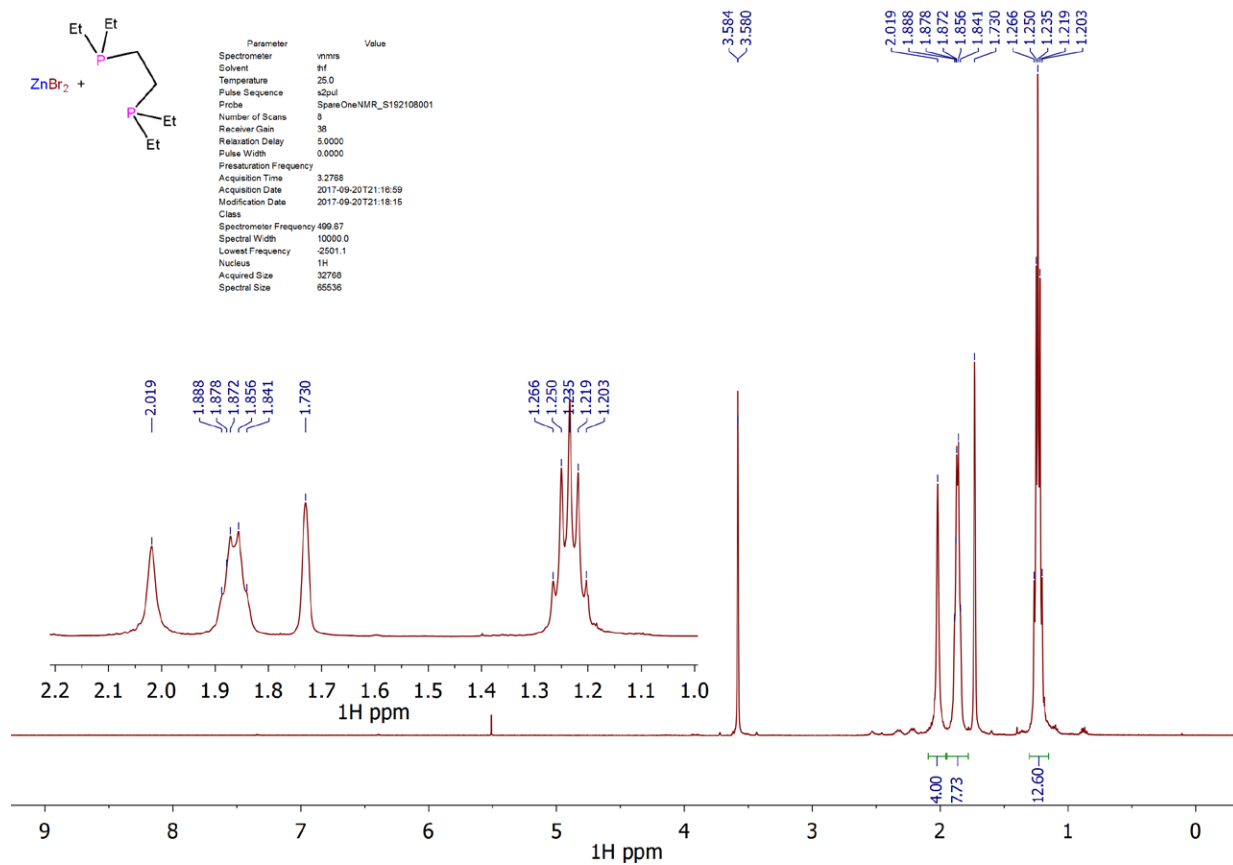
Supplementary Figure 116. ¹³C NMR spectrum (126 MHz, THF-*d*₈) of **12i**.



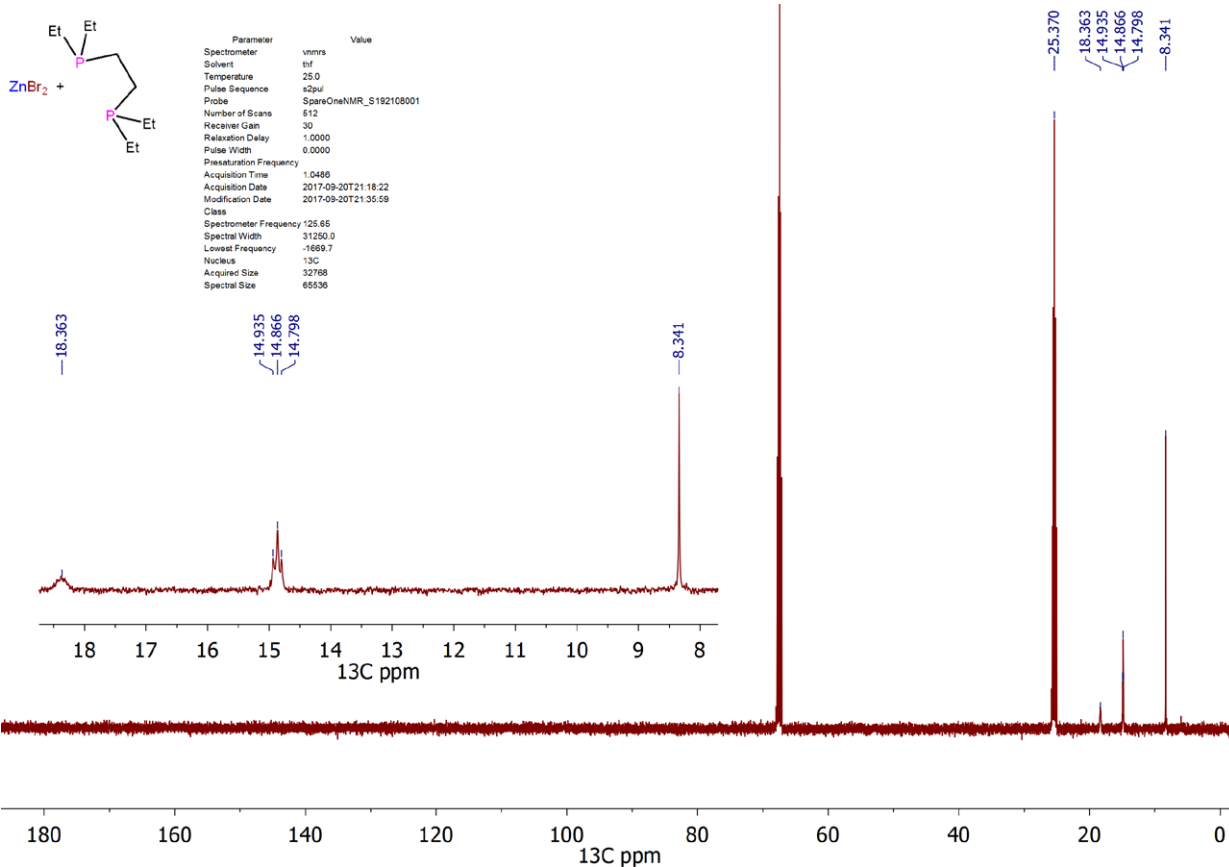
Supplementary Figure 117. ³¹P NMR spectrum (202 MHz, THF-*d*₈) of **12i**.

7.10 Reaction between ZnBr₂ and depe

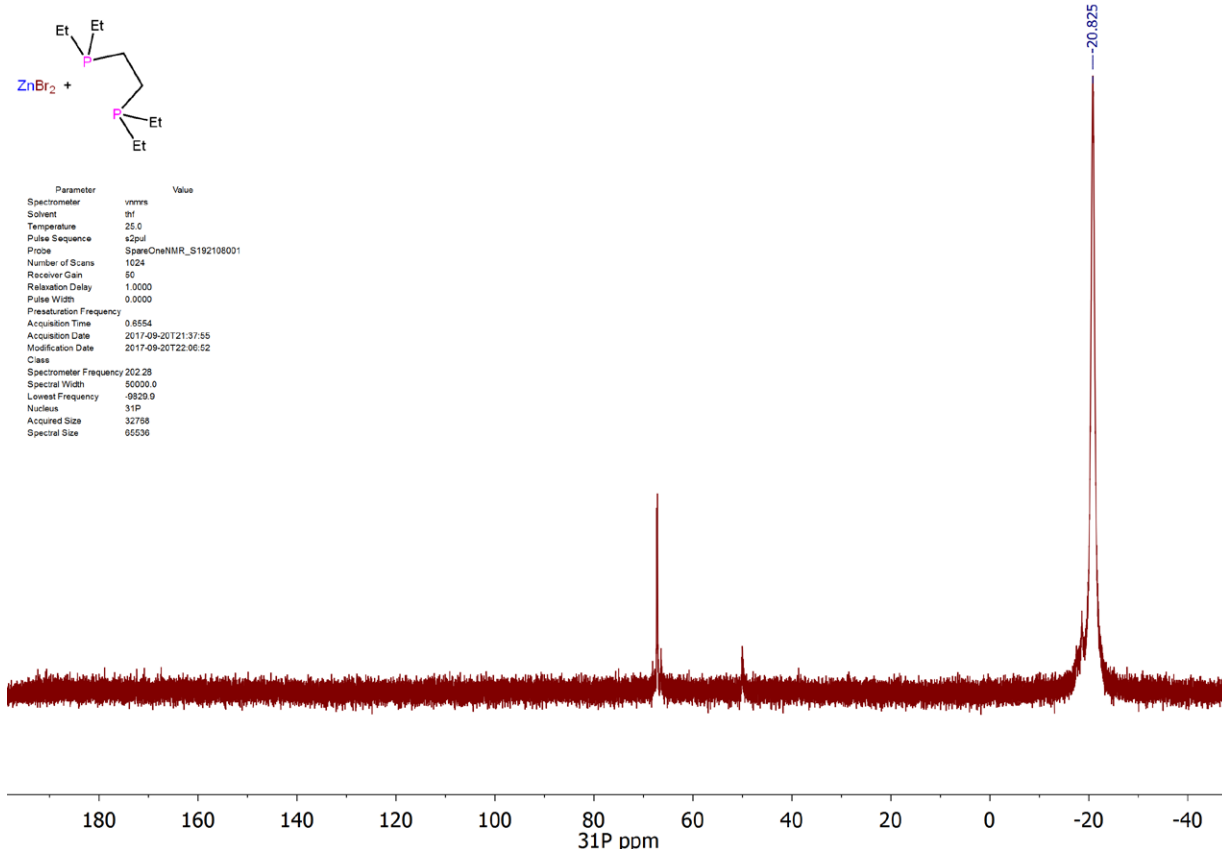
In an argon filled glove box, a vial was loaded with depe (100.0 mg, 0.485 mmol), ZnBr₂ (109.2 mg, 0.485 mmol) and CH₂Cl₂ (2 mL). After standing for 12 hours a colourless solution formed which was filtered and layered with hexane (4 mL). After 24 hours, a colourless oil had formed. NMR data were obtained from a deuterated THF solution of a 1:1 mixture of ZnBr₂ and depe. ¹H NMR (500 MHz, THF-d₈) δ = 2.02 (s, 4H), 1.86 (q, J=7.9, 8H), 1.23 (p, J=7.8, 12H). ¹³C NMR (126 MHz, THF-d₈) δ = 18.36, 14.87 (t, J=8.7), 8.34. ³¹P NMR (202 MHz, THF-d₈) δ = -20.8.



Supplementary Figure 118. ¹H NMR spectrum (500 MHz, THF-d₈) of ZnBr₂ + depe.



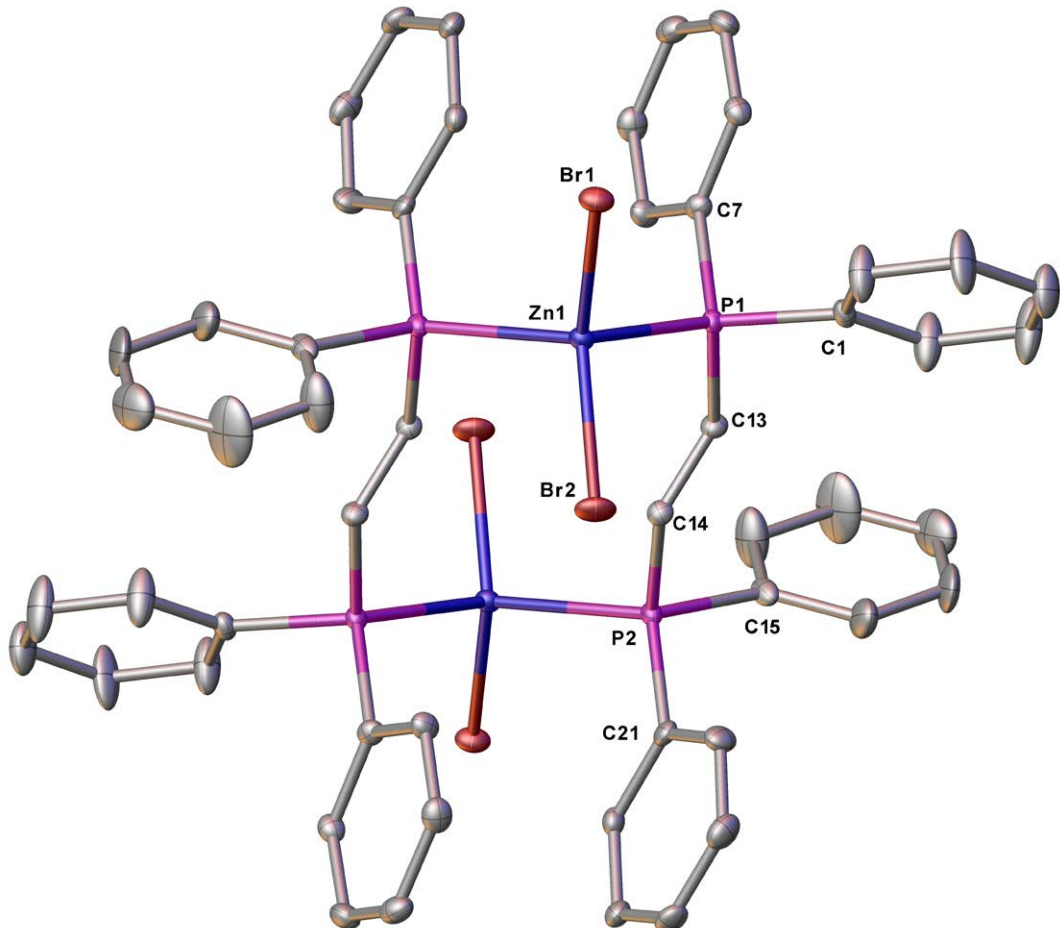
Supplementary Figure 119. ¹³C NMR spectrum (126 MHz, THF-*d*₈) of ZnBr₂ + depe.



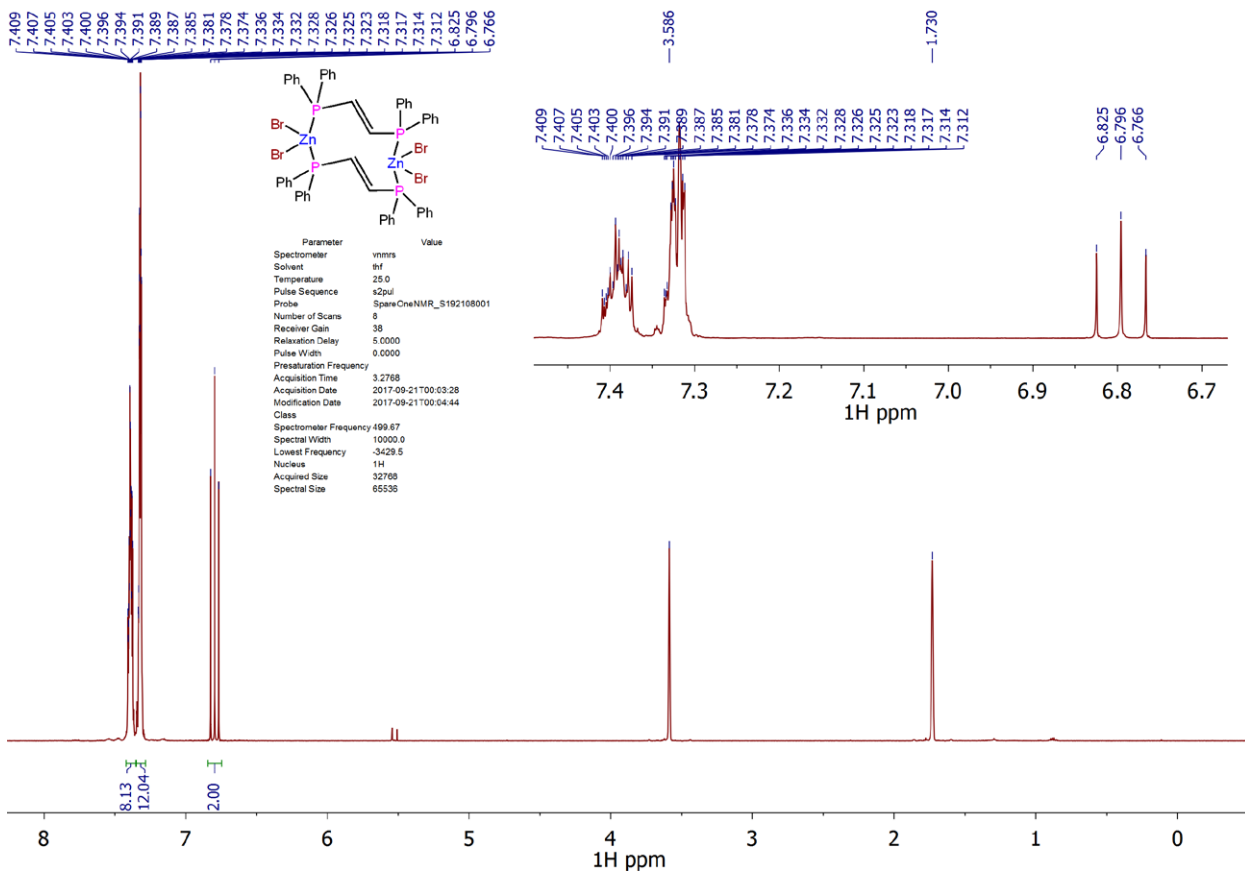
Supplementary Figure 120. ³¹P NMR spectrum (202 MHz, THF-*d*₈) of ZnBr₂ + depe.

7.11 [{ZnBr₂(*μ-trans*-dppen)}₂] (**13**)

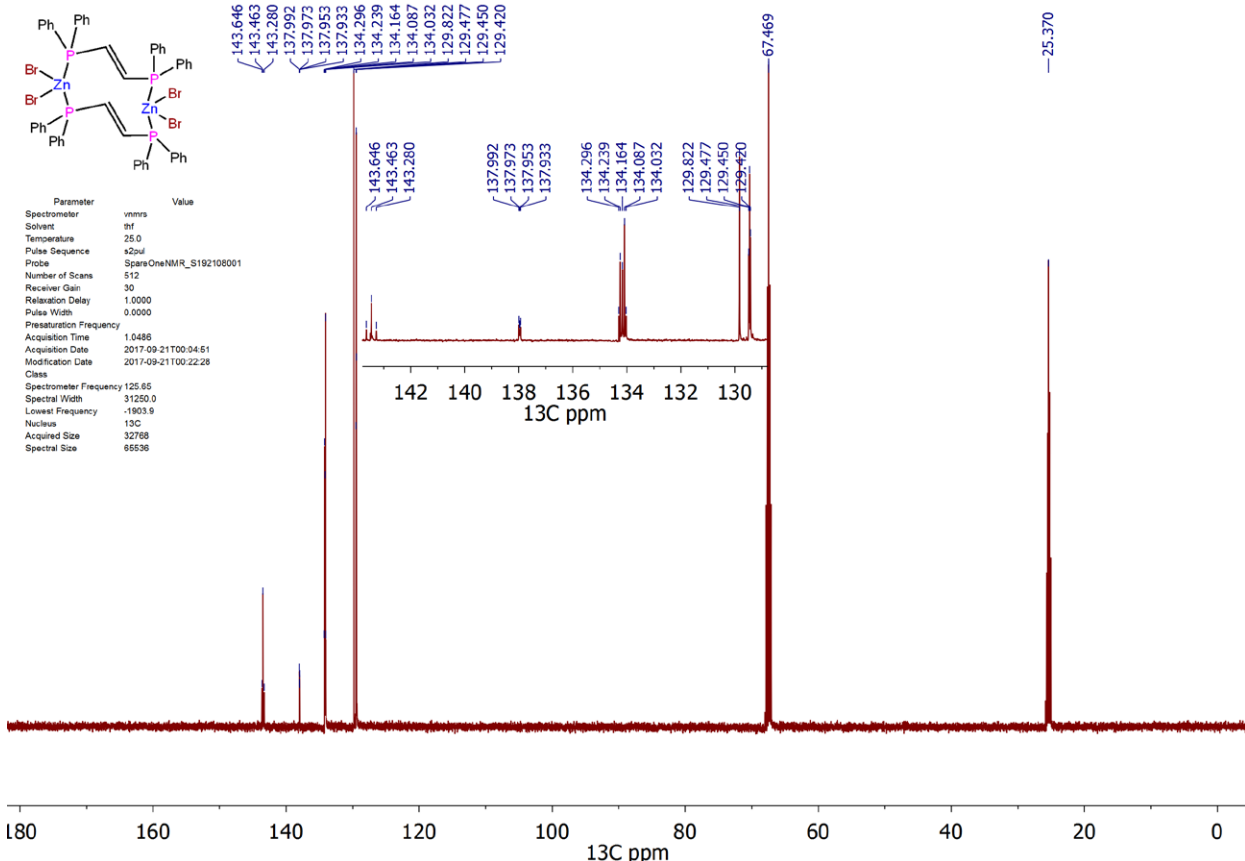
In an argon filled glove box, a vial was loaded with *trans*-dppen (116.7 mg, 0.294 mmol), ZnBr₂ (66.3 mg, 0.294 mmol), CH₂Cl₂ (2 mL) and 7 drops of THF. After standing for 12 hours colourless crystals were obtained. The crystals were dissolved by addition of THF and heating, the solution was filtered while still hot and once cool layered with hexane (4 mL). After 24 hours, colourless crystals formed which were isolated by decanting the supernatant solution, dried under reduced pressure, ground and further dried under reduced pressure for 12 hours to give **13** (174.7 mg, 95%) as a white powder. Crystals suitable for a crystallographic analysis were obtained by layering a THF solution of the compound with hexane. ¹H NMR (500 MHz, THF-*d*₈) δ = 7.42-7.37 (m, 8H), 7.35-7.30 (m, 12H), 6.86-6.70 (t, *J*=14.4, 2H). ¹³C NMR (126 MHz, THF-*d*₈) δ = 143.5 (t, *J*=22.9), 138.0 (dd, *J*=5.0, *J*=2.40), 134.4-133.9 (m), 129.8, 129.5 (t, *J*=3.6). ³¹P NMR (202 MHz, THF-*d*₈) δ = -7.4. Anal. Calcd for C₂₆H₂₂Br₂P₂Zn: C, 50.24; H, 3.57 Found: C, 50.21; H, 3.78. HRMS (ESI/Q-TOF) m/z: No [M]⁺ or [M+A]⁺ peak observed.

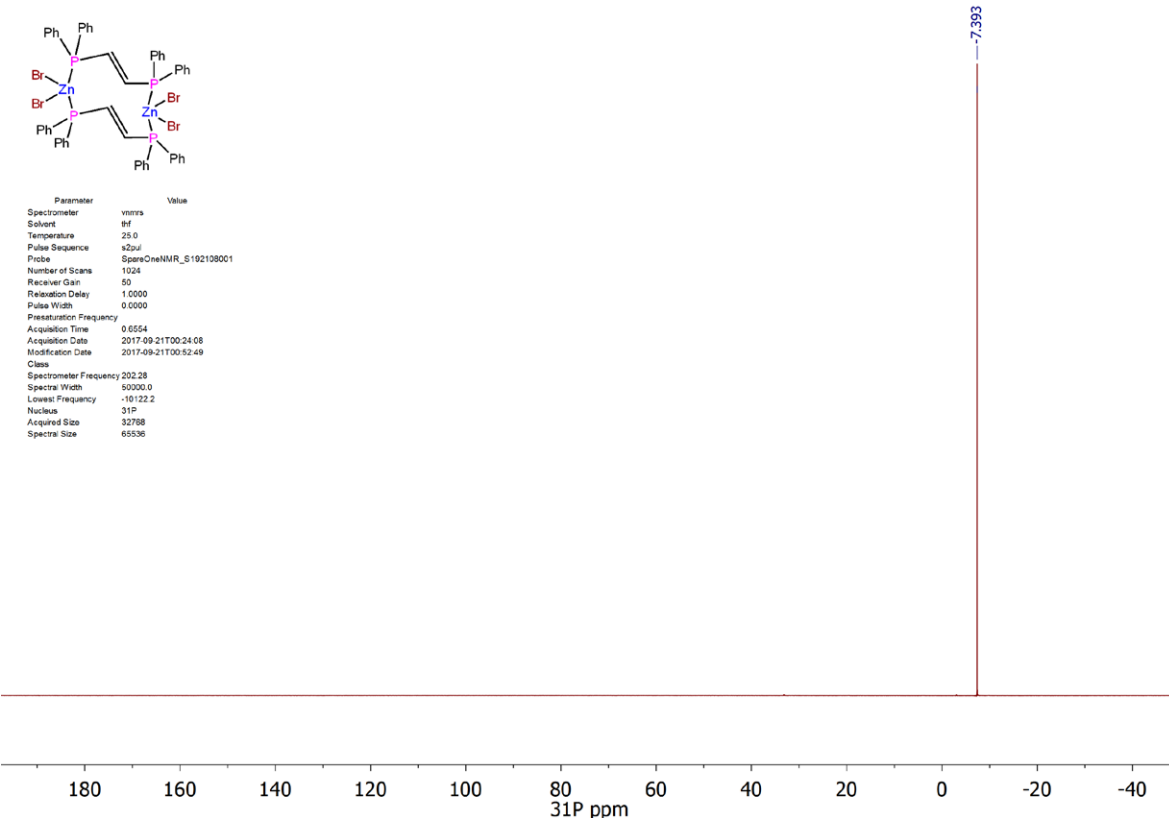


Supplementary Figure 121. Single-crystal X-ray structure of **13**. Hydrogen atoms and solvent molecules are omitted for clarity. Thermal ellipsoids are set at the 50% probability level.



Supplementary Figure 122 ^1H NMR spectrum (500 MHz, $\text{THF}-d_8$) of **13**.

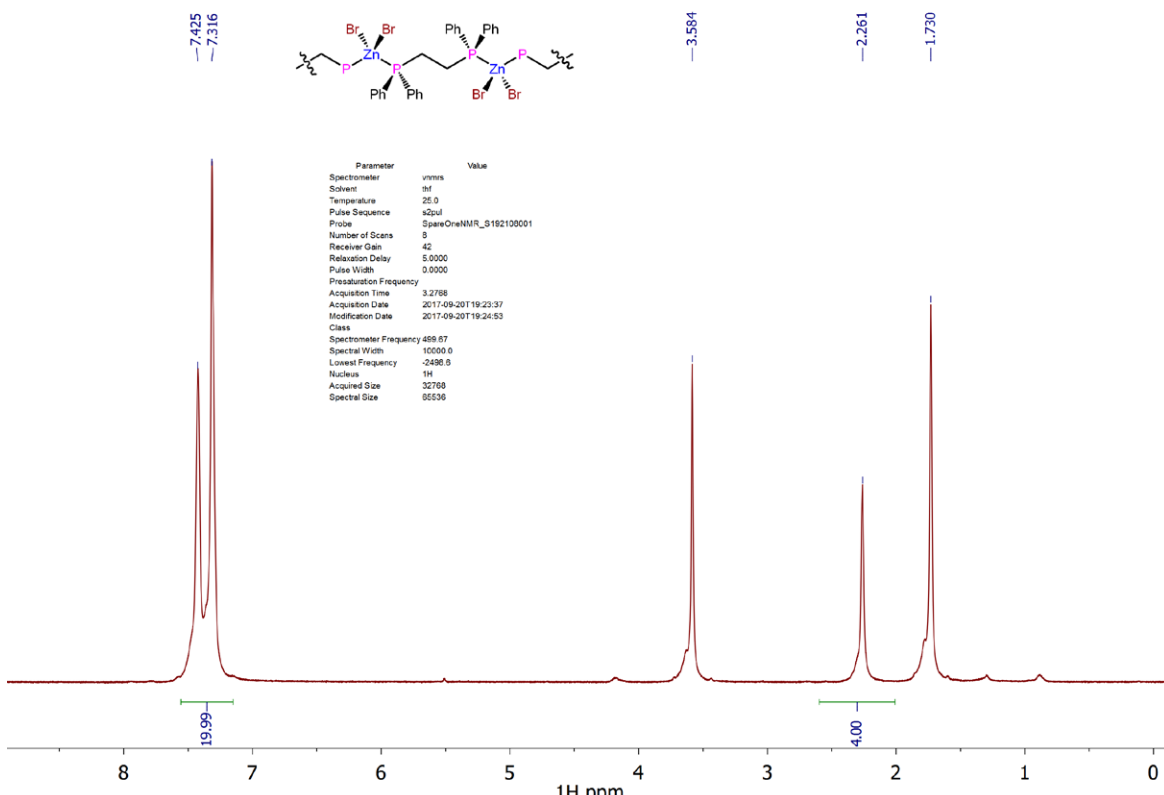




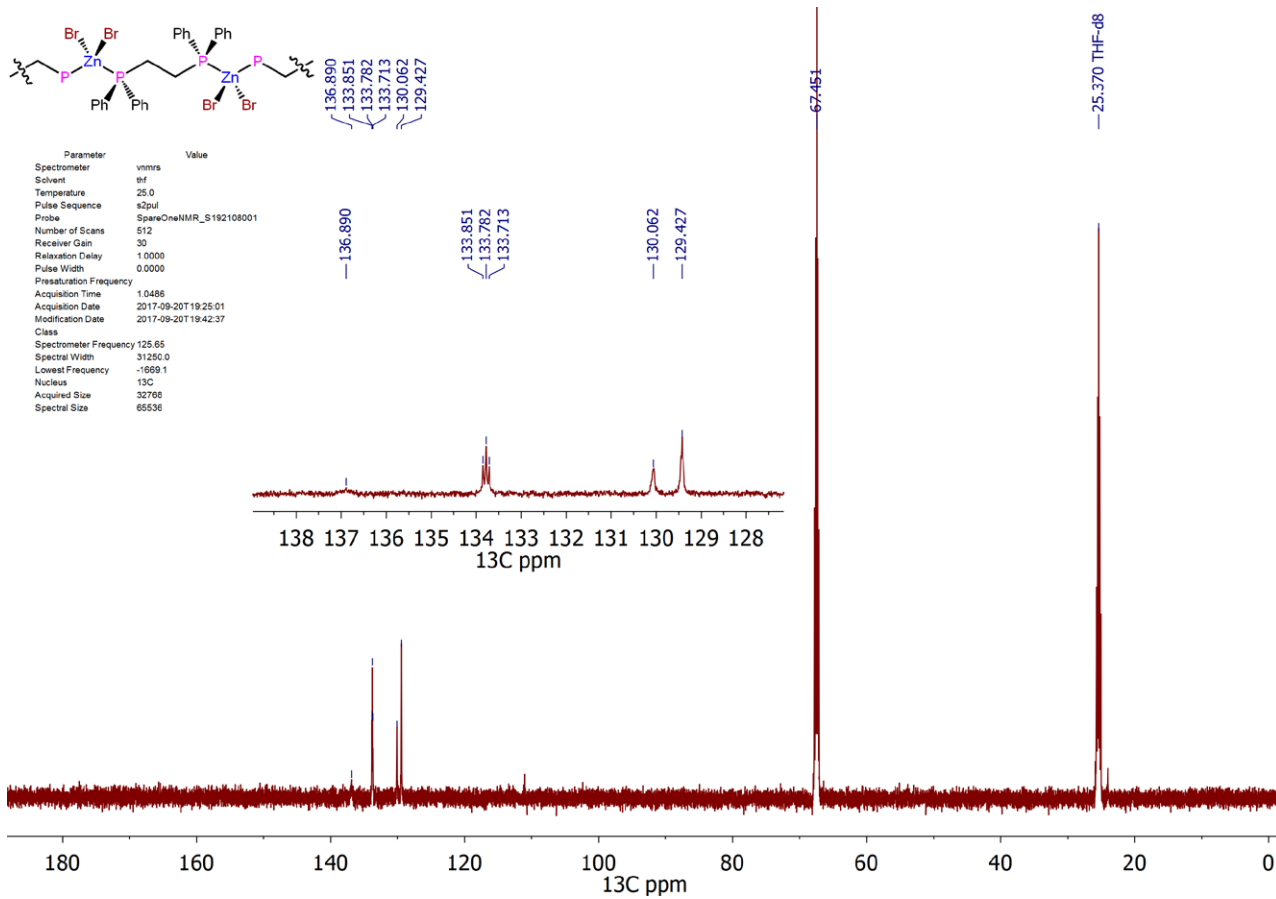
Supplementary Figure 124: ^{31}P NMR spectrum (202 MHz, THF- d_8) of **13**.

7.12 $\{[\text{ZnBr}_2(\mu^2\text{-dppe})]_n\}$ (14)

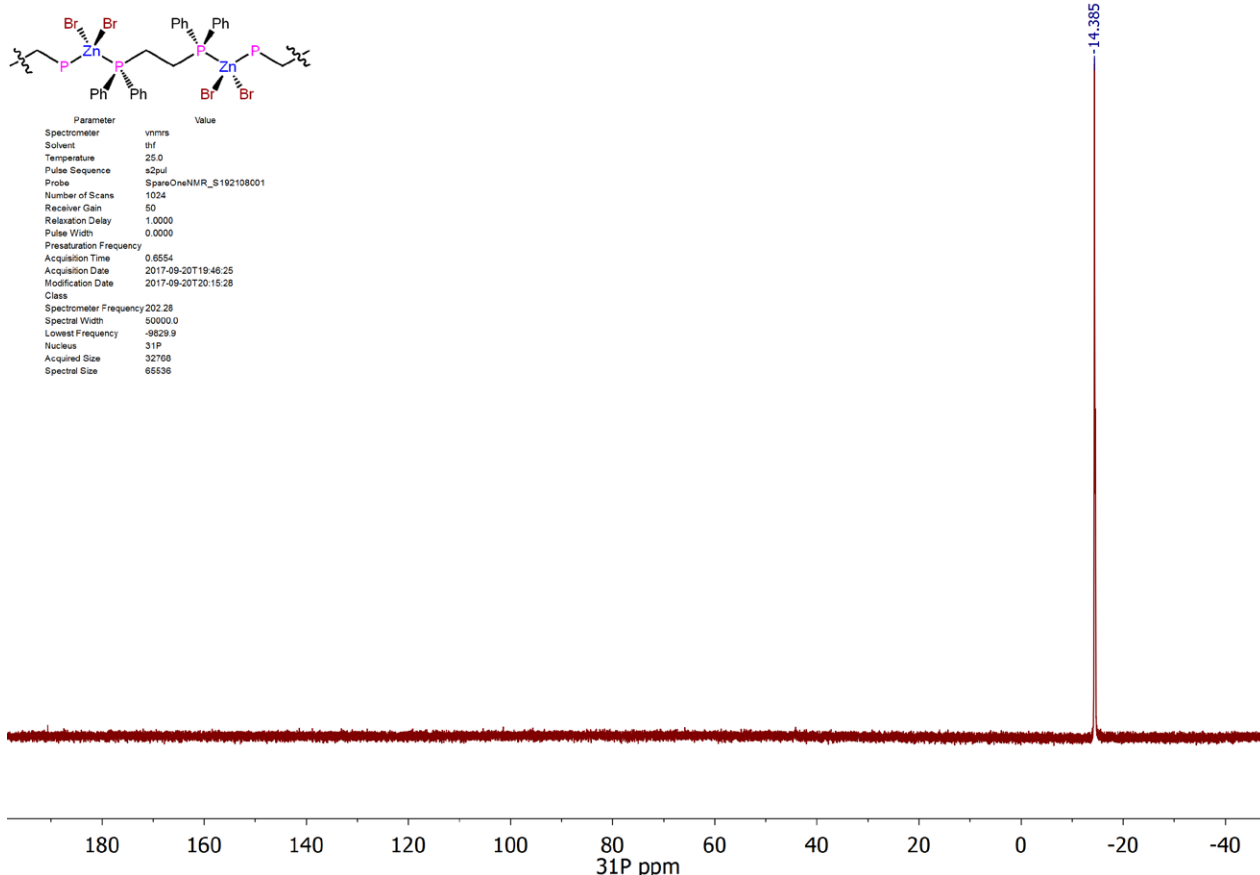
$\{[\text{ZnBr}_2(\mu^2\text{-dppe})]_n\}$ (14) was prepared according to a reported procedure.³² ^1H NMR (500 MHz, THF- d_8) δ = 7.43 (s, 10H), 7.32 (s, 10H), 2.26 (s, 4H). ^{13}C NMR (126 MHz, THF- d_8) δ = 136.9 (br s, weak), 133.8 (t, $J=8.7$), 130.1 (br s, 9.44), 129.4 (br s, 9.44), 24.0 (br s, 11.88). ^{31}P NMR (202 MHz, THF- d_8) δ = -14.4.



Supplementary Figure 125. ^1H NMR spectrum (500 MHz, THF- d_8) of **14**.



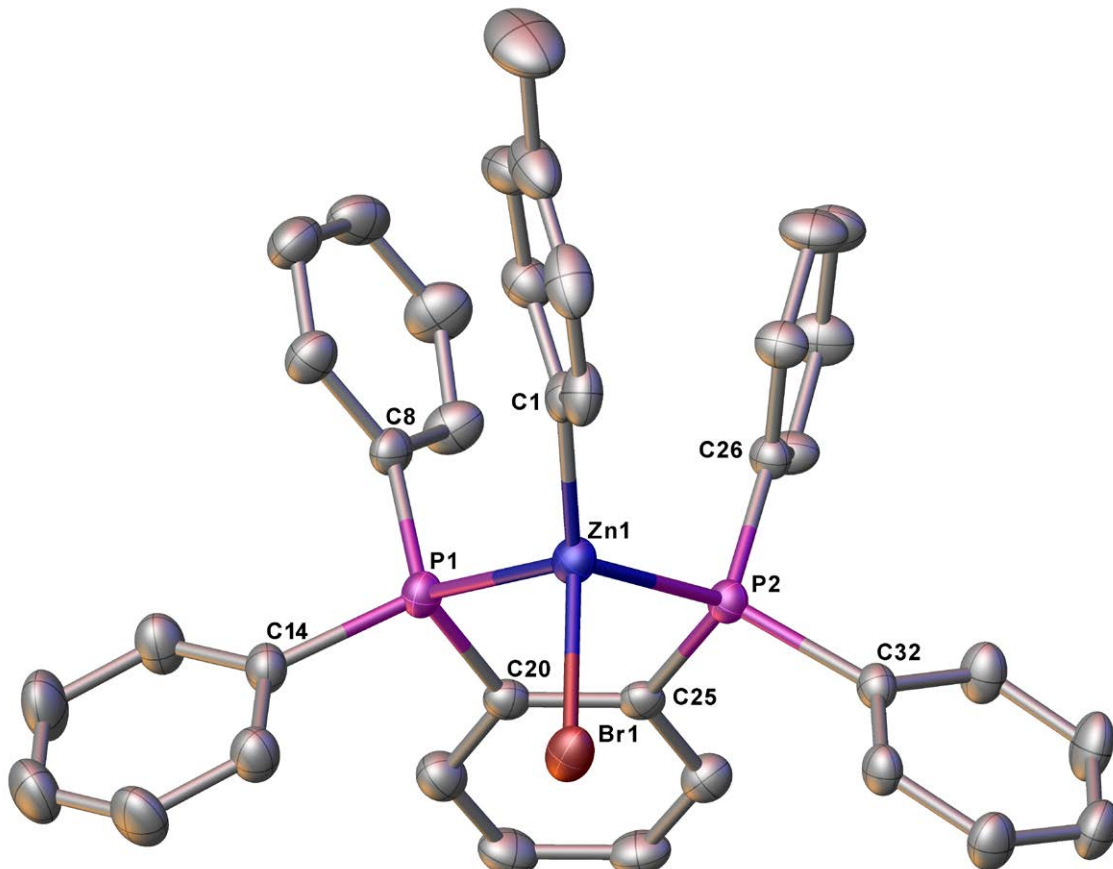
Supplementary Figure 126: ¹³C NMR spectrum (126 MHz, THF-*d*₈) of **14**.



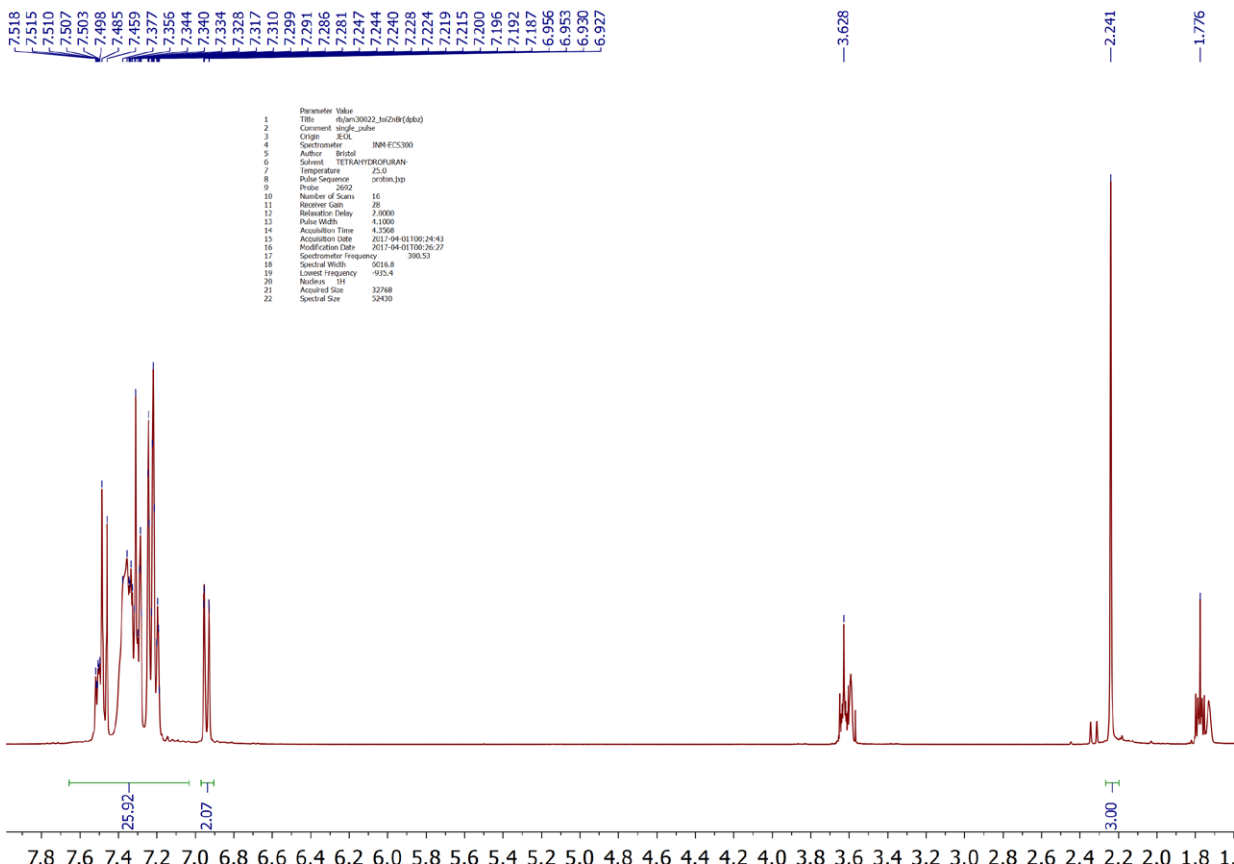
Supplementary Figure 127: ³¹P NMR spectrum (202 MHz, THF-*d*₈) of **14**.

7.13 [ZnBr(4-tolyl)(dpbz)] (15a)

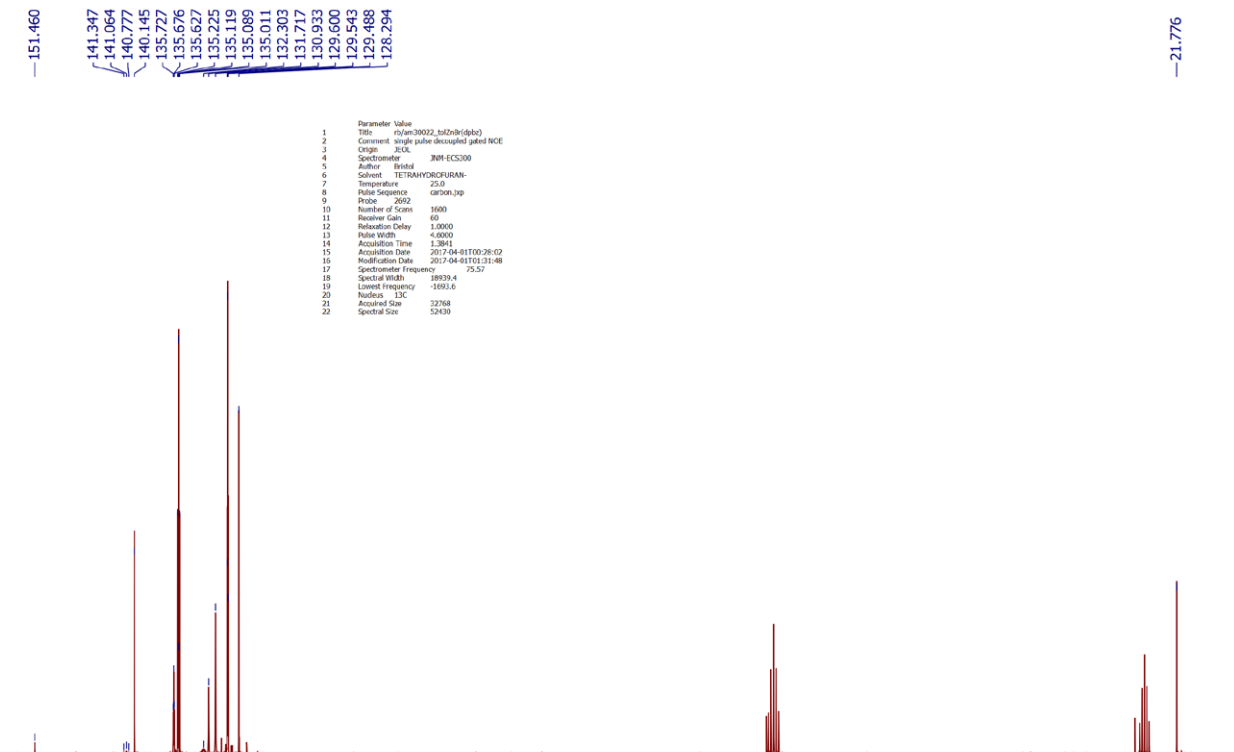
In an argon filled glove box, a vial was loaded with ZnBr₂ (25.2 mg, 0.112 mmol), Zn(4-tolyl)₂ (27.8 mg, 0.112 mmol), dpbz (100.0 mg, 0.224 mmol) and CH₂Cl₂ (3 mL). The resultant solution was filtered and layered with hexane. After 12 hours, a white powder as well as colourless crystals suitable for an X-ray crystallographic analysis formed which were isolated by decanting the supernatant solution, dried under reduced pressure, ground and further dried under reduced pressure for 12 hours to give **15a·½CH₂Cl₂** (89.0 mg, 55%) as a white powder. ¹H NMR (300 MHz, THF-*d*₈) δ = 2.24 (s, 6H; CH₃), 6.94 (d, ³J(H,H) = 7.7, 2H; tolyl CH_{arom}), 7.17-7.44 (m, 22H; dpbz CH_{arom}), 7.47 (d, ³J(H,H) = 7.9, 2H; tolyl CH_{arom}), 7.50-7.54 (m, 2H; dpbz CH_{arom}); ¹³C NMR (76 MHz, THF-*d*₈) δ = 21.8 (s), 128.3 (s), 129.5 (t, *J* = 4.7), 130.9 (br s), 131.7 (br s), 132.8-131.9 (br weak s), 135.1 (t, *J* = 8.1), 135.1 (s), 135.7 (t, *J* = 3.8), 140.2 (s), 140.7-141.5 (br weak m), 151.5 (s); ³¹P NMR (122 MHz, THF-*d*₈) δ = -19.4 (s). Anal. Calcd for C₃₈H₃₂BrClP₂Zn: C, 62.10; H, 4.45 Found: C, 62.32; H, 4.43. HRMS (ESI/Q-TOF) m/z: No [M]⁺ or [M+A]⁺ peak observed.



Supplementary Figure 128. Single-crystal X-ray structure **15a**. Hydrogen atoms and solvent molecules are omitted for clarity while thermal ellipsoids are set at the 50% probability level.



Supplementary Figure 129. ^1H NMR spectrum (300 MHz, THF- d_8) of **15a**.

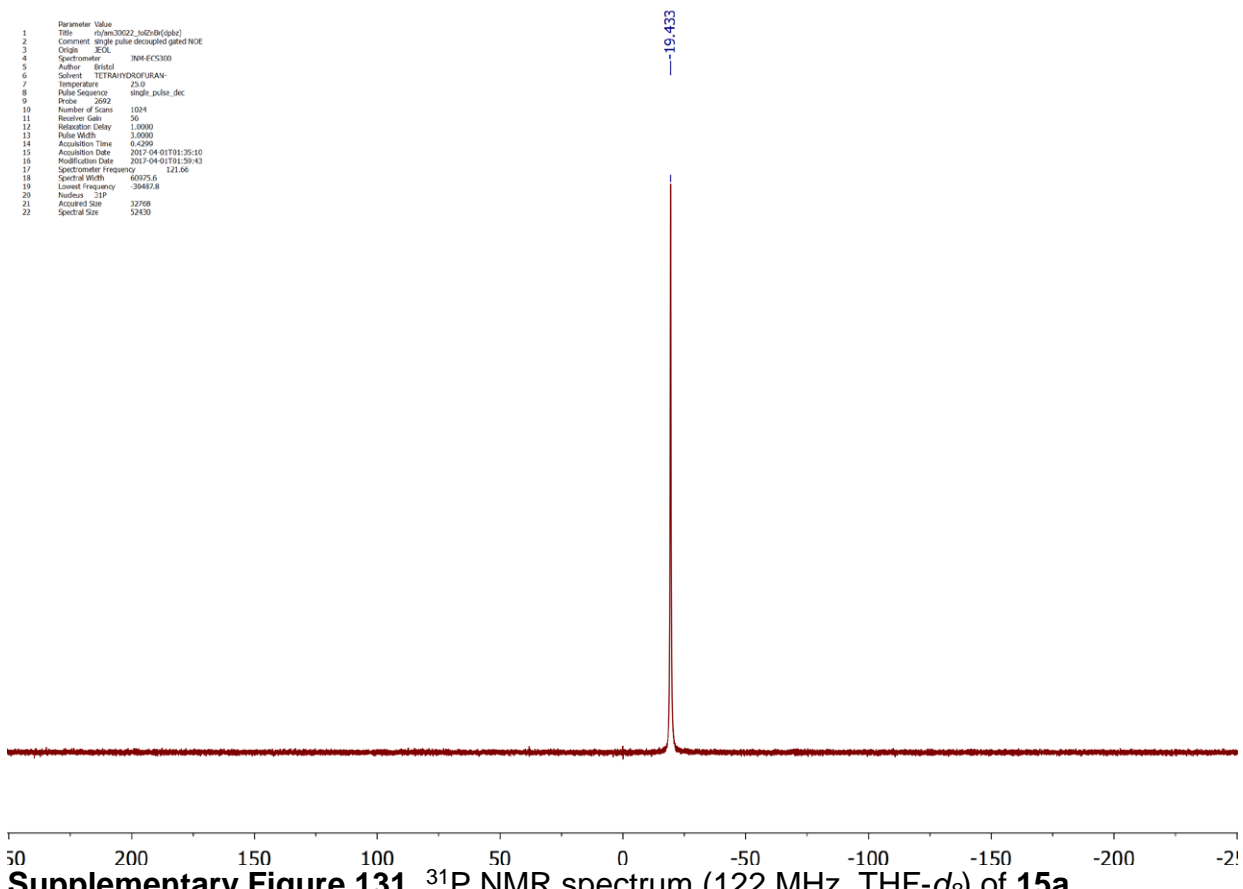


Supplementary Figure 130. ^{13}C NMR spectrum (76 MHz, THF- d_8) of **15a**.

```

Parameter Value
1 Title 31P_122MHz_15a_20170409_122MHz(p�)
2 Comment single pulse decoupled gated NOE
3 Operator JEOL
4 Spectrometer INN-EC5300
5 Author Bristol
6 Software STRAIGHTFORWARD
7 Temperature 23.0
8 Pulse Sequence single_pulse_dec
9 ProbeID 2692
10 Number of Scans 1024
11 RelaxationTime 1.0000
12 RelaxationDelay 1.0000
13 PulseWidth 1.0000
14 AcquisitionTime 0.4299
15 AcquisitionDate 2017-04-09T01:35:10
16 NumberofTransients 1024
17 SpectrometerFrequency 121.66
18 SpectralWidth 600.0
19 LineBreadth 3.00
20 Nucleus 31P
21 AccruedSize 32708
22 SpectralSize 52430

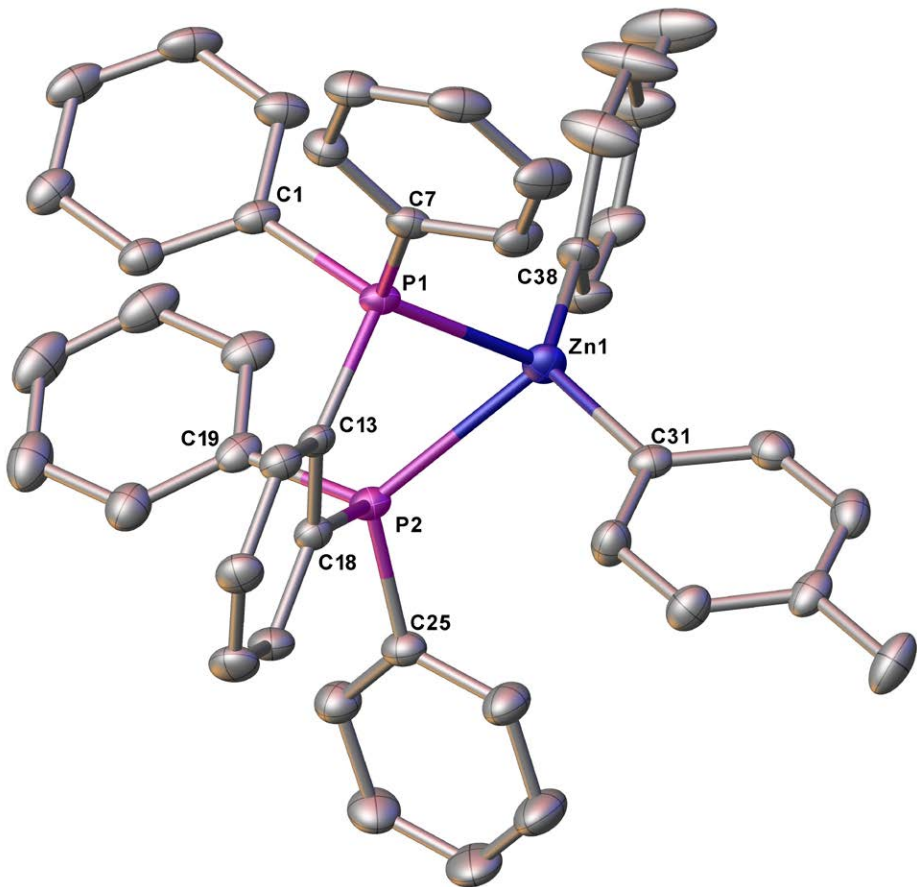
```



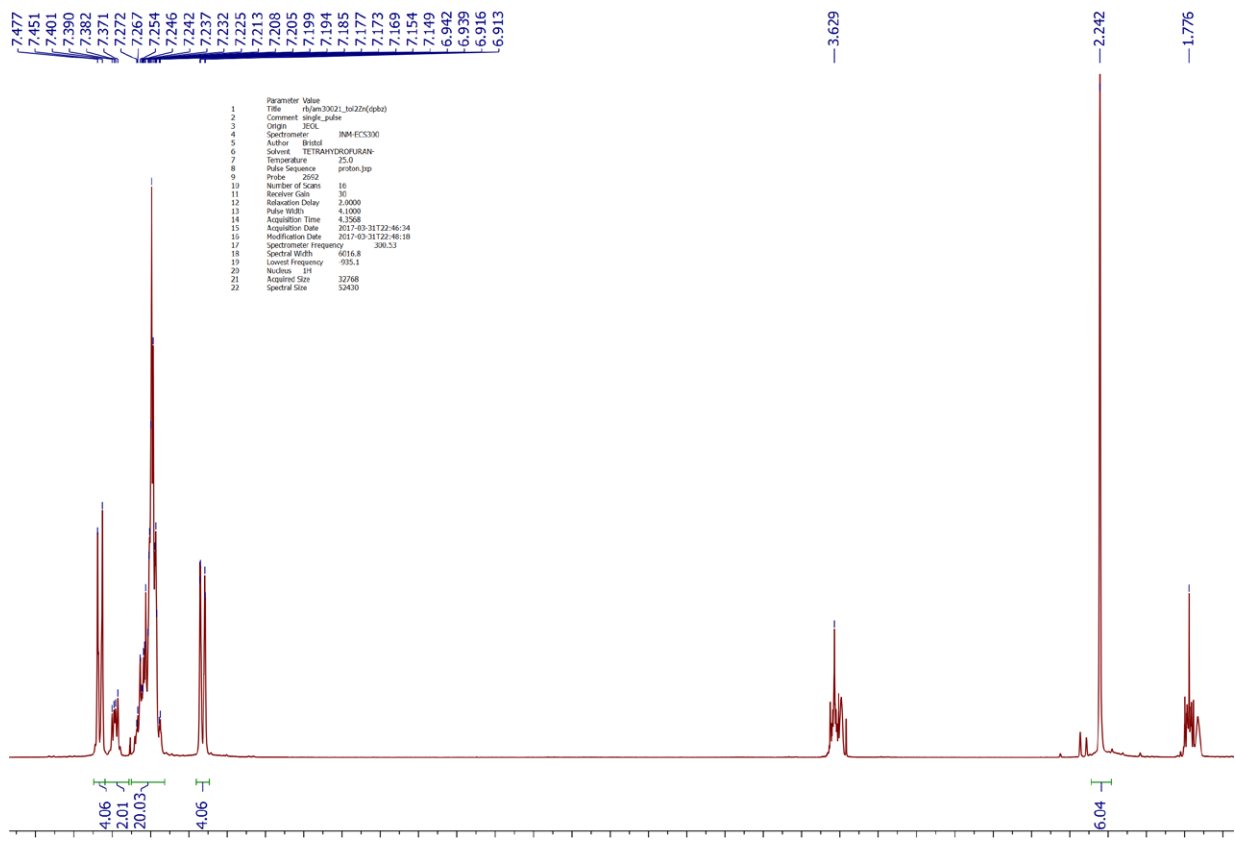
Supplementary Figure 131. ^{31}P NMR spectrum (122 MHz, THF- d_8) of **15a**.

7.14 [Zn(4-tolyl)₂(dpbz)] (16a)

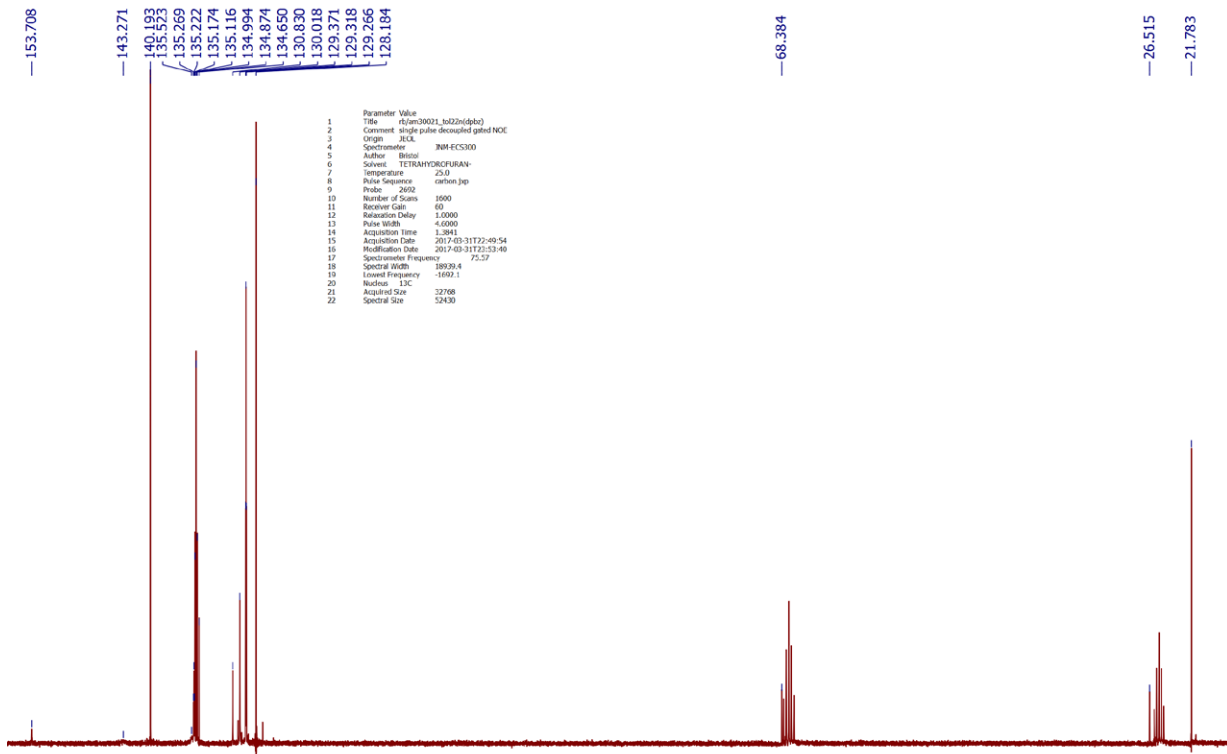
In an argon filled glove box, a vial was loaded with dpbz (99.7 mg, 0.223 mmol), Zn(4-tolyl)₂ (55.3 mg, 0.223 mmol) and toluene (2 mL). The resultant solution was filtered and layered with hexane. After 12 hours, colourless crystals formed which were isolated by decanting the supernatant solution, dried under reduced pressure, ground and further dried under reduced pressure for 12 hours to give **16a·½CH₂Cl₂** (110.2 mg, 71%) as a white powder. Crystals suitable for an X-ray crystallographic analysis were grown by layering a solution of the compound in CHCl₃ with hexane. ^1H NMR (300 MHz, THF- d_8) δ = 2.24 (s, 6H; CH₃), 6.93 (d, $^3J(\text{H},\text{H})$ = 7.1, 4H; tolyl CH_{arom}), 7.13-7.33 (m, 20H; dpbz CH_{arom}), 7.35-7.42 (m, 2H; dpbz CH_{arom}), 7.46 (d, $^3J(\text{H},\text{H})$ = 7.7, 4H; tolyl CH_{arom}); ^{13}C NMR (76 MHz, THF- d_8) δ = 21.8 (s), 128.2 (s), 129.3 (t, J = 4.0), 130.0 (br s), 130.8 (br s), 134.7 (s), 135.0 (t, J = 9.0), 135.2 (t, J = 3.6), 135.3-135.7 (br weak s), 140.2 (s), 142.8-143.8 (br weak s), 153.7 (s); ^{31}P NMR (122 MHz, THF- d_8) δ = -15.9 (s).



Supplementary Figure 132. Single-crystal X-ray structure of **16a**. Hydrogen atoms and solvent molecules are omitted for clarity while thermal ellipsoids are set at the 50% probability level.



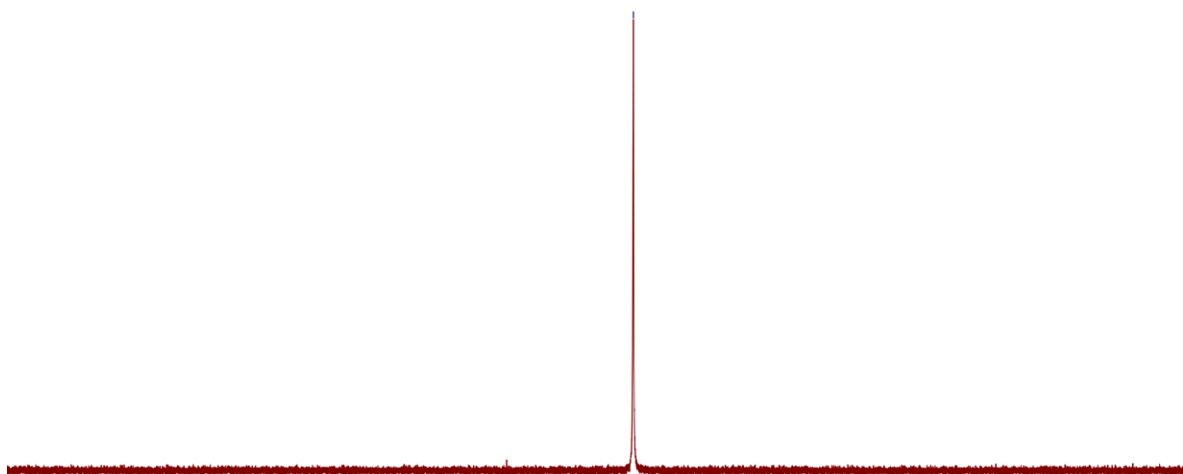
Supplementary Figure 133. ^1H NMR spectrum (300 MHz, $\text{THF}-d_8$) of **16a**.



Supplementary Figure 134. ^{13}C NMR spectrum (75 MHz, THF- d_8) of **16a**.

Parameter Value

- Title $\text{r2pm30021_1s122c(qdp)}$
- Comment single pulse decoupled gated NOE
- Origin JECI
- SpectrumType 3NM-FC500
- Author Brinol
- Solvent TETRAHYDROFURAN-
- Temperature 25.0
- PulseSequence carbon_jdp
- Pulse 2692
- Number of Scans 1000
- Receiver Gain 50
- Relaxation Delay 1.0000
- Pulse Width 4.0000
- Acquisition Time 0.4396
- Acquisition Date 2017-04-01T22:57:53
- Modification Date 2017-04-01T00:21:39
- Sample Name requirement 121.56
- Spectral Width 60075.6
- Locked Frequency -30487.8
- Noise 1.3%
- Acquired Size 32768
- Spectral Size 52430

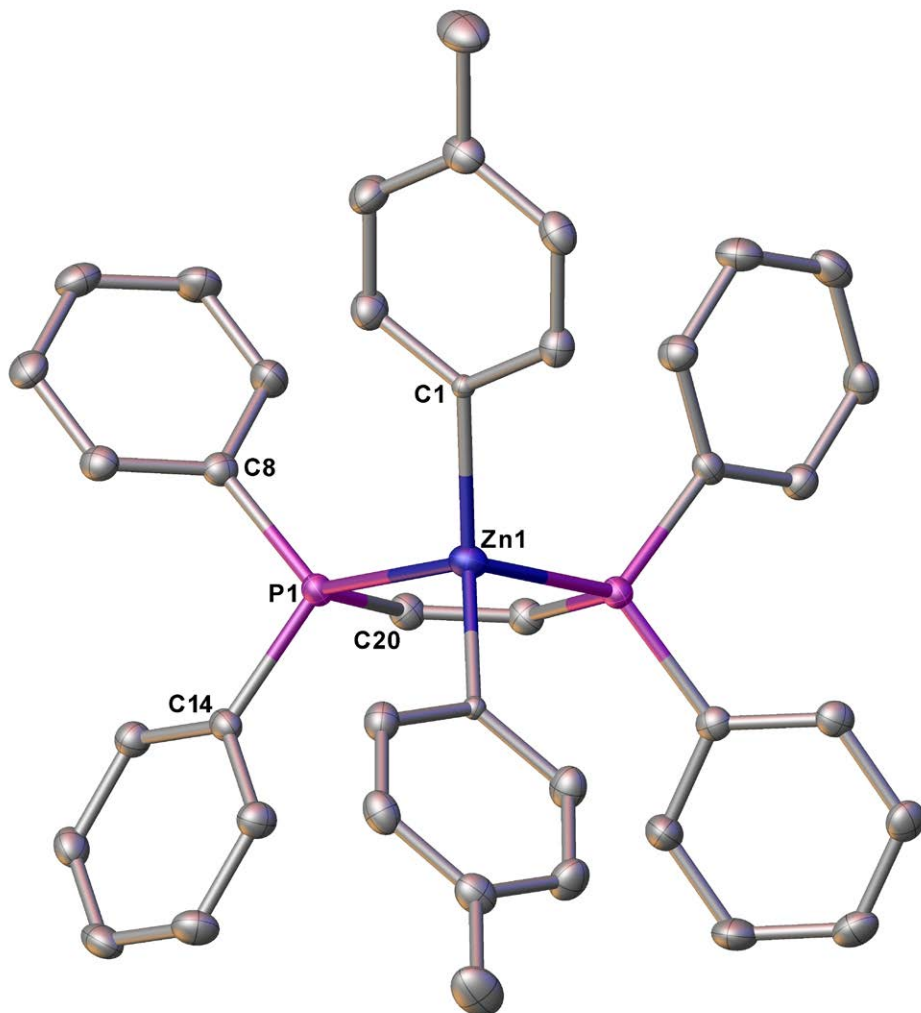


Supplementary Figure 135. ^{31}P NMR spectrum (122 MHz, THF- d_8) of **16a**.

7.15 [Zn(4-tolyl)₂(*cis*-dppen)] (**16b**)

In an argon filled glove box, a vial was loaded with *cis*-dppen (96.2 mg, 0.243 mmol), Zn(4-tolyl)₂ (60.1 mg, 0.243 mmol), CH₂Cl₂ (2 mL) and 7 drops of THF. After standing for 12 hours

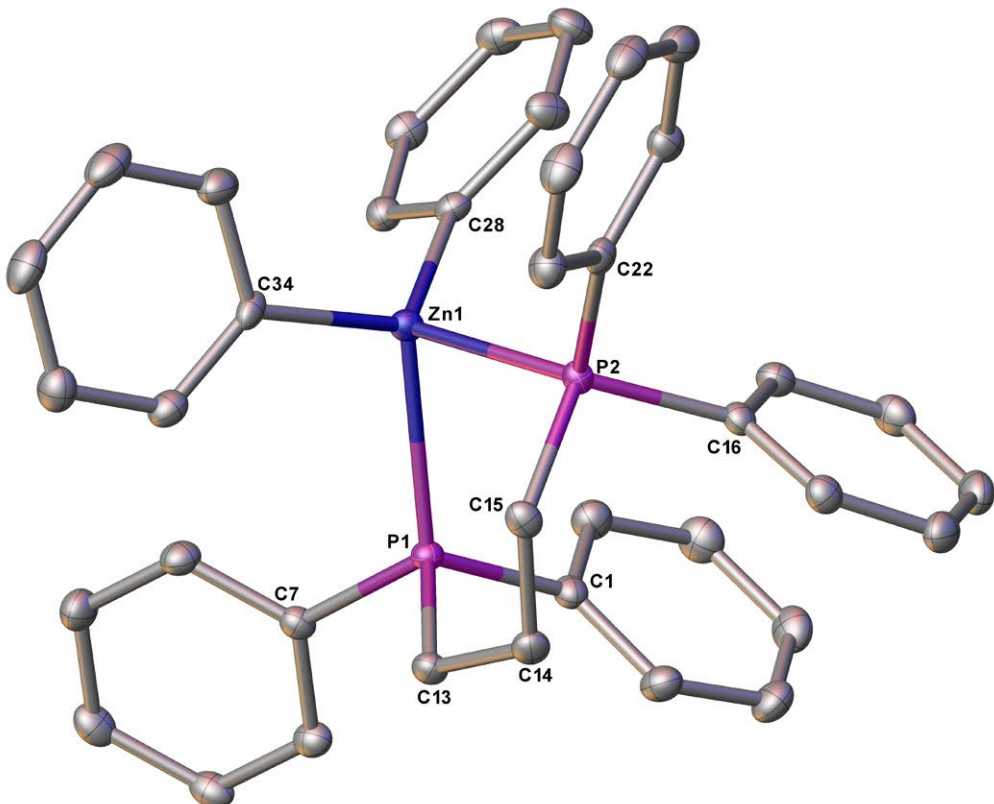
a colourless solution formed which was filtered and layered with hexane (4 mL). After 24 hours, colourless crystals suitable for an X-ray crystallographic analysis formed which were isolated by decanting the supernatant solution, dried under reduced pressure, ground and further dried under reduced pressure for 12 hours to give **16b**^{·½ CH₂Cl₂} (114.0 mg, 68%) as a white powder. Anal. Calcd for C_{40.5}H₃₇ClP₂Zn: C, 70.86; H, 5.43 Found: C, 70.81; H, 5.85. HRMS (ESI/Q-TOF) m/z: No [M]⁺ or [M+A]⁺ peak observed.



Supplementary Figure 136. Single-crystal X-ray structure of **16b**. Hydrogen atoms are omitted for clarity and thermal ellipsoids are set at the 50% probability level.

7.16 [ZnPh₂(dppp)] (16c)

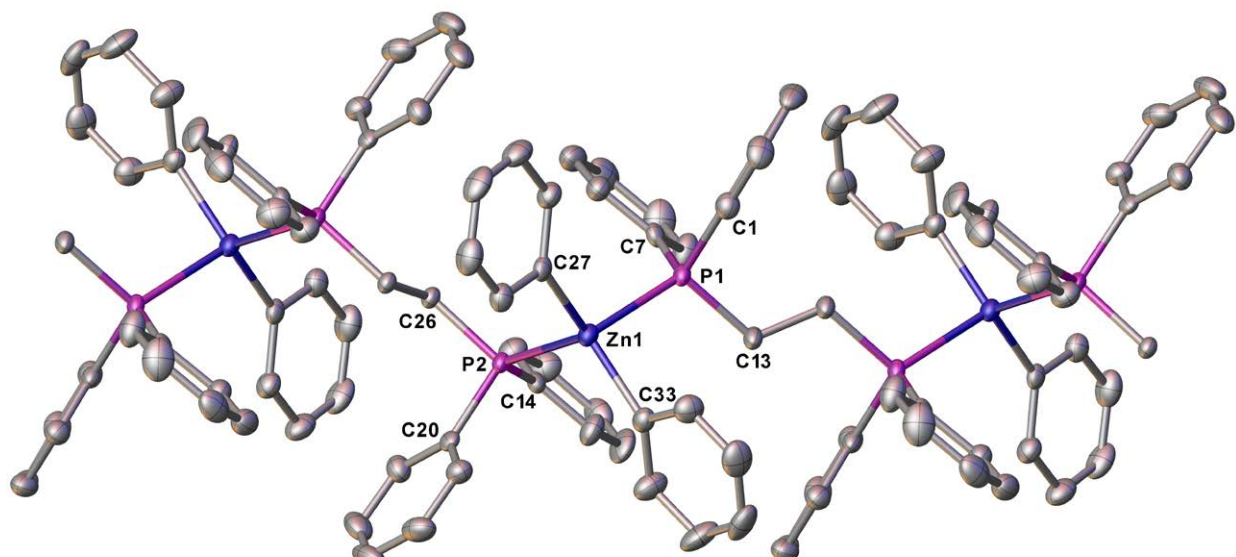
In an argon filled glove box, a vial was loaded with dppp (100.0 mg, 0.242 mmol), ZnPh₂ (59.9 mg, 0.242 mmol), CH₂Cl₂ (2 mL) and 7 drops of THF. After standing for 12 hours a colourless solution formed which was filtered and layered with hexane (4 mL). After 24 hours, colourless crystals suitable for an X-ray crystallographic analysis formed (Supplementary Figure 137).



Supplementary Figure 137. Single-crystal X-ray structure of **16c**. Hydrogen atoms are omitted for clarity and thermal ellipsoids are set at the 50% probability level.

7.17 $\{[\text{ZnPh}_2(\mu^2\text{-dppe})]_n\}$ (17)

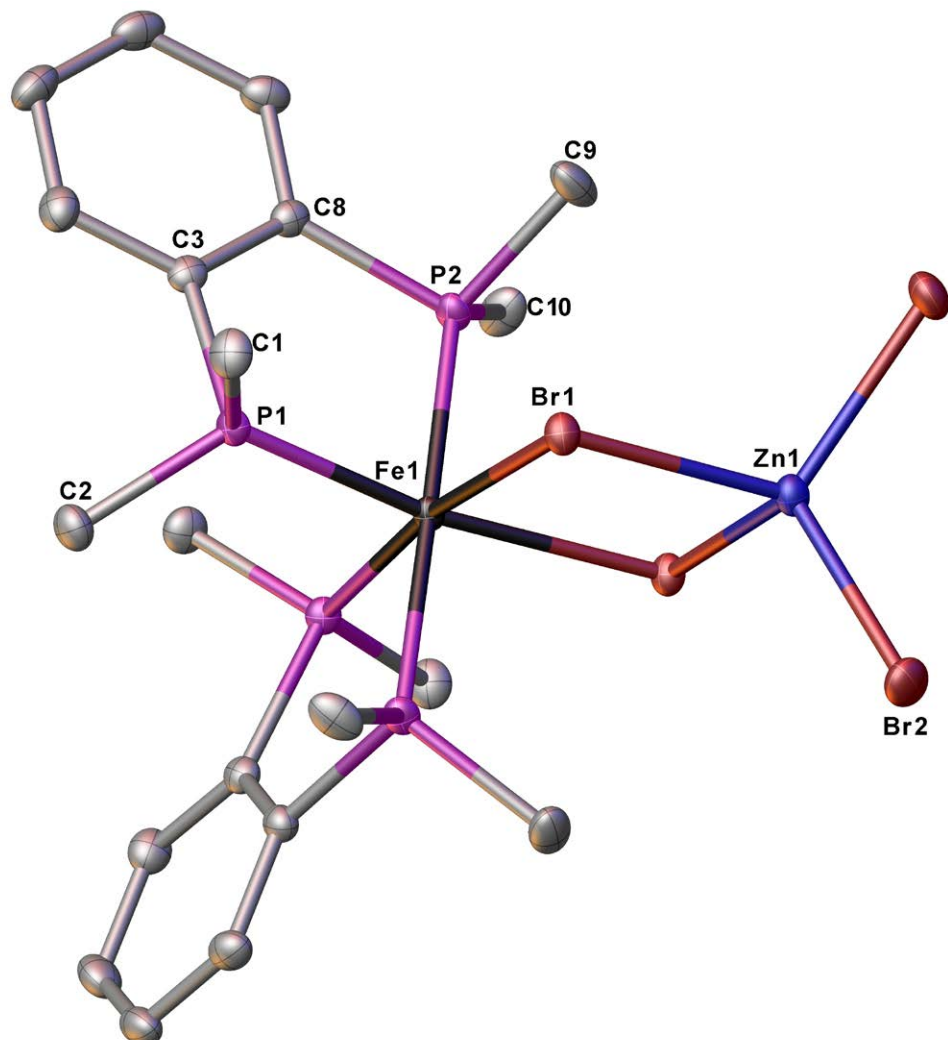
In an argon filled glove box, a vial was loaded with dppe (181.4 mg, 0.455 mmol), ZnPh_2 (100.0 mg, 0.455 mmol), CH_2Cl_2 (2 mL) and 7 drops of THF. After standing for 12 hours a colourless solution formed which was filtered and layered with hexane (4 mL). After 24 hours, colourless crystals suitable for an X-ray crystallographic analysis formed. The crystallographic analysis that followed revealed formation of $\{[\text{ZnPh}_2(\mu^2\text{-dppe})]_n\}$ (17) (Supplementary Figure 138).



Supplementary Figure 138. Single-crystal X-ray structure of **17**. Hydrogen atoms are omitted for clarity and thermal ellipsoids are set at the 50% probability level.

7.18 Reaction of $\text{FeBr}_2(\text{dmbz})_2$ with ZnBr_2 to give $[(\text{dmbz})_2\text{Fe}(\mu\text{-Br})_2\text{ZnBr}_2]$ (18)

An NMR tube was loaded with FeBr_2 (600 μL , 25 mM stock solution, 0.15 mmol) followed by addition of a stock solution of dmbz (200 μL , 75 mM stock solution, 0.15 mmol) in THF-d_8 to form an insoluble green precipitate. Subsequently, ZnBr_2 (16.9 mg, 0.15 mmol) was added and the mixture was shaken until the ZnBr_2 dissolved. The mixture was subject to an ^1H NMR spectroscopic analysis, but no signals were observed between 1500 and -200 ppm. After 12 h of standing at room temperature, the green precipitate was replaced by small dark red crystals which were found to be $[(\text{dmbz})_2\text{Fe}(\mu\text{-Br})_2\text{ZnBr}_2]$ (18) according to an X-ray crystallographic analysis (Supplementary Figure 139).



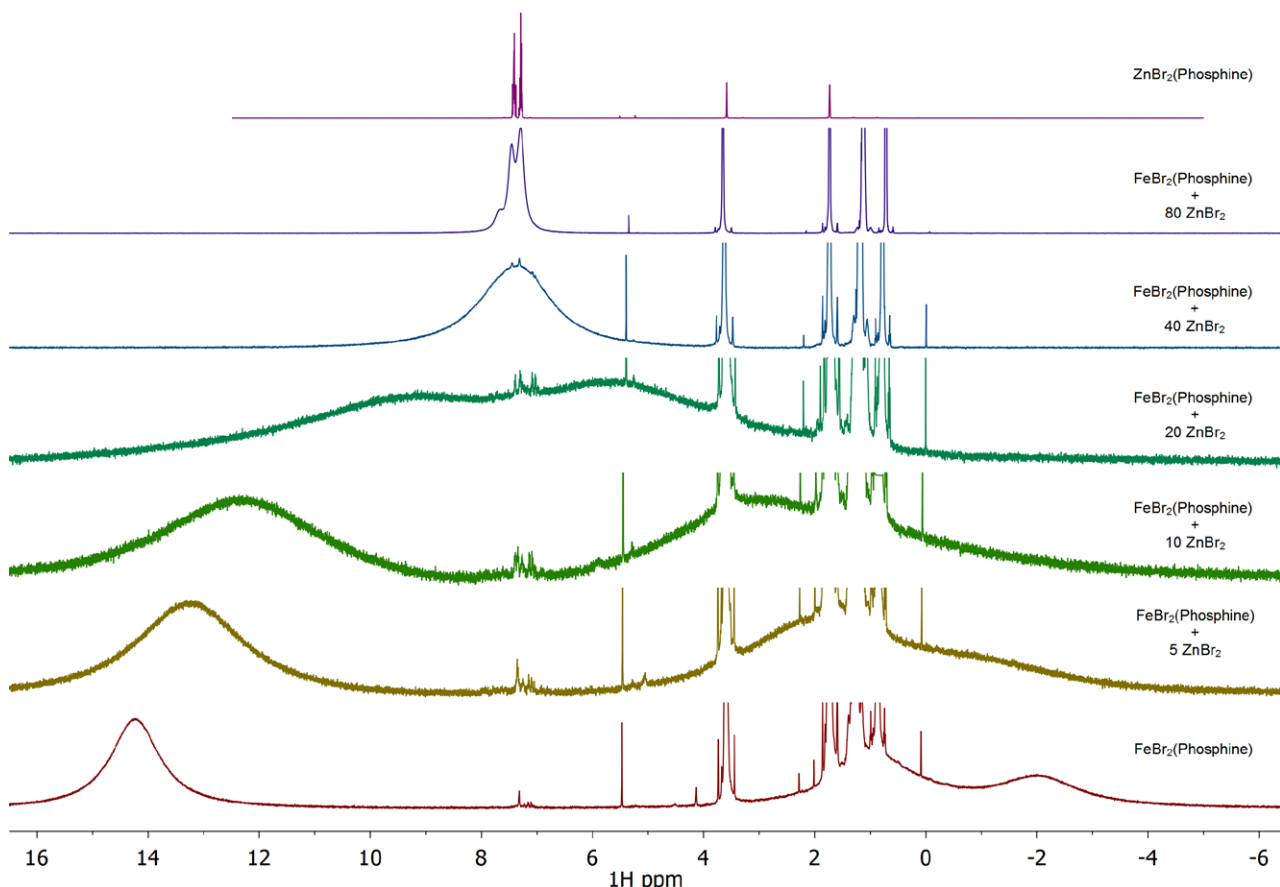
Supplementary Figure 139. Single-crystal X-ray structure of **18**. Hydrogen atoms are omitted for clarity and thermal ellipsoids are set at the 50% probability level.

8 Competition for diphosphine coordination between FeBr₂ and excess ZnBr₂.

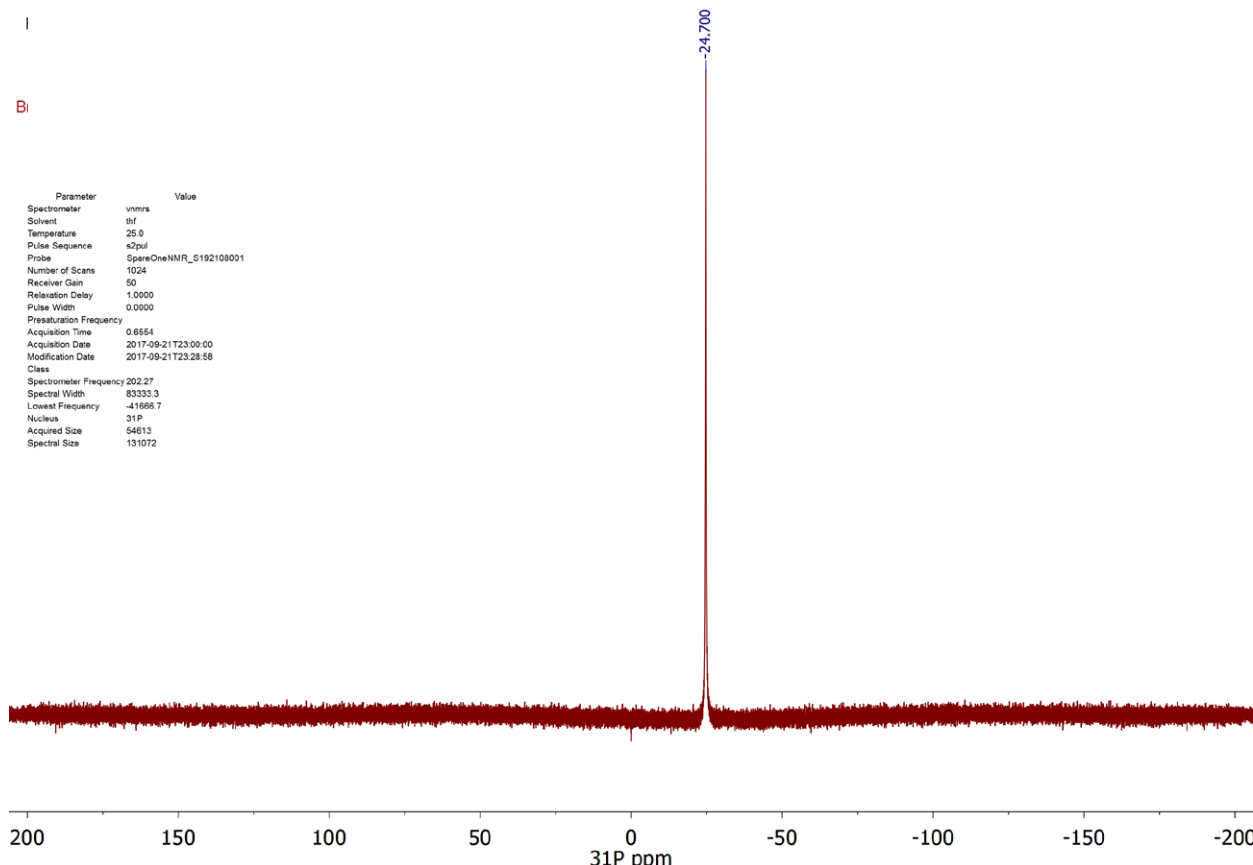
8.1 Competition reactions

In order to establish the preference of each phosphine to coordinate to Zn(II) or Fe(II), competition reactions of the diphosphines with FeBr₂ and increasing amounts of ZnBr₂ in THF were performed as follows: 12 NMR tubes were loaded with 600 µL of a stock solution of FeBr₂ (25 mM) and *n*-dodecane (internal standard, 25 mM) in THF-*d*₈ followed by addition of 200 µL of a stock solution of each diphosphine (75 mM) in THF-*d*₈ and the portionwise additions of ZnBr₂ of 16.9 mg (5 eq. in Zn), 16.9 mg (10 eq. in Zn), 33.8 mg (20 eq. in Zn), 67.6 mg (40 eq. in Zn) and 135.1 mg (80 eq. in Zn), with the ¹H NMR spectrum recorded after each addition, with a relaxation delay of 5 s.* The ³¹P NMR spectra were also collected for the mixtures with 80 eq. of ZnBr₂. The NMR spectra obtained are shown in Supplementary Figure 140 to Supplementary Figure 161.

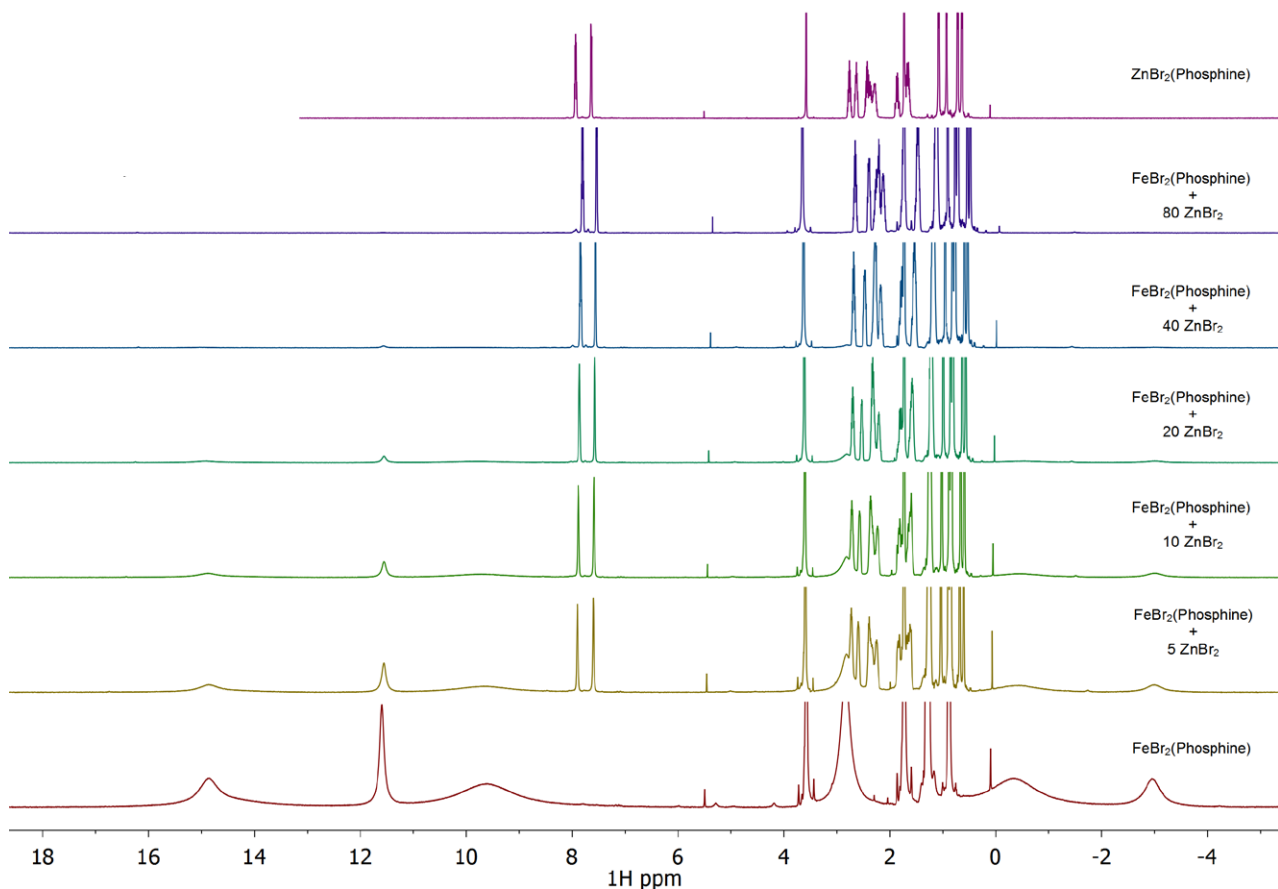
* The maximum relaxation delay of the [ZnBr₂(dpbz)] resonances in THF-*d*₈ was found to be 2.5 s. Therefore, a d1 = 5 s was used for ¹H NMR acquisition in order for the collected data to be quantifiable. Note that presence of paramagnetic species such as FeBr₂ will further reduce the relaxation delay of the various components in the mixture.



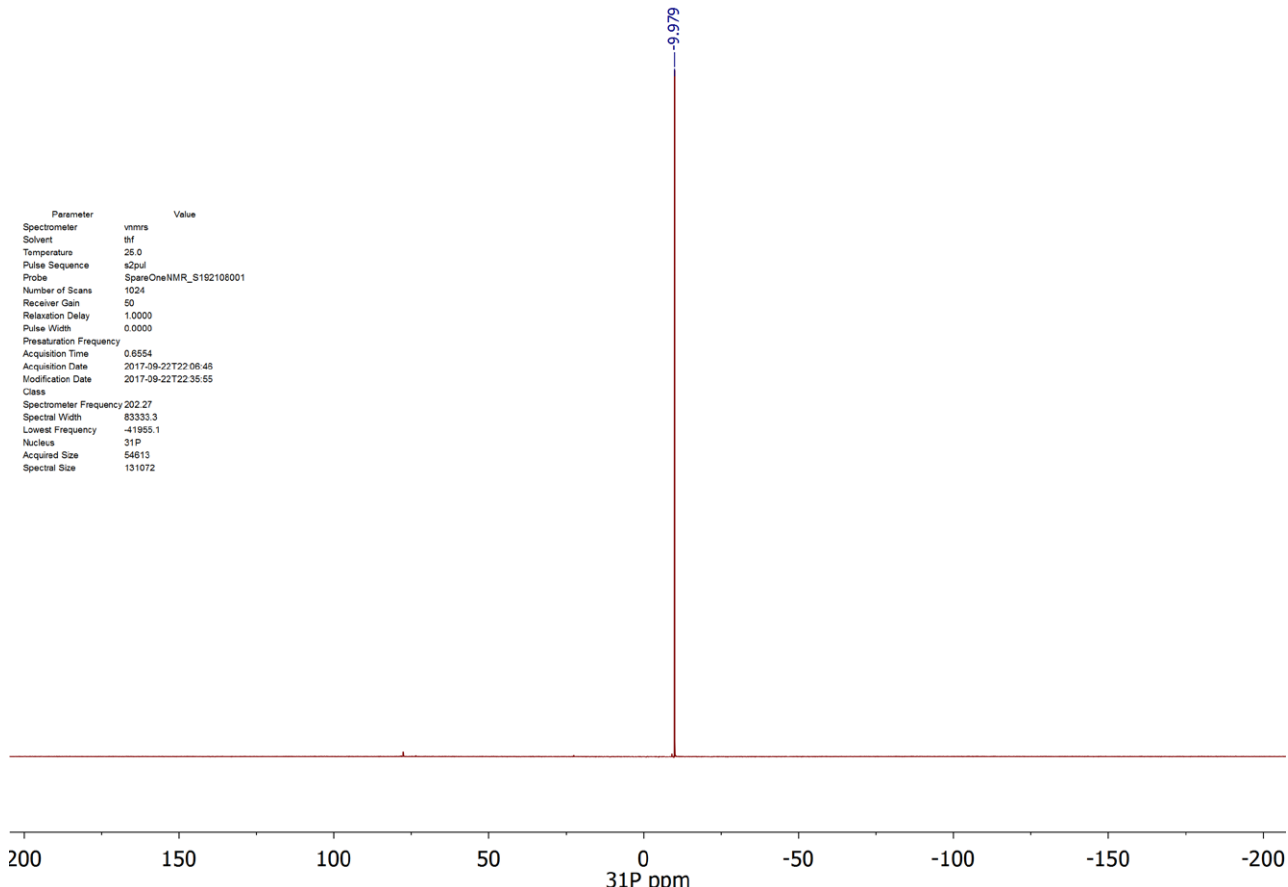
Supplementary Figure 140. Stacked ¹H NMR spectra (500 MHz, THF-*d*₈) of the reaction between FeBr₂, *cis*-dppen and varying eq. of ZnBr₂.



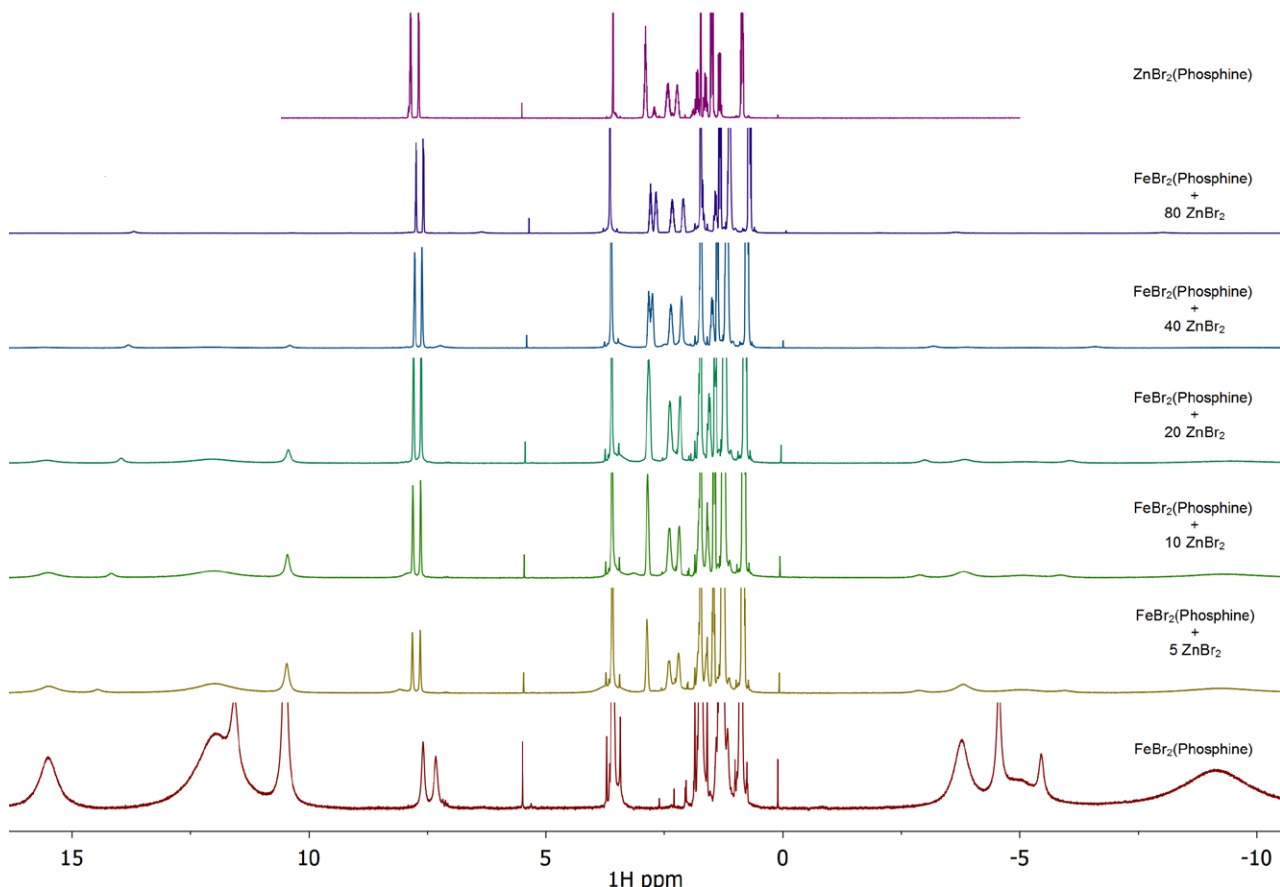
Supplementary Figure 141. ³¹P NMR spectrum (202 MHz, THF-*d*₈) of the reaction between FeBr₂, *cis*-dppen and 80 eq. of ZnBr₂.



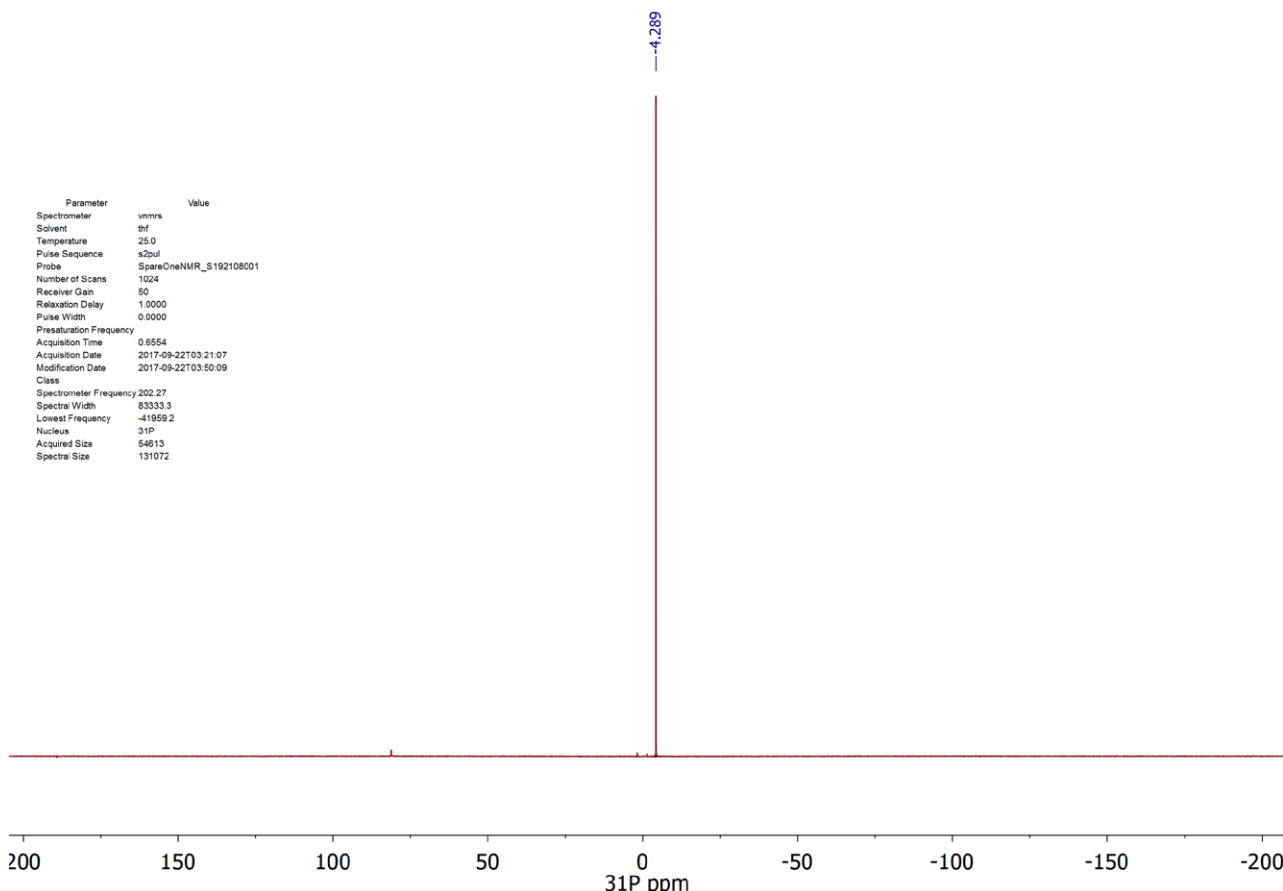
Supplementary Figure 142. Stacked ¹H NMR spectra (500 MHz, THF-*d*₈) of the reaction between FeBr₂, iPrDuphos and varying eq. of ZnBr₂.



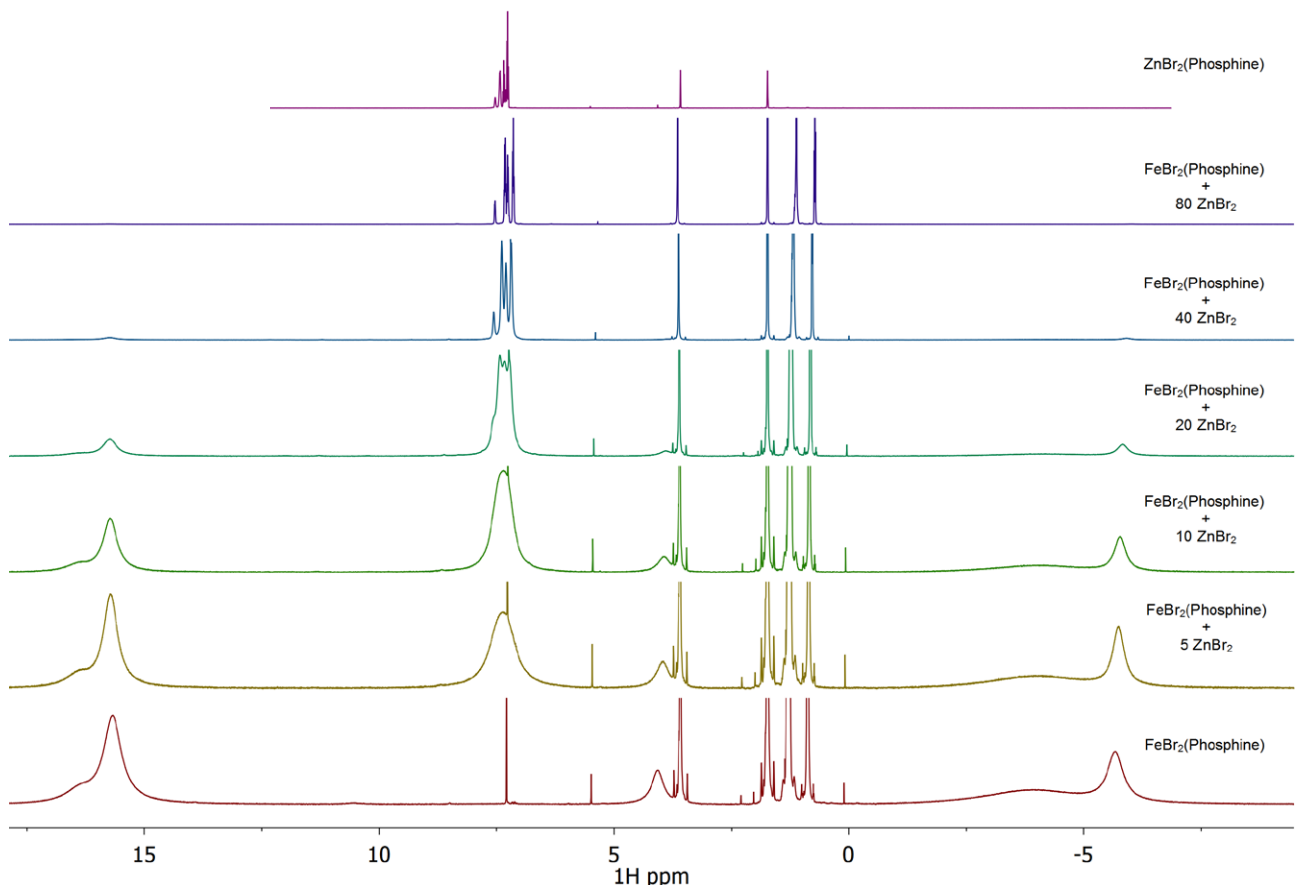
Supplementary Figure 143. ³¹P NMR spectrum (202 MHz, THF-*d*₈) of the reaction between FeBr₂, iPrDuphos and 80 eq. of ZnBr₂.



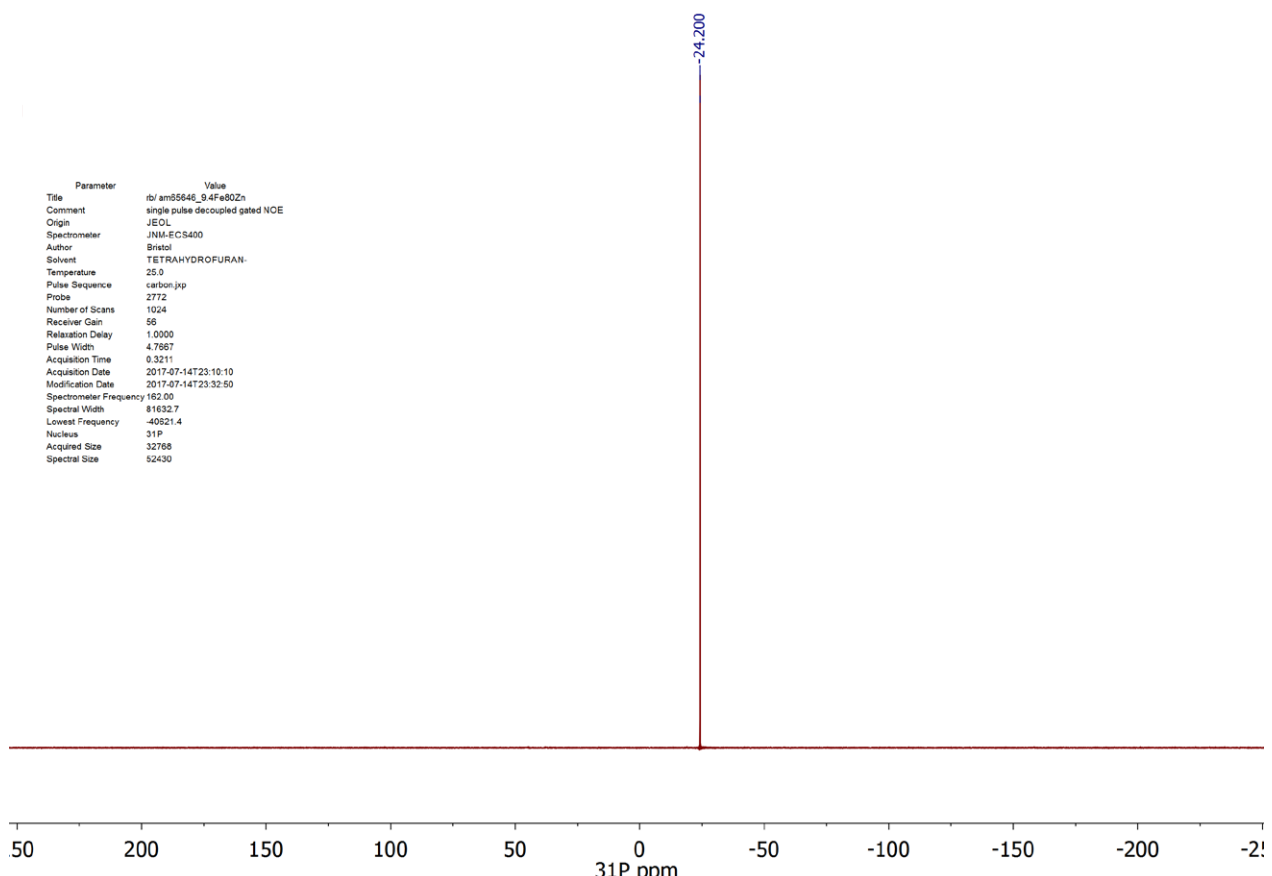
Supplementary Figure 144. Stacked ¹H NMR spectra (500 MHz, THF-*d*₈) of the reaction between FeBr₂, MeDuphos and varying eq. of ZnBr₂.



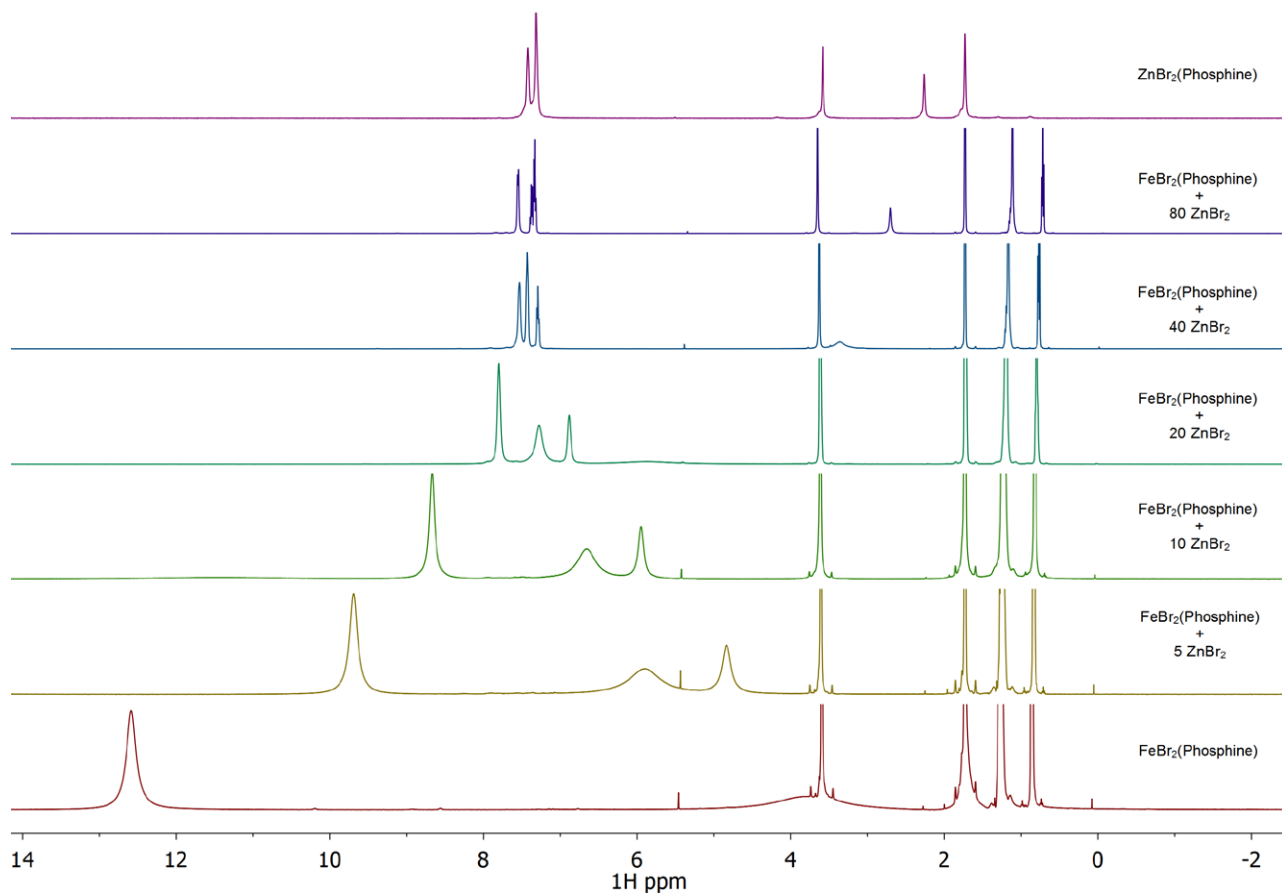
Supplementary Figure 145. ³¹P NMR spectrum (202 MHz, THF-*d*₈) of the reaction between FeBr₂, MeDuphos and 80 eq. of ZnBr₂.



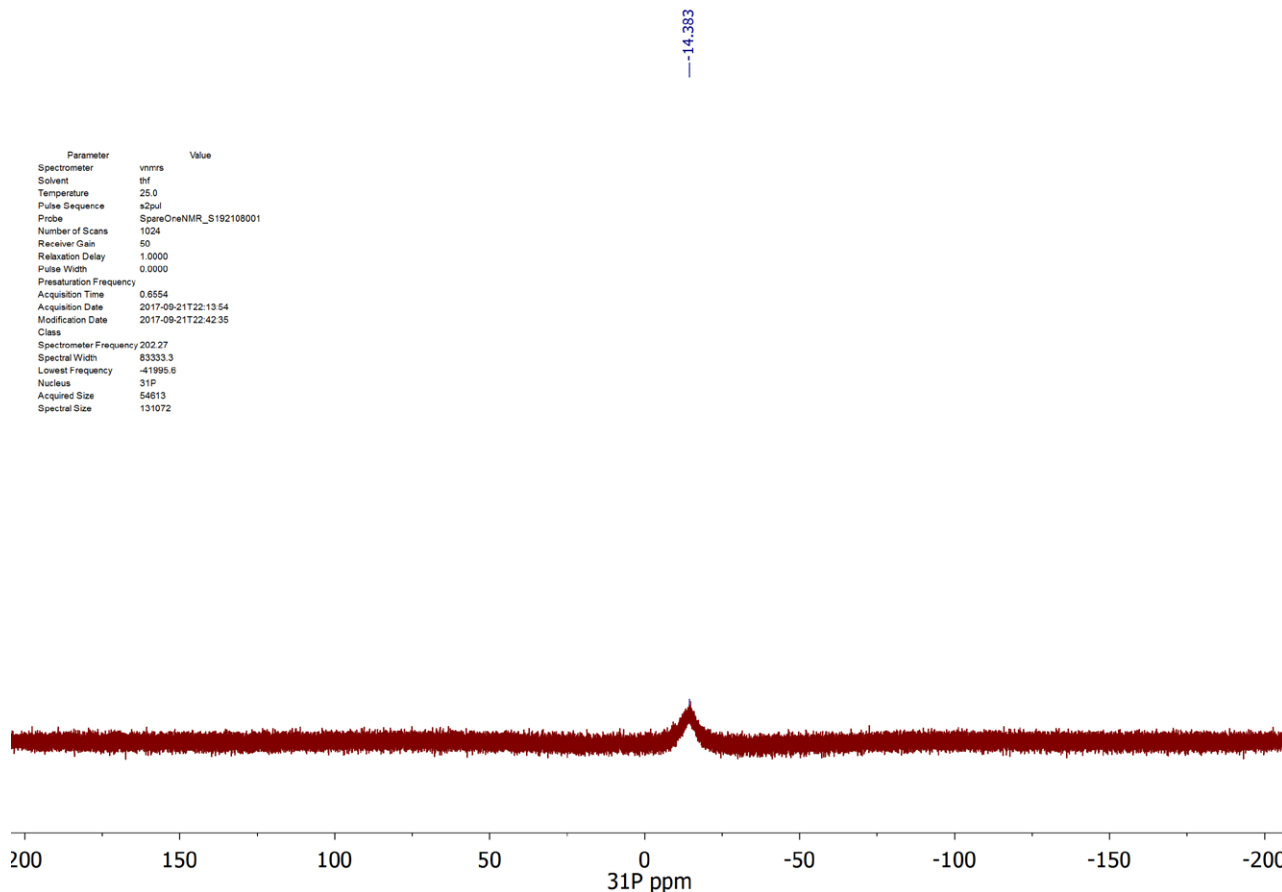
Supplementary Figure 146. Stacked ${}^1\text{H}$ NMR spectra (500 MHz, THF- d_8) of the reaction between FeBr_2 , dpbz and varying eq. of ZnBr_2 .



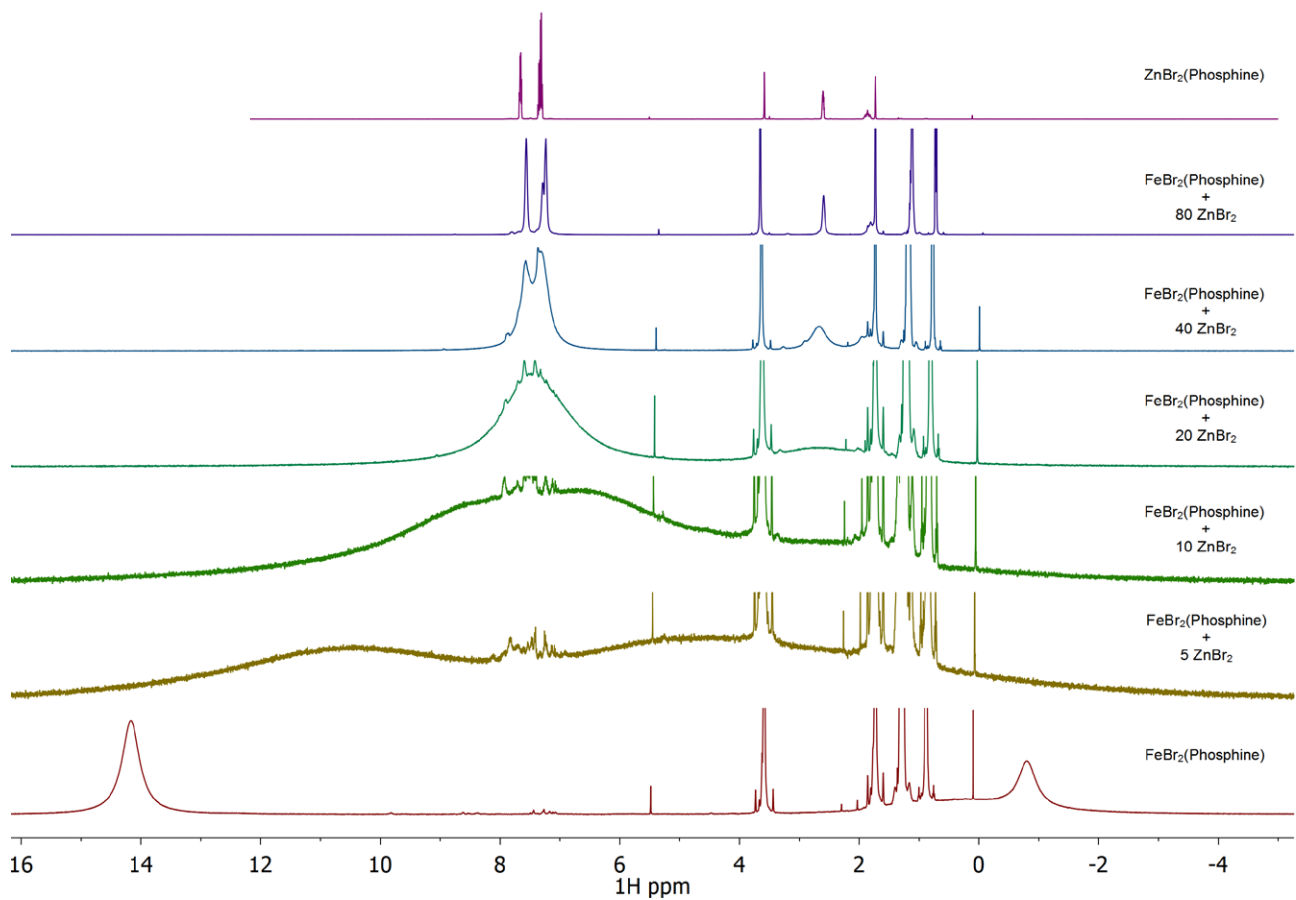
Supplementary Figure 147. ${}^{31}\text{P}$ NMR spectrum (202 MHz, THF- d_8) of the reaction between FeBr_2 , dpbz and 80 eq. of ZnBr_2 .



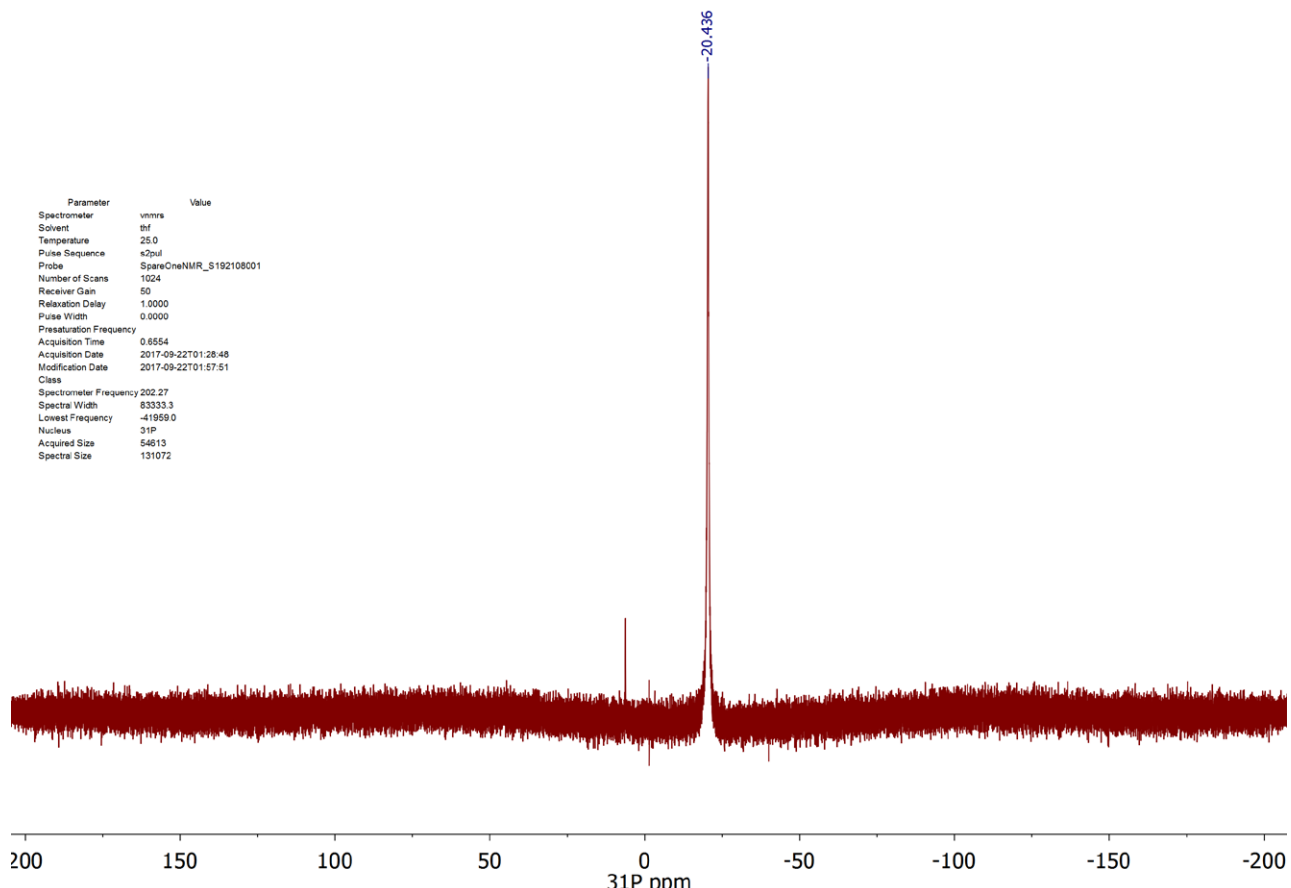
Supplementary Figure 148. Stacked ${}^1\text{H}$ NMR spectra (500 MHz, THF- d_8) of the reaction between FeBr_2 , dppe and varying eq. of ZnBr_2 .



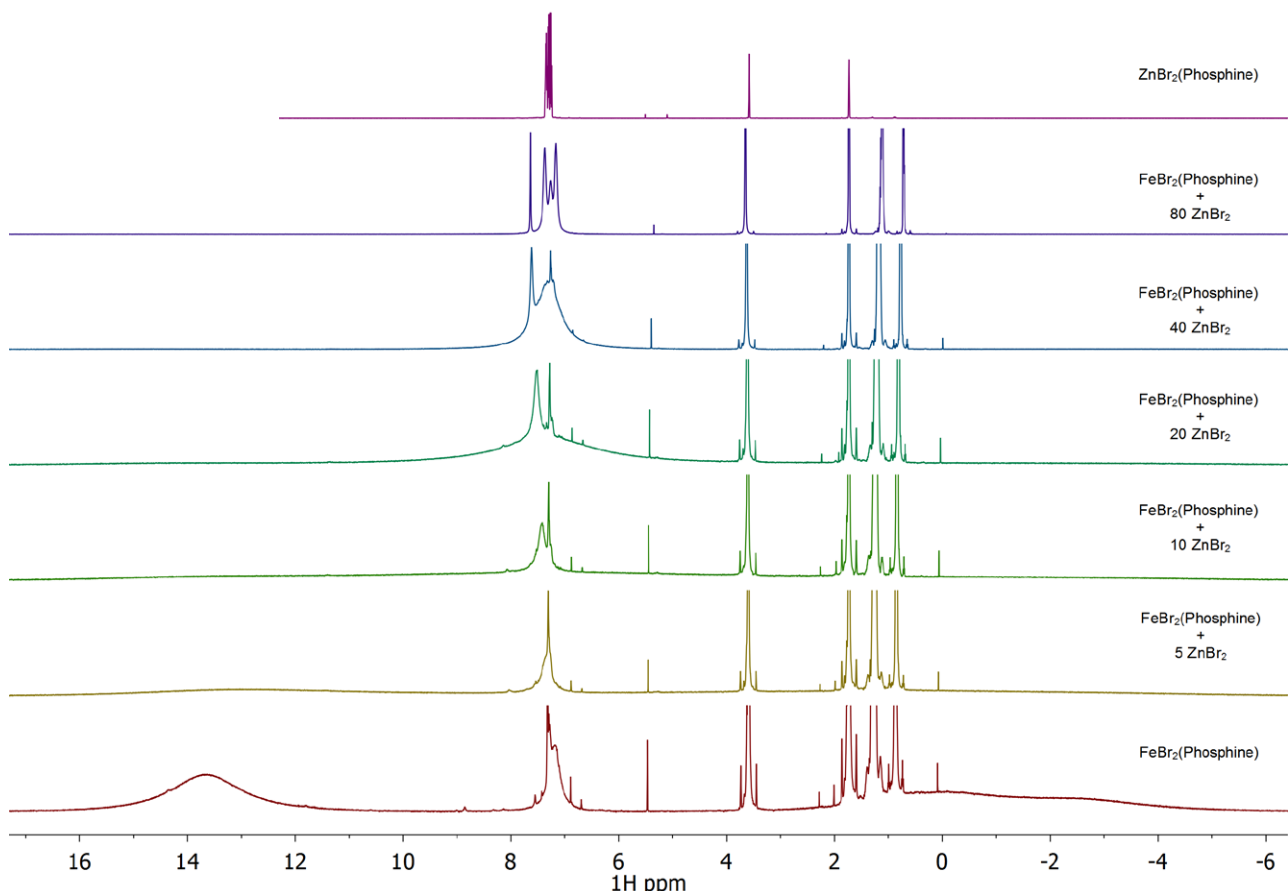
Supplementary Figure 149. ${}^{31}\text{P}$ NMR spectrum (202 MHz, THF- d_8) of the reaction between FeBr_2 , dppe and 80 eq. of ZnBr_2 .



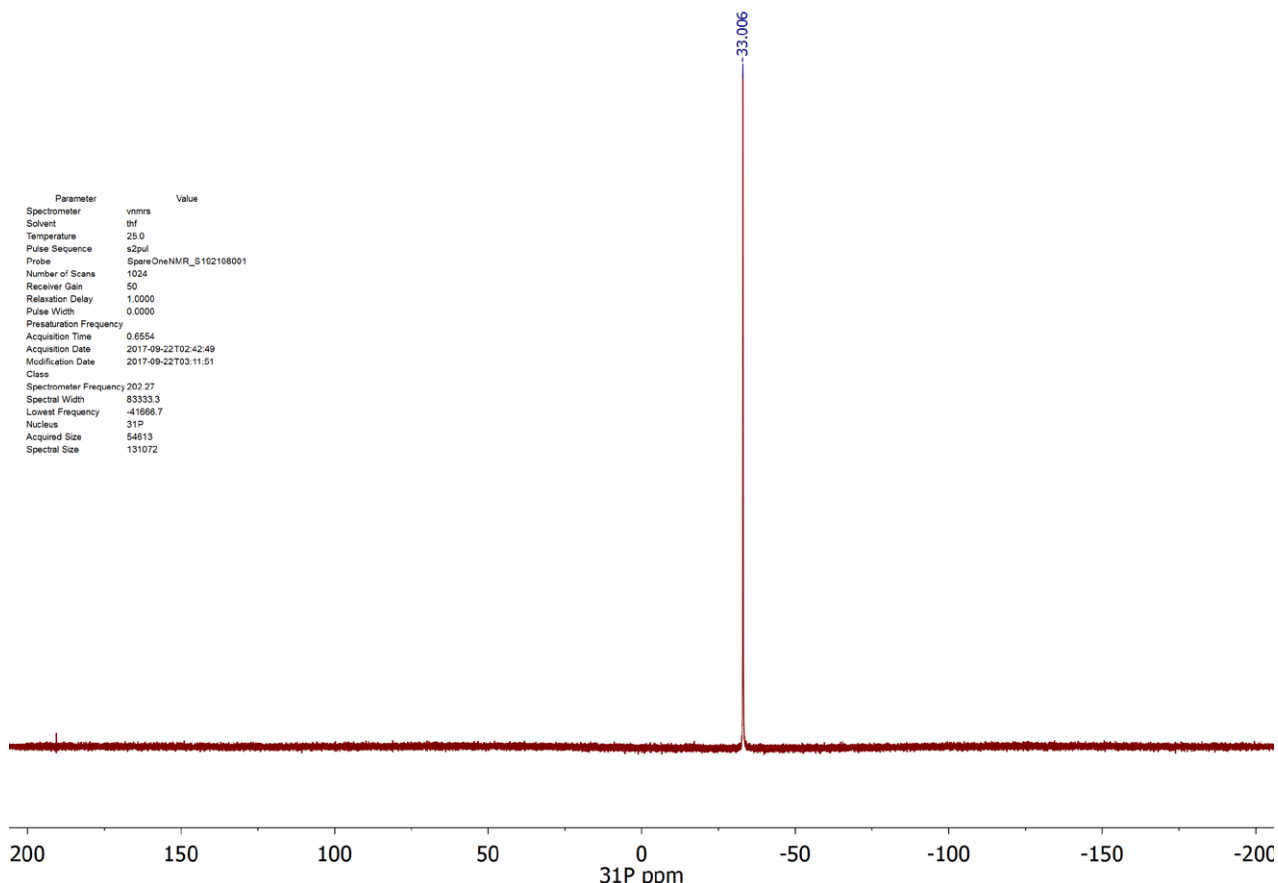
Supplementary Figure 150. Stacked ${}^1\text{H}$ NMR spectra (500 MHz, THF- d_8) of the reaction between FeBr₂, dppp and varying eq. of ZnBr₂.



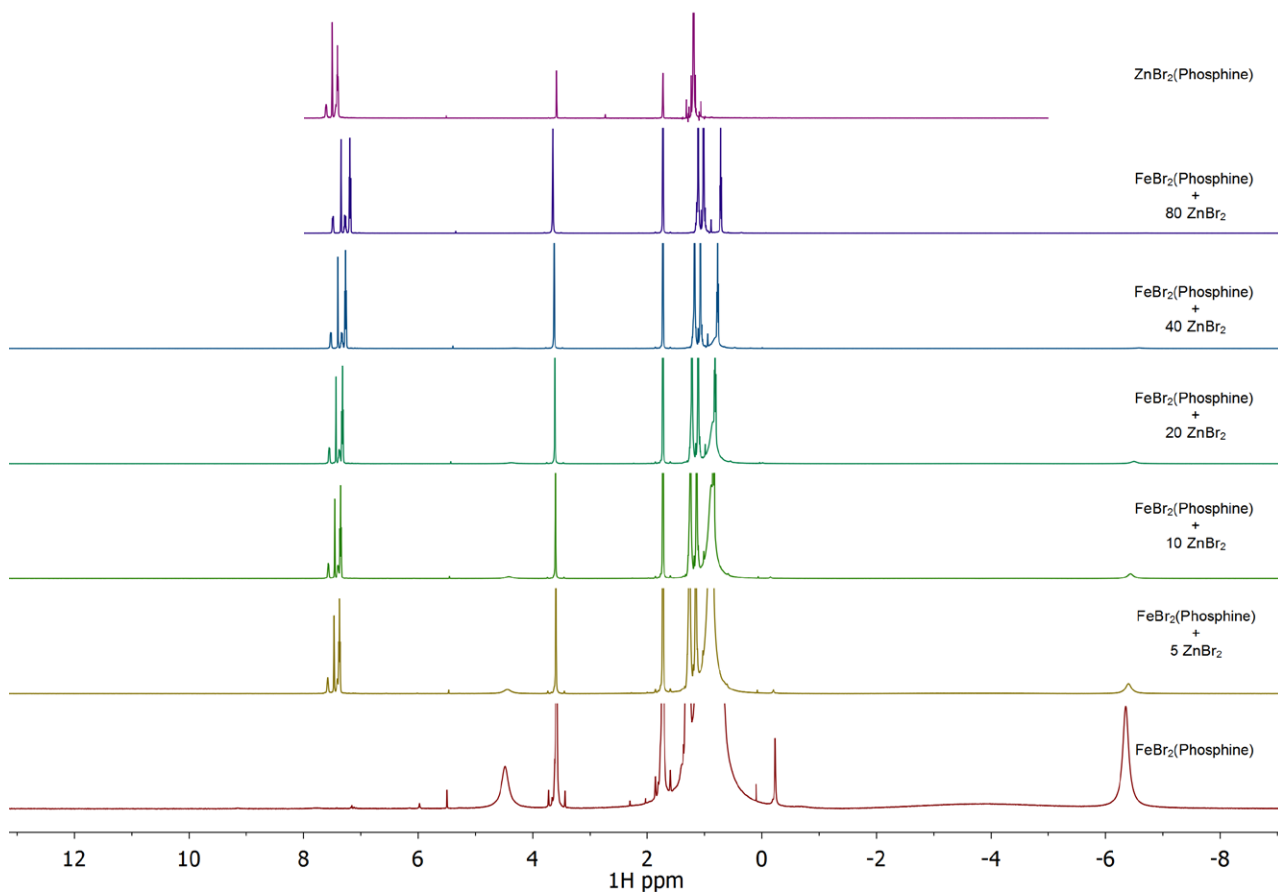
Supplementary Figure 151. ${}^{31}\text{P}$ NMR spectrum (202 MHz, THF- d_8) of the reaction between FeBr₂, dppp and 80 eq. of ZnBr₂.



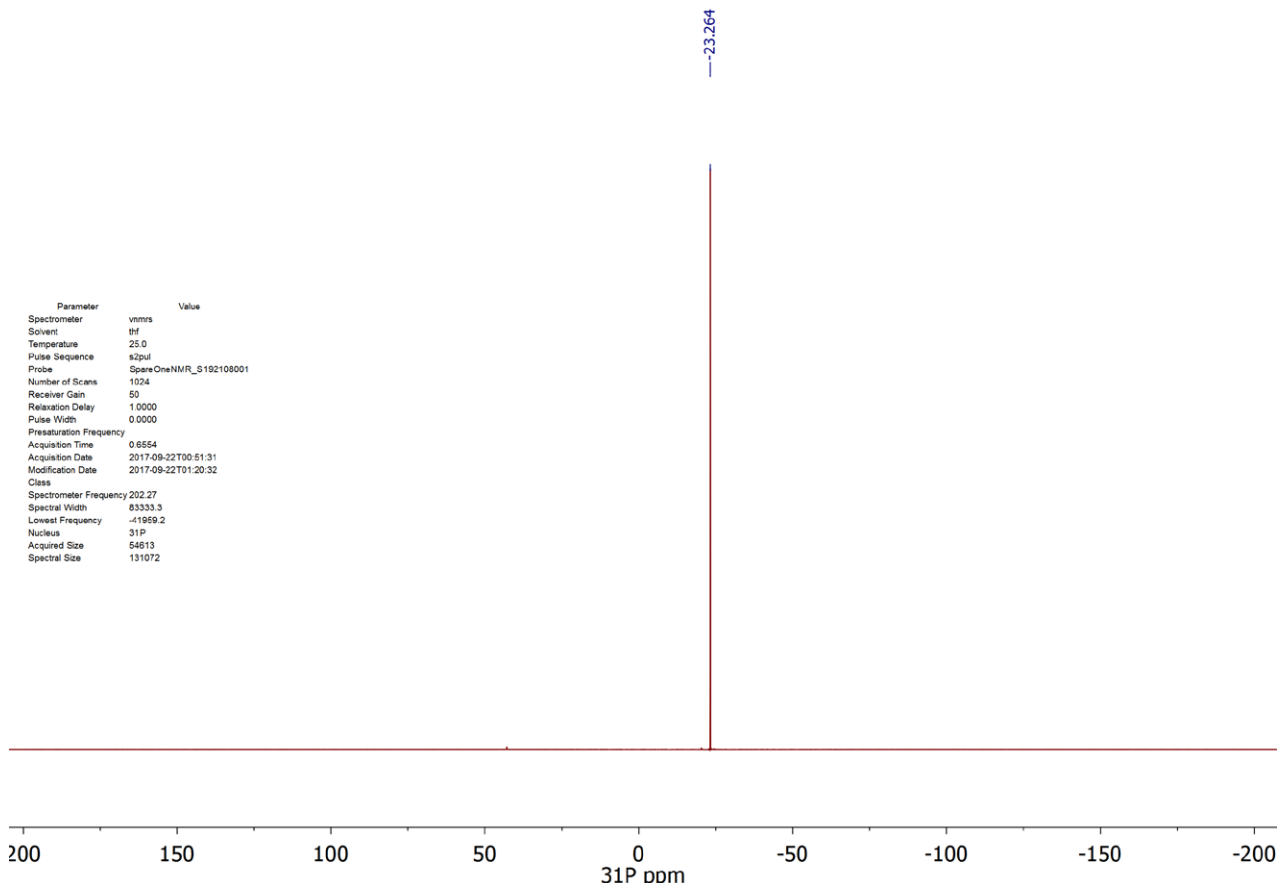
Supplementary Figure 152. Stacked ¹H NMR spectra (500 MHz, THF-*d*₈) of the reaction between FeBr₂, dpth and varying eq. of ZnBr₂.



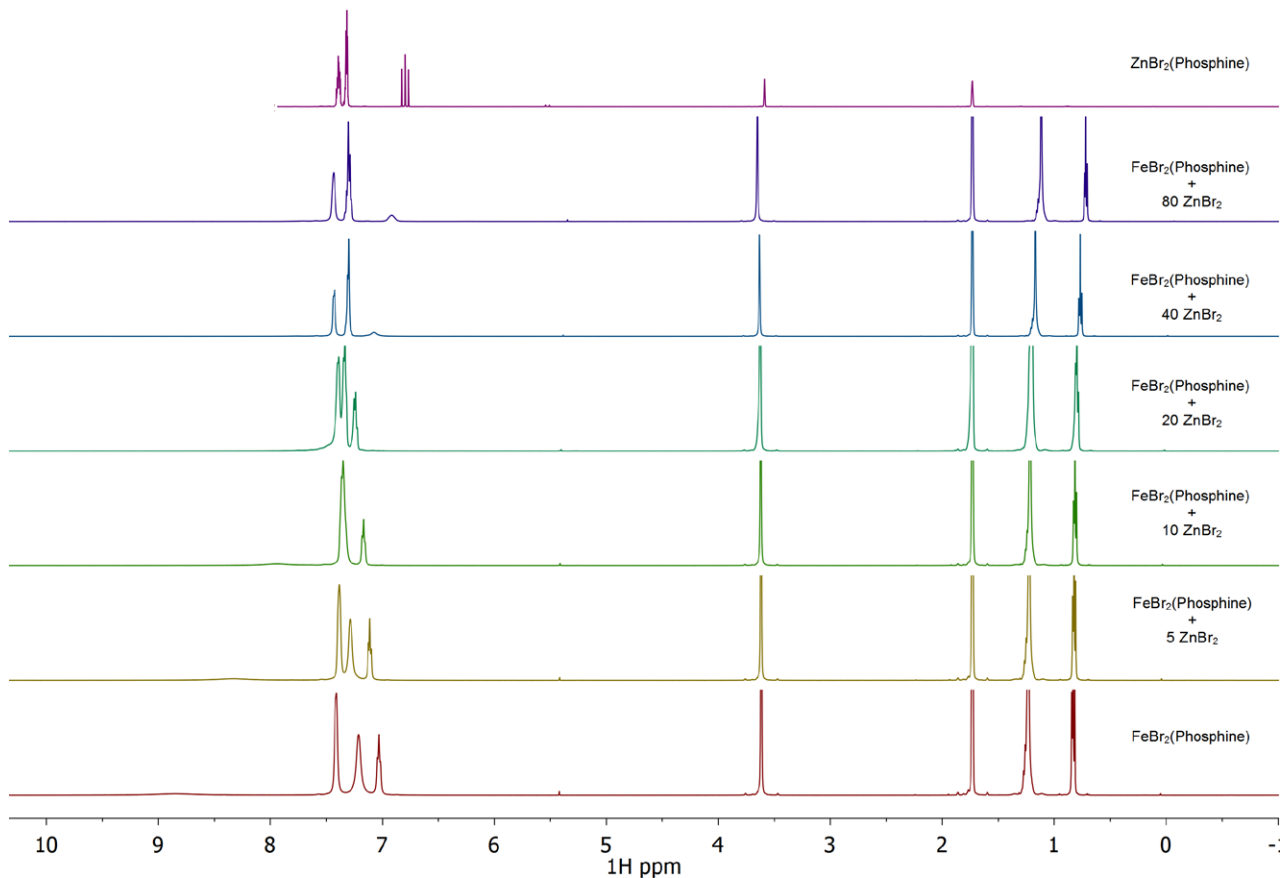
Supplementary Figure 153. ³¹P NMR spectrum (202 MHz, THF-*d*₈) of the reaction between FeBr₂, dpth and 80 eq. of ZnBr₂.



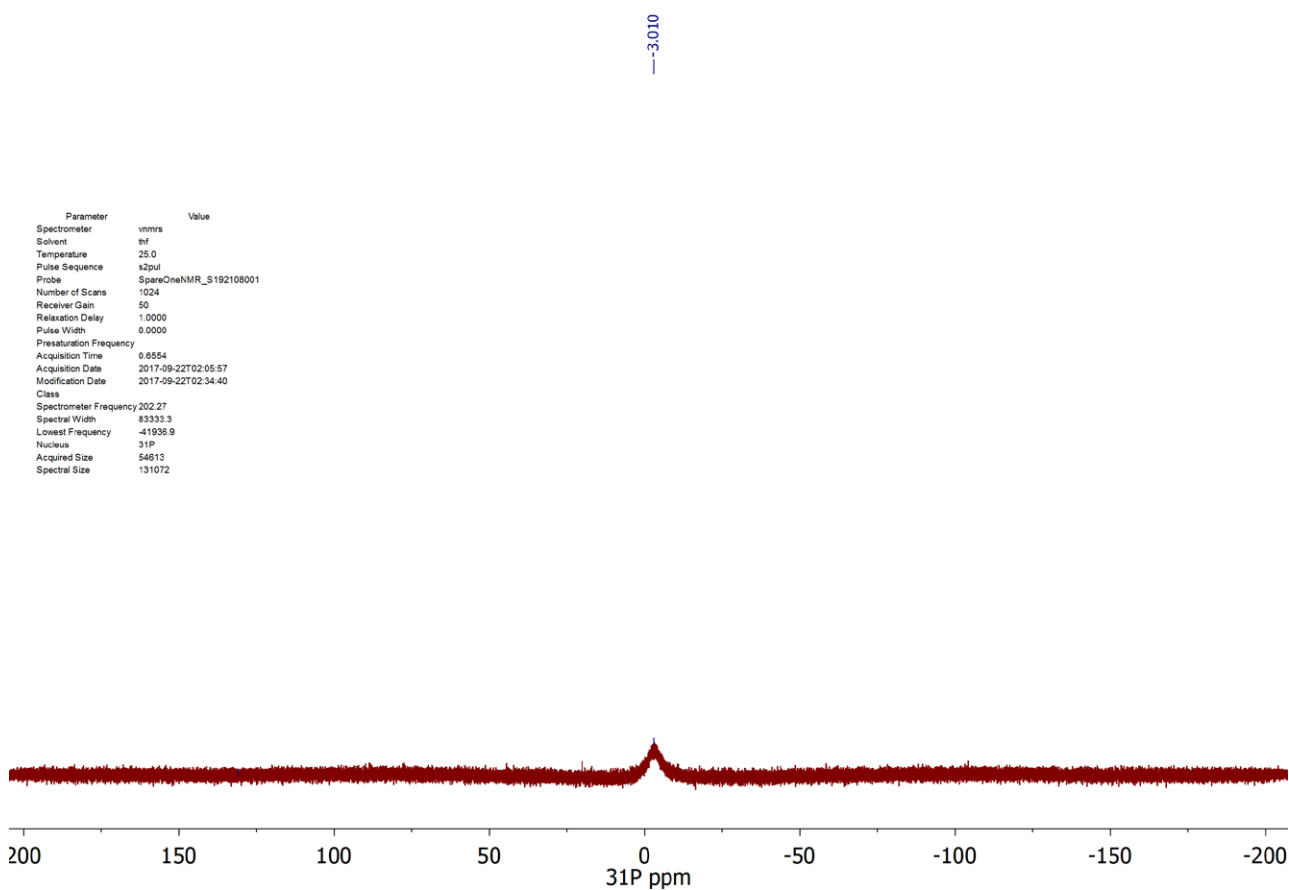
Supplementary Figure 154. Stacked ^1H NMR spectra (500 MHz, THF- d_8) of the reaction between FeBr_2 , sciopp and varying eq. of ZnBr_2 .



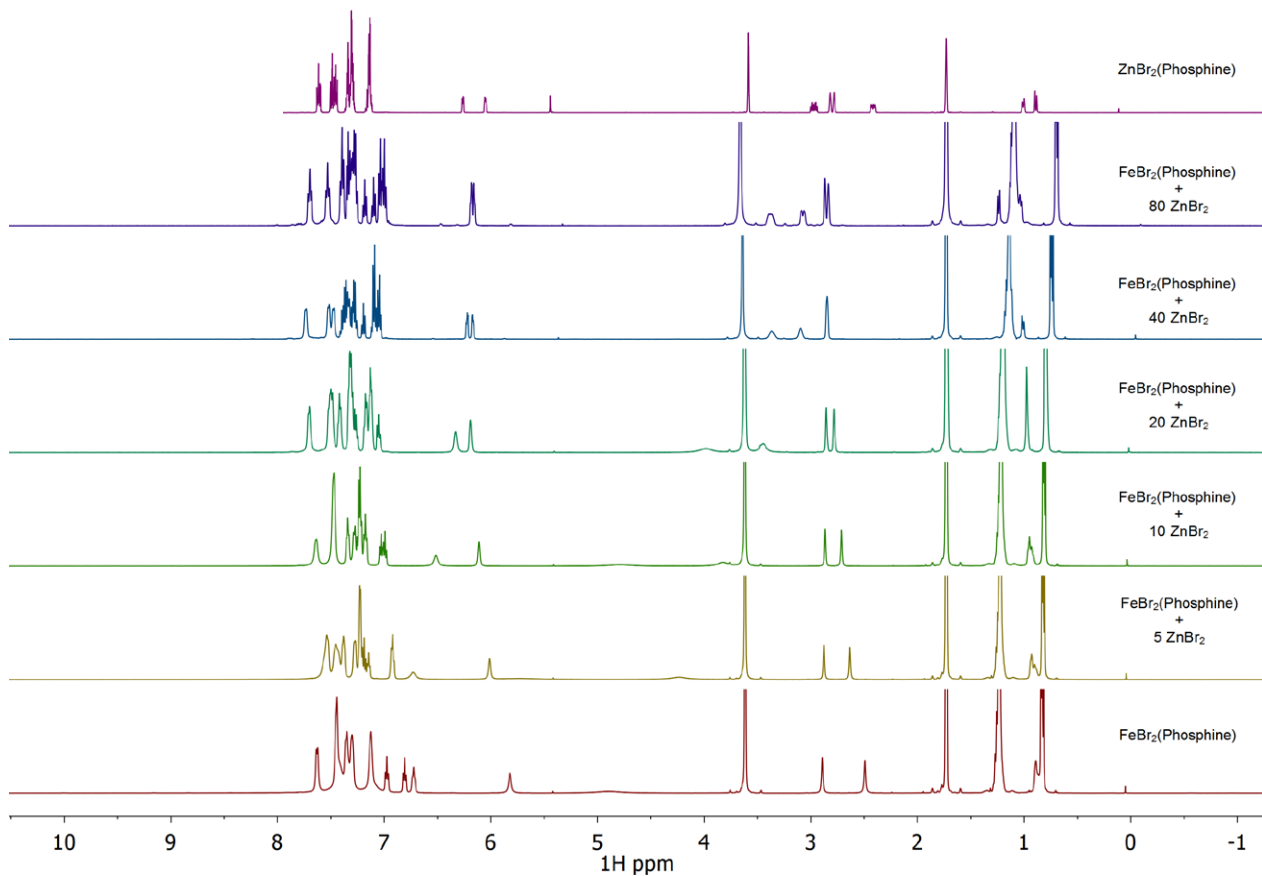
Supplementary Figure 155. ^{31}P NMR spectrum (202 MHz, THF- d_8) of the reaction between FeBr_2 , sciopp and 80 eq. of ZnBr_2 .



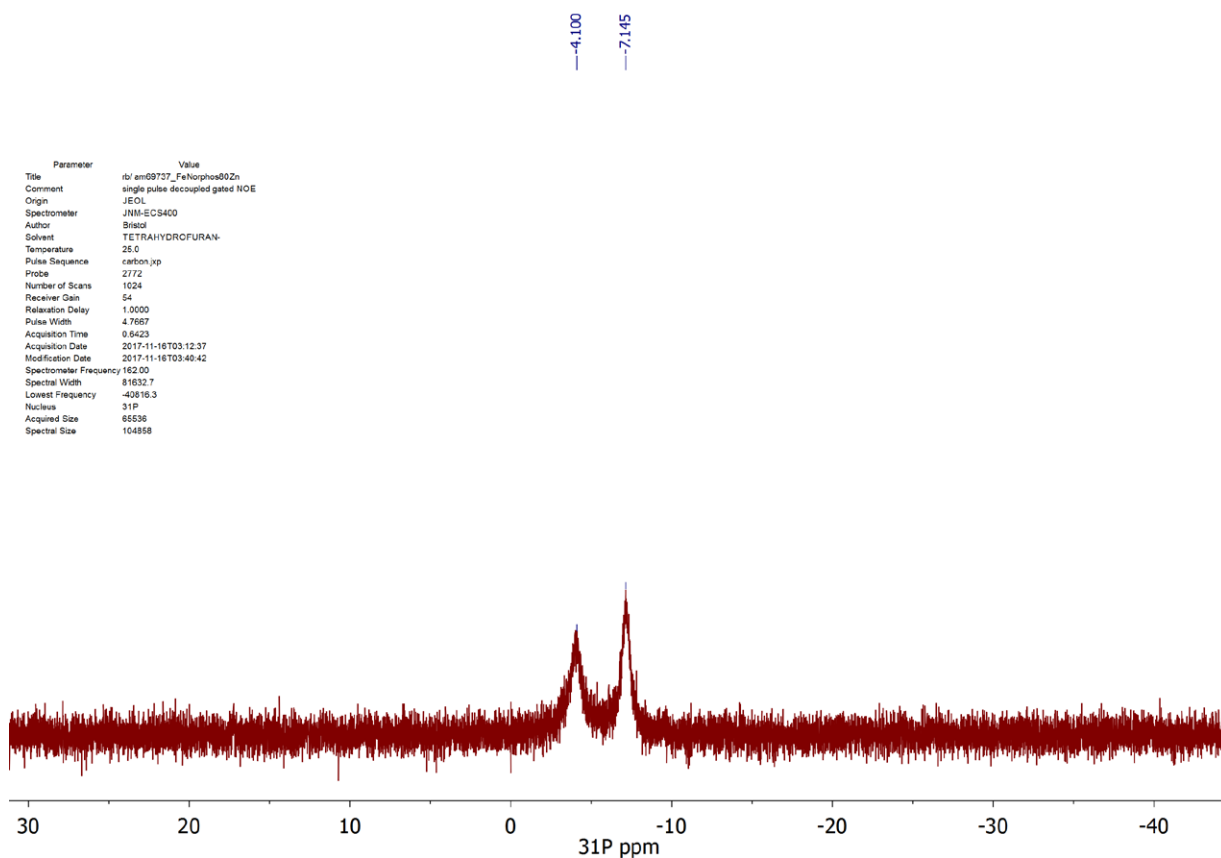
Supplementary Figure 156. Stacked ^1H NMR spectra (500 MHz, THF- d_8) of the reaction between FeBr_2 , *trans*-dppen and varying eq. of ZnBr_2 .



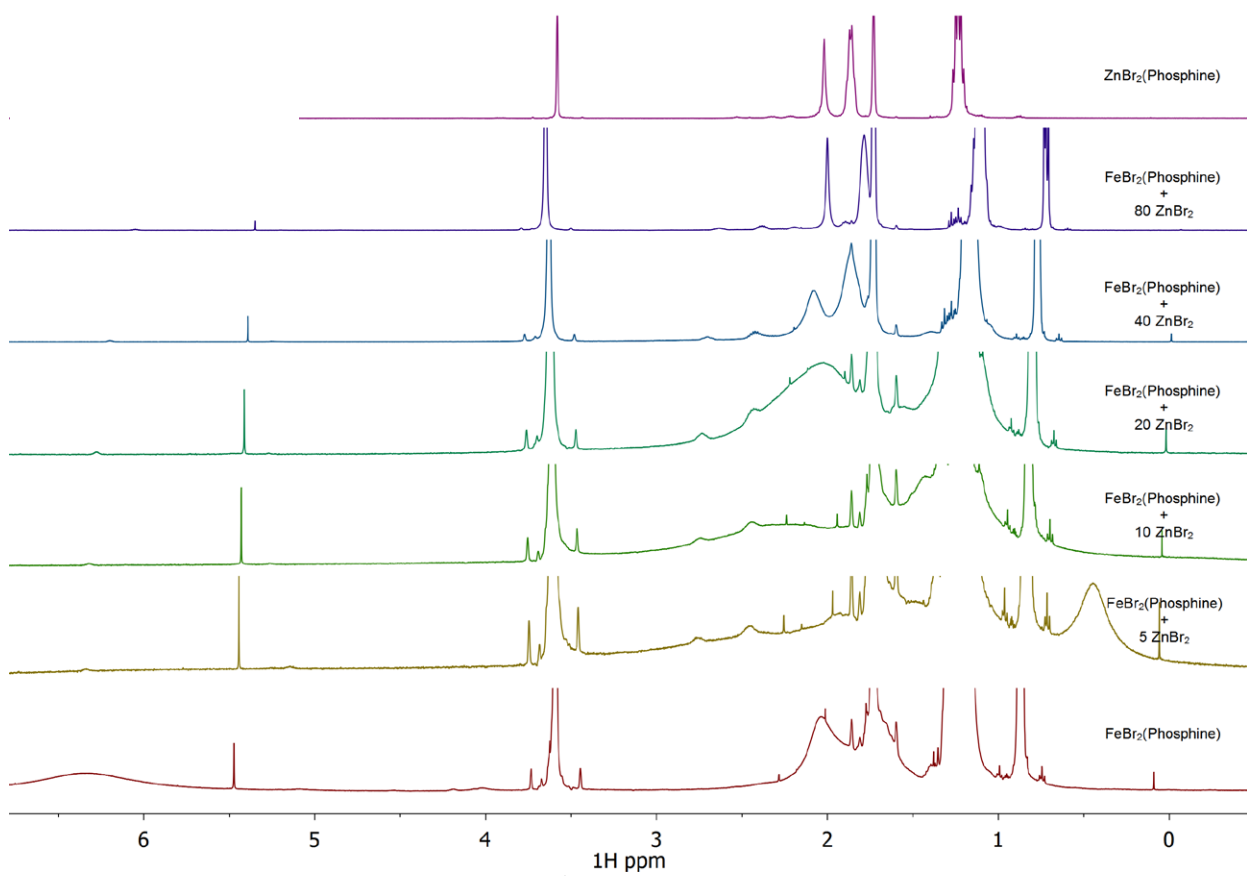
Supplementary Figure 157. ^{31}P NMR spectrum (202 MHz, THF- d_8) of the reaction between FeBr_2 , *trans*-dppen and 80 eq. of ZnBr_2 .



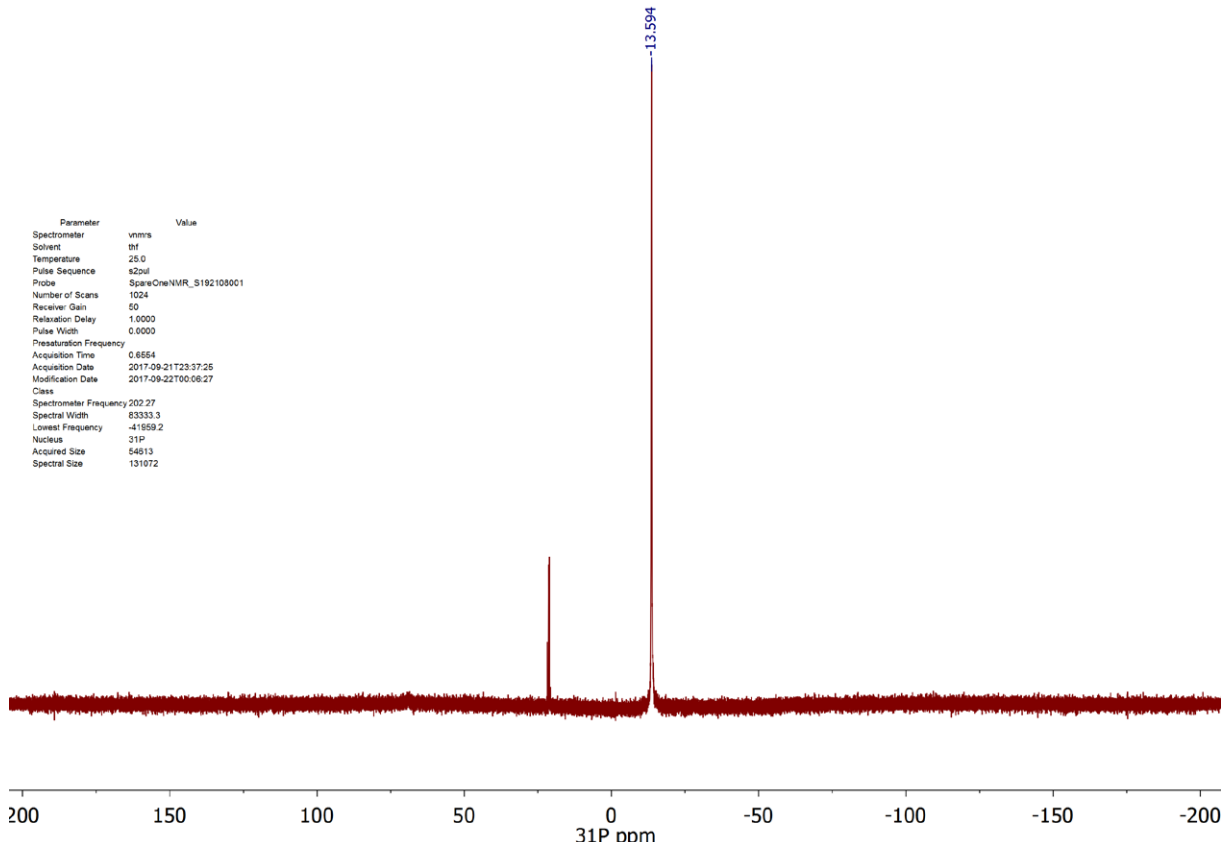
Supplementary Figure 158. Stacked ^1H NMR spectra (500 MHz, THF- d_8) of the reaction between FeBr_2 , norphos and varying eq. of ZnBr_2 .



Supplementary Figure 159. ^{31}P NMR spectrum (202 MHz, THF- d_8) of the reaction between FeBr_2 , norphos and 80 eq. of ZnBr_2 .



Supplementary Figure 160. Stacked ^1H NMR spectra (500 MHz, THF- d_8) of the reaction between FeBr_2 , depe and varying eq. of ZnBr_2 .



Supplementary Figure 161. ^{31}P NMR spectrum (202 MHz, THF- d_8) of the reaction between FeBr_2 , depe and 80 eq. of ZnBr_2 .

The equilibrium constants between the Fe-bound and Zn-bound diphosphines could not be established here due to the possible presence of one or more NMR silent paramagnetic iron-diphosphine species.

Depending on the diphosphine used the equilibrium between Fe-bound and Zn-bound phosphine can be slow (iPrDuphos, MeDuphos, dpbz, dpth and sciopp) or fast (*cis*-dppe, dppe, dppp, *trans*-dppe and norphos) compared with the NMR timescale. In the former case, addition of ZnBr₂ resulted in the gradual disappearance of the Fe-bound diphosphine paramagnetic resonances and the appearance of ZnBr₂(phosphine) resonances while in the latter the averaged resonances between Fe-bound phosphine and ZnBr₂(phosphine) were observed shifting towards the ZnBr₂(phosphine) resonances as the concentration of ZnBr₂ increased.

For the case of slow equilibration where discrete resonances can be observed for both Fe-bound and Zn-bound phosphine species, the ¹H NMR resonances corresponding to the ZnBr₂(phosphine) complex can be integrated against the *n*-dodecane internal standard in order to obtain an estimate of the percentage of that phosphine that is not bound to paramagnetic iron (Supplementary Equation 1).

$$\% \text{ Phosphine on Zn} = \frac{n_{P \text{ on Zn}}}{n_{P \text{ tot.}}} \times 100 = \frac{\frac{\int P \text{ on Zn}/Hs}{\int \text{dodecane}/20} \times n_{\text{dodecane}}}{n_{P \text{ tot.}}} = \frac{20 \times \int P \text{ on Zn}}{\int \text{dodecane} \times Hs}$$

Supplementary Equation 1. Calculation of the % phosphine not coordinated to the Fe from the ¹H NMR data obtained from the reactions between FeBr₂(phosphine) and *n* eq. of ZnBr₂ where a slow equilibrium between the Zn-bound and Fe-bound phosphine is established.

On the other hand, in case where a fast equilibrium between Fe-bound and Zn-bound phosphine is established, the percentage of phosphine not coordinated on the Fe can be calculated by dividing the difference between the observed chemical shift of the averaged resonance and the chemical shift of the isolated ZnBr₂(phosphine) complex with the difference between the chemical shift of the isolated FeBr₂(phosphine) complex and the isolated ZnBr₂(phosphine) complex and finally multiply by 100 (Supplementary Equation 2).

$$\% \text{ Phosphine on Zn} = \frac{\delta_{P \text{ on Fe}} - \delta_{\text{observed}}}{\delta_{P \text{ on Fe}} - \delta_{P \text{ on Zn}}} \times 100$$

Supplementary Equation 2. Calculation of the % of phosphine bound to Zn from the ¹H NMR data obtained from the reactions between FeBr₂(phosphine) and *n* eq. of ZnBr₂ where a fast equilibrium between the Zn-bound and Fe-bound phosphine is established.

According to the results from the calculations from Supplementary Equation 1 and Supplementary Equation 2 presented in Supplementary Table 11, it is suggested that although the equilibrium between Fe-bound and Zn-bound phosphine lies towards the Fe-bound side, at high concentrations of ZnBr₂ the majority of the phosphine is not coordinated to the Fe(II) centre. This is also evident from simple inspection of the ¹H NMR spectra of the FeBr₂(phosphine) + 80 ZnBr₂ mixtures which resemble the ¹H NMR spectra of the isolated ZnBr₂(diphosphine) complexes rather than those of the FeBr₂(diphosphine). Similarly, the ³¹P NMR chemical shifts of the FeBr₂(diphosphine) + 80 ZnBr₂ mixtures approximately coincide with the ³¹P NMR chemical shifts of the pure ZnBr₂(diphosphine) complexes in most cases (Supplementary Table 12). These results are consistent with the results from the XAFS studies using dpbz as the diphosphine, where it was found that the majority of the phosphine is not bound to the Fe, which is reasonable considering that during catalysis the molar ratio of Zn to Fe is 100 to 1.

Supplementary Table 11. Percentage of phosphine bound to Zn(II) in the mixtures of FeBr₂ + diphosphine + n eq. of ZnBr₂.^a

Equiv. ZnBr ₂	dpbz	sciopp	MeDuphos	iPrDuphos	<i>cis</i> - dppen	dppe	dppp	<i>trans</i> - dppen
5	25	29	29	39	14	55	51	28
10	37	42	43	52	28	74	81	48
20	56	60	64	71	74	91	97	72
40	79	79	84	84	98	98	99	94
80	90	92	91	88	100	100	100	95

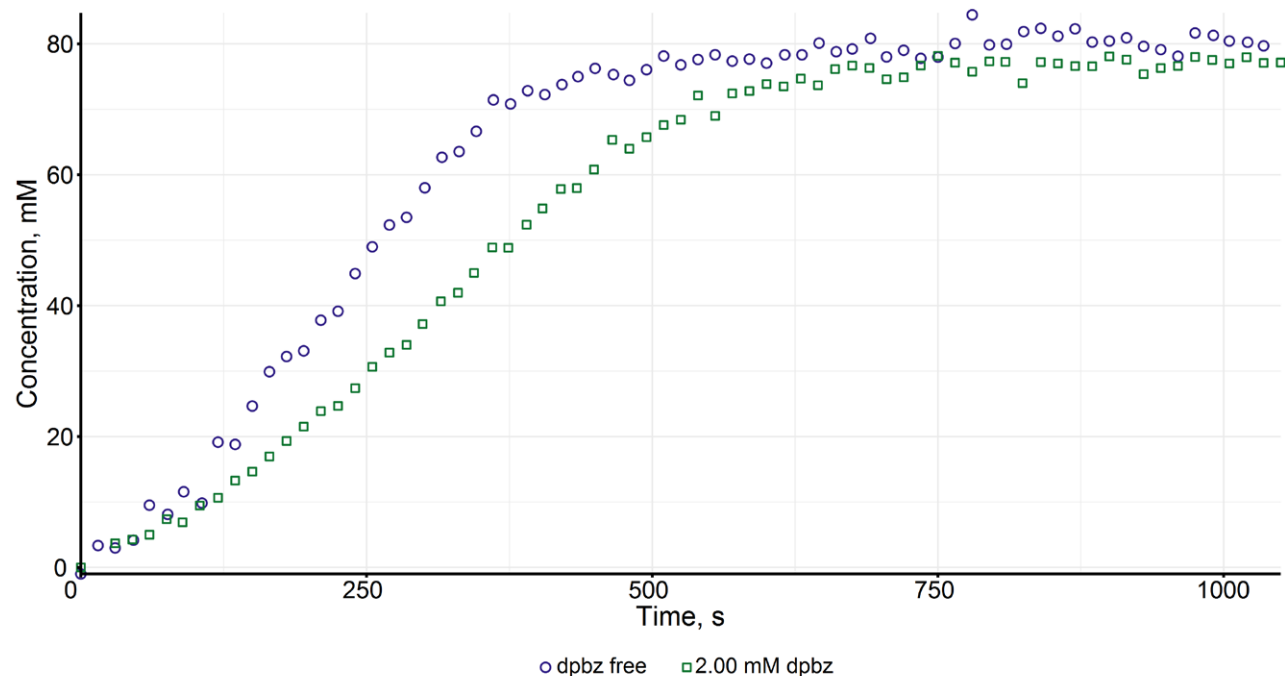
^aCalculation of the % phosphine bound on Zn for dpth was not possible due to the overlap between the paramagnetic resonances with the diamagnetic resonances in the ¹H NMR spectra for this system. Similarly, the calculation for norphos and depe was prevented by the complexity of the ¹H NMR spectra which made difficult to track the various shifting resonances.

Supplementary Table 12. ^{31}P NMR chemical shifts (ppm) of $[\text{ZnBr}_2(\text{phosphine})]$ complexes and $\text{FeBr}_2 + \text{diphosphine} + 80 \text{ ZnBr}_2$ mixtures in $\text{THF}-d_8$.

Phosphine	^{31}P NMR chemical shift of $\text{ZnBr}_2(\text{phosphine})$	^{31}P NMR chemical shift of $\text{FeBr}_2 + \text{diphosphine} + 80 \text{ ZnBr}_2$
cis-dppen	-24.2	-24.7
dppe	-14.4	-14.4 (weak br, 1125)
dppp	-21.5	-20.4
dpth	-27.2	-33.0
iPrDuphos	-10.2	-10.0
MeDuphos	-5.1	-4.3
norphos	-1.1, -3.2	-4.1, -7.1 (weak br, 156, 101)
depe	-20.8	-13.6
sciopp	-23.8	-23.3
trans-dppen	-7.4	-3.0 (weak br, 1073)
dpbz	-22.2	-24.2

8.2 Effect of dpbz on the FeBr_2 free coupling of **1** and MgBr_2 -free **2a**

The profiles of the reaction between **1** (100 mM) and MgBr_2 -free **2** (100 mM) with and without dpbz (2.00 mM) were collected according to the method described in section 2 using PhCl instead of THF at 7 °C and a total volume of 10.0 mL.³³ the results are summarised in Supplementary Figure 162.



Supplementary Figure 162. Comparison of the FeBr_2 -free coupling between **1** (100 mM) and **2** (100 mM) at 7.00 °C with and without dpbz and a total volume of 10.0 mL.

9 DFT calculations on equilibration of dpbz between Fe(II) and Zn(II)

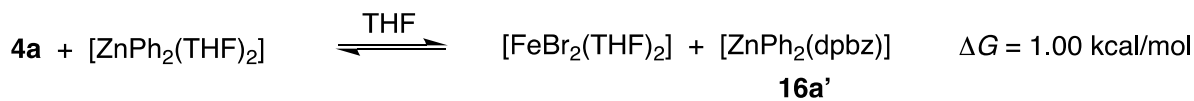
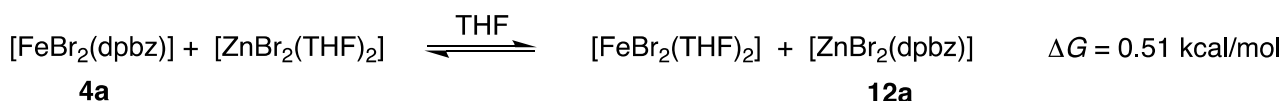
All DFT calculations were performed using Gaussian 09, Rev. D,⁸ using the B3LYP functional,²³⁻²⁶ with Grimme's D3-dispersion correction.³⁴ All calculations were performed without symmetry constraints. Geometry optimisation was performed using the 6-31G* basis set^{35,36} on all atoms except iron and zinc, for which the Stuttgart–Dresden effective core potential and associated basis set were used.³⁷ The final xyz coordinates and electronic energies of the optimised structures are given below. A frequency calculation was performed on each optimised structure, which confirmed it was a minimum with no imaginary stretching frequencies obtained. Solvent effects were modelled by performing a single point calculation on each of the optimised structures using the standard implementation of the SMD solvent model.³⁸ A further single point calculation was performed on each optimised structure using the 6-311+G* basis set on all atoms. The free energy of each species, G was calculated using Supplementary Equation 3 and the results are summarised in Supplementary Table 13 and Supplementary Figure 163.

$$G = G_{small} + E_{solv.} + E_{large} - 2 E_{small}$$

Supplementary Equation 3. Formula for the calculation of free energy, G. G_{small} = free energy calculated using 6-31G*/SDD, $E_{solv.}$ = solvation energy (6-31G*/SDD), E_{large} = electronic energy calculated using 6-311+G* basis set, E_{small} = electronic energy calculated using 6-31G*/SDD.

Supplementary Table 13. Calculated electronic and free energies (values in Hartrees).

	E_{small}	E_{solv}	E_{large}	G_{small}	G
[FeBr ₂ (dpbz)]	-7107.33679	-7107.37267	-8252.91451	-7106.95551	-8252.56607
[ZnBr ₂ (THF) ₂]	-5835.07868	-5835.07868	-7392.86252	-5834.86541	-7392.68799
[FeBr ₂ (THF) ₂]	-5731.86053	-5731.88135	-6877.23723	-5731.67101	-6877.06549
[ZnBr ₂ (dpbz)]	-7210.53209	-7210.56972	-8768.53620	-7210.14905	-8768.18776
[ZnPh ₂ (THF) ₂]	-1155.40212	-1155.42604	-2707.82919	-1155.03906	-2707.48702
[ZnPh ₂ (dpbz)]	-2530.86866	-2530.91219	-4083.49796	-2530.31621	-4082.98601



Supplementary Figure 163. Calculated free energies for the exchange of dpbz between iron and zinc complexes.

Optimised Cartesian Coordinates (B3LYP-D3/6-31G*/SDD)

[FeBr₂(dpbz)] (4a)

SCF Energy: -7107.33679101 a.u.

Fe	-0.03051	-0.95840	1.44182
P	1.61234	0.02515	-0.15920
P	-1.54707	-0.06186	-0.29973
C	1.73632	1.85598	-0.18296
C	1.44841	2.56274	0.99315
H	1.16351	2.02592	1.89328
C	1.49021	3.95825	0.99694
H	1.24896	4.49770	1.90822
C	1.82282	4.65473	-0.16538
H	1.84830	5.74117	-0.16048
C	2.11065	3.95518	-1.34093
H	2.36277	4.49465	-2.25009
C	2.06177	2.56228	-1.35294
H	2.26248	2.02381	-2.27486
C	3.31940	-0.61859	-0.32129
C	4.43424	0.20332	-0.54243
H	4.31353	1.27877	-0.62420
C	5.70738	-0.35991	-0.65361
H	6.56635	0.28417	-0.82188
C	5.87658	-1.74154	-0.54744
H	6.86883	-2.17619	-0.63358
C	4.76901	-2.56341	-0.32133
H	4.89563	-3.63841	-0.22785
C	3.49560	-2.00854	-0.20173
H	2.63904	-2.64845	-0.00752
C	-1.78539	1.75180	-0.19763
C	-1.57084	2.61132	-1.28447
H	-1.26068	2.20871	-2.24386
C	-1.73277	3.98852	-1.12927

H	-1.54990	4.64973	-1.97177
C	-2.11867	4.51495	0.10511
H	-2.23935	5.58843	0.22374
C	-2.33561	3.66239	1.19020
H	-2.62247	4.06809	2.15636
C	-2.16237	2.28659	1.04503
H	-2.28329	1.63227	1.90326
C	-3.20306	-0.76177	-0.63762
C	-4.27736	0.02072	-1.08683
H	-4.14862	1.08952	-1.23037
C	-5.51401	-0.57388	-1.34359
H	-6.34407	0.03690	-1.68844
C	-5.68396	-1.94769	-1.15624
H	-6.64844	-2.40737	-1.35487
C	-4.61628	-2.72914	-0.70665
H	-4.74719	-3.79663	-0.55271
C	-3.37923	-2.14184	-0.44170
H	-2.55087	-2.74712	-0.08276
C	0.81985	-0.34712	-1.78502
C	-0.59419	-0.34396	-1.85392
C	-1.22361	-0.60594	-3.07760
H	-2.30810	-0.61835	-3.13174
C	-0.46844	-0.86978	-4.22138
H	-0.96990	-1.07514	-5.16308
C	0.92536	-0.88356	-4.15022
H	1.51575	-1.10154	-5.03595
C	1.56547	-0.62514	-2.93707
H	2.64979	-0.65125	-2.88077
Br	-0.23164	0.18932	3.50196
Br	0.05967	-3.29562	0.96470

[ZnBr₂(THF)₂]

SCF Energy: -5835.05779037 a.u.

Zn	-0.54850	0.63575	0.56762
Br	-2.75506	-0.10827	0.65741
Br	0.90400	1.92821	1.83383
C	1.23296	1.21193	-1.82849
C	-0.98734	0.66325	-2.52596
C	1.26093	0.72786	-3.28311
H	1.77436	0.54374	-1.15549
H	1.58779	2.23439	-1.68541
C	-0.00949	-0.13427	-3.38000
H	-1.40206	1.52038	-3.07035
H	-1.80318	0.09085	-2.08157
H	1.19452	1.57520	-3.97485
H	2.17632	0.17480	-3.51199
H	-0.36220	-0.27315	-4.40598
H	0.16034	-1.12053	-2.93283
C	1.31179	-1.67866	1.43072
C	-0.16545	-2.35975	-0.20592
C	0.26663	-2.49399	2.19158
H	1.67782	-0.79214	1.94834
H	2.15715	-2.29395	1.09319
C	-0.59496	-3.12406	1.06378
H	0.49186	-2.95803	-0.84996
H	-1.00286	-1.97323	-0.78669
H	0.72081	-3.23806	2.85194
H	-0.34395	-1.82010	2.80038
H	-0.40917	-4.19669	0.95452
H	-1.65881	-2.97175	1.25741
O	-0.17456	1.16869	-1.43235
O	0.59454	-1.21459	0.25828

[FeBr₂(THF)₂]

SCF Energy: -5731.86053018 a.u.

Fe	-0.52435	-0.77386	0.72120
O	-2.62466	-0.62453	1.01784
C	-3.33954	0.34737	0.20209
C	-3.35833	-1.89119	1.02201
C	-4.11211	-0.50373	-0.79495
H	-4.00087	0.92733	0.85888
H	-2.59082	1.00409	-0.24160
C	-4.55471	-1.68964	0.08053
H	-2.67019	-2.66369	0.66763
H	-3.63743	-2.11194	2.05529
H	-3.42978	-0.83522	-1.58424
H	-4.95084	0.03288	-1.24783
H	-4.77051	-2.59070	-0.50006
H	-5.45421	-1.42972	0.65011
O	-0.42892	1.30402	1.25473
C	0.83968	1.94757	0.97267
C	-0.74850	1.62214	2.63751
C	1.66195	1.69355	2.23470
H	1.22570	1.49347	0.05819
H	0.65247	3.01624	0.80107
C	0.60555	1.74747	3.36948
H	-1.31227	2.56286	2.63985
H	-1.38243	0.81436	3.00427
H	2.46660	2.42311	2.36219
H	2.09689	0.69155	2.18631
H	0.65547	2.68684	3.92841
H	0.74804	0.91940	4.06681
Br	0.37552	-1.89235	2.60766
Br	-0.31644	-0.82942	-1.64035

[ZnBr₂(dpbz)] (12a)

SCF Energy: -7210.5320871 a.u.

C	0.69643	-0.22737	1.86830
C	1.39387	-0.43673	3.06538
C	0.70511	-0.67283	4.25568
C	-0.69011	-0.71267	4.25897
C	-1.39759	-0.51002	3.07332
C	-0.71947	-0.25943	1.87372
H	2.47979	-0.42907	3.06183
H	1.25898	-0.83545	5.17609
H	-1.22910	-0.90799	5.18192
H	-2.48259	-0.55827	3.07560
C	-3.28216	-0.66405	0.54845
C	-4.40855	0.13073	0.80778
C	-3.41806	-2.06134	0.46797
C	-5.65550	-0.46780	0.99820
H	-4.31661	1.21119	0.85603
C	-4.66645	-2.65006	0.66567
H	-2.55272	-2.67922	0.24222
C	-5.78557	-1.85644	0.93160
H	-6.52482	0.15341	1.19636
H	-4.76466	-3.73010	0.60171
H	-6.75790	-2.31873	1.07915
C	-1.77514	1.85165	0.22393
C	-1.55949	2.49778	-1.00197
C	-2.05825	2.61250	1.37068
C	-1.63237	3.89011	-1.07637
H	-1.30636	1.91897	-1.88598
C	-2.13777	4.00134	1.28736
H	-2.20116	2.11932	2.32816
C	-1.92322	4.64119	0.06291
H	-1.44736	4.38466	-2.02544

H	-2.35674	4.58472	2.17774
H	-1.97315	5.72508	0.00166
C	3.24673	-0.65401	0.52033
C	4.33878	0.15449	0.86994
C	3.42322	-2.03835	0.35594
C	5.59603	-0.42017	1.06257
H	4.20746	1.22653	0.98467
C	4.68247	-2.60395	0.55584
H	2.58003	-2.66250	0.07026
C	5.76822	-1.79802	0.90821
H	6.44051	0.20892	1.33087
H	4.81555	-3.67435	0.42652
H	6.74901	-2.24189	1.05648
C	1.75448	1.82737	0.07029
C	2.02365	2.31026	-1.22101
C	1.59819	2.73093	1.13134
C	2.15332	3.68139	-1.43891
H	2.09123	1.61935	-2.05624
C	1.71537	4.10215	0.90313
H	1.36830	2.36608	2.12789
C	1.99746	4.57801	-0.37934
H	2.35663	4.04821	-2.44107
H	1.57933	4.79831	1.72609
H	2.08397	5.64707	-0.55430
P	-1.61160	0.02885	0.28654
P	1.56954	0.01937	0.26675
Zn	-0.01775	-0.97428	-1.34494
Br	-0.03245	-3.30134	-0.86372
Br	0.04274	0.02176	-3.47083

[ZnPh₂(THF)₂]

SCF Energy: -1155.40212268 a.u.

Zn	0.00003	0.00010	-0.42472
C	1.45790	1.16431	2.20165
C	0.61328	2.81869	0.83426
C	2.70198	1.84319	1.58815
H	1.51214	0.07585	2.22995
H	1.23993	1.54587	3.20912
C	2.11877	2.83305	0.54408
H	0.33614	3.55772	1.60088
H	-0.02437	2.95635	-0.04209
H	3.28645	2.35542	2.35866
H	3.34380	1.10598	1.10108
H	2.54231	3.83868	0.62440
H	2.30752	2.45910	-0.46558
C	-1.45732	-1.16635	2.20122
C	-0.61402	-2.81950	0.83154
C	-2.70198	-1.84414	1.58769
H	-1.51116	-0.07791	2.23078
H	-1.23891	-1.54912	3.20814
C	-2.11970	-2.83318	0.54230
H	-0.33657	-3.55946	1.59716
H	0.02303	-2.95638	-0.04538
H	-3.28624	-2.35692	2.35799
H	-3.34377	-1.10620	1.10170
H	-2.54345	-3.83877	0.62198
H	-2.30902	-2.45827	-0.46690
O	0.35006	1.49741	1.33971
O	-0.35010	-1.49886	1.33827
C	-1.85098	0.51829	-0.84269
C	-2.59994	1.38429	-0.02100
C	-2.52844	-0.04134	-1.94517

C	-3.94620	1.66783	-0.27160
H	-2.12173	1.83926	0.84418
C	-3.87538	0.22953	-2.20725
H	-1.99355	-0.71360	-2.61535
C	-4.59023	1.08576	-1.36645
H	-4.49391	2.33912	0.38716
H	-4.36661	-0.22523	-3.06512
H	-5.63780	1.30031	-1.56427
C	1.85109	-0.51770	-0.84301
C	2.52890	0.04354	-1.94446
C	2.59977	-1.38494	-0.02239
C	3.87593	-0.22694	-2.20649
H	1.99426	0.71681	-2.61381
C	3.94611	-1.66812	-0.27297
H	2.12128	-1.84119	0.84197
C	4.59050	-1.08441	-1.36673
H	4.36745	0.22910	-3.06352
H	4.49359	-2.34040	0.38497
H	5.63814	-1.29867	-1.56452

[ZnPh₂(dpbz)] (16a')

SCF Energy: -2530.86865691 a.u.

C	0.80856	-0.26669	1.76437
C	1.51009	-0.48013	2.95896
C	0.82787	-0.77212	4.14084
C	-0.56520	-0.85441	4.13867
C	-1.27508	-0.63744	2.95691
C	-0.60532	-0.34021	1.76301
H	2.59497	-0.43480	2.96065
H	1.38527	-0.94257	5.05794
H	-1.10059	-1.09176	5.05406
H	-2.35768	-0.72018	2.95687

C	-3.13937	-0.80152	0.42593
C	-4.33309	-0.07276	0.31497
C	-3.20078	-2.19122	0.64313
C	-5.56595	-0.71960	0.42767
H	-4.30311	0.99865	0.14332
C	-4.43489	-2.82841	0.75962
H	-2.28898	-2.77371	0.72010
C	-5.62057	-2.09633	0.65132
H	-6.48359	-0.14345	0.34148
H	-4.46385	-3.90182	0.92547
H	-6.58133	-2.59705	0.73740
C	-1.77623	1.77866	0.22166
C	-1.49470	2.52512	-0.93143
C	-2.21675	2.44127	1.37933
C	-1.65678	3.91200	-0.92790
H	-1.12721	2.02708	-1.82306
C	-2.38025	3.82557	1.37851
H	-2.42254	1.87440	2.28309
C	-2.10018	4.56277	0.22366
H	-1.42026	4.48069	-1.82252
H	-2.72086	4.33049	2.27884
H	-2.22005	5.64306	0.22699
C	3.39095	-0.52363	0.44651
C	4.39523	0.33444	0.91980
C	3.70260	-1.86450	0.16528
C	5.68973	-0.14686	1.12143
H	4.16465	1.37632	1.12340
C	4.99640	-2.34243	0.37594
H	2.93176	-2.52949	-0.21679
C	5.99074	-1.48487	0.85343
H	6.46353	0.52336	1.48643
H	5.22889	-3.38118	0.15798

H	7.00000	-1.85627	1.00968
C	1.74733	1.83709	-0.01341
C	2.01143	2.36160	-1.28927
C	1.51271	2.71408	1.05622
C	2.05461	3.74160	-1.48506
H	2.15070	1.69411	-2.13365
C	1.54604	4.09380	0.85240
H	1.28459	2.32038	2.04202
C	1.81989	4.60952	-0.41624
H	2.25282	4.13530	-2.47824
H	1.34693	4.76496	1.68328
H	1.83822	5.68479	-0.57316
P	-1.49059	-0.03874	0.16640
P	1.66384	0.01295	0.15440
Zn	0.20737	-1.25023	-1.56115
C	0.28736	-0.22595	-3.25438
C	1.50684	-0.02938	-3.93430
C	-0.84692	0.38560	-3.82418
C	1.60012	0.75043	-5.09188
H	2.41559	-0.48753	-3.54274
C	-0.77208	1.16861	-4.98140
H	-1.81822	0.25408	-3.34761
C	0.45707	1.35903	-5.61675
H	2.56167	0.88263	-5.58460
H	-1.67119	1.62904	-5.38686
H	0.52276	1.96875	-6.51491
C	-0.10370	-3.06795	-0.81309
C	-0.94925	-3.92316	-1.55080
C	0.28858	-3.52917	0.45992
C	-1.39570	-5.14927	-1.04801
H	-1.28376	-3.61485	-2.54041
C	-0.14657	-4.75409	0.97658

H	0.92863	-2.91182	1.08630
C	-0.99903	-5.56689	0.22481
H	-2.05613	-5.77517	-1.64495
H	0.17248	-5.06967	1.96822
H	-1.34599	-6.51688	0.62490

10 Operando NMR spectroscopic investigation of the dpbz-complex speciation in the Negishi cross-coupling

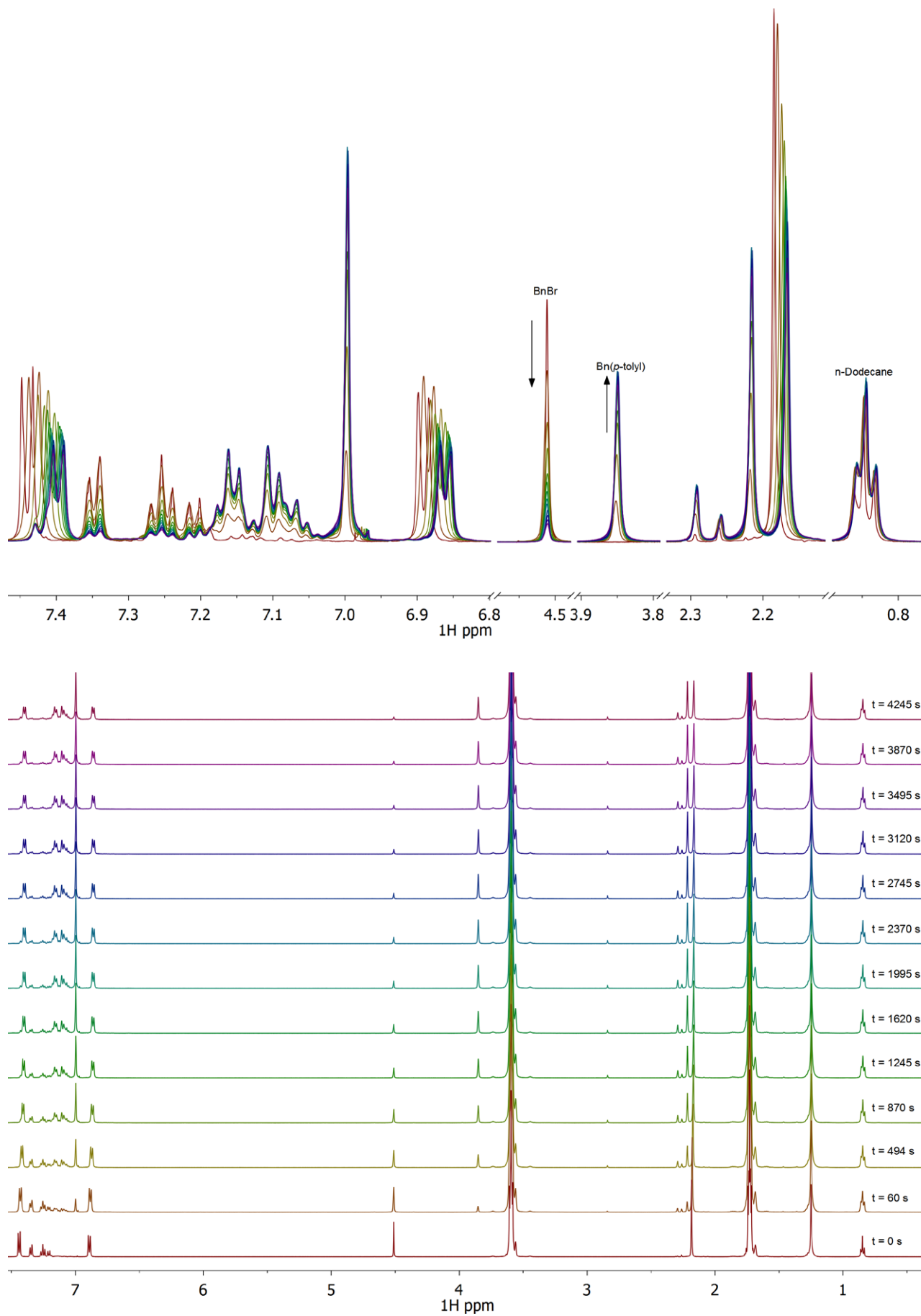
10.1 ^1H NMR spectroscopic investigation

10.1.1 Calculation of the ^1H NMR T_1 spin-lattice relaxation for BnBr and Bn(4-tolyl)

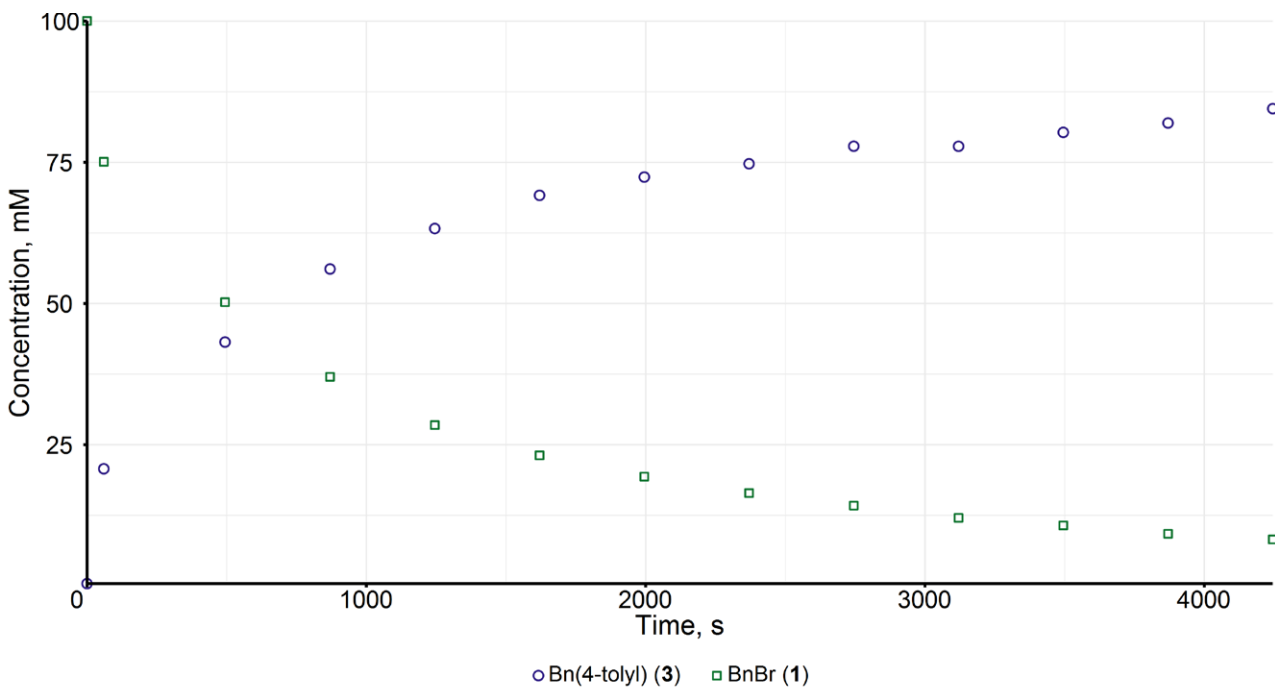
In order to determine the ^1H T_1 relaxation of BnBr (**1**) and Bn(4-tolyl) (**3**) under reaction conditions, an NMR tube was loaded with FeBr_2 (40.0 μL , 20.0 mM stock solution in $\text{THF-}d_8$, 0.80 μmol), dodecane (80.0 μL , 500 mM stock solution in $\text{THF-}d_8$, 40.0 μmol), ZnBr_2 (400 μL , 200 mM stock solution in $\text{THF-}d_8$, 80.0 μmol), dpbz (20.0 μL , 80.0 mM stock solution in $\text{THF-}d_8$, 1.60 μmol), benzyl bromide (32.0 μL , 2500 mM stock solution in $\text{THF-}d_8$, 80.0 μmol), Bn(4-tolyl) (14.7 μL , neat, 80.0 μmol) and $\text{THF-}d_8$ (213 μL) to give a solution with a total volume of 800 μL . A T_1 experiment was then performed. The calculated T_1 spin-lattice relaxation delays for **1** and **3** were found to be 7.98 ± 0.1063 s and 4.235 ± 0.07352 s respectively. Due to the resulting time required for the sample to fully relax between scans (5 x longest T_1 = 40 s) all ^1H NMR spectra were recorded as single scan experiments performed more than 40 s apart for achieving quantitation.

10.1.2 Negishi reaction profile determination by ^1H NMR spectroscopic monitoring

In an argon filled glovebox, FeBr_2 (40.0 μL , 20.0 mM stock solution in $\text{THF-}d_8$, 0.80 μmol) was applied to the head of a screw-top NMR tube and left horizontally so as to allow for the solvent to evaporate within the head region of the tube, leaving behind a thin film of FeBr_2 located on the top of the NMR tube. Subsequently, the NMR tube was carefully loaded with dpbz (20.0 μL , 80.0 mM stock solution in $\text{THF-}d_8$, 1.60 μmol), benzyl bromide (32.0 μL , 2500 mM stock solution in $\text{THF-}d_8$, 80.0 μmol), dodecane (80.0 μL , 500 mM stock solution in $\text{THF-}d_8$, 40.0 μmol), $\text{Zn(4-tolyl)}_2/2\text{MgBr}_2$ (400 μL , 200 mM stock solution in $\text{THF-}d_8$, 80.0 μmol) and $\text{THF-}d_8$ (268 μL) to give a solution with a total volume of 800 μL . A capillary containing $[\text{NiCl}_2(\text{dppe})]$ (50.0 μL , 16.0 mM stock solution in CDCl_3 , 0.80 μmol) was added and the NMR tube sealed, with the FeBr_2 residue remaining undisturbed at the head of the tube. The ^1H and ^{31}P NMR spectra at $t = 0$ s were then recorded providing the initial concentrations of the starting materials as well as locking and shimming the sample. The tube was then ejected, and the reaction initiated by quickly and carefully shaking the NMR tube so that the FeBr_2 residue quickly dissolved. The sample was quickly replaced and an NMR spectra collection array was initiated whereby the ^1H and ^{31}P spectra were recorded over time, with pre-calculated relaxation delays. The collected ^1H NMR spectra and the reaction profile obtained from the integrated spectra are presented in Supplementary Figure 164 and Supplementary Figure 165 respectively.



Supplementary Figure 164. Overlaid (top) and stacked (bottom) ¹H NMR (500 MHz, THF-*d*₈) spectra of the Negishi reaction between BnBr (**1**) (100 mM) and Zn(4-tolyl)₂/2 MgBr₂ (**2a**) (100 mM) catalyzed by FeBr₂ (1.00 mM) in presence of dpbz (2.00 mM) at 25 °C collected at various times during turnover.



Supplementary Figure 165. Reaction profile of the Negishi coupling between **1** (100 mM) and **2a** (100 mM) catalysed by FeBr_2 (1.00 mM) + dpbz (2.00 mM) at 25.0 °C and a total volume of 800 μL in an NMR tube, concentrations determined by ^1H NMR spectroscopy.

10.2 ^{31}P NMR spectroscopic investigation

10.2.1 Calculation of the ^{31}P NMR T_1 spin-lattice relaxation for zinc-phosphine complexes and the $[\text{NiCl}_2(\text{dppe})]$ capillary standard

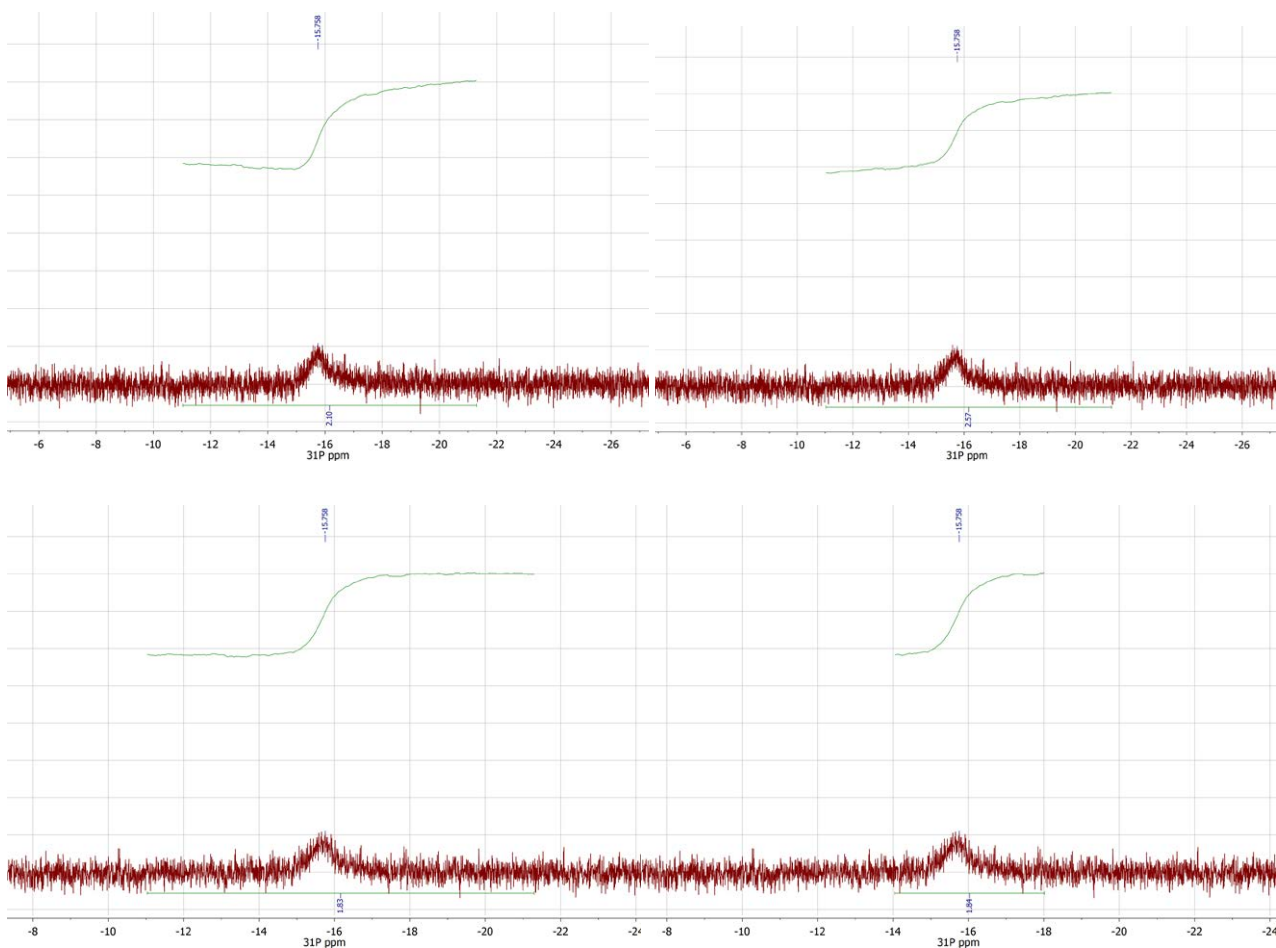
In order to determine a representative ^{31}P T_1 relaxation for the Zn(II)-dpbz complexes formed during catalysis in the presence of Fe(II), an NMR tube was loaded with FeBr_2 (40.0 μL , 20.0 mM stock solution in $\text{THF}-d_8$, 0.80 μmol), dpbz (20.0 μL , 80.0 mM stock solution in $\text{THF}-d_8$, 1.60 μmol), ZnBr_2 (400 μL , 200 mM stock solution in $\text{THF}-d_8$, 80.0 μmol) and $\text{THF}-d_8$ (340 μL) to give a solution with a total volume of 800 μL . A capillary containing $[\text{NiCl}_2(\text{dppe})]$ was added as a reference and standard with a resonance at 58.7 ppm. A T_1 experiment was then run and the relaxation delay of the peak at -26.6 ppm corresponding to the $[\text{ZnBr}_2(\text{dpbz})]$ complex in presence of iron was found to be 0.07487 ± 0.01232 s (202 MHz, 298 K, 2 mM in dpbz) while the one for $[\text{NiCl}_2(\text{dppe})]$ was 0.233 ± 0.03011 s (202 MHz, 298 K, 16 mM in CDCl_3). Accordingly, the relaxation delay for all quantitative ^{31}P experiments was set to 1.5 s. It must be noted that all ^{31}P NMR spectra involved in quantitative studies were acquired with the ^1H decoupling turned off.

10.2.2 ^{31}P NMR spectroscopic examination of the phosphorus speciation during the Negishi cross coupling

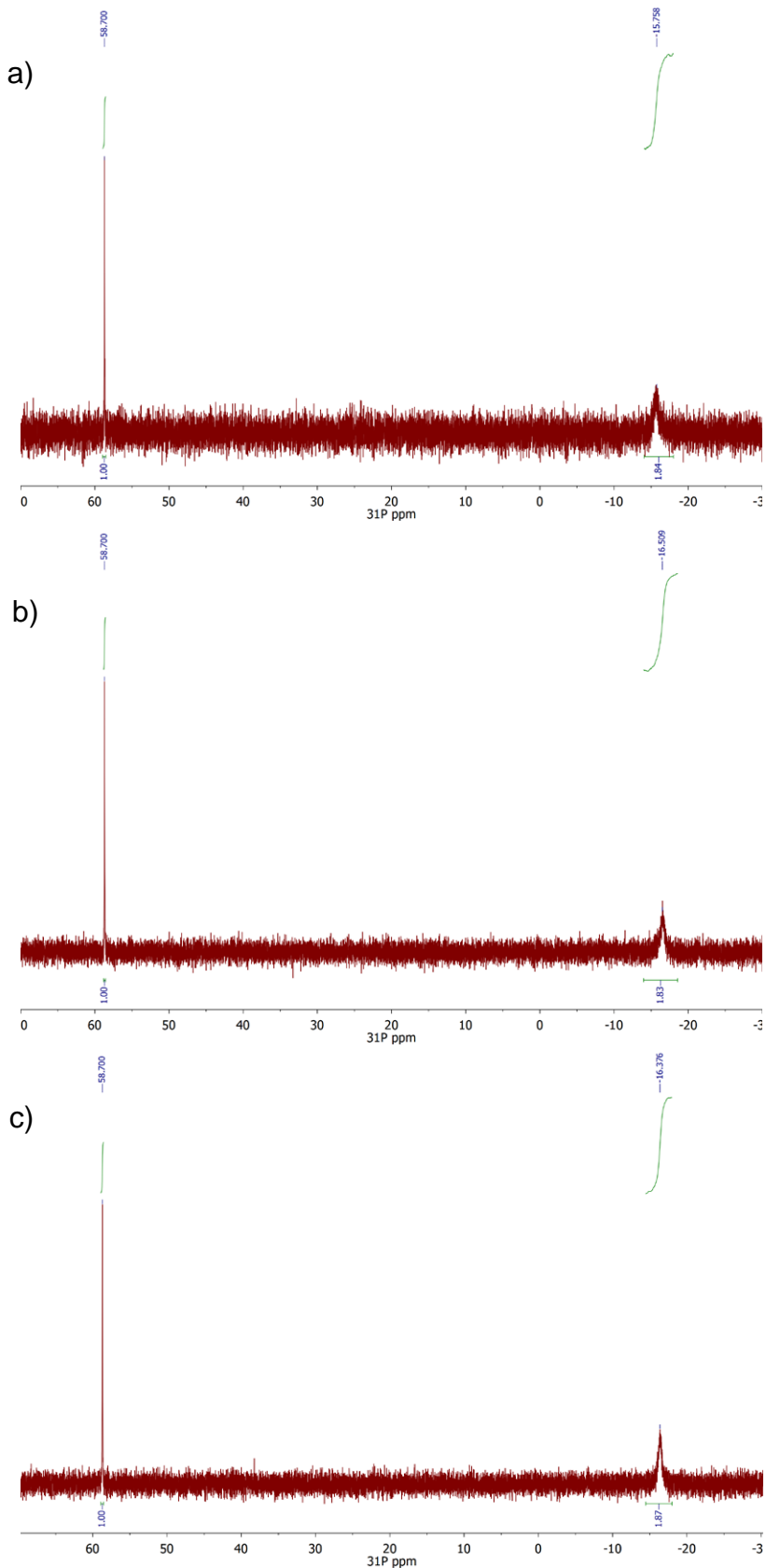
The same reaction protocol was used as described in section 10.1. However, due to the weak ^{31}P NMR signals as a result of the low phosphine concentration during catalysis (2.00 mM) in combination with peak broadening it was necessary to record the ^{31}P NMR spectrum over the first 40 minutes of the reaction (1024 scans) in order to obtain reasonable signal to noise ratios suitable for reliable integration. According to an ^1H NMR that followed after the

aforementioned ^{31}P NMR spectrum was recorded, the yield of $\text{Bn}(p\text{-tolyl})$ (**3**) was 87% signaling the end of the reaction. Subsequently, the same ^{31}P NMR measurement was repeated after the first 40 minutes of reaction providing information on the catalytic reaction's endpoint. Therefore, the observed ^{31}P NMR signal corresponding to the phosphorus species not bound on iron will be the average signal throughout the whole catalysis region. A separate ^{31}P NMR experiment was then performed by filling the same NMR tube in which the aforementioned catalysis took place and equipped with the same $[\text{NiCl}_2(\text{dppe})]$ -filled capillary with: dpbz (20.0 μL , 80.0 mM stock solution in THF-d_8 , 1.60 μmol), dodecane (80.0 μL , 500 mM stock solution in THF-d_8 , 40.0 μmol), $\text{Zn}(4\text{-tolyl})_2/2\text{MgBr}_2$ (300 μL , 200 mM stock solution in THF-d_8 , 60.0 μmol), $\text{Bn}(4\text{-tolyl})$ (7.3 μL , 40.0 μmol), ZnBr_2 (40 μL , 500 mM stock solution in THF-d_8 , 20.0 μmol), MgBr_2 (7.3 mg, 40.0 μmol) and THF-d_8 (353 μL) to give a solution with a total volume of 800 μL . The resultant solution, which mimics the catalytic reaction's composition at 50% conversion but excludes FeBr_2 , was submitted for a ^{31}P NMR experiment on the same instrument and with the same parameters used for the ^{31}P NMR study of the catalytic reaction under examination. The only difference in this case was the extremely high relaxation delay (60 s) necessary for ensuring that the collected spectrum can be quantified as a result of the absence of paramagnetic FeBr_2 in the mixture.

In the three spectra collected, two resonances were observed at 58.7 and -16.4 to -15.8 ppm corresponding to $[\text{NiCl}_2(\text{dppe})]$ and Zn-phosphine species respectively. When quantifying spectra with low signal to noise ratio it is crucial that baseline and phase corrections are performed very carefully so that the integral curve plateaus correctly on both sides of each NMR peak in a way that the integral doesn't change significantly when it is expanded. Therefore, spectra were baseline corrected using a polynomial fit with the help of MestReNova software, phase corrected and integrated by expanding the integration region just before the integral line plateaued on both sides of the peak. In Supplementary Figure 166 an example of the integration process is presented. Each collected ^{31}P NMR spectrum (reference reaction without FeBr_2 ; Negishi reaction collected during the first 40 minutes of reaction and reaction endpoint) was then processed in the way described above and the results are presented in Supplementary Figure 167. Clearly, the integral ratios between $[\text{NiCl}_2(\text{dppe})]$ and Zn-phosphine species are very similar in all cases demonstrating that during catalysis the vast majority of the phosphine is coordinated to the Zn.



Supplementary Figure 166. Example of NMR data processing of sample a) of Supplementary Figure 167 involving (top left to bottom right) phase correction, baseline correction using a 2nd order polynomial and trimming of the integration region to give the final integral value.



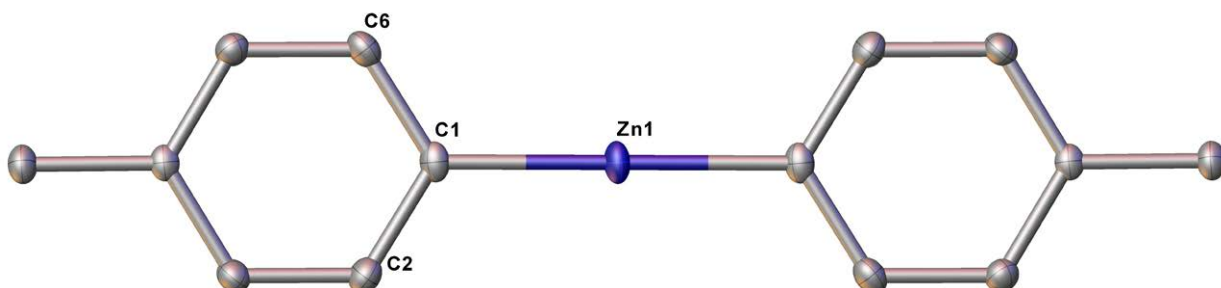
Supplementary Figure 167. a) ^{31}P NMR spectrum (202 MHz, $\text{THF}-d_8$) of a control experiment representing a 50% conversion mixture of the Negishi reaction (no FeBr_2 present), b) and c) ^{31}P NMR spectra (202 MHz, $\text{THF}-d_8$) of the Negishi cross coupling between **1** (100 mM) and **2a** (100 mM) catalyzed by FeBr_2 (1.00 mM) and dpbz (2 mM) at 25 °C over the period between 0 and 40 minutes (b) and the end point of the reaction ($t > 40$ min) (c).

11 Examining Aryl-Zn/Fe transmetallation

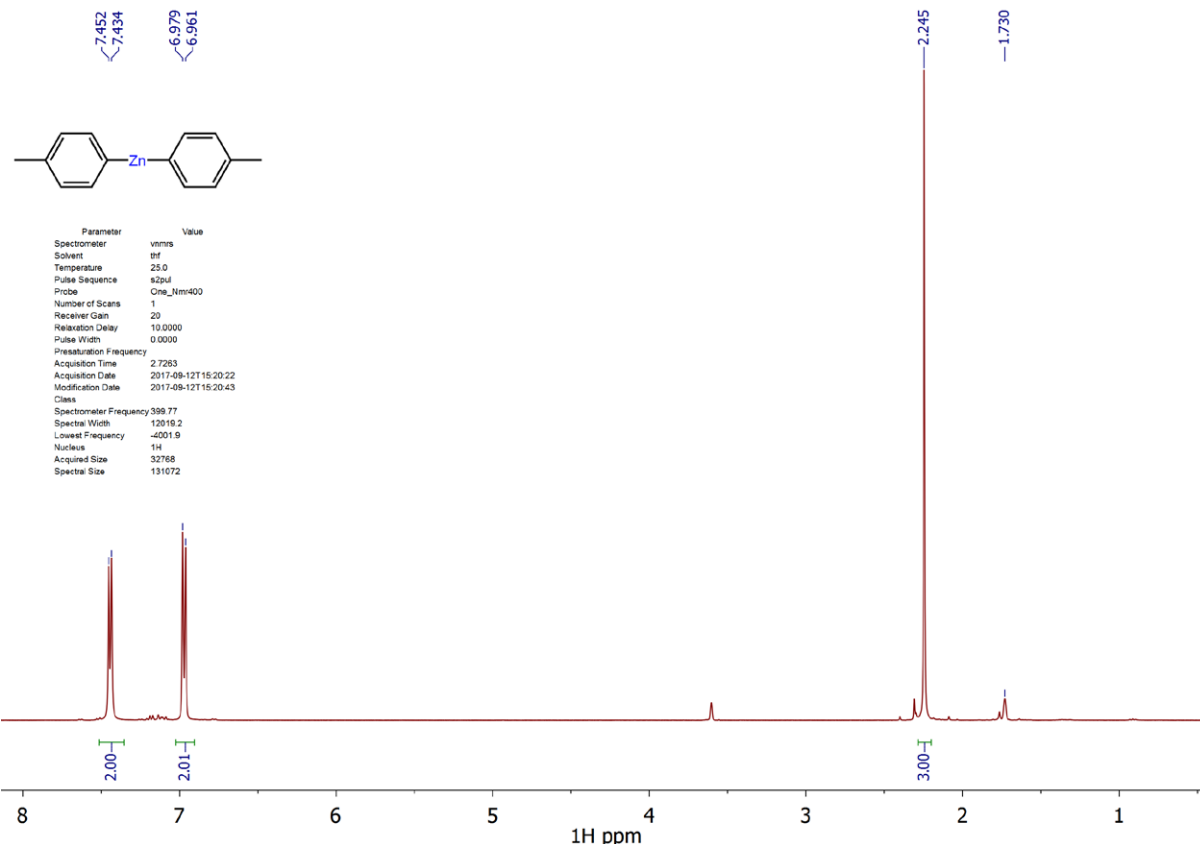
11.1 Transmetallation studies with Zn(4-tolyl)₂

11.1.1 Synthesis of Mg-free Zn(4-tolyl)₂ (Mg-free **2a**)

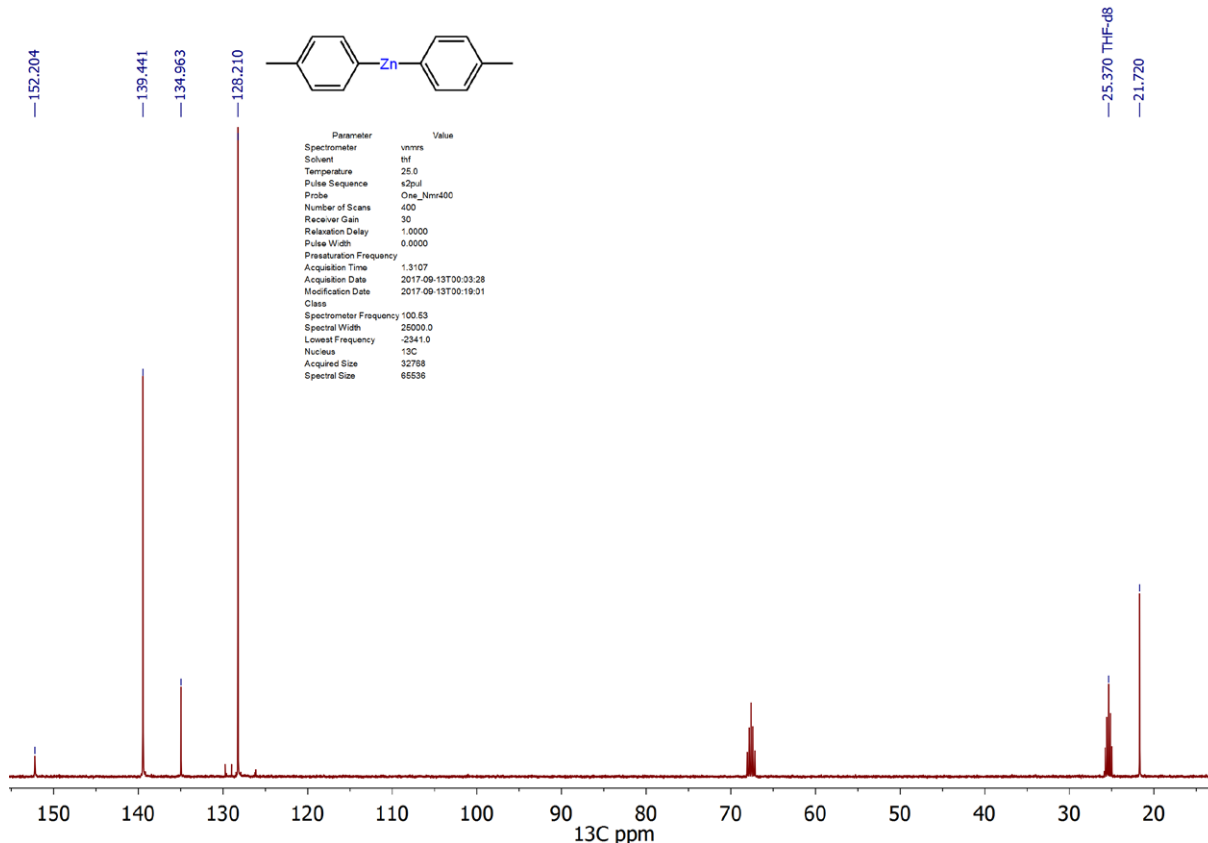
Magnesium-free Zn(4-tolyl)₂ (Mg-free **2a**) was prepared using a modification of the procedure reported by Sheverdina *et. al.*³⁹ A Schlenk was loaded with Li(4-tolyl) (9.000 g, 91.74 mmol), ZnCl₂ (6.066 g, 44.53 mmol), *m*-xylene (72 mL) and diethyl ether (20 mL). A reflux condenser was fitted and the mixture was heated at reflux temperature with vigorous stirring for 3 h during which time an exothermic reaction occurred along with formation of a grey precipitate. The resultant mixture was filtered while still hot and the yellow filtrate was dried under reduced pressure to give a solid which was first washed with cold (-35°C) toluene (3×10 mL) and then extracted with hot (~100 °C) toluene. The extracts were then left to cool to room temperature for 12 h to give a white crystalline solid which was filtered, washed with cold (-35°C) toluene (10 mL) and dried under reduced pressure. The recrystallisation procedure was repeated a second time to give Zn(4-tolyl)₂ (7.05 g, 63%) as a colourless crystalline solid. Crystals suitable for an X-ray crystallographic analysis were grown by allowing a saturated solution of the compound in toluene at 110 °C to cool to room temperature over a period of 12 h. ¹H NMR (400 MHz, THF-*d*₈) δ = 7.44 (d, *J*=7.2, 4H), 6.97 (d, *J*=7.3, 4H), 2.25 (s, 6H). ¹³C NMR (101 MHz, THF-*d*₈) δ = 152.2, 139.4, 135.0, 128.2, 21.7.



Supplementary Figure 168. Single-crystal X-ray structure of magnesium-free Zn(4-tolyl)₂ (Mg-free **2a**). Hydrogen atoms are omitted for clarity and thermal ellipsoids are set at the 50% probability level.



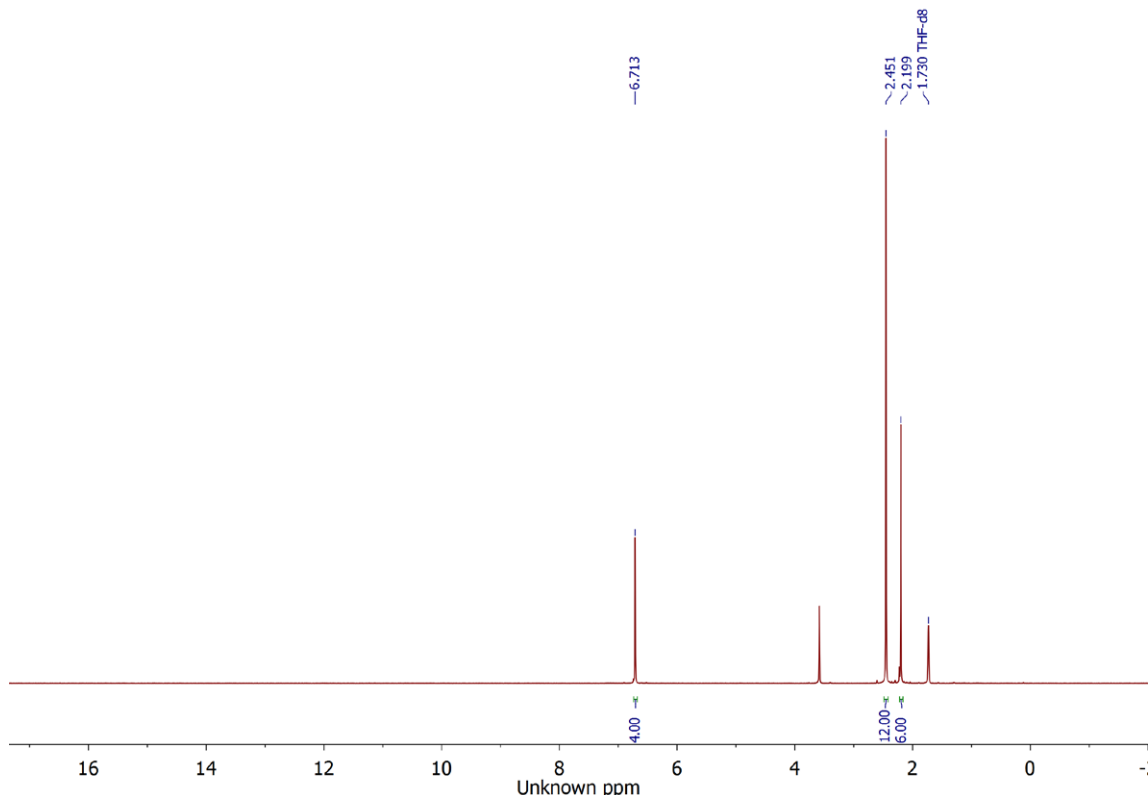
Supplementary Figure 169. ^1H NMR spectrum (400 MHz, THF- d_8) of Mg-free **2a**.



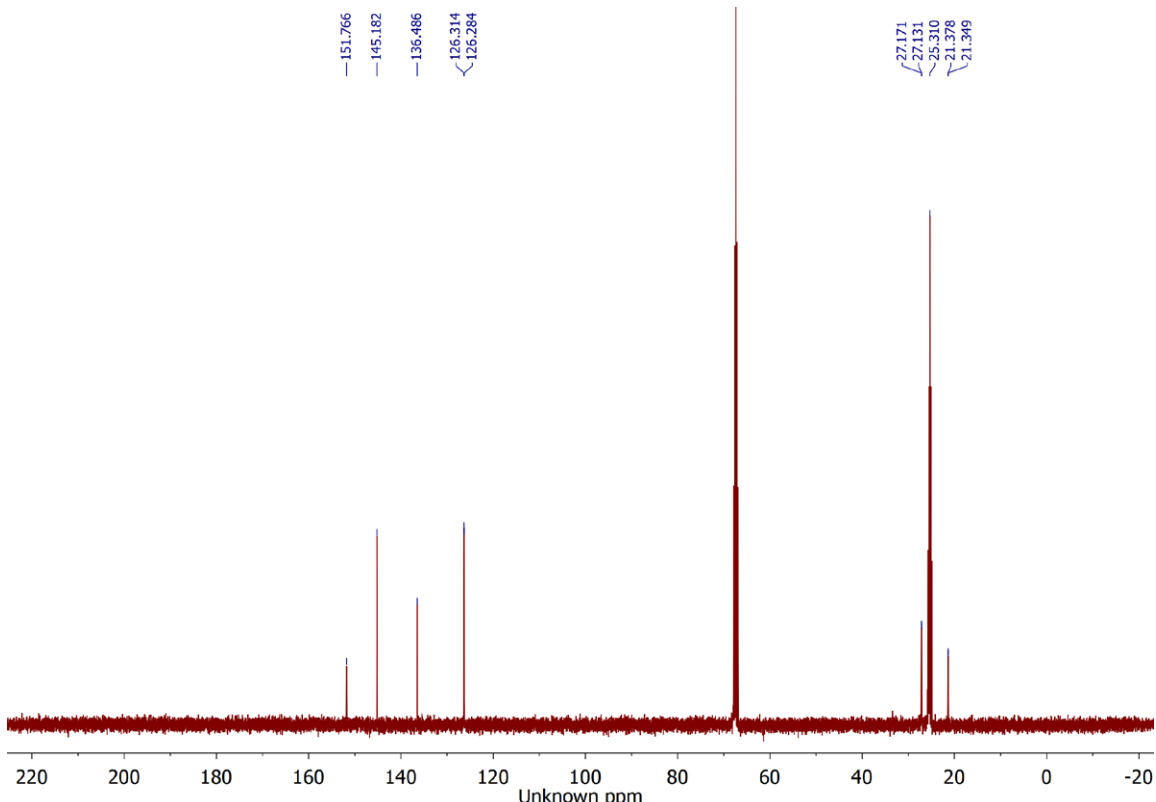
Supplementary Figure 170. ^{13}C NMR spectrum (100 MHz, THF- d_8) Mg-free **2a**.

11.1.2 Synthesis of Mg-free Zn(mes)₂ (Mg-free 2b)

A Schlenk was loaded with LiMes (1.000 g, 7.92 mmol), ZnCl₂ (540.2 mg, 3.96 mmol) *m*-xylene (15 mL) and diethyl ether (4 mL). A reflux condenser was fitted and the mixture heated to reflux temperature with vigorous stirring for 16 h, during which time a grey precipitate formed. After removing from the hotplate, the resulting mixture was filtered and left to cool to room temperature. The title product crystallised as colourless needles (795 mg, 66%). ¹H NMR (400 MHz, THF-*d*₈) δ = 6.71 (s, 4H), 2.45 (s, 12H), 2.20 (s, 6H). ¹³C NMR (101 MHz, THF-*d*₈) δ = 151.95, 145.37, 136.67, 126.48, 27.33, 21.55.



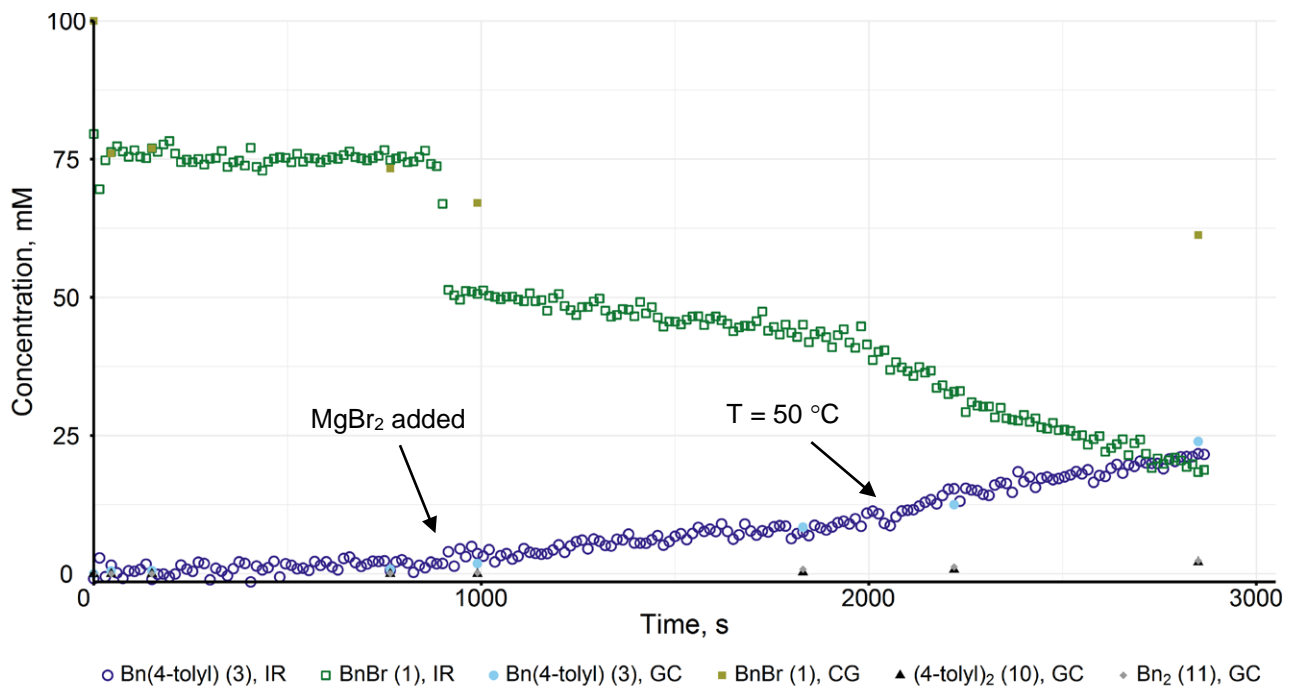
Supplementary Figure 171. ¹H NMR spectrum (400 MHz, THF-*d*₈) of Mg-free **2b**.



Supplementary Figure 172. ^{13}C NMR spectrum (100 MHz, THF- d_8) of Mg-free **2b**.

11.1.3 Effect of MgBr_2 on the Negishi cross coupling

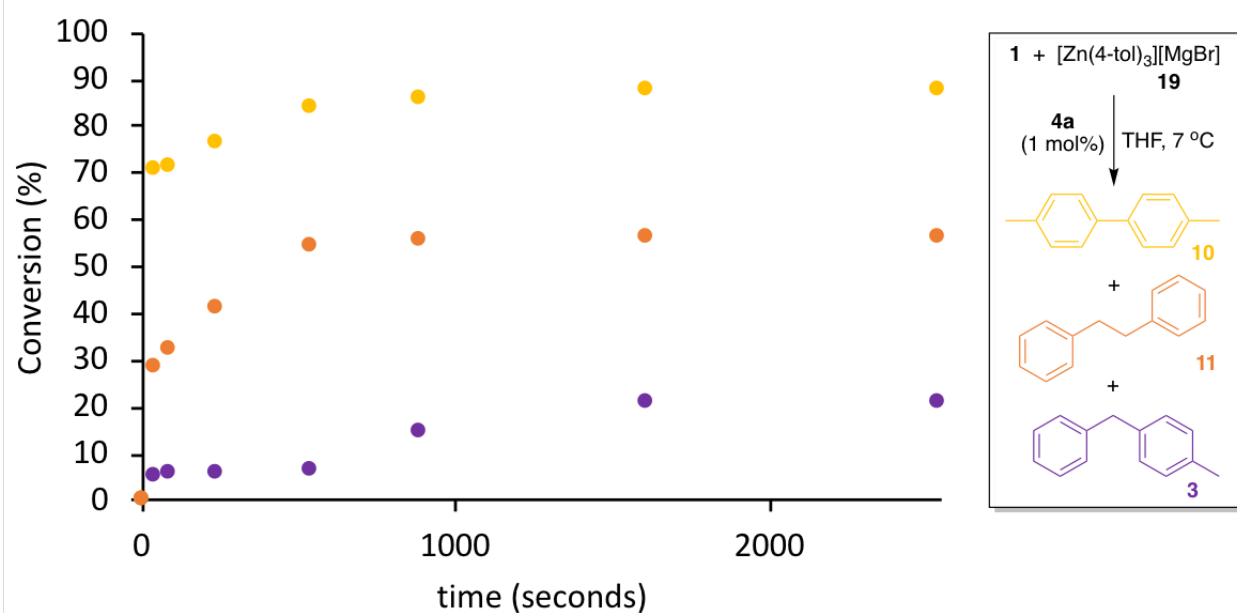
The profile of the reaction between **1** and Mg-free **2a** was obtained as described in section 2 with **1** (1.00 mmol), Mg-free **2a** (1.00 mmol in Zn), FeBr_2 (0.0100 mmol), dpbz (0.0200 mmol) and *n*-dodecane (internal standard, 0.5 mmol) at a total volume of 10.0 mL. The reaction was initiated by the addition of the FeBr_2 and after 915 s MgBr_2 (2.00 mmol) was added. At 1815 s the reaction temperature was increased to 50 °C. The reaction profile obtained is shown in Supplementary Figure 173.



Supplementary Figure 173. Negishi coupling between **1** (100 mM) and Mg-free **2a** (100 mM) catalysed by FeBr₂ (1.00 mM) + dpbz (2.00 mM) in a total volume of 10.0 mL, followed after 915 s by the addition of MgBr₂ (200 mM) at 7.00 °C. After 1815 s the temperature was increased at 50 °C.

11.1.4 Negishi reaction between **1** and *in situ*-formed [Zn(4-tolyl)₃][MgBr] (**19a**) catalysed by FeBr₂ + dpbz

A jacketed Schlenk equipped with a cooling coil was loaded with THF (2.10 mL), *n*-dodecane (internal standard, 1.00 mL, 500 mM solution in THF, 0.50 mmol), **2a** (5.00 mL, 200 mM solution in THF, 1.00 mmol), (4-tolyl)MgBr (1.00 mL, 1000 mM solution in THF, 1.00 mmol), dpbz (0.250 mL, 80.0 mM solution in THF, 0.0200 mmol) and BnBr (1) (0.40 mL, 2500 mM solution in THF, 1.00 mmol). The temperature was set at 7.00 °C and stirring at 500 rpm. Catalysis was initiated with addition of FeBr₂ (0.250 mL, 20.0 mM solution in THF, 0.0100 mmol) accompanied by a colour change to dark red and formation of a white precipitate. The reaction was sampled (0.1 mL - 0.2 mL aliquots) over the course of 40 minutes. Each sample was quenched with HCl solution (0.5 M) and the time recorded resulting in the reaction profile shown in Supplementary Figure 174.



Supplementary Figure 174. Reaction profile of the Negishi reaction between **1** and **19a** catalyzed by FeBr_2 and dpbz.

11.1.5 Reaction of FeBr_2 with magnesium-free $\text{Zn}(4\text{-tolyl})_2$ (**Mg-free 2a**) (Figure 7(a)(i)).

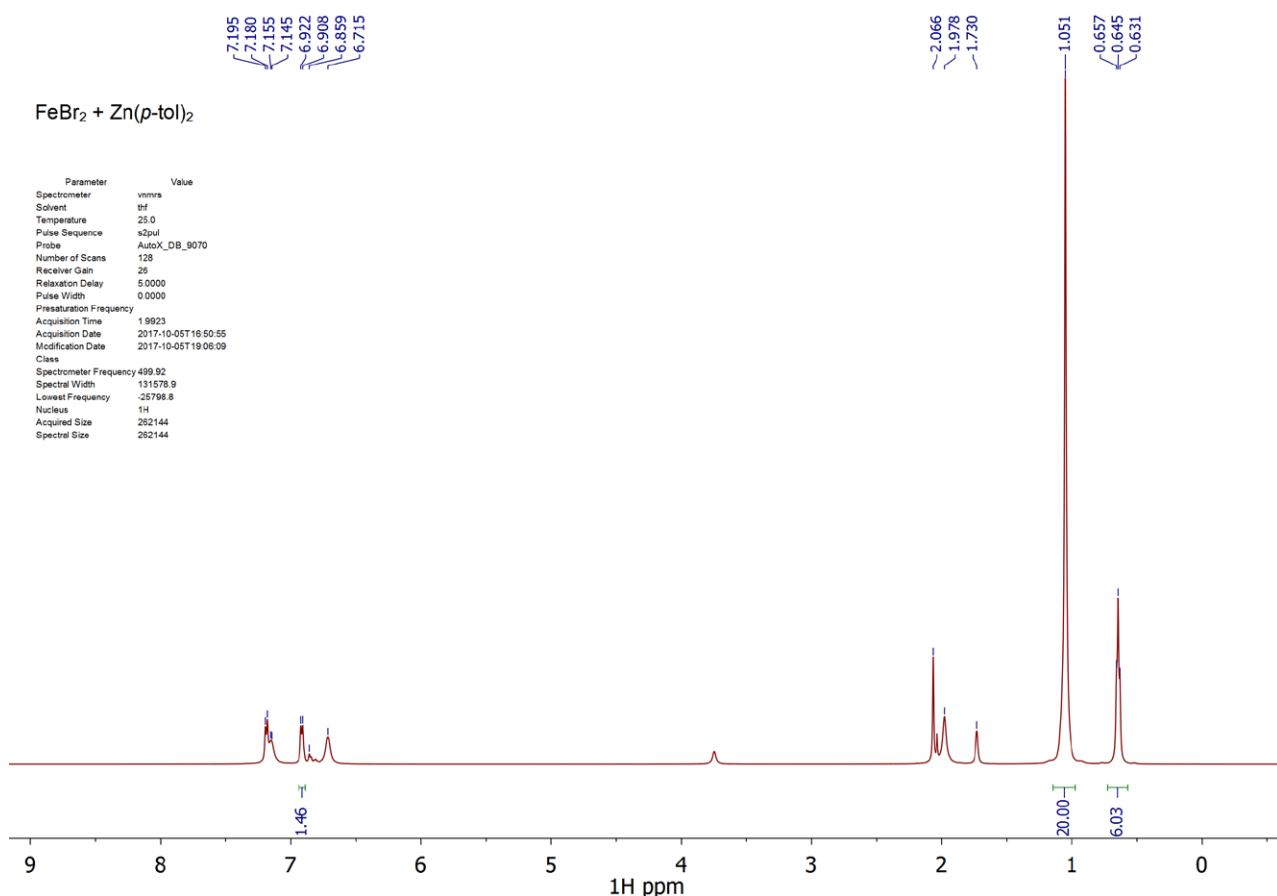
In an argon filled glove box, three vials were loaded with FeBr_2 (54.0 mg, 0.25 mmol), *n*-dodecane (internal standard, 42.6 mg, 0.25 mmol) and THF-d_8 (2.00 mL). The three mixtures were then heated to reflux until all FeBr_2 dissolved and left to cool to room temperature (approximately 21 °C). Subsequently, Mg-free **2a** (61.9 mg, 0.25 mmol) was added to the first vial, (123.8 mg, 0.50 mmol) to the second and (185.7 mg, 0.75 mmol) to the third. The initially pale-yellow solutions gradually turned darker after 5-10 minutes accompanied by the gradual formation of an insoluble black magnetic precipitate. The mixtures were then briefly heated at reflux temperature (approx. 2 min), sonicated for 2 h and stirred for another 12 h at approximately 21 °C in order for the reaction to reach completion. In order to determine the amount of 4,4'bitolyl **10** formed from the reactions, each mixture was filtered and 0.8 mL of each filtrate was loaded in a J. Youngs tap NMR tube and analysed by ^1H NMR spectroscopy (Supplementary Figure 175 and Supplementary Figure 176) while the rest was quenched with HCl solution 0.5 M, extracted with CH_2Cl_2 and analysed by GC-FID. The results are summarized in Supplementary Table 14.

Supplementary Table 14. Amount of **10** detected by GC-FID and ^1H NMR for the reactions between FeBr_2 and $\text{Zn}(4\text{-tolyl})_2$ (Mg-free **2a**).

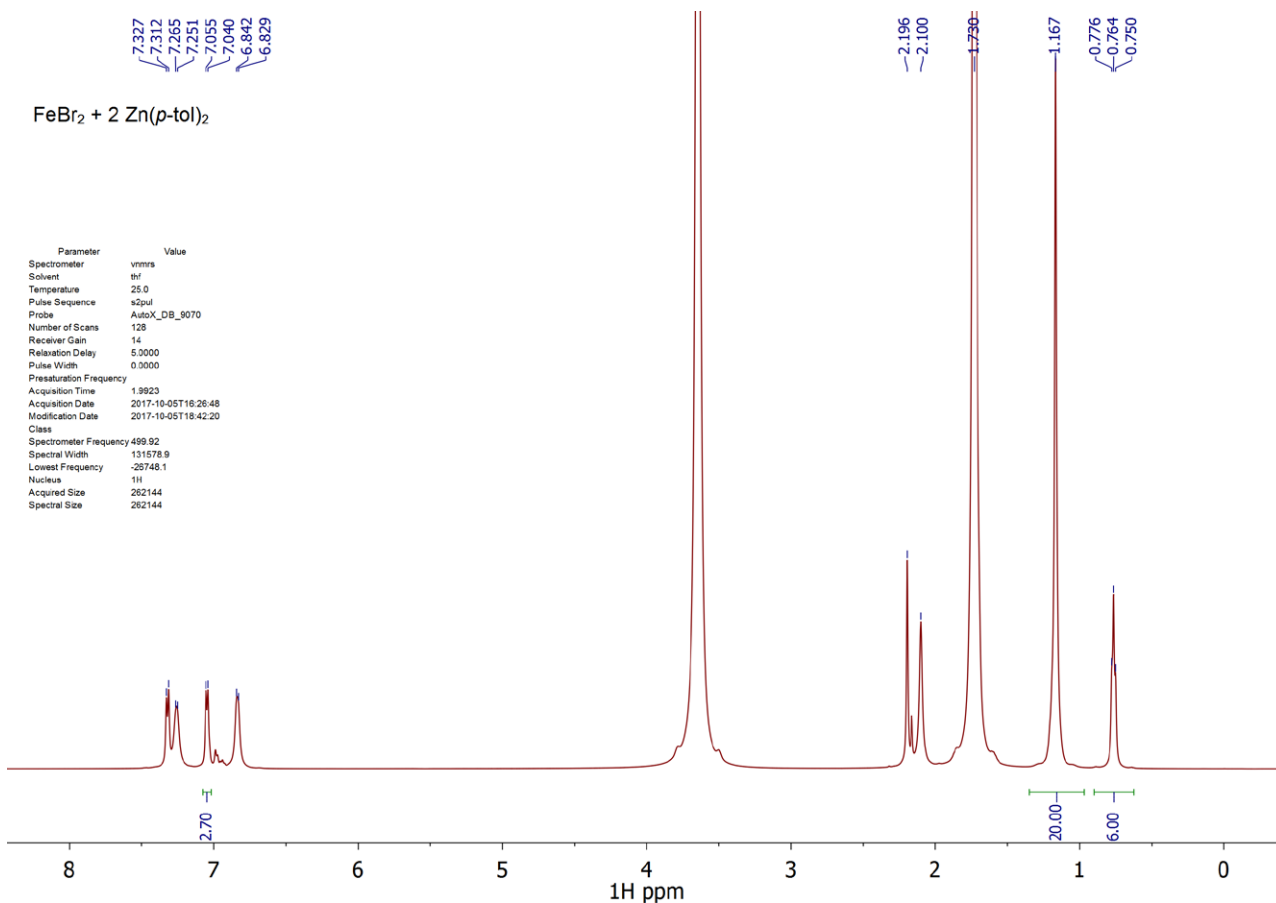
	$\text{Zn}(4\text{-tolyl})_2$ eq.	1 $\text{Zn}(4\text{-tolyl})_2$ eq.	2 $\text{Zn}(4\text{-tolyl})_2$ eq.	3 $\text{Zn}(4\text{-tolyl})_2$ eq.
(4-tolyl) ₂ mmol by GC-FID	0.083	0.161	0.206	-
(4-tolyl) ₂ mmol by ^1H NMR	0.091	0.169	-	-

$\text{FeBr}_2 + \text{Zn}(p\text{-tolyl})_2$

Parameter	Value
Spectrometer	vnmrs
Solvent	thf
Temperature	25.0
Pulse Sequence	s2pul
Probe	AutoX_DB_9070
Number of Scans	128
Receiver Gain	25
Repetition Delay	5.0000
Pulse Width	0.0000
Presaturation Frequency	
Acquisition Time	1.9923
Acquisition Date	2017-10-05T16:50:55
Modification Date	2017-10-05T19:06:09
Class	
Spectrometer Frequency	499.92
Spectral Width	131578.9
Lowest Frequency	-25798.8
Nucleus	^1H
Acquired Size	262144
Spectral Size	262144



Supplementary Figure 175. ^1H NMR spectrum(500 MHz, $\text{THF}-d_8$) of the filtrate from the reaction between FeBr_2 and Mg-free **2a** in THF.



Supplementary Figure 176. ¹H NMR spectrum (500 MHz, THF-*d*₈) of the filtrate from the reaction between FeBr₂ and 2 Mg-free **2a** in THF.

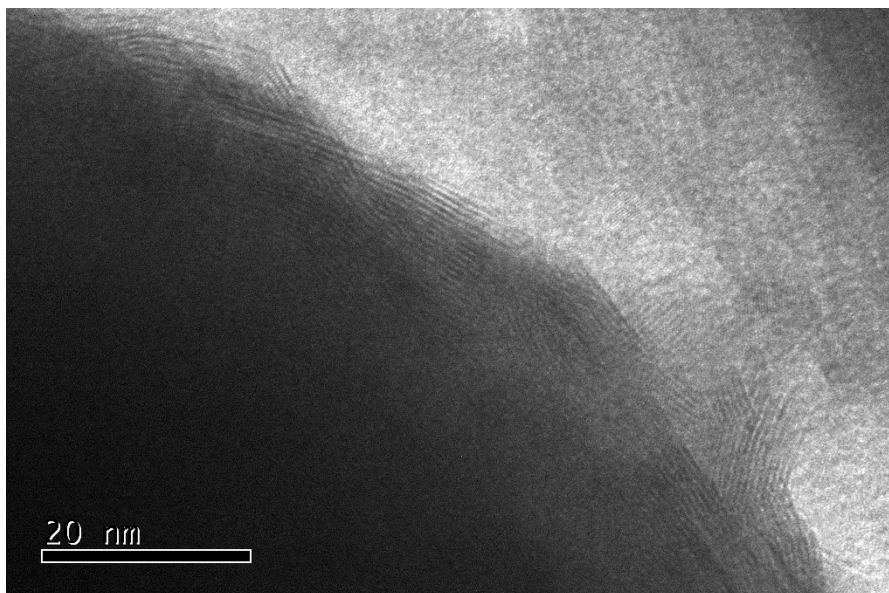
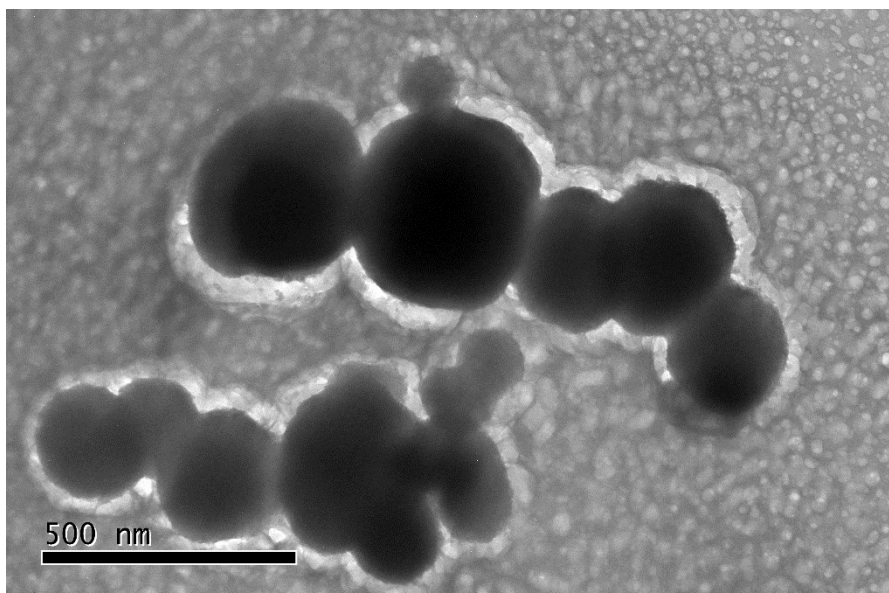
In order to characterise the magnetic precipitate formed from the reaction between FeBr₂ and Mg-free **2a**, the reaction was repeated as follows. In an argon filled glovebox, a vial was loaded with FeBr₂ (13.5 mg, 0.0625 mmol) and THF (0.5 ml). The mixture was heated to reflux temperature until all the FeBr₂ was dissolved and the solution allowed to cool to room temperature. Addition of Mg-free **2a** (31.0 mg, 0.125 mmol) followed and the reaction mixture was frequently agitated manually for a period of 2 h, during which time an insoluble black magnetic precipitate formed (magnetic stirring was avoided in order to minimise aggregation of magnetically responsive particles). Samples for TEM analysis were prepared either directly from the reaction mixture or after 3 washing cycles with deoxygenated and distilled water (magnetic separation, decantation of supernatant, resuspension in water). Specimens were drop-cast onto carbon covered 3 mm Cu grids washed with deoxygenated deionised water and the solvent was allowed to evaporate. The grids were stored in an inert atmosphere and loaded into a double-tilt specimen holder with minimal exposure to air before transfer into the transmission electron microscope (TEM) column.

TEM analysis of the unwashed samples revealed polydisperse, electron-dense particles with diameters typically ranging from 100 nm to 600 nm closely associated with a patchy network of deposited salts (Supplementary Figure 177). Higher magnification images of smaller, more electron-transparent particles suggest they might be nanostructured. In addition, layered structures with an interlamellar spacing of 0.62 nm were observed at the

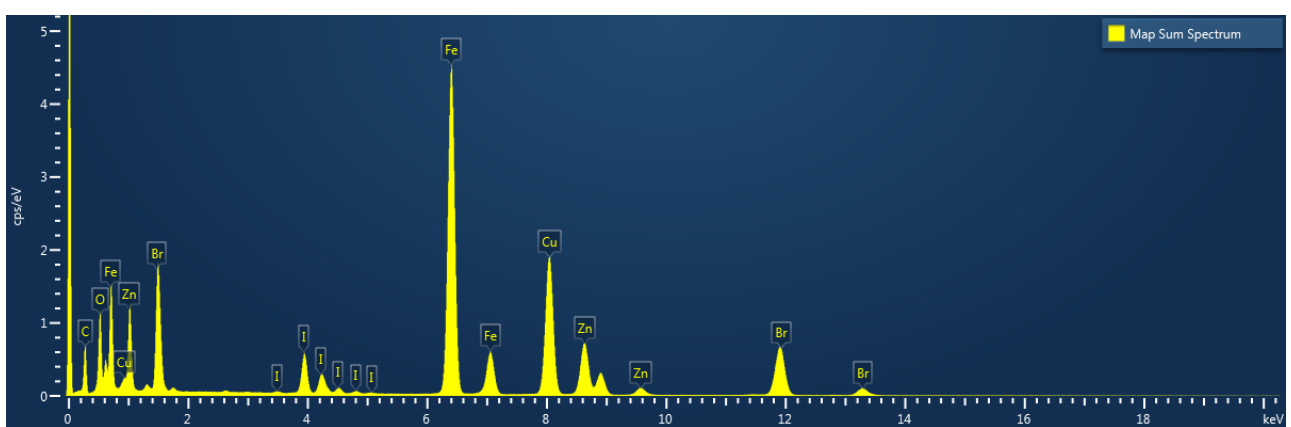
surface of the particles. EDX analysis indicated the sample contained predominantly Fe along with Zn, Br and I (Supplementary Figure 178) with the latter presumably originating from the synthesis of Li(4-tolyl) reagent, which is made from 4-tolyliodide, used for obtaining $Zn(4\text{-tolyl})_2$. Elemental mapping confirmed the particles were composed of Fe and closely associated I. In contrast Zn and Br were more concentrated around the edge of the particles presumably due to excess material depositing during the drying process (Supplementary Figure 179). To try and minimize these potential artefacts the samples were washed extensively with deoxygenated deionised water prior to grid preparation and the analysis repeated.

TEM of the washed sample revealed particles with similar dimensions to the unwashed samples (Supplementary Figure 180). Generally, there was less background material and the sub-micron particles were clearly nanostructured, possibly as aggregates of crystalline nanoparticles (5-10 nm in diameter). There was no evidence of large interlamellar spacings in the surface nanoparticles. EDX analysis indicated the sample contained predominantly Fe along with Zn, trace Br and negligible I (Supplementary Figure 181). Elemental mapping confirmed the particles were composed of Fe with both Zn and the trace Br signals also closely associated with the particles, in contrast to unwashed samples (Supplementary Figure 182). The absence of a core/shell structure to the particles, as seen with the unwashed samples, was further confirmed by linescan analysis which shows the surface is not enriched in Zn (Supplementary Figure 183). These data are consistent with excess Zn and Br depositing around the iron-rich particles during sample preparation of unwashed samples.

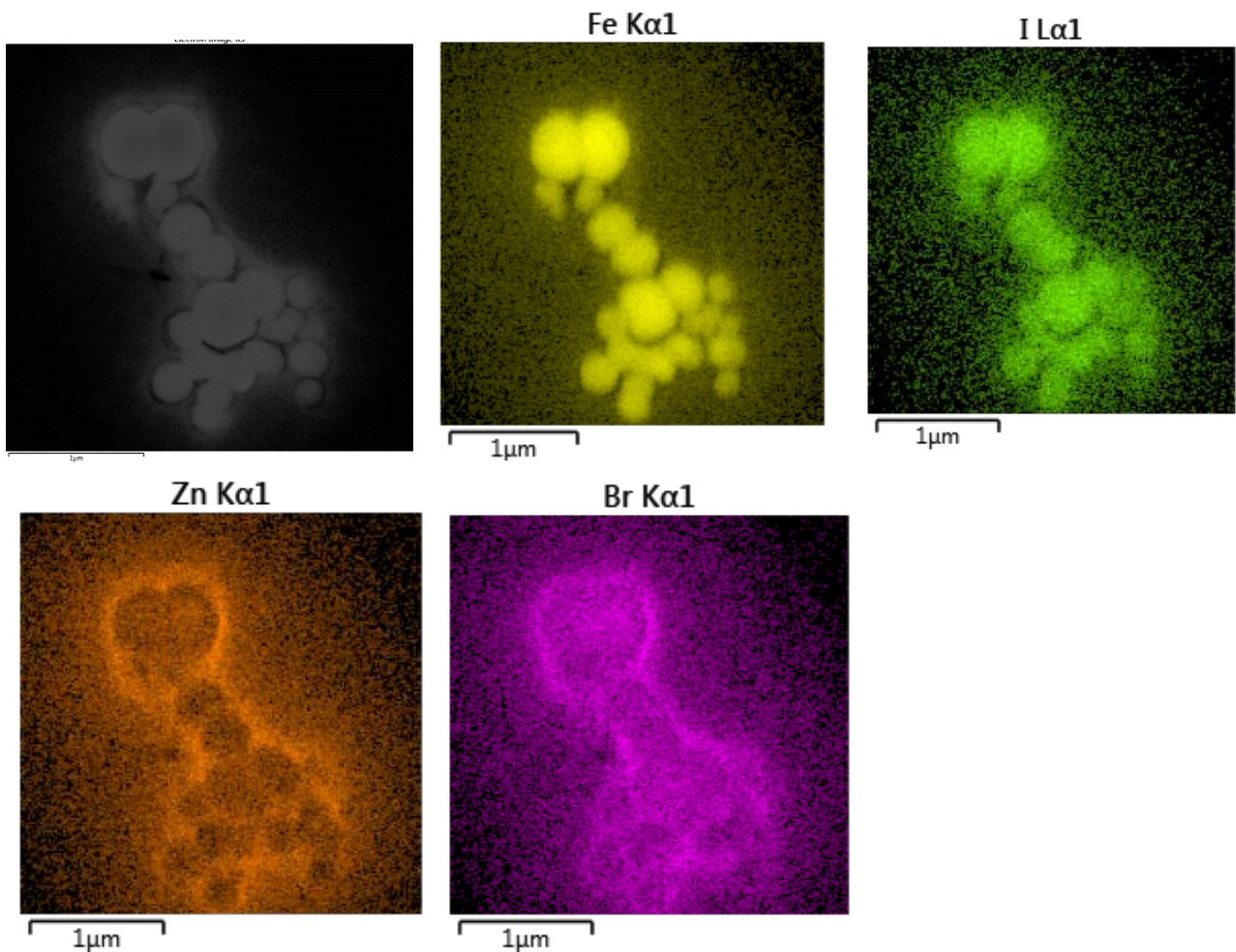
The formation of 4,4'-dimethylbiphenyl (**10**) was also monitored against time for the reaction between $FeBr_2$ and 2 Mg-free **2a** as follows. A jacketed Schlenk was charged with Mg-free **2a** (309.6 mg, 1.25 mmol) and dodecane (internal standard, 142 μ l, 0.625 mmol) followed by addition of $FeBr_2$ (5 ml, 0.125 M in THF, 0.625 mmol). The reaction was stirred at 21 °C 500 minutes during which time aliquots (0.1 ml) were collected and quenched with HCl solution (1.0 M, 0.5 ml). The organics were extracted from the aqueous layer with CH_2Cl_2 and analysed by GC-FID. The results are summarised in Supplementary Figure 184.



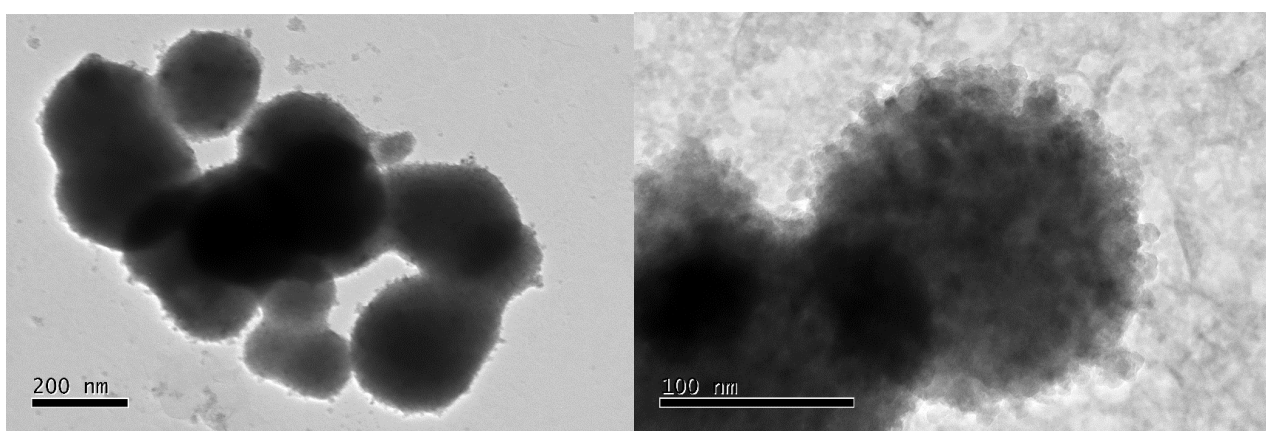
Supplementary Figure 177. TEM images of the unwashed iron nanoparticles isolated from the reaction between FeBr_2 and Mg-free **2a**.

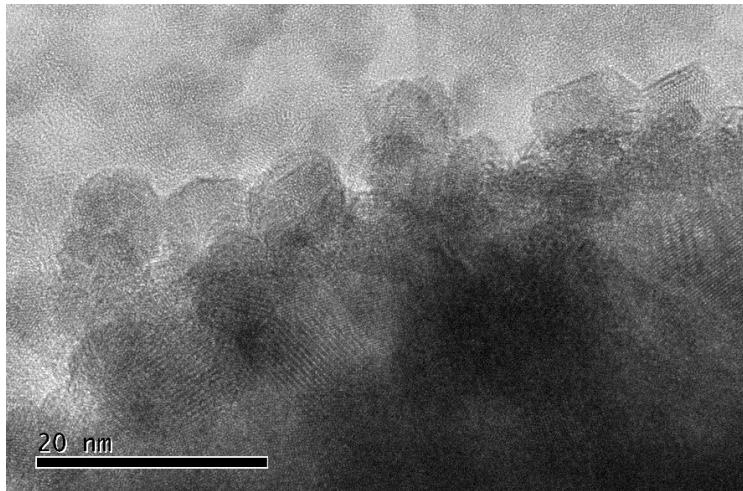


Supplementary Figure 178. EDX spectrum of unwashed iron nanoparticles isolated from the reaction between FeBr_2 and Mg-free **2a** indicating presence of Fe, Zn, Br and I (Cu signal is due to specimen support grid).

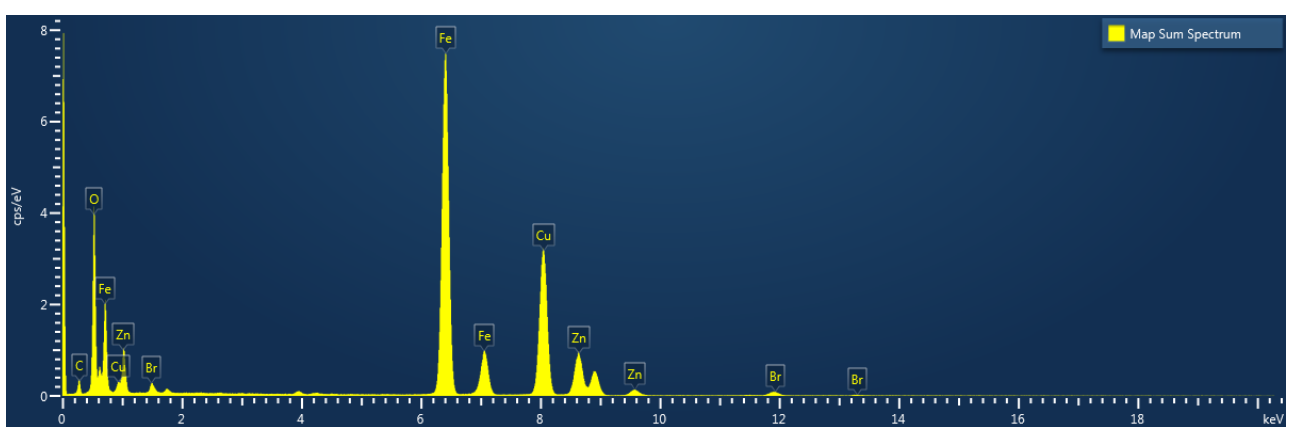


Supplementary Figure 179. HAADF-STEM image of unwashed iron nanoparticles isolated from the reaction between FeBr_2 and Mg-free **2a** and corresponding elemental maps for Fe, I, Zn and Br.

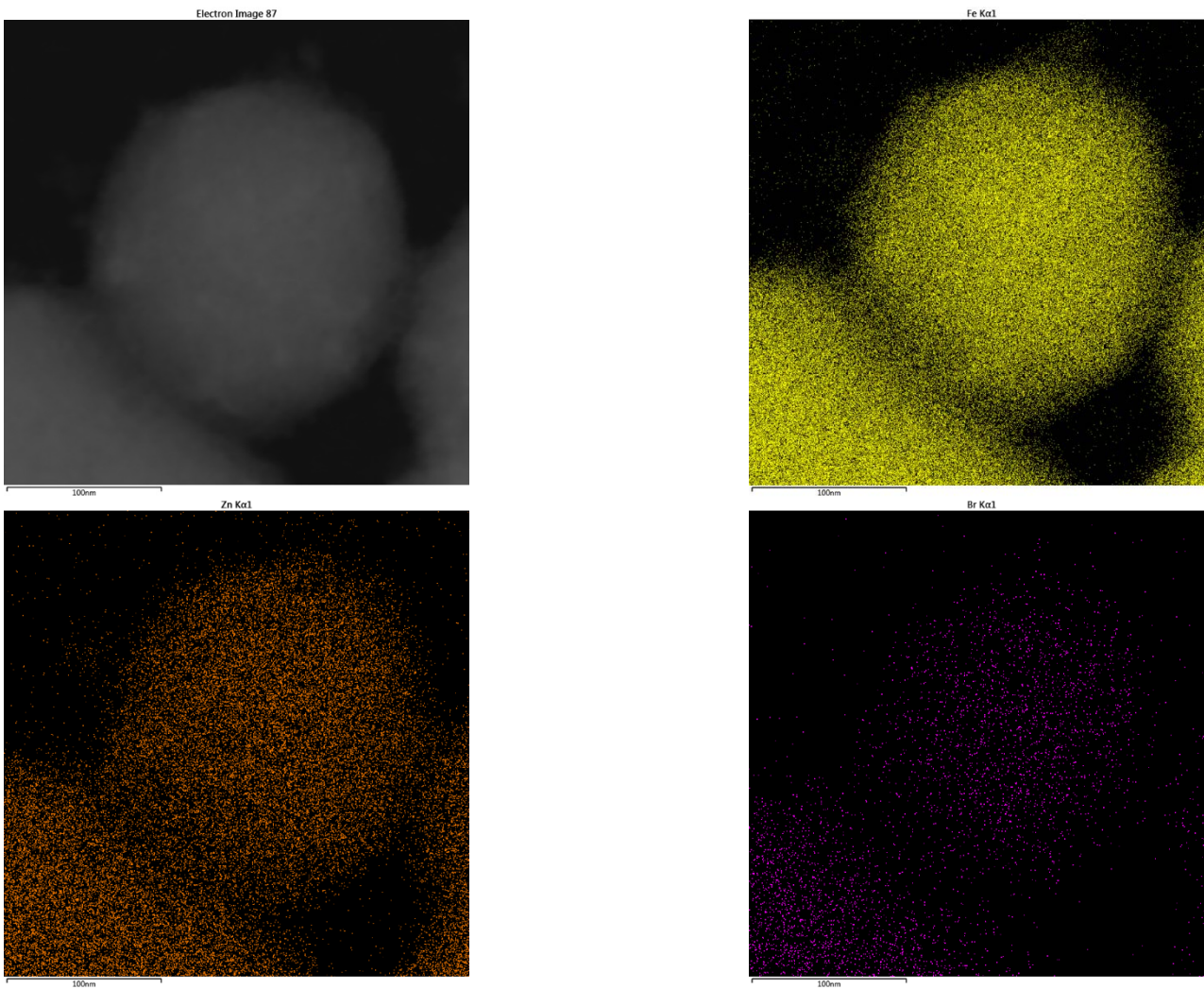




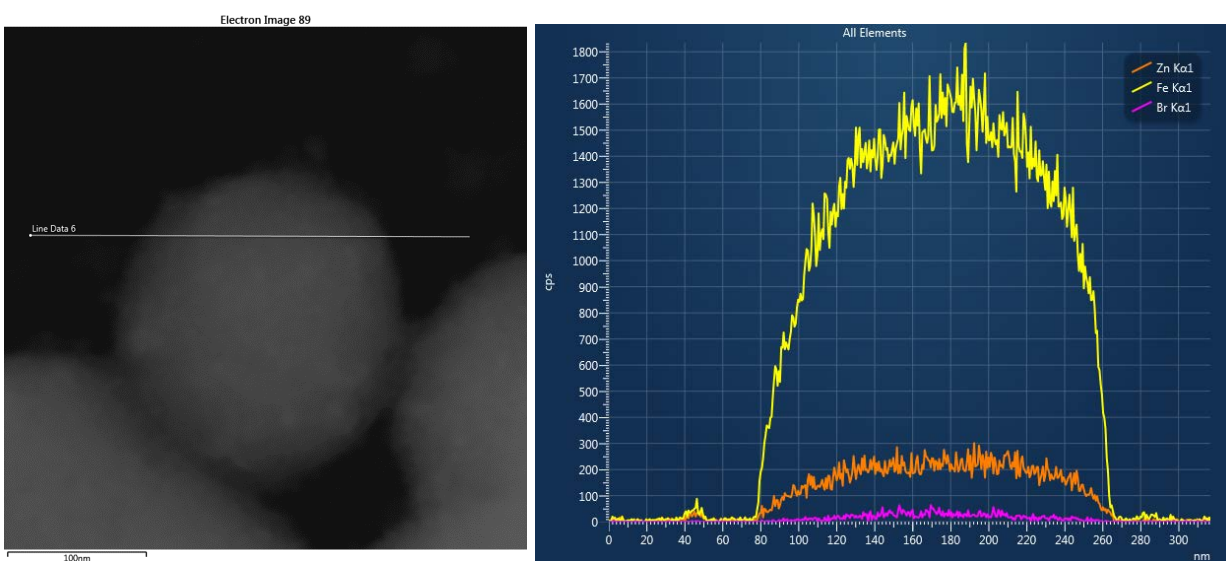
Supplementary Figure 180. TEM images of the iron nanoparticles isolated from the reaction between FeBr_2 and Mg-free **2a** after washing with deoxygenated deionised water.



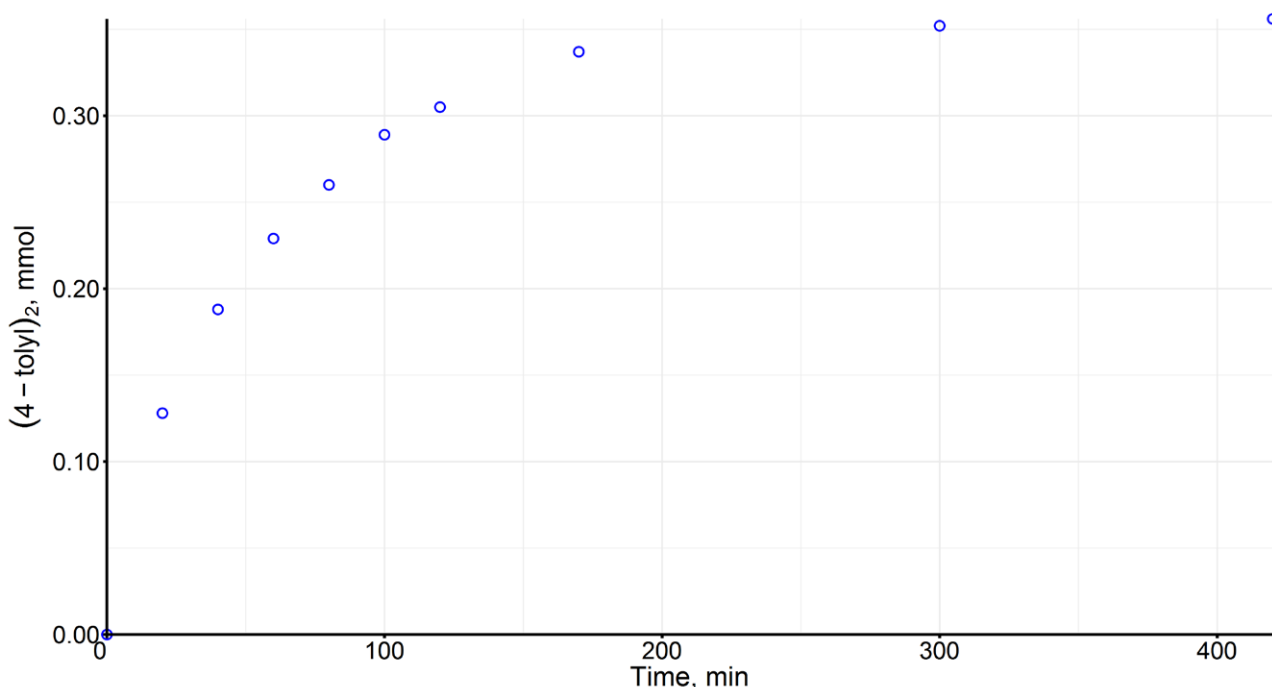
Supplementary Figure 181. EDX spectrum of iron nanoparticles isolated from the reaction between FeBr_2 and Mg-free after washing with deoxygenated and deionised water indicating presence of Fe, Zn and Br (Cu signal is due to specimen support grid).



Supplementary Figure 182. HAADF-STEM image of iron nanoparticles isolated from the reaction between FeBr_2 and Mg-free **2a** after washing with deoxygenated deionised water and corresponding elemental maps for Fe, Zn and Br.



Supplementary Figure 183. HAADF-STEM image and corresponding linescans for Fe, Zn and Br of iron nanoparticles isolated from the reaction between FeBr_2 and Mg-free **2a** after washing with deoxygenated deionised water.

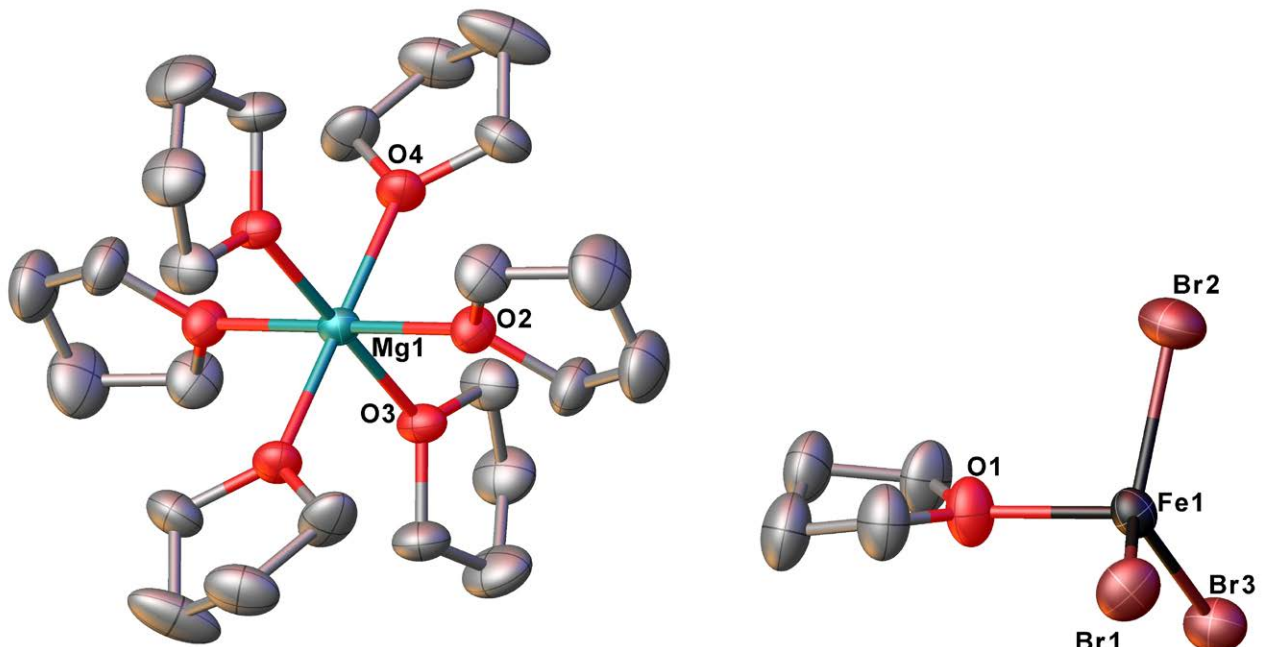


Supplementary Figure 184. Formation of **10** over the course of the reaction between FeBr_2 and Mg-free **2a**.

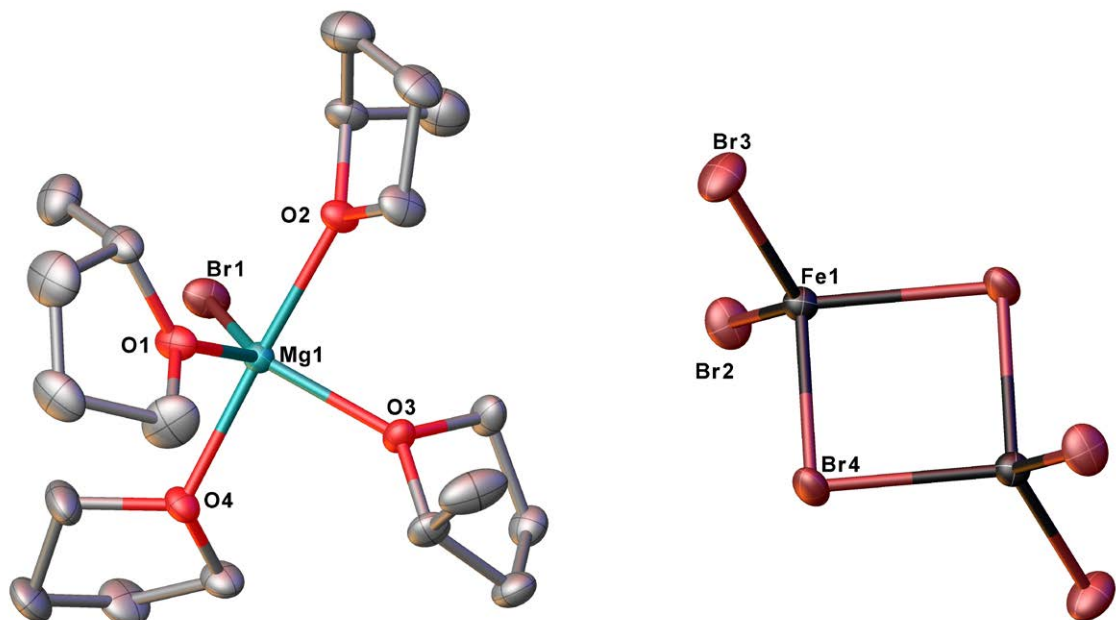
11.1.6 Reaction between $\text{FeBr}_2 + \text{Zn}(4\text{-tolyl})_2/2\text{MgBr}_2$ (**2a**) (Figure 7(a)(ii)).

A Schlenk was loaded with FeBr_2 (215.7 mg, 1 mmol), n-dodecane (internal standard, 68.1 μL , 0.3 mmol) and THF (5 mL). The mixture was heated at reflux temperature until the FeBr_2 dissolved. Once cool, $\text{Zn}(4\text{-tolyl})_2/2\text{MgBr}_2$ (**2a**) (5 mL, 200 mM, 1 mmol in Zn) was added at room temperature with vigorous stirring. This resulted in the instantaneous formation of an off-white precipitate which was separated from the solution *via* cannula filtration, washed with THF (2 x 3 mL) and dried under reduced pressure. The isolated white precipitate was extremely air-sensitive (changing colour to orange within seconds of exposure to air), partially soluble in THF and insoluble in CH_2Cl_2 , toluene, fluorobenzene and hexane. NMR characterisation of this precipitate in $\text{THF}-d_8$ showed only broad resonances due to THF. However, it was possible to grow crystals suitable for an X-ray crystallographic analysis by allowing a hot solution of the material to slowly cool to room temperature resulting in the formation of colourless crystals which were found to be $[\text{Mg}(\text{THF})_6][\text{FeBr}_3(\text{THF})]_2$ (**20**) (551.2 mg, 93 %) (Supplementary Figure 185). Anal. Calcd for $\text{C}_{32}\text{H}_{64}\text{Br}_6\text{Fe}_2\text{MgO}_8$: C, 32.24; H, 5.41 Found: C, 33.00; H, 5.38.

Complex $[\text{Mg}(\text{THF})_6][\text{FeBr}_3(\text{THF})]_2$ (**20**) could also be dissolved in 2-MeTHF. Layering a 2-MeTHF solution of **20** with hexane yielded colourless crystals of $[\text{MgBr}(2\text{-MeTHF})_3(\text{THF})]_2[\text{Fe}_2\text{Br}_6]$ (**21**) according to the X-ray crystallographic analysis (Supplementary Figure 186).

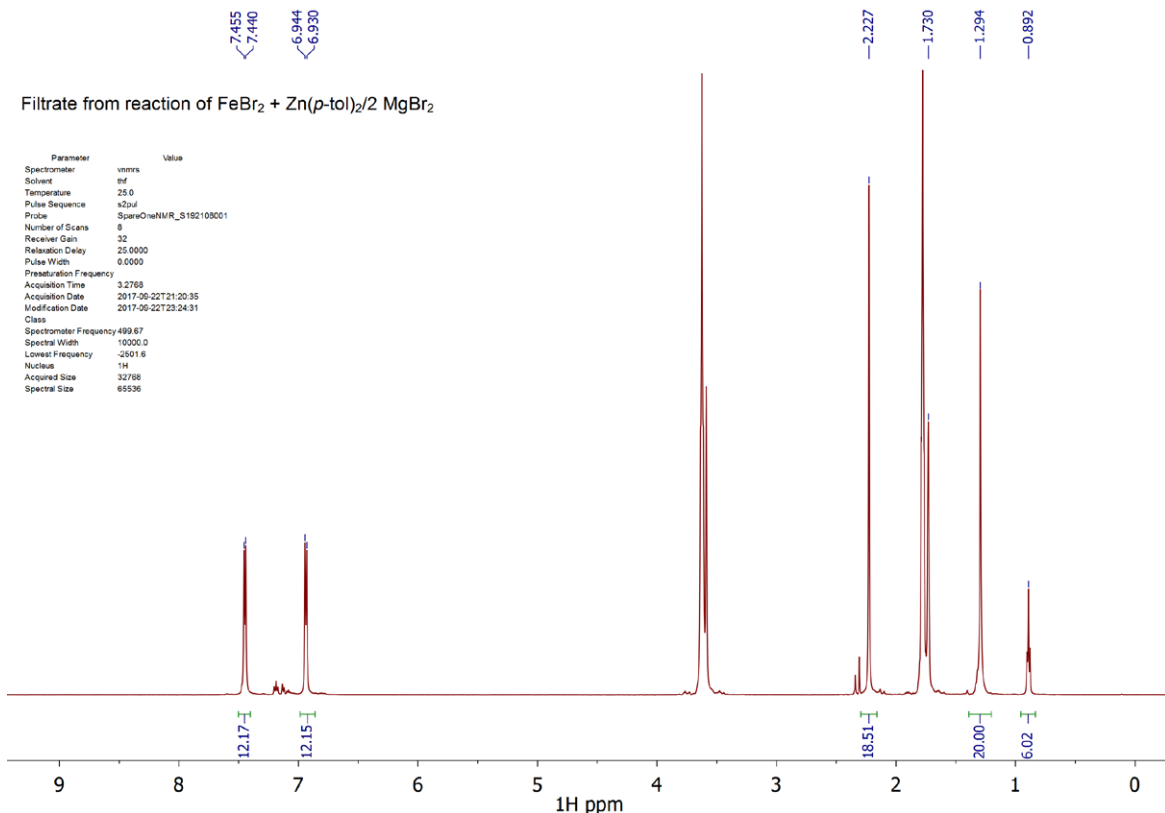


Supplementary Figure 185. Single-crystal X-ray structure of $[\text{Mg}(\text{THF})_6][\text{FeBr}_3(\text{THF})_2]$ (**20**). Hydrogen atoms and solvent molecules are omitted for clarity while thermal ellipsoids are set at the 50% probability level.



Supplementary Figure 186. Single-crystal X-ray structure of $[\text{MgBr}(2\text{-MeTHF})_3(\text{THF})_2][\text{Fe}_2\text{Br}_6]$ (**21**). Hydrogen atoms are omitted for clarity and thermal ellipsoids are set at the 50% probability level.

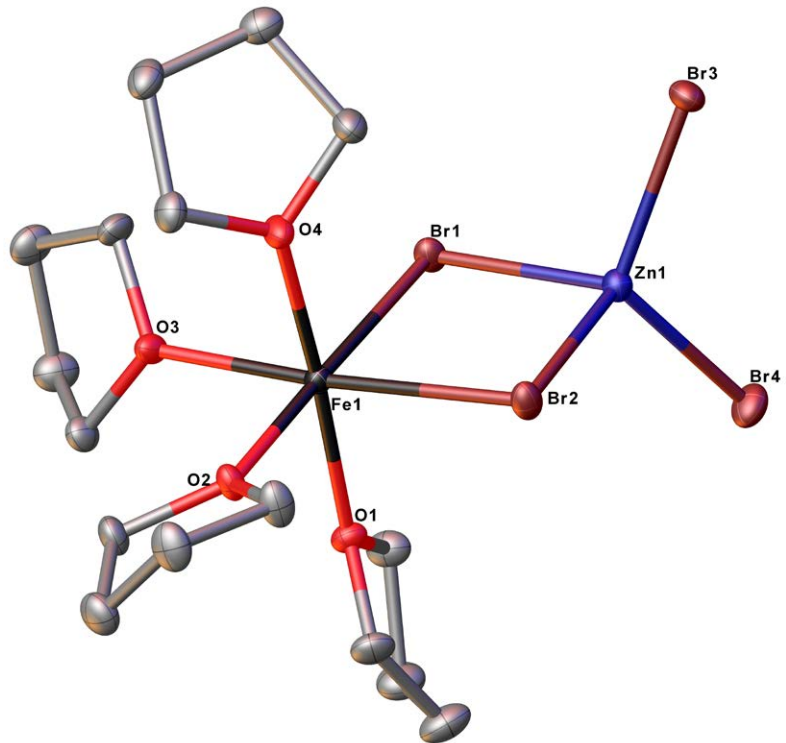
An aliquot (1 mL) of the filtrate obtained from the above synthesis of compound **20** was dried under reduced pressure to give a pale grey solid which was re-dissolved in $\text{THF}-d_8$ and analysed by ^1H and ^{13}C NMR spectroscopy. Both ^1H and ^{13}C NMR spectra revealed tolyl resonances due to residual **2a** (92%) (Supplementary Figure 187).



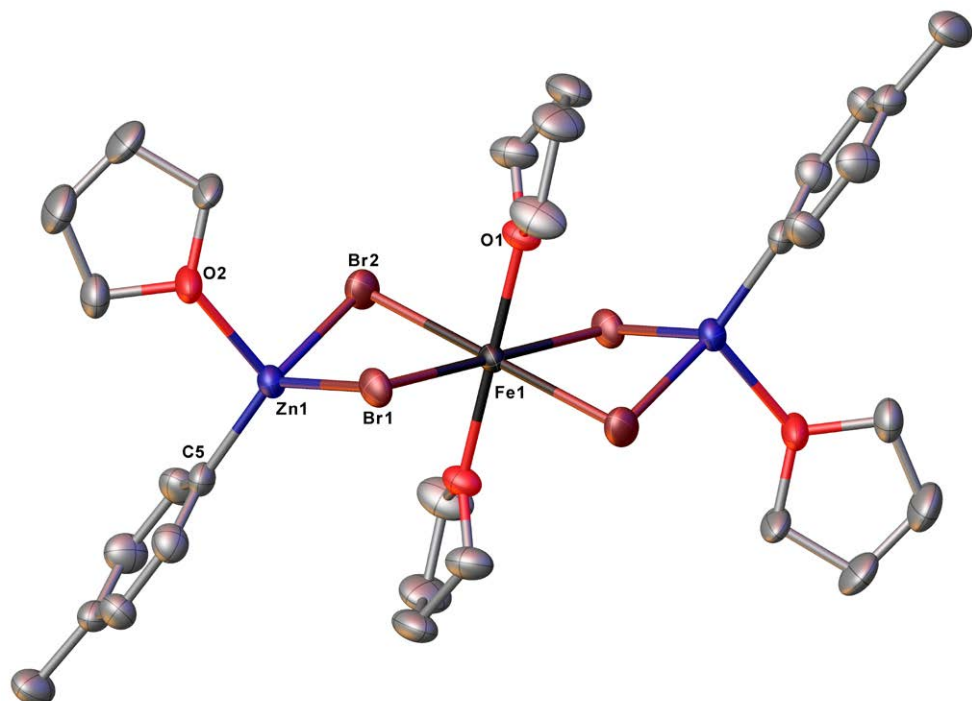
Supplementary Figure 187. ^1H NMR (500 MHz, THF- d_8) of the filtrate from the reaction between FeBr_2 and **2a** in THF in presence of *n*-dodecane as the internal standard.

The reaction was repeated a second time, except that the reaction mixture was heated at reflux temperature. A magnetic black powder of $\text{Fe}(0)$ formed instantly. The reaction was repeated a third time and the mixture was left to stand at room temperature. After two days of standing the mixture started turning darker with small amount of $\text{Fe}(0)$ formed. After a week a large amount of $\text{Fe}(0)$ was observed.

11.1.7 Reaction of FeBr_2 with magnesium-free $\text{Zn}(4\text{-tolyl})_2$ and ZnBr_2 (Figure 7(a)(iii)).
In an argon filled glove box, a vial was loaded with FeBr_2 (54.0 mg, 0.25 mmol), $\text{Zn}(4\text{-tolyl})_2$ (61.9 mg, 0.25 mmol), ZnBr_2 (56.3 mg, 0.25 mmol), *n*-dodecane (internal standard, 42.6 mg, 0.25 mmol) and THF (2 mL). The mixture was stirred until all of the FeBr_2 dissolved and then heated at reflux for 30 minutes to give a pale-yellow solution which was stirred for another 12 h at room temperature and then heated at reflux temperature for another 3 h. An aliquot of the solution was subjected to GC-FID analysis which revealed that no **10** had formed. The remaining solution was filtered and the filtrate layered with hexane (3 mL). After 18 hours two types of light yellow crystals suitable for an X-ray crystallographic analysis were obtained which corresponded to $[(\text{THF})_4\text{Fe}(\mu\text{-Br}_2)\text{ZnBr}_2]$ (**22**) and $[\text{Fe}(\text{THF})_2\{(\mu\text{-Br}_2)\text{Zn}(4\text{-tolyl})(\text{THF})\}_2]$ (**23**), Supplementary Figure 188 and Supplementary Figure 189.



Supplementary Figure 188. Single-crystal X-ray structure of $[(\text{THF})_4\text{Fe}(\mu\text{-Br}_2)\text{ZnBr}_2]$ (**22**). Hydrogen atoms are omitted for clarity while thermal ellipsoids are set at the 50% probability level.



Supplementary Figure 189. Single-crystal X-ray structure of $[\text{Fe}(\text{THF})_2\{(\mu\text{-Br})_2\text{Zn}(4\text{-tolyl})(\text{THF})\}_2]$ (**23**). Hydrogen atoms are omitted for clarity while thermal ellipsoids are set at the 50% probability level.

11.1.8 Effect of added dpbz on (4-tolyl)-Zn to Fe transmetallation

11.1.8.1 Determination of the amount of 4,4'-bitolyl (**10**) produced

In an argon filled glove box, three vials were loaded with FeBr_2 (54.0 mg, 0.25 mmol), $\text{Zn}(4\text{-tolyl})_2/2 \text{MgBr}_2$ (**2a**) (1.25 mL, 200 mM in THF, 0.25 mmol), *n*-dodecane (internal standard, 500 μL , 500 mM in THF, 0.25 mmol) and THF (1.00 mL). The three mixtures were stirred

for 3 minutes to give a white precipitate. Two equivalents of dpbz (223.2 mg, 0.50 mmol) per iron were added to the second vial while one equivalent of dpbz (111.6 mg, 0.25 mmol) was added to the third vial under stirring resulting in the instantaneous formation of dark red mixtures indicative of Fe(I) formation (see below). The reaction mixtures were left to react at approximately 21 °C and were sampled at 0.5 and 12 hours after the addition of dpbz. A final sample was also collected after the mixtures were heated at 66 °C for an additional 12 hours. The samples were quenched with HCl solution (0.5 M), extracted with CH₂Cl₂ and the extracts analysed by GC-FID in order to calculate the amount of 4,4'-bitolyl (**10**) present. The results are summarised in Supplementary Table 15.

Supplementary Table 15: Amount of **10** detected by GC-FID for the reactions between FeBr₂, **2a** and one or two equivalents of dpbz.

Time (h)	Vial 1: 0 eq. dpbz; amount (mmol) of 10	Vial 2: 2 eq. dpbz; amount (mmol) of 10	Vial 3: 1 eq. dpbz; amount (mmol) of 10
0.5	0.000	0.097	0.056
12	0.010	0.117	0.068
24 ^a	0.087	0.132	0.136

^aThe mixtures were heated at 66 °C for the last 12 hours of stirring.

11.1.8.2 Determination of the amount of Fe(I) produced

The production of Fe(I) in the reactions was determined as follows. Under an atmosphere of argon, a vial was loaded with FeBr₂ (53.7 mg, 0.25 mmol), **2a** (1.24 mL, 200 mM in THF, 0.249 mmol) and THF (1.26 mL). The mixture was stirred for 3 minutes to give a white precipitate and two equivalents of dpbz (222.4 mg, 0.48 mmol) was added with stirring resulting in the instantaneous formation of a dark red mixture indicative of Fe(I) formation. After 30 minutes stirring, 0.12 mL of the resultant solution was added to a 1.00 cm quartz glass cuvette fitted with a J. Youngs tap, along with THF (2.88 mL). The solution in the cuvette was diluted to half its original concentration (1.9 mM) and the UV-Vis spectrum recorded. The amount of [FeBr(dpzb)₂] (**9a**) was determined to be 0.25 mmol (quantitative).

The reaction was also repeated but adding the reagents in a different order: **2a**, two equivalents of dpbz and THF, stirred for 3 minutes before addition of FeBr₂, which again resulted in the instantaneous formation of a dark red mixture. After 30 minutes of stirring, 0.12 mL of the resultant solution was treated and analysed as above. The amount of [FeBr(dpzb)₂] (**9a**) was determined to be 0.26 mmol (quantitative).

11.1.8.3 Effect of added dpbz on the reaction of FeBr₂ with magnesium-free Zn(4-tolyl)₂ and ZnBr₂ (Figure 7(a)(iii)).

11.1.8.3.1 One equivalent of dpbz

In an argon filled glove box a vial was loaded with FeBr₂ (54.0 mg, 0.25 mmol) dissolved in THF (1 mL) followed by addition of Mg-free **2a** (61.9 mg, 0.25 mmol) and ZnBr₂ (56.3 mg, 0.25 mmol) both dissolved in THF (1 mL) to give a pale yellow solution which was briefly heated at reflux temperature. Dpbz (111.6 mg, 0.25 mmol) was added and the mixture was stirred for 24 hours to form an orangish-red solution which was filtered to remove trace amounts of insoluble material. The filtrate was layered with hexane (4 mL) and after 18 hours pale orange crystals formed. A representative crystal was found to have the same unit cell as [FeBr₂(dpbz)] (**4a**). The crystals were then separated by decanting the supernatant and the resultant solution was layered with hexane which after 18 h gave a second crop of crystals one of which was found to be [(THF)₄Fe(μ -Br)₂ZnBr₂] (**22**) according to an X-ray crystallographic study.

11.1.8.3.2 Two equivalents of dpbz

In an argon filled glove box a vial was loaded with FeBr₂ (54.0 mg, 0.25 mmol) and THF (1 mL) and was heated at reflux until FeBr₂ dissolved. A second vial was loaded with Mg-free **2a** (61.9 mg, 0.25 mmol), ZnBr₂ (56.3 mg, 0.25 mmol), *n*-dodecane (42.6 mg, 0.25 mmol) and THF (1 mL) and stirred until a colourless solution was obtained which was subsequently added to the FeBr₂ solution at room temperature. The resultant mixture was stirred and heated at reflux temperature for 30 minutes to give a pale yellow solution. Subsequent addition of dpbz (223.2 mg, 0.50 mmol) resulted in a colour change from pale yellow to orangish-red and the mixture was heated at reflux temperature for 30 minutes. The resulting solution was filtered and a sample of the filtrate was analysed by GC-FID which indicated the presence of **10** (0.004 mmol). After 24 hours a white solid formed in the remaining filtrate which was isolated by filtration, dissolved in THF and layered with hexane to give pale orangish-yellow crystals. The unit cells of three representative crystals were determined by an X-ray crystallographic analysis and were found to be the same as that for [FeBr₂(dpbz)] (**4a**).

The reaction was repeated as described above but this time the final pale-yellow solution was heated at reflux temperature for 30 minutes, filtered and left to stand for 4 days, after which time an off-white precipitate and a red solution was obtained. The supernatant was isolated by filtration and layered with hexane. After 18 hours, a mixture of pale orange, colourless and dark red crystals formed. The unit cells of a representative example of each one of the crystal types was crystallographically determined and matched with the unit cells of [FeBr₂(dpbz)] (**4a**), [ZnBr(4-tolyl)(dpbz)] (**15a**) and [FeBr(dpzb)₂] (**9a**) respectively.

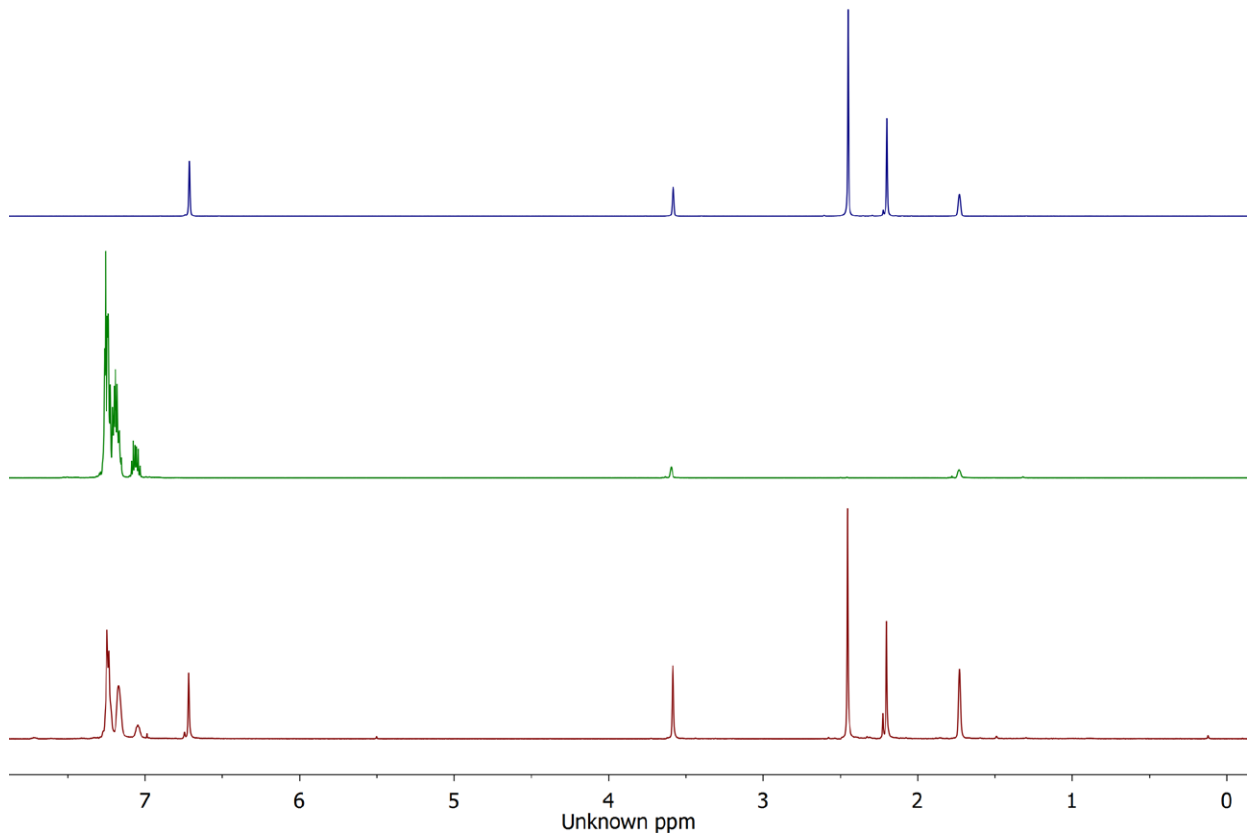
11.1.9 Reaction of *in situ*-formed [FeBr₂(dpbz)₂] with magnesium-free Zn(4-tolyl)₂

In an argon filled glove box, a vial was loaded with FeBr₂ (54.0 mg, 0.25 mmol), dpbz (223.2 mg, 0.5 mmol), *n*-dodecane (internal standard, 500 µL, 500 mM in THF, 0.25 mmol) and THF (2 mL) and the mixture was heated at reflux temperature until the FeBr₂ dissolved. After cooling, Mg-free **2a** (61.9 mg, 0.25 mmol) was added and the mixture was stirred for 0.5 hours to give a dark red solution which upon standing for 24 hours at room temperature gave dark red crystals isolated by filtration. A crystallographic study of one of the red crystals revealed it to be [FeBr(dp₂bz)₂] (**9a**).¹⁹ The filtrate was heated at 60 °C for 3 hours and then an aliquot was analysed by CG-FID. This indicated the presence of **10** (0.085 mmol). Meanwhile the rest of the filtrate was layered with hexane. After 48 hours dark red and pale-yellow crystals were obtained. Both types of crystals were subject to a crystallographic study and found to be [FeBr(dp₂bz)₂] (**9a**) and [FeBr₂(dpbz)] (**4a**) respectively.

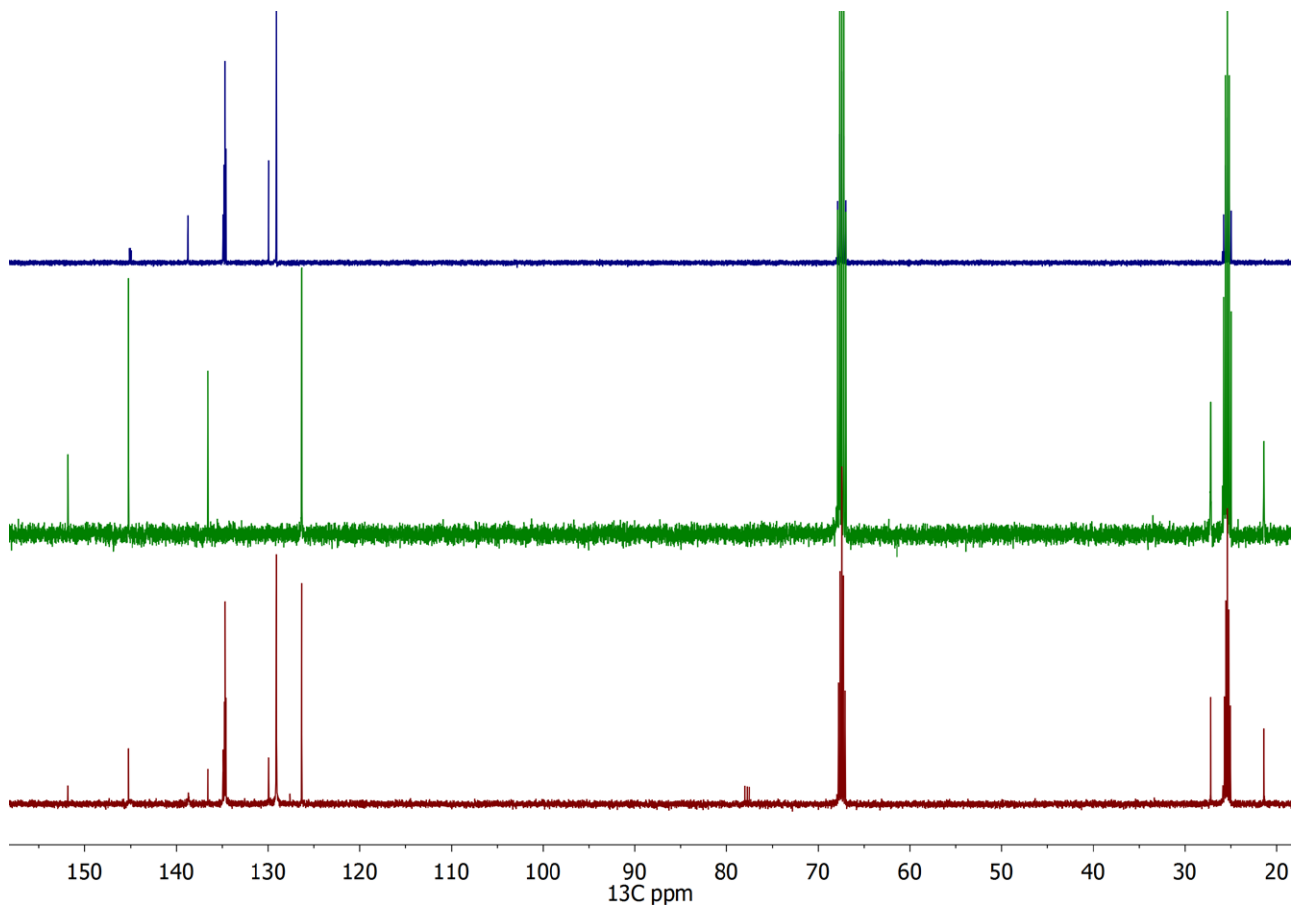
11.2 Transmetallation studies with Zn(mes)₂

11.2.1 Reaction of Zn(mes)₂ (Mg free **2b) with dpbz**

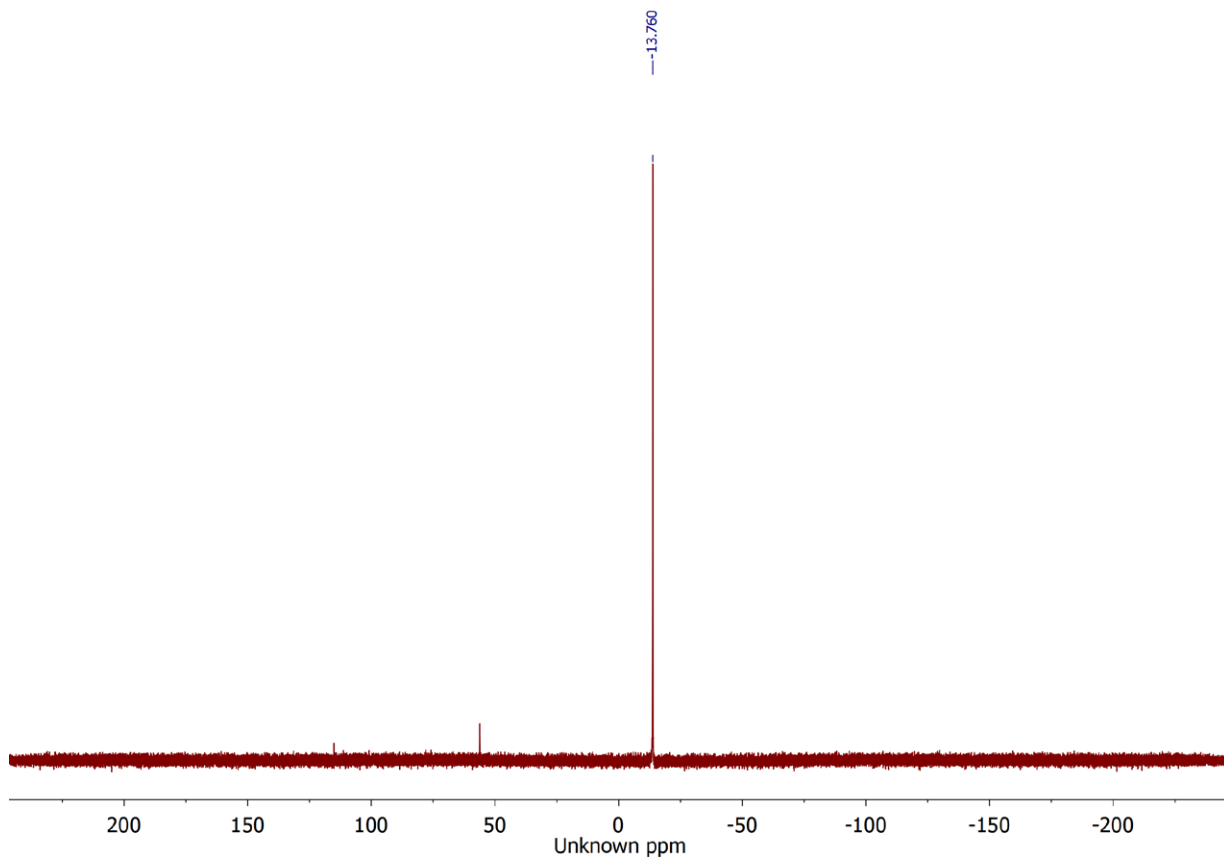
Under an atmosphere of argon, a 7 mL screwtop vial was charged with ZnMes₂ (Mg-free **2b**) (15.0 mg, 0.049 mmol), dpbz (22.0 mg, 0.049 mmol) and THF-*d*₈ (1.00 mL). The resulting mixture was heated inside the glovebox at 70 °C for 5 hours to give a clear, colourless solution. An aliquote of that solution was added to a J. Youngs tap NMR tube and subject to an NMR spectroscopic investigation. The ¹H and ¹³C NMR spectra collected (below) display peaks corresponding to free dpbz and Zn(mes)₂, while the ³¹P NMR spectrum displays a single resonance corresponding to free dpbz implying that no reaction occurred.



Supplementary Figure 190. Stacked ^1H NMR spectra (400 MHz, $\text{THF}-d_8$) of solutions of a $\text{Zn}(\text{mes})_2 + \text{dpbz}$ mixture (red, bottom), pure $\text{Zn}(\text{mes})_2$ (blue, top) and pure dpbz (green).



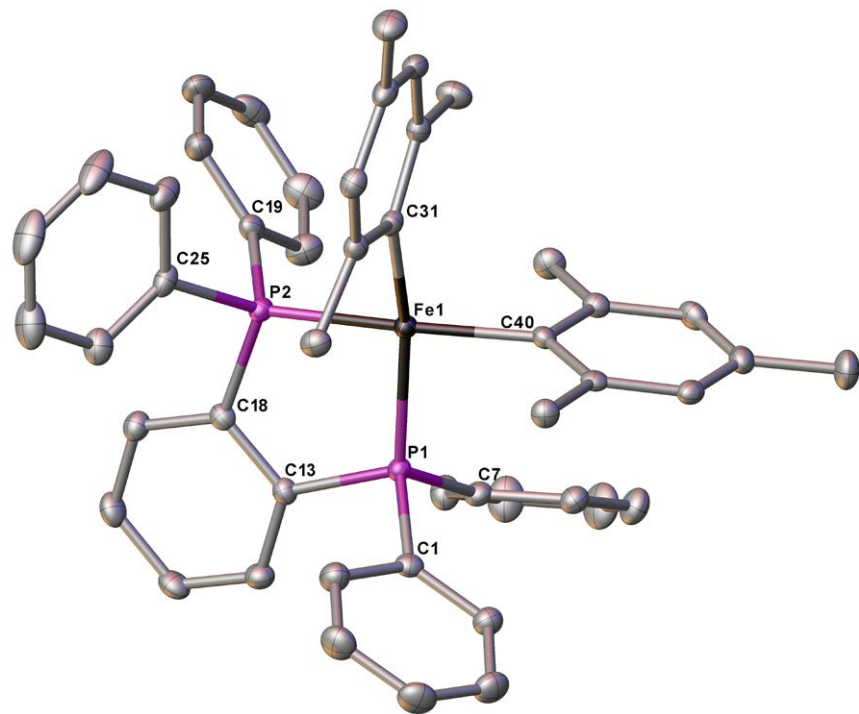
Supplementary Figure 191. Stacked ^{13}C NMR spectra (100 MHz, $\text{THF}-d_8$) of solutions of a $\text{Zn}(\text{mes})_2 + \text{dpbz}$ mixture (green), pure $\text{Zn}(\text{mes})_2$ (red) and pure dpbz (blue).



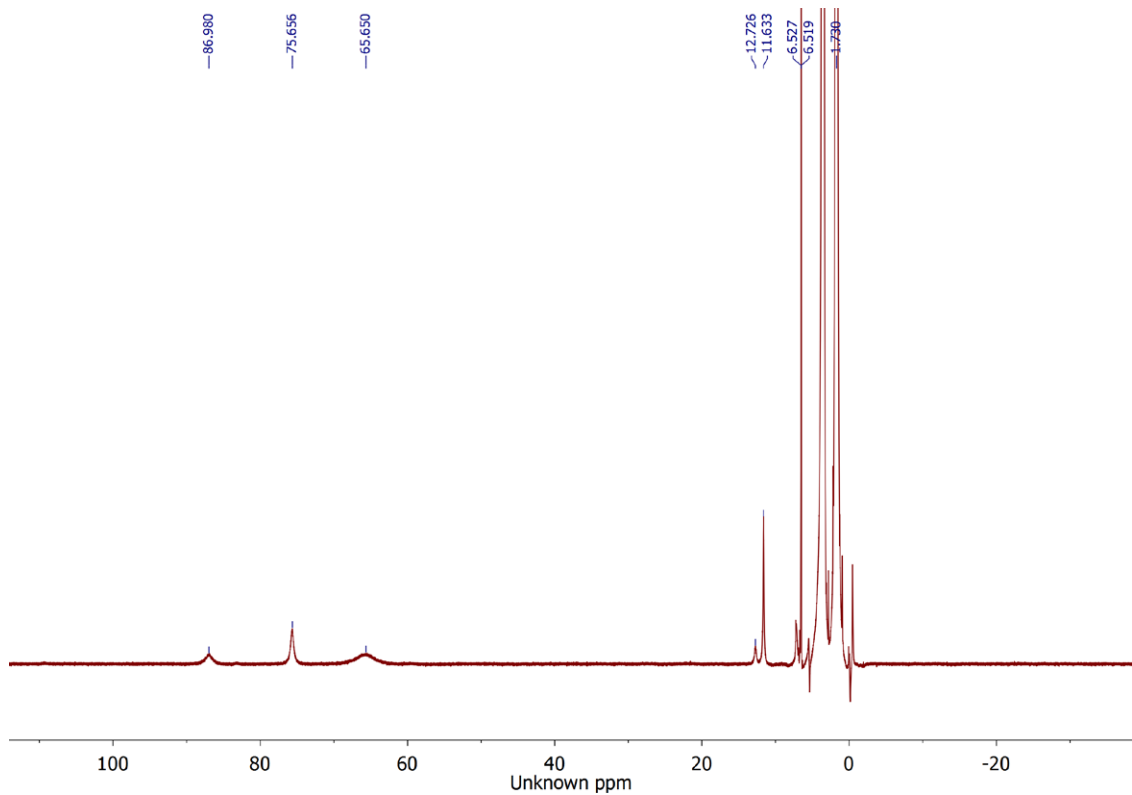
Supplementary Figure 192. ^{31}P NMR spectrum (202 MHz, THF- d_8) of a $\text{Zn}(\text{mes})_2 + \text{dpbz}$ solution.

11.2.2 Synthesis of $[\text{Fe}(\text{mes})_2(\text{dpbz})]$ (24) (Figure 7(b)(i))

In an argon filled glovebox, a vial was loaded with $[\{\text{Fe}(\text{mes})_2\}_2]$ (5.0 mg, 8.49 μmol), dpbz (7.58 mg, 17.0 μmol) and THF (2 mL). The resulting dark red solution was filtered through a Millipore filter and layered with hexane (5 mL) resulting in dark red crystals of the title compound (4.7 mg, 37%) which were suitable for an X-ray crystallographic study. ^1H NMR (500 MHz) δ 86.9 (s), 75.7 (s), 65.7 (s), 12.7 (s), 11.6 (s).



Supplementary Figure 193. Single-crystal X-ray structure of $[\text{Fe}(\text{mes})_2(\text{dpbz})]$ (**24**). Hydrogen atoms and solvent molecules are omitted for clarity. Thermal ellipsoids are set at the 50% probability level.

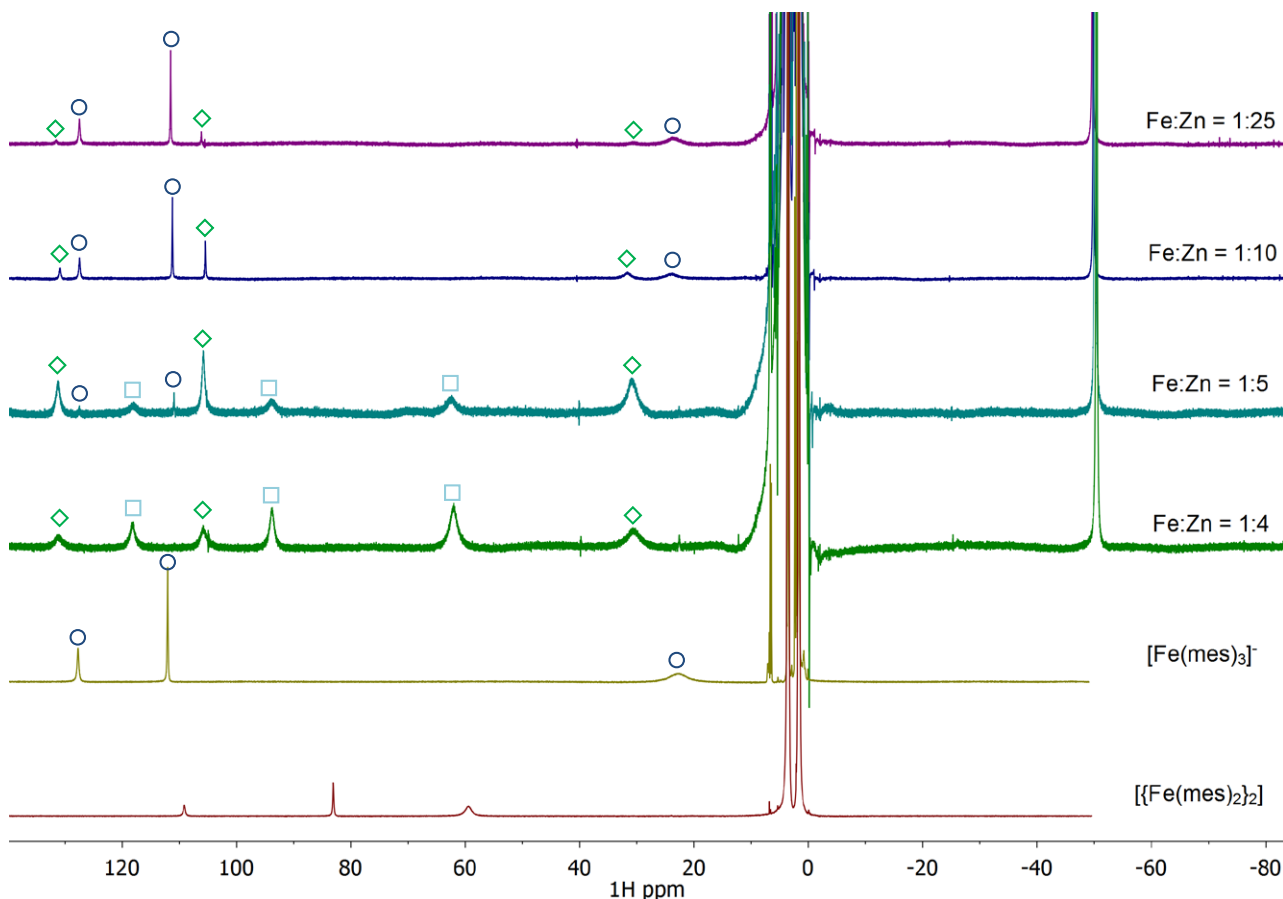


Supplementary Figure 194. ^1H NMR spectrum (500 MHz, THF) of $[\text{Fe}(\text{mes})_2(\text{dpbz})]$ (**24**).

11.2.3 Reaction of FeBr_2 with increasing amounts of $\text{Zn}(\text{mes})_2/2 \text{MgBr}_2$ (**2b**) (Figure 7(b)(ii))

In an argon filled glovebox, seven solutions of FeBr_2 and **2b** in THF were prepared at concentrations of: 15 mM/15 mM, 15 mM/30 mM, 15 mM/45 mM, 15 mM/60 mM, 14 mM/70 mM, 7.0 mM/70 mM and 2.8 mM/68.8 mM. In the first three cases (1:1, 1:2 and 1:3 ratios)

a fine white precipitate was formed, in the remaining four a solution was obtained. Subsequently, 800 μ L of each solution was added to a J. Youngs NMR tube. A sealed capillary containing a CDCl_3 solution of CoCp_2 (200 mM, 100 μ L, 20 μ mol) was added as an internal standard and reference and the ^1H NMR spectra recorded (Supplementary Figure 195). Upon addition of 4 equivalents of **2b** the $[\{\text{Fe}(\text{mes})_2\}_2]$ starting material is completely consumed producing a mixture of compounds assigned as $[\text{FeBr}(\text{mes})_2]^-$ (**26**, ◇) and $[\text{FeBr}_2(\text{mes})]^-$ (**25**, □) (also see next section for assignment of **26**). Further addition of one more equivalent of **2b** ($\text{Fe:Zn} = 1:5$) led to increased formation of $[\text{FeBr}(\text{mes})_2]^-$ (**26**, ◇) and a trace amount of $[\text{Fe}(\text{mes})_3]^-$ (**27**, ○). As expected at $\text{Fe:Zn} = 1:10$, only $[\text{Fe}(\text{mes})_3]^-$ (**27**, ○) and $[\text{FeBr}(\text{mes})_2]^-$ (**26**, ◇) are observed while at $\text{Fe:Zn} = 1:25$ the major species is $[\text{Fe}(\text{mes})_3]^-$ (**27**, ○) with a minor amount of $[\text{FeBr}(\text{mes})_2]^-$ (**26**, ◇) being also present.

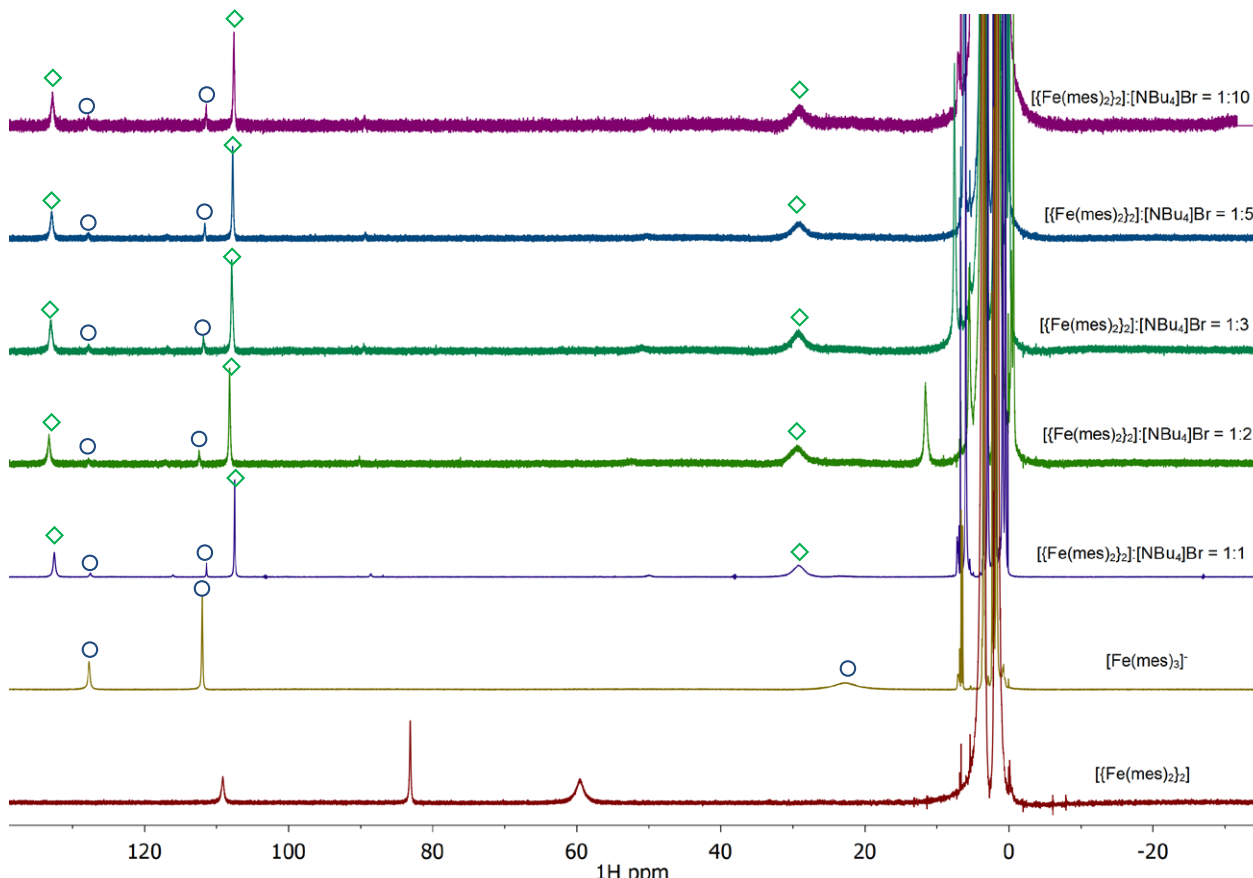


Supplementary Figure 195. Stacked ^1H NMR spectra (500 MHz, THF) of isolated $[\{\text{Fe}(\text{mes})_2\}_2]$ and $[\text{Fe}(\text{mes})_3]^-$ (○) as well as mixtures of FeBr_2 and **2b** at various molar Fe:Zn ratios. A capillary tube with a CDCl_3 solution of CoCp_2 was also used ($\delta = -49.3$ ppm) during data acquisition for reference and standardisation. Compound key: ○ = $[\text{Fe}(\text{mes})_3]^-$ (**27**), ◇ = $[\text{FeBr}(\text{mes})_2]^-$ (**26**), □ = $[\text{FeBr}_2(\text{mes})]^-$ (**25**).

11.2.4 Reaction of $[\{\text{Fe}(\text{mes})_2\}_2]$ with $[\text{NBu}_4]\text{Br}$

In an argon filled glovebox, a series of solutions were prepared in five vials by adding a solution of $[\{\text{Fe}(\text{mes})_2\}_2]$ (100 μ L, 85 mM stock solution, 8.5 μ mol) and THF (900 μ L). Subsequently, the following amounts of $[\text{NBu}_4]\text{Br}$ were added to the iron-containing vials respectively: (5.5 mg, 16.98 μ mol), (10.9 mg, 33.96 μ mol), (21.9 mg, 67.92 μ mol), (27.4 mg,

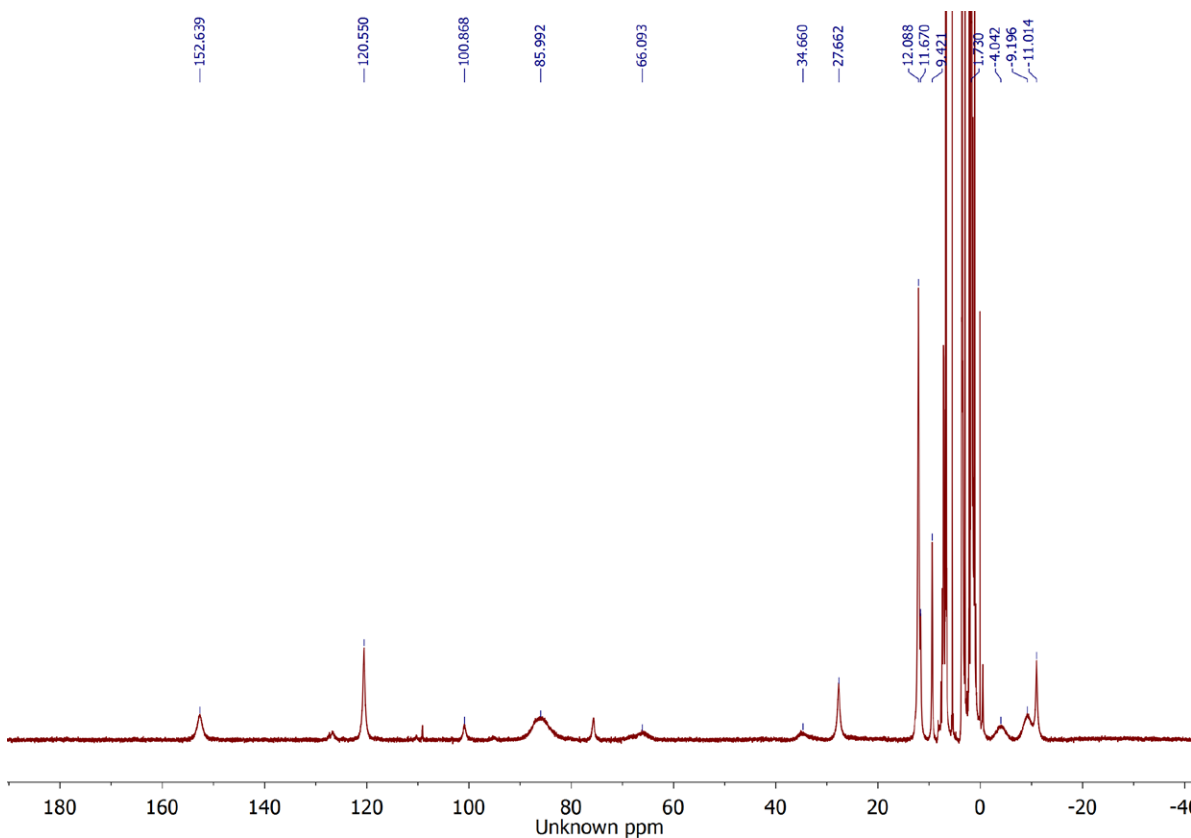
84.9 µmol) and (54.7 mg, 169.8 µmol) to give five solutions at $\{[\text{Fe}(\text{mes})_2]_2\}$: $[\text{NBu}_4]\text{Br}$ molar ratios of 1:1, 1:2, 1:3, 1:5 and 1:10 respectively. Each solution was passed through a Millipore filter directly into a J. Youngs NMR tube and the ^1H NMR spectra recorded (Supplementary Figure 196). In all cases a colour change from deep red to pale yellow was observed.



Supplementary Figure 196. Stacked ^1H NMR (500 MHz, THF) spectra of isolated $\{[\text{Fe}(\text{mes})_2]_2\}$ and $[\text{Fe}(\text{mes})_3]^-$ as well as mixtures of $\{[\text{Fe}(\text{mes})_2]_2\}/[\text{NBu}_4]\text{Br}$ at various molar ratios. Compound key: $\circ = [\text{Fe}(\text{mes})_3]^-$ (**27**), $\diamond = [\text{FeBr}(\text{mes})_2]^-$ (**26**).

11.2.5 Synthesis of $[\text{FeBr}(\text{mes})(\text{dpbz})]$ (**28**)

In an argon filled glovebox, a vial was loaded with $[\text{FeBr}_2(\text{dpbz})]$ (**4a**) (5.0 mg, 7.6 µmol), THF (2 mL) and 2-mesitylmagnesium bromide (0.97 M, 7.8 µL, 7.6 µmol). The resulting orange solution was filtered through a Millipore filter and layered with hexane (5 mL) resulting in formation of yellow crystals of the title compounds (2.3 mg, 43%). ^1H NMR (500 MHz) δ 120.6 (s), 100.9 (s), 86.0 (s), 66.1 (s), 34.7 (s), 27.7 (s), 12.1 (s), 11.7 (s), 9.4 (s), -4.0 (s), -9.2 (s), -11.0 (s).

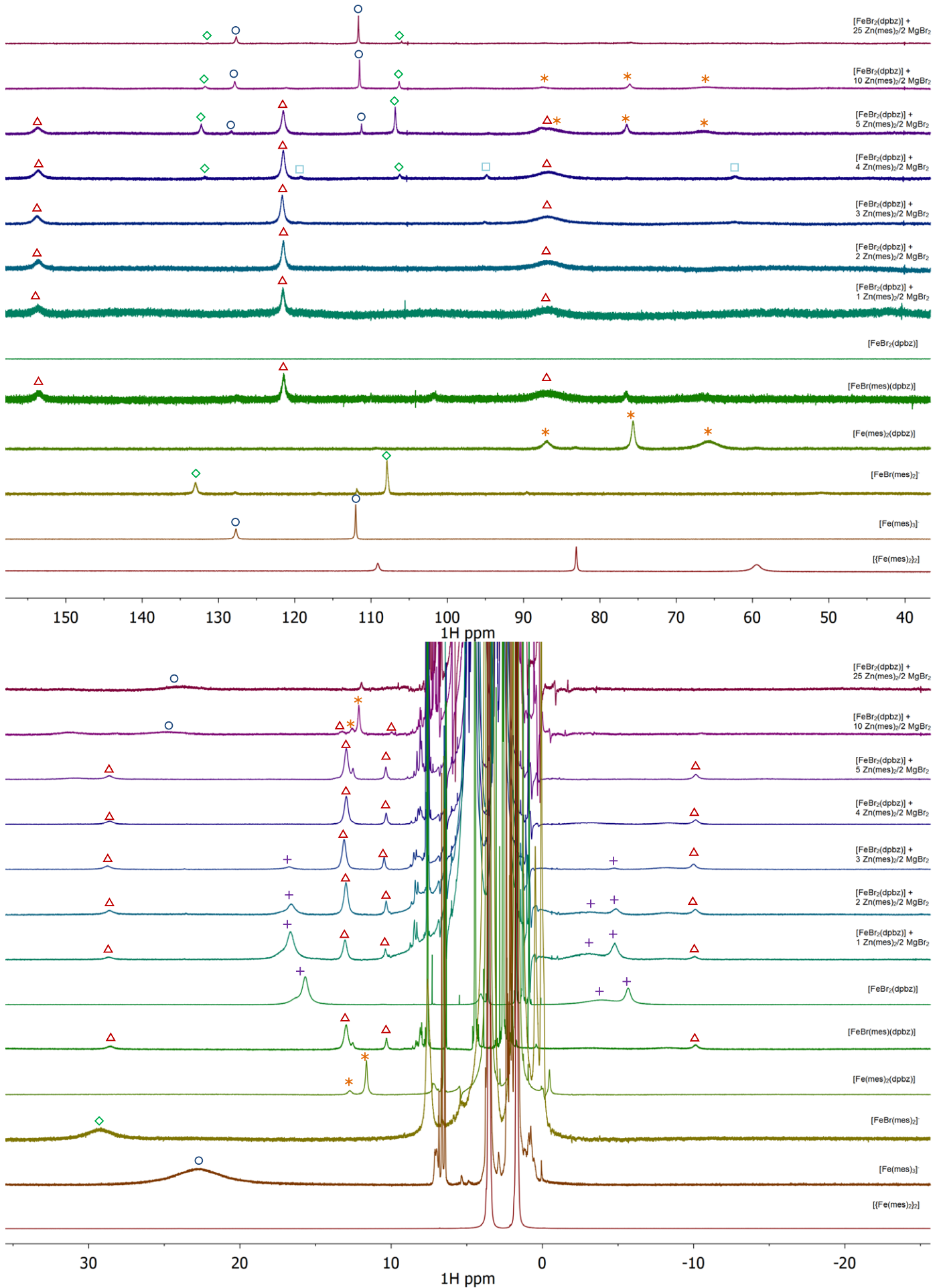


Supplementary Figure 197. ^1H NMR spectrum (500 MHz, THF) of $[\text{FeBr}(\text{mes})(\text{dpbz})]$ (**28**).

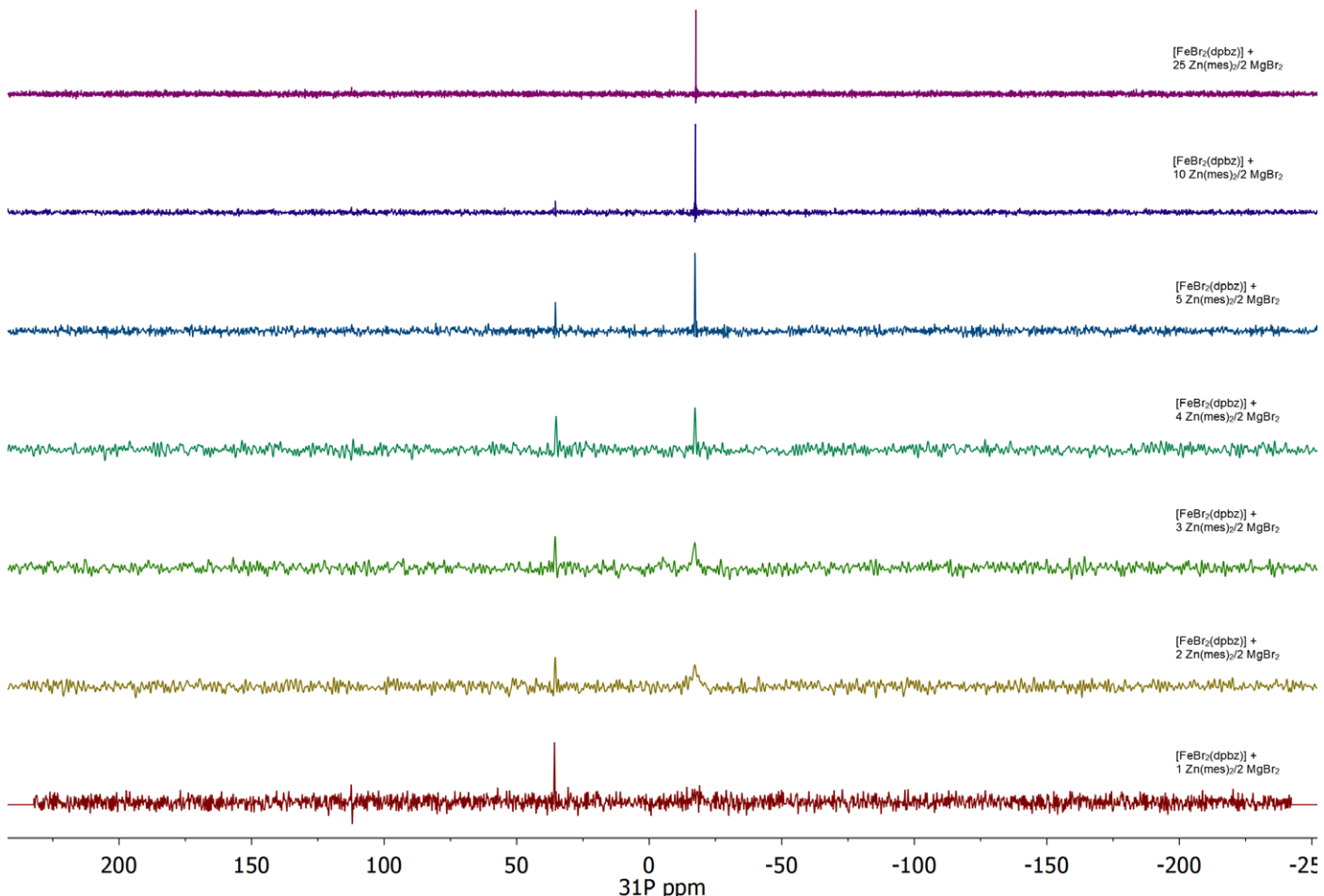
11.2.6 Reaction of $[\text{FeBr}_2(\text{dpbz})]$ (**4a**) with increasing amounts of $\text{Zn}(\text{mes})_2/2 \text{MgBr}_2$ (**2b**) (Figure 7(b)(iii))

In an argon filled glovebox, seven solutions of $[\text{FeBr}_2(\text{dpbz})]$ (**4a**) and **2b** in THF were prepared at concentrations of: 15 mM/15 mM, 15 mM/30 mM, 15 mM/45 mM, 15 mM/60 mM, 14 mM/70 mM, 7.0 mM/70 mM and 2.8 mM/68.8 mM. In all cases a solution was obtained. Subsequently, 800 μL of each solution was added to a J. Youngs NMR tube. A sealed capillary containing a CDCl_3 solution of CoCp_2 (200 mM, 100 μL , 20 μmol) was added for reference and standardisation and the ^1H and ^{31}P NMR spectra recorded (Supplementary Figure 198 and Supplementary Figure 199). Reaction of one equivalent of **2b** with $\text{FeBr}_2(\text{dpbz})$ (**4a**) leads to a mixture of $[\text{FeBr}_2(\text{dpbz})]$ (**4a**, $\textcolor{blue}{+}$), and $[\text{FeBr}(\text{mes})(\text{dpbz})]$ (**28**, $\textcolor{red}{\Delta}$). Addition of a second and third equivalent of **2b** increases the amount of $[\text{FeBr}(\text{mes})(\text{dpbz})]$ (**28**, $\textcolor{red}{\Delta}$) in solution while simultaneously decreasing the concentration in $[\text{FeBr}_2(\text{dpbz})]$ (**4a**, $\textcolor{blue}{+}$). At four equivalents of **2b** the predominant species is $[\text{FeBr}(\text{mes})(\text{dpbz})]$ (**28**, $\textcolor{red}{\Delta}$) with small amounts of $[\text{FeBr}(\text{mes})_2]$ (**26**, $\textcolor{green}{\diamond}$) and $[\text{FeBr}_2(\text{mes})]$ (**25**, $\textcolor{lightblue}{\square}$) becoming apparent. At **4a** : **2b** ratios of 1:5 the two major species observed are $[\text{FeBr}(\text{mes})_2]$ (**26**, $\textcolor{green}{\diamond}$) and $[\text{FeBr}(\text{mes})(\text{dpbz})]$ (**28**, $\textcolor{red}{\Delta}$) with minor amounts of $[\text{Fe}(\text{mes})_3]$ (**27**, $\textcolor{blue}{\circ}$) and $[\text{Fe}(\text{mes})_2(\text{dpbz})]$ (**24**, $\textcolor{orange}{*}$) being present. At 10 equivalents of **2b**, the major species present is $[\text{Fe}(\text{mes})_3]$ (**27**, $\textcolor{blue}{\circ}$) while $[\text{Fe}(\text{mes})_2(\text{dpbz})]$ (**24**, $\textcolor{orange}{*}$) and $[\text{FeBr}(\text{mes})_2]$ (**26**, $\textcolor{green}{\diamond}$) are minor. Lastly, when 25 of **2b** is added to $[\text{FeBr}_2(\text{dpbz})]$ (**4a**), $[\text{Fe}(\text{mes})_3]$ (**27**, $\textcolor{blue}{\circ}$) is the dominating species in solution with a trace of $[\text{FeBr}(\text{mes})_2]$ (**26**, $\textcolor{green}{\diamond}$) being present as well.

In the ^{31}P NMR spectra of the title reaction a resonance of increasing intensity with the amount of **2b** added is observed at -17.3 ppm which is tentatively assigned as $[\text{ZnBr}(\text{mes})(\text{dpbz})]$ (**15b**), judging by its chemical shift similar to that of $[\text{ZnBr}(4\text{-tolyl})(\text{dpbz})]$ (**15a**). In contrast, the species at 35.4 ppm resonates at a frequency too high to be attributed to a simple Zn(II) – phosphine species. It is very tentatively suggested that this may be due to the formation of a (dpbz)Zn-Br-Fe adduct reminiscent of the Zn – Fe adducts observed in section 11.1.7.



Supplementary Figure 198. ^1H NMR (500 MHz, THF) spectra (high chemical shifts on top stack) of: $\{[\text{Fe}(\text{mes})_2]_2\}$, $[\text{Fe}(\text{mes})_3]$, $\{[\text{Fe}(\text{mes})_2]_2 + [\text{NBu}_4]\text{Br}\}$, $[\text{Fe}(\text{mes})_2(\text{dpBz})]$ (**24**), $[\text{FeBr}(\text{mes})(\text{dpBz})]$ (**28**), $[\text{FeBr}_2(\text{dpBz})]$ (**4a**), and a series of $[\text{FeBr}_2(\text{dpBz})]$ (**4a**)/ n **2b** mixtures at molar ratios between 1:1 and 1:25. Compound key: \circ = $[\text{Fe}(\text{mes})_3]^-$ (**27**), \diamond = $[\text{FeBr}(\text{mes})_2]^-$ (**26**), \square = $[\text{FeBr}_2(\text{mes})]^-$ (**25**), $+$ = $[\text{FeBr}_2(\text{dpBz})]$ (**4a**), \triangle = $[\text{FeBr}(\text{mes})(\text{dpBz})]$ (**28**), $*$ = $[\text{Fe}(\text{mes})_2(\text{dpBz})]$ (**24**).



Supplementary Figure 199. ^{31}P NMR spectra (202 MHz, THF) of a series of $[\text{FeBr}_2(\text{dpbz})]$ (**4a**) and **2b** mixtures at molar Fe:Zn ratios between 1:1 and 1:25 with resonances observed at 35.4 ppm and -17.3 ppm.

11.2.7 Negishi cross coupling between BnBr (**1**) and $\text{Zn}(\text{mes})_2/2 \text{MgBr}_2$ (**2b**) catalysed by FeBr_2 and dpbz

The reaction was performed in line with the general procedure outlined in section 2.2 using **2b** in place of **2a**. An oven dried jacketed Schlenk was loaded with THF (3.10 mL), dodecane (1.00 mL, 500 mM stock solution in THF, 0.50 mmol), BnBr (0.40 mL, 2500 mM stock solution in THF, 1.00 mmol), $\text{Zn}(\text{mes})_2/2 \text{MgBr}_2$ (5.00 mL, 200 mM stock solution in THF, 1.00 mmol) and dpbz (0.250 mL, 80.0 mM stock solution in THF, 0.020 mmol) and the temperature set at 7.00 °C using a cryostat. Subsequently, FeBr_2 (0.25 mL, 40.0 mM stock solution in THF, 0.010 mmol) was added and the mixture left to react for one hour. An aliquote of the reaction was then collected, quenched with $\text{HCl}_{(\text{aq})}$ and extracted with CH_2Cl_2 . A GC-MS analysis of the collected sample indicated presence of starting materials and mesitylene from the hydrolysis of **2b**. The reactions temperature was then raised to 50.00 °C and left to react for 17 hours. An aliquote of the reaction was again analysed by GC-MS revealing presence of starting materials only.

12 Kinetic investigations on the Negishi coupling of 1 with 2a using *in situ* FT-IR spectroscopy

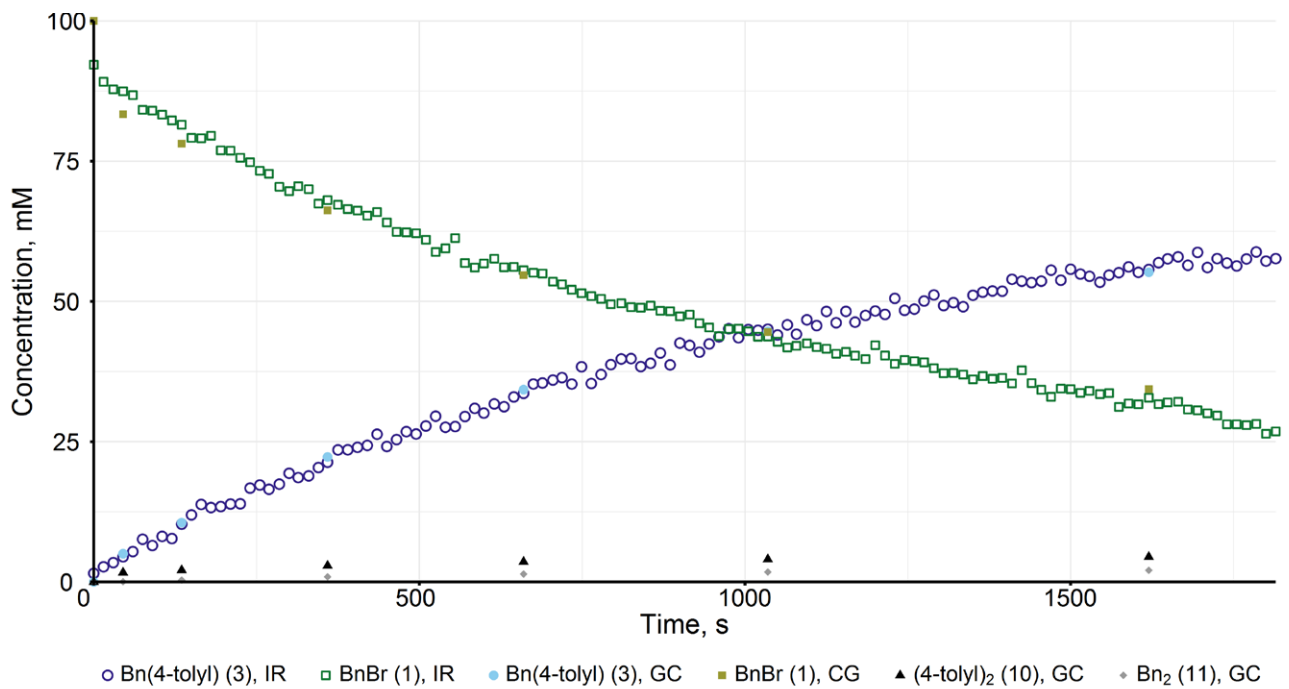
12.1 Reaction profiles

All reaction profiles were collected according to the method described in section 2; the individual experiments performed are summarised in Supplementary Table 16; and the data presented in Supplementary Figure 200 to Supplementary Figure 218.

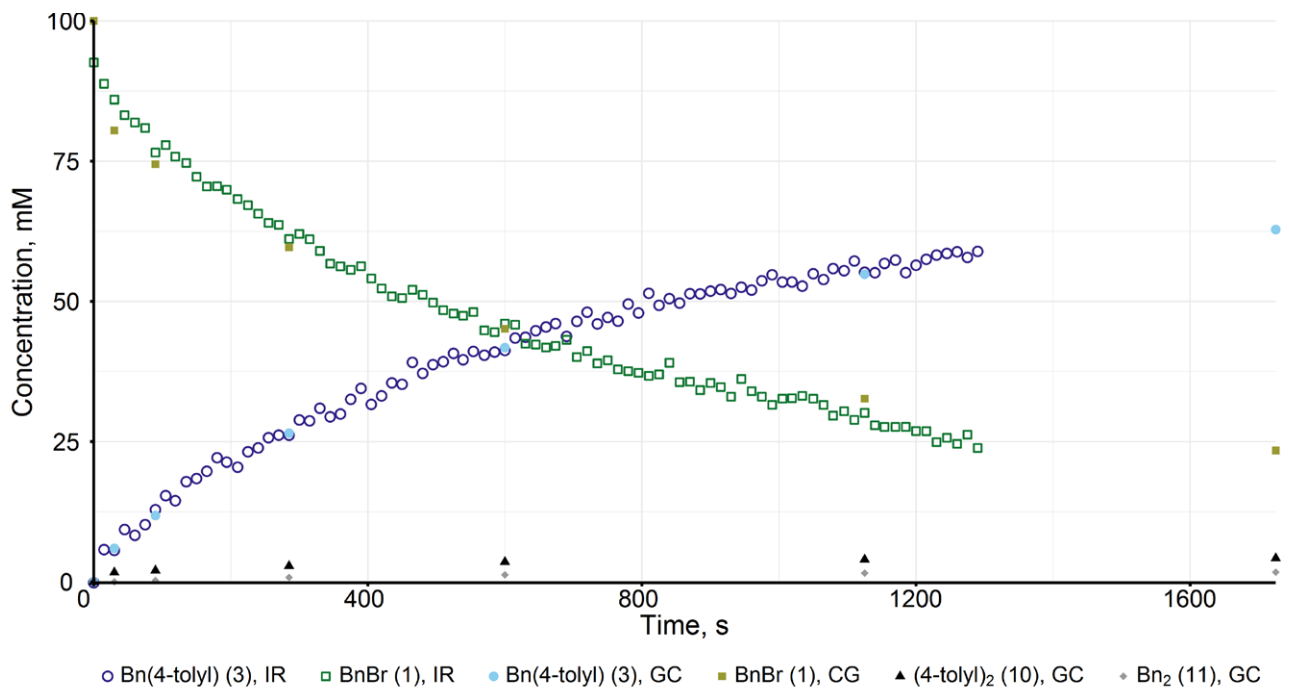
Supplementary Table 16: Summary of catalytic reactions monitored with *in situ* FT-IR spectroscopy for the kinetic study of the reaction between **1** and **2a** catalysed by FeBr₂ and dpbz.^a

Entry #	Pro-initiator (mM)	Nucleophile (mM)	BnBr (mM)	Phosphine (mM)
S1	FeBr ₂ (0.50)	2a (100)	100	dpbz (2.00)
S2	FeBr ₂ (0.75)	2a (100)	100	dpbz (2.00)
S3	FeBr ₂ (1.50)	2a (100)	100	dpbz (2.00)
S4	FeBr ₂ (2.00)	2a (100)	100	dpbz (2.00)
S5	FeBr ₂ (dpbz) ₂ (1.00)	2a (100)	50	–
S6	FeBr ₂ (dpbz) ₂ (1.00)	2a (100)	200	–
S7	FeBr ₂ (dpbz) ₂ (1.00)	2a (100)	400	–
S8	FeBr ₂ (dpbz) ₂ (1.00)	2a (100)	600	–
S9	FeBr ₂ (dpbz) ₂ (1.00)	2a (50)	100	–
S10	FeBr ₂ (dpbz) ₂ (1.00)	2a (75)	100	–
S11	FeBr ₂ (dpbz) ₂ (1.00)	2a (125)	100	–
S12	FeBr ₂ (dpbz) ₂ (1.00)	2a (162)	100	–
S13	FeBr ₂ (1.00)	2a (100)	100	dpbz (0.50)
S14	FeBr ₂ (1.00)	2a (100)	100	dpbz (0.75)
S15	FeBr ₂ (1.00)	2a (100)	100	dpbz (1.00)
S16	FeBr ₂ (1.00)	2a (100)	100	dpbz (1.50)
S17	FeBr ₂ (1.00)	2a (100)	100	dpbz (5.00)
S18	FeBr ₂ (1.00)	2a (100)	100	dpbz (10.0)
S19	FeBr ₂ (1.00)	2a (100)	100	dpbz (20.0)

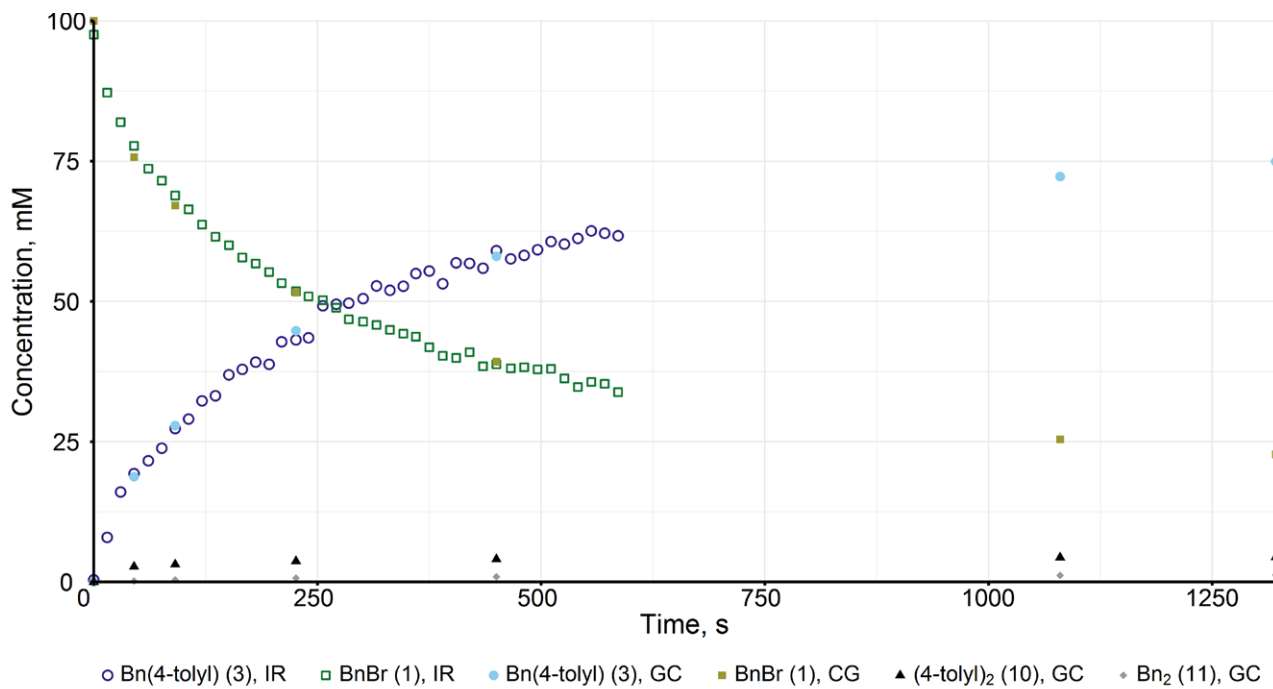
^a General conditions: Reactions were performed in THF at a total volume of 10 mL and monitored with FT-IR spectroscopy at 7.00 °C. BnBr stock solution = 2500 mM, Zn stock solutions = 200 mM, 0.5 mmol of *n*-dodecane added as a 500 mM stock solution, Fe stock solution = 20 mM. All reactions were initiated by addition of the Fe stock solution. ^b Reaction was performed in PhCl and initiated by addition of BnBr.



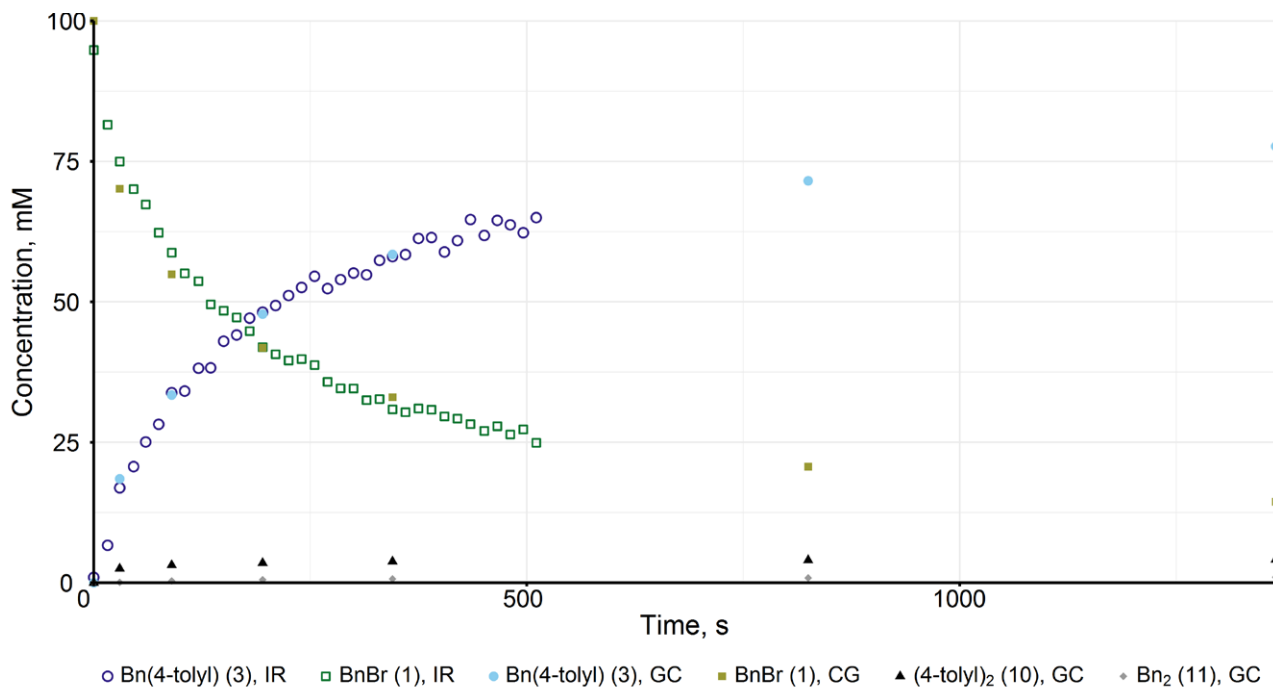
Supplementary Figure 200. Negishi coupling between **1** (100 mM) and **2a** (100 mM) catalysed by FeBr_2 (0.50 mM) + dpbz (2.00 mM) at 7.00 °C and a total volume of 10.0 mL (entry S1, Supplementary Table 16).



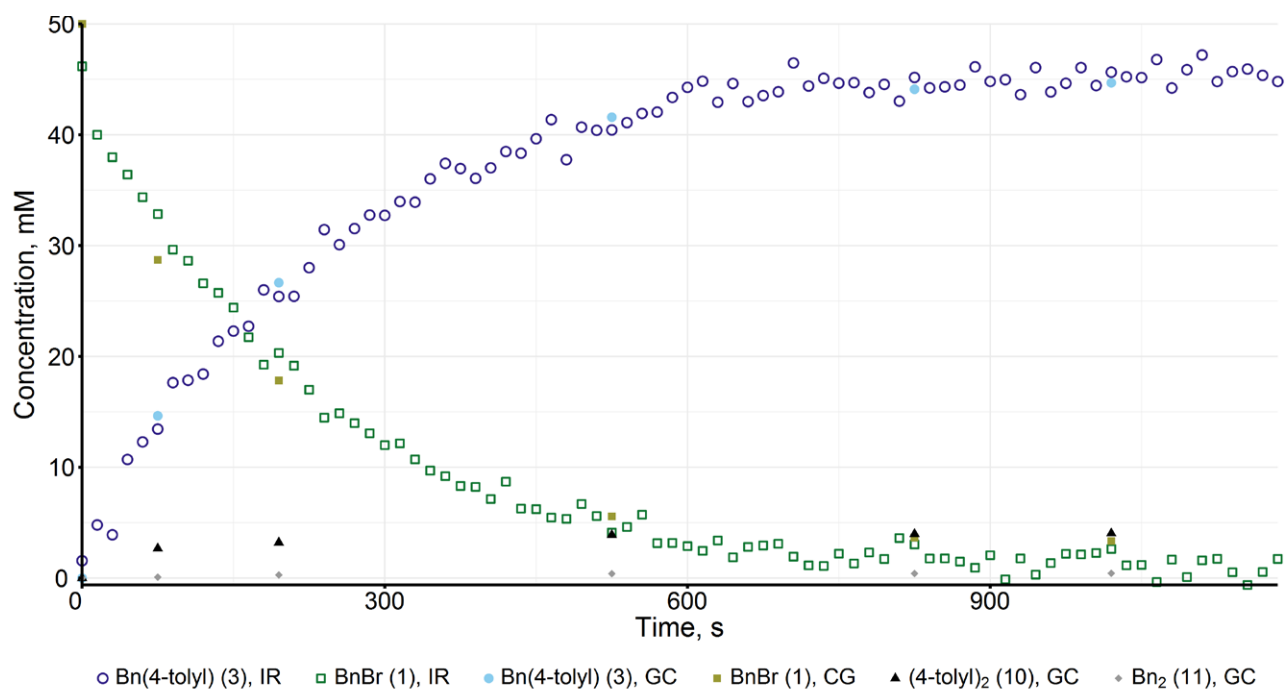
Supplementary Figure 201. Negishi coupling between **1** (100 mM) and **2a** (100 mM) catalysed by FeBr_2 (0.75 mM) + dpbz (2.00 mM) at 7.00 °C and a total volume of 10.0 mL (entry S2, Supplementary Table 16).



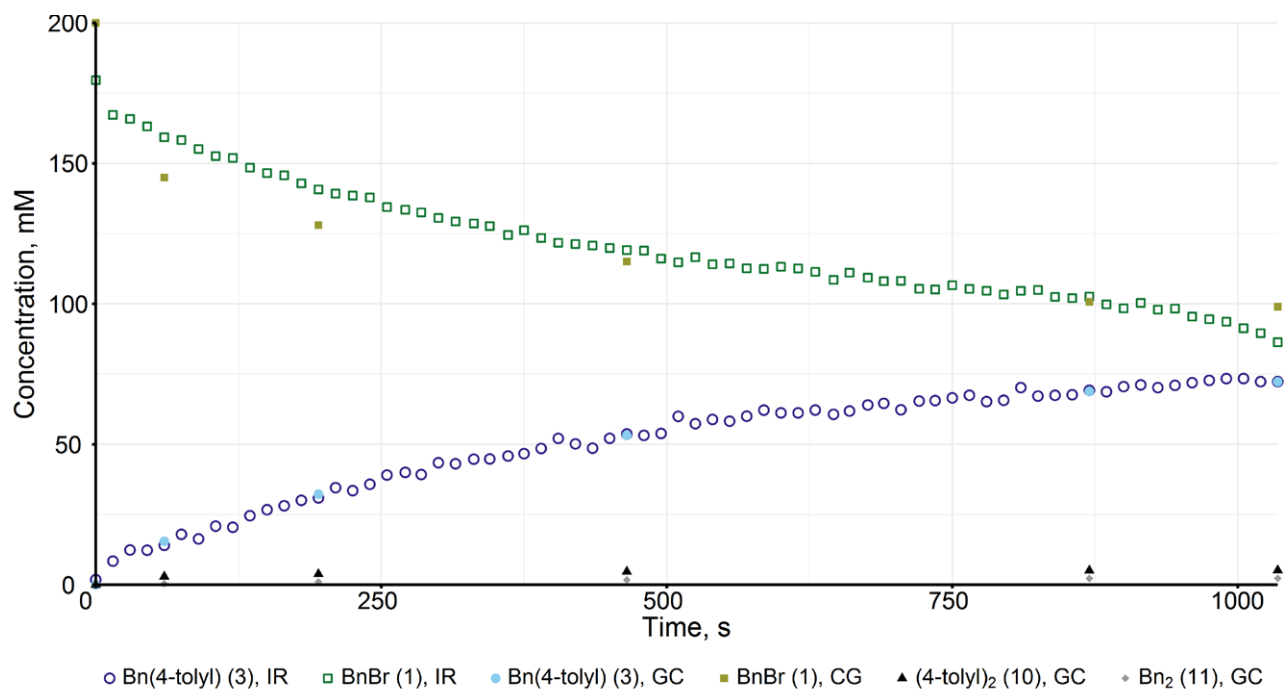
Supplementary Figure 202. Negishi coupling between **1** (100 mM) and **2a** (100 mM) catalysed by FeBr_2 (1.50 mM) + dpbz (2.00 mM) at 7.00 °C and a total volume of 10.0 mL (entry S3, Supplementary Table 16).



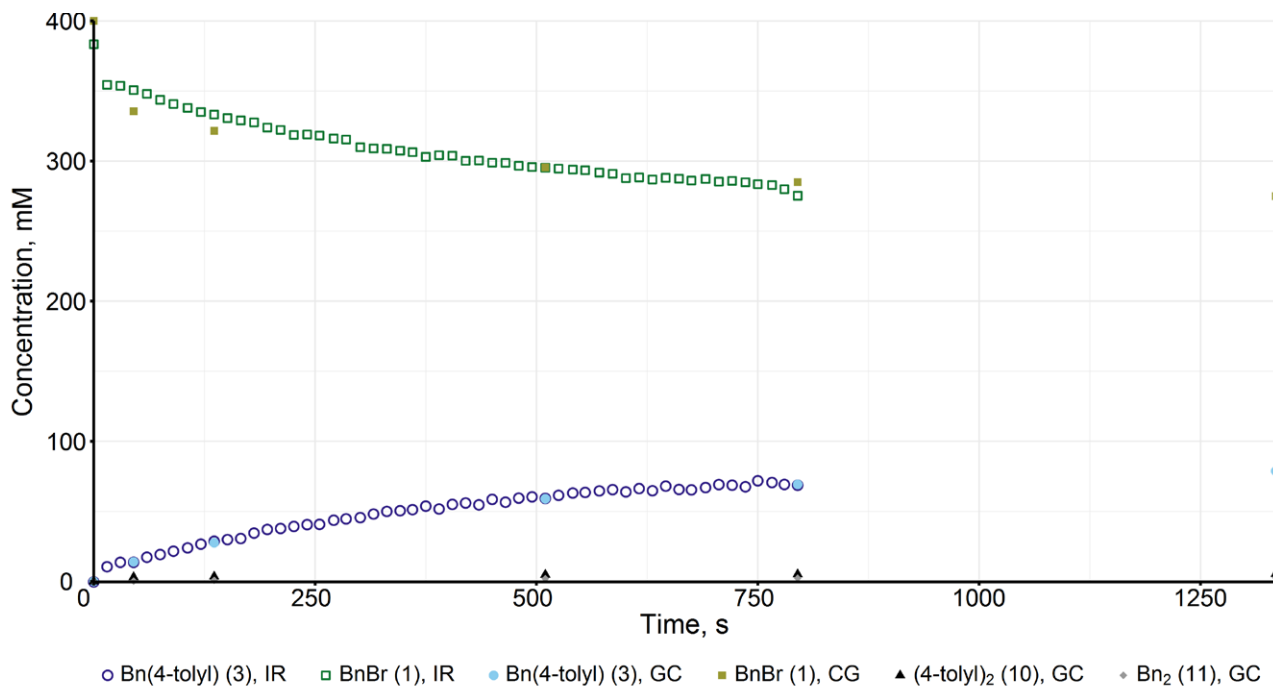
Supplementary Figure 203. Negishi coupling between **1** (100 mM) and **2a** (100 mM) catalysed by FeBr_2 (2.00 mM) + dpbz (2.00 mM) at 7.00 °C and a total volume of 10.0 mL (entry S4, Supplementary Table 16).



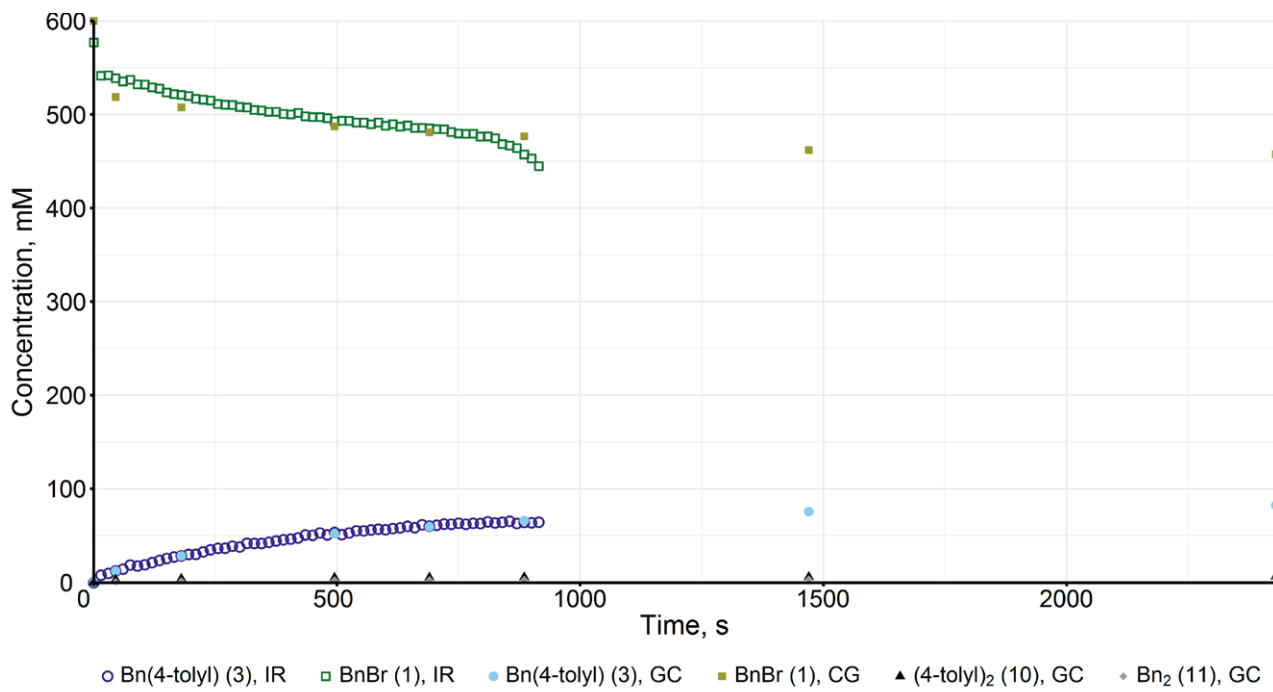
Supplementary Figure 204. Negishi coupling between **1** (50.0 mM) and **2a** (100 mM) catalysed by **7a** (1.00 mM) at 7.00 °C and a total volume of 10.0 mL (entry S5, Supplementary Table 16).



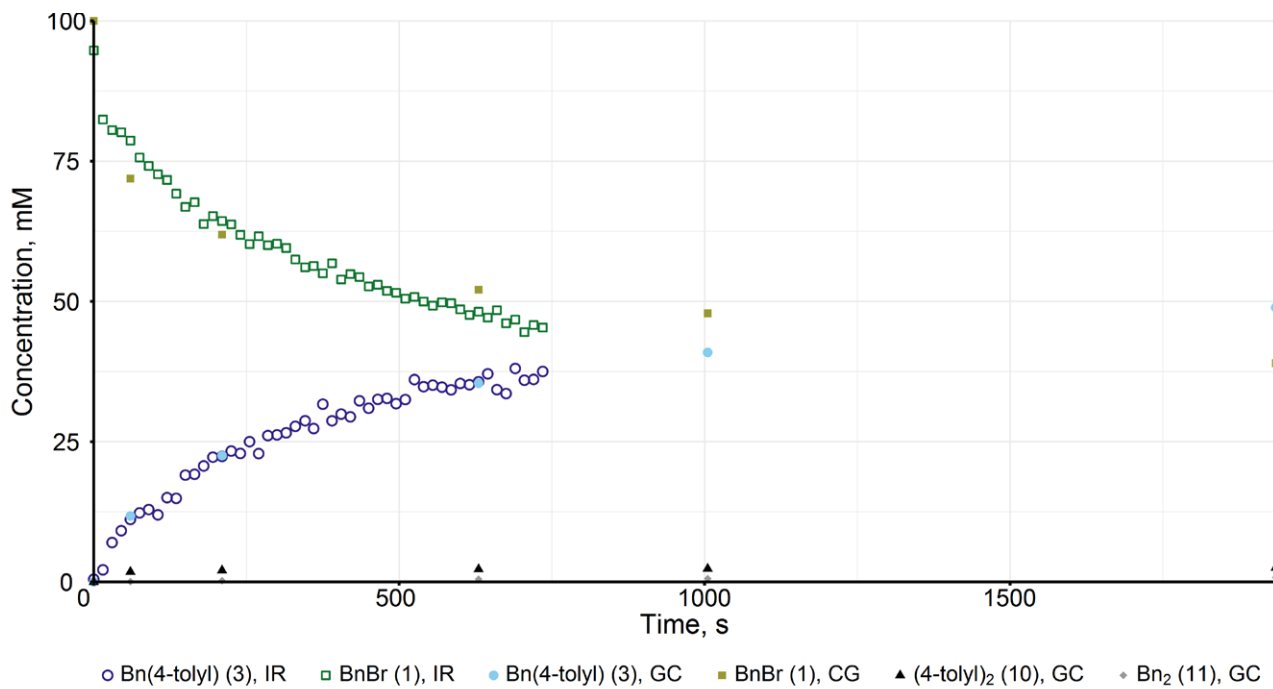
Supplementary Figure 205. Negishi coupling between **1** (200 mM) and **2a** (100 mM) catalysed by **7a** (1.00 mM) at 7.00 °C and a total volume of 10.0 mL (entry S6, Supplementary Table 16).



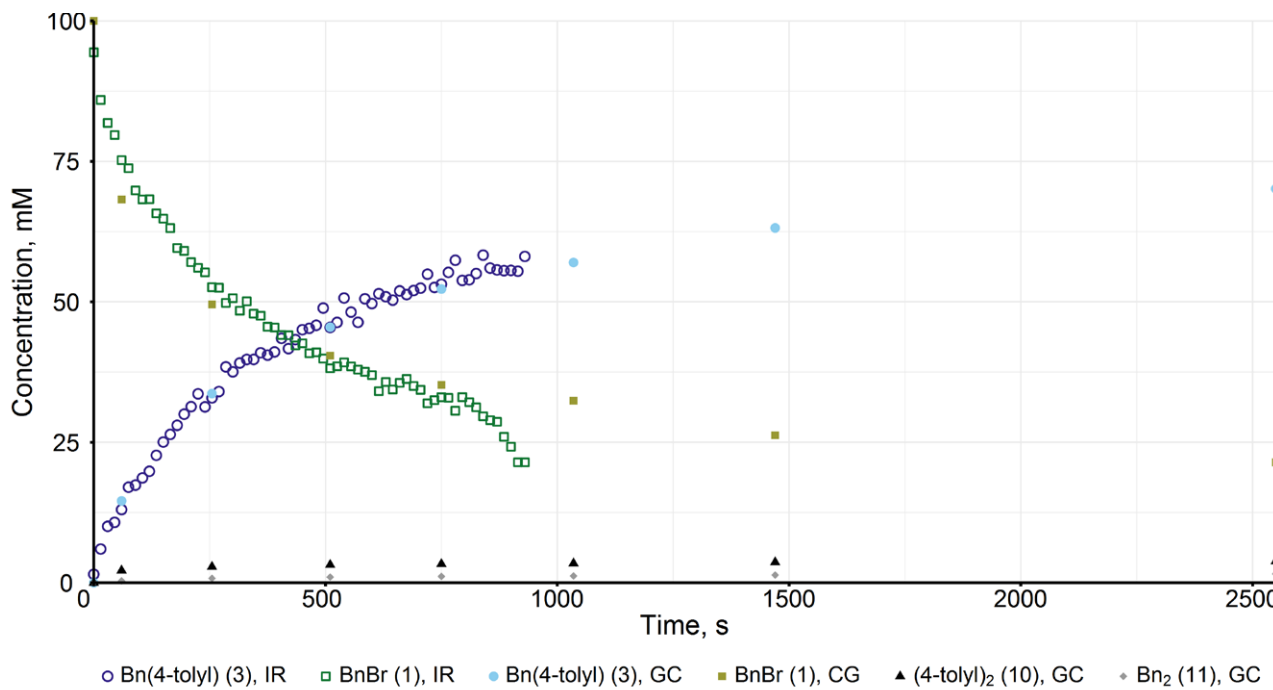
Supplementary Figure 206. Negishi coupling between **1** (400 mM) and **2a** (100 mM) catalysed by **7a** (1.00 mM) at 7.00 °C and a total volume of 10.0 mL (entry S7, Supplementary Table 16).



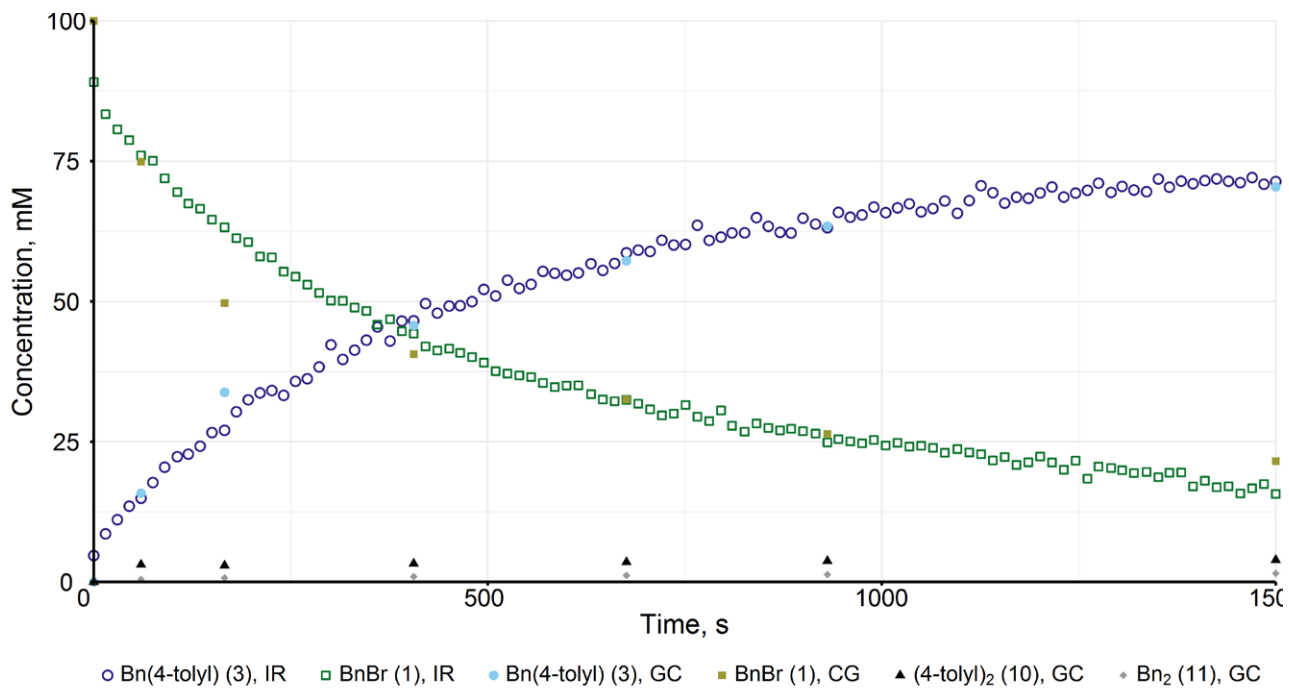
Supplementary Figure 207. Negishi coupling between **1** (600 mM) and **2a** (100 mM) catalysed by **7a** (1.00 mM) at 7.00 °C and a total volume of 10.0 mL (entry S8, Supplementary Table 16).



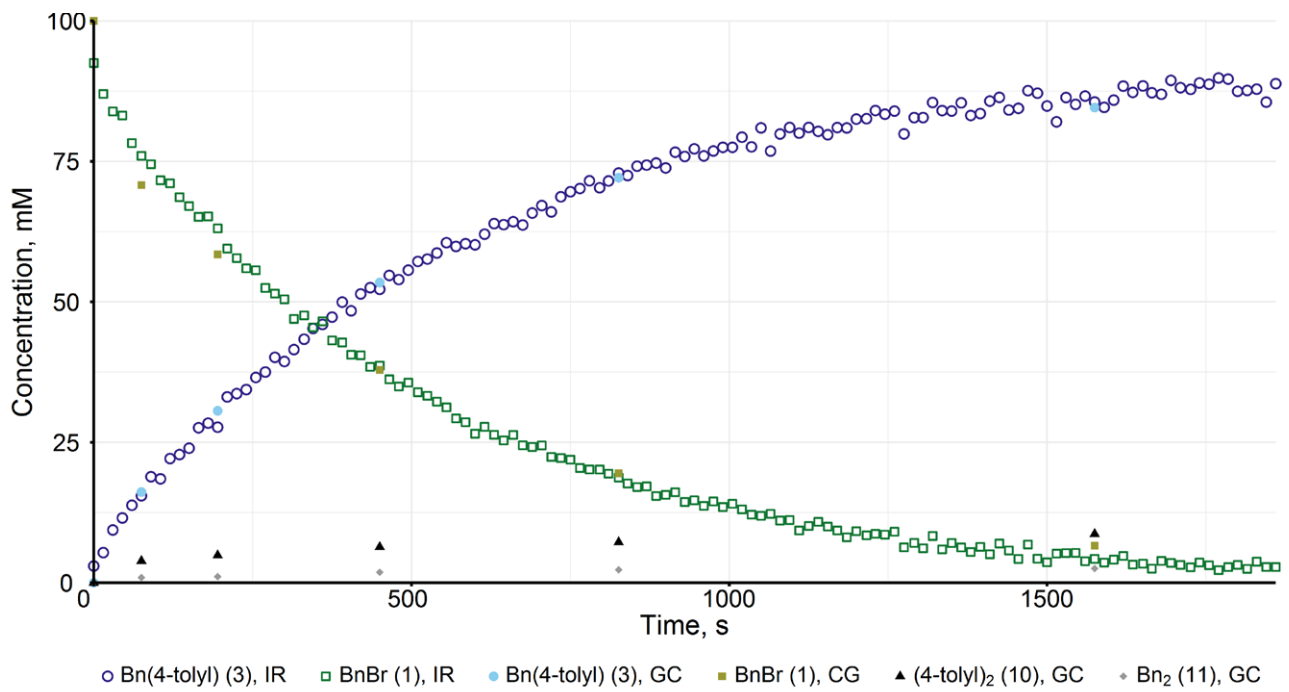
Supplementary Figure 208. Negishi coupling between **1** (100 mM) and **2a** (50.0 mM) catalysed by **7a** (1.00 mM) at 7.00 °C and a total volume of 10.0 mL (entry S9, Supplementary Table 16).



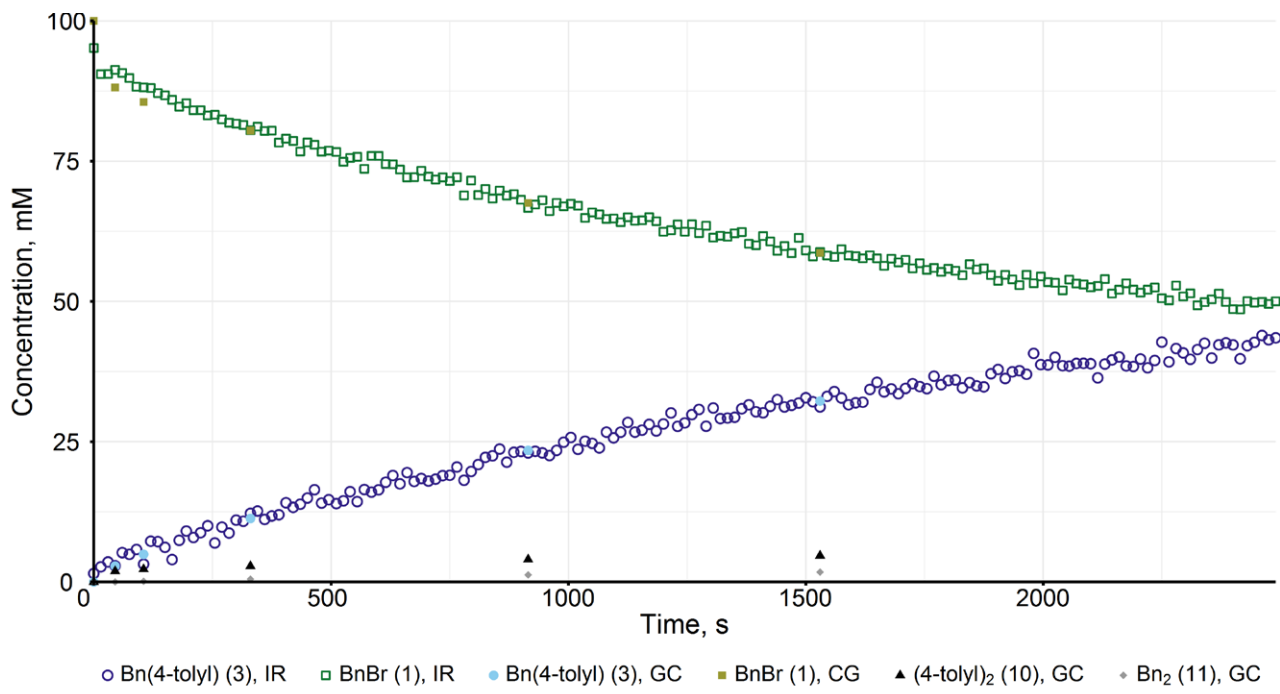
Supplementary Figure 209. Negishi coupling between **1** (100 mM) and **2a** (75.0 mM) catalysed by **7a** (1.00 mM) at 7.00 °C and a total volume of 10.0 mL (entry S10, Supplementary Table 16).



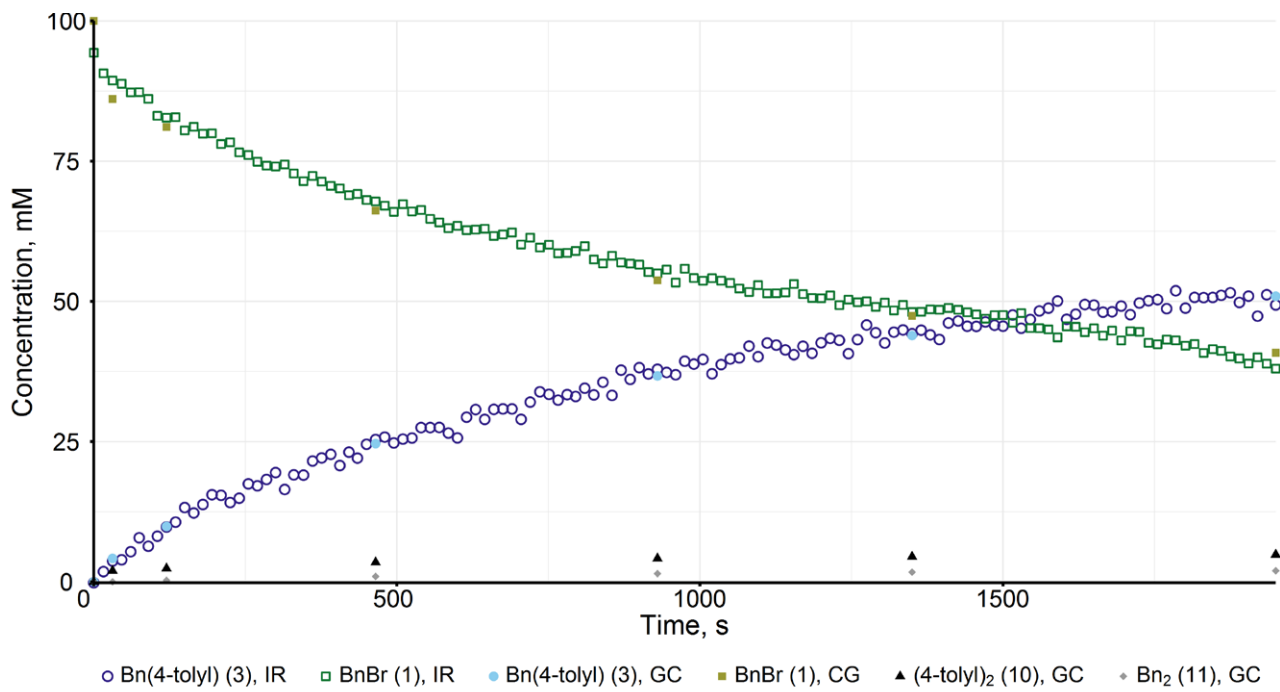
Supplementary Figure 210. Negishi coupling between **1** (100 mM) and **2a** (125 mM) catalysed by **7a** (1.00 mM) at 7.00 °C and a total volume of 10.0 mL (entry S11, Supplementary Table 16).



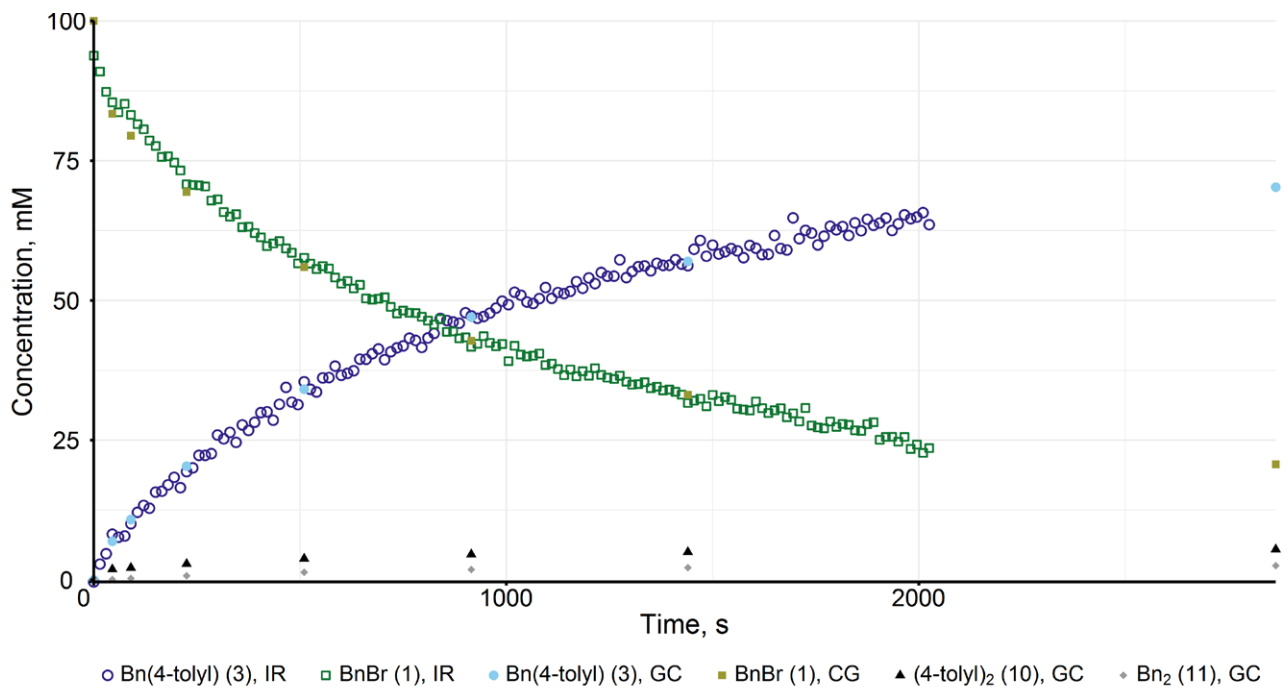
Supplementary Figure 211. Negishi coupling between **1** (100 mM) and **2a** (162 mM) catalysed by **7a** (1.00 mM) at 7.00 °C and a total volume of 10.0 mL (entry S12, Supplementary Table 16).



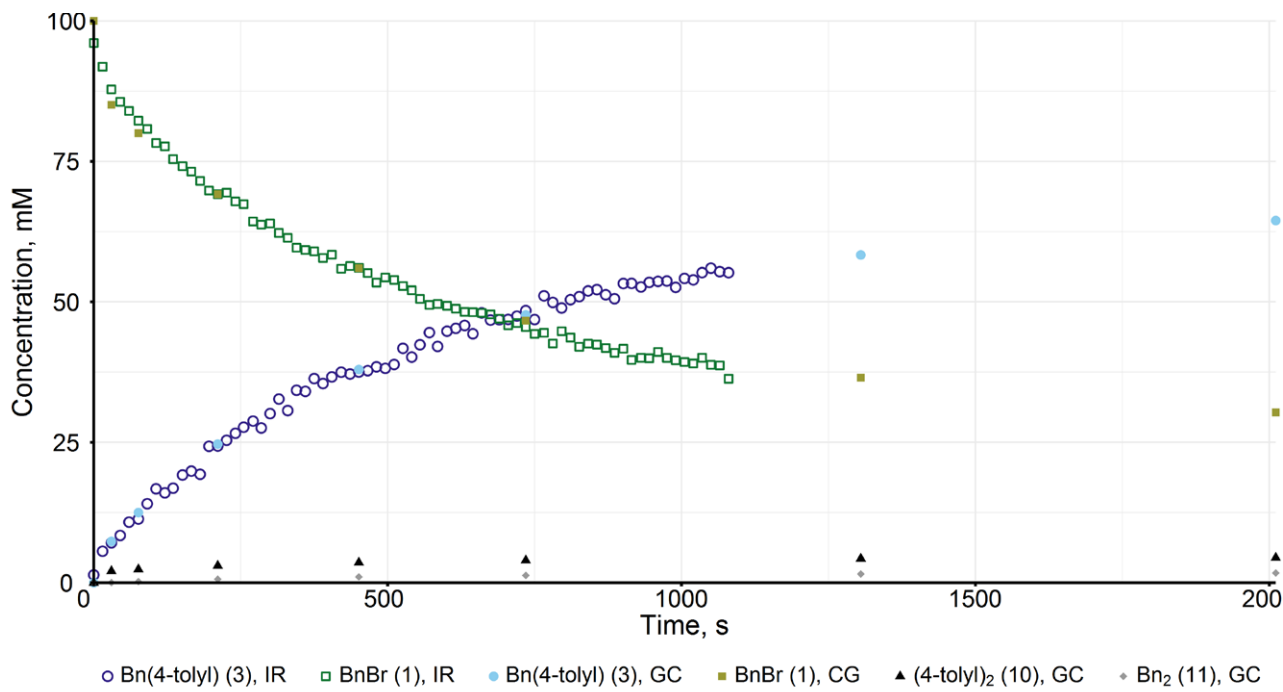
Supplementary Figure 212. Negishi coupling between **1** (100 mM) and **2a** (100 mM) catalysed by FeBr_2 (1.00 mM) + dpbz (0.50 mM) at 7.00 °C and a total volume of 10.0 mL (entry S13, Supplementary Table 16).



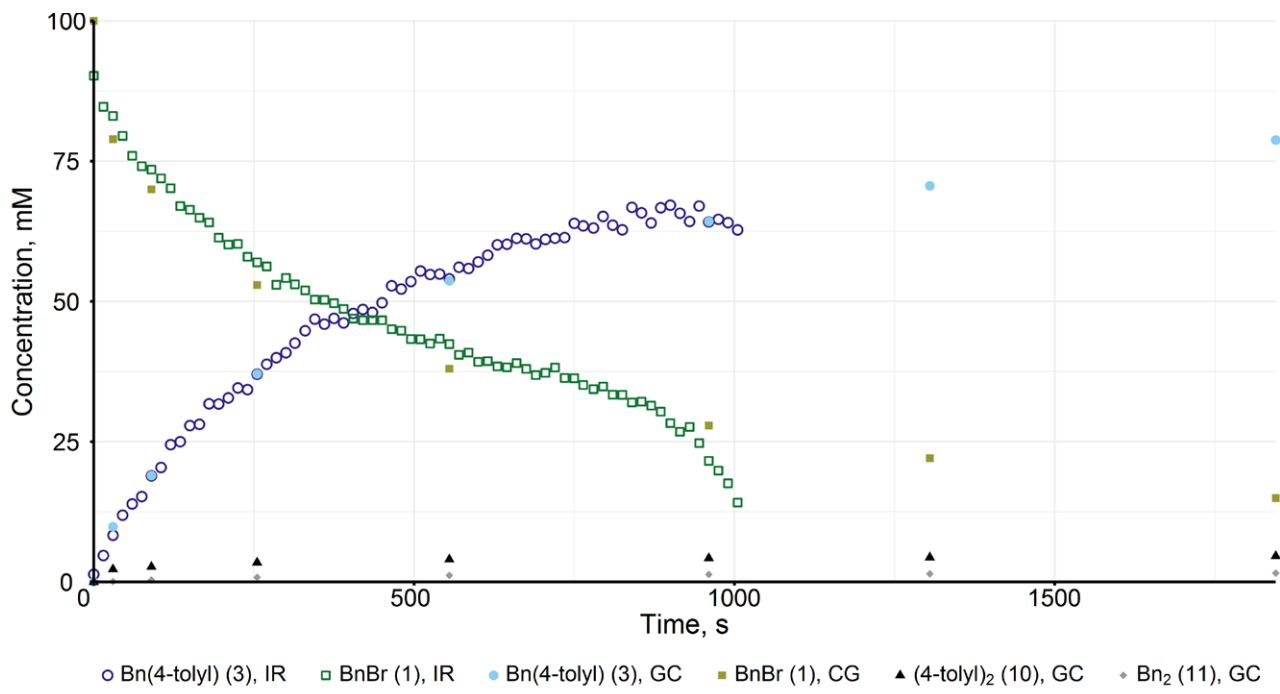
Supplementary Figure 213. Negishi coupling between **1** (100 mM) and **2a** (100 mM) catalysed by FeBr_2 (1.00 mM) + dpbz (0.75 mM) at 7.00 °C and a total volume of 10.0 mL (entry S14, Supplementary Table 16).



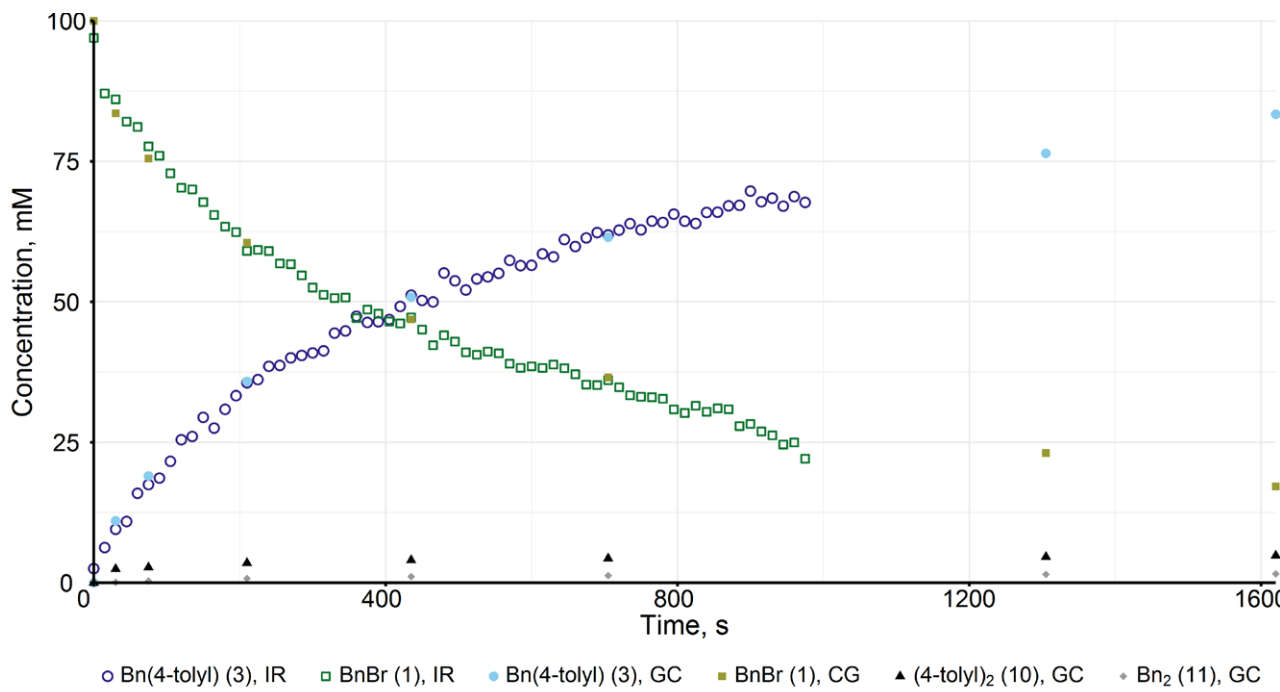
Supplementary Figure 214. Negishi coupling between **1** (100 mM) and **2a** (100 mM) catalysed by FeBr_2 (1.00 mM) + dpbz (1.00 mM) at 7.00 °C and a total volume of 10.0 mL (entry S15, Supplementary Table 16).



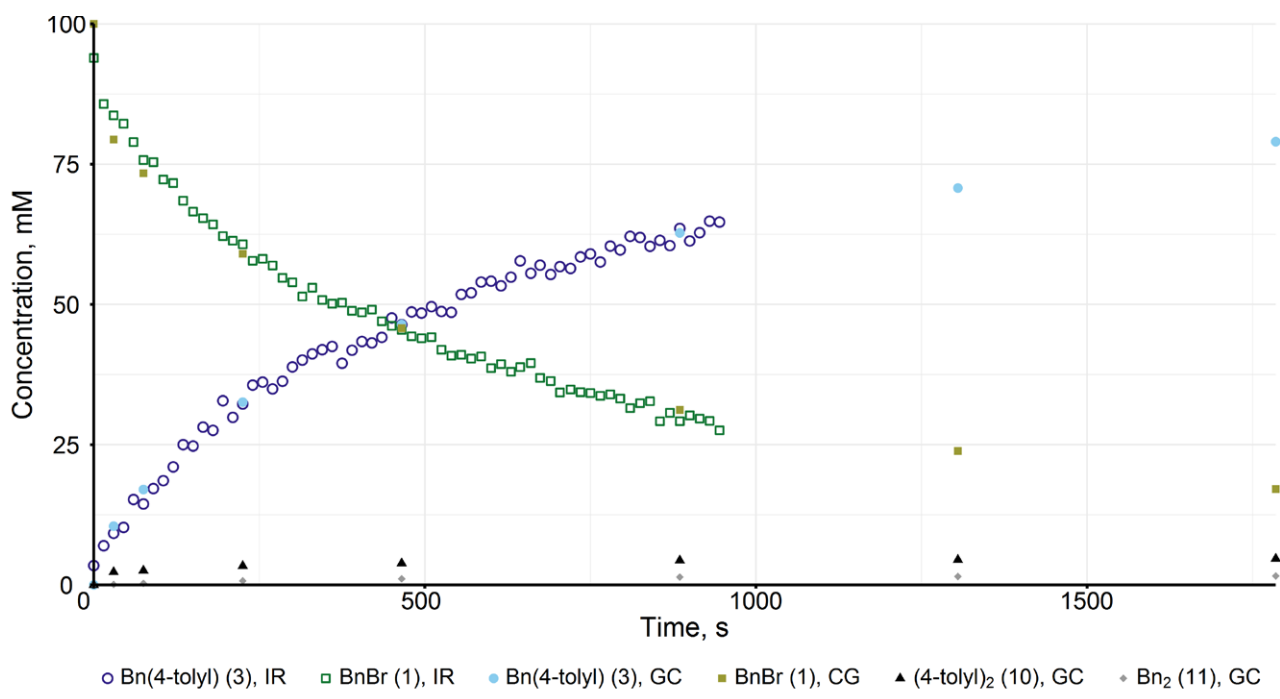
Supplementary Figure 215. Negishi coupling between **1** (100 mM) and **2a** (100 mM) catalysed by FeBr_2 (1.00 mM) + dpbz (1.50 mM) at 7.00 °C and a total volume of 10.0 mL (entry S16, Supplementary Table 16).



Supplementary Figure 216. Negishi coupling between **1** (100 mM) and **2a** (100 mM) catalysed by FeBr_2 (1.00 mM) + dpbz (5.00 mM) at 7.00 °C and a total volume of 10.0 mL (entry S17, Supplementary Table 16).



Supplementary Figure 217. Negishi coupling between **1** (100 mM) and **2a** (100 mM) catalysed by FeBr_2 (1.00 mM) + dpbz (10.0 mM) at 7.00 °C and a total volume of 10.0 mL (entry S18, Supplementary Table 16).

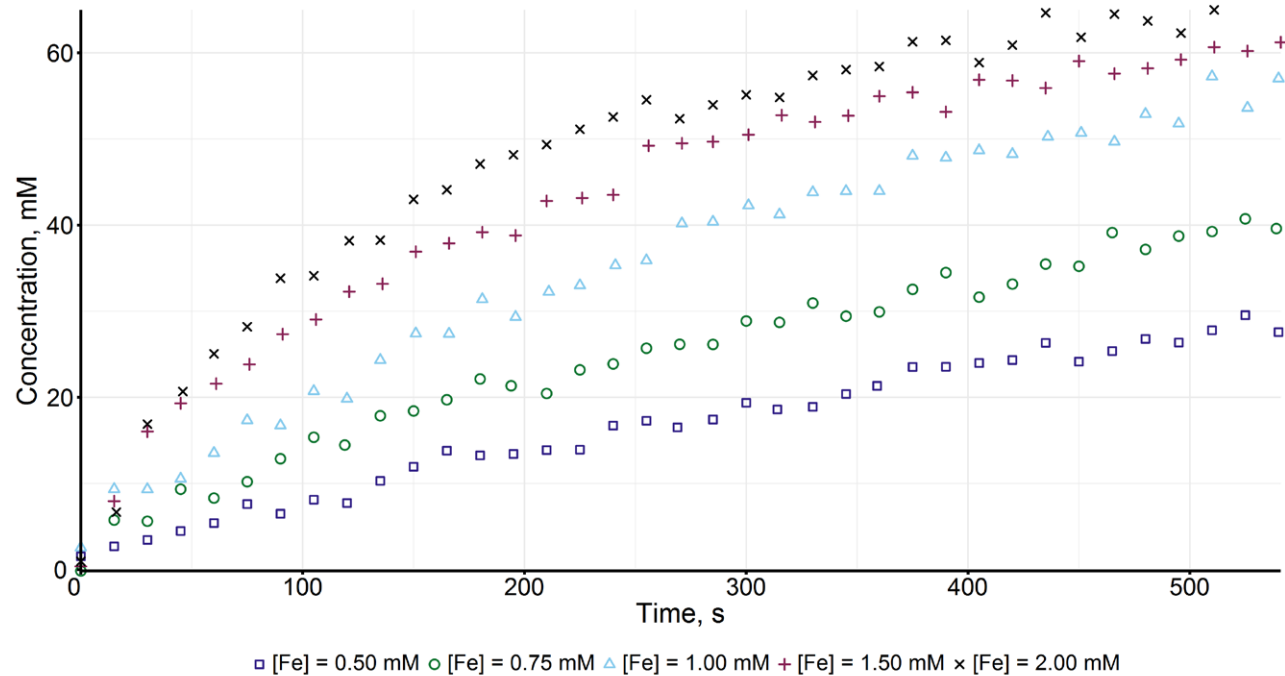


Supplementary Figure 218. Negishi coupling between **1** (100 mM) and **2a** (100 mM) catalysed by FeBr_2 (1.00 mM) + dpbz (20.0 mM) at 7.00 °C and a total volume of 10.0 mL (entry S19, Supplementary Table 16).

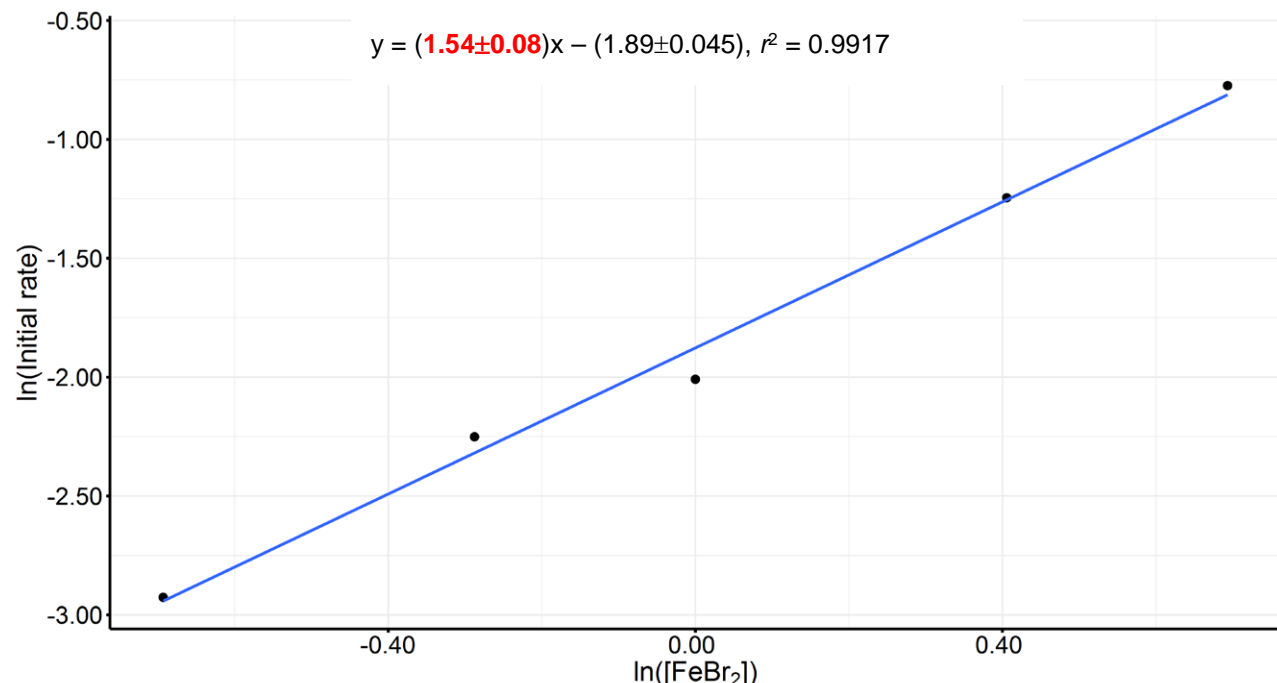
12.2 Kinetic analysis of the reaction between **1** and **2a** catalysed by FeBr_2 and dpbz in THF at 7.00 °C and a total volume of 10 mL.

The orders in Fe, BnBr, Zn and dpbz were calculated using the method of initial rates or/and the variable time normalisation analysis method reported by Jordi Bures.^{40,41} The t = 0 point was excluded from the calculation of the initial rate due to the presence of a burst phase at the beginning of the reaction.

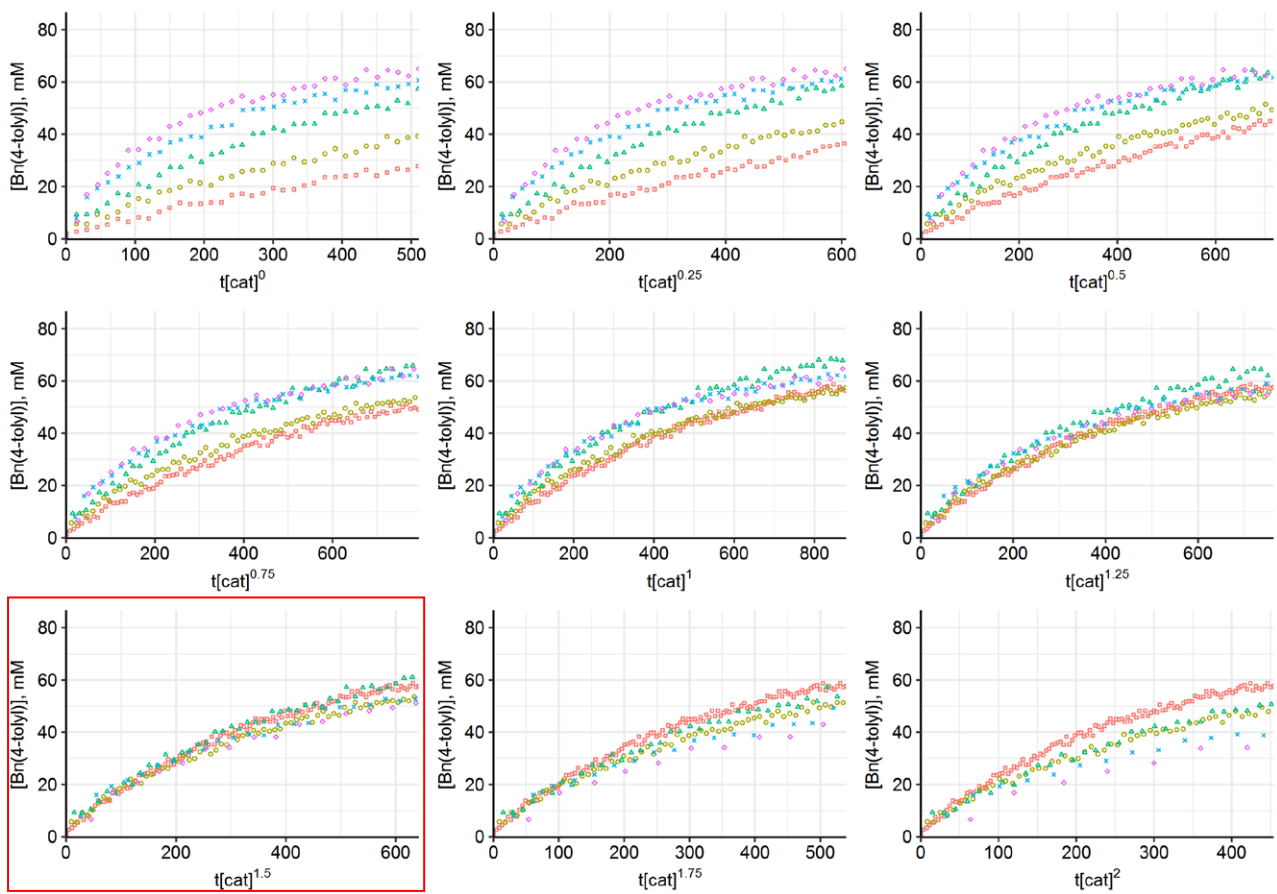
Determination of the order in Fe.



Supplementary Figure 219. Reaction progress for the Negishi coupling between **1** and **2a** catalysed by $\text{FeBr}_2 + \text{dpbz}$ at varying concentrations of FeBr_2 .

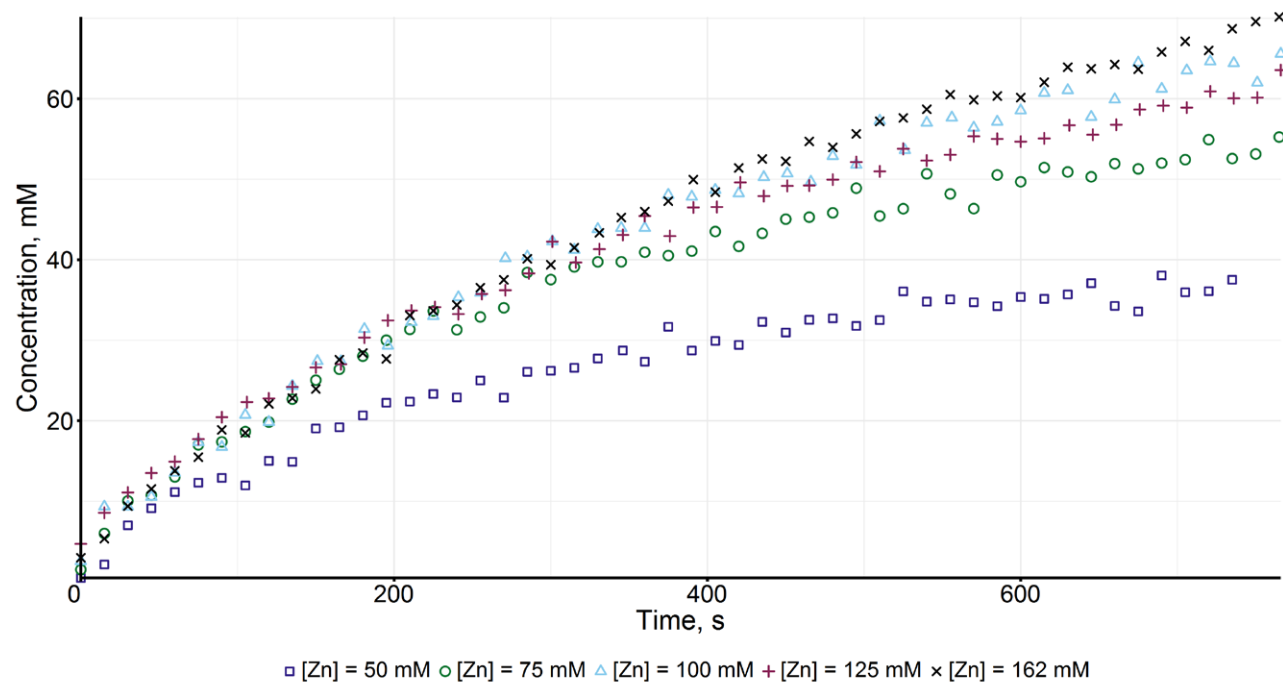


Supplementary Figure 220. Ln-In plot for the Negishi coupling between **1** and **2a** catalysed by $\text{FeBr}_2 + \text{dpbz}$ at varying concentrations of FeBr_2 . Standard errors are included in the fitted equation.

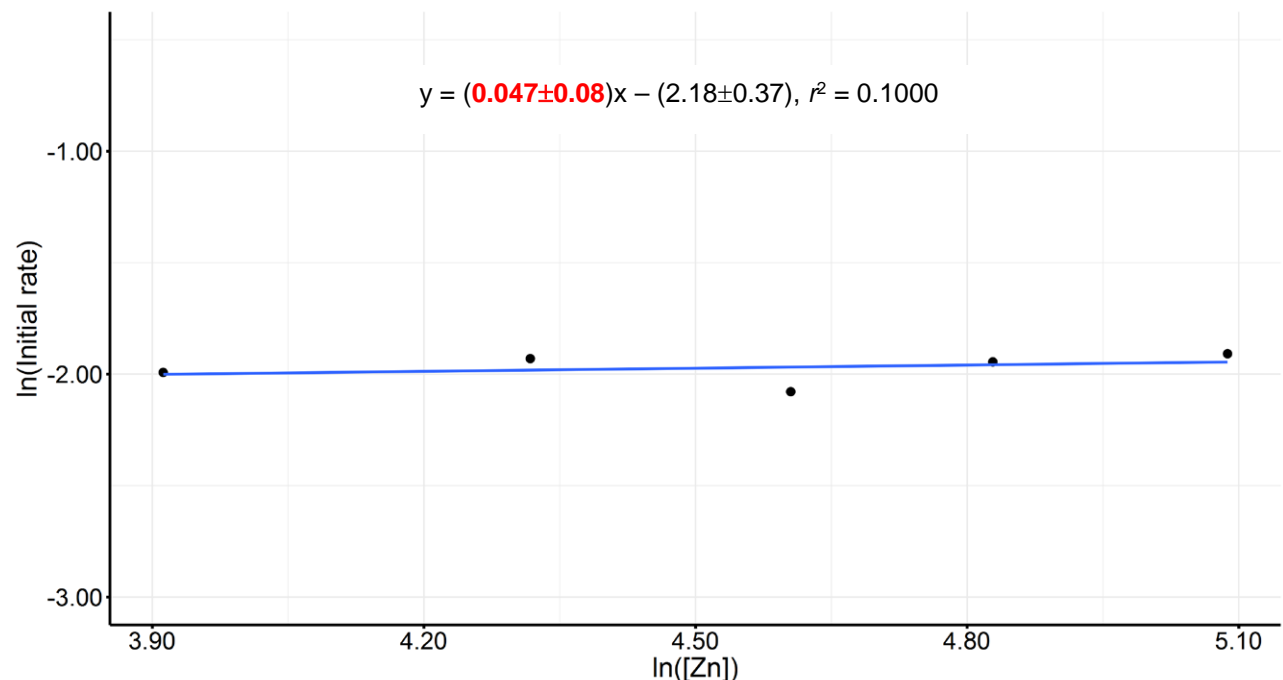


Supplementary Figure 221. Variable time normalisation analysis for determination of the order in Fe in the Negishi coupling between **1** and **2a** catalysed by $\text{FeBr}_2 + \text{dpbz}$.

Determination of the order in Zn:

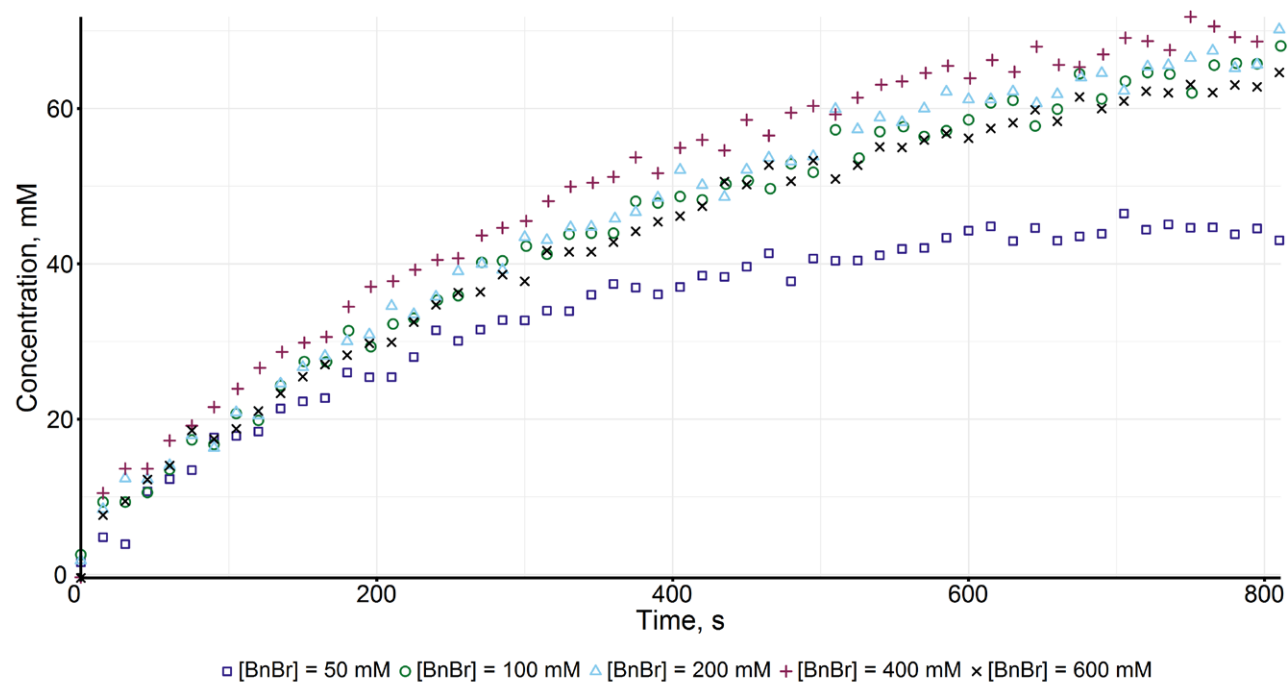


Supplementary Figure 222. Reaction progress for the Negishi coupling between **1** and **2a** catalysed by $\text{FeBr}_2 + \text{dpbz}$ at varying concentrations of **2a**.

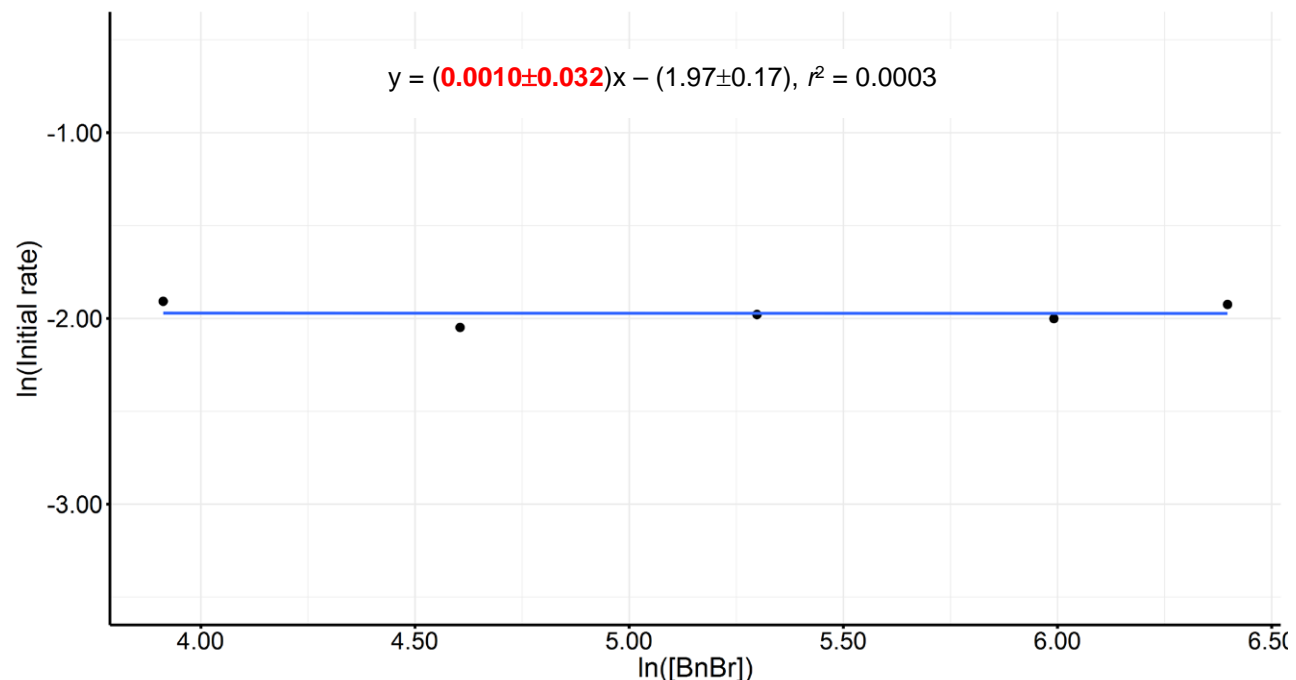


Supplementary Figure 223. Ln-Ln plot for the Negishi coupling between **1** and **2a** catalysed by $\text{FeBr}_2 + \text{dpbz}$ at varying concentrations of **2a**. Standard errors are included in the fitted equation.

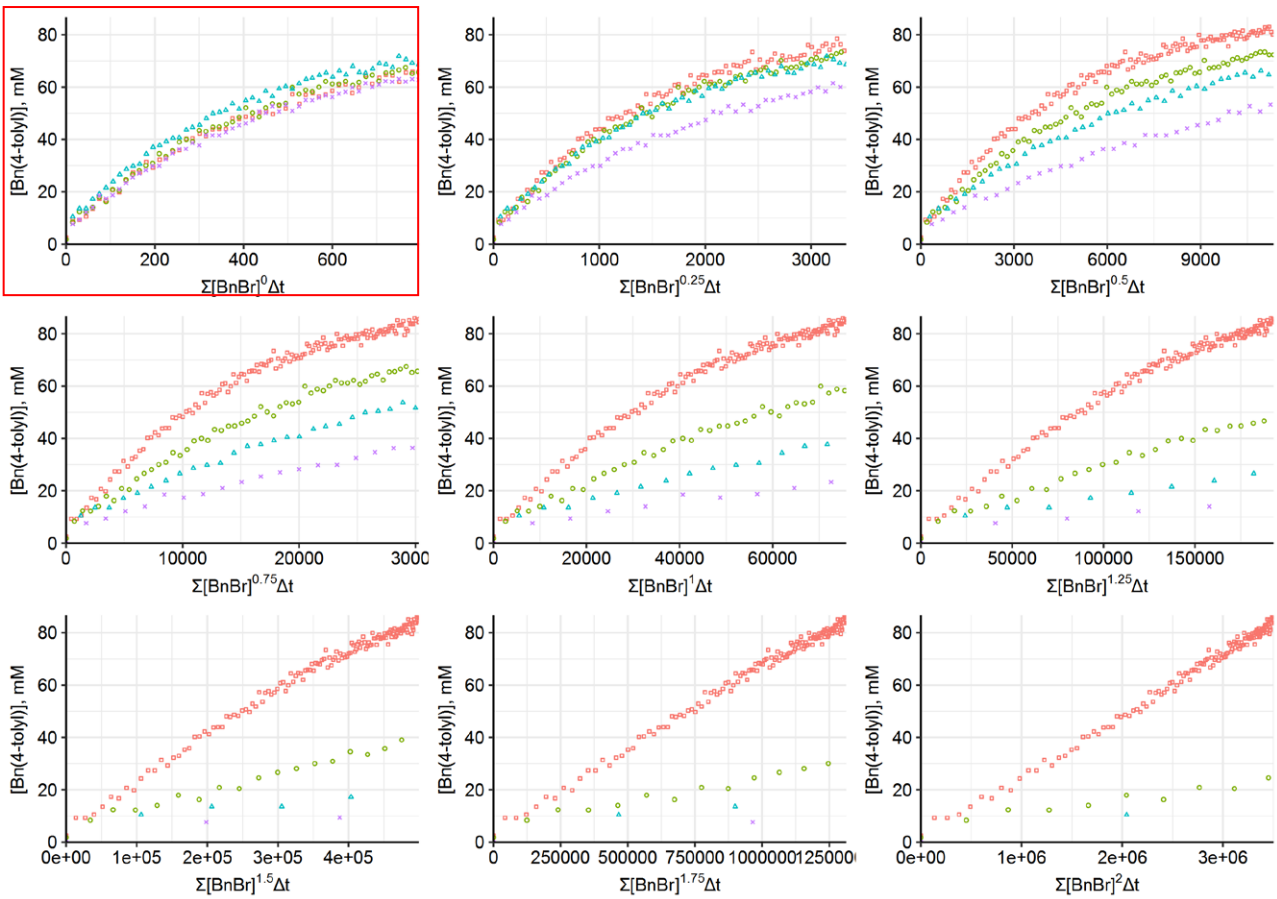
Determination of the order in BnBr:



Supplementary Figure 224. Reaction progress for the Negishi coupling between **1** and **2a** catalysed by $\text{FeBr}_2 + \text{dpbz}$ at varying concentrations of **1**.

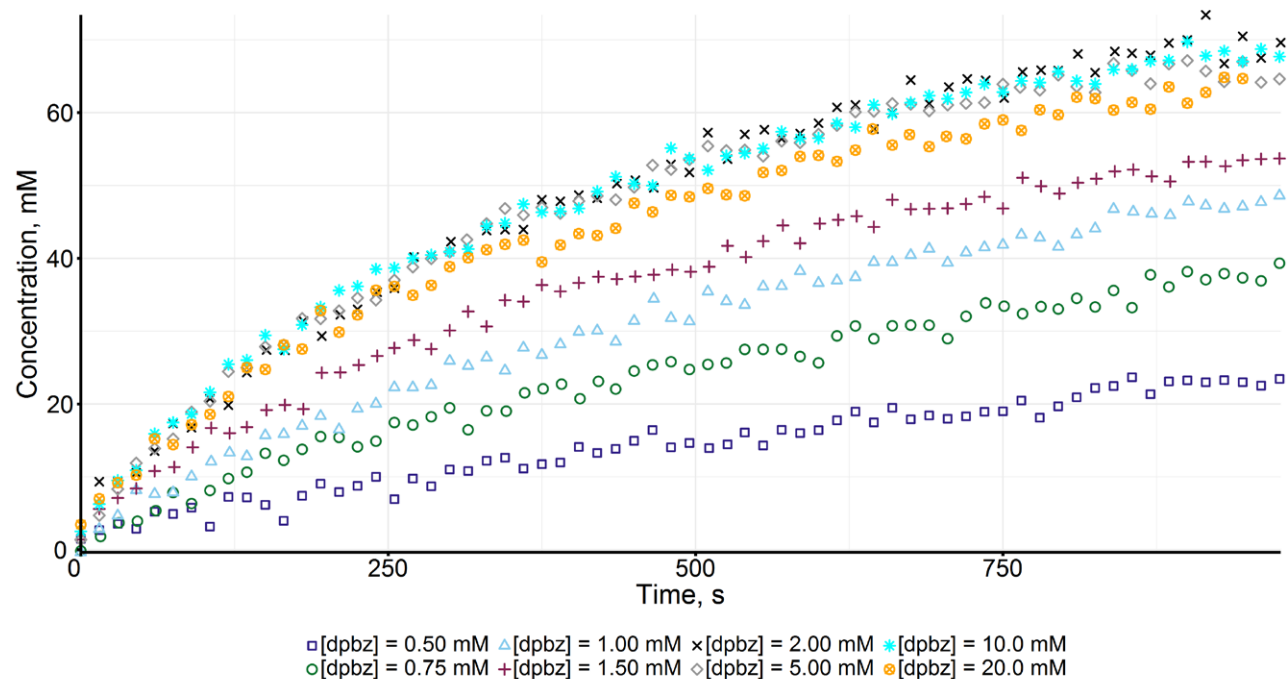


Supplementary Figure 225. Ln-Ln plot for the Negishi coupling between **1** and **2a** catalysed by $\text{FeBr}_2 + \text{dpbz}$ at varying concentrations of **1**. Standard errors are included in the fitted equation.

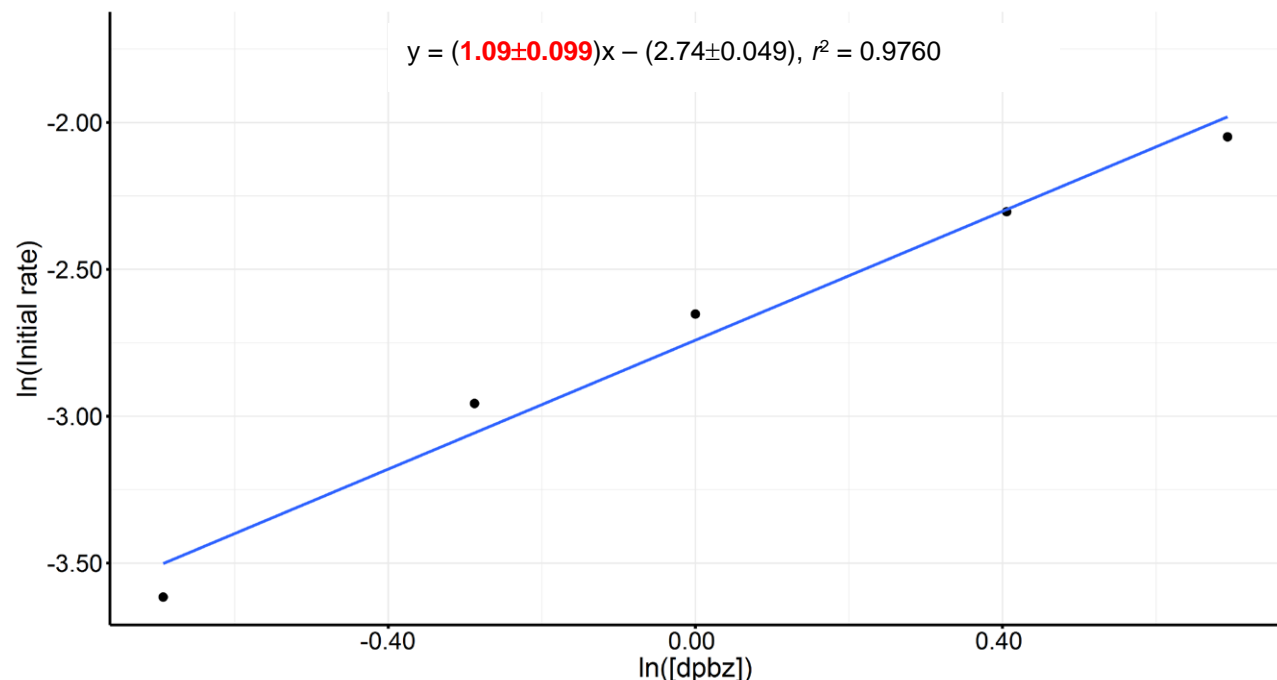


Supplementary Figure 226. Variable time normalisation analysis for determination of the order in **1** in the Negishi coupling between **1** and **2a** catalysed by $\text{FeBr}_2 + 2 \text{ dpbz}$.

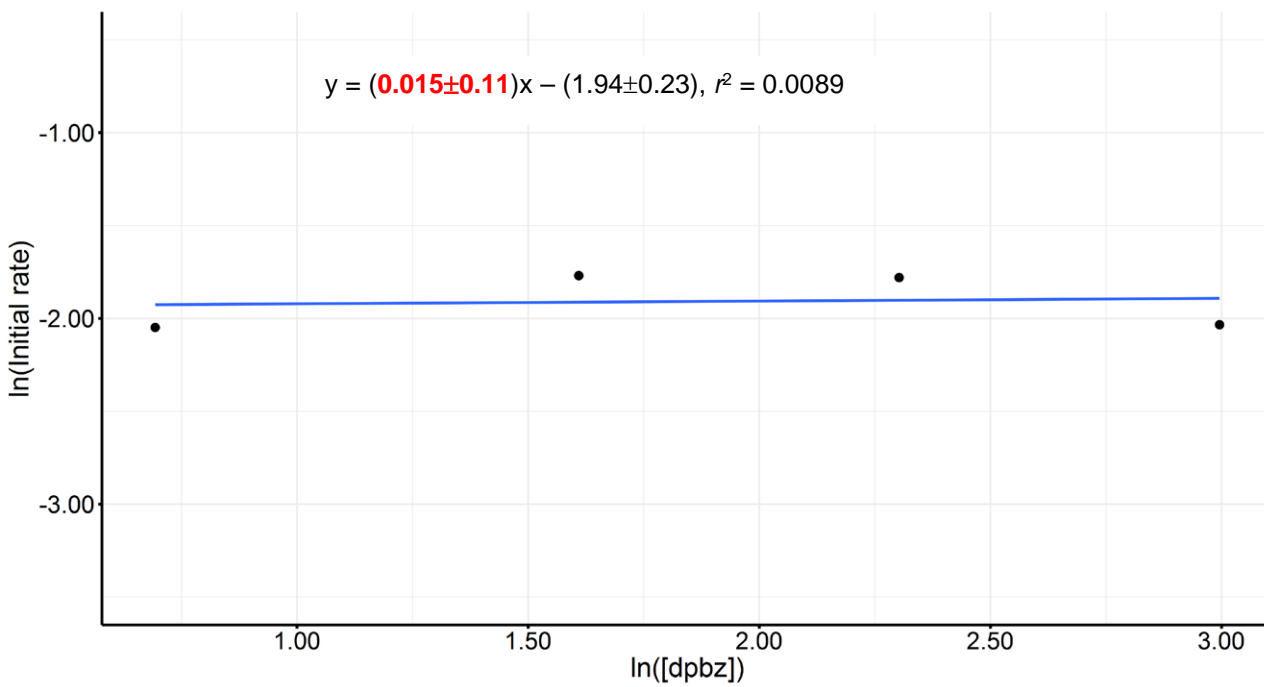
Determination of the order in dpbz:



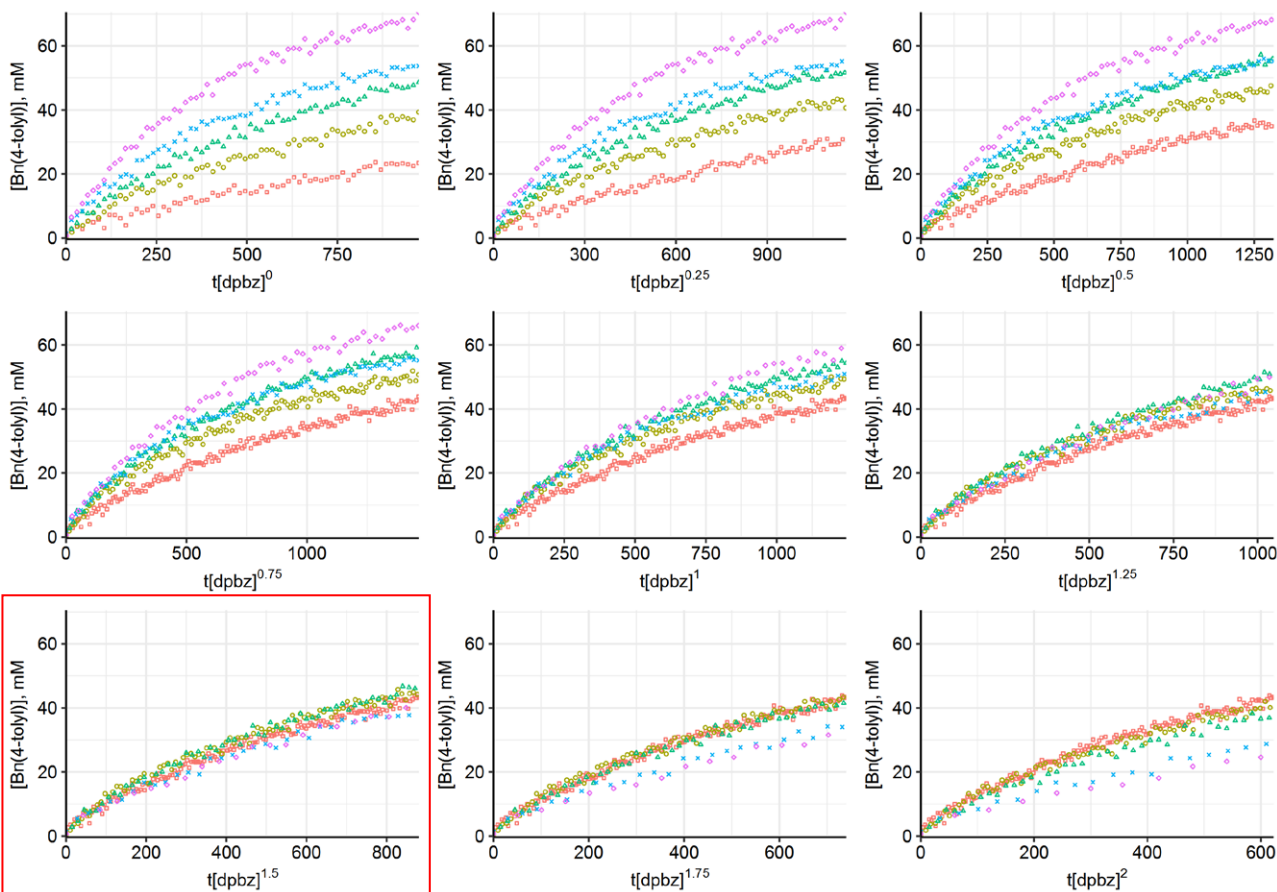
Supplementary Figure 227. Reaction progress for the Negishi coupling between **1** and **2a** catalysed by $\text{FeBr}_2 + \text{dpbz}$ at varying concentrations of dpbz.



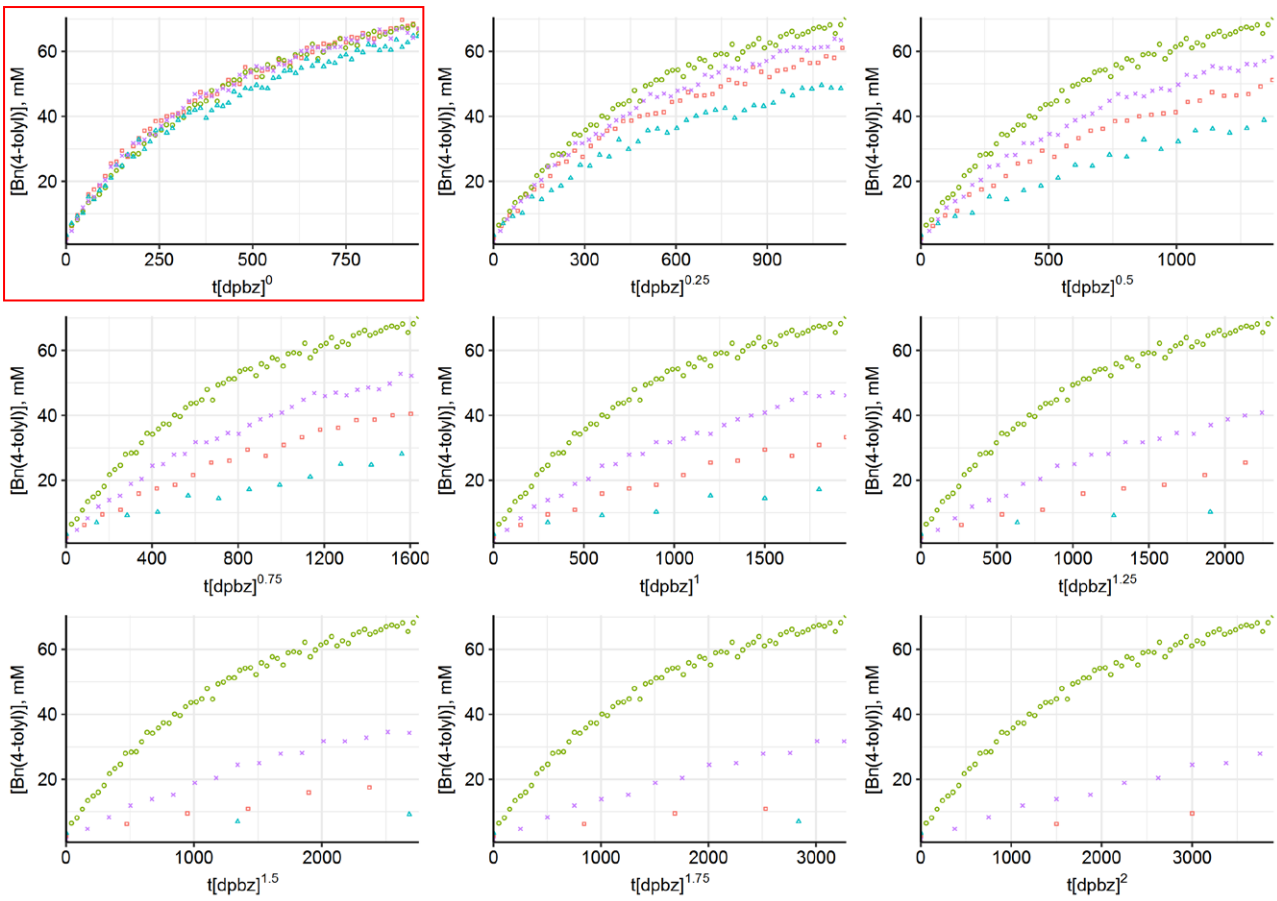
Supplementary Figure 228. Ln-Ln plot for the Negishi coupling between **1** and **2a** catalysed by $\text{FeBr}_2 + \text{dpbz}$ at concentrations of dpbz between 0.50 mM and 2.00 mM. Standard errors are included in the fitted equation.



Supplementary Figure 229. Ln-Ln plot for the Negishi coupling between **1** and **2a** catalysed by $\text{FeBr}_2 + \text{dpbz}$ at concentrations of dpbz between 2.00 mM and 20.0 mM. Standard errors are included in the fitted equation.



Supplementary Figure 230. Variable time normalisation analysis for determination of the order in dpbz in the Negishi coupling between **1** and **2a** catalysed by $\text{FeBr}_2 + \text{dpbz}$ at concentrations of dpbz between 0.50 mM and 2.00 mM.



Supplementary Figure 231: Variable time normalisation analysis for determination of the order in dpbz in the Negishi coupling between **1** and **2a** catalysed by $\text{FeBr}_2 + \text{dpbz}$ at concentrations of dpbz between 2.00 mM and 20.0 mM.

13 Crystallographic data

Crystals of each compound included in this section could be grown as described in sections 2.1, 4, 7 and 11. X-ray diffraction experiments for all of the compounds were carried out at 100(2) K, or 240(2) K (**7a**) or 200(2) K (**12b**, **12h**, **20**, **23**) on a Bruker APEX II diffractometer using Mo-K α radiation ($\lambda = 0.71073 \text{ \AA}$) apart from complex $[(\text{dmbz})_2\text{Fe}(\mu\text{-Br})_2\text{FeBr}_2]$ (**8**) which was analysed on a Bruker Proteum Microstar diffractometer using Cu-K α radiation ($\lambda = 1.54178 \text{ \AA}$) at 200(2) K. Data collections were performed using a CCD area detector from a single crystal mounted on a glass capillary. Intensities were integrated⁴² and absorption corrections based on equivalent reflections were applied using SADABS.⁴³ The structures were all solved using SHELXT,⁴⁴ apart from $\text{FeBr}_2(\text{dpbz})_2$ (**7a**) and $[\text{ZnBr}_2(\text{dpbz})]$ (**12a**) which was solved using Superflip,^{45,46} and refined against all F^2 in SHELXL^{47,48} using Olex 2.⁴⁹ All of the non-hydrogen atoms were refined anisotropically while the hydrogen atoms were located geometrically and refined using a riding model unless otherwise detailed under the specific details for each structure. If appropriate, additional refinement details for specific structures are detailed below and crystal structure and refinement data are given in Supplementary Table 17 to Supplementary Table 23. Crystallographic data for the compounds have been deposited with the Cambridge Crystallographic Data Centre as supplementary publication CCDC 1836928-1836960. Copies of the data can be obtained free of charge on application to CCDC, 12 Union Road, Cambridge CB2 1EZ, UK (fax(+44) 1223 336033, e-mail: deposit@ccdc.cam.ac.uk).

13.1 Specific refinement details

[FeBr₂(dpbz)] (4a). The THF solvent molecule in the lattice displayed disorder in two of the carbon atoms over two positions. The occupancies of the two positions were refined with the sum set to equal 1, resulting in relative occupancies of 63:37 for the two parts. Restraints were applied to maintain similar bond lengths for the two parts and similar anisotropic displacement parameters for the atoms in the THF.

[FeBr₂(dpth)] (4b). The molecule displayed disorder in two of the phenyl rings, the sum of the occupancies of each of the phenyl rings were set to equal 1 and refined. Both phenyl rings refined to similar values and were subsequently linked to the same free variable with refined occupancies of 78:22. Restraints were applied to maintain sensible anisotropic displacement parameters. The CH_2Cl_2 in the lattice was also disordered over three positions, the sum of the occupancies of the three parts was set to equal 1 and refined to 48:37:15. Restraints were applied to the C-Cl distances and the anisotropic displacement parameters to maintain sensible values.

[FeBr₂(norphos)] (4e). The cage C13-C19 was disordered across a symmetry element so the occupancies were necessarily fixed at 50%. Restraints were applied to maintain sensible C-C distances and anisotropic displacement parameters. Disorder was also identified in one of the phenyl rings, the sum of the occupancies was set to equal 1 and refined to 74:26. The carbon atoms were refined as a rigid group. Restraints were applied to the P-C distances and the anisotropic displacement parameters to maintain sensible values. The Squeeze routine within Platon^{50,51} was used to remove disordered solvent in the lattice that could not be sensibly modelled.

[{FeBr₂(μ²-dppe)}_n] (5). One of the phenyl rings, one of the Br atom positions and one of the CH₂Cl₂ molecules displayed disorder. In all cases the sum of the occupancies of the two parts were set to equal 1 and refined to ~50:50 (phenyl ring), 94:6 (Br) and 88:13 (CH₂Cl₂). Restraints and constraints were applied to maintain sensible thermal and geometric parameters for the disordered atoms.

[ZnBr₂(dpbz)] (12a). The toluene was disordered across a symmetry element; the occupancies were therefore necessarily fixed at 50%.

[ZnBr₂(dpth)] (12b). The Squeeze routine within Platon^{50,51} was used to remove disordered solvent in the lattice that could not be sensibly modelled.

[ZnBr₂(sciopp)] (12c). Three of the *tert*-Butyl groups were found to be disordered over two positions. The occupancies of the pairs of *tert*-butyl carbon atoms were refined with their sum set to equal 1 and refined to 87:13, 63:37 and 60:40. Restraints were applied to maintain sensible C-C distances and anisotropic displacement parameters for the disordered atoms. The Squeeze routine within Platon^{50,51} was used to remove disordered solvent in the lattice that could not be sensibly modelled.

[ZnBr₂(dmbz)] (12h). The solvent THF in the lattice was found to be disordered over three positions and across a symmetry element. The occupancies of the 3 sites were refined with their sum set to equal 1 giving values of 375:375:250. Restraints were applied to maintain sensible geometric and thermal parameters.

[{ZnBr₂(μ-*trans*-dppe)}₂] (13). The data were twinned and refined against an hklf 5 format hkl file. The twin scale factor refined to 16.1(2) %. The THF in the lattice was found to be disordered over two positions across a symmetry element and the occupancies were necessarily fixed at 50%. Restraints and constraints were applied to maintain sensible thermal and geometric parameters.

[ZnBr(4-tolyl)(dpbz)] (15a). The THF in the lattice was disordered over two positions. The occupancies were refined with their sum set to equal 1. Restraints were applied to maintain sensible thermal and geometric parameters.

[Zn(4-tolyl)₂(dpbz)] (16a). The chloroform in the lattice was found to be disordered across a symmetry element. The occupancies were necessarily fixed at 50%. Restraints were applied to maintain sensible geometric parameters.

[Mg(THF)₆][FeBr₃(THF)]₂ (20). Disorder was identified in the THF molecule coordinated to the Fe centre and the occupancies of the disordered atoms were refined with the sum set to equal 1. The refined values were 58:42 and restraints were applied to the bond lengths around the ring and also the anisotropic displacement parameters. The free THF in the lattice was also disordered over two positions across a symmetry element, the occupancies were fixed at 50% and restraints were applied to both bond lengths and anisotropic displacement parameters. The anisotropic displacement parameters for the free THF are slightly larger than ideal and it is likely that there is either further disorder that could not be sensibly modelled or the total occupancy of the THF is currently slightly high.

[MgBr(2-MeTHF)₃(THF)][Fe₂Br₆] (21). Disorder was identified in two of the THF molecules coordinated to the Mg centre and the occupancies of the disordered atoms were refined with their sums set to equal 1. The refined occupancies were 58:42, 89:11 and 78:22. Restraints and constraints were applied to maintain sensible geometric parameters and anisotropic displacement parameters.

[Fe(THF)₂{(μ -Br)₂Zn(4-tolyl)(THF)}₂] (23). The zinc atom and coordinated THF were found to be disordered over two positions. The sum of the occupancies was set to 1 and refined to 0.69:0.31 while restraints were applied to the geometric parameters to maintain sensible values. Restraints and constraints were applied to the anisotropic displacement parameters to maintain sensible values as well.

[MgBr(THF)₅][{ZnBr(4-tolyl)(μ -Br)}₂] (24). The Br1 atom was found to be disordered over two positions, the occupancies refined to 87:13 and the anisotropic displacement parameters for the two positions were constrained to be identical.

13.2 Tables of crystal data and structure refinement

Supplementary Table 17: Crystal data and structure refinement for Zn(4-tolyl)₂ (**Mg-free 2**), [FeBr₂(dpbz)] (**4a**), [FeBr₂(dpth)] (**4b**), [FeBr₂(MeDuphos)] (**4c**) and [FeBr₂(dppp)] (**4d**).

Compound	Zn(4-tolyl) ₂ (Mg-free 2a)	[FeBr ₂ (dpbz)] (4a)	[FeBr ₂ (dpth)] (4b)	[FeBr ₂ (MeDuphos)] (4c)	[FeBr ₂ (dppp)] (4d)
Empirical formula	C ₁₄ H ₁₄ Zn	C ₃₄ H ₃₂ Br ₂ FeOP ₂	C ₂₉ H ₂₄ Br ₂ Cl ₂ FeP ₂ S	C ₁₈ H ₂₈ Br ₂ FeP ₂	C ₂₇ H ₂₆ Br ₂ FeP ₂
Formula weight	247.62	734.20	753.05	522.01	628.09
Temperature/K	100(2)	100(2)	100(2)	100(2)	100(2)
Crystal system	monoclinic	triclinic	monoclinic	monoclinic	monoclinic
Space group	P2 ₁ /c	P-1	P2 ₁ /n	P2 ₁	P2 ₁ /n
a/Å	9.7313(3)	9.3634(2)	11.7937(2)	14.0539(4)	9.5111(2)
b/Å	4.91110(10)	10.1562(2)	22.5640(4)	9.7474(2)	15.8439(4)
c/Å	11.4464(4)	18.5426(3)	11.9402(2)	17.0496(4)	17.1007(4)
$\alpha/^\circ$	90	100.0110(10)	90	90	90
$\beta/^\circ$	91.470(2)	96.9930(10)	100.3170(10)	112.3236(13)	93.572(2)
$\gamma/^\circ$	90	110.7150(10)	90	90	90
Volume/Å ³	546.86(3)	1591.76(5)	3126.07(9)	2160.56(9)	2571.95(10)
Z	2	2	4	4	4
$\rho_{\text{calcd}}/\text{cm}^3$	1.504	1.532	1.600	1.605	1.622
μ/mm^{-1}	2.205	3.110	3.397	4.542	3.832
F(000)	256.0	740.0	1496.0	1048.0	1256.0
Crystal size/mm ³	0.63 × 0.522 × 0.298	0.39 × 0.132 × 0.072	0.31 × 0.295 × 0.16	0.466 × 0.393 × 0.206	0.505 × 0.497 × 0.298
Radiation	MoKα ($\lambda = 0.71073$)	MoKα ($\lambda = 0.71073$)	MoKα ($\lambda = 0.71073$)	MoKα ($\lambda = 0.71073$)	MoKα ($\lambda = 0.71073$)
2θ range for data collection/°	4.186 to 55.004	4.41 to 55.148	3.948 to 55.138	2.582 to 55.242	3.508 to 55.012
Index ranges	-12 ≤ h ≤ 12, -6 ≤ k ≤ 6, -14 ≤ l ≤ 14	-12 ≤ h ≤ 12, -13 ≤ k ≤ 13, -24 ≤ l ≤ 24	-15 ≤ h ≤ 15, -28 ≤ k ≤ 29, -15 ≤ l ≤ 15	-18 ≤ h ≤ 18, -12 ≤ k ≤ 12, -22 ≤ l ≤ 22	-12 ≤ h ≤ 11, -20 ≤ k ≤ 20, -22 ≤ l ≤ 22
Reflections collected	8916	28343	55033	77156	44666
R _{int} / R _{sigma}	0.0122 / 0.0072	0.0238 / 0.0226	0.0397 / 0.0242	0.0257 / 0.0144	0.0230 / 0.0131
Data/restraints/parameters	1258/0/71	7354/79/380	7235/409/464	10029/1/423	5898/0/289
Goodness-of-fit on F ²	1.166	1.033	1.126	1.028	1.035
Final R indexes [$ I >= 2\sigma(I)$]	R ₁ = 0.0176, wR ₂ = 0.0466	R ₁ = 0.0262, wR ₂ = 0.0623	R ₁ = 0.0413, wR ₂ = 0.0980	R ₁ = 0.0169, wR ₂ = 0.0406	R ₁ = 0.0178, wR ₂ = 0.0410
Final R indexes [all data]	R ₁ = 0.0184, wR ₂ = 0.0469	R ₁ = 0.0326, wR ₂ = 0.0649	R ₁ = 0.0517, wR ₂ = 0.1021	R ₁ = 0.0175, wR ₂ = 0.0408	R ₁ = 0.0216, wR ₂ = 0.0421
Largest diff. peak/hole / e Å ⁻³	0.37/-0.27	0.63/-0.54	0.84/-1.01	0.41/-0.22	0.38/-0.21
Flack parameter	-	-	-	0.005(3)	-

Supplementary Table 18: Crystal data and structure refinement for [FeBr₂(norphos)] (**4e**), [FeBr₂(*cis*-dppen)] (**4f**), [FeBr₂(*iPrDuphos*)] (**4g**), [{FeBr₂(μ²-dppe)}_n] (**5**) and [{FeBr₂(μ-*trans*-dppen)}₂] (**6**).

Compound	[FeBr ₂ (norphos)] (4e)	[FeBr ₂ (<i>cis</i> -dppen)] (4f)	[FeBr ₂ (<i>iPrDuphos</i>)] (4g)	[{FeBr ₂ (μ ² -dppe)} _n] (5)	[{FeBr ₂ (μ- <i>trans</i> -dppen)} ₂] (6)
Empirical formula	C ₃₁ H ₂₉ Br ₂ FeP ₂	C ₂₆ H ₂₂ Br ₂ FeP ₂	C ₂₆ H ₄₄ Br ₂ FeP ₂	C ₂₈ H ₂₈ Br ₂ Cl ₄ FeP ₂	C ₅₄ H ₄₈ Br ₄ Cl ₄ Fe ₂ P ₄
Formula weight	678.14	612.04	634.22	783.91	1393.94
Temperature/K	100(2)	100(2)	100(2)	100(2)	100(2)
Crystal system	hexagonal	monoclinic	orthorhombic	monoclinic	triclinic
Space group	<i>P</i> 6 ₂	<i>P</i> 2 ₁ / <i>m</i>	<i>P</i> 2 ₁ 2 ₁	<i>P</i> 2 ₁ / <i>c</i>	<i>P</i> -1
<i>a</i> /Å	18.503(2)	7.6048(2)	9.3258(8)	14.3401(14)	10.2256(3)
<i>b</i> /Å	18.503(2)	18.9975(5)	15.1966(12)	16.4378(15)	12.4439(3)
<i>c</i> /Å	10.1266(14)	8.4442(2)	20.2410(16)	15.0242(15)	13.1152(3)
<i>α</i> /°	90	90	90	90	64.7110(10)
<i>β</i> /°	90	100.665(2)	90	116.761(2)	88.7250(10)
<i>γ</i> /°	120	90	90	90	69.4670(10)
Volume/Å ³	3002.6(8)	1198.88(5)	2868.6(4)	3162.2(5)	1396.93(6)
Z	3	2	4	4	1
ρ _{calc} g/cm ³	1.125	1.695	1.469	1.647	1.657
μ/mm ⁻¹	2.466	4.108	3.435	3.461	3.721
F(000)	1020.0	608.0	1304.0	1560.0	692.0
Crystal size/mm ³	0.515 × 0.42 × 0.348	0.374 × 0.18 × 0.078	0.609 × 0.458 × 0.439	0.6 × 0.472 × 0.344	0.356 × 0.324 × 0.318
Radiation	MoKα (λ = 0.71073)	MoKα (λ = 0.71073)	MoKα (λ = 0.71073)	MoKα (λ = 0.71073)	MoKα (λ = 0.71073)
2θ range for data collection/°	4.402 to 51.35 -22 ≤ <i>h</i> ≤ 22, -22 ≤ <i>k</i> ≤ 22, -12 ≤ <i>l</i> ≤ 12	4.288 to 55.04 -9 ≤ <i>h</i> ≤ 9, -24 ≤ <i>k</i> ≤ 24, -10 ≤ <i>l</i> ≤ 10	3.352 to 55.154 -12 ≤ <i>h</i> ≤ 12, -19 ≤ <i>k</i> ≤ 19, -26 ≤ <i>l</i> ≤ 26	3.918 to 55.036 -18 ≤ <i>h</i> ≤ 18, -21 ≤ <i>k</i> ≤ 21, -19 ≤ <i>l</i> ≤ 19	3.474 to 55.25 -13 ≤ <i>h</i> ≤ 13, -16 ≤ <i>k</i> ≤ 16, -16 ≤ <i>l</i> ≤ 17
Reflections collected	93171	21244	101491	27327	24576
R _{int} / R _{sigma}	0.0342 / 0.0102	0.0273 / 0.0161	0.0224 / 0.0081	0.0314 / 0.0291	0.0143 / 0.0130
Data/restraints/parameters	3807/352/226	2836/0/145	6615/0/288	7261/247/400	6455/0/307
Goodness-of-fit on F ²	1.019	1.055	1.118	1.037	1.160
Final R indexes [<i>I</i> >=2σ (<i>I</i>)]	R ₁ = 0.0279, wR ₂ = 0.0708	R ₁ = 0.0181, wR ₂ = 0.0399	R ₁ = 0.0121, wR ₂ = 0.0299	R ₁ = 0.0332, wR ₂ = 0.0778	R ₁ = 0.0220, wR ₂ = 0.0517
Final R indexes [all data]	R ₁ = 0.0299, wR ₂ = 0.0720	R ₁ = 0.0215, wR ₂ = 0.0411	R ₁ = 0.0123, wR ₂ = 0.0300	R ₁ = 0.0407, wR ₂ = 0.0808	R ₁ = 0.0235, wR ₂ = 0.0521
Largest diff. peak/hole / e Å ⁻³	0.39/-0.25	0.38/-0.26	0.24/-0.20	1.13/-0.86	0.57/-0.30
Flack parameter	0.004(3)	-	-0.0023(12)	-	-

Supplementary Table 19: Crystal data and structure refinement for [FeBr₂(dpbz)₂] (**7a**), [FeBr₂(dmbz)₂] (**7b**), [(dmbz)₂Fe(μ-Br)₂FeBr₂] (**8**), [ZnBr₂(dpbz)] (**12a**) and [ZnBr₂(dpth)] (**12b**).

Compound	[FeBr ₂ (dpbz) ₂] (7a)	[FeBr ₂ (dmbz) ₂] (7b)	[(dmbz) ₂ Fe(μ-Br) ₂ FeBr ₂] (8)	[ZnBr ₂ (dpbz)] (12a)	[ZnBr ₂ (dpth)] (12b)
Empirical formula	C ₆₀ H ₄₈ Br ₂ FeP ₄	C ₂₀ H ₃₂ Br ₂ FeP ₄	C ₂₁ H ₃₄ Br ₄ Cl ₂ Fe ₂ P ₄	C _{33.5} H ₂₈ Br ₂ P ₂ Zn	C ₂₈ H ₂₂ Br ₂ P ₂ SZn
Formula weight	1108.53	612.00	912.60	71.69	677.64
Temperature/K	240(2)	100(2)	200(2)	100(2)	200(2)
Crystal system	monoclinic	monoclinic	monoclinic	triclinic	triclinic
Space group	P2 ₁ /n	P2 ₁ /n	C2/c	P-1	P-1
a/Å	11.0317(2)	9.0697(2)	12.6109(18)	9.3305(3)	9.3840(2)
b/Å	12.7696(3)	8.7187(2)	15.334(2)	10.0923(3)	10.0199(2)
c/Å	18.0365(5)	15.1999(3)	16.894(2)	17.3404(6)	17.2184(4)
α/°	90	90	90	83.930(2)	81.8150(10)
β/°	92.7928(17)	96.4570(10)	102.963(4)	83.701(2)	79.9890(10)
γ/°	90	90	90	69.116(2)	69.2600(10)
Volume/Å ³	2537.79(10)	1194.32(4)	3183.5(8)	1512.49(9)	1485.27(6)
Z	2	2	4	1	2
ρ _{calc} g/cm ³	1.451	1.702	1.904	1.576	1.515
μ/mm ⁻¹	2.037	4.250	16.725	3.581	3.709
F(000)	1128.0	616.0	1784.0	718.0	672.0
Crystal size/mm ³	0.407 × 0.192 × 0.156	0.383 × 0.179 × 0.174	0.275 × 0.255 × 0.184	0.543 × 0.262 × 0.194	0.616 × 0.4 × 0.371
Radiation	MoKα (λ = 0.71073)	MoKα (λ = 0.71073)	CuKα (λ = 1.54178)	MoKα (λ = 0.71073)	MoKα (λ = 0.71073)
2θ range for data collection/°	3.91 to 55.938	4.996 to 55.244	9.222 to 133.874	4.33 to 56.116	4.684 to 55.062
Index ranges	-12 ≤ h ≤ 14, -16 ≤ k ≤ 15, -20 ≤ l ≤ 23	-11 ≤ h ≤ 11, -11 ≤ k ≤ 11, -19 ≤ l ≤ 19	-14 ≤ h ≤ 15, -13 ≤ k ≤ 18, -18 ≤ l ≤ 20	-12 ≤ h ≤ 12, -13 ≤ k ≤ 13, -22 ≤ l ≤ 22	-12 ≤ h ≤ 11, -13 ≤ k ≤ 13, -22 ≤ l ≤ 22
Reflections collected	22913	20482	17920	28215	26468
R _{int} / R _{sigma}	0.0503 / 0.0514	0.0184 / 0.0106	0.0646 / 0.0402	0.0238 / 0.0225	0.0185 / 0.0166
Data/restraints/parameters	6088/0/304	2784/0/128	2817/0/155	7297/0/379	6845/0/307
Goodness-of-fit on F ²	1.016	1.062	1.035	1.039	1.036
Final R indexes [I>=2σ (I)]	R ₁ = 0.0377, wR ₂ = 0.0707	R ₁ = 0.0186, wR ₂ = 0.0491	R ₁ = 0.0602, wR ₂ = 0.1653	R ₁ = 0.0244, wR ₂ = 0.0603	R ₁ = 0.0220, wR ₂ = 0.0553
Final R indexes [all data]	R ₁ = 0.0629, wR ₂ = 0.0784	R ₁ = 0.0200, wR ₂ = 0.0496	R ₁ = 0.0615, wR ₂ = 0.1672	R ₁ = 0.0312, wR ₂ = 0.0629	R ₁ = 0.0269, wR ₂ = 0.0571
Largest diff. peak/hole / e Å ⁻³	0.39/-0.52	0.51/-0.40	1.31/-1.42	0.91/-0.77	0.48/-0.39
Flack parameter	-	-	-	-	-

Supplementary Table 20: Crystal data and structure refinement for [ZnBr₂(sciopp)] (**12c**), [ZnBr₂(iPrDuphos)] (**12d**), [ZnBr₂(*cis*-dppen)] (**12e**), [ZnBr₂(dppp)] (**12f**) and [ZnBr₂(morphos)] (**12g**).

Compound	[ZnBr ₂ (sciopp)] (12c)	[ZnBr ₂ (iPrDuphos)] (12d)	[ZnBr ₂ (<i>cis</i> -dppen)] (12e)	[ZnBr ₂ (dppp)] (12f)	[ZnBr ₂ (morphos)] (12g)
Empirical formula	C ₆₂ H ₈₈ Br ₂ P ₂ Zn	C ₂₆ H ₄₄ Br ₂ P ₂ Zn	C ₂₆ H ₂₂ Br ₂ P ₂ Zn	C ₂₇ H ₂₆ Br ₂ P ₂ Zn	C ₃₂ H ₃₀ Br ₂ Cl ₂ P ₂ Zn
Formula weight	1120.45	643.74	621.56	637.61	772.59
Temperature/K	100(2)	100(2)	100(2)	100(2)	100(2)
Crystal system	monoclinic	orthorhombic	monoclinic	monoclinic	orthorhombic
Space group	C ₂ /c	P ₂ ₁ 2 ₁ 2 ₁	P ₂ ₁ /m	P ₂ ₁ /n	P ₂ ₁ 2 ₁ 2 ₁
a/Å	27.2207(6)	9.3230(7)	7.6072(4)	9.5796(7)	10.0172(2)
b/Å	19.8006(4)	15.2142(12)	18.9050(9)	15.7374(11)	16.1729(4)
c/Å	24.5953(5)	20.1478(16)	8.4230(4)	17.1338(13)	19.2813(5)
α/°	90	90	90	90	90
β/°	104.1110(10)	90	100.656(3)	94.0090(10)	90
γ/°	90	90	90	90	90
Volume/Å ³	12856.5(5)	2857.8(4)	1190.46(10)	2576.7(3)	3123.71(13)
Z	8	4	2	4	4
ρ _{calc} g/cm ³	1.158	1.496	1.734	1.644	1.643
μ/mm ⁻¹	1.708	3.780	4.535	4.192	3.640
F(000)	4720.0	1320.0	616.0	1272.0	1544.0
Crystal size/mm ³	0.467 × 0.461 × 0.336	0.516 × 0.428 × 0.298	0.292 × 0.27 × 0.269	0.665 × 0.467 × 0.312	0.446 × 0.316 × 0.214
Radiation	MoKα (λ = 0.71073)				
2θ range for data collection/°	3.962 to 55.112 -35 ≤ h ≤ 35, -25 ≤ k ≤ 25, -31 ≤ l ≤ 31	3.354 to 55.126 -12 ≤ h ≤ 12, -19 ≤ k ≤ 19, -25 ≤ l ≤ 26	4.31 to 55.104 -9 ≤ h ≤ 9, -24 ≤ k ≤ 24, -10 ≤ l ≤ 10	4.736 to 54.924 -12 ≤ h ≤ 8, -20 ≤ k ≤ 20, -22 ≤ l ≤ 21	4.582 to 55.214 -13 ≤ h ≤ 13, -21 ≤ k ≤ 21, -25 ≤ l ≤ 25
Reflections collected	112540	50325	20921	22163	111181
R _{int} / R _{sigma}	0.0410 / 0.0247	0.0272 / 0.0156	0.0235 / 0.0132	0.0267 / 0.0247	0.0257 / 0.0098
Data/restraints/parameters	14820/252/706	6569/0/288	2824/0/145	5902/0/289	7227/0/352
Goodness-of-fit on F ²	1.021	1.045	1.068	1.031	1.107
Final R indexes [I>=2σ (I)]	R ₁ = 0.0344, wR ₂ = 0.0846	R ₁ = 0.0141, wR ₂ = 0.0310	R ₁ = 0.0220, wR ₂ = 0.0567	R ₁ = 0.0201, wR ₂ = 0.0435	R ₁ = 0.0205, wR ₂ = 0.0553
Final R indexes [all data]	R ₁ = 0.0481, wR ₂ = 0.0911	R ₁ = 0.0153, wR ₂ = 0.0313	R ₁ = 0.0234, wR ₂ = 0.0573	R ₁ = 0.0252, wR ₂ = 0.0448	R ₁ = 0.0211, wR ₂ = 0.0555
Largest diff. peak/hole / e Å ⁻³	1.16/-1.10	0.26/-0.17	0.91/-0.52	0.33/-0.32	0.40/-0.66
Flack parameter	-	-0.0075(18)	-	-	0.0008(13)

Supplementary Table 21: Crystal data and structure refinement for [ZnBr₂(dmbz)] (**12h**), [{ZnBr₂(μ -trans-dppen)}₂] (**13**), [ZnBr(4-tolyl)(dpbz)] (**15a**), [Zn(4-tolyl)₂(dpbz)] (**16a**) and [Zn(4-tolyl)₂(*cis*-dppen)] (**16b**).

Compound	[ZnBr ₂ (dmbz)] (12h)	{ZnBr ₂ (μ -trans-dppen)} ₂ (13)	[ZnBr(4-tolyl)(dpbz)] (15a)	[Zn(4-tolyl) ₂ (dpbz)] (16a)	[Zn(4-tolyl) ₂ (<i>cis</i> -dppen)] (16b)
Empirical formula	C ₁₄ H ₂₄ Br ₂ OP ₂ Zn	C ₅₆ H ₅₀ Br ₄ OP ₄ Zn ₂	C ₄₁ H ₃₉ BrOP ₂ Zn	C _{44.5} H _{38.5} Cl _{1.5} P ₂ Zn	C ₄₀ H ₃₆ P ₂ Zn
Formula weight	495.46	1313.22	754.94	753.74	644.00
Temperature/K	200(2)	100(2)	100(2)	100(2)	100(2)
Crystal system	orthorhombic	monoclinic	monoclinic	monoclinic	monoclinic
Space group	<i>Pnma</i>	<i>C2/c</i>	<i>P2₁/c</i>	<i>P2₁/n</i>	<i>C2/c</i>
<i>a</i> /Å	16.4278(3)	22.9831(8)	16.6539(6)	10.8092(4)	18.5804(9)
<i>b</i> /Å	10.0759(2)	12.6681(4)	12.6983(5)	21.8902(8)	7.9589(4)
<i>c</i> /Å	12.1134(2)	21.4872(7)	17.5103(6)	15.9922(6)	23.1437(14)
$\alpha/^\circ$	90	90	90	90	90
$\beta/^\circ$	90	118.055(2)	107.972(2)	94.679(2)	111.327(2)
$\gamma/^\circ$	90	90	90	90	90
Volume/Å ³	2005.07(6)	5520.9(3)	3522.3(2)	3771.4(2)	3188.1(3)
<i>Z</i>	4	4	4	4	4
$\rho_{\text{calc}}/\text{g/cm}^3$	1.641	1.580	1.424	1.327	1.342
μ/mm^{-1}	5.364	3.917	1.954	0.873	0.899
F(000)	984.0	2616.0	1552.0	1564.0	1344.0
Crystal size/mm ³	0.672 × 0.443 × 0.303	0.311 × 0.211 × 0.194	0.6 × 0.21 × 0.112	0.6 × 0.579 × 0.532	0.371 × 0.352 × 0.154
Radiation	MoKα ($\lambda = 0.71073$)	MoKα ($\lambda = 0.71073$)	MoKα ($\lambda = 0.71073$)	MoKα ($\lambda = 0.71073$)	MoKα ($\lambda = 0.71073$)
2θ range for data collection/°	4.178 to 55.14	3.79 to 55.088	4.034 to 54.968	3.16 to 55.992	4.706 to 55.124
Index ranges	-21 ≤ <i>h</i> ≤ 21, -13 ≤ <i>k</i> ≤ 13, -15 ≤ <i>l</i> ≤ 15	-29 ≤ <i>h</i> ≤ 26, -16 ≤ <i>k</i> ≤ 16, -21 ≤ <i>l</i> ≤ 27	-21 ≤ <i>h</i> ≤ 21, -16 ≤ <i>k</i> ≤ 16, -21 ≤ <i>l</i> ≤ 22	-14 ≤ <i>h</i> ≤ 14, -28 ≤ <i>k</i> ≤ 28, -21 ≤ <i>l</i> ≤ 18	-24 ≤ <i>h</i> ≤ 24, -10 ≤ <i>k</i> ≤ 10, -30 ≤ <i>l</i> ≤ 30
Reflections collected	34280	6341	30737	68017	27447
R _{int} / R _{sigma}	0.0351 / 0.0144	0.0390 / 0.0261	0.0561 / 0.0589	0.0392 / 0.0227	0.0251 / 0.0145
Data/restraints/parameters	2453/224/146	6341/35/310	8071/165/456	9013/3/462	3689/42/196
Goodness-of-fit on F ²	1.063	1.156	0.854	1.038	1.110
Final R indexes [<i>I</i> >=2σ (<i>I</i>)]	R ₁ = 0.0318, wR ₂ = 0.0842	R ₁ = 0.0453, wR ₂ = 0.1168	R ₁ = 0.0398, wR ₂ = 0.1139	R ₁ = 0.0370, wR ₂ = 0.0980	R ₁ = 0.0349, wR ₂ = 0.0945
Final R indexes [all data]	R ₁ = 0.0398, wR ₂ = 0.0890	R ₁ = 0.0500, wR ₂ = 0.1184	R ₁ = 0.0617, wR ₂ = 0.1297	R ₁ = 0.0493, wR ₂ = 0.1045	R ₁ = 0.0367, wR ₂ = 0.0955
Largest diff. peak/hole / e Å ⁻³	0.65/-0.78	1.02/-1.17	0.88/-0.72	0.62/-0.60	1.26/-0.40
Flack Parameter	-	-	-	-	-

Supplementary Table 22: Crystal data and structure refinement for $[\text{ZnPh}_2(\text{dppp})]$ (**16c**), $\{[\text{ZnPh}_2(\mu\text{-dppe})]_n\}$ (**17**), $[(\text{dmbz})_2\text{Fe}(\mu\text{-Br})_2\text{ZnBr}_2]$ (**18**), $[\text{Mg}(\text{THF})_6][\text{FeBr}_3]_2$ (**20**) and $[\text{MgBr}(\text{THF})(2\text{-MeTHF})_3][\text{Fe}_2\text{Br}_6]$ (**21**).

Compound	$[\text{ZnPh}_2(\text{dppp})]$ (16c)	$\{[\text{ZnPh}_2(\mu\text{-dppe})]_n\}$ (17)	$[(\text{dmbz})_2\text{Fe}(\mu\text{-Br})_2\text{ZnBr}_2]$ (18)	$[\text{Mg}(\text{THF})_6][\text{FeBr}_3]_2$ (20)	$[\text{MgBr}(\text{THF})(2\text{-MeTHF})_3][\text{Fe}_2\text{Br}_6]$ (21)
Empirical formula	$\text{C}_{39}\text{H}_{36}\text{P}_2\text{Zn}$	$\text{C}_{38}\text{H}_{34}\text{P}_2\text{Zn}$	$\text{C}_{20}\text{H}_{32}\text{Br}_4\text{FeP}_4\text{Zn}$	$\text{C}_{36}\text{H}_{72}\text{Br}_6\text{Fe}_2\text{MgO}_9$	$\text{C}_{38}\text{H}_{76}\text{Br}_8\text{Fe}_2\text{Mg}_2\text{O}_8$
Formula weight	631.99	617.96	837.19	1264.40	1460.58
Temperature/K	100(2)	100(2)	100(2)	200(2)	100(2)
Crystal system	monoclinic	triclinic	monoclinic	monoclinic	monoclinic
Space group	$P2_1/n$	$P-1$	$C2/c$	$C2/c$	$P2_1/c$
$a/\text{\AA}$	10.1851(5)	10.6785(5)	14.3827(4)	16.1245(4)	13.6591(4)
$b/\text{\AA}$	16.1790(7)	12.5107(6)	11.2990(4)	12.4410(3)	10.2503(3)
$c/\text{\AA}$	19.4108(9)	14.4745(7)	18.4404(7)	25.1083(6)	19.6297(6)
$\alpha/^\circ$	90	114.529(3)	90	90	90
$\beta/^\circ$	95.597(3)	90.482(3)	112.253(3)	95.5540(10)	98.715(2)
$\gamma/^\circ$	90	114.197(3)	90	90	90
Volume/ \AA^3	3183.4(3)	1567.05(14)	2773.55(17)	5013.2(2)	2716.62(14)
Z	4	2	4	4	2
$\rho_{\text{calc}}/\text{cm}^3$	1.319	1.310	2.005	1.675	1.786
μ/mm^{-1}	0.899	0.911	7.390	5.417	6.483
F(000)	1320.0	644.0	1632.0	2536.0	1448.0
Crystal size/mm ³	$0.458 \times 0.357 \times 0.352$	$0.335 \times 0.238 \times 0.159$	$0.265 \times 0.134 \times 0.085$	$0.538 \times 0.444 \times 0.184$	$0.575 \times 0.323 \times 0.264$
Radiation	MoK α ($\lambda = 0.71073$)	MoK α ($\lambda = 0.71073$)	MoK α ($\lambda = 0.71073$)	MoK α ($\lambda = 0.71073$)	MoK α ($\lambda = 0.71073$)
2 θ range for data collection/ $^\circ$	3.284 to 55.144 -13 \leq h \leq 13, -20 \leq k \leq 20, -25 \leq l \leq 24	3.168 to 55.798 -14 \leq h \leq 14, -16 \leq k \leq 16, -19 \leq l \leq 19	4.728 to 55.226 -18 \leq h \leq 18, - 14 \leq k \leq 14, -23 \leq l \leq 23	3.26 to 55.052 -15 \leq h \leq 20, -16 \leq k \leq 15, -32 \leq l \leq 32	4.198 to 55.052 -17 \leq h \leq 17, -13 \leq k \leq 13, -24 \leq l \leq 25
Reflections collected	55010	27550	24070	32397	42530
$R_{\text{int}} / R_{\sigma\text{igma}}$	0.0258 / 0.0150	0.0551 / 0.0564	0.0497 / 0.0257	0.0318 / 0.0232	0.0355 / 0.0222
Data/restraints/parameters	7330/0/379	7467/0/370	3205/0/141	5775/195/302	6252/142/310
Goodness-of-fit on F^2	1.035	1.025	1.049	1.038	1.030
Final R indexes [$ I >= 2\sigma(I)$]	$R_1 = 0.0243$, $wR_2 = 0.0606$	$R_1 = 0.0372$, $wR_2 = 0.0744$	$R_1 = 0.0239$, $wR_2 = 0.0529$	$R_1 = 0.0381$, $wR_2 = 0.0892$	$R_1 = 0.0284$, $wR_2 = 0.0650$
Final R indexes [all data]	$R_1 = 0.0288$, $wR_2 = 0.0627$	$R_1 = 0.0573$, $wR_2 = 0.0811$	$R_1 = 0.0323$, $wR_2 = 0.0554$	$R_1 = 0.0541$, $wR_2 = 0.0975$	$R_1 = 0.0385$, $wR_2 = 0.0684$
Largest diff. peak/hole / e \AA^{-3}	0.60/-0.25	0.45/-0.36	0.64/-0.42	0.78/-0.58	0.99/-0.90
Flack parameter	-	-	-	-	-

Supplementary Table 23: Crystal data and structure refinement for $[(\text{THF})_4\text{Fe}(\mu\text{-Br}_2)\text{ZnBr}_2]$ (22), $[\text{Fe}(\text{THF})_2\{(\mu\text{-Br})_2\text{Zn}(4\text{-tolyl})(\text{THF})\}_2]$ (23), $[\text{Fe}(\text{mes})_2(\text{dpbz})]$ (24), and $[\text{MgBr}(\text{THF})_5]\{[\text{ZnBr}(4\text{-tolyl})(\mu\text{-Br})\}_2\}$ (29).

Compound	$[(\text{THF})_4\text{Fe}(\mu\text{-Br}_2)\text{ZnBr}_2]$ (22)	$[\text{Fe}(\text{THF})_2\{(\mu\text{-Br})_2\text{Zn}(4\text{-tolyl})(\text{THF})\}_2]$ (23)	$[\text{Fe}(\text{mes})_2(\text{dpbz})]$ (24)	$[\text{MgBr}(\text{THF})_5]\{[\text{ZnBr}(4\text{-tolyl})(\mu\text{-Br})\}_2\}$ (29)
Empirical formula	$\text{C}_{16}\text{H}_{32}\text{Br}_4\text{FeO}_4\text{Zn}$	$\text{C}_{30}\text{H}_{46}\text{Br}_4\text{FeO}_4\text{Zn}_2$	$\text{C}_{48}\text{H}_{46}\text{FeP}_2$	$\text{C}_{54}\text{H}_{94}\text{Br}_6\text{Mg}_2\text{O}_{10}\text{Zn}_2$
Formula weight	729.27	976.90	740.64	1562.11
Temperature/K	100(2)	200(2)	100(2)	100(2)
Crystal system	monoclinic	triclinic	triclinic	triclinic
Space group	$P2_1/c$	$P-1$	$P-1$	$P-1$
$a/\text{\AA}$	16.5169(3)	7.9953(2)	10.9171(2)	10.3520(11)
$b/\text{\AA}$	9.8109(2)	11.1216(2)	11.1389(2)	12.3057(12)
$c/\text{\AA}$	16.2491(3)	12.1154(2)	16.8884(4)	13.8393(14)
$\alpha/^\circ$	90	100.5590(10)	91.3980(10)	93.313(5)
$\beta/^\circ$	114.2620(10)	109.0900(10)	101.9070(10)	102.603(5)
$\gamma/^\circ$	90	109.0940(10)	106.1100(10)	112.191(5)
Volume/ \AA^3	2400.53(8)	909.82(3)	1923.31(7)	1573.8(3)
Z	4	1	2	1
$\rho_{\text{calc}}/\text{g/cm}^3$	2.018	1.783	1.279	1.648
μ/mm^{-1}	8.279	6.124	0.509	4.642
F(000)	1424.0	484.0	780.0	792.0
Crystal size/ mm^3	$0.522 \times 0.301 \times 0.197$	$0.601 \times 0.534 \times 0.378$	$0.362 \times 0.251 \times 0.194$	$0.581 \times 0.55 \times 0.399$
Radiation	MoK α ($\lambda = 0.71073$)	MoK α ($\lambda = 0.71073$)	MoK α ($\lambda = 0.71073$)	MoK α ($\lambda = 0.71073$)
2 θ range for data collection/ $^\circ$	4.956 to 55.104 -21 $\leq h \leq 21$, -12 $\leq k \leq 12$, -21 $\leq l \leq 21$	3.762 to 55.15 -10 $\leq h \leq 10$, -14 $\leq k \leq 14$, -15 $\leq l \leq 15$	2.474 to 56.022 -13 $\leq h \leq 14$, -14 $\leq k \leq 14$, -22 $\leq l \leq 22$	3.618 to 55.868 -11 $\leq h \leq 13$, -16 $\leq k \leq 15$, -18 $\leq l \leq 17$
Index ranges				
Reflections collected	41454	16070	35907	28745
$R_{\text{int}} / R_{\text{sigma}}$	0.0266 / 0.0151	0.0224 / 0.0227	0.0367 / 0.0336	0.0244 / 0.0215
Data/restraints/parameters	5535/0/235	4212/163/231	9268/0/466	7530/0/339
Goodness-of-fit on F^2	1.050	1.023	1.022	1.034
Final R indexes [$ I \geq 2\sigma(I)$]	$R_1 = 0.0208$, $wR_2 = 0.0530$	$R_1 = 0.0246$, $wR_2 = 0.0600$	$R_1 = 0.0343$, $wR_2 = 0.0811$	$R_1 = 0.0250$, $wR_2 = 0.0566$
Final R indexes [all data]	$R_1 = 0.0249$, $wR_2 = 0.0544$	$R_1 = 0.0314$, $wR_2 = 0.0631$	$R_1 = 0.0453$, $wR_2 = 0.0863$	$R_1 = 0.0291$, $wR_2 = 0.0582$
Largest diff. peak/hole / e \AA^{-3}	1.26/-0.71	0.79/-0.57	0.44/-0.37	1.49/-1.12
Flack parameter	-	-	-	-

13.3 Selected bond lengths and angles for the Fe and Zn phosphine complexes

Supplementary Table 24: Selected bond lengths (\AA) and angles ($^\circ$) for the phosphine complexes of FeBr_2 .^a

Bond length (\AA) or angle ($^\circ$)	dpth	dpbz	sciopp	Dppn	MeDuphos	iPrDuphos
Fe-P1	2.4298(10)	2.4350(5)	2.4252(8)	2.3980(5)	2.4269(7)	2.4224(5)
Fe-P2	2.4569(10)	2.4192(6)	2.4612(8)	2.3793(5)	2.3992(7)	2.4110(5)
Fe-Br1	2.3537(6)	2.3680(3)	2.3721(5)	2.3672(3)	2.3550(4)	2.3602(3)
Fe-Br2	2.3632(6)	2.3652(3)	2.3533(5)	2.3666(3)	2.3677(5)	2.3724(3)
P1-Fe-P2	82.88(3)	80.899(18)	81.47(3)	84.751(16)	84.10(2)	84.508(16)
	cis-dppen	dppp	dppe	trans-dppen	norphos	dmbz
Fe-P1	2.4390(4)	2.4207(4)	2.4620(7)	2.4464(5)	2.4777(12)	2.2316(4)
Fe-P2	2.4390(4) ^b	2.4148(4)	2.4739(7)	2.4520(2)	2.4777(12) ^b	2.2351(4)
Fe-Br1	2.3539(4)	2.3632(2)	2.3860(5)	2.3729(3)	2.3516(7)	2.47533(18)
Fe-Br2	2.3659(4)	2.3917(2)	2.3812(5)	2.3711(3)	2.3516(7) ^b	2.47533(18) ^b
P1-Fe-P2	81.239(19)	93.983(14)	104.34(2)	100.865(18)	86.85(6)	85.961(16)

^a The values reported for $[\text{FeBr}_2(\text{sciopp})]$ (**4h**) were obtained from the work of Masaharu *et al.*¹⁶ ^b Symmetry related bond lengths.

Supplementary Table 25: Selected bond lengths (\AA) and angles ($^\circ$) for the complexes of ZnBr_2 with various phosphines.^a

Bond length (\AA) or angle ($^\circ$)	dpth	dpbz	sciopp	norphos	iPrDuphos
Zn-P1	2.4436(4)	2.4495(5)	2.4347(3)	2.4751(8)	2.3947(6)
Zn-P2	2.4447(5)	2.4206(5)	2.4459(5)	2.4656(8)	2.4112(6)
Zn-Br1	2.3511(3)	2.3488(3)	2.3391(3)	2.3513(4)	2.3724(3)
Zn-Br2	2.3403(3)	2.3613(3)	2.3447(3)	2.3522(5)	2.3547(3)
P1-Zn-P2	83.166(15)	81.395(18)	82.040(18)	90.41(3)	87.335(19)
	cis-dppen	dppp	dppe	trans-dppen	dmbz
Zn-P1	2.4405(5)	2.4029(5)	2.519(2)	2.4107(14)	2.3855(8)
Zn-P2	2.4405(5) ^b	2.4060(5)	2.502(2)	2.4203(14)	2.3856(7)
Zn-Br1	2.3480(4)	2.4053(3)	2.4372(16)	2.3644(7)	2.3814(6)
Zn-Br2	2.3428(4)	2.3579(3)	2.419(2)	2.3714(8)	2.3301(6)
P1-Zn-P2	82.73(2)	97.054(15)	110.05(8)	105.13(5)	85.53(4)

^a The values reported for the coordination polymer $\{[\text{ZnBr}_2(\mu\text{-dppe})]_n\}$ (**14**) were obtained from the work of Liu *et al.*³² ^b Symmetry related bond lengths.

Supplementary References

- 1 Hoye, T. R., Eklov, B. M. & Voloshin, M. No-D NMR Spectroscopy as a Convenient Method for Titration Organolithium (RLi), RMgX , and LDA Solutions. *Org. Lett.* **6**, 2567-2570 (2004).
- 2 Schwindt, M. A., Lejon, T. & Hegedus, L. S. Improved synthesis of (aminocarbene)chromium(0) complexes with use of C_8K -generated $\text{Cr}(\text{CO})_5$. Multivariate optimization of an organometallic reaction. *Organometallics* **9**, 2814 (1990).
- 3 Clifton, J., Habraken, E. R. M., Pringle, P. G. & Manners, I. Subtle effects of ligand backbone on the efficiency of iron-diphos catalysed Negishi cross-coupling reactions. *Catal. Sci. Technol.* **5**, 4350-4353 (2015).
- 4 Wehman, E., Jastrzebski, J. T. B. H., Ernsting, J.-M., Grove, D. M. & van Koten, G. Structural investigation of aryllithium clusters in solution I. A ^{13}C and ^7Li NMR study of phenyllithium and some methyl-substituted phenyllithium derivatives. *J. Organomet. Chem.* **353**, 133-143 (1988).
- 5 Hatakeyama, T. et al. Iron-catalyzed Suzuki-Miyaura coupling of alkyl halides. *J. Am. Chem. Soc.* **132**, 10674-10676 (2010).
- 6 Fulmer, G. R. et al. NMR Chemical Shifts of Trace Impurities: Common Laboratory Solvents, Organics, and Gases in Deuterated Solvents Relevant to the Organometallic Chemist. *Organometallics* **29**, 2176-2179 (2010).
- 7 Falivene, L. et al. SambVca 2. A Web Tool for Analyzing Catalytic Pockets with Topographic Steric Maps. *Organometallics* **35**, 2286-2293 (2016).
- 8 Gaussian 09, Revision D.01, Frisch, M. J. et al, Gaussian, Inc., Wallingford CT, 2010..
- 9 Perdew, J. P. Density-functional approximation for the correlation energy of the inhomogeneous electron gas. *Phys. Rev. B* **33**, 8822-8824 (1986).
- 10 Becke, A. D. Density-functional exchange-energy approximation with correct asymptotic behavior. *Phys. Rev. A* **38**, 3098-3100 (1988).
- 11 Schäfer, A., Huber, C. & Ahlrichs, R. Fully optimized contracted Gaussian basis sets of triple zeta valence quality for atoms Li to Kr. *J. Chem. Phys.* **100**, 5829-5835 (1994).
- 12 Leininger, T., Nicklass, A., Stoll, H., Dolg, M. & Schwerdtfeger, P. The accuracy of the pseudopotential approximation. II. A comparison of various core sizes for indium pseudopotentials in calculations for spectroscopic constants of InH , InF , and InCl . *J. Chem. Phys.* **105**, 1052-1059 (1996).
- 13 Flener Lovitt, C., Frenking, G. & Girolami, G. S. Donor-Acceptor Properties of Bidentate Phosphines. DFT Study of Nickel Carbonyls and Molecular Dihydrogen Complexes. *Organometallics* **31**, 4122-4132 (2012).
- 14 Newland, R. J. et al. Accessing Alkyl- and Alkenylcyclopentanes from Cr-Catalyzed Ethylene Oligomerization Using 2-Phosphinophosphinine Ligands. *Organometallics* **37**, 1062-1073 (2018).
- 15 Jover, J. et al. Expansion of the Ligand Knowledge Base for Chelating P,P-Donor Ligands (LKB-PP). *Organometallics* **31**, 5302-5306 (2012).
- 16 Hikaru, T. et al. Investigation of Organoiron Catalysis in Kumada-Tamao-Corriu-Type Cross-Coupling Reaction Assisted by Solution-Phase X-ray Absorption Spectroscopy. *Bull. Chem. Soc. Jpn.* **88**, 410-418 (2015).
- 17 Barclay, J. E., Leigh, G. J., Houlton, A. & Silver, J. Mossbauer and preparative studies of some iron(II) complexes of diphosphines. *J. Chem. Soc., Dalton Trans.*, 2865-2870 (1988).
- 18 Bennett, M. A. et al. Coordination and organometallic complexes of iron containing o-phenylenebis(dimethylphosphine) (pdmp). Crystal and molecular structure of $[\text{Fe}(\eta^2\text{-C}_2\text{H}_4)(\text{pdmp})_2]$. *J. Chem. Soc., Dalton Trans.*, 1733-1741 (2000).
- 19 Adams, C. J. et al. Iron(I) in Negishi cross-coupling reactions. *J. Am. Chem. Soc.* **134**, 10333-10336 (2012).
- 20 Newville, M. IFEFFIT : interactive XAFS analysis and FEFF fitting. *J. Synchrotron Radiat.* **8**, 322-324 (2001).
- 21 Ravel, B. & Newville, M. ATHENA, ARTEMIS, HEPHAESTUS: data analysis for X-ray absorption spectroscopy using IFEFFIT. *J. Synchrotron Radiat.* **12**, 537-541 (2005).
- 22 Neese, F. The ORCA program system. *Wiley Interdiscip. Rev. Comput. Mol. Sci.* **2**, 73-78 (2012).
- 23 Becke, A. D. Density functional thermochemistry. III. The role of exact exchange. *J. Chem. Phys.* **98**, 5648-5652 (1993).
- 24 Lee, C., Yang, W. & Parr, R. G. Development of the Colle-Salvetti correlation-energy formula into a functional of the electron density. *Phys. Rev. B* **37**, 785-789 (1988).
- 25 Vosko, S. H., Wilk, L. & Nusair, M. Accurate spin-dependent electron liquid correlation energies for local spin density calculations: a critical analysis. *Can. J. Phys.* **58**, 1200-1211 (1980).
- 26 Stephens, P. J., Devlin, F. J., Chabalowski, C. F. & Frisch, M. J. Ab Initio Calculation of Vibrational Absorption and Circular Dichroism Spectra Using Density Functional Force Fields. *J. Phys. Chem.* **98**, 11623-11627 (1994).
- 27 Lenthe, E. v., Baerends, E. J. & Snijders, J. G. Relativistic regular two - component Hamiltonians. *J. Chem. Phys.* **99**, 4597-4610 (1993).
- 28 Pantazis, D. A., Chen, X.-Y., Landis, C. R. & Neese, F. All-Electron Scalar Relativistic Basis Sets for Third-Row Transition Metal Atoms. *J. Chem. Theory. Comput.* **4**, 908-919 (2008).

- 29 Wüllen, C. v. Molecular density functional calculations in the regular relativistic approximation: Method, application to coinage metal diatomics, hydrides, fluorides and chlorides, and comparison with first-order relativistic calculations. *J. Chem. Phys.* **109**, 392-399 (1998).
- 30 Neese, F., Wennmohs, F., Hansen, A. & Becker, U. Efficient, approximate and parallel Hartree–Fock and hybrid DFT calculations. A ‘chain-of-spheres’ algorithm for the Hartree–Fock exchange. *Chem. Phys.* **356**, 98-109 (2009).
- 31 Tromp, M., Moulin, J., Reid, G. & Evans, J. Cr K - Edge XANES Spectroscopy: Ligand and Oxidation State Dependence — What is Oxidation State? *AIP Conference Proceedings* **882**, 699-701 (2007).
- 32 Liu, X., Liu, Y., Hao, Y., Yang, X.-J. & Wu, B. Square helix versus zigzag chain of group 12 metal coordination polymers with 1,2-bis(diphenylphosphino)ethane (dppe). *Inorg. Chem. Commun.* **13**, 511-513 (2010).
- 33 Dunsford, J. J., Clark, E. R. & Ingleson, M. J. Direct C(sp₂)-C(sp₃) Cross - Coupling of Diaryl Zinc Reagents with Benzylic, Primary, Secondary, and Tertiary Alkyl Halides. *Angew. Chem. Int. Ed.* **54**, 5688-5692 (2015).
- 34 Grimme, S., Ehrlich, S. & Goerigk, L. Effect of the damping function in dispersion corrected density functional theory. *J. Comput. Chem.* **32**, 1456-1465 (2011).
- 35 Hariharan, P. C. & Pople, J. A. The influence of polarization functions on molecular orbital hydrogenation energies. *Theor. chim. acta* **28**, 213-222 (1973).
- 36 Frisch, M. J., Pople, J. A. & Binkley, J. S. Self-consistent molecular orbital methods 25. Supplementary functions for Gaussian basis sets. *J. Chem. Phys.* **80**, 3265-3269 (1984).
- 37 Andrae, D., Häußermann, U., Dolg, M., Stoll, H. & Preuß, H. Energy-adjusted *ab initio* pseudopotentials for the second and third row transition elements. *Theor. chim. acta* **77**, 123-141 (1990).
- 38 Marenich, A. V., Cramer, C. J. & Truhlar, D. G. Universal Solvation Model Based on Solute Electron Density and on a Continuum Model of the Solvent Defined by the Bulk Dielectric Constant and Atomic Surface Tensions. *J. Phys. Chem. B* **113**, 6378-6396 (2009).
- 39 Sheverdina, N. I., Abramova, A. V. & Kocheshkov, K. A. Complexes in the Series of Aromatic Organo-zinc Compounds Corresponding to the General Formula ArZnX. *Doklady Akademii Nauk Sssr* **134**, 853-855 (1960).
- 40 Burés, J. A Simple Graphical Method to Determine the Order in Catalyst. *Angew. Chem. Int. Ed.* **55**, 2028-2031 (2016).
- 41 Burés, J. Variable Time Normalization Analysis: General Graphical Elucidation of Reaction Orders from Concentration Profiles. *Angew. Chem. Int. Ed.* **55**, 16084-16087 (2016).
- 42 Bruker, SAINT+ v8.38A Integration Engine, Data Reduction Software, Bruker Analytical X-ray Instruments Inc., Madison, WI, USA, 2015.
- 43 Bruker, SADABS 2014/5, Bruker AXS area detector scaling and absorption correction, Bruker Analytical X-ray Instruments Inc., Madison, Wisconsin, USA, 2014/5.
- 44 Sheldrick, G. SHELXT - Integrated space-group and crystal-structure determination. *Acta Cryst. A* **71**, 3-8 (2015).
- 45 Palatinus, L. & Chapuis, G. SUPERFLIP - a computer program for the solution of crystal structures by charge flipping in arbitrary dimensions. *J Appl Crystallogr.* **40**, 786-790, doi:doi:10.1107/S0021889807029238 (2007).
- 46 Palatinus, L., Prathapa, S. J. & van Smaalen, S. EDMA: a computer program for topological analysis of discrete electron densities. *J Appl Crystallogr.* **45**, 575-580 (2012).
- 47 Sheldrick, G. Crystal structure refinement with SHELXL. *Acta Cryst. C* **71**, 3-8 (2015).
- 48 Sheldrick, G. A short history of SHELX. *Acta Cryst. A* **64**, 112-122 (2008).
- 49 Dolomanov, O. V., Bourhis, L. J., Gildea, R. J., Howard, J. A. K. & Puschmann, H. OLEX2: a complete structure solution, refinement and analysis program. *J. Appl. Crystallogr.* **42**, 339-34 (2009).
- 50 Spek, A. Structure validation in chemical crystallography. *Acta Cryst. D* **65**, 148-155 (2009).
- 51 Spek, A. Single-crystal structure validation with the program PLATON. *J. Appl. Crystallogr.* **36**, 7-13 (2003).